

ANNUAL REVIEW OF NUCLEAR SCIENCE

EMILIO SEGRÈ, *Editor*
University of California

GERHART FRIEDLANDER, *Associate Editor*
Brookhaven National Laboratory

WALTER E. MEYERHOF, *Associate Editor*
Stanford University

VOLUME 11

1961

ANNUAL REVIEWS, INC.
PALO ALTO, CALIFORNIA, U.S.A.

ENGINEERING
QC
T70
.A65
v.11

ANNUAL REVIEWS, INC.
PALO ALTO, CALIFORNIA, U.S.A.

© 1961 BY ANNUAL REVIEWS, INC.
ALL RIGHTS RESERVED

Library of Congress Catalogue Number: 53-995

FOREIGN AGENCY
Maruzen Company, Limited
6 Tori-Nichome Nihonbashi
Tokyo

PRINTED AND BOUND IN THE UNITED STATES OF AMERICA BY
GEORGE BANTA COMPANY, INC.

PREFACE

This volume follows the pattern established in previous ones. We repeat a cordial invitation to our readers to suggest topics they would like to see reviewed. The Editorial Committee welcomes this cooperation.

We gratefully thank all our contributors. The laborious task of writing good review articles should be considered as a distinct contribution to scientific welfare.

We thank again Joann Huddleston for her indefatigable editorial help.

E. SEGRÈ, *Editor*

ERRATA

Volume 10 (1960):

p. 382 Eq. 38 *read*

$$\frac{e\hbar}{2mc} \sqrt{\frac{3}{4\pi}} \sum_i (g_i l_i + g_s s_i) \text{ for } \frac{e\hbar}{2mc} \sqrt{\frac{3}{4\pi}} (g_l l + g_s s)$$

Eq. 40 *read*

$$1.16 \times 10^{-2} E_\gamma^3 \Lambda (M1) \text{ ev} \quad \text{for} \quad 2.76 \times 10^{-3} E_\gamma^3 \Lambda (M1) \text{ ev}$$

Eq. 41 *read*

$$1.04 \times E_\gamma^3 \Lambda (E1) \text{ ev} \quad \text{for} \quad 2.50 \times 10^{-1} E_\gamma^3 \Lambda (E1) \text{ ev}$$

p. 383 Eq. 42 *read*

$$8.06 \times 10^{-6} E_\gamma^5 \Lambda (E2) \text{ ev} \quad \text{for} \quad 8.02 \times 10^{-6} E_\gamma^5 \Lambda (E2) \text{ ev}$$

CONTENTS

	PAGE
STATISTICAL METHODS IN HIGH-ENERGY PHYSICS, <i>Martin Kretzschmar</i>	1
STRONG INTERACTIONS AND REACTIONS OF HYPERONS AND HEAVY MESONS, <i>G. Morpurgo</i>	41
THEORIES OF NUCLEON-NUCLEON ELASTIC SCATTERING, <i>Michael J. Moravcsik and H. Pierre Noyes</i>	95
NUCLEAR ORIENTATION, <i>Louis D. Roberts and J. W. T. Dabbs</i> . . .	175
SHIELDING OF HIGH-ENERGY ACCELERATORS, <i>S. J. Lindenbaum</i> . .	213
NEUTRON CAPTURE GAMMA RAYS, <i>G. A. Bartholomew</i>	259
NEUTRON DIFFRACTION, <i>M. K. Wilkinson, E. O. Wollan, and</i> <i>W. C. Koehler</i>	303
NUCLEAR EFFECTS OF COSMIC RAYS IN METEORITES, <i>James R. Arnold</i>	349
DETECTION OF NUCLEAR EXPLOSIONS, <i>R. Latter, R. F. Herbst, and</i> <i>K. M. Watson</i>	371
HEAVY-ION ACCELERATORS, <i>Edward L. Hubbard</i>	419
ISOTOPE EFFECTS IN CHEMICAL REACTIONS, <i>Ralph E. Weston, Jr.</i> .	439
INDUSTRIAL USES OF ISOTOPES, <i>W. F. Libby</i>	461
RELATED ARTICLES APPEARING IN OTHER ANNUAL REVIEWS . . .	483
AUTHOR INDEX	485
SUBJECT INDEX	497
CUMULATIVE INDEX OF CONTRIBUTING AUTHORS, VOLUMES 7 TO 11 .	510
CUMULATIVE INDEX OF CHAPTER TITLES, VOLUMES 7 TO 11 . . .	511

Annual Reviews, Inc., and the Editors of this publication assume no responsibility for the statements expressed by the contributors to this *Review*.

STATISTICAL METHODS IN HIGH-ENERGY PHYSICS^{1,2}

BY MARTIN KRETZSCHMAR³

Lawrence Radiation Laboratory, University of California, Berkeley, California

CONTENTS

I. INTRODUCTION.....	1
II. BASIC THEORETICAL IDEAS.....	2
A. FORMULATION OF THE FERMI MODEL AND GENERAL SURVEY..	2
B. FINAL-STATE INTERACTIONS.....	11
C. INELASTICITY AND PERIPHERAL COLLISIONS.....	13
D. METHODS FOR THE CALCULATION OF PHASE-SPACE INTEGRALS.	14
E. THERMODYNAMIC APPROXIMATION.....	19
F. ISOTOPIC SPIN CONSERVATION AND ANALYSIS OF CHARGE STATES.....	20
III. APPLICATIONS TO SPECIAL PROCESSES.....	22
A. MESON PRODUCTION IN NUCLEON-ANTINUCLEON ANNIHILATION	22
B. MESON PRODUCTION IN PION-NUCLEON COLLISIONS.....	27
C. MESON PRODUCTION IN NUCLEON-NUCLEON COLLISIONS AT ENERGIES BELOW 30 BEV.....	29
D. MESON PRODUCTION IN NUCLEON-NUCLEON COLLISIONS AT COSMIC RAY ENERGIES.....	33
LITERATURE CITED.....	35

I. INTRODUCTION

In the 25 years since the theoretical prediction of the meson by Yukawa, it has not been possible in spite of great efforts to develop a satisfactory theory for a general description of the interactions of pi mesons and nucleons. The most promising approach today uses the method of dispersion relations (53) but is as yet restricted to the treatment of a few simple processes. In this method as in earlier ones the complexity of the mathematical formalism grows rapidly when one goes to higher energies (>1 Bev) and considers reactions with three or more particles in the final state. At present there is little hope that a quantitative theory of multiple-particle production based

¹ The survey of the literature pertaining to this review was completed in February 1961.

² This work was done under an appointment supported by the International Cooperation Administration under the Visiting Research Scientists Program administered by the National Academy of Sciences of the United States of America; and it was supported in part by the United States Air Force under Contract No. AF 49(638)-327 monitored by the AF-Office of Scientific Research of the Air Research and Development Command and the Office of Naval Research under Contract No. r-222(60) (NR 041-221).

³ Permanent address: Max-Planck-Institut für Physik und Astrophysik, München 23/Germany.

on fundamental principles can be developed in the near future. Therefore, for a long time to come we shall have to use models of various kinds for the interpretation of experimental results on multiple-particle production.

Inherent in the nature of such a model is its property of overemphasizing certain aspects of the reaction and neglecting certain others. Since, to some extent, which aspects an author considers most significant depends on his personal taste, we are faced in this branch of physics with a large number of differing models (connected with the names of Bhabha, Fermi, Heisenberg, Landau, Lewis, Oppenheimer, Wouthuyzen, and many others), each of which has at least some qualitative justification from experimentally observed facts. Most of these models are formulated for multiple-pion production in nucleon-nucleon collisions at extremely high energies. The basic assumptions of these models [apart from a recent one based on analogies to the Cherenkov effect (61, 62, 192)] and their interconnections were reviewed recently by Koba & Takagi (114) and earlier in somewhat more detail by Rozental & Chernavskii (170).

In this article we shall restrict the discussion to the Fermi model and its various refinements because it is distinguished from the others by two important features.

(a) Its formulation is sufficiently general to allow an application to many different processes such as nucleon-antinucleon annihilation, and production of pions and strange particles in meson-nucleon and in nucleon-nucleon collisions. This generality is obtained because one starts with a general cross-section formula and inserts into it a simplifying assumption about the matrix element of the process, which amounts to saying that many features of these high-energy reactions are dominated by the density in phase space of the final states that are accessible from the given initial state under consideration of all conservation laws. For this reason the Fermi model is frequently called the "statistical model" or the "statistical theory."

(b) Preferably the Fermi model is to be applied in the "low"-energy range (as compared with cosmic ray energies) between 1 or 2 and 30 Bev of laboratory energy and is thus of great interest in connection with the big accelerators. At the lower end of this energy range, the model becomes unreliable because only a few final states are accessible and their details are important; at the higher end, deviations occur because of insufficient consideration of peripheral interactions.

II. BASIC THEORETICAL IDEAS

A. FORMULATION OF THE FERMI MODEL AND GENERAL SURVEY

The general problem from the point of view of scattering theory.—Let i be a uniquely defined initial state describing the collision of two elementary particles with masses m'_k and four-momenta⁴ $p'_k = (\omega'_k, \mathbf{p}'_k)$, where

⁴ Throughout this paper we use units such that $\hbar = c = 1$. The scalar product of two four-vectors $x = (x_0, \mathbf{x})$ and $y = (y_0, \mathbf{y})$ is defined as $xy = x_0y_0 - \mathbf{x} \cdot \mathbf{y}$. For example $p'_k{}^2 = \omega'_k{}^2 - \mathbf{p}'_k{}^2 = m'_k{}^2$.

$\omega_k'^2 = m_k'^2 + p_k'^2$ and $k=1,2$; then we obtain from S -matrix theory for the cross section of the reaction leading to any state out of a set Φ of final states f (107):

$$\sigma_{\Phi} = \frac{(2\pi)^2 \cdot \omega_1' \omega_2'}{\sqrt{(p_1' p_2')^2 - m_1'^2 m_2'^2}} \sum_{f \in \Phi} \delta^4(P_f - p_1' - p_2') |M_{fi}|^2 \quad 1.$$

Here P_f is the total four-momentum in the final state f ; and \sum stands for integration over continuous, and summation over discrete, variables. Denoting by I the unity operator, the matrix elements M_{fi} can be related to the scattering matrix S by

$$S_{fi} = I_{fi} + i \cdot \delta^4(P_f - p_1' - p_2') M_{fi} \quad 2.$$

This is a rigorous formula; the matrix element M_{fi} , however, is essentially unknown. The calculation of its numerical value is the as yet unsolved, basic problem of quantum field theory. Most of what we do know about M_{fi} follows from its invariance with regard to certain groups of transformations such as translations, Lorentz transformations, and rotations in isotopic spin space. Each such invariance requires M_{fi} to satisfy a corresponding conservation law. We know that in all strong interactions the following quantities are conserved: total four-momentum P , total angular momentum J (including spin), total isotopic spin T , total baryon number N , total strangeness S , and total electric charge, the latter being described as conservation of the three-component T_3 of the total isotopic spin.

Therefore, M_{fi} may be represented as

$$M_{fi} = \delta_{N_f N_i} \delta_{S_f S_i} \delta_{T_3 f T_3 i} \sum_{\alpha, J, T} \sum_{\alpha', J', T'} \langle f | J, T, \alpha \rangle \delta_{JJ'} \delta_{TT'} M(\alpha, \alpha', J, T) \langle J', T', \alpha' | i \rangle \quad 3.$$

The unspecified quantum numbers α, α' serve to make the states $|N_i, S_i, T_{3i}, J', T', \alpha'\rangle$ and $|N_f, S_f, T_{3f}, J, T, \alpha\rangle$ uniquely determined. All dynamical effects are now contained in the unknown matrix element $M(\alpha, \alpha', J, T)$. The transformation coefficients $\langle f | \dots, J, T, \alpha \rangle$ and $\langle \dots, J', T', \alpha' | i \rangle$ can be factored into an isotopic-spin-dependent part, which will be discussed in Section II F, and a second part, which can in principle be derived from the kinematics of the reaction. In practice, however, this second part is never calculated. Since initial and final states are usually given in a momentum representation, one is forced by computational difficulties to neglect angular momentum conservation (see also p. 10).

Introduction of the statistical hypothesis.—The purpose of the statistical theory is to investigate the usefulness of certain simple assumptions about the dependence of $M(\alpha, \alpha', J, T)$ on the conserved quantities and on the masses, momenta, and quantum numbers of the final-state particles. To obtain reliable answers it is important to evaluate the contents of Equations 1 and 3 as far as feasible without further approximations. However, to work out the essential points let us disregard for the moment all spins,

charges, etc., and all conservation laws except the one for total four-momentum. For σ_Φ as given by 1 to be Lorentz-invariant, M_{fi} must have the form

$$M_{fi} = \left(\frac{m'_1 \cdot m'_2 \cdot m_1 \cdot m_2 \cdot \dots \cdot m_n}{\omega'_1 \cdot \omega'_2 \cdot \omega_1 \cdot \omega_2 \cdot \dots \cdot \omega_n} \right)^{1/2} \cdot M'_{fi} \quad 4.$$

where m_1, \dots, m_n and $\omega_1, \dots, \omega_n$ denote masses and energies of the particles in the final state and M'_{fi} now depends only on Lorentz-invariant quantities. In the nonrelativistic limit we have $M_{fi} = M'_{fi}$.

According to Fermi (76, 77) we may assume

$$|M'_{fi}|^2 \propto (2\pi)^{-3(n-1)} \Omega^{n-1} \quad 5.$$

where Ω is a quantity of the dimensions of a volume that is independent of the individual momenta of particles in the final state, but is eventually dependent on the total center-of-mass energy E . The summations in 1 are thus greatly simplified; e.g., the cross section of the reaction, which leads from the given initial state to a final state with n particles with masses m_1, \dots, m_n and nonspecified momenta, is proportional to

$$\sigma(E; m_1, \dots, m_n) \propto P(E; m_1, \dots, m_n) = (\Omega/V)^{n-1} \cdot (V/8\pi^2)^{n-1} \rho(E, 0; m_1, \dots, m_n) \quad 6.$$

where V is a large, but arbitrary normalization volume whose role will become clear later on and $\rho(E, 0; m_1, \dots, m_n)$ stands for the phase-space integral [Neuman (150), Srivastava & Sudarshan (179)]

$$\rho_S(E, P; m_1, \dots, m_n) = \int d\mathbf{p}_1 \dots \int d\mathbf{p}_n \frac{m_1 m_2 \dots m_n}{\omega_1 \omega_2 \dots \omega_n} \delta \left(E - \sum_{i=1}^n \sqrt{m_i^2 + \mathbf{p}_i^2} \right) \delta^3 \left(\mathbf{P} - \sum_{i=1}^n \mathbf{p}_i \right) \quad 7.$$

Lepore, Neuman & Stuart (127; see also 145) proposed a theory based on somewhat different assumptions, that leads to phase-space integrals in which the denominator $(\omega_1 \cdot \omega_2 \cdot \dots \cdot \omega_n)^{-1}$ in Equation 7 is replaced by $(\omega_1 \cdot \omega_2 \cdot \dots \cdot \omega_n)^{-3/2}$. Earlier only phase-space integrals of the following form were considered

$$\rho_F(E, P; m_1, \dots, m_n) = \int d\mathbf{p}_1 \dots \int d\mathbf{p}_n \delta \left(E - \sum_{i=1}^n \sqrt{m_i^2 + \mathbf{p}_i^2} \right) \delta^3 \left(\mathbf{P} - \sum_{i=1}^n \mathbf{p}_i \right) \quad 8.$$

which corresponds to $M_{fi} \approx M'_{fi}$.

The latter version is used in all calculations before 1958 and in recent work at the CERN and Dubna laboratories, the ρ_S version mainly by the Berkeley group in investigations of antinucleon annihilation. With the same Ω the phase-space integral ρ_S favors smaller average energies and higher multiplicities of the final particles than ρ_F , but the use of a slightly larger Ω in connection with ρ_F may partly compensate these differences. Since the presently available numerical material is too scarce, a systematic comparison is not possible. The numerical evaluation of ρ_S is comparatively easy, because its Lorentz invariance permits the use of simple recurrence formulas (cf. Eq. 24 and 25); on the other hand, in view of the crude approximation 5, the property of Lorentz invariance by itself does not necessarily guarantee better agreement with experiment.

Relations 5 and 6 are interpreted as describing the following physical picture: To an observer in the center-of-mass system each of the two incoming particles appears to have the shape of a Lorentz-contracted sphere. At the moment of collision the two particles penetrate each other, and the total energy E of the system is concentrated in a small space region of volume Ω . Because of the strong interactions a rapid succession of transitions now sets in, particles of various kinds are created and annihilated, and if the total energy is sufficiently high, there will be a large number of possible final states and each one can be arrived at in a great many different ways. This circumstance suggests that some sort of statistical equilibrium will be attained, so that each state which is accessible from the given initial state via strong interactions will finally be excited to its average statistical strength. Transitions by electromagnetic or weak interactions are much too slow to contribute to the statistical equilibrium. Therefore, all final states involving the production of photons, electrons, muons, and neutrinos or violation of strangeness and isotopic spin conservation have to be dropped from the considerations. To be more specific, the system finally reaches a state in which it looks as if the n final particles could be considered as a gas of free particles confined to the large normalization volume V ; i.e. the cross section of each final state should be proportional first to $(\Omega/V)^{n-1}$, the probability that all n particles will be found simultaneously assembled inside the volume⁵ Ω ; second to the density (with regard to the total energy E) of final states in the phase space.⁶ As was remarked by Fermi (76) this approach in a sense represents the extreme opposite of perturbation theory.

According to this picture, Ω is assumed to be the volume of the larger of the two Lorentz-contracted spheres, which are occupied by the incoming particles. For all practical purposes, at least one of them will be a baryon or antibaryon, which as a result of its strong interaction with the pion field is surrounded by a pion cloud. The size of Ω will therefore be approximately determined by the pion Compton wavelength as

$$\Omega \approx \Lambda \cdot \Omega_0 = \Lambda \cdot (4\pi/3\mu^3) \quad 9.$$

where μ is the pion mass and the Lorentz-contraction factor is given by ($m'_1 \geq m'_2$)

$$\Lambda = m'_1/\omega'_1 = 2m'_1 E / (E^2 + m'^2_1 - m'^2_2) \quad 10.$$

The justification of this factor is occasionally doubted and the factor com-

⁵ The exponent $n-1$ instead of n indicates that the position of Ω inside V is undetermined. Originally in 5 it followed from dimensional reasons, because the number of degrees of freedom of the final state is not $3n$, but $3(n-1)$ because of three-momentum conservation.

⁶ It is sometimes argued that the right-hand side of 6 is the phase-space density of final states for a system, which is enclosed in Ω . Because the integrations in 7 and 8 represent summations over the possible momentum eigenstates of free particles in infinite space, this argument is not correct; because of the extremely small size of Ω , not even approximately. For further discussion of this point cf. Lewis (129, p. 243), Koba & Takagi (114, p. 27), and others (4, 118, 149).

pletely omitted or replaced by other E -dependent terms (150, 157). However, the successful application of the Fermi model to pion-nucleon and nucleon-nucleon collisions at various energies supports Fermi's original suggestion. As Fermi has already emphasized, Equation 9 is only an order-of-magnitude estimate, and in practice Ω should be looked at as a parameter which can be varied in certain limits to give best agreement with experiments.

The simple physical picture described above has over the years been a constant source for refinements and implementations of the theory; on the other hand, it has been subject to a number of objections which outline its limits of validity:

(a) A certain fraction of the collisions of the initial particles will be peripheral. Then, at first, only the overlap region of the two meson clouds will be excited. The time necessary for the excitation to propagate with the velocity of light to the outer edges of the particles ($\approx \mu^{-1}$) is Λ^{-1} times longer than the collision time ($\approx \Lambda \cdot \mu^{-1}$). For nucleon-nucleon collisions at 29-Bev laboratory energy, we have $\Lambda^{-1} = 4$; for cosmic ray energies, Λ^{-1} may be much larger. For large Λ^{-1} it would be unreasonable to assume the physical system will remain in Ω until the whole volume is uniformly excited and an equilibrium established. Rather, one would expect two highly excited particles ("fireballs") to emerge from the collision region. Evidence from cosmic ray events supports this point of view (cf. III D).

(b) At extremely high energy densities the particle concept itself may become questionable because of continuous creation and reannihilation (166). One expects the energy concentration to expand like a fluid beyond the initial collision volume Ω , until the energy density has become so low that the mean free path of a particle in the "fluid" is of the order of magnitude of its range of interaction with other particles (e.g. one pion Compton wavelength). Only in this last stage does the assignment of definite particle numbers make sense. Pomeranchuk (166) suggests replacing Ω^{n-1} in Equation 6 by $(n\Omega)^{n-1}$ to take the expansion stage cursorily into account. Alternatively, the agreement with experiment can be greatly improved by detailed consideration of all resonant final-state interactions that occur in the pion-nucleon, pion-hyperon, and pion-pion system (cf. II B). At very high energies, where high multiplicities prevail, the expansion of the energy "fluid" can be described by the formalism of relativistic hydrodynamics [Landau (124); for further developments see (27)].

(c) The interactions of K mesons with other particles are somewhat weaker and of shorter range than the corresponding interactions of pions; moreover, K mesons probably originate closer to the nucleon core than pions. Strange particles will therefore not fully attain statistical equilibrium and their production will be less copious. As was first pointed out by Haber-Schaim & Yekutieli (94), such effects can be accounted for in an approximate way by generalizing 5 and 9 to⁷

⁷ This *ansatz* seems to be more natural than the one used by Barashenkov *et al.* (12), which involves linear combinations of different volumes. Also compare Hagedorn (101).

$$|M'_{fi}|^2 \propto (2\pi)^{-3(n-1)} \Lambda^{n-1} (\Omega_0^{(1)} \Omega_0^{(2)} \dots \Omega_0^{(n)})^{n-1/n} \quad 11.$$

where now the size of $\Omega_0^{(i)}$ depends on the nature of the i th particle. It seems reasonable to use the same volume Ω_π for all pions and nucleons, the same volume Ω_Y for all hyperons, and Ω_K for K mesons. In particular, the following choices have been discussed: (1) $\Omega_\pi = \Omega_0 = 4\pi/3\mu^3$, $\Omega_Y = \Omega_\pi$, and $0.1 < (\Omega_K/\Omega_\pi) < 0.3$. This corresponds roughly to Gell-Mann's global symmetry hypothesis and is the choice that gave best agreement with experimental data of various kinds. Earlier calculations using $\Omega_K = (\mu/m_K)^3 \Omega_0 = 0.02\Omega_0$, where m_K is the K -meson mass, led to an insufficient amount of K -meson production. For more detailed discussion see the papers by Barashenkov and co-workers (5, 11, 12, 14, 15, 144). (2) $\Omega_\pi = \Omega_0 = 4\pi/3\mu^3$ and $\Omega_Y = \Omega_K = (\mu/m_K)^3 \Omega_0$. This corresponds to weak pion-hyperon interaction and greatly underestimates strange-particle production cross sections. (3) $\Omega_\pi = \Omega_Y = \Omega_K = \Omega_0$, which represents the unmodified Fermi model and greatly overestimates strange-particle production. Figure 1 demonstrates the influence of such assumptions on hyperon production and on the K/\bar{K} ratio. Much more numerical material of this kind can be found in the articles of Hagedorn (98, 99).

(d) Even though angular momentum conservation is neglected, the number of spin states and the statistics of the produced particles must somehow be taken into consideration. As already proposed by Fermi (79), one adds to Equation 6 for the spins a factor $\prod_{i=1}^n (2s_i + 1)$, where s_i is the spin of the i th particle and, to estimate the effects of statistics, another factor $(n_\alpha! n_\beta! n_\gamma! \dots)^{-1}$ indicating that among the final particles there are groups of $n_\alpha, n_\beta, n_\gamma, \dots$ identical particles ($n_\alpha + n_\beta + n_\gamma + \dots = n$). Having introduced isotopic spin, all final-state particles belonging to the same isotopic multiplet form such a group; e.g., $n_\alpha, n_\beta, n_\gamma$ might be the numbers of pions, nucleons, and antinucleons respectively. In an investigation which uses the correct statistics for each type of particles from the beginning, Magalinski & Terletskii (138) confirm this result. In addition, they find small correction terms (1 to 10 per cent in a special case discussed by them) which increase the statistical weights of Bose particles and decrease them for Fermi particles.

Scope of the model and a general formula.—Collecting our above results we replace 6 by the more complete formula

$$P(E; m_1, \dots, m_n) = \frac{g_{k_1 k_2 k_3}(T) \prod_{i=1}^n (2s_i + 1)}{(2\pi)^{3(n-1)} \prod_\alpha n_\alpha!} \left(\prod_{i=1}^n \Lambda \cdot \Omega_0^{(i)} \right)^{n-1/n} \cdot \rho(E, 0; m_1, \dots, m_n) \quad 12.$$

In writing the weight factor $g_{k_1 k_2 k_3}(T)$ we have anticipated a result following from isotopic spin conservation (cf. II F) and have assumed that the initial state is an eigenstate of total isotopic spin T and that we have summed over all possible charge distributions in the final state. Also we like to mention that resonant final-state interactions can be treated by assuming formation of isobars, which leave the interaction region and decay outside (for more details cf. II B). As far as expression 12 is concerned, isobars are treated just like elementary particles with their respective masses inserted into ρ .

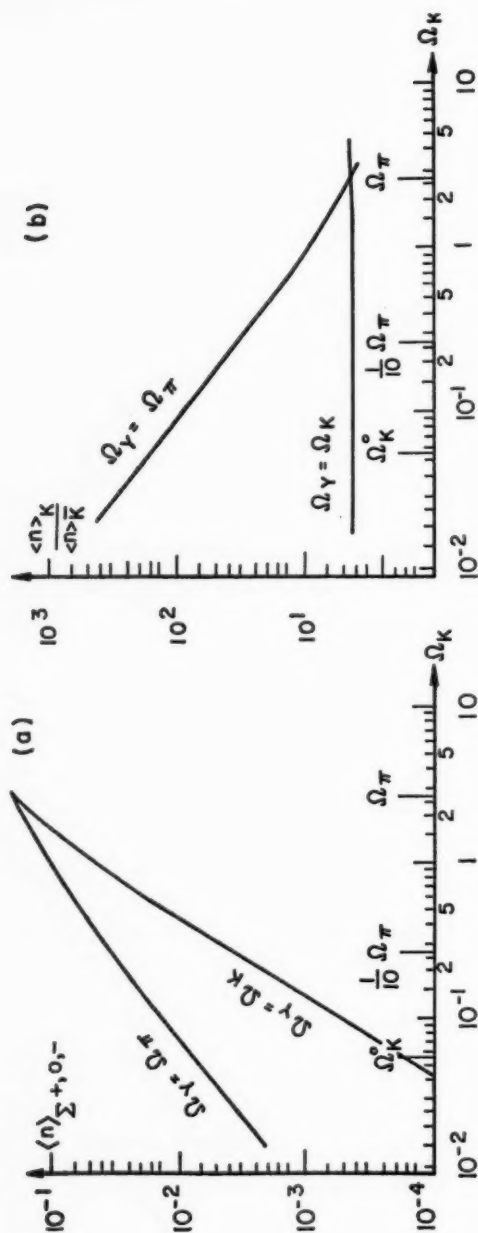


FIG. 1. Dependence on the choice of production volumes of (a) the total number of Σ hyperons and (b) the ratio of the number of K mesons to the number of \bar{K} mesons, both in nucleon-nucleon collisions at 6.2 Bev [Hagedorn (98)]. Here Ω_K^0 is the volume corresponding to the K -meson Compton wavelength.

The production volume for pion-nucleon and pion-pion isobars is usually chosen to be Ω_π ; their decay must be considered in a second step.

Now, what can the statistical model be expected to predict? It is clear from 11 that no absolute, but only relative, cross sections (i.e. branching ratios) can be calculated. If, however, some inelastic cross section (e.g., the total cross section excluding diffraction scattering) is known experimentally, all others (partial cross sections) can be related to it by the model.

Many formulas like 12 can be written down; in particular, the momentum and Q -value distributions in the reaction channel leading to m_1, \dots, m_n are obtained essentially by omitting one or two momentum integrations, respectively, in evaluating $\rho(E, 0; m_1, \dots, m_n)$. The shape of these distributions is, of course, independent of the $\Omega_0^{(i)}$. In displaying experimental results one is often forced to combine the data from several reaction channels (e.g., because neutral particles escaped observation). In this situation, to compare with the model one has to combine the theoretical predictions from the same set of channels, weighing them with the $P(E; m_1, \dots, m_n)$ given by 12. In this way one can also derive mean multiplicities, mean kinetic energies, and other averaged quantities. Explicit formulas including proper normalization are given in the recent review by Hagedorn (101). Furthermore, the model makes definite predictions for the energy dependence of branching ratios and all other quantities mentioned above. These seem to be, generally, in good agreement with experiment; however, in the future more detailed studies might serve to discriminate between ρ_S and ρ_F and to test the justification of the Lorentz-contraction factor Λ and the validity of various modifications of the original theory.

Computational difficulties arise not only because the evaluation of the phase-space integrals becomes extremely complex with increasing particle number, but also because of the rapid increase of the number of final states with the total center-of-mass energy. For example, in the case of a nucleon-nucleon collision, the number of statistical weights (as given by 12) to be calculated is 10 at 2.75 BeV, 50 at 6.2 BeV, and 600 at 25 BeV (99). Therefore, at higher energies the use of electronic computers is an absolute necessity; even so, calculations become unfeasible at energies above 50 BeV (apart from limitations intrinsic to the model) so that other methods have to be used (cf. II E and III D). The general procedure and detailed programs for such calculations have been described in three reports by Hagedorn [(96, 97); also cf. Hoang & Young (103)]. Another very general and versatile program is now being worked out in Berkeley by Lepore & Riddell (128).

Taking our model literally, we would predict isotropy for all angular distributions. This prediction, however, cannot seriously be expected to be correct, because peripheral collisions were treated insufficiently, angular momentum conservation was neglected, and spins entered only through the weight factors $\prod_i (2s_i + 1)$. Just these things would have been most relevant.⁸ Because of the mathematical complexity of the problem, only quali-

⁸ In Hagedorn's derivation (99, 101), the M'_{fi} as given by 5 are not proper S -matrix elements, but averages of such over all angular coordinates. Thus, the prediction of angular distributions is expressly excluded.

tative indications are available for the effect of possible correction terms accounting for angular momentum conservation (76, 78). As shown below, the situation with regard to angular correlations is somewhat more hopeful.

Formulation of the model in terms of spherical waves.—To account for selection rules in nucleon-antinucleon annihilation, the consideration of energy and angular momentum conservation at the expense of neglecting three-momentum conservation was recently attempted [Cook & Lepore (59), Koba (112)]. This reaction is particularly favorable because only spinless particles are produced. One argues that each factor Ω/V in 6 stands actually for $\int_0^\infty |\psi(x)|^2 dx$, where $\psi(x)$ is the wave function of a spinless particle, normalized in V . This is clear in a momentum representation, where the $\psi(x)$ are plane waves; in a description by spherical waves, however, when we correlate the particles only through energy conservation and neglect three-momentum, we have to make the following replacement⁹ in 6 for each final particle.

$$\frac{\Omega_0}{V} \frac{V}{(2\pi)^3} \int d\mathbf{p} \cdots \rightarrow \frac{2}{\pi} \sum_{l,m} \int_0^\infty p^2 dp \int_{\Omega_0} r^2 dr d\omega |j_l(pr) Y_l^m(\omega)|^2 \cdots \quad 13.$$

where the j_l are spherical Bessel functions and the Y_l^m , spherical harmonics. To account for angular momentum conservation too, the wave function to be squared must describe the complete n -particle final state and must be an eigenfunction of total angular momentum L , and $L_z = M$. Then we obtain, instead of 12, for the statistical weights (R is the radius of Ω_0):¹⁰

$$P(E, L, M; m_1, \dots, m_n) = \frac{g_{k_1 k_2} \cdots (T)}{\prod_{\alpha} n_{\alpha}!} \cdot \frac{2^n}{\pi^n} \sum_{(L)} \int_0^R r_1^2 dr_1 \int d\omega_1 \cdots \int_0^R r_n^2 dr_n \int d\omega_n \int_0^\infty p_1^2 dp_1 \cdots \int_0^\infty p_n^2 dp_n \delta(E - \omega_1 - \omega_2 - \cdots - \omega_n) \left| \sum_{m_1, \dots, m_n} K_n(L, M, l_1, \lambda_1, \dots, l_{n-2}, \lambda_{n-2}, l_{n-1}, l_n) Y_{l_1}^{m_1}(\omega_1) \cdots Y_{l_n}^{m_n}(\omega_n) j_{l_1}(p_1 r_1) \cdots j_{l_n}(p_n r_n) \right|^2 \quad 14.$$

The K_n are composed of Clebsch-Gordan coefficients and describe the coupling of the individual angular momenta l_1, \dots, l_n to total angular momentum L ; the quantum numbers $\lambda_1, \dots, \lambda_{n-2}$ distinguish the various ways in which this can be done. The summation $\sum_{(L)}$ extends over all possible combinations $l_1, \dots, l_n, \lambda_1, \dots, \lambda_{n-2}$. Using orthogonality properties, 14 can then be reduced to

$$P(E, L, M; m_1, \dots, m_n) = \frac{g_{k_1 k_2} \cdots (T)}{\prod_{\alpha} n_{\alpha}!} \cdot \frac{2^n}{\pi^n} \sum_{(L)} \int_0^R r_1^2 dr_1 \cdots \int_0^R r_n^2 dr_n \cdot \int_0^\infty p_1^2 dp_1 \cdots \int_0^\infty p_n^2 dp_n \delta(E - \omega_1 - \omega_2 - \cdots - \omega_n) |j_{l_1}(p_1 r_1) \cdots j_{l_n}(p_n r_n)|^2 \quad 15.$$

⁹ Since by neglect of three-momentum conservation there are $3n$ degrees of freedom, we have as many factors Ω/V as we have final particles.

¹⁰ We may eventually insert additional energy-dependent factors as in Equation 4.

In this outline we have followed Koba's (112) presentation, which differs in some details from that of Cook & Lepore (59).

Angular correlations.—Similar ideas have been used by Goldhaber *et al.* (90) to explain the angular correlations of pions emitted in nucleon-anti-nucleon annihilation. It is observed that pion pairs with like charges have greater preference for small angles than pion pairs with unlike charges (89), which is explained as an effect of Bose statistics causing a clustering of pions with like charges in states with similar momenta. Whereas so far statistics have entered only through the weight factor $(\prod_{\alpha} n_{\alpha}!)^{-1}$, for the derivation of angular correlation functions the symmetry of the wave functions must be used explicitly. For example, for a pair of like pions we write (the normalization constant N is chosen so that $\phi(\mathbf{x}_1, \mathbf{x}_2)$ is normalized in V).

$$\phi(\mathbf{x}_1, \mathbf{x}_2) = (\sqrt{2} \cdot NV)^{-1} \{ \exp [i\mathbf{p}_1\mathbf{x}_1 + i\mathbf{p}_2\mathbf{x}_2] + \exp [i\mathbf{p}_2\mathbf{x}_1 + i\mathbf{p}_1\mathbf{x}_2] \} \quad 16.$$

and with this we make the replacement

$$\left(\frac{\Omega}{V} \right)^2 \rightarrow \int_{\Omega} d\mathbf{x}_2 \int_{\Omega} d\mathbf{x}_1 |\phi(\mathbf{x}_1, \mathbf{x}_2)|^2 = \frac{1}{N^2} \left(\frac{\Omega}{V} \right)^2 \left[1 + 9 \left(\frac{\cos t}{t^2} - \frac{\sin t}{t^3} \right)^2 \right] \quad 17.$$

where $t = R|\mathbf{p}_1 - \mathbf{p}_2|$. From this the correlation functions are easily obtained.

Various theoretical investigations.—Despite different starting points, we find similarities in the final formulas when we compare Fermi's statistical model to the bremsstrahlung theory of Lewis, Oppenheimer & Wouthuyzen (130). This connection has been investigated in the framework of S -matrix theory by numerous Japanese authors, whose work is briefly reviewed by Koba & Takagi (114). On the other hand, the problem of a consistent covariant formulation of the Fermi model and of relativistic conservation theorems (e.g., angular momentum tensor) has been discussed by Neuman (150) from the viewpoint of the theory of the microcanonical ensemble.

B. FINAL-STATE INTERACTIONS

As the final particles emerge from the collision region and separate from each other, the long-range parts of the forces will make themselves felt. In particular, pion-nucleon, pion-hyperon, or pion-pion resonances will strongly influence the observed multiplicities and branching ratios. Such effects were predicted very early by Belinfante (32) and Peaslee (159) and found to be important from an analysis of the first experiments on multiple-meson production [Fowler *et al.* (82)]. The original Fermi model disagreed strongly with these experiments but was improved by Kovacs (120), who supplemented the Fermi matrix element, Equation 5, by a term that describes pion-nucleon scattering in the framework of the static theory of Chew & Low. This modification was derived for low energies and low multiplicities (one or two) only. A mathematically much simpler proposal was made by Belenkii & Nikishov (30). They suggested that a resonating pion-nucleon system because of the small width of the $J = T = \frac{3}{2}$ resonance at 195 Mev behaves like a metastable particle N^* (isobar) with a lifetime just long enough to allow escape from the reaction region Ω . For the purposes of the statistical model, N^* has to be treated just like an elementary particle with

spin $\frac{3}{2}$, isospin $\frac{3}{2}$, and mass 1.31 (nucleon masses), which decays later on into a nucleon (N) and a pion.¹¹ For example, in a nucleon-nucleon collision, one considers, as possible final states leading to production of n pions, $2N+n\pi$, $N+N^*+(n-1)\pi$, $2N^*+(n-2)\pi$ plus states with strange particle, anti-nucleon, and anti-isobar formation. In proton-proton collisions at 2.75 Bev (36), one observes a branching ratio $(2N+\pi):(2N+2\pi):(2N+3\pi)$ of 36:48:16 compared with 31:50:19 according to the statistical theory with isobars and 69:29:2 without isobars [Cerulus & Hagedorn (48)]. The isobar hypothesis is also strongly reflected in the calculated momentum spectra of secondary particles.

Related to this is another model created by Lindenbaum & Sternheimer (131, 132), which differs from the modified statistical model in that pion production occurs exclusively through isobar formation and in that the detailed shape of the pion-nucleon $J=T=\frac{3}{2}$ resonance enters [see also (125)]. Their model makes predictions on the production of one additional pion in pion-nucleon collisions and of one or two pions in nucleon-nucleon collisions. In the latter case the ratio of single to double production is an additional parameter. There is also room for various assumptions on the angular distributions for isobar production and decay. Most of the experimental material at energies below 3 Bev is being compared to this Lindenbaum-Sternheimer model instead of the modified statistical model, the agreement being moderately good, though some discrepancies seem to exist (50, 65).

The question arises whether the higher resonances of the pion-nucleon system in the $T=\frac{3}{2}$ state at 600 Mev and 900 Mev have to be considered in such models. [For the appropriate generalization of the Lindenbaum-Sternheimer model see (133).] Cerulus & Hagedorn (48, 98, 99) conclude from calculations for proton-proton collisions at 2.75, 6.2, and 25 Bev, using a statistical model with $J=T=\frac{3}{2}$ isobar, that this is indeed unnecessary. Experimentally, a fairly weak effect of these resonances on the momentum spectra has been found only at energies higher than 2 Bev (51). In the meson-theoretic picture an explanation for this might be that the excitation of the isobars is effected by pion exchange, as a consequence of which the excitation cross section contains a factor $(q^2-\mu^2)^{-2}$, where q is the four-momentum transfer between the nucleons. The larger q^2 , the smaller this factor is, and it therefore tends to dampen the effect of higher resonances (176). Also, the resonances might be so broad that the lifetime of the isobars is too short to allow escape from the reaction region.

Apart from resonant interactions, the possibility of final-state annihilation of nucleon-antinucleon pairs with small relative momenta (98, 99) and the possibility of deuteron formation from final-state neutron-proton pairs have been discussed. The latter is expected, if the attention is fixed on a particular reaction channel, to enhance the meson production cross section near

¹¹ A similar proposal was made by Yamamoto (189). Pion-pion, pion-hyperon, and other resonances can be considered in the same fashion. In a later paper Belenkii (26) has given additional theoretical support to this picture.

the threshold of that channel (41). On the other hand, for the interpretation of observations made at the 25-Bev CERN accelerator (57, 58), the relative cross section for deuteron production in proton-proton collisions at that energy is needed. In a calculation by Hagedorn (100) which gave the right order of magnitude, the deuteron was treated like an elementary particle; however, in 12 the production volume $\Omega_0^{(d)}$ was assumed to be ($\Omega_0 = 4\pi/3\mu^3$)

$$\Omega_0^{(d)} = \Omega_0 \int_{\Omega_0} |\psi_d|^2 d\tau \approx \frac{1}{5} \Omega_0 \text{ to } \frac{1}{10} \Omega_0 \quad 18.$$

where ψ_d is a Hulthén-type deuteron wave function with a hard core. This expression essentially reflects the small probability that the big deuteron can be squeezed into a volume as small as Ω_0 . Schiff (175) confirmed this result by a more detailed treatment of the neutron-proton final-state interaction [see also Ishida (105)].

C. INELASTICITY AND PERIPHERAL COLLISIONS

The statistical model as such pertains only to completely inelastic collisions, in which the total available energy is supplied for the production of secondary particles. Most central collisions are of this type, but they constitute only a part of the actual events. As already mentioned, peripheral collisions at high energies are likely to result in the formation of two radiating centers moving along the original directions of the incoming particles. An important, but as yet not satisfactorily solved, problem is the description of events that lie in between these two extremes and the estimation of the relative probabilities of the various types of collisions.

If we define the inelasticity K of a nucleon-nucleon collision as the percentage of total kinetic energy of the incoming nucleons in the center-of-mass system that is spent for production of secondary particles,¹² then we observe, experimentally, inelasticities of $K = 50 \pm 5$ per cent throughout the laboratory energy range 3–10 Bev (38, 42, 63, 108, 185), while the statistical theory would predict, e.g. at 6.2 Bev, $K = 74$ per cent (23). This discrepancy is also reflected in the fact that, at least at 6 Bev and above, experimentally observed nucleon momentum spectra are much more energetic, meson spectra much softer than those predicted by theory (cf. Fig. 6). Furthermore, the higher the energy, the more the angular distributions of nucleons and mesons become anisotropic with a peaking in the forward and backward directions (38, 108, 109).

To get an indication of what fraction of the actual events the statistical model might be applicable to, v. Behr & Cerulus (23) assume that a nucleon-nucleon collision at 6.2 Bev results in either (a) a central collision describable by the statistical model, (b) excitation of one nucleon to an isobar in the $J = T = \frac{3}{2}$ state without changing the nucleon's initial direction, or (c) excitation of both nucleons to such isobars. The relative probabilities of the

¹² Cosmic ray physicists use a different notion of inelasticity, namely, the fraction of kinetic energy of the primary particle in the laboratory system that is carried away by secondary particles.

three types of reaction are introduced as additional parameters. Assuming that about 50 per cent of all events are central collisions and the others peripheral, v. Behr & Cerulus can fit almost within the limits of error all available experimental data, including angular distributions (cf. Table I).

The same problems for nucleon-nucleon collisions at 9 Bev were discussed by Barashenkov *et al.* (8, 18, 19, 20) by means of a rough model without free parameters, which, however, overestimates the amount of central collisions and is difficult to reconcile with the observed low inelasticities.¹³ In this model, peripheral nucleon-nucleon collisions are viewed essentially as collisions between one of the nucleons and a pion in the cloud surrounding the other one, and their outcome is related, by using rough field-theoretical estimates on the momentum distribution in the pion cloud, to experimental data or to a statistical model for pion-nucleon collisions at a corresponding energy. Similar calculations, including pion-pion interactions, have been made for pion-nucleon collisions at 5 Bev and 6.8 Bev [Barashenkov (6, 8, 9)]. A presumably better way to describe the physical picture outlined above is indicated by the recently much discussed field-theoretical approach based on the assumption of one-pion exchange, which explains many important features of such collisions at least qualitatively. Extensive references to most of the work in this direction can be found in the papers of Salzman & Salzman (174) and of Yajima *et al.* (187).

D. METHODS FOR THE CALCULATION OF PHASE-SPACE INTEGRALS

As soon as the first systematic attempts were made to compare the predictions of the statistical theory and experimental data, it was realized that the use of approximate expressions for the phase-space integrals $\rho(E, \mathbf{P}; m_1, \dots, m_n)$ (cf. Eqs. 7 and 8) may give quite misleading results. [Unpublished work by C. N. Yang & R. Christian, Brookhaven Cosmotron internal report, cited in (82, footnote 22).]

In his original paper Fermi (76) treats heavy particles such as nucleons, K mesons as nonrelativistic [i.e., their total energy is given by $M + (p^2/2M)$], and light particles such as pions as extreme-relativistic (i.e., essentially massless). He then argues that the kinetic energy is approximately equipartitioned among the various types of particles, that, consequently, the heavy particles have the largest momenta, and that it is therefore sufficient to assume momentum conservation only for them. This leads to the formula¹⁴

$\rho F, \text{ approx}(E, 0; M_1, \dots, M_r, m_1, \dots, m_s)$

$$= \left[\frac{(2\pi)^{r-1} \cdot \prod_{i=1}^r M_i}{\sum_{i=1}^r M_i} \right]^{3/2} \cdot [8\pi]^s \cdot \frac{T^{3/2 \cdot (r-1) + 3s-1}}{\Gamma[3/2 \cdot (r-1) + 3s]} \quad 19.$$

¹³ Another simple model, which deviates in the opposite direction, has been described by Hagedorn (101).

¹⁴ An elegant derivation is given in Milburn's review (145). Belenkii *et al.* (28, p. 540) give a geometric interpretation.

TABLE I
DATA ON NUCLEON-NUCLEON COLLISIONS AT 6.2 BEV

	Mean number of prongs	Mean number of charged pions	Mean kinetic energy of charged pions (in units 0.938 Mev)	Mean kinetic energy of protons (in units 0.938 Mev)	Inelasticity (in per cent)
Statistical theory, central collisions only	N^* , no π^*	3.25	2.04	388	287
	N^* and π^*	3.72	2.51	302	240
Statistical theory, central (50 per cent) and periph- eral (50 per cent) collisions	N^* , no π^*	2.73	1.50	364	502
	N^* and π^*	2.96	1.73	304	479
Experimental data	Kalbach <i>et al.</i> (108)	—	1.9 ± 0.3	252 ± 21	$550 \pm ?$
	Daniel <i>et al.</i> (63)	—	1.51 ± 0.18	309 ± 48	636 ± 96
	Winzeler <i>et al.</i> (185)	2.8 ± 0.3	—	—	—

Comparison of theoretical calculations of v. Behr & Cerulus (23) with some experimental data. N^* denotes the $J = T = \frac{1}{2}$ pion-nucleon isobar, π^* a $J = T = 1$ pion-pion isobar with mass 4μ . The possible effect of the latter has been considered in the second and fourth row, but not in the first and third one.

where M_i and m_i are the masses of the nonrelativistic and the extreme-relativistic particles, respectively, and $T = E - \sum_i M_i$ is the total kinetic energy. The case of nonrelativistic particles only follows from 19 by putting $s=0$; the case of extreme-relativistic particles only, by putting $r=1$ and $M_1=0$.¹⁵ Later, Lepore & Stuart (126; see also 145) and, independently, Rozenal (169)¹⁶ have shown that with neglect of momentum conservation for the extreme-relativistic particles, one greatly overestimates the weight of high multiplicities. Their result, rigorous in the extreme-relativistic limit, is¹⁵

$$\rho_{F, \text{ extr relat}}(E, 0; s) = \frac{(2s-1)(4s-4)!}{2^{4(s-1)}[(2s-1)!]^2} \cdot \frac{(8\pi)^{s-1}}{(3s-4)!} E^{3s-4} \quad 20.$$

where the second part of the right-hand side is Fermi's approximate expression with momentum conservation cursorily taken into account by replacing, in 19, $s \rightarrow s-1$. The deviation of expression 20 from the rigorous one is shown in Figure 2a.

Milburn (145) has given explicit formulas for calculating exact numerical values of the phase-space integrals ρ_F as given in 8 in a step-by-step calculation for a case where one has a particle of mass M and up to three massless relativistic particles, a situation applicable in inelastic pion-nucleon scattering. Also, Block (35) has reduced ρ_F , for two, three, four, and five particles in the final state, to forms suitable for exact numerical evaluation by hand computation with only the restriction $m_4=m_1$ and $m_5=m_2$. He also gives rigorous formulas for momentum spectra and Q -value distributions. These methods are, however, cumbersome in practice.

It may be more advantageous to start out from another exact expression for ρ_F , which was first given by Lepore & Stuart (126):¹⁷

$$\rho(E, 0; m_1, \dots, m_n) = \rho_{F, \text{ extr relat}}(E, 0; n) \cdot f_n(\nu_1, \dots, \nu_n) \quad 21$$

$$f_n(\nu_1, \dots, \nu_n) = 2 \cdot (4\pi)^{n-2} \cdot \frac{[(2n-1)!]^2 (3n-4)!}{(2n-1) \cdot (4n-4)!} \cdot \left(\prod_{i=1}^n \nu_i^2 \right) \cdot \int_{-\infty-i\epsilon}^{+\infty-i\epsilon} d\alpha \cdot \alpha^n e^{i\alpha} \int_0^\infty \frac{d\lambda \cdot \lambda^2}{(\alpha^2 - \lambda^2)^n} \cdot \prod_{i=1}^n H_2^{(2)}(\nu_i \sqrt{\alpha^2 - \lambda^2}) \quad 22.$$

where $\nu_i = m_i/E$ and $H_2^{(2)}(z)$ is a Hankel function. The functions $f_n(\nu_1, \dots, \nu_n)$ depend on the energy only through the ratios $\nu_i = m_i/E$. The remaining integrations in 22 are difficult because of essential singularities of the integrand in the complex α plane at $\pm\lambda$.¹⁸ Maksimenko & Rozenal

¹⁵ Pion production may be kept in energetically feasible limits by the replacement $T = E - \sum_i M_i \rightarrow T = E - \sum_i M_i - \sum_j m_j$ in 19 and $E \rightarrow E - \sum_j m_j$ in 20, which corresponds to $\sqrt{m_j^2 + p_j^2} \approx m_j + p_j$ instead of $\approx p_j$ (126, 145).

¹⁶ Rozenal gives expressions also for nonvanishing total momentum P .

¹⁷ A slightly simpler derivation in terms of the invariant singular functions $\Delta^{(1)}(z, \mu^2)$ and $\Delta(z, \mu^2)$ is found in (143) and in (28, App. III).

¹⁸ Lepore & Riddell (128) recently carried out one more integration and developed methods to evaluate the last remaining integral on an electronic computer.

(28, 143) therefore suggested a series expansion of $f_n(\nu_1, \dots, \nu_n)$ in terms of ν_i^2 and $\nu_i^2 \ln \nu_i^{-1}$ [see also Maksimenko (139); Zastavenko (194, App.)]. The expressions for the coefficients are fairly complicated and may be found in the original papers. The first term in this expansion is 1, which gives the extreme-relativistic approximation 20. The series does not converge very well for large values of ν_i and for total kinetic energies $T \approx \sum_i m_i$ (even 10 to 15 terms of the series are not sufficient), i.e., in the case when a nonrelativistic treatment of heavy particles (M_i) might be a good approximation. The authors therefore give another series expansion for this region in powers of $(E - \sum_i M_i / \sum_i M_i)$, of which the first term is 19 [see in particular (28)]. This expansion corresponds to taking the convolution of two phase-space integrals, one for extreme-relativistic particles and one for nonrelativistic particles, with momentum conservation for all particles rigorously taken into account

$$\rho_{F, \text{mixed}}(E, 0; M_1, \dots, M_r, m_1, \dots, m_s) \quad 23.$$

$$= \int d\epsilon \int d\mathbf{p} \rho_{F, \text{extr relativ}}(E - \epsilon, -\mathbf{p}; \mathbf{s}) \cdot \rho_{F, \text{nonrelativ}}(\epsilon, \mathbf{p}; M_1, \dots, M_r)$$

This is about the best one can do with such approximate expressions, the degree of validity of the approximation being shown on Figure 2b.

Zastavenko (194) proposed a different method for exploiting 22 that is particularly suited for low multiplicities. It consists first in calculating $f_n^{(1)}(x) = f_n(x, 0, 0, \dots, 0)$, $f_n^{(2)}(x) = f_n(x/2, x/2, 0, \dots, 0)$, \dots , $f_n^{(n)}(x) = f_n(x/n, x/n, \dots, x/n)$ with the formulas of Maksimenko & Rozenal (143) and second in an interpolation procedure to obtain $f_n(\nu_1, \dots, \nu_n)$ for all other arguments. This method has been used in recent Russian work (18), and its accuracy is 5 per cent and better.

Fialho (81), on the other hand, calculates (Eq. 22) by means of a saddle-point method similar to that used in statistical mechanics. By its very nature this procedure is most accurate for high multiplicities, but correction terms for low multiplicities are also worked out. The final numerical results then are identical with those of rigorous calculations on electronic computers. In Fialho's method concepts like temperature, entropy, and free energy appear.

As we saw earlier (cf. p. 7), the integral ρ_F as given by 8 and 21, 22 represents the phase-space density only when the particles obey Boltzmann statistics. To remove this limitation, Magalinskii & Terletsii (138) started from the appropriate microcanonical distributions and obtained general formulas for Fermi, Bose, and Boltzmann statistics with arbitrary total momentum of the system, which contain Eqs. 21, 22 as a special case and are useful in discussion of corrections to ρ_F due to the use of the proper statistics.

While all the work mentioned above is based on the Lepore-Stuart formula, Cerulus & Hagedorn (47) gave a detailed description of a Monte Carlo method for a direct evaluation of the phase-space integrals as given in 8. This method is particularly suited for electronic computers and can be coupled with other programs to yield all desirable information in a single

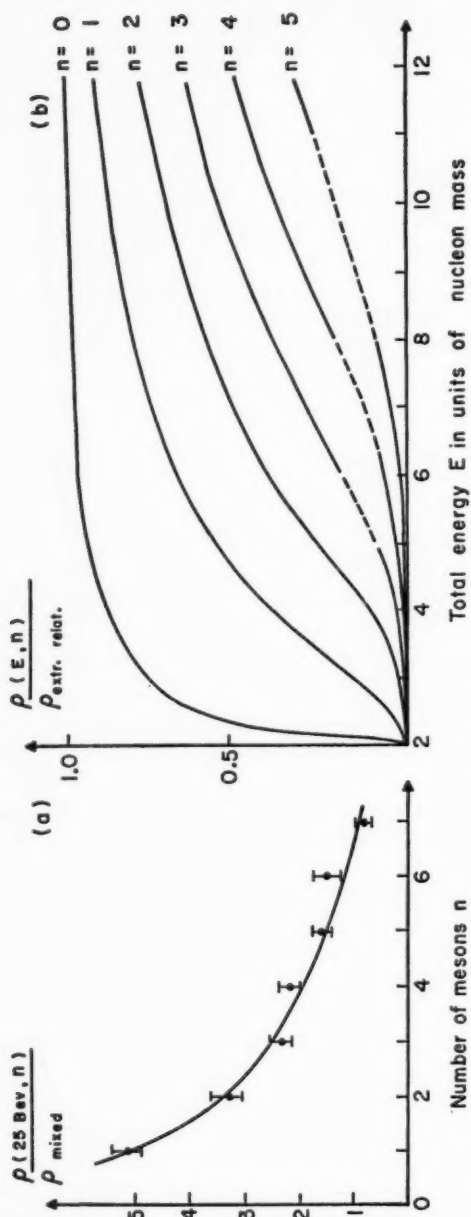


FIG. 2. Deviation of approximate expressions for the phase-space integrals (of Eq. 23 in Fig. 2a, of Eq. 20 in Fig. 2b) from the rigorous expressions in the case of pion production in nucleon-nucleon collisions. The exact values of the phase-space integrals were calculated in Figure 2a by a Monte Carlo method with errors as indicated [Cerulus & Hagedorn (47)], in Figure 2b from the series expansions of Maksimenko & Rozenal [Belenkii *et al.* (28)].

computer run (cf. p. 9). This Monte Carlo method is based essentially on random distribution of the available kinetic energy to the n final particles.

Monte Carlo methods are also used in constructing "random-stars" as proposed by Kopylov (116). From a set of random variables the momentum vectors of a possible event are reconstructed, and in this way a table of "stars" can be drawn up which represents the prediction of the statistical model and can be compared with actually observed events. By this method, quantities that are difficult to calculate otherwise, like angular correlations, can easily be compared with experiment; also, various assumptions concerning the matrix elements can be investigated.

Finally, a word must be said about the covariant form of phase-space integrals (Eq. 7) introduced by Srivastava & Sudarshan (179). Because of Lorentz invariance they fulfill the condition

$$\rho_S(E, \mathbf{P}; m_1, \dots, m_n) = \rho_S(\sqrt{E^2 - \mathbf{P}^2}, 0; m_1, \dots, m_n) \quad 24.$$

and from this one obtains the recurrence relation

$$\rho_S(E, 0; m_1, \dots, m_n) = \int d\mathbf{p}_n \cdot \frac{m_n}{\sqrt{m_n^2 + \mathbf{p}_n^2}} \cdot \rho_S(\sqrt{E^2 + m_n^2 - 2E(m_n^2 + \mathbf{p}_n^2)^{1/2}}, 0; m_1, \dots, m_{n-1}) \quad 25.$$

Contrary to the Fermi formulation, lower phase-space integrals for only zero total momentum enter into the recurrence formula, and this circumstance greatly facilitates numerical computations.^{19,20}

E. THERMODYNAMIC APPROXIMATION

As the energy which is available for the production of secondary particles increases, more and more final states become accessible and larger and larger numbers of particles will be produced, so that at very high energies computations along the lines described above become unfeasibly long (cf. p. 9). Since, on the other hand, approximations to the phase-space integrals, which are valid for large n , become more and more useful [cf. Fialho (81)], Fermi (76) suggested that the formalism of thermodynamics might be used for the calculation of momentum spectra and the average multiplicities.²¹ One then asserts that after the collision the total energy E of the system is uniformly distributed over the interaction volume $\Lambda \cdot \Omega_0$ and the equilibrium state of the system is characterized by a certain temperature T (measured in units of the pion mass μ), which is determined from the equation

$$E = \Lambda \cdot \Omega_0 [\epsilon_\pi(T) + \epsilon_N(T) + \epsilon_K(T) + \dots] \quad 26.$$

¹⁹ A paper by Yakovlev (188) on the details of such calculations contains several errors, as pointed out by Kopylov (117).

²⁰ Programs for an IBM 650 computer have been described by Hoang & Young (103). A more general program is being worked out by Lepore & Riddell (128).

²¹ Neuman (150) discussed for some special cases the relation of this formalism to the methods described above. Cf. also the last paragraph of (138).

Here $\epsilon_\pi(T)$, $\epsilon_N(T)$, $\epsilon_K(T)$, \dots denote the energy densities of the pion gas, the nucleon gas, the K -meson gas, etc., calculated from the formulas of relativistic thermodynamics with variable particle number (i.e., with particle creation and annihilation).²² Once the temperature T is known, the densities $n_\pi(T)$, $n_N(T)$, \dots of the pion gas, nucleon gas, etc., can be calculated and from this, the average multiplicities $[\Lambda\Omega_0 \cdot n_\pi(T), \dots]$ and the average energies $[\epsilon_\pi(T)/n_\pi(T), \dots]$. In doing so, a proper consideration of conservation of charge, nucleon number, and strangeness is extremely important, especially at low temperatures ($T \approx \mu$), because it has great influence on the relative frequency with which various types of particles appear (25, 27, 68, 111, 137).

These methods applied to nucleon-antinucleon annihilation lead to almost the same results as the formalism discussed earlier (large interaction volume, temperature $\mu/T = 1.4$; cf. p. 23) (122, 186). However, for nucleon-nucleon collisions at high energies one obtains extremely high temperatures and, consequently, an unreasonably large proportion of strange particles, nucleons, and antinucleons among the secondary particles; and also the transverse momenta come out too large (39, 76, 122). All these difficulties can be avoided by assuming that the system undergoes, before its decay into the observed secondary particles, an expansion until a final temperature of $\mu/T \approx 1.2$ is reached (25, 27, 29, 68). This numerical value may be understood on the basis of a large pion-pion cross section ($\sigma_{\pi\pi} \approx \mu^{-2}$) (110).

A detailed theory for the expansion process has been worked out by Landau *et al.* (2, 27, 29, 124) using the formalism of relativistic hydrodynamics. The expansion is mainly one-dimensional and in the direction of the primary particle, and it conserves the entropy of the system. Therefore, the average multiplicities and the transverse momenta can be determined from thermodynamical relations alone, while the angular distributions and longitudinal momentum spectra are strongly affected by the details of the hydrodynamical stage (cf. p. 33). For the rather complicated mathematical details we must refer to the original literature. The present status of this theory is described in the report by Feinberg (75).

F. ISOTOPIC SPIN CONSERVATION AND ANALYSIS OF CHARGE STATES

For simplicity let us assume that the initial state is a pure eigenstate of isotopic spin T_i and three-component T_{3i} . (If this is not the case, calculations have to be carried out for several values of total isotopic spin separately, and the results have to be weighed according to the weight of the various total isotopic spin eigenvalues in the initial state.) The reaction then can lead only to final states with the same quantum numbers. For the probability to produce a final state containing n particles with masses m_i and isotopic spin t_i ($i = 1, 2, \dots, n$), which are in an exact eigenstate of total iso-

²² The basic formulas of relativistic thermodynamics are collected in (25, 27, 29). In connection with Equation 26 compare also footnote 6.

topic spin T_f and three-component T_{3f} , we obtain according to 1, 3 and 7 or 8

$$P(E, T_f, T_{3f}; m_1 t_1, \dots, m_n t_n) \propto \sum_{\nu} \delta_{N_f N_i} \delta_{S_f S_i} \delta_{T_f T_i} \delta_{T_{3f} T_{3i}} |M'(\nu, T_f, m_1, \dots, m_n)|^2 \rho(E, 0; m_1, \dots, m_n) \quad 27.$$

Here ν distinguishes the various possibilities to form isotopic spin T_f , T_{3f} by vector addition of t_1, \dots, t_n . According to the statistical hypothesis, $M'(\nu, T, m_1, \dots, m_n)$ is assumed to be independent of ν and T and to be given by 11. The summation over ν then simply results in a weight factor $g_{k_1 k_2 k_3} \dots (T)$, denoting the number of linearly independent eigenfunctions of total isotopic spin T and T_3 which can be formed from k_1 particles of isotopic spin $\frac{1}{2}$ (nucleons, K mesons), k_2 particles of isotopic spin 1 (pions), k_3 particles of isotopic spin $\frac{3}{2}$ (nucleon isobars), etc. ($k_1 + k_2 + k_3 + \dots = n$). The weights $g_{k_1 k_2 k_3} \dots (T)$ can be taken from published tables, which have been computed partly by using closed algebraic expressions (123, 191) or from recurrence formulas²³ (10). The principles for calculations as outlined above were first formulated by Fermi (79) [see also Yeivin (190)].

These weight factors are of use only for the calculation of the multiplicity distribution regardless of charge. Experimentally, however, this distribution is frequently not well known because of difficulties in detecting neutral particles; therefore, a comparison of theoretical and experimental prong distributions or even a detailed charge analysis is often much more informative. Then we cannot characterize the final states f in Equations 1 and 3 by a unique eigenvalue of total isotopic spin, but we must state which particles have which charge. From Equation 3 we then obtain

$$|M'_{fi}|^2 = \delta_{N_f N_i} \delta_{S_f S_i} \delta_{T_f T_i} \delta_{T_{3f} T_{3i}} \left\{ \sum_{\nu} |\langle f | T_f, \nu \rangle|^2 \cdot |M'(\nu, T_f, m_1, \dots, m_n)|^2 + \sum_{\substack{\nu, \nu' \\ \nu \neq \nu'}} \langle f | T_f, \nu \rangle \langle f | T_f, \nu' \rangle^* M'(\nu, T_f, m_1, \dots, m_n) M'^*(\nu', T_f, m_1, \dots, m_n) \right\} \quad 28.$$

where again the initial state was assumed to be a pure isotopic spin state. The usual statistical model calculations assume, as above, the independence from ν and T of the matrix elements $M'(\nu, T, m_1, \dots, m_n)$ and neglect the second sum, which represents interference terms. The problem of calculating charge distributions thus essentially reduces to finding the values of the sums $\sum_{\nu} |\langle f | T_f, \nu \rangle|^2$. One way of doing this is by using Clebsch-Gordan coefficients. Cerulus (45) and Belenkii *et al.* (28) have thus calculated tables of the numerical values of these sums for all cases of practical interest.²⁴ Alternatively, group-theoretical methods may be used to find general alge-

²³ Some misprints in the tables of Yeivin & De-Shalit (191) are corrected by Barashenkov & Barbashov (10).

²⁴ These two papers describe all details of the calculation, cf. in particular the appendices of (28). We note that by summing the expressions $\sum_{\nu} |\langle f | T_f, \nu \rangle|^2$ over the various final charge states, one obtains the above defined weights $g_{k_1 k_2 k_3} \dots (T)$.

braic expressions directly (46, 158, 164). [A partial result giving the weight of a system consisting of π^0 mesons only has already been obtained by Goebel (88, App.).] For such considerations it is important how the set of quantum numbers ν is chosen. In particular, for a many-pion system ν may characterize the permutation symmetry of the complete isotopic-spin wave function (3, 154). Belenkii *et al.* (28, App. II) and Pais (158) emphasized that these symmetries may well have physical significance and that, because the charge distribution may be very different for different ν 's (as can be seen from the numerous tables in these two papers), deviations from the statistical model predictions may give hints on dynamical effects which eventually cause a preponderance of certain of these symmetries. In this connection, however, it should be remembered that the neglect of interference terms in 28 may not always be a good approximation and may also be responsible for certain deviations. Some examples of this kind have been discussed by Nikishov (155), who points out, e.g., that such effects may cause deviations of the individual π^+ , π^- , π^0 momentum spectra from the statistical model prediction, while all three spectra taken together are in good agreement.

III. APPLICATIONS TO SPECIAL PROCESSES

A. MESON PRODUCTION IN NUCLEON-ANTINUCLEON ANNIHILATION

Annihilation at rest or at low kinetic energies is eminently well suited to testing the basic premises and the degree of validity of the statistical model since, on the one hand, a large amount of energy is provided for meson production, sufficient for the creation of up to 13 pions and, on the other hand, the process is particularly simple: only bosons are produced, it is 100 per cent inelastic, and there are no uncertainties with regard to Lorentz-contraction factors.

Experimentally this annihilation has been studied in emulsions [cf. the literature survey in (71)], in propane (1, 91, 102) and hydrogen bubble chambers (104, 135), both at rest and at appreciable kinetic energies of the incident antiproton (up to 1.99 Bev/c, corresponding to a total energy of 2.42 Bev in the center-of-mass system). Among the measured quantities to be compared with theoretical predictions, we have multiplicity distributions of pions, probability of K -meson production, prong distributions, momentum spectra, and angular correlations; and all these quantities are studied in their dependence on the energy of the incident antinucleons.

The most striking features of the annihilation process are the observed high pion multiplicities (4.9 ± 0.2 at rest) and the low probability for K -meson production (4 ± 1 per cent at rest). Earlier statistical calculations (31, 86, 180) were improved by Barkas *et al.* (22) and Maksimenko (139) by using exact values for the phase-space integrals. The result is that with $\Omega_\pi = \Omega_K = \Omega_0 = (4\pi/3\mu^3)$, an average of 3.4 pions in each annihilation is predicted, together with a K -meson pair in more than 40 per cent of all cases. By choosing $\Omega_\pi = \Omega_K = 15\Omega_0$, corresponding to a radius of $2.46\mu^{-1}$, at least the

pion multiplicity can be fitted, while one still obtains about 12 per cent probability for K -meson production. Almost identical results are obtained by using the thermodynamical formalism (122, 186). Although Equation 9 is only an order-of-magnitude estimate, an interaction volume as large as $15\Omega_0$ is hardly compatible with the most simple version of the physical picture underlying the statistical model.

Most proposals to explain or to avoid such a large volume are based in one way or another on the possibility of strong final-state pion-pion interactions. The simplest way is to follow Pomeranchuk [(166) cf. p. 6] and calculate the statistical weight of an n -particle final state with an effective volume $\Omega = n\Omega_0$ instead of $\Omega = \Omega_0$. As shown by Maksimenko (139) and Frautschi (84), the results depend sensitively on assumptions for the possible K -meson-pion interaction.²⁵ Best agreement with experiment is obtained with the hypothesis that pions interact strongly with each other and weakly with K mesons, but both are produced in the same volume $\Omega = (\delta_{0,n\pi} + n_\pi)\xi^3\Omega_0$, where $\xi \approx 1$ and n_π is the number of produced pions. This method is related to Landau's (27) picture in which one would assume an expansion after the annihilation proper, until the mean free path of the produced mesons has become larger than the linear dimensions of the system. Only then are the decay characteristics determined and can they be described in terms of a decay temperature T . Assuming strong pion-pion and pion- K -meson interaction with a total cross section close to the geometrical one ($\sigma_{\pi\pi} \approx \pi\mu^{-2}$) [i.e. a picture similar to Frautschi's (84) model $P(c)$], one obtains the estimate $1 < (\mu/T) < 2$ and, in particular, with $\mu/T = 1.4$ (corresponding to $\Omega = 15\Omega_0$) an average pion multiplicity of 5 and 8 per cent probability for K -meson production (122, 186).

So far, the meson-meson cross section has been supposed only to be large (smooth or resonant). The particular case of a resonant interaction may be treated in the formalism of Belenkii & Nikishov (30). The predictions depend sensitively on the assumed spin and isotopic spin of the pion-pion isobar (93, Table IV). Current theoretical studies of the nucleon electromagnetic form-factor and of pion-nucleon scattering in the framework of dispersion theory (53) have strongly suggested the existence of a pion-pion resonance in the $T=J=1$ state at 4.5μ total center-of-mass energy of the two-pion system. Assuming an isobar with these quantum numbers and mass 4μ , and a reaction volume $\Omega_\pi = \Omega_0$, Cerulus (44) obtained excellent agreement with experimental data [for similar results cf. (173)]. On the whole, the predictions of the isobar model are similar to those of the conventional Fermi model with large radius. For example, Agnew *et al.* (1) observed in 127 hydrogen-like annihilations (events with K -meson production excluded) a ratio of 2-prong:4-prong:6-prong events of 42.5:52.8:4.7. Cerulus (44) calculated 45.9:52.0:2.1 from the isobar model and 35.8:56.7:7.5 from the

²⁵ From a comparison with Barkas *et al.* (22), Frautschi (84), and Cerulus (44), it seems that Maksimenko overestimates K -meson production.

conventional Fermi model with large volume (also cf. Fig. 3); his calculations definitely favor an isobar of mass 4μ over one of mass 3μ . In the isobar model, K -meson production is satisfactorily described with $\Omega_K/\Omega_0 = 0.5$. The assumption of a $T=J=0$ pion-pion isobar would give considerably poorer results [Eberle (69)]. Apart from the small differences in the prong and multiplicity distributions, the isobar model predicts a small bump with a width determined by the lifetime of the pion-pion isobar at the upper end of the two-prong momentum spectrum, which can be detected only with accurate data. Also, characteristic differences are to be expected in Q -value distributions (89, 165) and small-angle correlations of unlike pions (92, 141); as yet, however, no direct experimental evidence for the existence of an isobar has been found in this way.

Cook & Lepore (59), neglecting three-momentum conservation, considered the effects of angular momentum conservation and of selection rules, using a method described above (cf. p. 10; for their results cf. Fig. 3). The effects of selection rules were also studied by Desai (66) in the framework of the conventional Fermi model with large volume; however, some additional assumptions are necessary to bring the selection rules into the play. While some influence on the pion multiplicity distribution is found, the prong distribution remains almost unaffected.

The angular correlation functions, i.e., the distribution of angles enclosed by the momenta of all possible pion pairs, are, on the whole, quite well described by the statistical model (cf. Fig. 4). If, however, one selects pion pairs with like charges, deviations at small angles are observed (89). A correction to account for the influence of Bose-Einstein statistics (cf. p. 11) would lie in the right direction, but would be large enough only for $\Omega = (0.75^3\Omega_0 = 0.43\Omega_0)$, while $\Omega = 8\Omega_0$ (covariant model) is required to obtain correct multiplicities [Goldhaber *et al.* (90)]. Thus the situation here is still unsatisfactory.

The data that were available at the time of the Rochester conference in 1960 (177) suggested that the pion multiplicity is almost independent of the momenta of the incoming antiprotons (measurements were made up to 1.99 Bev/c antiproton laboratory momentum). A careful reanalysis, in particular of K -meson events, revealed a slight increase of the pion multiplicity with antiproton momentum which, however, still might be a little less than predicted by the covariant statistical model (135). In any case, it does not seem advisable to drop the Lorentz-contraction factor from the calculation. No calculations of the energy dependence with the old noncovariant model have been published, though a comparison would be interesting, because the absence of energy denominators might favor higher momenta and lower multiplicities. Belenkii *et al.* (28) claim an energy dependence of a multiplicity proportional to $\bar{E}_4^{\frac{1}{2}}$, where \bar{E} is the total energy of the nucleon-antinucleon pair in the laboratory system. It is not clear, however, in what limits and with what accuracy this is to hold.

The probability for annihilation with K -meson production was found to

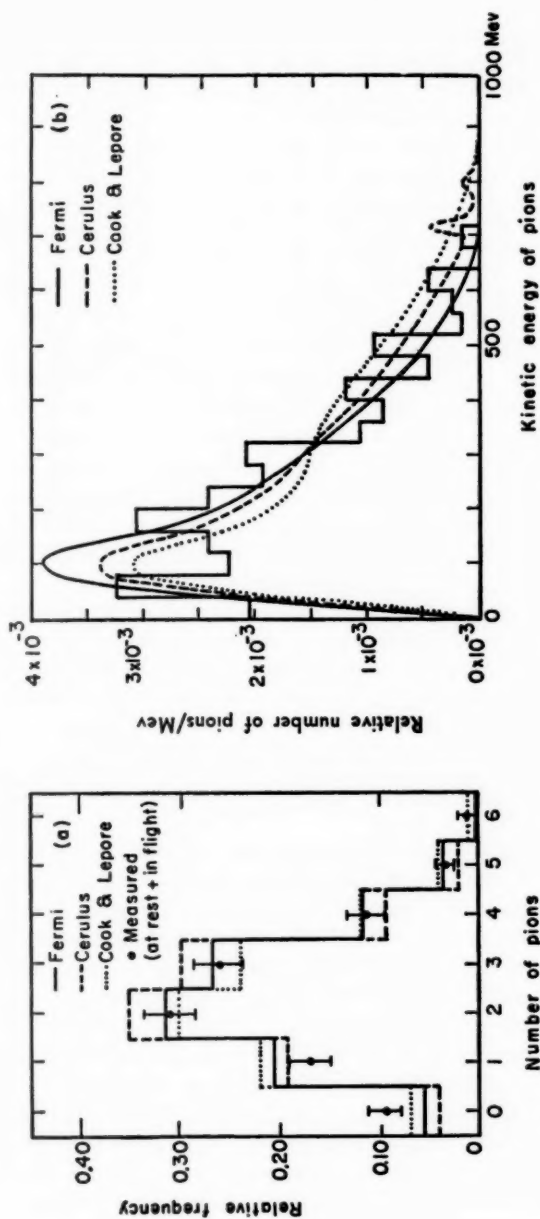


FIG. 3. Comparison of three versions of the statistical model (Fermi: conventional model with large volume; Cerulus: model with pion-pion isobar; Cook & Lepore: model with angular momentum conservation and selection rules) with (a) the observed multiplicity distribution of charged pions, (b) the observed pion momentum spectrum corrected for detection efficiency, pion absorption, and inelastic scattering [Ekspong *et al.* (71)].

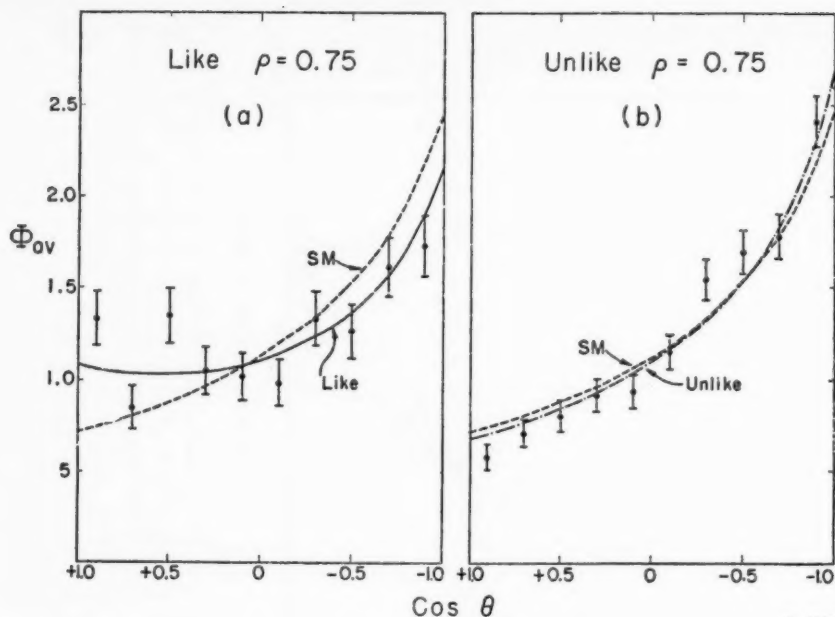


FIG. 4. Distribution of the angles between pairs of pions, that have (a) like charges or (b) unlike charges, averaged over the multiplicities 4, 5, and 6 [Goldhaber *et al.* (90)]. The dashed line *SM* represents a statistical model prediction, which takes into account only angular correlations arising from conservation of four-momentum. The solid and the dashed-dotted lines include in addition the correlations due to Bose-Einstein statistics. Calculations were done with an interaction volume of radius $\sigma\mu^{-1}$; the maximum correlation effect was obtained for $\sigma=0.75$.

rise from 4 ± 1 per cent at rest to 8 ± 1 per cent at 1.05 BeV/c antiproton momentum (91, 102), while at the same time the pion multiplicity shows relatively little increase. Using the covariant theory the data can be fitted just within the limits of error by choosing $\Omega_\pi = 8\Omega_0$ and $\Omega_K/\Omega_\pi = 0.11$, wherein it is important that the Lorentz-contraction factor Λ be included in the calculation. The momentum spectra of *K* mesons and of pions associated with *K* mesons agree fairly well with the model.

A model, originally invented by Koba & Takeda (115; also cf. 84) to explain the large pion multiplicity, predicts a much lower increase of pion multiplicity with energy than the conventional Fermi model and might also explain the anisotropy of the pion angular distribution, which is observed to develop at higher energies with a peaking in the forward and backward directions (102). The model pictures the annihilation as a two-stage process: At first the nucleon core and the antinucleon core annihilate each other with emission of pions and *K* mesons; then the two meson clouds fly off, having lost their attracting centers. The first stage is described by statistical theory with an interaction volume of radius $2/3\mu$, inferred from the Stanford electron

scattering experiments, and is assumed to occur much faster than a typical oscillation of the meson cloud, so that the meson clouds remain relatively undisturbed during the annihilation proper. The composition of the meson cloud is estimated from meson theory (e.g., from a static, intermediate coupling theory), a procedure which is subject to some uncertainty since the influence on the final state of the interaction between core pions and cloud pions, which is necessary to lift the cloud pions from their virtual states to the mass shell, is not accounted for by this method.

B. MESON PRODUCTION IN PION-NUCLEON COLLISIONS

This reaction has been investigated at various pion energies up to 16 Bev. Near 1 Bev some features of the reaction, e.g. angular distributions, seem to change rapidly with energy, so that neither the statistical model nor the Lindenbaum-Sternheimer model can give a satisfactory description of all the finer details (163). These changes are not yet well understood, but they may be due to the influence of the $T = \frac{1}{2}$ resonances at 600 and 900 Mev in the pion-nucleon system. The possible effects of interference terms have been studied (33), and Lindenbaum & Sternheimer (133) investigated an extended isobar model including the 600-Mev and 900-Mev pion-nucleon resonances. Also, some evidence for a pion-pion resonance has been reported from an investigation of events with backward emission of the nucleon (162).

At 1.37 Bev (70) we probably have more favorable conditions for the application of a purely statistical model. As is clear already from much lower energies, a strong influence of the $J = T = \frac{3}{2}$ pion-nucleon resonance on the final state is present, which must be taken into account in any statistical calculation. This becomes clear from Table II, where we have compared a calculation by Milburn (145), which neglects this resonance, with one by Nikishov (152), which includes isobar production by using the formalism of Belenkii & Nikishov (30).²⁶

Nikishov's pion momentum spectra show a characteristic two-peak structure similar to those of the Lindenbaum-Sternheimer model.

Most of the theoretical work, however, has concentrated on the energy region of 4.5 to 5 Bev (136, 183) because it is sufficiently high above the threshold for multiple production so that many final states are accessible and all assumptions of the statistical theory seem to be fulfilled. The work of Nikishov (153), containing a detailed charge analysis and treating pions as extreme-relativistic particles, and more rigorous calculations by Maksimenko (140) led to satisfactory agreement with experiment (cf. Table II). This includes momentum spectra, too, e.g., the predicted average momentum of charged secondary pions is 0.55 Bev/c compared with the measured value 0.54 Bev/c. The corresponding numbers for secondary protons are 0.75 Bev/c and 0.74 Bev/c. Such close agreement is the more remarkable as the angular distributions deviate sharply from isotropy. Nucleons are emitted

²⁶ Milburn used exact values for the phase-space integrals and thus improved the first calculations for this process, made by Fermi (76, 80). For a calculation including a pion-pion resonance cf. Ruskin (172).

TABLE II

RELATIVE FREQUENCIES OF PRONG DISTRIBUTIONS IN PION-NUCLEON COLLISIONS

	Observed charged particles	Experi- mental data	Theory with isobar	Theory without isobar
1.37 Bev	$(\pi^- + p)_{el}$	0.11	0.15	0.27
π^- -Proton collisions	$(\pi^- + p)_{inel}$	0.35	0.29	0.30
[Eisberg <i>et al.</i> (70)]	$\pi^+ + \pi^-$	0.50	0.50	0.39
	$\pi^+ + 2\pi^- + p$	0.04	0.06	0.04
5 Bev	2-prong	0.58	0.60	0.66
π^- -Proton collisions	4-prong	0.40	0.37	0.33
[Maenchen <i>et al.</i> (136)]	6-prong	0.02	0.03	0.01

$(\pi^- + p)_{el}$ denotes incoherent elastic scattering (i.e., diffraction scattering excluded). Columns 4 and 5 give the result of a statistical theory with and without consideration of final-state pion-nucleon interaction through the $J = T = \frac{3}{2}$ resonance. The theoretical data at 1.37 Bev come from Nikishov (152) and Milburn (145); the latter recalculated for a volume with a radius of one pion Compton wavelength. The data at 5 Bev come from Maksimenko (140).

preferentially in the backward, pions in the forward, directions. This circumstance suggests that a great fraction of the incident pions collides with the meson cloud of the nucleon, thus demonstrating a sizable pion-pion interaction.²⁷ Barashenkov (6) estimates that at least 20 to 30 per cent of the total inelastic cross section must be ascribed to such peripheral collisions to explain the asymmetry of the nucleon and meson emission; the estimate is based on the assumption of a certain momentum distribution of the pions in the cloud.

Similar observations are made in experiments at 7 Bev (161). Again, prong distribution, mean number of charged particles, and the pion momentum spectrum are in excellent agreement with the statistical theory, the calculated proton momentum spectra are somewhat too soft, and the angular asymmetries have become even more marked. Barashenkov (9) finds, comparing all these data to theory, that at least 55 per cent of the total cross section must now be peripheral to explain the angular asymmetry.

It thus appears that the good agreement of the statistical model with some of the experimental observations is due to a balance of the neglect of pion-pion interaction and the neglect of peripheral collisions (8, 9). It would seem desirable to invent a more detailed model into which a pion-pion interaction is built explicitly. However, simply to add production of pion-pion isobars to the above statistical calculations would be too simple a proposal,

²⁷ Certain similarities, e.g. angular asymmetries, are found in multiple-pion photo-production. [Cf. (52), where comparisons with phase-space predictions can be found.] The $J = T = \frac{3}{2}$ pion-nucleon resonance has a large influence, but the energies (≤ 1 Bev) may still be too low to justify the assumptions of the statistical model.

which would lead to too high pion multiplicities and considerably worsen the agreement with experiment (8, 9, 17, 171, 172, 173).

Finally, let us discuss strange-particle production. The predictions will depend sensitively on what choice is made for the production volumes Ω_π , Ω_K , and Ω_Y (cf. the discussion on p. 6). Barashenkov & Maltsev (14) have worked out in great detail the consequences of the three choices (1), (2), (3) (cf. p. 7) for π^-p and π^+p collisions at 5 and 7 Bev. However, because of the limited statistics available, a comparison with experiment is difficult. By carrying out a charge analysis for π^-p collisions at 5 Bev, Mikhul (144) found probabilities of 3.34 and 0.66 per cent for K^+ and K^- production, respectively, according to hypothesis (1) with $\Omega_K = (\mu/m_K)^3 \Omega_0$, and probabilities of 0.40 and 0.74 per cent with hypothesis (2), compared with the experimental values 2.8 ± 1.2 and 1.2 ± 0.6 per cent, respectively (34). At 7 Bev the neutral hyperon and the K -meson pair production cross sections have been measured as $\sigma(Y^0K) = 0.8 \pm 0.25$ mb and $\sigma(K\bar{K}) = 1.2 \pm 0.3$ mb (178). Their ratio $\sigma(Y^0K)/\sigma(K\bar{K}) = 0.7 \pm 0.2$ may be used to fix the value of Ω_K/Ω_Y . One finds $\Omega_K/\Omega_Y = 0.25 \pm 0.07$; i.e., with $\Omega_Y = \Omega_\pi$ [hypothesis (1)] a similar value is obtained for Ω_K/Ω_π as in the case of antinucleon annihilation. [With $\Omega_K = (\mu/m_K)^3 \Omega_0$ one would have $\sigma(Y^0K)/\sigma(K\bar{K}) = 7.5$.] Ruskin & Usik (171, 173, cf. also 8, 17) tried to avoid the use of different production volumes by introducing a pion-pion resonance, thus enlarging the statistical weight for pion production relative to strange-particle production. The results, however are not too promising.

Figure 5 summarizes some characteristic data for inelastic pion-nucleon collisions over the whole energy range that is accessible today.

C. MESON PRODUCTION IN NUCLEON-NUCLEON COLLISIONS AT ENERGIES BELOW 30 BEV

The cloud chamber experiments performed by Fowler *et al.* (82) on inelastic neutron-proton interactions at energies up to 2.2 Bev established the existence of multiple-meson production for the first time on the basis of evidence other than cosmic ray data. Although the neutron beam had a considerable energy spread and little was known about its spectrum, the strong influence on the final state of the $J=T=\frac{1}{2}$ pion-nucleon resonance was clearly demonstrated, as had been predicted by Belinfante (32) and Peaslee (159). The resulting sharp disagreement with the statistical theory as originally formulated by Fermi (76) led to the proposals of Belenkii & Nikishov (30)—production of nucleon isobars according to statistical laws—which we discussed in detail in Section II B [also cf. (142, 151)]. Multiplicity distributions observed in proton-proton interactions (with well-defined beam energy) at 0.8, 1.5, 2.75, and 3.0 Bev (49, 83, 184, 193) agree well with the predictions of the thus-modified model [Maksimenko (140); Cerulus & Hagedorn (48) also calculate momentum spectra for 2.75 Bev].

Alternatively, experiments in this energy region may be interpreted in terms of the Lindenbaum-Sternheimer model (131), which assumes pion production to occur exclusively via isobar formation. The not too abundant

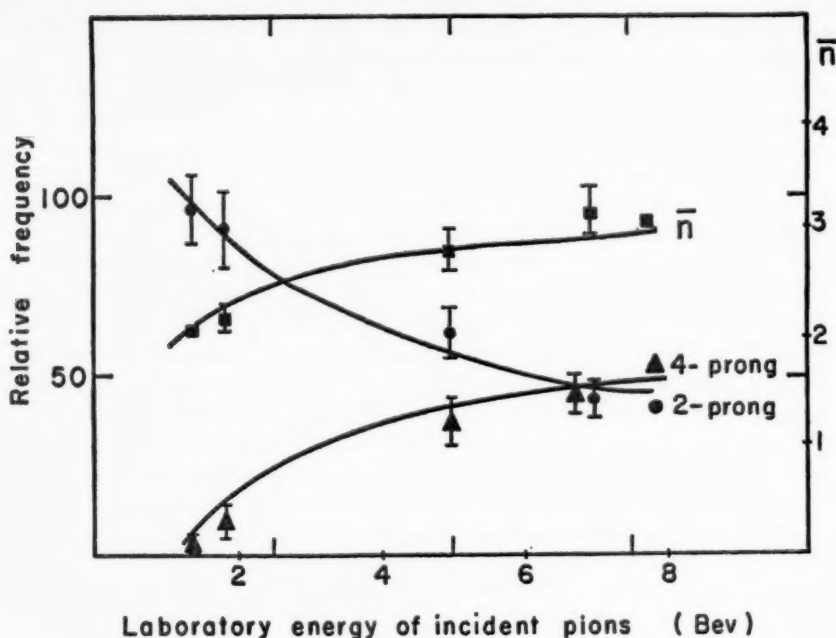


FIG. 5. Average number of charged secondary particles and of two-prong and four-prong events in π^- -proton collisions at various energies. The solid curve represents a statistical model, which includes the $J=T=\frac{3}{2}$ pion-nucleon isobar [Barashenkov (7)]; the points at 6.8 Bev are taken from Petržilka (161).

data previously available were in reasonable agreement with this model, especially at lower energies, where only a single nucleon can be excited to an isobar state. However, a more recent experiment at 1.6 Bev (50) failed, in spite of a sizable fraction of double-meson production events, to exhibit one peak in the proton momentum distribution, which is caused by excitation of two isobars. The latter process would be the only one in this model that can lead to double-meson production,²⁸ whereas in the statistical theory most of the double production would occur through formation of one isobar and direct production of the other pion. According to the statistical model, at 2.75 Bev only 15.4 per cent of the total cross section for meson production is due to formation of one or two isobars without direct pion production, 34.2 per cent is due to direct meson production without isobar formation, and 50.4 per cent is due to simultaneous direct production and isobar formation [Cerulus & Hagedorn (48), Table I; see also (140)].

Comparing experimental data around 6 Bev (63, 108, 168, 185) with Hagedorn's (98) detailed theoretical analysis, we find that even though iso-

²⁸ The influence of higher pion-nucleon resonances seems to be small at this energy. According to the extended isobar model (133), these resonances would open new channels for double-meson production.

bar formation has been included, the theory predicts too high values for the pion momenta, too low values for the proton momenta (cf. Table I); in addition, the observed anisotropy of nucleons and pions with a peaking in the forward and backward directions remains unexplained. According to theory, 74 per cent of the kinetic energy available in the center-of-mass system should be spent for meson production; experimentally one finds 49 ± 5 per cent. Only the mean multiplicities and the mean prong number are predicted in approximate agreement with the experimental numbers. Hagedorn assumed all collisions to be central, whereas the above results suggest that peripheral collisions play a vital role. Indeed, assuming that only 50 per cent of all collisions are central, the others peripheral, a phenomenological calculation made by v. Behr & Cerulus (23), the principles of which are described in Section II C, led to agreement with all available data. The authors also discussed whether or not the formation of pion-pion isobars should be assumed in the calculation of the central collision part, but because of the wide experimental errors they could not come to an unambiguous decision.

The same features listed above persist at 9 Bev and become even more pronounced (21, 38) (cf. Fig. 6). [For extensive references to experimental work, cf. Barashenkov *et al.* (18, 20) and Bogachev *et al.* (37, 38). For a sur-

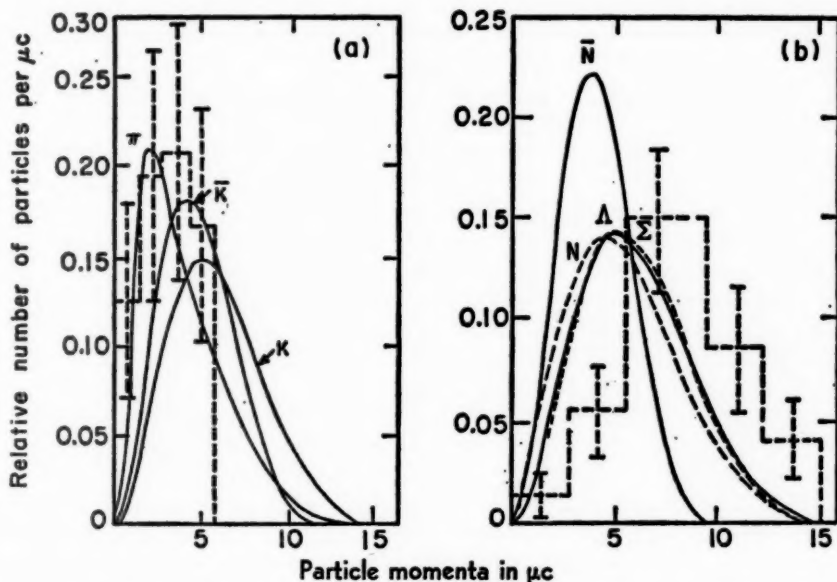


FIG. 6. Center-of-mass momentum spectra of secondary particles in proton-proton collisions at 9 Bev. The theoretical curves (dotted lines nucleons and Σ hyperons respectively) represent a statistical model without accounting for peripheral interactions; the experimental histograms are for pions and nucleons, respectively [Barashenkov, Maltsev & Wang Pei (21)].

vey of data at all energies up to 9 Bev cf. Barashenkov (7).] The two-prong events are much more frequent, many-prong events are somewhat less frequent than predicted by theory, and, in particular, low-multiplicity events are generally associated with the largest anisotropies (forward and backward peaking) (18, 19, 20). Earlier statistical calculations in terms of central collisions only (11, 13) had to be revised, therefore, to allow for peripheral interactions too. Because of the rough theoretical method (cf. p. 14) no quantitative agreement could be obtained. It is, however, interesting that the charge asymmetry observed in proton-neutron interactions (the proton tends to keep its charge) can be understood on the assumption that in a peripheral collision the nucleons are excited to the $J = T = \frac{3}{2}$ state and continue their flight in their original direction of motion (20).

Hagedorn's (99) theoretical predictions for collisions at 25 Bev were highly useful for planning the experiments. The available data are still scarce. The pion and γ -ray (from π^0 decay) energy spectra are in fair agreement with the theoretical curves of v. Behr & Hagedorn (24) at small angles (0° to 6°) in the laboratory system; deviations occur at larger angles (16°) and again show the importance of peripheral collisions (57, 64). A mean multiplicity of charged secondary particles of 4.1 ± 0.6 was observed in proton-free-proton collisions at 22.6 Bev (60) compared with the theoretical value of 4.7 at 25 Bev. As in the case of pion-nucleon collisions, it again seems that as far as integrated quantities like mean multiplicities are concerned, the neglect of pion-pion interactions and further resonances makes up for the neglect of peripheral collisions.

Some remarks on the predicted rate of antiproton production are appropriate. Hagedorn (98, 99) calculated a ratio of antiproton: π^- mesons of 10^{-5} at 6.2 Bev and approximately 10^{-1} at 25 Bev. In doing so, he allowed for final-state annihilation of those antinucleons, which were produced with small momentum relative to one of the three final nucleons. [A detailed description of this procedure is given in (98), cf. especially Appendix II.] This correction reduced the antinucleon yield by a factor of 4 at 6.2 Bev and by only a factor of $\frac{4}{3}$ at 25 Bev (because here antinucleons are produced with higher kinetic energies). The predicted ratio at 25 Bev is larger by a factor of 10 to 400 than the ratio observed in recent experiments at CERN (57). This may be partly due to the use of metal targets instead of hydrogen, but it is doubtful that the whole effect can be explained by annihilation of the missing antiprotons with other nucleons in the target nucleus, since no dependence on the atomic weight of the target is observed.

At 25 Bev also, a sizable fraction of high-energy deuterons and smaller amounts of H^3 and He^3 have been observed (57). The deuteron production (at least its order of magnitude) can be understood on the basis of a statistical model with final-state nucleon-nucleon interaction (100) (cf. p. 13); the same holds true in principle for H^3 and He^3 , if antinucleons are created simultaneously. The experimental situation, however, needs further clarification—in particular, by use of hydrogen targets—before more detailed conclusions can be drawn.

Little is known about strange-particle production. The theoretical prediction using hypothesis (1) (cf. p. 7) of 4.6 per cent probability for hyperon production (1.2 mb) in nucleon-nucleon collisions at 3 Bev [Barashenkov *et al.* (15, 16)] is too high by an order of magnitude if the recent measurement of $130 \pm 30 \mu\text{b}$ (134) is correct.²⁹ At 3 Bev one is not much above the strange-particle production threshold and therefore, presumably, the statistical assumptions are not yet applicable. Barashenkov *et al.* have also made predictions for 5 Bev (12) and for 7 and 10 Bev (11), Hagedorn for 6.2 Bev (98); however, no good experimental data are available for comparison. For 25 Bev the existing experimental evidence indicates agreement with Hagedorn's (99) calculations at least insofar as the ratios $K^+:\pi^+$ and $K^-:\pi^-$ at various laboratory angles are concerned (57, 64). In these calculations hypothesis (1) was used with $\Omega_\pi = \Omega_\pi$ and $\Omega_K = 0.2\Omega_\pi$, which led also to good agreement for nucleon-antinucleon annihilation and pion-nucleon collisions. However, in this experiment some of the observed K mesons may have been created by secondary collisions within the target nucleus.

D. MESON PRODUCTION IN NUCLEON-NUCLEON COLLISIONS AT COSMIC RAY ENERGIES

Meson production in cosmic ray events is a phenomenon of considerable complexity, and an adequate coverage is beyond the scope of this article. We restrict ourselves to a few outstanding facts.

The experimental situation in this field was summarized recently by Powell *et al.* (160, 167). As for the theory, it is evident that the simple thermodynamical model proposed by Fermi (76) (cf. Sect. II E) is quite inadequate for the description of experimental details; at best it can roughly reproduce the dependence of the mean energy of the emitted mesons on the primary nucleon energy (122). A subsequent version (78) incorporating angular momentum conservation has been criticized on theoretical (cf. p. 6) and experimental grounds (e.g., the degree of anisotropy of the predicted angular distribution of shower particles is much too small). Some of these difficulties are avoided in the theory of Landau (27, 124) (cf. Sect. II E). Here the predicted increase with primary energy of the average anisotropy of the angular distributions is in fair agreement with experiment (55, 160). Also, the observed low transverse momenta and their independence from primary energy can be accounted for, if the hydrodynamical treatment is restricted to the one-dimensional expansion of the system in the direction of the primary particle so that transverse momenta arise solely from thermal motion and are determined by the decay temperature T_k [$1 < (\mu/T_k) < 2$] (39, 146, 147). In accordance with observation, the theory predicts that a few particles emitted in the forward direction carry away most of the primary energy (the first and second particles carry 58 and 22 per cent of the primary energy at 1000 Bev, and 33 and 15 per cent, respectively, at 10^7 Bev) (106). Most of these fast particles are nucleons, which may theoretically be explained by

²⁹ Earlier calculations (40, 95, 119) did not consider strangeness conservation and used approximate expressions for the phase-space integrals.

the somewhat singular role that they play in the hydrodynamical expansion process (72). For further details cf. the review articles of Feinberg (75) and Koba & Takagi (114).

There are, however, a number of experimental facts which contradict this theory. For example, it predicts the emission of about equal numbers of particles in the forward and backward directions in the center-of-mass system; and until recently the assumption that this prediction was correct had been used, among others, as a criterion for determining the primary energy. This may be misleading; in fact, a new method for direct determination of the primary energy made it possible to show that in the region of several hundred Bev the above forward-backward symmetry is observed only in about 50 per cent of the events, the others showing emission mainly in the forward, or mainly in the backward, direction (67). A study of the inelasticities revealed that the asymmetric events may be explained as peripheral collisions of one of the nucleons with a meson in the cloud of the other one. These observations, as well as the great fluctuation of the multiplicities at a given energy, suggest that the hydrodynamical theory cannot be used as a description of every single event, but only as a phenomenological model to derive average values for some of the observed quantities. Eventually one must restrict oneself to only such events as might be the outcome of central collisions and use different models for peripheral interactions.

Among these the so-called "two-center" models have been most thoroughly discussed. Here it is assumed, as already suggested on p. 6, that after the collision two highly excited meson-emitting centers fly away, in the center-of-mass system, in opposite directions parallel to that of the primary particle. In the first such models (74, 111, 113, 121, 181) the emitting centers were considered to be excited nucleons which decay isotropically in their own rest systems according to statistical (or thermodynamical) laws or simply by emission of mesons of a single momentum. The details of the decay process are relatively unimportant, since the main features of these models are determined by the kinematics of the two independent emitting centers. One obtains definite relations among the degree of anisotropy, the multiplicity, and the inelasticity. Experimentally, in particular at energies above 1000 Bev, one finds clear evidence, from the absence of particles emitted near 90° , for a division of the emitted particles into two groups, with an angular distribution consistent with the assumption of emission from two independent centers. In general, however, the degree of anisotropy is such that according to the excited nucleon model, the nucleon had to travel rather slowly and, consequently, to be very highly excited, which would result in multiplicities much larger than the observed ones. Likewise the occurrence of very-high-energy nucleons would not be accounted for. It was therefore suggested (54, 55, 56, 156) that as a result of the collision the meson clouds of the nucleons are highly excited and then break off, travelling slowly behind the nucleons, which continue their path with very high velocity. The secondary mesons would then originate from decay of the excited

meson clouds; also forward-backward asymmetries would be easily understandable. A large part, but not all, of the experimental material is consistent with this model. [Further aspects are discussed in (43, 85, 87, 148, 182, 187).] It should be mentioned that the hydrodynamical model could also produce, at not too high energies ($<10^4$ Bev), the two-hump structure of the angular distributions, which is characteristic for the two-center models, by assuming fluctuations in the size of the interaction volume or in the decay temperature (73).

LITERATURE CITED

1. Agnew, L. E., Jr., Elioff, T., Fowler, W. B., Lander, R. L., Powell, W. M., Segrè, E., Steiner, H. M., White, H. S., Wiegand, C., and Ypsilantis, T., *Phys. Rev.*, **118**, 1371-91 (1960)
2. Amai, S., Fukuda, H., Iso, C., and Sato, M., *Progr. Theoret. Phys. (Kyoto)*, **17**, 241-87 (1957)
3. Amati, D., and Vitale, B., *Nuovo cimento*, [10]2, 719-27 (1955)
4. Auluck, F. C., and Kothari, D. S., *Phys. Rev.*, **90**, 1002-3 (1953)
5. Barashenkov, V. S., *Zhur. Ekspl. i Teoret. Fiz.*, **34**, 1016-17 (1958); *Soviet Phys. JETP*, **7**, 701 (1958); *Nuclear Phys.*, **7**, 146-47 (1958)
6. Barashenkov, V. S., *Zhur. Ekspl. i Teoret. Fiz.*, **37**, 1464-66 (1959); *Soviet Phys. JETP*, **10**, 1038-39 (1960); *Nuclear Phys.*, **15**, 486-94 (1960)
7. Barashenkov, V. S., *Nuovo cimento*, [10]14, 656-58 (1959)
8. Barashenkov, V. S., *Fortschr. Physik*, **9**, 29-41 (1961)
9. Barashenkov, V. S., *Nuclear Phys.*, **22**, 71-77 (1961)
10. Barashenkov, V. S., and Barbashov, B. M., *Nuovo cimento, Suppl.*, [10]7, 19-24 (1958)
11. Barashenkov, V. S., Barbashov, B. M., and Bubelev, E. G., *Nuovo cimento, Suppl.*, [10]7, 117-28 (1958)
12. Barashenkov, V. S., Barbashov, B. M., Bubelev, E. G., and Maksimenko, V. M., *Nuclear Phys.*, **5**, 17-22 (1958)
13. Barashenkov, V. S., Belyakov, V. A., Bubelev, E. G., Wang Shou Feng, Maltsev, V. M., Ten Gyn, and Tolstov, K. D., *Nuclear Phys.*, **9**, 74-82 (1958)
14. Barashenkov, V. S., and Maltsev, V. M., *Acta Phys. Polon.*, **17**, 177-82 (1958)
15. Barashenkov, V. S., and Maltsev, V. M., *Acta Phys. Polon.*, **17**, 397-400 (1958)
16. Barashenkov, V. S., and Maltsev, V. M., *Zhur. Ekspl. i Teoret. Fiz.*, **36**, 933-34 (1959); *Soviet Phys. JETP*, **9**, 659-60 (1959)
17. Barashenkov, V. S., and Maltsev, V. M., *Zhur. Ekspl. i Teoret. Fiz.*, **37**, 884-86 (1959); *Soviet Phys. JETP*, **10**, 630-31 (1960)
18. Barashenkov, V. S., and Maltsev, V. M., *Nuclear Phys.*, **17**, 377-87 (1960)
19. Barashenkov, V. S., Maltsev, V. M., and Mikhul, E. K., *Zhur. Ekspl. i Teoret. Fiz.*, **37**, 1484-86 (1959); *Soviet Phys. JETP*, **10**, 1052-54 (1960)
20. Barashenkov, V. S., Maltsev, V. M., and Mikhul, E. K., *Nuclear Phys.*, **13**, 583-93 (1959)
21. Barashenkov, V. S., Maltsev, V. M., and Wang Pei, *Zhur. Ekspl. i Teoret. Fiz.*, **38**, 650-52 (1960); *Soviet Phys. JETP*, **11**, 467-68 (1960)
22. Barkas, W. H., Birge, R. W., Chupp, W. W., Eksping, A. G., Goldhaber, G., Goldhaber, S., Heckman, H. H., Perkins, D. H., Sandweiss, J., Segrè, E., Smith, F. M., Stork, D. H., van Rossum, L., Amaldi, E., Baroni, G., Castagnoli, C., Franzinetti, C., and Manfredini, A., *Phys. Rev.*, **105**, 1037-58 (1957)
23. v. Behr, J., and Cerulus, F., *Nuovo cimento*, [10]16, 1046-67 (1960); **17**, 807 (1960)
24. v. Behr, J., and Hagedorn, R., *Graphs of Lab.-Spectra [at different angles (1° , 3° , 5° , 10° , 20°)] of particles produced in 25 GeV p-p collisions according to a statistical theory* (Unpublished Rept. CERN 60-20, May 6th, 1960)
25. Belenkii, S. Z., *Zhur. Ekspl. i Teoret. Fiz.*, **28**, 111-13 (1955); *Soviet Phys. JETP*, **1**, 161-62 (1955)
26. Belenkii, S. Z., *Zhur. Ekspl. i Teoret. Fiz.*, **32**, 1171-75 (1957); *Soviet Phys. JETP*, **5**, 952-56 (1957);

- Nuclear Phys.*, **2**, 259-66 (1956-57)
27. Belenkii, S. Z., and Landau, L. D., *Uspekhi Fiz. Nauk*, **56**, 309-48 (1955); *Fortschr. Physik*, **3**, 536-73 (1955); *Nuovo cimento, Suppl.*, [10] **3**, 15-31 (1956)
 28. Belenkii, S. Z., Maksimenko, V. M., Nikishov, A. I., and Rozental, I. L., *Uspekhi Fiz. Nauk*, **62**, 1-36 (1957); *Fortschr. Physik*, **6**, 524-64 (1958)
 29. Belenkii, S. Z., and Milekhin, G. A., *Zhur. Ekspil. i Teoret. Fiz.*, **29**, 20-32 (1955); *Soviet Phys. JETP*, **2**, 14-22 (1956)
 30. Belenkii, S. Z., and Nikishov, A. I., *Zhur. Ekspil. i Teoret. Fiz.*, **28**, 744-46 (1955); *Soviet Phys. JETP*, **1**, 593-96 (1955)
 31. Belenkii, S. Z., and Rozental, I. L., *Zhur. Ekspil. i Teoret. Fiz.*, **30**, 595-96 (1956); *Soviet Phys. JETP*, **3**, 786-87 (1956-57)
 32. Belinfante, F. J., *Phys. Rev.*, **92**, 145-52 (1953)
 33. Bergia, S., Bonsignori, F., and Stanghellini, A., *Nuovo cimento*, [10] **16**, 1073-84 (1960)
 34. Besson, C., Crussard, J., Fouché, V., Hennessy, J., Kayas, G., Parikh, V. R., and Trilling, G., *Nuovo cimento*, [10] **6**, 1168-88 (1957)
 35. Block, M. M., *Phys. Rev.*, **101**, 796-99 (1956)
 36. Block, M. M., Harth, E. M., Cocconi, V. T., Hart, E., Fowler, W. B., Shutt, R. P., Thorndike, A. M., and Whittemore, W. L., *Phys. Rev.*, **103**, 1483-89 (1956)
 37. Bogachev, N. P., Bunyatov, S. A., Vishki, T., Merkov, Yu. P., Sidorov, V. M., and Yarba, V. A., *Zhur. Ekspil. i Teoret. Fiz.*, **38**, 432-40 (1960); *Soviet Phys. JETP*, **11**, 317-22 (1960)
 38. Bogachev, N. P., Bunyatov, S. A., Merkov, Yu. P., Sidorov, V. M., and Yarba, V. A., *Zhur. Ekspil. i Teoret. Fiz.*, **38**, 1346-48 (1960); *Soviet Phys. JETP*, **11**, 968-70 (1960)
 39. Boos, E. G., and Takibaev, Zh. S., *Zhur. Ekspil. i Teoret. Fiz.*, **38**, 1276-84 (1960); *Soviet Phys. JETP*, **11**, 920-26 (1960)
 40. Brovetto, P., and Ferroni, S., *Nuovo cimento*, [10] **3**, 1387-93 (1956)
 41. Brueckner, K. A., and Kovacs, J. S., *Phys. Rev.*, **94**, 726-27 (1954)
 42. Bugg, W. M., and King, D. T., *Phys. Rev.*, **119**, 1408-10 (1960)
 43. Burmeister, J., Lanius, K., and Meyer, H. W., *Nuovo cimento*, [10] **11**, 12-20 (1959)
 44. Cerulus, F., *Nuovo cimento*, [10] **14**, 827-35 (1959); *K-Meson Production in N-N Annihilation Computed with a Statistical Theory* (Unpublished Rept. CERN 60-10, March 25th, 1960)
 45. Cerulus, F., *Nuovo cimento, Suppl.*, [10] **15**, 402-25 (1960)
 46. Cerulus, F., *Nuovo cimento*, [10] **19**, 528-36 (1961)
 47. Cerulus, F., and Hagedorn, R., *Nuovo cimento, Suppl.*, [10] **9**, 646-58, 659-77 (1958)
 48. Cerulus, F., and Hagedorn, R., *Multiple Meson Production from p-p Collisions at 2.75 Gev According to a Statistical Theory* (Unpublished Rept. CERN 59-3, 1959)
 49. Cester, R., Hoang, T. F., and Kernan, A., *Phys. Rev.*, **100**, 940-42 (1955); **103**, 1443-49 (1956)
 50. Chadwick, G. B., Collins, G. B., Swartz, C. E., Roberts, A., De Benedetti, S., Hien, N. C., and Duke, P. J., *Phys. Rev. Letters*, **4**, 611-13 (1960)
 51. Chadwick, G. B., Collins, G. B., Fujii, T., Hien, N. C., and Duke, P. J., *Bull. Am. Phys. Soc.*, **6**, 63 (1961)
 52. Chasan, B. M., Cocconi, G., Cocconi, V. T., Schectman, R. M., and White, D. H., *Phys. Rev.*, **119**, 811-14 (1960)
 53. Chew, G. F., *Ann. Rev. Nuclear Sci.*, **9**, 29-60 (1959); *Double Dispersion Relations and Unitarity as the Basis for a Dynamical Theory of Strong Interactions* (UCRL Rept. 9289, June 1960)
 54. Ciok, P., Coghen, T., Gierula, J., Hołyński, R., Jurak, A., Mięso-wicz, M., Saniewska, T., Stanis, O., and Perneg, J., *Nuovo cimento*, [10] **8**, 166-69 (1958)
 55. Ciok, P., Coghen, T., Gierula, J., Hołyński, R., Jurak, A., Mięso-wicz, M., and Saniewska, T., *Nuovo cimento*, [10] **10**, 741-54 (1958)
 56. Cocconi, G., *Phys. Rev.*, **111**, 1699-706 (1958)
 57. Cocconi, G., *Proc. Ann. Rochester Conf. High Energy Phys.*, 799-808 (Univ. Rochester, Rochester, N. Y., 1960)
 58. Cocconi, V. T., Fazzini, T., Fidecaro, G., Legros, M., Lipman, N. H.,

- and Merrison, A. W., *Phys. Rev. Letters*, **5**, 19-21 (1960)
59. Cook, R. F., and Lepore, J. V., *Phys. Rev.*, **120**, 1028-40 (1960)
 60. Cvijanovich, G., Dayton, B., Egli, P., Klaiber, B., Koch, W., Nikolić, M., Schneeberger, R., Winzeler, H., Combe, J. C., Gibson, W. M., Lock, W. O., Schneeberger, M., and Vanderhaeghe, G., *Helv. Phys. Acta*, **33**, 546-50 (1960); *Nuovo cimento*, [10]20, 1012-16 (1961)
 61. Czyż, W., Ericson, T., and Glashow, S. L., *Nuclear Phys.*, **13**, 516-24 (1959)
 62. Czyż, W., and Glashow, S. L., *Nuclear Phys.*, **20**, 309-12 (1960)
 63. Daniel, R. R., Kameswara Rao, N., Malhotra, P. K., and Tsuzuki, Y., *Nuovo cimento*, [10]16, 1-25 (1960)
 64. v. Dardel, G., Mermod, R. M., Weber, G., and Winter, K., *Proc. Ann. Rochester Conf. High Energy Phys.*, 837-39 (Univ. Rochester, Rochester, N. Y., 1960)
 65. Derado, I., and Schmitz, N., *Phys. Rev.*, **118**, 309-15 (1960)
 66. Desai, B. R., *Phys. Rev.*, **119**, 1385-89, 1390-94 (1960)
 67. Dobrotin, N. A., and Slavatskiy, S. A., *Proc. Ann. Rochester Conf. High Energy Phys.*, 819-28 (Univ. Rochester, Rochester, N. Y., 1960)
 68. Domokos, G., *Acta Phys. Hung.*, **9**, 49-62 (1958)
 69. Eberle, E., *Nuovo cimento*, [10]8, 610-14 (1958)
 70. Eisberg, R. M., Fowler, W. B., Lea, R. M., Shephard, W. D., Shutt, R. P., Thorndike, A. M., and Whittemore, W. L., *Phys. Rev.*, **97**, 797-808 (1955)
 71. Ekspong, A. G., Frisk, A., Nilsson, S., and Ronne, B. E., *Nuclear Phys.*, **22**, 353-409 (1961)
 72. Emelyanov, A. A., and Rozental, I. L., *Zhur. Ekspl. i Teoret. Fiz.*, **33**, 808-9 (1957); *Soviet Phys. JETP*, **6**, 622-23 (1958)
 73. Emelyanov, A. A., and Rozental, I. L., *Zhur. Ekspl. i Teoret. Fiz.*, **38**, 194-97 (1960); *Soviet Phys. JETP*, **11**, 142-44 (1960)
 74. Farley, F. J. M., *Nuovo cimento*, [10]16, 209-26 (1960)
 75. Feinberg, E. L., *Uspekhi Fiz. Nauk*, **70**, 333-50 (1960); *Soviet Phys. Uspekhi*, **3**, 147-58 (1960)
 76. Fermi, E., *Progr. Theoret. Phys. (Kyoto)*, **5**, 570-83 (1950)
 77. Fermi, E., *Elementary Particles*, 79-87 (Yale Univ. Press, New Haven, Conn., 110 pp., 1951)
 78. Fermi, E., *Phys. Rev.*, **81**, 683-87 (1951)
 79. Fermi, E., *Phys. Rev.*, **92**, 452-53 (1953); **93**, 1434 (1954)
 80. Fermi, E., *Anais acad. brasil. cienc.*, **26**, 61-63 (1954)
 81. Fialho, G. E. A., *Phys. Rev.*, **105**, 328-37 (1957)
 82. Fowler, W. B., Shutt, R. P., Thorndike, A. M., and Whittemore, W. L., *Phys. Rev.*, **95**, 1026-44 (1954)
 83. Fowler, W. B., Shutt, R. P., Thorndike, A. M., Whittemore, W. L., Cocconi, V. T., Hart, E., Block, M. M., Harth, E. M., Fowler, E. C., Garrison, J. D., and Morris, T. W., *Phys. Rev.*, **103**, 1489-501 (1956)
 84. Frautschi, S. C., *Progr. Theoret. Phys. (Kyoto)*, **22**, 15-24 (1959)
 85. Friedländer, E. M., *Phys. Rev. Letters*, **5**, 212-13 (1960)
 86. Gatto, R., *Nuovo cimento*, [10]3, 468-72 (1956)
 87. Gierula, J., Mięsowicz, M., and Zielinski, P., *Nuovo cimento*, [10]18, 102-19 (1960)
 88. Goebel, C., *Phys. Rev.*, **103**, 258-61 (1956)
 89. Goldhaber, G., Fowler, W. B., Goldhaber, S., Hoang, T. F., Kalogeropoulos, Th. E., and Powell, W. M., *Phys. Rev. Letters*, **3**, 181-83 (1959)
 90. Goldhaber, G., Goldhaber, S., Lee, W., and Pais, A., *Phys. Rev.*, **120**, 300-12 (1960)
 91. Goldhaber, G., Goldhaber, S., Powell, W. M., and Silberberg, R., *Phys. Rev.*, **121**, 1525-33 (1961)
 92. Goldhaber, G., and Lee, W., *Revs. Mod. Phys.*, **33**, 402-6 (1961)
 93. Gotō, T., *Nuovo cimento*, [10]8, 625-31 (1958)
 94. Haber-Schaim, U., and Yekutieli, G., *Phil. Mag.*, **43**, 997-98 (1952)
 95. Haber-Schaim, U., Yeivin, Y., and Yekutieli, G., *Phys. Rev.*, **94**, 184-85 (1954)
 96. Hagedorn, R., *Calculating High Energy Particle Production According to Statistical Theories on an Electronic Computer* (Unpublished Rept. CERN 59-25, July 2nd, 1959, and Internal Rept. 7580/Th. 62 CERN, 1959)
 97. Hagedorn, R., *A Program for Calculating Multiple Phase Space Integrals by a Monte Carlo Method on the*

- Ferranti-Mercury Computer* (Internal Rept. 6381, CERN, 1959)
98. Hagedorn, R., *Nuovo cimento*, [10]15, 246-68 (1960)
 99. Hagedorn, R., *Nuovo cimento*, [10]15, 434-61, 462-64 (1960)
 100. Hagedorn, R., *Phys. Rev. Letters*, 5, 276-77 (1960)
 101. Hagedorn, R., *Fortschr. Physik*, 9, 1-28 (1961)
 102. Hoang, T. F., *Phys. Rev.*, 121, 1523-24 (1961); *Analysis of K-Meson Production by \bar{p} Annihilation* (UCRL Rept. 8994 Rev., July 29, 1960)
 103. Hoang, T. F., and Young, J., *Covariant Phase Space Factors for Reactions Involving Four to Six Secondary Particles* (UCRL Rept. 9050, January 1960)
 104. Horwitz, N., Miller, D., Murray, J., and Tripp, R., *Phys. Rev.*, 115, 472-77 (1959)
 105. Ishida, S., *Progr. Theoret. Phys. (Kyoto)*, 22, 207-12 (1960)
 106. Iwadare, J., *Nuovo cimento*, [10]12, 630-32 (1959)
 107. Jauch, J. M., and Rohrlich, F., *The Theory of Photons and Electrons*, 167 (Addison-Wesley Publ. Co., Inc., Cambridge, Mass., 488 pp., 1955)
 108. Kalbach, R. M., Lord, J. J., and Tsao, C. H., *Phys. Rev.*, 113, 330-37 (1959)
 109. King, D. T., *Phys. Rev.*, 109, 1344-46 (1958)
 110. Koba, Z., *Progr. Theoret. Phys. (Kyoto)*, 15, 294-95, 461-72 (1956)
 111. Koba, Z., *Progr. Theoret. Phys. (Kyoto)*, 17, 288-302 (1957)
 112. Koba, Z., *Nuovo cimento*, [10]18, 608-12 (1960)
 113. Koba, Z., and Takagi, S., *Nuovo cimento*, [10]10, 755-62 (1958)
 114. Koba, Z., and Takagi, S., *Fortschr. Physik*, 7, 1-47 (1959)
 115. Koba, Z., and Takeda, G., *Progr. Theoret. Phys. (Kyoto)*, 19, 269-84, 594-95 (1958)
 116. Kopylov, G. I., *Zhur. Ekspl. i Teoret. Fiz.*, 35, 1426-34 (1958); 36, 1598-600 (1959); 39, 1091-98 (1960). *Soviet Phys. JETP*, 8, 996-1002 (1959); 9, 1136-37 (1959); 12, 761-65 (1961)
 117. Kopylov, G. I., *Zhur. Ekspl. i Teoret. Fiz.*, 39, 209 (1960); *Soviet Phys. JETP*, 12, 150 (1961)
 118. Kothari, D. S., *Nature*, 173, 590 (1954)
 119. Kothari, L. S., *Nature*, 171, 309 (1953); *Phys. Rev.*, 90, 1087-89 (1953)
 120. Kovacs, J. S., *Phys. Rev.*, 101, 397-409 (1956)
 121. Kraushaar, W. L., and Marks, L. J., *Phys. Rev.*, 93, 326-30 (1954)
 122. Kretzschmar, M., *Z. Physik*, 150, 247-63 (1958)
 123. Kretzschmar, M., *Z. Physik*, 157, 554-57 (1960)
 124. Landau, L. D., *Izvest. Akad. Nauk SSSR, Ser. Fiz.*, 17, 51-64 (1953)
 125. Lebedev, A. E., and Petrunin, V. A., *Zhur. Ekspl. i Teoret. Fiz.*, 38, 1337-39 (1960); *Soviet Phys. JETP*, 11, 962-64 (1960)
 126. Lepore, J. V., and Stuart, R. N., *Phys. Rev.*, 94, 1724-27 (1954)
 127. Lepore, J. V., Neuman, M., and Stuart, R. N., *Phys. Rev.*, 94, 788 (1954)
 128. Lepore, J. V., and Riddell, R. J., Jr. (Private communication)
 129. Lewis, H. W., *Revs. Mod. Phys.*, 24, 241-48 (1952)
 130. Lewis, H. W., Oppenheimer, J. R., and Wouthuyzen, S. A., *Phys. Rev.*, 73, 127-40 (1948)
 131. Lindenbaum, S. J., and Sternheimer, R. M., *Phys. Rev.*, 105, 1874-99 (1957)
 132. Lindenbaum, S. J., and Sternheimer, R. M., *Phys. Rev.*, 106, 1107-8 (1957); 109, 1723-33 (1958)
 133. Lindenbaum, S. J., and Sternheimer, R. M., *Phys. Rev. Letters*, 5, 24-26 (1960); *Phys. Rev.*, 123, 333-76 (1961); *Proc. Ann. Rochester Conf. High Energy Phys.*, 73, 205-7, 640 (Univ. Rochester, Rochester, N. Y., 1960)
 134. Louttit, R. I., Morris, T. W., Rahm, D. C., Rau, R. R., Thorndike, A. M., and Willis, W. J., *Proc. Ann. Rochester Conf. High Energy Phys.*, 372-76 (Univ. of Rochester, Rochester, N. Y., 1960)
 135. Lynch, G. R., *Revs. Mod. Phys.*, 33, 395-401 (1961)
 136. Maenchen, G., Fowler, W. B., Powell, W. M., and Wright, R. W., *Phys. Rev.*, 108, 850-64 (1957)
 137. Magalinskii, V. B., and Terletskii, Ya. P., *Zhur. Ekspl. i Teoret. Fiz.*, 29, 151-57 (1955); *Soviet Phys. JETP*, 2, 143-47 (1956)
 138. Magalinskii, V. B., and Terletskii, Ya. P., *Zhur. Ekspl. i Teoret. Fiz.*, 32, 584-91 (1957); *Soviet Phys. JETP*, 5, 483-88 (1957)

139. Maksimenko, V. M., *Zhur. Eksptl. i Teoret. Fiz.*, **33**, 232-37 (1957); *Soviet Phys. JETP*, **6**, 180-83 (1958)
140. Maksimenko, V. M., *Zhur. Eksptl. i Teoret. Fiz.*, **35**, 1302-4 (1958); *Soviet Phys. JETP*, **8**, 909-10 (1959)
141. Maksimenko, V. M., *Zhur. Eksptl. i Teoret. Fiz.*, **38**, 652-54 (1960); *Soviet Phys. JETP*, **11**, 469-70 (1960)
142. Maksimenko, V. M., and Nikishov, A. I., *Zhur. Eksptl. i Teoret. Fiz.*, **31**, 727-29 (1956); *Soviet Phys. JETP*, **4**, 614-16 (1957)
143. Maksimenko, V. M., and Rozental, I. L., *Zhur. Eksptl. i Teoret. Fiz.*, **32**, 658-66 (1957); *Soviet Phys. JETP*, **5**, 546-51 (1957)
144. Mikhul, E. K., *Zhur. Eksptl. i Teoret. Fiz.*, **35**, 298-99 (1958); *Soviet Phys. JETP*, **8**, 205-6 (1959)
145. Milburn, R. H., *Revs. Mod. Phys.*, **27**, 1-14 (1955)
146. Milekhin, G. A., *Zhur. Eksptl. i Teoret. Fiz.*, **35**, 1185-97 (1958); *Soviet Phys. JETP*, **8**, 829-37 (1959)
147. Milekhin, G. A., and Rozental, I. L., *Zhur. Eksptl. i Teoret. Fiz.*, **33**, 197-99 (1957); *Soviet Phys. JETP*, **6**, 154-56 (1958); *Nuovo cimento, Suppl.*, [10] **8**, 770-74 (1958)
148. Nagai, H., and Ito, D., *Progr. Theoret. Phys. (Kyoto)*, **23**, 966-67 (1960)
149. Nanda, V. S., *Progr. Theoret. Phys. (Kyoto)*, **11**, 605-6 (1954)
150. Neuman, M., *Anais acad. brasil. cienc.*, **31**, 361-79, 487-506 (1959)
151. Nikishov, A. I., *Zhur. Eksptl. i Teoret. Fiz.*, **29**, 246 (1955); *Soviet Phys. JETP*, **2**, 161-62 (1956)
152. Nikishov, A. I., *Zhur. Eksptl. i Teoret. Fiz.*, **30**, 601-3 (1956); *Soviet Phys. JETP*, **3**, 634-36 (1956)
153. Nikishov, A. I., *Zhur. Eksptl. i Teoret. Fiz.*, **30**, 990-91 (1956); *Soviet Phys. JETP*, **3**, 783-84 (1956)
154. Nikishov, A. I., *Zhur. Eksptl. i Teoret. Fiz.*, **30**, 1149-50 (1956); *Soviet Phys. JETP*, **3**, 976-77 (1956)
155. Nikishov, A. I., *Zhur. Eksptl. i Teoret. Fiz.*, **38**, 509-12 (1960); *Soviet Phys. JETP*, **11**, 369-71 (1960)
156. Niu, K., *Nuovo cimento*, [10] **10**, 994-1021 (1958)
157. Ono, K., and Yokoi, K., *Progr. Theoret. Phys. (Kyoto)*, **13**, 101-2 (1955)
158. Pais, A., *Ann. phys.*, **9**, 548-602 (1960)
159. Peaslee, D. C., *Phys. Rev.*, **94**, 1085 (1954); **95**, 1580-81 (1954)
160. Perkins, D. H., in *Progr. in Elementary Particle and Cosmic Ray Phys.*, **5**, 257-363 (1960)
161. Petrzilka, V., *Proc. Ann. Rochester Conf. High Energy Phys.*, 82-91 (Univ. Rochester, Rochester, N. Y., 1960)
162. Pickup, E., Ayer, F., and Salant, E. O., *Phys. Rev. Letters*, **5**, 161-63 (1960)
163. Pickup, E., *Proc. Ann. Rochester Conf. High Energy Phys.*, 69-73 (Univ. Rochester, Rochester, N. Y., 1960)
164. Pilkuhn, H., *Nuclear Phys.*, **22**, 168-76 (1961)
165. Pinski, G., *Phys. Rev. Letters*, **6**, 136-38 (1961)
166. Pomeranchuk, I. Ya., *Doklady Akad. Nauk SSSR*, **78**, 889-91 (1951); German Transl. in *Abhandl. Sowjet. Physik*, **4**, 78-81 (Verlag Kultur und Fortschritt, Berlin, Germany, 1954)
167. Powell, C. F., Fowler, P. H., and Perkins, D. H., *The Study of Elementary Particles by the Photographic Method*, 519-76 (Pergamon Press, New York-London-Paris-Los Angeles, 669 pp., 1959)
168. Rajopadhye, V. Y., *Phil. Mag.*, [8] **5**, 537-51 (1960)
169. Rozental, I. L., *Zhur. Eksptl. i Teoret. Fiz.*, **28**, 118-20 (1955); *Soviet Phys. JETP*, **1**, 166-69 (1955)
170. Rozental, I. L., and Chernavskii, D. S., *Uspekhi Fiz. Nauk*, **52**, 185-238 (1954); *Fortschr. Physik*, **4**, 560-609 (1956)
171. Ruskin, V. I., *Zhur. Eksptl. i Teoret. Fiz.*, **36**, 164-68 (1959); *Soviet Phys. JETP*, **9**, 113-15 (1959)
172. Ruskin, V. I., *Zhur. Eksptl. i Teoret. Fiz.*, **37**, 105-8 (1959); *Soviet Phys. JETP*, **10**, 74-76 (1959)
173. Ruskin, V. I., and Usik, P. A., *Zhur. Eksptl. i Teoret. Fiz.*, **38**, 929-33 (1960); *Soviet Phys. JETP*, **11**, 669-72 (1960)
174. Salzman, F., and Salzman, G., *Phys. Rev. Letters*, **5**, 377-79 (1960); *Phys. Rev.*, **120**, 599-608 (1960); **121**, 1541-44 (1961)
175. Schiff, L. I., *Note on the Calculation of Deuteron Production in High Energy Events* (Unpublished CERN

- Rept. 60-32, August 23rd, 1960)
176. Selove, W., *Phys. Rev. Letters*, **5**, 163-65 (1960)
177. Solmitz, F., *Proc. Ann. Rochester Conf. High Energy Phys.*, 164-72 (Univ. Rochester, Rochester, N. Y., 1960)
178. Soloviev, M. I., *Proc. Ann. Rochester Conf. High Energy Phys.*, 388-402 (Univ. Rochester, Rochester, N. Y., 1960)
179. Srivastava, P. P., and Sudarshan, E. C. G., *Phys. Rev.*, **110**, 765-66 (1958)
180. Sudarshan, E. C. G., *Phys. Rev.*, **103**, 777-79 (1956)
181. Takagi, S., *Progr. Theoret. Phys. (Kyoto)*, **7**, 123-25 (1952)
182. Takibaev, Zh. S., *Doklady Akad. Nauk SSSR*, **127**, 67-69 (1959); *Soviet Phys. Doklady*, **4**, 817-18 (1960)
183. Walker, W. D., *Phys. Rev.*, **108**, 872-77 (1957)
184. Wallenmeyer, W. A., *Phys. Rev.*, **105**, 1058-67 (1957)
185. Winzeler, H., Klaiber, B., Koch, W., Nikolić, M., and Schneeberger, M., *Nuovo cimento*, [10]**17**, 8-34 (1960)
186. Yajima, N., and Kobayakawa, K., *Progr. Theoret. Phys. (Kyoto)*, **19**, 192-200 (1958)
187. Yajima, N., Takagi, S., and Kobayakawa, K., *Progr. Theoret. Phys. (Kyoto)*, **24**, 59-80 (1960)
188. Yakovlev, L. G., *Zhur. Eksptl. i Teoret. Fiz.*, **37**, 1041-45 (1959); *Soviet Phys. JETP*, **10**, 741-43 (1960)
189. Yamamoto, Y., *Progr. Theoret. Phys. (Kyoto)*, **18**, 81-86 (1957)
190. Yeivin, Y., *Phys. Rev.*, **97**, 1084-85 (1955)
191. Yeivin, Y., and De-Shalit, A., *Nuovo cimento*, [10]**1**, 1146-51 (1955)
192. Yekutieli, G., *Nuovo cimento*, [10]**13**, 446-47 (1959)
193. Yuan, L. C. L., and Lindenbaum, S. J., *Phys. Rev.*, **103**, 404-12 (1956)
194. Zastavenko, L. G., *Zhur. Eksptl. i Teoret. Fiz.*, **37**, 1319-23 (1959); *Soviet Phys. JETP*, **10**, 939-42 (1960); (Unpublished Dubna-Repts)

STRONG INTERACTIONS AND REACTIONS OF HYPERONS AND HEAVY MESONS

BY G. MORPURGO

*Istituto di Fisica dell'Università di Firenze,
Istituto Nazionale di Fisica Nucleare-Sottosezione di Firenze, Italy*

1. INTRODUCTION

The purpose of this article is to review the large amount of work in the field covered by the above title during the last few years, a work which has been accompanied by relatively little progress in understanding.

The expression "little progress" here refers to the sad fact that we are still unable to make specific predictions on the strong strange-particle reactions, except for those predictions which follow from the general principles of quantum mechanics (in particular from the theory of nuclear reactions) and from some well-established conservation laws.

Foreseeing future developments is difficult, but it becomes more and more apparent that the study of the strong interactions of elementary particles is likely to proceed for a while along phenomenological lines similar in many respects to those of the physics of nuclear reactions. Indeed, on one hand, ambitious attempts to find a simple description incorporating high symmetries (attempts guided by the idea that, after all, we should be dealing with simple or "elementary" phenomena) have not led to positive results. On the other hand, no definite dynamical prediction is possible as yet for any of the strange-particle strong reactions. The most recent techniques, based on the study of the analytical properties of the S matrix, may change this situation; however, they have not yet changed it and the question of whether such techniques will evolve into a general method where many different processes are predicted with a clearly defined approximation in terms of a few parameters is a question the answer to which is highly problematical.

In this review we shall consider symmetry problems first and next the dynamical problems, discussion of which we shall essentially limit to the phenomenological treatment of the K^- reactions at low energy, which is certainly the process that has received the greater amount of attention in the last few years. As far as the symmetry properties are concerned, we shall consider: (a) the experiments proposed to determine the relative parities of the strange particles, (b) those speculations in which some new kind of symmetry is postulated, and (c) the problem of parity conservation of the strong interactions.

The period from the beginning of 1958 to the end of 1960 is surveyed; several review articles (1 to 5) appeared before this period and one (6) during it. We have also been greatly helped by the reports of the Geneva (7a, b),

Kiev (8a, b), and Rochester conferences (9a, b, c); also reference (10) can be consulted usefully.

It must be stressed that it has not been possible to illustrate the main problems and, at the same time, to give a detailed list of cross sections and a discussion of all the reactions involving strange particles. We have chosen to use the space at our disposal to illustrate the main problems, but we think that a compilation of the reactions involving elementary particles, like the famous Ajzenberg and Lauritsen compilation for the light nuclei, would soon begin to be useful.

Also, we shall not discuss the very-high-energy region, for which a separate review will certainly be needed in a short time because of the relatively recent entrance in operation of the Dubna and Cern accelerators.

2. TABLE OF PARTICLES

The 1960 table of particles, compiled by Barkas & Rosenfeld (11), is reproduced below (Table I). Detailed comments and references are given in (11) as to how the various data in the table have been obtained; we do not reproduce them here, but list instead the following points which it appears appropriate to insert as a complement to the table.

2.1 *Additions to the list of observed particles.*—One possible example of Ξ^0 (12) has been observed; examples of antihyperons $\bar{\Lambda}^0$ (13), $\bar{\Sigma}^-$ (14), $\bar{\Sigma}^+$ (15), and $\bar{\Xi}^0$ (16) have also been established through their decay and the recognition of the antinucleonic nature of the heavy decay product.

2.2 *Search for new particles.*—Resonances due to strong interactions will be excluded in the following discussion. For the hyperon-pion ($Y-\pi$) and $K-\pi$ systems, preliminary evidence on these resonances will be described later; for the pion-pion ($\pi-\pi$) system, (17) contains a summary of the present situation. The exclusion of pure strong interaction resonances implies that when considering, as in the next paragraph, the neutral bosons with isotopic spin $T=0$, we restrict our discussion to those neutral bosons whose decay cannot take place without the participation, real or virtual, of a photon. This restriction is artificial and is motivated by historical reasons and by our preference not to discuss here the question of the $\pi-\pi$ resonances, which, as is apparent from (17), is still in a very fluid state.

(a) *Neutral boson:* The search for a neutral boson was initiated for a number of reasons: the most important one is that, under the assumption of maximum charge 1 and maximum hypercharge 1, a neutral boson with $T=0$ is the only particle compatible with the scheme of Gell-Mann & Nishijima which has not yet been found. Of course, such a $T=0$ boson can be a simple strong resonance, as mentioned above; but if its mass is less than $2m_\pi$ or if it is a vector boson with a mass less than $3m_\pi$, the presence of a γ ray is needed in the decay (18), so that the boson is "long-lived" ($\tau \sim 10^{-20}s$ instead of $\sim 10^{-23}s$ as expected for a pure strong resonance). In

TABLE I
MASSES AND MEAN LIVES OF ELEMENTARY PARTICLES, SEPTEMBER 1960

Particle	Spin	Mass (Errors represent standard deviation) (Mev)	Mass difference (Mev)	Mean life (sec)
Photon γ	1	0	γ	γ Stable
Leptons				
ν	$\frac{1}{2}$	0	ν	ν Stable
e^\pm	$\frac{1}{2}$	0.510976 ± 0.000007	e^\pm	e^\pm Stable
μ^\pm	$\frac{1}{2}$	105.655 ± 0.010	μ^\pm	μ^\pm $(2.212 \pm 0.001) \times 10^{-6}$
Mesons				
π^\pm	0	139.59 ± 0.05	$\left. \begin{array}{l} 33.93 \pm 0.05 \\ 4.59 \pm 0.01 \end{array} \right\}$	π^\pm $(2.55 \pm 0.03) \times 10^{-8}$
π^0	0	135.00 ± 0.05		
K^\pm	0	493.9 ± 0.2	$\left. \begin{array}{l} 3.9 \pm 0.6 \\ (1.5 \pm 0.5) \eta / \tau (K_1) \end{array} \right\}$	K^+ $(1.224 \pm 0.013) \times 10^{-8}$ K^0 50% K_1 , 50% K_2 K_1 $(1.00 \pm 0.038) \times 10^{-10}$ K_2 $6.1 (+1.6/-1.1) \times 10^{-8}$
K^0	0	497.8 ± 0.6		
K_1	0			
K_2	0			
Baryons				
p	$\frac{1}{2}$	938.213 ± 0.01	$\left. \begin{array}{l} 1.2939 \pm 0.0004 \end{array} \right\}$	p Stable n $(1.013 \pm 0.029) \times 10^8$
n	$\frac{1}{2}$	939.507 ± 0.01		
Λ	$\frac{1}{2}$	1115.36 ± 0.14	$\left. \begin{array}{l} \Lambda \dots \dots \dots \\ 6.56 \pm 0.22 \\ 4.45 \pm 0.4 \end{array} \right\}$	Λ $(2.51 \pm 0.09) \times 10^{-10}$ Σ^+ $0.81 (+0.06/-0.05) \times 10^{-10}$ Σ^- $1.61 (+0.1/-0.09) \times 10^{-10}$ Σ^0 $< 0.1 \times 10^{-10}$
Σ^+	$\frac{1}{2}$	1189.40 ± 0.20		
Σ^-	$\frac{1}{2}$	1195.96 ± 0.30		
Σ^0	$\frac{1}{2}$	1191.5 ± 0.5		
Ξ^-	?	1318.4 ± 1.2	$\left. \begin{array}{l} \Xi^- \dots \dots \dots \\ \Xi^0 \dots \dots \dots \end{array} \right\}$	Ξ^- $1.28 (+0.38/-0.30) \times 10^{-10}$ Ξ^0 1.5×10^{-10} (1 event)
Ξ^0	?	1311.0 ± 8.0		

* A value of $1.9 \pm 0.5 \times 10^{-10}$ sec has been obtained by Glaser *et al.* (Preprint, Naval Research Lab., Washington 25, D. C.). This paper also contains references to previous work.

particular, the existence of a π_0^0 , a pseudoscalar boson with $T=0$ having a mass near to that of the ordinary π^0 , was postulated by Baldin (19a) and Yamaguchi (19b) to explain some apparent inconsistencies in low-energy pion physics; and a vector ρ_0 meson with mass $<3m_\pi$ was postulated by Nambu (18) in connection with the problem of the nucleon's electromagnetic structure. Though the reasons invoked by Baldin, Yamaguchi, and Nambu are not too convincing, these reasons and the intrinsic interest of the problem did stimulate a number of experimenters to look for such hypothetical bosons or for similar ones. Most of these experiments were summarized by Pontecorvo (20). The most interesting work, because of the general character of the method used, is: a search for the reaction $D+D \rightarrow \text{He}^4 + \pi_0^0$ (21), which, while forbidden by charge symmetry for the normal π^0 , would not be forbidden by charge symmetry for a $T=0$ boson; and photoproduction experiments (22, 23). No evidence for a neutral boson with a mass less than $2.5m_\pi$ has been obtained from the first experiment, nor (with a mass less than $3.5m_\pi$) from the second; upper limits of the cross sections have, of course, been set, but for their appreciation a complete discussion of the above experiments, which is out of place here, is needed. For other experiments in the search for neutral bosons (long-lived in the sense of this paragraph), compare (24) and (25).

(b) Charged particles with mass $550 m_e$: The experiments performed (26a, b, c) to confirm the existence of such particles, for which evidence was originally reported by Alikhanian *et al.* (26d) in a cosmic ray experiment, have all given negative results. For a survey compare (27).

(c) The heavy charged boson:¹ If the assumption of maximum hypercharge 1 is abandoned, but that of maximum charge 1 is maintained, the Gell-Mann—Nishijima scheme admits the existence of a few new particles which have already been listed on several occasions [compare, e.g. (1)]. One of these is a positive boson with strangeness $S=2$ and its conjugate with $S=-2$; these have been called D^\pm . A systematic attempt to attribute to these bosons various events, which had been reported in the past as difficult to interpret on the basis of known particles, was made by Yamanouchi (29) in November 1959. The situation was interpreted in (29) as indicative of the existence of a D^+ boson with $S=2$ and mass ~ 720 Mev; however, an essential part of this identification was based on two events, reported by the Bristol (30) and Columbia (31) groups. Such events, which look like a decay of some positive particle into a π^+ and a neutral particle, correspond to a π^+ with 60 Mev energy. Interpreted as a D^+ decay, the mass of the D^+ should be 720 Mev. However, Prowse (32) remarked later that the mass of these hypothetical D^+ particles, which, by the way, had been observed during the scanning of a K^+ beam, is not consistent with the above value, but is instead entirely consistent with the mass of a K^+ . This makes Yamanouchi's

¹ Heavy charged and possibly neutral bosons have also been introduced to transmit the weak four fermion interactions; compare (28) for a possible scheme.

interpretation untenable, although the nature of these anomalous K^+ decays is not yet clear (33), as the uniqueness and the value of the π^+ energy in both events need an explanation.

Recently, a Soviet group (34) has obtained, in studying π^- collisions at 7 GeV/c in a propane bubble chamber, several events [the Dubna event listed in (29) is of this kind] which allow the two following interpretations: either they can be attributed to a reaction of the kind



(the incident K^+ being produced in the primary collision of the π^- with a very small momentum transfer to the neutron (n); or, if they are attributed to a decay: $D^+ \rightarrow K^0 + \pi^+$ they correspond to values of M_D ranging from 750 to 950 Mev. Presumably an experiment with a beam of K^+ may lead to the correct interpretation. The recent discovery (compare Sect. 6.7) of a K - π resonance makes it possible that we are dealing with reaction 2.1, but with the final K^0 and π^+ produced in such a resonant state.

To summarize, the scattered existing evidence is insufficient to prove the existence of a charged long-lived boson heavier than the K meson.

No evidence exists for new baryons; in particular, as remarked, e.g., in (35), there is indirect evidence against the existence of a baryon with $S=1$. This would be one of the baryons compatible with the scheme of Gell-Mann and Nishijima if the hypercharge could assume values larger than 1.

2.3 Mass.—²The methods which have been used to determine the masses

² On the theoretical side, attempts have been made to understand the masses of the hyperons and heavy mesons. There are two different kinds of problems here. One consists in assuming that in some zero-order approximation, e.g., one in which the K -baryon interactions are left out, all the baryon masses are equal, and in trying to explain the mass differences among the different baryon multiplets as a consequence of the strong (supposedly only moderately so) K -baryon interactions. On the whole, this kind of problem, though much work has been devoted to it [e.g. (38, 39, 40)], does not seem promising at the moment.

The other problem is that of explaining the differences in mass within each multiplet, which are presumably of electromagnetic origin. It is well known that because the inner parts of the charge distribution may contribute to such an effect, the neutron-proton ($n-p$) mass difference problem is far from a quantitative solution, so that there is no reason to think the situation may be more favourable for the $\Sigma^-, \Sigma^0, \Sigma^+$ or for the K^0, K^+ mass difference problem. In this last case, however, a qualitative explanation of the fact that $m_{K^0} > m_{K^+}$, contrary to a straightforward application of perturbation theory (41) and to the expectation from the fact that $m_{\pi^+} > m_{\pi^0}$, can be given (42a, b, c). This explanation is based on the observation that, unlike the π^0 , the K^0 is a particle with a nonzero charge density; the charge density may be chosen so that the electrostatic self energy may explain in principle that $m_{K^0} > m_{K^+}$. Concerning the Σ multiplet, there have been calculations (43, 44) in the direction of connecting the Σ mass differences with the K mass differences, by calculating perturbatively the effect which the observed K mass difference has on the Σ multiplet masses. Qualitatively, one can find agreement, but this is certainly only part of the story.

are described in (11); here we mention only the main changes in the mass situation during the period covered by this review, as follows. A slight increase of the hyperon (Λ) mass and a better determination of the masses of the Σ multiplet; the mass of the Ξ^- is now known with a much smaller error ($\sim 50 \Xi^-$ are known), but the study of the Ξ^- properties still proceeds slowly because of the small production cross section of this particle [in associated production $3.6_{-2.1}^{+2.5} \mu\text{b}$ per nucleon for 7 GeV/c π^- ; $10.6_{-3.2}^{+4.4} \mu\text{b}$ per nucleon for 8 GeV/c π^- (34); in production from K^- (36), reaction $K^- + N \rightarrow \Xi^- + K$, $18 \pm 5 \mu\text{b}$ per nucleon with 1.17 GeV/c K^-].

A mass difference of 3.9 ± 0.6 Mev between K^0 and K^+ has been established, the neutral K^0 being heavier, and it has been recognized (37a, b) that the mass difference between the K_1^0 and K_2^0 components of the neutral K is of the order $\hbar/\tau(K_1^0)$. Except for this last result, all the others have been obtained using energy and momentum conservation in the appropriate processes; the last-mentioned result has been established with high precision in an ingenious experiment (37a) based on the study of the forward regeneration of K_1^0 in a beam of K^0 which passes through a dense material.

2.4 Spin.—The values of the spin of the hyperons indicated in Table I have been deduced, from the Adair and Lee & Yang arguments, in associated production; and from the Treiman argument in K^- absorption, taking into account the Day, Snow & Sucher (45) conclusion that K^- is absorbed, in hydrogen, from S states. A proposal for a *direct* K^0 spin determination is made in (46).

2.5 Magnetic moment.—No experimental data exist on the magnetic moments of any one of the strange particles, nor on the magnetic moments of hyperfragments. The only relations which can be stated (47a, b, c) independently of perturbation theory by a simple use of charge independence are: (a) $\mu_{\Sigma^+} + \mu_{\Sigma^-} = 2 \mu_{\Sigma^0}$ (mirror theorem); (b) the Λ^0 and Σ^0 moments do not receive a contribution from the pion currents and are therefore expected to be smaller than those of the other hyperons or of the nucleons. A perturbative calculation by Holladay (48) shows that values of μ_{Λ^0} or μ_{Σ^0} larger than 0.5 nm are improbable and that the actual values may well be a great deal smaller than this.

Following the line described in the introduction, we shall examine the symmetry properties which characterize the interactions of the strange particles. We divide this presentation into three parts: (a) the relative parities of the strange particles (Sect. 3); (b) the assumption and the consequence of particular "internal symmetries" (Sect. 4); and (c) the question of parity conservation of the strong interactions (Sect. 5).³

3. THE RELATIVE PARITIES OF THE STRANGE PARTICLES

We assume here that parity is conserved in strong interactions of strange particles, a question we shall discuss later, and we shall examine the methods

³ The questions (a) and (b) [and very shortly (c)] have also been reviewed in (6).

that have been proposed to determine the relative parities of the new particles.

It is, first of all, clear that, because of conservation of strangeness in strong interactions and the nonconservation of parity in weak interactions, only the relative parity $P_{\Lambda KN}$ of the Λ - K system with respect to the nucleon is a well-defined quantity. Of course, we may conventionally define the parity of the Λ as positive just like that of the nucleon and speak of the parity of the K ; this is often done, so that when one speaks, e.g., of a pseudo-scalar K , the parity for the Λ is assumed to be positive.

The other quantities of interest, in addition to $P_{\Lambda KN}$, are the parity of the Σ - K system with respect to the nucleon $P_{\Sigma KN}$ and the relative parity of Λ and Σ or of Ξ and N indicated respectively by $P_{\Lambda\Sigma}$, $P_{\Xi N}$. The fact that $P_{\Xi N}$ is a well-defined quantity is shown clearly in the reaction $K^- + p \rightarrow \Xi^- + K^+$ or (49) $\Xi^- + p \rightarrow \Lambda + \Lambda$, both of which may serve in the future for its practical determination. It is also evident that only two among the three quantities $P_{\Lambda KN}$, $P_{\Sigma KN}$, $P_{\Lambda\Sigma}$ are independent. Finally, it must be mentioned that the particles belonging to the same isotopic spin multiplet must have the same space-time properties, and in particular the same parity, so that a question like that of the parity of the Σ^- relative to the Σ^0 does not arise. The question of the relative parity of the K^+ and K^0 will be considered later.

The interest in the determination of relative parities of the strange particles lies, of course, in the same general reasons which stimulated, ten years ago, the determination of the parity of the pion; this interest, however, has been made more acute by the circumstance that a particular kind of symmetry can be imposed on the Lagrangian of strange particles only if $P_{\Lambda\Sigma}$ is even.

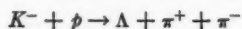
A number of experiments have been proposed, and in part performed, to determine the parities; those proposals which in our opinion have the greater chance of leading to a definite answer will be discussed below.⁴

DETERMINATION OF RELATIVE PARITY OF Λ , N , K

3.1 Okun & Pomeranchuk's method.—The reaction

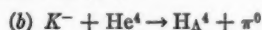
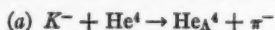
⁴ Among other proposed methods, we list those of reference (50a to e) which all involve, however, either polarized targets or rather difficult polarization measurements. In (50e) a general rule is established associating the relative parities with the polarizations of the particles involved in two-body reactions. We quote this rule here, since some of the following methods can be considered consequences of it; call \mathbf{p}_i and \mathbf{p}_f the relative momenta of the two initial and final particles, \mathbf{n} the normal to the plane formed by \mathbf{p}_i and \mathbf{p}_f , S_{ni} and S_{nf} the sum of the spin components of the initial and final particles along \mathbf{n} , P_i and P_f the products of the intrinsic parities of the particles in initial and final states; then $\Delta S_n = S_{ni} - S_{nf}$ must be even or odd depending on whether $P_i P_f = \pm 1$.

The perturbative calculations may also allow in some cases a determination of parities (compare, e.g., Sect. 6.9 for photoproduction), but it is always difficult to assess the reliability of such conclusions.



with bound K^- or at very low (positive) energy in the continuum gives an appropriate method of determining $P_{\Lambda KN}$. This method has been proposed by Okun & Pomeranchuk (51). Since the absorbed K^- should be in an S state (45), the two pions will go into an S state of relative motion because of the low value of their relative momentum (the situation is reminiscent of that existing in the τ decay); the Λ will therefore go into a P state if $P_{\Lambda KN}$ is odd or into an S state if $P_{\Lambda KN}$ is even. The angular distribution of the Λ momentum with respect to the two-pion total momentum will, therefore, give the required information. The difficulty of this method lies in the very low rate of occurrence of the process: one case in about 10^3 absorption events at rest (8a). Notice also that the relative momentum of the two pions may be as large as 130 Mev/c so that the assumption that only a two-pion S state intervenes, though not unreasonable, has to be checked using sufficient statistics.

3.2 Dalitz's method.—The existence of the following reactions has been established in helium bubble chamber experiments (52):



So far, 15 cases of (a) and 5 cases of (b) have been observed (53). If one can be sure that the spin state of He_Λ^4 (or H_Λ^4) through which the above reactions proceed is zero, then the mere observation of such reactions implies odd $P_{\Lambda KN}$ (5). Notice also that if the state of He_Λ^4 through which the reactions proceed has instead spin one no prediction is, in general, possible; however, if the absorption of the K^- takes place entirely from an S state, then $P_{\Lambda KN}$ must be even.

To know the spin state of He_Λ^4 (or H_Λ^4) through which the reactions (a) and (b) proceed is, therefore, important (5). This question may be divided into two: (a) Does there exist an excited state of He_Λ^4 ? (b) If not, can we be sure that the spin of He_Λ^4 is zero?

It is clear that a positive answer to the first question would ruin the method since if the ground state has spin zero, such an excited state would have spin one and vice versa. Also, a negative answer to question (b) would reduce the effectiveness of the method since any conclusion would be subordinate to the assumption of S -state absorption. As the discussion by Dalitz & Downs (54) and Dalitz (8c) shows, the balance is so delicate that it is impossible at present to predict or exclude the existence of an excited bound state of He_Λ^4 (or H_Λ^4); however, it seems clear from the above phenomenological analysis that if such a state exists, its binding energy should be less than 0.1 Mev. If this is so, Dalitz & Downs, as well as Block *et al.* (53), argue that the relatively large rate of formation of He_Λ^4 (or H_Λ^4) in K^- capture may indicate whether such formation takes place in the ground state or in this hypothetical excited state with $B_\Lambda < 0.1$ Mev. Indeed, the probability⁵ r

⁵ Here, r is defined as $(\text{yield of } \text{He}_\Lambda^4 + \pi^-) / [(\text{yield of } n + \text{He}^3 + \pi^-) + (\text{yield of } \text{He}^4 + \pi^-)]$.

that a Λ which is produced in the K^- capture remains bound and gives rise to a He_Λ^4 , the so-called sticking probability, evidently increases with increasing B_Λ . Dalitz & Downs have computed r as a function of B_Λ (making the simplifications typical of this kind of problems). They conclude that while r is 4.5 per cent for $B_\Lambda = 0.1$ Mev, it is four times as large for $B_\Lambda = 2$ Mev so that the possibility of a discrimination exists. The experimental value of r is, according to (53), 20 ± 7 per cent (only 15 He_Λ^4 hypernuclei were effectively seen, but use was made in this evaluation of a corrected number of 25 ± 7 per cent to take into account the losses). This represents rather preliminary evidence in favour of the formation of He_Λ^4 in its ground state.

On the other hand, there is practically no evidence on the question of the spin of the ground state.⁶ Of course, this question may be answered by measuring the angular distribution of the π^- with respect to the direction of the momentum of the H_Λ^4 in the decay $\text{H}_\Lambda^4 \rightarrow \text{He}^4 + \pi^-$; the details of the angular distributions are discussed, e.g., in (5) and (54, 85). The number of observed H_Λ^4 is now much too small to allow such an analysis; however, a clear answer to questions (a) and (b) above is essential before $P_{\Lambda KN}$ can be established by this method.

Another reaction, of the same kind, to determine $P_{\Lambda KN}$ is (56) $\pi^- + \text{He}^4 \rightarrow \text{H}_\Lambda^4 + K^0$. So far, no example of this reaction, which even if allowed is expected to be rare [1 event per 10^4 π^- interactions at 1 Gev (54)], has been detected; only preliminary results are available (57).

3.3 Dispersion relations.—The forward dispersion relations for K^\pm proton scattering can in principle be used to determine $P_{\Lambda KN}$ and $P_{\Sigma KN}$; at present, no conclusion can be obtained without making an assumption for $P_{\Lambda \Sigma}$; and, assuming $P_{\Lambda \Sigma}$ to be even, the indication is that $P_{\Lambda KN}$ is odd. This is, however, only an indication since the analysis is complicated and depends on some assumptions concerning the extrapolation of the \bar{K} - p cross section into the unphysical region. We shall not reproduce this analysis, since the essential points have been reviewed recently by Amati & Vitale (6), Dalitz (7b), and Matthews (9c); we therefore refer the interested reader to the above papers, in the order mentioned, for an adequate introduction to this subject, and to papers by Amati (58), Kerth *et al.* (59), and Selleri (60) for a discussion based on the most recent data and leading to the above conclusion.

3.4 Extrapolation method.—Taylor (61) has suggested that an extrapolation method of the Chew & Low type (62) may determine $P_{\Lambda KN}$ in a photoproduction experiment. It is well known that the Chew & Low method, when applied to photoproduction of a charged pion, consists in extrapolating the cross section up to the nonphysical angle $\cos \theta = c/v_\pi$ where v_π is the velocity of the photoproduced pion in the center-of-mass system. The value

⁶ A method proposed by Dalitz & Liu (55) for differentiating between spin zero and one does not give as clear-cut an answer as one would like in this kind of problem [compare also (53)].

of the residue of the production amplitude at such an angle is then related to the pion-nucleon coupling constant. Application of the method to pion photoproduction experiments was discussed in detail by Taylor and co-workers (62) as a tool for determining the π - N coupling constant. The result of (62) was that a determination of the π - N coupling constant accurate to 10 per cent with 260-Mev photons (for which $\cos\theta = 1.33$) implies measuring the cross section near the forward direction every 5° with an accuracy of 1 to 2 per cent. In the case of photoproduced K^+ at a photon energy of 1000 Mev, the above value of $\cos\theta$ is 2.7 so that the extrapolation has to extend over a much wider region than in the pion case. However, the essence of Taylor (61) and Moravcsik's (63) proposal is that only the sign of the residue at $\cos\theta = c/v_K$ is sufficient to discriminate between scalar and pseudoscalar K , so that one may hope to reach a conclusion when the experimental data improve. Such improvement should, in fact, allow a more definite determination than is now possible of the number of partial waves required and, therefore, of the order of the extrapolating polynomial, according to Moravcsik (63).

This method and also that of Okun & Pomeranchuk can be extended to a direct determination of $P_{\Sigma NK}$; this is essentially all that can be said with respect to such a direct determination.

DETERMINATION OF RELATIVE PARITY OF Λ AND Σ HYPERONS

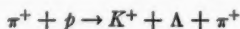
3.5 Correlations of polarizations and momenta.—For a direct determination of $P_{\Lambda\Sigma}$ the following methods have been suggested:

(a) Use of the reaction $\Sigma^- + p \rightarrow \Lambda + K^0$ with polarized Σ^- absorbed at rest or from an S state in the continuum (64); if the absorption is from an S state, a dependence of the hyperon polarization on its direction of emission can occur only for odd $P_{\Lambda\Sigma}$. The hyperon polarization can be detected through its decay asymmetry; the main difficulty is having polarized Σ^- brought to rest in hydrogen.

(b) Use of the correlation of hyperon polarization and gamma polarization in the decay of a polarized Σ^0 [Feldman & Fulton (65)].

(c) A measurement of the correlation between the spin of Λ and the plane of the electron positron pair in the Dalitz decay $\Sigma \rightarrow \Lambda + e^+ + e^-$ of a polarized Σ^0 (66, 67). According to (66) the study of 10^2 to 10^3 Dalitz decays of Σ^0 should determine $P_{\Lambda\Sigma}$ unambiguously, if a source of appreciably polarized Σ^0 can be found. A Dalitz decay of the Σ^0 takes place in about 175 γ decays [more precisely, 184 for even $P_{\Lambda\Sigma}$, 165 for odd $P_{\Lambda\Sigma}$ (68)].

3.6 The Y - π resonance method.—The existence of a Y - π resonance ($= Y^*$) with a total energy of ~ 1380 Mev has been suggested recently (compare Sect. 6.7). Assume (but unfortunately the preliminary indications are not in favour of this) that Y^{*+} can decay both in $\Lambda + \pi^+$ and in $\Sigma^+ + \pi^0$ with reasonable probability. Assume also that in a reaction like, e.g.,



and

$$\pi^+ + p \rightarrow K^+ + \Sigma^+ + \pi^0$$

we can separate those events for which $\Lambda + \pi^+$ and $\Sigma^+ + \pi^0$ are produced through the "decay" of the resonance Y^{*+} . Assume finally that the Y^* is strongly polarized (perpendicularly to its "production plane") and that interference effects from events not passing through the resonance are not dominating the picture. Consider those events where the Y^* (or equivalently the K^+) goes in a given direction; then the Λ^0 and Σ^+ from Y^* decay are polarized. Call $\bar{\mathcal{P}}_\Lambda$ and $\bar{\mathcal{P}}_\Sigma$ the average polarization for all Λ and, respectively, all Σ^+ , the average referring to events produced in the conditions described above. Then it can be shown (69) that $\bar{\mathcal{P}}_\Lambda/\bar{\mathcal{P}}_\Sigma$ is a positive quantity if the $\Lambda\Sigma$ relative parity is even, a negative quantity if it is odd. To measure $\bar{\mathcal{P}}_\Lambda$ and $\bar{\mathcal{P}}_\Sigma$, use can be made of the asymmetry in the $\Lambda \rightarrow p + \pi^-$, $\Sigma^+ \rightarrow p + \pi^0$ decays. Indeed, though at present only the absolute value of the ratio between the parameters α_Λ and α_0 is known, the same experiment, as shown in (69), should provide a determination of the sign of this ratio α_Λ/α_0 . The present experimental situation with respect to the Y^* (compare Sect. 6.7) is still too preliminary to permit judgment on the chances of this method.

3.7 The "cusp" method.—The "cusp" effect was first considered by Wigner (71a) and Breit (71b). A recent survey appears in a preprint by Fonda (71c). We describe this method in some detail, following the treatment of Baz & Okun (70), because experiments are now being done (9a). Consider the process (a) $\pi^- + p \rightarrow \Lambda + K^0$ at an energy E immediately above the threshold E_t for the process (b) $\pi^- + p \rightarrow \Sigma^0 + K^0$. Call $M_{\ell'}^{\ell}$ the S -matrix element for the process (a) in a state having the same quantum numbers (parity J and T) as those which, immediately above the threshold, characterize the S state of $\Sigma^0 + K^0$ in process (b). Define k as

$$k = \hbar^{-1} \sqrt{2\mu |E - E_t|} \quad \mu = \frac{m_\Lambda m_{K^0}}{m_\Lambda + m_K}$$

One can then prove that for $E > E_t$ one has

$$M_0^{1/2}(E) = M_0^{1/2}(E_t) + ak + \dots \quad \text{if } P_{\Lambda\Sigma} = 1 \quad 3.7-1$$

or

$$M_1^{1/2}(E) = M_1^{1/2}(E_t) + ak + \dots \quad \text{if } P_{\Lambda\Sigma} = -1 \quad 3.7-2$$

and in addition that $M_0^{1/2}$ or, respectively, $M_1^{1/2}$ are the only matrix elements which have, immediately above the threshold E_t , a linear dependence on k . In the above formulas, a is a complex coefficient.⁷ If we remark that the analyticity of the S matrix implies that the matrix elements for the process (a) below the threshold are obtained from those above by the substitution $k \rightarrow +ik$, we may express the result contained in Equations 3.7-1 or

⁷ $a = \lim_{k \rightarrow 0} S(\pi^- + p \rightarrow \Lambda^0 + K^0) \cdot S(\pi^- + p \rightarrow \Sigma^0 + K^0) / 2k$, where the $S(a \rightarrow b)$ are the corresponding S -matrix elements.

3.7-2 as follows: the matrix elements for process (a), in a state having the same quantum numbers as those characterizing reaction (b) immediately above the threshold, have an infinite first derivative with respect to E at $E = E_t$. Although it is not possible, for reasons of space, to give the derivation of Equations 3.7-1 or 3.7-2, it can be stated that in (70) they are derived simply, using only the unitarity of the S matrix, its symmetry in a J, M representation, the analyticity property already mentioned, and the fact that the outgoing $\Sigma^0 + K^0$ wave, near threshold, is produced in an S state and therefore has a matrix element proportional to $k^{1/2}$ (while in general the matrix element for an l wave behaves as $k^{l+1/2}$).

The interesting quantities are the cross section $\sigma(\theta, E)$ and the polarization $\mathcal{P}(\theta, E)$; it is quite generally

$$\sigma(\theta, E) = |g(\theta, E)|^2 + |h(\theta, E)|^2$$

and

$$\mathcal{P}(\theta, E) = 2 \operatorname{Im} \frac{h(\theta, E) g^*(\theta, E)}{\sigma(\theta, E)}$$

where

$$g(\theta, E) = (2ik_1)^{-1} \sum_l ((l+1)M_l^{l+1/2} + lM_l^{l-1/2})P_l(\theta) \quad 3.7-3$$

$$h(\theta, E) = -(2ik_1)^{-1} \sum_l (M_l^{l+1/2} - M_l^{l-1/2})P_l^{(1)}(\theta) \quad 3.7-4$$

In 3.7-3, 4, $P_l(\theta)$ and $P_l^{(1)}(\theta)$ are the conventional Legendre functions and k_1 is the wave number (in the center-of-mass system) of the incident π^- . The behaviour of $M_0^{1/2}$ or $M_1^{1/2}$ at $E = E_t$ is reflected in the behaviour of $\sigma(\theta, E)$ and $\mathcal{P}(\theta, E)$ as is clear on inserting 3.7-1 or 3.7-2 in 3.7-3 and 3.7-4 and confining ourselves to terms of first order in k . If we put:

$$\sigma(\theta, E_t) \equiv \sigma(\theta), \quad \mathcal{P}(\theta, E_t) \equiv \mathcal{P}(\theta)$$

the following formulas are easily obtained in the two cases of even and odd relative $P_{\Lambda\Sigma}$ parity; for $P_{\Lambda\Sigma} = 1$ the expressions of $G_+(\theta)$, $F_+(\theta)$ have to be taken; for $P_{\Lambda\Sigma} = -1$ those of $G_-(\theta)$, $F_-(\theta)$:

$$\begin{aligned} \sigma(\theta, E) &= \sigma(\theta) + \frac{k}{k_1} \begin{cases} -\operatorname{Im} G_{\pm}(\theta)a^* & E > E_t \\ \operatorname{Re} G_{\pm}(\theta)a^* & E < E_t \end{cases} \\ \mathcal{P}(\theta, E) &= \mathcal{P}(\theta) + \frac{k}{k_1} \begin{cases} \operatorname{Re} F_{\pm}(\theta)a^* & E > E_t \\ \operatorname{Im} F_{\pm}(\theta)a^* & E < E_t \end{cases} \end{aligned} \quad 3.7-4a$$

where

$$G_+(\theta) = g(\theta), \quad F_+(\theta) = (h(\theta) - i\mathcal{P}(\theta)g(\theta))/\sigma(\theta) \quad 3.7-5$$

and

$$G_-(\theta) = g(\theta) \cos \theta + h(\theta) \sin \theta, \quad F_-(\theta) = (h(\theta) \cos \theta - g(\theta) \sin \theta - i\mathcal{P}(\theta)G_-(\theta))/\sigma(\theta) \quad 3.7-6$$

The above formulas show that in principle one can determine $P_{\Lambda\Sigma}$ if $\sigma(\theta, E)$ and $\mathcal{P}(\theta, E)$ may be accurately measured at all angles at some E above

and below E_t . Indeed, the angular dependence of the term linear in k which one has thus determined is different, both for σ and for Φ , in the two cases of even and odd parity. As the formulas 3.7-5 and 3.7-6 show, $G_-(\theta)$ contains a power of $\cos \theta$ higher than $G_+(\theta)$, and $F_-(\theta)$ similarly contains a power of $\cos \theta$ higher than $F_+(\theta)$. Assuming that it is possible to know from an analysis of $\sigma(\theta)$ how many powers of $\cos \theta$ are needed in $g(\theta)$ and $h(\theta)$, one can decide the sign of $P_{\Lambda\Sigma}$.

Experimentally, the method is exceedingly difficult; in fact it is difficult to detect the presence of the singularity⁸ at E_t and much more difficult to measure angular distributions and polarizations on both sides of the singularity⁹ so as to establish the sign of $P_{\Lambda\Sigma}$. As usual, the polarization has to be determined through the asymmetry of the hyperon decay. One has to make measurements near, below, and above E_t with the highest possible energy resolution. How near to E_t is a difficult question to answer. It is necessary, of course, for the validity of 3.7-1 and 3.7-2 that $kR \leq 1$ where R is some radius of interaction, let us say m_K^{-1} . This condition is certainly not sufficient because if the contribution of the singularity to the total cross section is small (that is, if the coefficient of the term linear in k is such that terms linear in k give a small contribution), the possibility of its detection decreases as one goes far from E_t . Thus, the wisest prescription, even if not the most illuminating, at present is to make measurements as near as possible to E_t .

It may be added that the situation is rather more complicated than is apparent in the above, because of the existence of the two thresholds for the $\Sigma^0 + K^0$ and $\Sigma^- + K^+$ channels, the second of which is (Table I) very near to the first (within 0.5 Mev). A treatment including both channels, but neglecting the $\Sigma^- - K^+$ Coulomb attraction, has recently been given by Day, Snow & Sucher (72).

Finally, it should be clear that the phenomenon discussed here is only an example of a more general phenomenon: a singular dependence on the energy exists in the S matrix for any channel at the threshold for another channel, provided only that the two channels are strongly coupled; in our case, for instance, in addition to the singularity discussed above, a singularity in the pion-nucleon elastic scattering can be expected at the thresholds for the $\Lambda - K$ and $\Sigma - K$ channels. A singularity is also expected at the threshold for $K^- + p \rightarrow \bar{K}^0 + n$ in all the $K^- + p \rightarrow \Sigma + \pi$ reactions, and so on.

⁸ Some irregularity in the behaviour of the angular distribution and polarization on passing through E_t has been experimentally noted [cf. (9a)].

⁹ Whether the singularity in σ is really a cusp or an S -shaped curve depends of course on the signs of the coefficients of the term linear in k in 3.7-4a; these signs can be determined only by using models or, better, by using the experimentally determined amplitudes when these are known. In the present case the amplitude for S and P waves given in (152) might allow a preliminary analysis. (Cf., however (88).)

4. LOOKING FOR NEW SYMMETRIES

If it is assumed that each particle is described by a different field, it is easy to construct all the possible trilinear interactions which are invariant under rotations in the usual three-dimensional isotopic spin space¹⁰ and conserve charge.

The Lagrangian interaction which one obtains was first written by d'Espagnat & Prentki (73); an elementary way to construct it is described in (1). If we restrict ourselves, quite arbitrarily, to trilinear interactions, eight elementary interaction terms corresponding to the eight processes $N \rightarrow N + \pi$, $\Sigma \rightarrow \Sigma + \pi$, $\Lambda \rightarrow \Sigma + \pi$, $\Xi \rightarrow \Xi + \pi$ and $N \rightarrow \Lambda + K$, $N \rightarrow \Sigma + K$, $\Xi \rightarrow \Lambda + \bar{K}$, $\Xi \rightarrow \Sigma + \bar{K}$ can be written; the process $\Lambda \rightarrow \Lambda + \pi^0$ is of course absent, since it does not conserve T ; eight coupling constants appear in the Lagrangian interaction below, corresponding to the eight above processes:

$$\begin{aligned} \mathcal{L}^{(\pi)} &= ig_1 \bar{N} \gamma_5 \tau N \pi + g_2 \bar{\Lambda} \cdot \Sigma \pi - \frac{g_3}{2} \bar{\Sigma} \gamma_5 \times \Sigma \pi + ig_4 \bar{\Xi} \gamma_5 \tau \Xi \pi + \text{h.c.} \\ \mathcal{L}^{(K)} &= f_1 \bar{N} \cdot \Lambda K + f_2 \bar{N} \cdot \tau \Sigma K + f_3 \bar{\Xi} \cdot \Lambda \tau_2 \bar{K} + f_4 \bar{\Xi} \cdot \tau \Sigma \tau_2 \bar{K} + \text{h.c.} \end{aligned} \quad 4.1$$

To be definite, in 4.1 we have assumed that all the hyperons have spin $\frac{1}{2}$, the nonderivative form of the interaction has been written, and the dot stays for 1 or $i\gamma_5$ according to the relative parity of the particles involved; the field operators have been indicated with the symbols of the particles they represent, according to standard conventions.¹¹

Even if the assumption of trilinearity were acceptable and if one knew the relative parities of all the particles involved, almost nothing could be done with the expression 4.1. Indeed, not much credit can be given to perturbative calculations, and reliable nonperturbative methods do not exist. One is, therefore, naturally led to ask whether, for some particular choice of the coupling constants in the interactions 4.1, the total Lagrangian possesses a particularly symmetrical form and gives rise, as a consequence, to predictions about physical processes which are independent of detailed dynamical calculations.

It is clear, however, that a high "internal" symmetry in the total

¹⁰ Some progress has been made in establishing the validity of charge independence for the interactions of strange particles; indeed, experiments of absorption of K^- at rest in deuterium show (74) that the ratio between the number of events in which one charged pion is produced and the number of events in which a neutral pion is produced is $2(1.06 \pm 0.05)$, in good agreement with the value 2 predicted by charge independence.

In addition, previous indications of a violation of one of the triangular inequalities in the production process $\pi + N \rightarrow \Sigma + K$ have disappeared (75), though the errors are still very large. Presumably, the K^- -He⁴ experiments (53) will soon produce additional evidence.

¹¹ In the following we shall sometimes use the notations $g_{NN\pi}$ and $g_{\Lambda\Sigma\pi}$ for g_1 and g_2 ; $f_{\Lambda NK}$, $f_{\Sigma NK}$ for f_1 and f_2 .

Lagrangian does not exist; in fact the highest possible symmetry would necessarily correspond to equal masses for all the baryons. The mass differences among the existing particles are, on the other hand, substantial: $(M_{\Xi} - M_N)/M_N = 40$ per cent.

Nevertheless, it is possible to start from a rather symmetrical free Lagrangian (in which at least some of the masses have been considered equal) and to assume that the interactions giving rise to the observed mass differences (let us call them the "perturbation") are relatively small as compared to the main part of the strong interactions which are assumed to have some particular symmetries. Of course, progress along the proposed line can be made only if the very strong interactions lead, as a consequence of their symmetry, to predictions independent of detailed dynamical calculations. One can then use these predictions in situations where the "perturbation" is expected to have negligible effects, and compare the predictions with the experiment.

4.1 *The doublet symmetry.*—A first negative, but important,¹² result along these lines is due to Pais (76, 77). His work is interesting because it does not assume a very high symmetry for the Lagrangian 4.1, but instead assumes the minimum possible symmetry which may lead to predictions independent of detailed dynamical calculations; and also because the perturbation is really small, the expansion parameter being $\delta = (M_{\Sigma} - M_{\Lambda})/M_{\Sigma} = 0.067$. Pais' conclusion is that even the rather modest symmetry that he assumes is in contradiction with the data. In detail, Pais assumes: (a) even $P_{\Lambda\Sigma}$, (b) negligible δ in dynamical calculations, (c) that the presently known baryon spectrum is complete, (d) that the symmetry of the very strong interactions is such that in 4.1:

$$g_2 = g_3 = g \quad f_1 = f_2 = f_I \quad f_3 = f_4 = f_{II} \quad 4.1-1$$

Here assumptions (a), (b), (c) do not need any special explanation except that all these speculations concerning new symmetries fail for odd $P_{\Lambda\Sigma}$. Notice also that nothing is postulated with respect to the Ξ , N , π , and K masses. The central assumption is expressed by 4.1-1. One may ask why, among all the possible choices of the coupling constants, attention is fixed only on the particular relations 4.1-1; indeed, one of the main points of Pais' arguments has been to show that these relations are a necessary condition for obtaining linear relations among matrix elements for different processes over and above those provided by charge independence. Reference is made to (77) for a proof of this. Here we shall derive only the physical consequences of the assumptions above. The symmetry properties of the Lagrangian under such assumptions become evident, introducing the symbols:¹³

$$N_2 = \begin{pmatrix} \Sigma^+ \\ Y^0 \end{pmatrix} \quad N_3 = - \begin{pmatrix} Z^0 \\ \Sigma^- \end{pmatrix}$$

¹² These results have ended a number of speculations in which very large symmetries were postulated at the start, violating them immediately afterwards.

¹³ The definition of N_3 differs by a sign from that of Pais (76).

where

$$Y^0 = 2^{-1/2}(\Lambda^0 - \Sigma^0) \quad Z^0 = 2^{-1/2}(\Lambda^0 + \Sigma^0)$$

On writing also, for uniformity of notation,

$$N_1 = \begin{pmatrix} p \\ n \end{pmatrix} \quad N_4 = \begin{pmatrix} \Xi^0 \\ \Xi^- \end{pmatrix}$$

the interaction Lagrangian may be rewritten as $\mathcal{L}^{(\pi)} + \mathcal{L}^{(K)}$ where

$$\mathcal{L}^{(\pi)} = i[g_1 \bar{N}_1 \gamma_5 N_1 + g(\bar{N}_2 \gamma_5 N_2 + \bar{N}_3 \gamma_5 N_3) + g_4 \bar{N}_4 \gamma_5 N_4] \pi + \text{h.c.} \quad 4.1-2a$$

$$\begin{aligned} \mathcal{L}^{(K)} = & \sqrt{2} f_{11} (\bar{N}_1 \eta N_2) K^0 - (\bar{N}_1 \eta N_3) K^+ \\ & + \sqrt{2} f_{11} [(\bar{N}_4 \eta' N_2) \bar{K}^+ + (\bar{N}_4 \eta' N_3) \bar{K}^0] + \text{h.c.} \end{aligned} \quad 4.1-2b$$

and $\eta = 1$ or $i\gamma_5$; $\eta' = 1$ or $i\gamma_5$.

It is evident that this expression, as well as the free Lagrangian, has two kinds of symmetry. First it is rotation invariant when one attributes "isotopic spin i " to the individual particles indicated in the first column of Table II below. This symmetry corresponds to the fact that under the above assumptions all the baryons may be treated as doublets, and the K^+ , K^0 (as well as their charge conjugate) as isoscalar particles ($i=0$). The second symmetry corresponds to rotations in the N_2 , N_3 plane; the corresponding isotopic spin k assignments are given in the third column of the table.

TABLE II
DOUBLET SYMMETRY ASSIGNMENTS OF i AND k

	i	i_3	k	k_3	$S_1 = \frac{1}{2}S + k_3$
π	1	1, 0, -1	0	0	0
N_1	$\frac{1}{2}$	$\frac{1}{2}(p), -\frac{1}{2}(n)$	0	0	0
N_2	$\frac{1}{2}$	$\frac{1}{2}(\Sigma^+), -\frac{1}{2}(Y^0)$	$\frac{1}{2}$	$+\frac{1}{2}(\Sigma^+, Y^0)$	0
N_3	$\frac{1}{2}$	$\frac{1}{2}(Z^0), -\frac{1}{2}(\Sigma^-)$	$\frac{1}{2}$	$-\frac{1}{2}(Z^0, \Sigma^-)$	-1
N_4	$\frac{1}{2}$	$\frac{1}{2}(\Xi^0), -\frac{1}{2}(\Xi^-)$	0	0	-1
$K^{+,0}$	0	0	$\frac{1}{2}$	$+\frac{1}{2}(K^+), -\frac{1}{2}(K^0)$	$1(K^+), 0(K^0)$

These two symmetries constitute what is usually called the "doublet symmetry."¹⁴ The situation may be described by the statement that if the doublet symmetry is true, there exist two isotopic spin vectors $I = \Sigma i$ and $K = \Sigma k$ which are separately conserved; $I(I+1)$ are the eigenvalues of I^2 , $K(K+1)$ those of K^2 ; I^2 and K^2 commute. It is readily seen from the table that the usual isotopic spin T is given by:

$$T = I + K$$

¹⁴ Such assignments were first considered by Tiomno (78) and somewhat later, but independently, by Dallaporta (79).

Of course, the separate conservation of I and K gives rise to selection rules for many processes as well as to relations between matrix elements for different processes in addition to those implied by charge independence (conservation of T). Many of these relations or selection rules can be derived using only the conservation of I_3 and K_3 ; therefore, we have also given in the table the individual values of i_3 and k_3 , and the value of $S_1 \equiv \frac{1}{2}S + k_3 = \frac{1}{2}S + (i_3 - t_3)$ which is more convenient to use. Here S is the ordinary strangeness and S_1 is conserved because of the conservation of S and k_3 .

Note also that a particular case of invariance under rotations in the N_2, N_3 plane is the invariance under the simultaneous substitutions

$$N_2 \rightleftharpoons N_3 \quad K^+ \rightleftharpoons -K^0 \quad -\bar{K}^0 \rightleftharpoons K^+ \quad 4.1-3$$

Using 4.1-3 and the conservation of S_1 , the following consequences, among others, may be easily established (76):

- (a) In the reactions $\pi^- + p \rightarrow \Lambda^0 + K^0$ and $\pi^- + p \rightarrow \Sigma^0 + K^0$

$$d\sigma(\Lambda^0 K^0) \simeq d\sigma(\Sigma^0 K^0)$$

- (b) Similarly, in the reactions $\pi^- + p \rightarrow \Sigma^- + K^+$ and $\pi^- + p \rightarrow \Sigma^0 + K^0$

$$d\sigma(\Sigma^- K^+) \simeq 2d\sigma(\Sigma^0 K^0) \quad 4.1-4$$

- (c) The processes $\pi^+ + p \rightarrow \Sigma^+ + K^+$, $K^+ + n \rightarrow K^0 + p$, and $K^- + p \rightarrow \Sigma^+ + \pi^-$ are forbidden.

These statements are strictly true only if the mass difference $m_\Sigma - m_\Lambda$ is neglected in the computation of the matrix elements and, therefore, they are subject to corrections of order δ or in some cases δ^2 . It is clear, however, that most of these conclusions are in violent disagreement with experiment; we refer the reader to Sections 6, 6.1, 6.9, where some relevant data are presented.

In writing down the Lagrangian 4.1-2, we have implicitly assumed that K^+ and K^0 have the same parity. At the price of losing K and T conservation, leaving only I conservation, no need exists for this assumption and one can as well assume that they have opposite parity. This means that in 4.1-2b a γ_5 has to be inserted either before N_2 or before N_3 . Pais (80) has explored the consequences of this assumption in detail. Of course, if $P_{K^+K^0} = -1$, the invariance property 4.1-3 is broken and, consequently, Equation 4.1-4 is no longer valid; however, the forbiddenness of the processes indicated before under c remains, as well as those other relations (some in violent disagreement with experiment) which arise from the separate conservation of S_1 and S . The separate conservation of S_1 and S may also be broken by some convenient interaction (in the case $P_{K^+K^0} = -1$, the interaction $K\bar{K}\pi$ is a possible, parity-nonviolating, one); but if one introduces symmetries and immediately afterwards violates them, one is back at the starting point.

In addition, if $P_{K^+K^0} = -1$ it is difficult to understand why two strongly interacting particles with opposite parity should have approximately the same mass. More details on this and related problems appear in (80). It is

noteworthy that the assumption $P_{K^+K^0} = -1$ implies, necessarily, a violation not only of charge independence (T conservation), but also of the charge symmetry. Such a violation would be most apparent in reactions in which real strange particles participate. As noted in this connection by Pais (81) and independently by Morpurgo (82), an ideal experiment to test such a possible violation of charge symmetry directly would be that of comparing at each energy and angle the cross section for associated production of new particles by π^- and π^+ in a self-conjugated nucleus (83); any deviation from charge symmetry would reflect in a deviation from unity in the ratio between the rates of mirror processes (due correction being made for Coulomb effects).

We conclude this section with the statement that not even the relatively modest symmetry 4.1-2 exists; that is, Σ and Λ cannot be simultaneously coupled symmetrically to K and π .

4.2 *Restricted and global symmetry.*—We must, therefore, be more modest. Continuing to assume even $P_{\Lambda\Sigma}$, we can suppose, for example, that only the pions are coupled symmetrically to Σ and Λ . Of course, the previous arguments show that in this case no prediction can be made which is independent of detailed dynamical calculations; but if we simultaneously assume that the K interactions are an order of magnitude smaller than the pion interactions and can, essentially, be treated perturbatively, some predictions can still be derived from this "restricted symmetry" (84).

In detail, the assumptions made now are: (a) weak K interactions, (b) $g_2 = g_3$ so that the interaction of pions with Λ and Σ can be written:

$$ig(\bar{N}_2 \epsilon \gamma_5 N_2 + \bar{N}_3 \epsilon \gamma_5 N_3) \pi + \text{h.c.}$$

in the notation previously introduced. If one prefers to be a little more ambitious, he can also assume that the pion-nucleon (and possibly the π - Ξ interaction) have the same coupling constant (always under the assumption of weak K couplings). This is the global symmetry first introduced by Gell-Mann and Schwinger; it corresponds to the following pion-baryon interaction (85):¹⁵

$$ig[\bar{N}_1 \epsilon \gamma_5 N_1 + \bar{N}_2 \epsilon \gamma_5 N_2 + \bar{N}_3 \epsilon \gamma_5 N_3 + \bar{N}_4 \epsilon \gamma_5 N_4] \pi + \text{h.c.}$$

The evidence for weak K interactions is certainly not strong. It is true that the values for the unrenormalized coupling constants $f_1^2/4\pi$ and $f_2^2/4\pi$ deduced from a perturbative treatment of K^+-p scattering and of Λ^0 and Σ^0 photoproduction, assuming a pseudoscalar K and $P_{\Lambda\Sigma} = 1$, are both ~ 2 .¹⁶ These

¹⁵ The opposite assumption that K are strongly coupled symmetrically to baryons, while pion interactions are weaker and unsymmetrical, is discussed by Sakurai (86) and called "cosmic symmetry."

¹⁶ Of course, values of the renormalized coupling constants can, in principle, be derived from the dispersion relations of K^+-p scattering (compare p. 49), but in practice this is not yet possible. Also, it appears useless to quote values of f_1 or f_2 derived perturbatively under the assumption of a scalar K and $P_{\Lambda\Sigma} = 1$ because the perturbative treatment for K^+-p scattering with a scalar K and $P_{\Lambda\Sigma} = 1$ is in disagreement with the experimental data.

values are certainly smaller than those of $g_1^2/4\pi$ or, as far as we can say, of the $g_2^2/4\pi$ coupling constants which both¹⁷ correspond to ~ 15 .

However, it is far from clear whether and when the above $f^2/4\pi$ are really the significant parameters to measure the strength of K interactions or, in other words, the relative importance of their physical effects; indeed (compare Sect. 6.6), in one case it can be shown that the effects of the K interactions cannot be treated perturbatively, unless the present values of the Dalitz & Tuan parameters undergo large changes.

Nevertheless, some work has been done to investigate the consequences of global or restricted symmetry and to compare them with the experiments; only brief comment on such work will be given below.

(a) Hyperon-nucleon scattering: This question has already been discussed in some detail in (7b) and (6). Here we say only that under the global symmetry assumption the Σ^+-p and Σ^-n potentials in triplet odd- l or singlet even- l states must be the same as the proton-proton ($p-p$) or neutron-neutron ($n-n$) potentials. Nothing can be said with respect to the other states since Pauli's principle forbids such states for the $p-p$ or $n-n$ system. Without additional special assumptions [e.g. (87)], only a few inequalities (88) can be stated, and they cannot as yet be checked. Considering bound states, in particular, the problem arises whether the Σ^-n state analogous to the $n-n$ singlet state, which is almost bound, can be expected to be bound. The balance is delicate here, since the difference from the $n-n$ case is due both to the difference in mass and to the K interactions. Even if these last are weak they may well be decisive in this problem, so that, again, no conclusion is really possible. It must be added that Σ^-n compounds have been carefully looked for; the present data do not show any such evidence either in K^-D absorption (89) or in complex nuclei (90, 91). The formation of such compounds is however forbidden in K^-D absorption by a selection rule for S -state capture if the $P_{\Sigma KN}$ is odd and the spin of the bound state is zero (64).

(b) A comparison of the rates of the reactions $\Sigma^-+p \rightarrow \Sigma^0+n$ and $\Sigma^-+p \rightarrow \Lambda^0+n$ would provide evidence of restricted symmetry—indeed, it is

¹⁷ Assuming that the main part of the $\Lambda-N$ force in hyperfragments is transmitted by 2 pions, the lowest-order perturbative calculations [Lichtenberg & Ross (157) and Dallaporta & Ferrari (158)], with $P_{\Lambda\Sigma}=1$, of Λ -nucleon potential lead to a value ≈ 15 for $g_{\Sigma\Lambda}^2/4\pi$. More direct determinations of the g_2, g_3 coupling constants will become possible when more is known on $Y-N$ scattering; at present only the following hydrogen data are available:

- (a) $\Lambda + p \rightarrow \Lambda + p$ (4 events) $\sigma = 40 \pm 20$ mb; $p_L^\Lambda = 500-1000$ Mev/c (159)
- (b) $\Lambda + p \rightarrow \Sigma^+ + n$ (2 events) $\sigma = 30 \pm 20$ mb; $p_L^\Lambda = 700-800$ Mev/c (160)
- (c) $\Sigma^+ + p \rightarrow \Sigma^+ + p$ (10 events) $\sigma = 38_{-14}^{+18}$ mb; $T_L^\Sigma = 100-700$ Mev
- (d) $\Sigma^- + p \rightarrow \Sigma^- + p$ (6 events) $\sigma = 10_{-4}^{+6}$ mb; $T_L^\Sigma = 100-700$ Mev [for (c) and (d) compare (160)].

More indirect evidence on $Y-N$ cross sections (in particular $\Sigma N \rightarrow \Lambda N$) is available from K^- absorption reactions in complex nuclei and especially in deuterium; the analysis of this last process (e.g., $K^-+D \rightarrow \Sigma^0+p+\pi^- \rightarrow \Lambda^0+p+\pi^-$) is given in (161a) and (161b).

straightforward to show that the matrix elements for these two reactions are equal under the assumption of restricted symmetry. However, as discussed in detail by Dalitz (7b), at low energy the Σ, Λ mass difference dominates the picture in this process, so that, again, restricted symmetry alone does not lead to any precise conclusion. The situation, as pointed out in (7b), would be clearer at high-energy and low-momentum transfer (to exclude the interaction region where the K meson may be important), but so far no experimental data exist in such regions.

(c) Tests of the validity of global or restricted symmetry in pion-hyperon scattering were discussed originally by Amati & Vitale (84); later work on similar lines was done by Salam (8b), D'Espagnat & Prentki (92), Gupta (93), Kawarabayashi (94), Capps (95), Ross & Shaw (96). Here we shall discuss only the question of strict global or restricted symmetry as defined previously, leaving for Section 6.8 the problem of the possible $p_{3/2}$ resonance in π - Y scattering where a looser concept of global symmetry has generally been used.

In practice the pion-hyperon state that we are considering is produced in K^- absorption reactions; if global or restricted symmetry is valid the final π - Σ or π - Λ states produced in K^- absorption can be described in two alternative ways: (a) in the conventional way as eigenstates of isotopic spin T 1 or 0; (b) as eigenstates of the isotopic spin I belonging to the eigenvalues $\frac{3}{2}$ and $\frac{1}{2}$. In this last description π - N_2 and π - N_3 scattering are identical; and since transitions between $I=\frac{1}{2}$ and $I=\frac{3}{2}$ states are forbidden, it is apparent that the number of independent matrix elements is reduced from 9 to 7 by restricted symmetry. Global symmetry would introduce a further limitation by requiring that the phases of the π - N scattering in a state with given J, l , and I are equal to the real part of those of pion-hyperon scattering in the same state; however, there is some ambiguity here concerning the energy at which the two cases have to be compared, because of the mass difference between Λ, Σ , and nucleons.

It must be stressed that global and restricted symmetry lose any meaning if the K interactions are strong. The effects of the K interactions show themselves in a nonconservation of I also in processes where real K 's do not intervene; if these effects are strong, those consequences of the hypothetical I conservation which would be present when the K interactions are switched off cannot be unambiguously determined (92, 93).

Now, in this problem, the presence of the K^- channels is strongly felt in pion-hyperon scattering in the energy region near $m_K + m_P$ under discussion here; therefore, there is not much profit in continuing this discussion. In case the reactive K^- effects on hyperon scattering should not be too large (which, in view of the results of Sect. 6.6, is unlikely at present), the original treatment of (84), which is unambiguously justifiable only if the $\pi Y \rightarrow \bar{K} N$ matrix elements are small with respect to the $\pi Y \rightarrow \pi Y$ matrix elements, is entirely adequate; and the resulting formulas can be applied to test global

or restricted symmetry. Particularly at low K^- energy (where the K^-p scattering phase shifts are small), the inequality

$$(W_{\Sigma^- \pi^+} + W_{\Sigma^+ \pi^-} - 4W_{\Sigma^0 \pi^0})^2 + 4W_{\Sigma^0 \pi^0}W_{\Lambda^0 \pi^0 \rho} - 4W_{\Sigma^- \pi^+}W_{\Sigma^+ \pi^-} \geq 0$$

has to be satisfied, the W being the branching ratios to the various final states in arbitrary units and $\rho = \rho_{\Sigma}/\rho_{\Lambda}$ being the ratio between the phase-space volumes for Σ and Λ production, which takes into account the kinematical aspects of the Σ , Λ mass difference. At present (8a) the experimental errors appear too large to allow a check of this inequality.

4.3 Weak doublet symmetry.—It appears from the previous survey that the assumption that strong interactions have symmetries stronger than charge independence does not lead to encouraging results; indeed, the doublet symmetry definitely leads to disagreement with experiment, and the predictions of global symmetry or restricted symmetry are in most cases ambiguous or not too fruitful.

Recently, however, Treiman (97) and especially Pais (98) have made an effort to determine whether or not the above symmetries are capable of showing themselves more clearly in some decay processes, in particular, in the nonleptonic decays of hyperons. It is evident that such processes are influenced, virtually, by the strong interactions; and if one assumes that in such processes the strong interactions behave as if the doublet symmetry were essentially true, it becomes possible to make specific predictions concerning the decay parameters of Σ 's and Λ . Consider, specifically, the parity properties of the Σ^\pm and Λ decay interactions. It is experimentally known that the decay Σ_+^+ (that is, $\Sigma^+ \rightarrow n + \pi^+$), as well as $\Sigma_-^-(\Sigma^- \rightarrow n + \pi^-)$, does conserve parity, whereas $\Sigma_0^+ \rightarrow p + \pi^0$ and $\Lambda \rightarrow p + \pi^-$ violate parity conservation very strongly. As Pais observes, this situation is remarkable because, even if one can construct weak decay interactions which imply the above properties and are in agreement with the $\Delta T = \frac{1}{2}$ rule, one might expect that virtual strong processes would change the situation completely. Consider, for instance, the Σ_-^- and suppose that the direct decay interactions conserve parity for this process. One may also, however, have a Σ_-^- decay through the sequence $\Sigma^- \rightarrow \Sigma^+ + 2\pi^- \rightarrow p + \pi^0 + 2\pi^- \rightarrow n + \pi^-$, which violates parity conservation due to parity violation in $\Sigma^+ \rightarrow p + \pi^0$. There is no way to exclude the above sequence if simple charge independence is assumed; but if doublet symmetry is postulated, the transition $\Sigma^- \rightarrow \Sigma^+ + 2\pi^-$ is forbidden. In a similar way, parity conservation in Σ_+^+ decay can be understood if we assume, in addition to doublet symmetry, that in the Z^0 (as well in the Y^0) decay, parity is conserved, parity nonconservation in Λ^0 decay being due to opposite parity waves in Z^0 and Y^0 decay.

It is outside the scope of this review to describe more fully the predictions which follow for hyperon decays from the above line of approach. It must be emphasized, however, as noted by Pais himself, that one cannot have confidence in the above approach until it is clear why the doublet symmetry

should fail to show itself directly in strong processes and should exhibit its power only indirectly in decay processes.

4.4 Compound models.—The idea that only a few particles are elementary and the remaining ones are compound is rather old. An attempt to describe the pion as a nucleon-antinucleon compound with a binding energy of ~ 1700 Mev was made by Fermi & Yang (99); Goldhaber (100) and Christy (101) considered the possibility of describing all the strange particles as nucleon K compounds. Sakata (102) remarked that an even simpler possibility might be one in which nucleons and Λ are regarded as elementary, all other strongly interacting particles being constructed through them. This last description has several simple features which have been summarized by Yamaguchi (103) and Ikeda *et al.* (104). It is particularly remarkable that the interactions do not change the kind of a particle; a neutron always remains a neutron, a proton remains a proton, and a Λ remains a Λ . The reason for this is simply the conservation of baryonic number, charge, and strangeness. The simplicity increases further if we assume that in some zero-order approximation, the validity of which is rather problematical, proton mass = neutron mass = Λ mass and that the theory is invariant with respect to arbitrary permutations of these three particles. In this approximation, where for instance the mass of the π ($\sim \bar{N}N$) is equal to that of the K ($\sim \bar{\Lambda}N$), a few predictions can be made, the strongest being that the K is pseudoscalar and has zero spin as the pion does.

In principle, one would like the theory to move in the future in the direction of compound schemes. But, at present, reliable dynamical relativistic calculations are unfeasible so that it is not possible to predict, assuming e.g. some quadrilinear interaction between $n, p, \Lambda, \bar{n}, \bar{p}, \bar{\Lambda}$, whether a given compound state is bound or not, and this is the first question a compound model should answer. Thus further speculation on these points appears useless here.

There is, however, a general idea originated by Fujii (105) and discussed recently by Sakurai (106) which it seems appropriate to mention. The idea arises, in Fujii's presentation, from the remark made above that in the Sakata model the three strongly interacting particles are separately conserved. This feature is shared by the electromagnetic interactions and suggests the construction of the interactions of the strongly interacting particles in analogy with the electromagnetic case. According to Fujii this can be done most simply by writing the interaction as $B_\mu J_\mu$, where

$$J_\mu = i \sum_\alpha g_\alpha \bar{\Psi}_\alpha \gamma_\mu \Psi_\alpha \quad (\alpha = p, n, \Lambda) \quad 4.4-1$$

and where B_μ is a vector neutral boson field of mass m , which satisfies the equation:

$$(\square - m^2)B_\mu = -J_\mu \quad 4.4-2$$

and the subsidiary condition,

$$\left(\frac{\partial B_\mu}{\partial x_\mu} + mB'\right)\Psi = 0 \quad 4.4-3$$

where B' is an auxiliary neutral scalar field¹⁸ with $(\square - m^2)B' = 0$. As a result of these equations we have $\partial J_\mu / \partial x_\mu = 0$. The theory can be formulated, following a method suggested by Stückelberg (107), in such a way that the interaction terms are obtained from the free Lagrangian, as in electrodynamics, through the substitutions

$$\frac{\partial}{\partial x_\mu} \rightarrow \frac{\partial}{\partial x_\mu} + ig_n B_\mu \quad 4.4-4$$

where g_p , g_n , g_Λ are three coupling constants for p , n , and Λ . If, in addition, we say

$$g_p = g_n = g_\Lambda = g^{(B)} \quad 4.4-5$$

$g^{(B)}$ may be interpreted, in analogy with the electromagnetic case, as the baryonic charge. As pointed out on several occasions [compare (108)] and emphasized by Sakurai, the analogy with the electric charge fails completely if this baryonic charge is identified with the coupling constant of the global symmetry pion-baryon Lagrangian, although the initial motivation for global symmetry was just that of giving equal baryonic charge to all the baryons (109).

Now, although interaction 4.4-1 conserves isotopic spin and hypercharge (or equivalently strangeness), the symmetry with respect to the neutron, proton, lambda permutations implied by 4.4-5 would produce a scheme in which all the baryons, and similarly π and K , have the same mass. This can be avoided, and, at the same time, the conservation of hypercharge and isotopic spin can be put on the same footing as the conservation of the baryonic number, if we introduce two other vector bosons $B^{(Y)}$ and $B^{(T)}$ in addition to the one previously introduced (which we shall call $B^{(B)}$ from now on, the upper index indicating that this is responsible for the conservation of the baryonic number). In the same way that $B^{(B)}$ is coupled to the baryonic current, $B^{(Y)}$ and $B^{(T)}$ are coupled, respectively, to the hypercharge and isotopic spin currents (for this to be possible, $B^{(T)}$ itself must have a unit isotopic spin). Then, in the same way that $g^{(B)}$ is the baryonic charge, the coupling constants $g^{(Y)}$ and $g^{(T)}$ of these two additional couplings are the hypercharge and the isotopic charge of the particles. This is essentially the scheme of Sakurai, except that he writes the currents considering all the particles as elementary [see, however (110)]. While the introduction of both $B^{(B)}$ and $B^{(Y)}$ seems essential in a theory of this kind, the introduction of $B^{(T)}$ does not appear to us strictly necessary, at least if the Sakata model is used; although, according to Sakurai, who writes down the interactions regarding all the particles as elementary, the explicit introduction of $B^{(T)}$ not

¹⁸ Because of 4.4-3, B' does not represent a physical field and can be eliminated through a canonical transformation.

only is needed to destroy an excessive Λ - Σ symmetry (equivalent to the doublet symmetry), but also seems to be an important point in the comparison of theory to experiment. Finally, three remarks must be added. (a) If one considers the quadrilinear interaction terms formed by the mutual interactions of two currents, a vector current presumably allows the binding of an N - \bar{N} pair to form a pion. (b) Either in a compound model description or in one where each particle is elementary, the B bosons are strongly decaying particles provided their mass is sufficiently large ($m > 2m_\pi$ for $B^{(T)}$; $B^{(B)}$ and $B^{(V)}$ behave like Nambu's ρ). This may explain why these particles have not yet been observed; but, simultaneously, the question arises of understanding the meaning of a Lagrangian containing a field B , where B is a strongly unstable particle, or, in other words, a "resonance." (c) The analogy with electrodynamics is more superficial than it may appear at first sight; although the interactions are generated as indicated in 4.4-4, gauge invariance, in the sense which it has in electrodynamics, is lost, since the B meson, unlike the photon, has a mass.

In (106) a preliminary discussion is given of some possible experimental tests of the theory, using only the static solutions (analogous to the Coulomb static potential in electrodynamics). It seems inappropriate to enter into this discussion here, first because the theory has to be understood better (e.g., the question of the meaning of a Lagrangian in which a strongly unstable particle appears must be clarified), and second because at present no firm conclusion can be drawn. Sakurai's method (106, p. 17) for judging whether a theory is or is not correct does not seem to be entirely bias free! Again we must end these considerations without arriving at any conclusion, leaving for the future the question whether the above ideas are or are not correct and useful.

5. DO THE STRONG INTERACTIONS CONSERVE PARITY?

There have recently been a number of experiments to answer this question; the most accurate among these try to determine the parity impurity of nuclear levels. Three methods have been used: (a) $M1$ - $E1$ interference in nuclear γ transitions; (b) search for terms odd in $\cos \theta$ in β - γ angular correlations; (c) angular distribution of γ rays emitted after absorption of thermal polarized neutrons.

A discussion of these experiments was recently given by Blin-Stoyle (111); though these experiments should be continued, it appears from the results obtained so far that the parity impurities of nuclear levels are very small: $F \leq 10^{-4}$ or 10^{-5} , where F is the impurity mixture coefficient in the wave function. This means that at least the dominant part of the nucleon-nucleon potential, that caused by pion exchange, must conserve parity. It is more difficult to say anything about the portion of the potential arising from the exchange of strange particles. Results of Fubini & Walecka (112) on low-energy pion-nucleon scattering show that, in such a case, the effects of

an assumed parity nonconservation of the interactions involving strange particles are small.

It is natural to ask whether one can find reasons for conservation of parity in strong interactions (or at least in the pion-nucleon interactions) and not in weak ones. The question is, therefore, "Does there exist some invariance property, more powerful than parity conservation, which the strong interactions must obey and which implies as a consequence parity conservation for all (or part of) the strong interactions?"

A step in this direction (although, for reasons which we shall mention later, it is probably a false step) was made independently by many people: Feinberg (113), Morpurgo & Touschek (114), Gupta (115), Soloviev (116). It was noticed that once time-reversal invariance is postulated (and weak interactions, so far, do agree with such an invariance), the pion-nucleon interaction automatically conserves parity if one assumes that: (a) it is a Yukawa-like coupling not involving derivatives; (b) it is charge independent (charge symmetry is in fact sufficient).

The proof is simple: write a three-linear interaction between neutron, proton, and pion without derivatives; calling n , p , π respectively the neutron, proton, and pion fields, the most general hermitian interaction with no derivatives is:

$$(n^+\gamma_4(a + b\gamma_5)p)\pi^+ + (p^+\gamma_4(a^* - b^*\gamma_5)n)\pi$$

Invariance under charge symmetry implies that, under the substitution $n \leftrightarrow p$, $\pi^+ \leftrightarrow \pi^-$ the above interaction must remain invariant or, at most, change sign. Therefore, one must have

$$a = \pm a^* \quad b = \mp b^* \quad 5.1$$

where either the upper or the lower signs are simultaneously taken. But time-reversal invariance implies:

$$a = \pm a^* \quad b = \pm b^* \quad 5.2$$

which is not compatible with 5.1 unless a or b vanishes. Therefore, parity is conserved. The proof is completed on remarking that for the π^0 nucleon interaction a similar property holds (as, in general for any nonderivative interaction bilinear in the *same* field).

If we now go to the strong interactions of strange particles and no additional assumption is made, it is clear from the proof just sketched that no similar theorem can be proved. For instance, the most general nonderivative $\Lambda\bar{N}K$ interaction satisfying the requirement of charge independence is

$$K^+\Lambda^+\gamma_4(a + b\gamma_5)p + K_0^+\Lambda^+\gamma_4(a + b\gamma_5)n + Kp^+\gamma_4(a^* - b^*\gamma_5)\Lambda + K_0n^+\gamma_4(a^* - b^*\gamma_5)\Lambda \quad 5.3$$

Time-reversal invariance implies again, as in 5.2, that a and b have the same phase, which in this case can very well be true without either of them vanishing.

In this situation three possibilities are suggested. (a) The present way of explaining parity conservation has no sense; it gives the correct answer in the pion-nucleon case, but this is just a chance determined by the restrictive assumptions we have made. (b) Pion-nucleon interactions do conserve parity but strange-particle strong interactions do not conserve parity. (c) The scheme is reasonable, but some additional assumption has to be made (besides time reversal and charge independence or charge symmetry) so that parity conservation follows from "more powerful" symmetries for the strong interactions involving strange particles, too.

Of course nothing more can be said if possibility (a) is the correct one. On the other hand, if (b) is correct one question arises: how could one detect a possible nonconservation of parity of strong interactions of strange particles, and what is the present experimental evidence on this point?

In principle the experiments mentioned at the beginning of this section on the parity purity of nuclear levels can give an answer to this question; we have, however, already mentioned that it is not easy to be sure of the amount of parity impurity in nuclear levels induced by a possible nonconservation of parity in strong interactions involving strange particles. An alternative method is that of studying reactions in which strange particles are directly involved.

Consider, for instance, a reaction like $K^- + p \rightarrow Y + \pi$ or $\pi + p \rightarrow Y + K$ and assume that parity is not conserved in these processes. One may then have a nonvanishing component of the hyperon polarization in the plane of production when such plane is defined, or simply a longitudinal polarization of the hyperon when the production plane is not defined. The justification for these statements is to be found in the well-known fact that a parity-conserving interaction can only produce a polarization normal to the production plane. The above-mentioned polarization can of course be tested by examining the angular distribution of the decay products of the hyperon, since $\Sigma^+ \rightarrow p + \pi^0$ and $\Lambda \rightarrow p + \pi^-$ are good analyzers of polarization. The experiments performed so far at low energy [reactions $K^- + p \rightarrow \Sigma^+ + \pi^-$ (117) with K^- absorbed at rest; or $K^- + \text{He}^4$ interactions (118); or $\pi^- + p \rightarrow \Lambda^0 + K^0$ (119) with 1.12 Gev/c pions] do not provide any evidence for parity nonconservation. The errors are still large, however; for instance, in the first-mentioned reaction, calling θ the angle between the line of flight of the p from the Σ^+ decay in the rest system of the Σ^+ and the line of flight of the Σ^+ , the angular distribution is given in (117) as $1 + A \cos \theta$ with $A = 0.02 \pm 0.19$.

It must be added, in connection with the associated production reaction, that a compilation of cosmic ray and Cosmotron events produced in complex nuclei (120) appears to give a statistically significant nonzero value for the longitudinal polarization of the Λ 's. Although it is difficult to understand how one could obtain a nonzero average longitudinal polarization mix-

ing so many kinds of events and, moreover, the effect is apparently not confirmed by some recent production events in complex nuclei at low energy (121, 122), it still seems important to improve the statistics in bias-free conditions at high energy, in view of the recently reported results of the Dubna groups (123). The indications from these groups, who have studied Λ production in a Xe bubble chamber and in a propane bubble chamber, with pions of 2.8 and 7–8 Gev, respectively, are in favour of a forward-backward asymmetry, although the statistics are still limited (~ 120 and ~ 200 Λ , respectively).

The situation is obscure, and a high-energy experiment in hydrogen for the purpose of clarifying the question would be appropriate. We may add that if parity is not conserved it may well be that the longitudinal polarization of the produced hyperon is significant only at a high energy of the hyperon or, in other words, is a relativistic effect. Also, the study of the polarization of the hyperon and the subsequent asymmetries in its decay is not the only way to detect a possible parity nonconservation of strong interactions; another way is to study a reaction in flight with three or more final products, one of which is a strange particle, and to look for a possible pseudo-scalar formed with the three momenta. A possible candidate for this might be the reaction $K^- + p \rightarrow Y + \pi^+ + \pi^-$. Other examples which illustrate the above statement, in reactions involving antibaryons, have been given in (124).

We now briefly consider the remaining possibility (c) (p. 66), confining our attention to nonderivative Yukawa couplings; the question is which additional symmetry has to be imposed on the strong interactions of strange particles, besides time reversal and charge independence, in such a way that parity conservation follows automatically. Obviously there is no unique answer to this question. If the doublet symmetry were valid one might consider it the answer (125). In fact, the doublet symmetry (with some additional restriction) plus time-reversal invariance implies, for nonderivative interactions, parity conservation. Since we know that the doublet symmetry is incorrect, we have really no guiding principle to answer the above question, so that if the strong interactions of the strange particles do indeed conserve parity (and until the contrary is experimentally demonstrated this should be, at least, the simplest attitude), it must be concluded that our "explanation" of parity conservation fails. This failure would not be too surprising because it must be admitted that an explanation of so fundamental a property as parity conservation, based on an assumption as restrictive as the one that the interaction is nonderivative is not really appealing. This is what we had in mind when we used the expression "false step" at the beginning of this discussion.

We still believe that conservation of parity (if it is true) has to be explained (together, admittedly, with many other things) and that the idea

that it must follow from some more powerful symmetry property is fundamentally correct, even if such symmetry property probably is not that considered in the above "explanation."

Notice that according to the Fujii-Sakurai prescriptions for constructing the interactions, parity conservation is automatically ensured, as already noted in (105). This is an interesting aspect of Fujii's scheme; it is similar to the fact that for the electromagnetic interaction parity conservation follows automatically from gauge invariance and the assumption of minimality.

6. DYNAMIC PROBLEMS

The only two-body reactions involving strange particles at "low energy" on which a reasonable amount of information now exists are the photo-production reactions, associated production by pions, and K^-N , \bar{K}^-N reactions. We shall concentrate almost exclusively on the K^-N reactions which, in recent times, have been the most carefully studied experimentally (8a) and theoretically. Only a few comments will be added on the reactions of associated production by photons and pions (Sect. 6.9) and on the K^+N reactions (this section); the situation in hyperfragments has been reviewed rather recently (8c) and will not be considered in this survey.

First, we must clarify briefly why little progress has been made in going beyond a phenomenological treatment; generally this depends (using the language of perturbation theory) on the large number and variety of intermediate states which are near the energy shell and on the large number of interaction terms about which nothing is known. The situation, in this respect, is certainly more complicated than that existing in low-energy pion physics. The case of K^+N scattering will show this clearly.

The low-energy K^+N scattering reactions are among the simpler of all the strange-particle reactions: below the threshold for π production only one channel exists for K^+p scattering ($T=1$) and two ($T=0, 1$) for K^+n scattering; but in the absence of a guiding principle, the interaction terms to be considered are at least: $(N-\Lambda-K)$, $(N-\Sigma-K)$, $(\pi-\pi-K-\bar{K})$, $(K-\bar{K}-N-N)$ where the four coupling constants and the relative parities of Λ , Σ are all unknown. One can understand how a treatment of the four interactions based on perturbative or Tamm-Dancoff-like methods has led, so far, only to tentative conclusions.¹⁹ This being the situation for the "simple" K^+N reactions, it is

¹⁹ The following remarks are appropriate here:

(a) The experimental data on K^+N reactions are reasonably accurate only for the K^+p reaction: $\sigma(K^+p \rightarrow K^+p)$ is ~ 14 mb for $T_K \leq 100$ Mev (7a, 162) and increases slightly (59, 162), if at all (163), above this value up to an energy of 400 Mev (59). The angular distribution (center-of-mass system) is consistent with isotropy, an analysis in terms of S waves being sufficient only up to 400 Mev (163); the K^+p potential is repulsive. For the $K^+n \rightarrow K^+n$ and $K^+n \rightarrow K^0p$ reactions, the experimental information is, in our opinion, essentially qualitative since it has been obtained indirectly through complicated analysis of scattering in complex nuclei (7a, 164, 165).

clear why it is not profitable to go beyond a phenomenological treatment in examining the K^-N reactions. We shall now give such a phenomenological description which, by the way, contains some new points of interest in this problem.

6.1 K^-N reactions.—The list of "low-energy" K^-p reactions is given in Table III. The phenomenological treatment of these reactions has been developed in great detail by Jackson *et al.* (129), Dalitz (7b), Dalitz & Tuan (130, 131), Salam (8b), Matthews (9c), and Ross & Shaw (132). There is

TABLE III

REACTIONS AND BRANCHING RATIOS FROM K^-p ABSORPTION AT REST (8a)*

$K^-p \rightarrow \Sigma^-\pi^+$	$\rightarrow \Sigma^+\pi^-$	$\rightarrow \Sigma^0\pi^0$	$\rightarrow \Lambda^0\pi^0$	$\rightarrow \Lambda^0\pi^+\pi^-$
0.44 ± 0.01	0.20 ± 0.01	0.28 ± 0.03	0.08 ± 0.02	0.0013 ± 0.0006

* For K^-n reactions (from K^-D scattering and absorption) compare (89).

little doubt that this problem, together with K^+N scattering, will play for strange-particle physics the same leading role that low-energy pion-nucleon scattering has for pion physics.

The treatment of low-energy KN reactions by the authors mentioned above has three points of particular interest: (a) it may give indications

The main qualitative features are a very small exchange versus nonexchange scattering at low energy which increases rapidly with the energy (162, 164) and, apparently, the necessity of a strong P wave in the $T=0$ state. The K^+D experiments (163) in connection with an analysis like that of (166, 167) will soon, presumably, allow a more quantitative determination of the behaviour of the K^+n reactions.

(b) The conclusion contained in (126) that the $\bar{N}\Lambda K$ and $\bar{N}\Sigma K$ interactions, treated by the Tamm-Dancoff method using both pseudoscalar couplings, are not in themselves sufficient to explain the K^+N scattering may well be correct; but it is based in (126) on the use of experimental data [summarized in (7a)] which, if true, would violate at low energy the relation $d\sigma(K^+n \rightarrow K^+n) + d\sigma(K^+n \rightarrow K^0p) \geq \frac{1}{2}d\sigma(K^+p \rightarrow K^+p)$ that is implied by charge independence.

(c) If a pseudoscalar interaction is assumed both for $\bar{N}\Lambda K$ and $\bar{N}\Sigma K$ and if a lowest-order perturbation calculation is made (127), the K^+p potential proves to be repulsive, as it is. Also, the energy and angular dependence of the K^+ process prove to be essentially correct, although the slight increase in $\sigma(K^+p \rightarrow K^+p)$ with energy is not reproduced. The exchange cross section does not show, however, the increase with energy and the strong angular dependence which it is asserted to have. A possible way for explaining the data perturbatively, assuming opposite Σ, Λ parity and a $K\bar{K}\pi\pi$ interaction has been suggested by Barshay (128).

(d) If some credit is given to the perturbative calculation with pseudoscalar K and $P_{\Lambda\Sigma}=1$, the value $(f^2/4\pi) \cong 2$ is obtained by fitting the K^+p elastic cross section and assuming $f_{NAK}^2 = f_{N\Sigma K}^2 = f^2$. It is this value which was mentioned at p. 58.

about the range of the \bar{K} - N interaction;²⁰ (b) it can make some predictions on the Y - π scattering matrix elements; (c) it may yield information concerning the degree of validity of perturbation theory at low energy.

The experimental situation in regard to these reactions is summarized by Table III and by Figures 1 and 2. A large amount of experimental data of considerable precision exists (135) in the region of momenta p_L from 300 Mev/c to 1.15 Gev/c, but we shall consider only the low-energy region under $p_L \sim 200$ Mev/c. The following statement describes the present experimental situation in this region: (a) The total cross section for elastic scattering σ_{el} decreases in this region from ~ 90 mb for $p_L = 100$ Mev/c to ~ 55 mb for $p_L = 250$ Mev/c with ~ 15 per cent errors. The charge-exchange cross section σ_{ex} is 6 to 7 times smaller than the elastic cross section. (b) The angular distributions for elastic scattering and for Σ - π production are, apart from Coulomb effects, consistent with isotropy up to at least $p_L = 250$ Mev/c. (c) The ratio Σ^-/Σ^+ changes from a value ~ 2.2 at rest to a value 1 at $p_L = 175$ Mev/c. Both the numerator and the denominator decrease with increasing p_L ; the Σ^- and Σ^+ production cross sections are given separately in Figure 2.

The phenomenological treatment which follows is based on the assumption that in the low-energy region it is sufficient to consider S waves of the \bar{K} - N system; such treatment may be conducted at four levels of accuracy, indicated in what follows as approximations 1, 2, 3, 4:

- (1) One simply introduces two scattering lengths (129):

$$A_0 = a_0 + ib_0 \quad A_1 = a_1 + ib_1$$

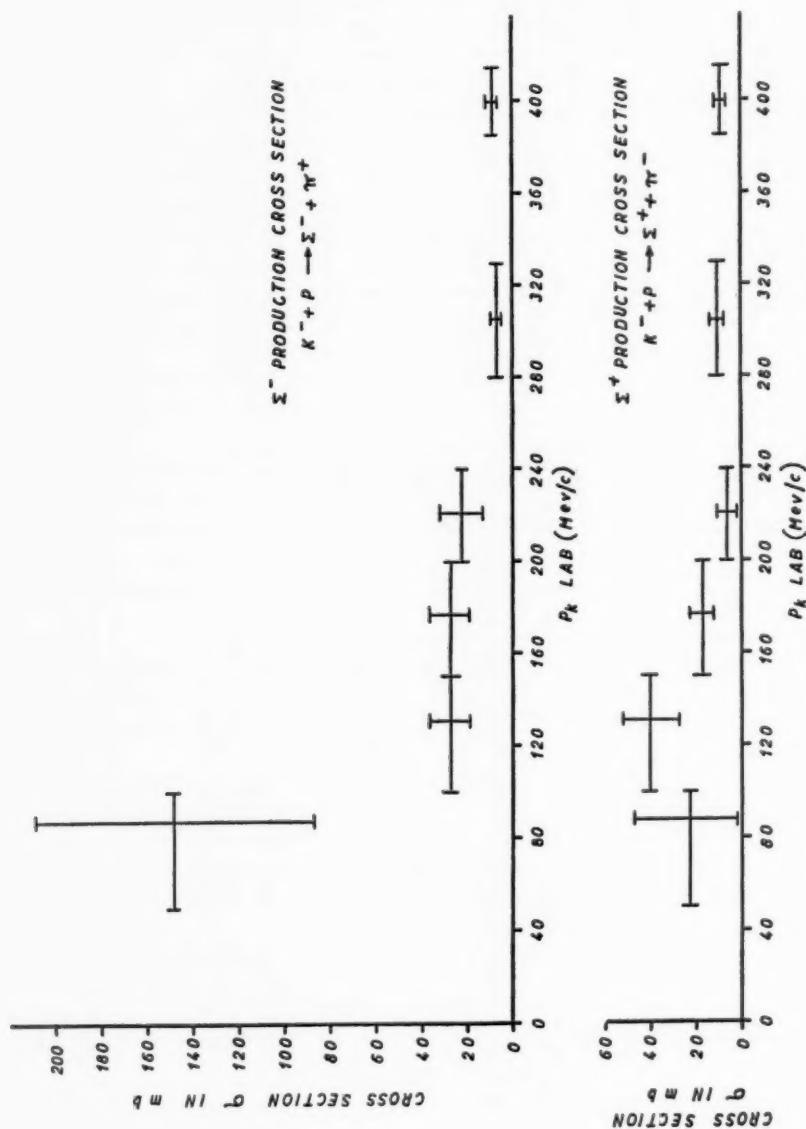
in the $T=0$ and $T=1$ states; one expresses the scattering, charge-exchange, and absorption cross sections in terms of A^0, A_1 ; the effects of the mass difference between K^0 and K^- and the Coulomb forces are neglected at this stage.

- (2) Proceeding along the same line as above, one takes into account the mass difference effect (130, 136).

- (3) The Coulomb forces are also included (131, 137).

- (4) The whole problem is reconsidered from the start (131) by using, instead of a scattering-length approximation, a reaction matrix description where more parameters are needed. It is then possible to have expressions for the absorption cross section and for the scattering cross sections in the various hyperon channels (138).

²⁰ Ferrari, Frye & Pusterla (133) have investigated the effect of a K - \bar{K} - π - π matrix element on low-energy \bar{K} - N reactions and, in particular, whether such a matrix element is compatible with the assumption of constant scattering length. Note that the two-pion exchange determines the longest-range part of the \bar{K} - N "potential." With the assumptions made in (133) in the estimate of the $(K$ - \bar{K} - π - $\pi)$ matrix element, the effective range term proves to be not negligible, but little justification yet exists for such an estimate which, according to calculations of Lee (134), appears to be in contrast with K^+ - p scattering.

FIG. 2. Σ^- and Σ^+ production cross sections from absorption of K^- (8a).

In the following we first give the formulas for σ_{so} and σ_{ex} , $\sigma_{abs}^{(0)}$, $\sigma_{abs}^{(1)}$ in approximation 2, next state their relation with the simple approximation 1 and briefly describe the problem of determining the scattering lengths from the experimental data. We next describe the predicted behaviour, as a function of energy of the quantities of interest and the methods that can be used to discriminate between the several sets of amplitudes which, at the present moment, are all compatible with the rough existing experimental data. We finally consider the more complete treatment, using the reaction matrix (approximation 4).

6.2 *The scattering-length approximation.*—As shown by Dalitz & Tuan (130) a scattering-length approximation is equivalent to a boundary condition on the logarithmic derivative of the radial S -wave function $u_T(r)$ ($T=0$, 1=isotopic spin index) for K^- -nucleon scattering: $[u_T'(r)/u_T(r)]_{r=0} = A_T^{-1}$.

From this boundary condition the cross sections are easily obtained in the approximation 2:

$$\sigma_{el} = \pi \left| \frac{A_1(1 - ik'A_0) + A_0(1 - ik'A_1)}{\Delta} \right|^2 \quad 6.2-1$$

$$\sigma_{ex} = \pi \frac{k'}{k} \left| \frac{A_1 - A_0}{\Delta} \right|^2$$

$$\sigma_{abs}^{(0)} = \frac{4\pi}{k} b_0 \left| \frac{1 - ik'A_1}{\Delta} \right|^2, \quad \sigma_{abs}^{(1)} = \frac{4\pi}{k} b_1 \left| \frac{1 - ik'A_0}{\Delta} \right|^2 \quad 6.2-2$$

where:

$$\Delta = 1 - \frac{1}{2}i(k + k')(A_1 - A_0) - kk'A_1A_0$$

$k = \sqrt{2\mu T_K}$ = wave number of the K^- in the center-of-mass system, and $k' = \sqrt{k^2 - k_0^2}$ or $i\sqrt{|k^2 - k_0^2|}$, respectively, for $k > k_0$ or $k < k_0$, k_0 being the wave number of the K^- at the (center-of-mass) \bar{K}_0 threshold.

The formulas in approximation 1 are immediately obtained, using $k' = k$, that is, $k_0 = 0$. Then if we also write:

$$k \cot \delta_T = A_T^{-1} \quad 6.2-3$$

thus defining (in the scattering-length approximation) a complex phase shift δ_T , it is easy to demonstrate that the formulas 6.2-1 and 6.2-2 reduce to the usual (129)

$$\sigma_{so} = \frac{\pi}{k^2} \left| \frac{1}{2}(1 - \exp 2i\delta_0) + \frac{1}{2}(1 - \exp 2i\delta_1) \right|^2 \quad 6.2-4$$

$$\sigma_{ex} = \frac{\pi}{k^2} \left| \frac{1}{2}(\exp 2i\delta_0 - \exp 2i\delta_1) \right|^2 \quad 6.2-5$$

and

$$\sigma_{abs}^{(T)} = \frac{\pi}{k^2} (1 - |\exp 2i\delta_T|^2) \quad 6.2-6$$

6.3 *The determination of the scattering lengths* (7b, 130).—Assuming we have the values of σ_{sc} , σ_{ex} , and $\sigma_{abs}^{(T)}$ ($T=0, 1$) at one energy, we can derive from the four equations 6.2-1, 6.2-2 values for A_0 , A_1 , that is, for (a_0, b_0) (a_1, b_1).

This would indeed be easy in approximation 1. In fact, writing $\delta T = \alpha T + i\beta T$, Equations 6.2-6 univocally determine β_0, β_1 ; and using next Equations 6.2-4 and 6.2-5 we can determine α_0 and α_1 . Four different pairs (α_0, α_1) are obtained in this way; two of them differ from the other two only in a simultaneous change in sign of α_0 and α_1 . Corresponding to these four solutions for δ_0, δ_1 , we obtain, using 6.2-3, four solutions for A_0, A_1 , two of which are obtained from the other two, changing simultaneously the sign of a_0, a_1 . As we shall see (Table IV), two of the solutions obtained using present data have a positive sign both for a_0 and a_1 ; they are called the $(a+)$ and $(b+)$ solutions. The solutions obtained by changing the sign of a_0, a_1 in the previous ones are respectively called $(a-)$ and $(b-)$.

The determination of A_0, A_1 , when formulas 6.2-1 and 6.2-2 valid in approximation 2 are used and when it is again assumed that the four cross sections $\sigma_{sc}, \sigma_{ex}, \sigma_{abs}^{(T)}$ are experimentally known at some energy $\gg k_0^2/2\mu$, is similar to that discussed above in approximation 1. Indeed, if $k \gg k_0$ the formulas of approximation 2 tend toward those of approximation 1. In addition, for $k > k_0$ the formulas possess the reflection property $A_0 \rightleftharpoons -A_0^*$, $A_1 \rightleftharpoons -A_1^*$ corresponding to the invariance under reversal of the sign of the real part of A_0, A_1 discussed above.

The determination of A_0, A_1 becomes, however, much more complicated

TABLE IV
DALITZ & TUAN VALUES OF THE \bar{K} -N SCATTERING AMPLITUDES*
(in 10^{-13} cm)

Solution α (130)	Solution β (131)
$(a+)A_0 = 0.20 + 0.76i$ $A_1 = 1.62 + 0.38i$	$A_0 = 0.2 + 0.8i$ $A_1 = 1.6 + 0.4i$
$(b+)A_0 = 1.88 + 0.82i$ $A_1 = 0.40 + 0.41i$	$A_0 = 1.6 + 1.6i$ $A_1 = 0.7 + 0.22i$
$(a-)A_0 = -0.20 + 0.76i$ $A_1 = -1.62 + 0.38i$	$A_0 = -0.3 + 1.6i$ $A_1 = -1.0 + 0.18i$
$(b-)A_0 = -1.88 + 0.82i$ $A_1 = -0.40 + 0.41i$	$A_0 = -1.8 + 0.6i$ $A_1 = -0.33 + 0.5i$

* *Note added in proof:* The more exact analysis mentioned in the text has been completed (R. H. Dalitz, *Revs. Mod. Phys.*, to be published) but is not available to the author. Corrected expressions for the $(a+)$, $(a-)$ sets, as reported by King *et al.* in *Phys. Rev. Letters*, **6**, 500 (1961), are:

$$\begin{aligned}
 (a+) & \left[A_0 = 0.05(\pm 0.2) + i1.10 \begin{pmatrix} +0.2 \\ -0.3 \end{pmatrix}; A_1 = 1.45(\pm 0.2) + i0.35 \begin{pmatrix} +0.09 \\ -0.07 \end{pmatrix} \right] \\
 (a-) & \left[A_0 \times -0.75 \begin{pmatrix} +0.35 \\ -0.45 \end{pmatrix} + i2.00(\pm 0.35); A_1 = -0.85(\pm 0.15) + i0.21(\pm 0.04) \right]
 \end{aligned}$$

in the present experimental situation; in fact, we have no knowledge of $\sigma_{\text{abs}}^{(0)}$, $\sigma_{\text{abs}}^{(1)}$ because

$$\begin{aligned}\sigma_{\text{abs}}^{(1)} &= 2\sigma(\Lambda) + 2\sigma(\Sigma^+) + 2\sigma(\Sigma^-) - 4\sigma(\Sigma^0) \\ \sigma_{\text{abs}}^{(0)} &= 6\sigma(\Sigma^0)\end{aligned}$$

and $\sigma(\Lambda^0)$, $\sigma(\Sigma^0)$ are not experimentally known.

All one can do (130) is to replace the two Equations 6.2-2 with two other relations connecting A_0 , A_1 to experimentally known quantities, by using some assumptions and information on the branching ratios from K^- absorption at rest (Table III). The first relation is the following:

$$\sigma(\Sigma^+) + \sigma(\Sigma^-) = \frac{1}{2}\sigma_{\text{abs}}^{(0)} + \frac{1}{2}(1 - \epsilon)\sigma_{\text{abs}}^{(1)} \quad 6.3-1$$

Here ϵ is the fraction of Λ hyperon production in the $T=1$ state: $\epsilon = 2\sigma(\Lambda)/\sigma_{\text{abs}}^{(1)}$; the assumption is made that ϵ is energy independent and, therefore, equal to its known value for K^- absorption at rest. The second usable relation is:

$$(\sigma_{\text{abs}}^{(0)}/\sigma_{\text{abs}}^{(1)})_{K^- \text{ at rest}} = R \quad 6.3-2$$

where R is again experimentally known. It should be noted that both 6.3-1 and 6.3-2 imply the assumption that the K^- absorption at rest takes place from S states. This is probably valid in view of the arguments by Day, Snow & Sucher (45); however, it would be preferable to have values, at, say, $p_L = 175$ Mev/c for $\sigma(\Sigma^0)$ and $\sigma(\Lambda^0)$ also or at least for their sum.

The use of 6.3-2 makes the determination of (A_0, A_1) more complicated; in fact, as formulas 6.2-6 show, at $k < k_0$ both $\sigma_{\text{abs}}^{(0)}$ and $\sigma_{\text{abs}}^{(1)}$ and their ratio lose the $A_0 \rightleftharpoons -A_0^*$, $A_1 \rightleftharpoons -A_1^*$ symmetry so that the four solutions for A_0, A_1 obtained in approximation 2 by the use of 6.3-2 are all unrelated.

Two actual determinations of A_0, A_1 have been made so far; both are based on the values of σ_{el} , σ_{ex} , $\sigma(\Sigma^+) + \sigma(\Sigma^-)$ at $p_L = 175$ Mev/c and on Equation 6.3-2 at rest. The values assumed for the above cross sections are those given in Figure 1b (8a). The values taken for R and for ϵ are, in one calculation (to be called α), based on approximation 1: $R=2$, $\epsilon=0.2$; in the other (to be called β), based on approximation 2: $R=4$, $\epsilon=0.2$. The values of A_0, A_1 for the four solutions are reported in each case in Table IV.

The best values for R and ϵ are $R \sim 6$, $\epsilon \sim 0.5$, so that a third determination of A_0, A_1 , which also takes into account the errors, would be needed. Apparently such a calculation is in progress (131, 139), but since no results are available now we shall simply report the results based on the sets of A_0, A_1 as determined above.

It is expected that most of the qualitative features of the conclusions to be reported below will continue to be valid in the more exact solution, but before a more quantitative investigation can be attempted it appears essential to reduce the experimental errors and obtain sufficient information to determine A_0, A_1 from data at one energy.

We end this section with a comment on the inclusion of the Coulomb

force (approximation 3). Although the formulas for the various cross sections are, of course, affected by the Coulomb force, the modifications at $p_L = 175$ Mev/c stay within present experimental errors (137). Also, the expression of R (6.3-2) in terms of A_0, A_1 is not affected by the Coulomb force so that, as far as the determination of A_0, A_1 is concerned, no error is made, with the present data, in neglecting the Coulomb force. It is essential, however, to make use of the Coulomb corrected formulas to compute the angular elastic distribution as well as the total elastic cross section at $p_L \leq 120$ Mev/c.

6.4 Comparison of the scattering-length approximation with experiment.—

The question now is which among the four solutions A_0, A_1 is the correct one. While in the ideal situation of no experimental errors this question could be answered immediately and, at the same time, the correctness of the scattering-length approximation might be checked, this is not so easy with the present data.

Let us examine some points in detail:

(a) The Coulomb nuclear interference in K^-p elastic scattering might allow a choice between the plus and minus solutions. The plus solutions imply positive interference, the minus solutions imply negative interference; these interferences change the angular distribution near the forward direction and increase or decrease the total elastic cross section (compare Figure 1b). Their effects are important for $p_L \leq 100$ Mev/c. The angular distribution data did initially appear to be in favour of the plus solutions, but it was later realized that the errors are still too large to allow a definite conclusion (8a).

Similarly, the behaviour of the total elastic K^-p cross section as a function of p_L for $p_L \leq 100$ Mev/c might permit a choice among the four solutions if reliable data in the low-momentum region were available. This is shown in Figure 1a. Figure 1b shows that if the preliminary evidence of a decrease in the elastic K^-p cross section at $p_L \leq 100$ Mev/c, based on emulsion work (7a, 140a), is confirmed [but the most recent emulsions results (140b), also included in Figure 1b, apparently do not provide such confirmation], the (a-) solution would be preferable to the other solutions. It can be seen that the cross sections of Figure 1a would all increase with decreasing p_L if the Coulomb force effect were not included. It is this last effect which, as shown in (137), substantially reduces σ_{el} at low momenta for the minus solutions and thus might produce agreement with experiment for the (a-) solution.

(b) The charge-exchange cross section does not make it possible to distinguish between the various sets of amplitudes; its energy dependence is in qualitative agreement with the predictions for all the sets.

(c) An interesting difference in the behaviour of π^-Y scattering is predicted with use of the various solutions (141). To see this clearly, however, a generalization of the simple scattering-length approximation used so far

is needed: the reaction matrix treatment (131) (approximation 4). This we shall consider next.

6.5 *The reaction matrix treatment: π -Y scattering and Σ^-/Σ^+ ratio.*—Above the energy $E_t = M_p + m_K$ two S matrices are necessary for a complete description of the phenomena, one for the $T=0$ and the other for the $T=1$ state. The first is a two-by-two matrix (states $\bar{K}N$, $\Sigma\pi$) with matrix elements S_{KK} , S_{KY} , S_{YY} ; the second is a three-by-three matrix (states $\bar{K}N$, $\Sigma\pi$, $\Lambda\pi$). Here we consider negative P_{KYN} so that only S waves intervene in all channels; we also fix our attention for simplicity on the $T=0$ states. If $E < E_t$ this $T=0$ matrix will consist of the single element S_{YY} which corresponds to π -Y scattering. The following is designed to show that S_{YY} for $E < E_t$ is related to the parameters characterizing the S matrix ($T=0$) for $E > E_t$. These parameters, if the following approximation is valid, are simply A_0 (the scattering length for the $T=0$ state of the previous section) plus an additional parameter which can be taken to be the π -Y($T=0$) phase shift at $E = E_t$. Some important features of the Y - π scattering at $E < E_t$ may be predicted with the knowledge of A_0 only.

The approximation referred to above will now be explained: introduce, instead of the S matrix, the reaction matrix K defined by the well-known equation:

$$S = \frac{1 + i\pi\delta(E - H_0)K}{1 - i\pi\delta(E - H_0)K} \quad 6.5-1$$

If time reversal is valid, K is a real symmetric matrix. The assumption now is that (for S waves) the matrix elements of K are energy independent. With this approximation, which is the generalization of the scattering-length approximation of the previous section, the result described at the beginning of this section can be proved as follows: call α , β , and γ the (energy-independent) matrix elements:

$$\alpha = \langle \bar{K}N | K | \bar{K}N \rangle, \quad \beta = \langle \bar{K}N | K | \pi Y \rangle, \quad \gamma = \langle Y\pi | K | Y\pi \rangle$$

With some algebraic calculations it then follows that, above E_t ,

$$S_{KK} = \frac{1 + ikA}{1 - ikA} \quad 6.5-2$$

where

$$A \equiv a + ib = \alpha + i\beta^2(M_\Sigma/E)q[1 - i(M_\Sigma/E)q\gamma]^{-1} \quad 6.5-3$$

Here q is the center-of-mass momentum of the π - Σ system corresponding to total (center-of-mass) energy E . Notice that A (and of course a , b) are functions of q ; but since q/E is a slowly varying function of E , the quantity A is a slowly varying function of E , and the scattering-length approximation of the previous section essentially corresponds, in this description, to the assumption of constant α , β , γ . We may identify the A_0 of the previous section with the A as given by 6.5-3, calculated, e.g., at $E = E_t$.

Now, using 6.5-1 again, one can similarly show that above E_t

$$S_{YY} = \frac{1 - ikA^*}{1 - ikA} \exp 2i\lambda \quad 6.5-4$$

where

$$\tan \lambda = (M_{\Sigma q}/E)\gamma \quad 6.5-5$$

The statement given at the beginning of this section, concerning the knowledge of S_{YY} below E_t from the parameters above E_t , follows immediately from 6.5-4 by the simple substitution of k with $+ik = i\sqrt{2\mu}|E - E_t|$ in 6.5-4. We obtain

$$S_{YY} = \frac{1 + kA^*}{1 + kA} \exp 2i\lambda \quad 6.5-6$$

Note that

$$|S_{YY}(E < E_t)|^2 = 1$$

The result 6.5-6 was obtained by Dalitz & Tuan (141). It is, of course, valid only not too far from E_t , because otherwise the assumption of constant α , β , γ breaks down.

We can now write the $Y\pi \rightarrow Y\pi$ cross section (below but not too far from E_t) as:²¹

$$\sigma_{YY}(E < E_t) = 4 \frac{\pi}{q^2} \frac{(-bk \cos \lambda + (1 + ka) \sin \lambda)^2}{(1 + ka)^2 + k^2 b^2} \quad 6.5-7$$

One can check that for $b \neq 0$ the above cross section reaches a maximum value, corresponding to a resonance, for

$$k_r = - \frac{1}{a + b \tan \lambda}$$

Now it can always happen, as this formula shows, that λ or equivalently γ has, accidentally, so to speak, a value such that a resonance exists for some preassigned k_r . This can not be excluded, but is not particularly interesting. The interesting conclusion is that independently of the value of γ , a resonance must exist²¹ in the interval from $m_\pi + m_Y$ to E_t if a is negative and sufficiently large (so that $k_r > 0$ but $k_r^2/2\mu < E_t - m_Y - m_\pi$ and not too far from E_t).²²

We recall now that if the $(b-)$ solution were the correct one, a_0 (as given in Table IV) is negative and rather large, so that in such a case a resonance in the $T=0$ state should presumably exist below E_t .

²¹ Notice that according to 6.5-3 and 6.5-5, b and $\sin \lambda$ go to zero together with q as of course they must do.

²² The physical argument underlying these Dalitz & Tuan resonances is (131) that if the real part of the scattering length is negative and large for $T=0$ or for $T=1$, a bound state of the $\bar{K}-N$ system in the corresponding T state can be expected. The existence of a coupling with the $Y-\pi$ system induces a more or less fast decay of such a state, which in the $Y-\pi$ scattering manifests itself as a (more or less broad) resonance.

So far we have considered the $T=0$ state for simplicity; but similar conclusions are valid for the $T=1$ state, though in this case the situation is much more complicated, because instead of the single indeterminate parameter γ (or λ), three unknown parameters appear in the formulas. One can nevertheless predict a resonance below E_t in this case also, provided that a_1 is negative and sufficiently large.²³ This happens to be true for the $(a-)$ solutions; so that, if this prediction is correct, a resonance should be expected in a $J=\frac{1}{2}$ state at some energy below E_t . Whether or not this is the π - Λ resonance recently discovered (compare Sect. 6.7) is a question which cannot yet be answered, because too little is known on such π - Λ resonance. Certainly, if the pion-lambda resonance proves to have $J=\frac{1}{2}$ and if more accurate future data confirm the large value of a_1 in the $(a-)$ solution, the minus solution will be more clearly indicated.

Summarizing, we can say that, presently, the energy dependence of the K^-p scattering cross section as well as the π - Λ resonance provides weak indications in favour of the $(a-)$ solution.

The Coulomb interference in the angular distribution (8a) provides a weak indication for the $(a+)$ or $(b+)$ solution. An additional argument for the $(a+)$ [or $(b-)$] solution which we cannot explain in detail here might be provided by the energy behaviour of the Σ^-/Σ^+ ratio if the points at $p_L \sim 90$ Mev/c in Figure 2 are believed. In fact, if the $(a+)$ or $(b-)$ solutions are correct, the strong energy dependence of $N(\Sigma^-)/N(\Sigma^+)$ might be explained (131) as a cusp effect (at the K^0 threshold).

Finally, the $\bar{K}-n$ scattering (which takes place entirely in a $T=1$ state) obviously might provide independent evidence for the determination of the amplitudes. In particular, the elastic cross section for an (a) -type solution is expected to be larger than that for the (b) -type solutions. Calculations (142 a, b) for K^-D elastic plus inelastic (but not absorptive) scattering at $p_L=200$ Mev/c appear to rule out the $(a+)$ solution if the preliminary value of $\sigma=100 \pm 25$ mb for K^-D nonabsorptive scattering is accepted. Again, the experimental evidence is only preliminary.

6.6 *The validity of perturbation theory in K^-p absorption processes.*—To complete this section we reproduce an observation of Dalitz & Tuan (131) which shows the nonvalidity of perturbation theory for $K-N-Y$ interactions, in this kind of phenomena at least, using the present solutions A_0 , A_1 . The observation is the following. One can show, using the K matrix formalism in a way similar to that by which 6.5-2 and 6.5-4 have been deduced, that the $\bar{K}N \rightarrow Y\pi$ transition matrix element T_{KY} in the $T=0$ state is given by:

$$q^{1/2}k^{-1/2}T_{KY} = \exp(i\lambda) \cdot b^{1/2}(1 - iak + bk)^{-1}$$

²³ This is true at least for some choice of the above three parameters; whether it is true for any choice is not clear from the treatment in (131). *Note added in proof:* Compare, however, R. Dalitz, *Phys. Rev. Letters*, **6**, 239 (1961). Also, if $P_{\Lambda\Sigma} = -1$ the possibility of S and P waves must be considered.

Call f the K - N - Y coupling constant; since the leading term of b in an expansion in f is of order f^2 , one is entitled to write, if a perturbative expansion in f is valid,

$$q^{1/2}k^{-1/2}T_{KY} = \exp(i\lambda)b^{1/2}(1 + iak - bk) + \dots \quad 6.6-1$$

Dalitz & Tuan observe that the term $b^{3/2}k$ for $p_L = 175$ Mev/c has, for any of the previously discussed solutions, a value not less than 0.4 and cannot be cancelled by any other terms of order f^3 because, in the expansion 6.6-1, it gives rise to the only term of order f^3 which is real and proportional to k . Therefore, a perturbative expansion of this T -matrix element is certainly not a fast convergent one.

THE Y - π (AND K - π) "RESONANCE"

6.7 A maximum in the Y - π cross section has been recently discovered (143a, b), through study of reactions like

$$K^- + p \rightarrow Y + \pi^+ + \pi^- \quad 6.7-1$$

The preliminary data refer to two momenta of the K meson, $p_L = 1.15$ Gev/c (143a) and $p_L = 760$ Mev/c (143b). Although the available data are still preliminary and things will rapidly change, it seems appropriate to give a description of this phenomenon here.^{22a} It appears that in the larger fraction of the events (130 over 170 at 1.15 Gev/c) the Y produced in 6.7-1 is a Λ .

For each of these events the kinetic energy of the π^+ and π^- can be inserted in a two-dimensional diagram; this should be uniformly populated inside a certain region if the phase space alone dominates the reaction (and if only S waves intervene in the final state). This plot is given in Figure 3. In addition, the separate T_{π^+} and T_{π^-} distributions are projected. The existence of a maximum at the energy $T_{\pi} = 280$ Mev is evident both in the π^+ and in the π^- distribution (as far as the first maximum in the π^- distribution is concerned, this is produced by the very existence of the π^+ maximum). The two maxima at T_{π^+} and $T_{\pi^-} = 280$ Mev are interpreted in (143a) as showing that a considerable fraction of the reactions 6-7.1 goes through

$$K^- + p \rightarrow Y^{*\pm} + \pi^\mp \quad 6.7-2$$

with a subsequent decay of the $Y^{*\pm}$: $Y^{*\pm} \rightarrow \Lambda^0 + \pi^\pm$. The resulting average mass of the Y^* is 1380 Mev; its (Breit-Wigner) half-width is 32 Mev.

The difference in height of the plus and minus peaks is interpreted as corresponding to different amplitudes for the two reactions 6.7-2; since the Y^* has $T=1$ and the initial state is a coherent superposition of $T=0$ and $T=1$ states, this is entirely possible.

Two important questions must be answered by the experiments:

(a) Which is the branching ratio for decay of the Y^* into $\Lambda + \pi$ and

^{22a} Note added in proof: The situation in March 1961 is described by M. Alston & M. Ferroluzzi (UCRL-9587) and Berge *et al.*, *Phys. Rev. Letters*, **6**, 557 (1961).

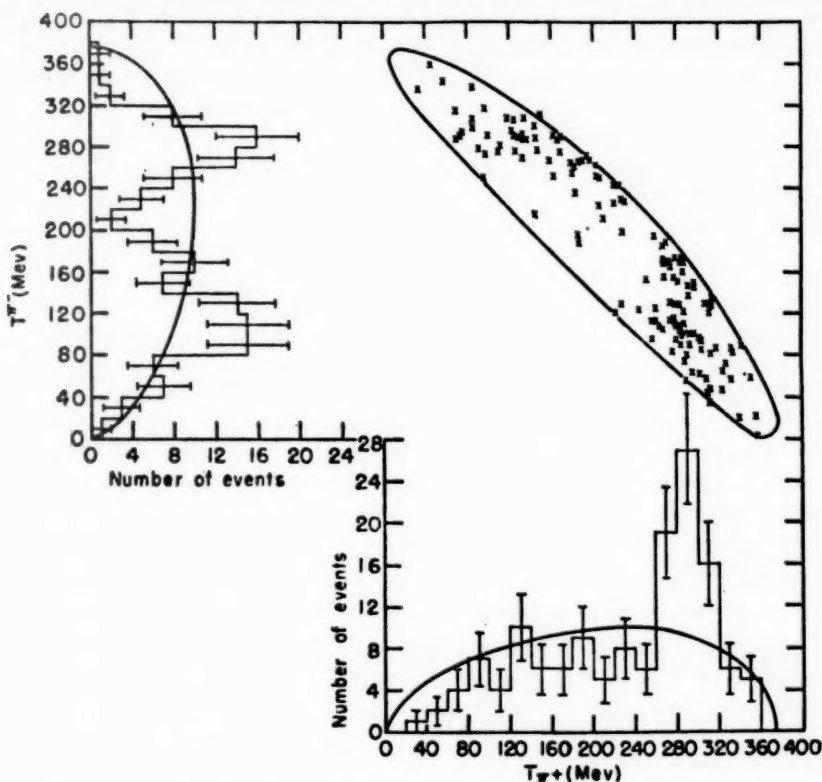


FIG. 3. The situation on the π - Y resonance: corresponding to each observed event with given T_{π^+} and T_{π^-} (the kinetic energy of π^+ and π^-), a point is plotted in the central diagram; the diagram is then projected on the T_{π^+} and T_{π^-} axes (143a).

$\Sigma^0 + \pi$; note that the figures given before ($\sim 130 \Lambda$ over 170 events of kind 6.7-1) do not answer this question because it is not known how many Σ^0 have been produced through the resonance. The above figures are only an indication of a small Σ^0 -to- Λ^0 ratio. We may remark that the product pR , where p is the center-of-mass momentum and R is the interaction radius, is $pR \sim 0.6$ if a Σ^0 is emitted and if the value m_{π}^{-1} is assumed for R , so that, if it could be established that the $Y^* \rightarrow \Lambda + \pi$ goes in an $S_{1/2}$ channel, a small branching ratio Λ -to- Σ^0 decay would be an indication, but certainly not a proof, of opposite Σ , Λ parities.

(b) The question of the spin Y^* is a fundamental one. It can be investigated with the methods discussed in detail in (1; cf. 144), namely, the Adair method, and the search for anisotropies in the standard angular distributions.

The data, so far, are too preliminary to be worth reporting. If the spin

proves to be $\frac{1}{2}$, the chance that we are dealing with the Dalitz & Tuan phenomenon increases considerably. Note that the Y^* has a mass ~ 50 Mev below the $M_p + m_K$ rest mass. If, on the other hand, the spin is $\frac{3}{2}$ (and $P_{\Lambda\Sigma} = 1$), this would be a point in favour of the identification of the Y^* with the resonance for the $Y-\pi$ system indicated by global-like symmetry arguments, as summarized in the next section. [Recently, evidence for a $K-\pi$ resonance K^{*-} at a total, center-of-mass energy of 885 Mev has been presented (145) through study of the reaction

$$K^- + p \rightarrow \bar{K}^0 + p + \pi^-$$

with incident K^- of 1.15 Gev/c and using methods of analysis similar to those described above in connection with the Y^* resonance. From the branching ratio in decay ($K^- + \pi^0$ versus $K^0 + \pi^-$), a value $\frac{1}{2}$ for the isotopic spin of the K^* is favoured, but the evidence is still preliminary; there is now little evidence on the spin. The $K-\pi$ resonance, because of its large mass, should not be important for low-energy $K-N$ scattering, but may soon contribute to an understanding of the $K-\bar{K}-\pi-\pi$ interaction. The results of (34), showing a cross section for $K-\bar{K}$ production larger than that for $Y-K$ production with high-energy 7 to 8 Gev π^- on propane, should also be taken into account in such an analysis.]

GLOBAL SYMMETRY AND Y^* RESONANCE

6.8 Which are the detailed predictions of global symmetry for $\pi-Y$ scattering in p states? The expression global symmetry is used here in a much looser sense than that used in Section 4.2. Several authors (85, 146a, b, 147a, b, c) have considered the following question: which are the predictions for $\pi-Y$ scattering of the fixed source model or of some more refined but essentially equivalent model, all these models being treated in analogy with what is normally done for P -wave pion-nucleon scattering? The assumptions are made (a) that both Λ and Σ interact with the pion only in P states ($P_{\Lambda\Sigma} = 1$) and (b) that diagrams involving K intermediate states can be entirely neglected in calculating $\pi-Y$ scattering. This is certainly untrue for S states, as the phenomenological treatment shows; it may (or may not) be reasonable for P states. While the Dalitz & Tuan resonance is a general phenomenon, the conclusions drawn in this section will be derived with the use of a model and of many assumptions. Also, the number of parameters is rather large so that the results are certainly too flexible; however, a typical conclusion of this kind of attempt will be briefly described here, following the treatment of Amati, Stanghellini & Vitale (146).

Define g_Λ and g_Σ through the matrix elements of the interaction for emission of a physical pion with momentum q in a transition between the physical Λ and Σ states, as specified below

$$\langle \Lambda | V_{qk} | \Sigma_k \rangle = i g_\Lambda \sqrt{\frac{2\pi}{\omega_q}} u(q) \delta \cdot q$$

$$\langle \Sigma_i | V_{qjk} | \Sigma_j \rangle = g_\Sigma \sqrt{\frac{2\pi}{\omega_q}} u(q) \delta \cdot q e_{ijk}$$

where $u(q)$ is a cutoff function; we next put $\Delta = M_\Sigma - M_\Lambda$ and

$$I(\omega) = \frac{1}{3\pi} \int_{m_\pi} d\omega' \frac{q'^2 u^2(q')}{\omega'^2(\omega' - \omega)}$$

Here and in the following, ω is defined as $\omega = E - m_\Lambda$, E being the total energy of the state. The matrix elements of the K matrix in the $T=0, 1, 2$ states with $J=\frac{1}{2}$ and $J=\frac{3}{2}$, respectively, may be calculated using the method of Bosco *et al.* (146c) and have the form $N_{\Sigma}^T/D_{\Sigma}^T$; the denominators D_s^T are reported below as given in (146a):²⁴

$$D_s^0 = 1 + 2(2g_\Sigma^2 - g_\Lambda^2)I\omega + 4(g_\Lambda^2 - g_\Sigma^2)I\Delta \quad 6.8-1$$

$$D_s^1 = [1 - 2(g_\Sigma^2 - g_\Lambda^2)I\omega + (2g_\Sigma^2 - 4g_\Lambda^2)I\Delta](1 - 2g_\Lambda^2I\omega - 2g_\Lambda^2I\Delta) - 8g_\Sigma^2g_\Lambda^2\omega^2I^2$$

$$D_s^2 = 1 - 2(g_\Lambda^2 + g_\Sigma^2)I\omega + 2(2g_\Lambda^2 + g_\Sigma^2)I\Delta$$

The resonance energies are simply the zeros of the above D_{Σ}^T . The existence and position of such zeros may be examined as a function of g_Λ , g_Σ or, equivalently, of the two parameters

$$\delta = \frac{g_\Lambda^2 - g_\Sigma^2}{g_\Lambda^2 + g_\Sigma^2} \quad \Omega = \frac{1}{2} \frac{1}{g_\Sigma^2 + g_\Lambda^2} \quad 6.8-2$$

The energy dependence of $I(\omega)$ is neglected. If $g_\Lambda^2 \sim g_\Sigma^2$ or, more precisely, if $\delta < 0.3$, only the $T=1$ and $T=2$ states with $J=\frac{3}{2}$ have resonances, there being no resonance either in the $T=0$, $J=\frac{3}{2}$ state or in the $J=\frac{1}{2}$ states. The $T=1$ and $T=2$ resonance energies may be written, as is clear from 6.8-1 and 6.8-2,

$$E_{\text{res}}^1 = m_\Lambda + \omega_{\text{res}}^1 = \Omega + m_\Lambda - \frac{1}{2}\Delta - \frac{1}{2}\delta\Delta \quad 6.8-3$$

$$E_{\text{res}}^2 = m_\Lambda + \omega_{\text{res}}^2 = \Omega + m_\Lambda + \frac{1}{2}\Delta + \frac{1}{2}\delta\Delta$$

Assuming that $\Omega = 290$ Mev as in the pion-nucleon case, one obtains for $\delta=0$ $E_{\text{res}}^1 = 1365$ Mev in reasonable agreement with the data. It does not seem appropriate to insist on the meaning of this coincidence; more interesting is a definite prediction which can be read from 6.8-3: if the resonance which has been found corresponds to E_{res}^1 , a resonance in a $T=2$ state must exist at an energy $E_{\text{res}}^1 + 2\Delta[1 + (2\delta/3)]$. Other predictions of the model are the widths of the resonances and the branching ratio for decay in Λ^0 or Σ^0 ; this last quantity depends sensitively on δ . The data are, however, still too preliminary to allow a discussion. We only add that if the condition $\delta < 0.3$ is not fulfilled and if, e.g., $g_\Lambda^2 \gg g_\Sigma^2$, the model predicts resonances in all the three $J=\frac{3}{2}$ states and in the states with $J=\frac{1}{2}$ having $T=1$.

If the spin of the Y^* proves to be $\frac{1}{2}$, this observation increases the interest of determining whether the Λ - π state is $S_{1/2}$ or $P_{1/2}$.

ASSOCIATED PRODUCTION BY PHOTONS AND PIONS

6.9 We shall complete this survey with some comments on the reactions

²⁴ Also the expression for D_s^T as well as those of N_s^T is given in (146a). *Note added in proof:* The same expressions for the D 's have been obtained by M. Islam, *Nuovo cimento*, 20, 161 (1961) using a different method; in addition Islam has estimated the effects of the \bar{K} interactions, neglected in (146a, b), finding them to be small.

of associated production of strange particles by photons and pions. This section is only a bibliographic introduction to the subject; it is inserted because, in conjunction with the remarks on the K^+-N scattering (p. 68), the reader may get an idea of the present status of the most extensively studied low-energy reactions.

(a) The reactions $\gamma + p \rightarrow Y + K$ (Fig. 4) have been considered perturbatively by Kawaguchi & Moravcsik (148), by Fujii & Marshak (149), and by Capps (150). Even if we assume that only the $\bar{N}-K-\Lambda$ and $\bar{N}-K-\Sigma$ interactions intervene in this problem, there are a number of unknown quantities: in addition to $P_{\Lambda NK}$ and $P_{\Sigma NK}$, the two coupling constants $f_{\Lambda NK}$ and $f_{\Sigma NK}$ and all the anomalous magnetic moments. If we consider only the reactions $\gamma + p \rightarrow \Sigma^0 + K^+$ or $\gamma + p \rightarrow \Lambda^0 + K^+$ [although, as pointed out in (150), the cross sections for some of the reactions with a charged hyperon may be larger than these], the intervening magnetic moments are μ_{Λ^0} , μ_{Σ^0} and μ_T , this last quantity being defined as the matrix element of the magnetic moment operator between the Λ and Σ states: $\mu_T = \langle \Lambda_0 | \mu | \Sigma_0 \rangle$. The above parameters are too many to allow any conclusion; but if the K interactions' contribution to the magnetic moments is neglected, we have $\mu_{\Lambda^0} = \mu_{\Sigma^0} = 0$. If, in addition, the assumption of global symmetry is made, we have $\mu_T = \mu_{\Sigma^+} = 1.8$ nm; therefore, the individual cross sections depend only on the value of $f_{\Lambda NK}$ and $f_{\Sigma NK}$ and on $P_{\Lambda NK}$, $P_{\Sigma NK}$. Capps assumes, for simplicity, that $f_{\Lambda NK}^2 = f_{\Sigma NK}^2$ and considers both parities and both the cases $f_{\Lambda NK}/f_{\Sigma NK} = 1$ and $f_{\Lambda NK}/f_{\Sigma NK} = -1$. The main difference between the cases of even or odd parity is that, for even $P_{Y NK}$, the strong dipole term in $\sin^2\theta$ is expected to be present even at low values of the photon energy (50 to 100 Mev above the threshold). Some evidence for this $\sin^2\theta$ term apparently exists (151a) in Σ^0 and not in Λ production, but the errors are still so large that any conclusion is extremely premature.

As far as the values of $f_{\Lambda NK}$ and $f_{\Sigma NK}$ are concerned, the results of McDaniel *et al.* (151) are compatible with $f_{\Lambda NK}/f_{\Sigma NK} = -1$; for odd $P_{\Lambda NK}$ one obtains $f_{\Lambda NK}^2/4\pi \sim 2$, for even $P_{\Lambda NK}$, $f_{\Lambda NK}^2/4\pi$ is only 0.063.

Whether or not a perturbative treatment has some validity for low-energy photoproduction cannot be said at the moment, but it would be a mistake to draw premature negative conclusions in this respect.

(b) The cross sections and angular distributions for reactions $\pi + p \rightarrow Y + K$ have been summarized in Figure 5; for information on the polarization of the hyperon at several energies and angles compare (27) and (152).

It appears from Figure 5 that the total cross section of $\pi^- + p \rightarrow \Lambda + K^0$ has a maximum somewhere in the interval $T_{\pi-L} \sim 910-1000$ Mev. This energy is near to that of the third $\pi^- - p$ scattering (~ 900 Mev) resonance, so that the presence of the maximum itself might be related to such resonance. If so, it is interesting that the angular distribution as well as the angular dependence of the polarization can be fitted in terms of s and p waves only [for such a fit compare (152)]; this would mean that the third resonance has at most $J = \frac{3}{2}$ for odd $P_{\Lambda NK}$. If, on the other hand, it could be established by independent methods that the $\pi^- - p$ resonance is $D_{3/2}$ (for odd $P_{\Lambda KN}$) or has

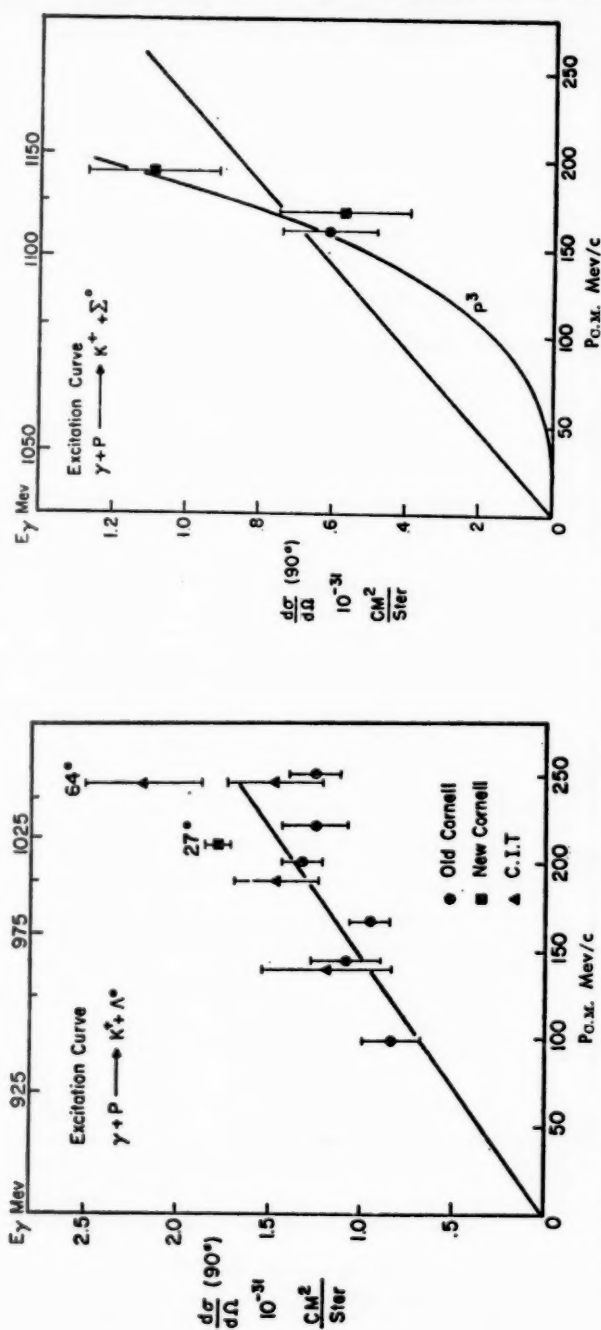


FIG. 4. The present status of associated photoproduction experiments. The $\Lambda^0 K^0$ angular distribution is in the region covered by the graph, consistent with isotropy; for the $\Sigma^0 K^0$ angular distribution compare the text (151a).

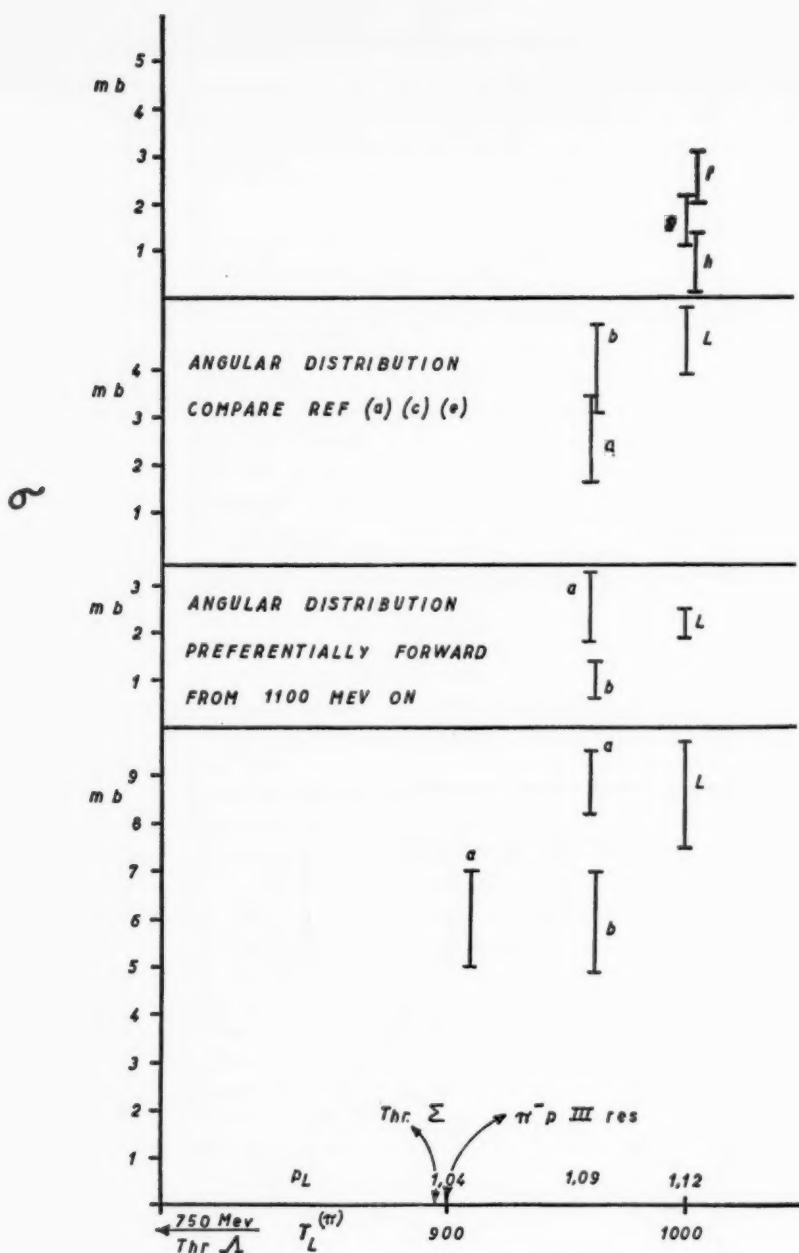
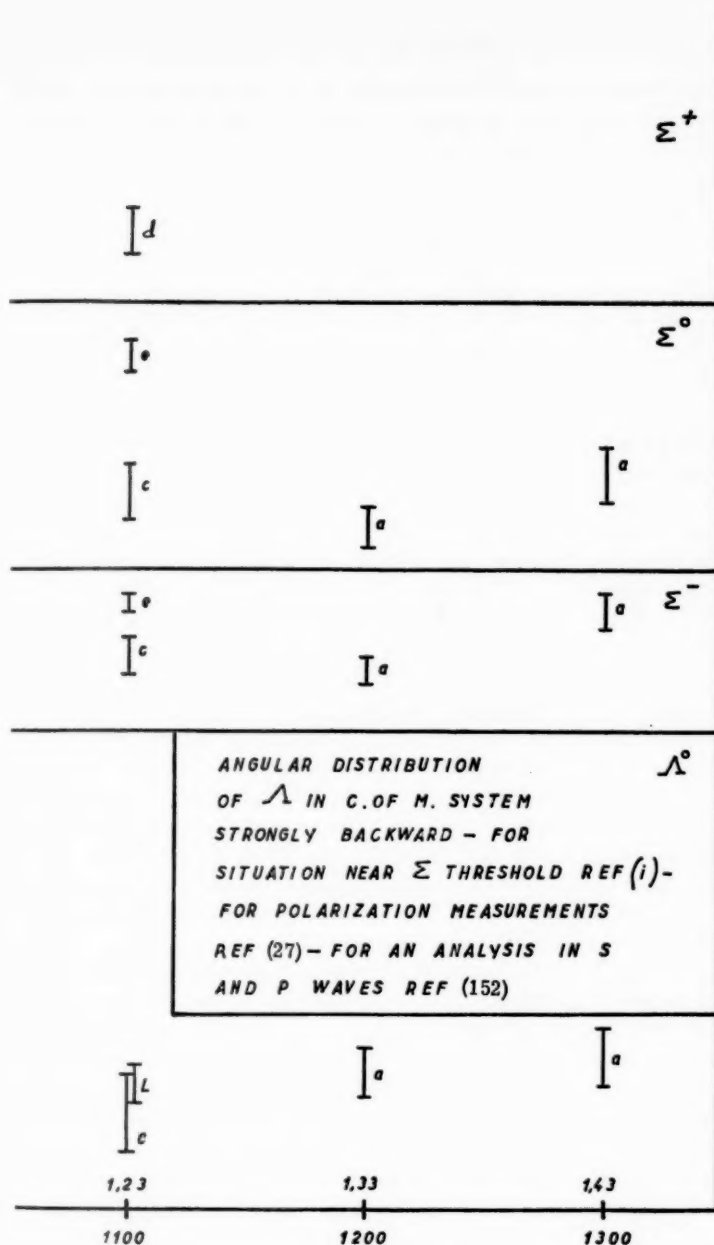


FIG. 5. The present data on the reactions $\pi^- + p \rightarrow \Lambda^0 + \pi$

- (a) Eisler, F., et al., *Nuovo cimento*, 10, 468 (1958)
- (b) Adair, R. K., and Leipuner, L. B., *Phys. Rev.*, 109, 1358 (1958)
- (c) Brown, J. L., et al., *Phys. Rev.*, 108, 1036 (1957)
- (d) Brown, et al., *Phys. Rev.*, 107, 906 (1957)
- (e) Crawford, F. S., Jr., et al., *Phys. Rev. Letters*, 3, 394 (1959)



$K^0; \rightarrow \Sigma^0 + K^0; \Sigma^- + K^+$ and $\pi^+ + p \rightarrow \Sigma^+ + K^+$.

- (f) Berthelot, A., *et al.*, *Proc. Rochester 1960*
- (g) Erwin, A. R., Jr., *et al.*, *Phys. Rev.*, **115**, 669 (1956)
- (h) Hannum, W. H., *et al.*, *Phys. Rev.*, **118**, 577 (1960)
- (i) Alston, M., *et al.*, *Proc. Rochester 1960*, 378
- (l) Crawford, F. S., Jr., *et al.*, quoted in ref. (27)

J higher than $\frac{3}{2}$ (there are indications of this), a strong presumption would exist for the unreliability of an analysis in terms of S and P waves only, and this would indirectly affect and complicate the determination of $P_{\Lambda\Sigma}$ by the "cusp" method.

The broad features of the angular distributions are noted in Figure 5 [cusp effects—compare (9a)—are not considered there]: the angular distribution of the Λ in the center-of-mass system is strongly peaked backward as soon as one goes ~ 100 Mev above the threshold; the angular distribution of the Σ^- is, instead, preferentially forward from 1100 Mev (laboratory energy) on. For the $\Sigma^0(\Sigma^+)$ reactions, although there is some backward (forward) preference, the experimental situation is not entirely clear.

Some time ago Goldhaber (153) remarked that perhaps the angular distribution could be understood in a model in which the incident pion dissociates into a \bar{K} - K pair and the K continues its flight while the \bar{K} is absorbed by the proton producing the hyperon. Of course, dissociation of the pion into a \bar{K} - K pair is not possible unless K and \bar{K} have opposite parities. Pais (80) discussed this question in more detail, concluding that the angular distributions can be understood, at least for the hyperon, by assuming a scalar $K^{(\text{charged})}$ and a pseudoscalar $K^{(\text{neutral})}$. As we have already mentioned, there is no particular reason to believe in an opposite charged-neutral K parity; however, Tiomno has recently remarked (154) that if the existence of a heavy scalar boson K' is postulated, with the same isotopic spin and hypercharge as those of the K , the mechanism of Goldhaber-Pais can be used in explaining the backward production of hyperons. Indeed, if the K' is scalar, the incident π^- can dissociate into a virtual K^0 - K'^- pair, the K'^- being next absorbed by the proton. Tiomno *et al.* (154) have made perturbative calculations of this process and obtained for the mass of this K' a value of ~ 605 Mev, in order to give the best fit to the observed hyperon angular distributions. It is possible that Tiomno's K' may be identified with the resonance recently suggested (Sect. 6.7) for the K - π system.

It must be emphasized that, even in the conventional formulation where only the \bar{N} - Λ - K and \bar{N} - Σ - K interactions are considered, the number of free parameters at our disposal is sufficiently large to fit the observed angular distributions, as pointed out by Warner (155) and by Ogimoto & Shimizu (156). According to the conclusions in (155) and (156), perturbative calculations can reproduce the angular distributions for a scalar or pseudoscalar K and $P_{\Lambda\Sigma}=1$ and for an appropriate choice of the coupling constants g_2, g_3, f_2, f_3 . It follows that it is not yet possible to assert that the Goldhaber-Pais-Tiomno mechanism is or is not chiefly responsible for the typical angular distribution of the Λ . Here we meet again, as in the K - N scattering problem, the question of determining the role of the three-linear versus the K - \bar{K} - π - π interactions; indeed, the \bar{K}' - K - π is essentially equivalent to some kind of K - \bar{K} - π - π interaction.

7. CONCLUSION

The general aspects of the conclusions to be drawn from the facts described in the previous pages have been considered in the introduction. We shall not come back to them here. As for the more specific aspects, they have been inserted at the appropriate places: essentially the titles of the main sections indicate an equivalent number of open problems. We list them again here: (a) to know definitely whether parity is or is not conserved in the strong strange-particle interactions; (b) to know $P_{\Lambda NK}$ and $P_{\Sigma NK}$; (c) to know whether the phenomenological analysis correctly represents the data in the low-energy region: which is the set of amplitudes to be used, and which are their precise numerical values; (d) to know the effects of the resonances that have been discovered (including all the pion-nucleon resonances) in the various coupled channels, etc. These are essentially experimental problems. To obtain answers to such questions is the first task for the future. Such answers should simplify the problem of getting at least qualitative ideas of which are the important vertices in the strange-particle interactions; it is clear from the preceding that little is now known about this. Not only is the relative importance of the trilinear couplings poorly understood, but the relative importance of quadrilinear and trilinear couplings is also not known. Only after such ideas have been formed and accompanied by accurate experimental measurements can one hope to make some step beyond a purely phenomenological treatment.

LITERATURE CITED¹

1. Franzinetti, C., and Morpurgo, G., *Nuovo cimento*, **6**, Suppl. 469 (1957)
2. Dalitz, R. H., *Repts. Progr. in Phys.*, **20**, 163 (1957)
3. Gell-Mann, M., and Rosenfeld, A. H., *Ann. Rev. Nuclear Sci.*, **7**, 407 (1957)
4. Markov, M. A., *Hyperons and K-Mesons* (State Publishers of Physical and Mathematical Literature, Moscow, USSR, 1958)
5. Dalitz, R. H. (Lectures given at the Brookhaven Natl. Lab., July-August 1957) (Unpublished)
6. Amati, D., and Vitale, B., *Fortschr. Physik*, **VII**, 375 (1959)
- 7a. Kaplon, M., *Proc. Geneva 1958*, 171¹
- 7b. Dalitz, R. H., *Proc. Geneva 1958*, 187¹
- 8a. Alvarez, L. W., *Univ. Calif. Rept. UCRL 9354* (August 11, 1960); compare also *Proc. Kiev 1959*
- 8b. Salam, A., *Proc. Kiev 1959*¹
- 8c. Dalitz, R. H., *Proc. Kiev 1959*¹
- 9a. Schwartz, M., *Proc. Rochester 1960*, 685¹
- 9b. Miller, D., *Proc. Rochester 1960*, 693¹
- 9c. Matthews, P. T., *Proc. Rochester 1960*, 700¹
10. d'Espagnat, B., Jauch, J. M., Yamaguchi, Y., Lederman, L., and Peyrou, C., *Cern 59-35* (Lectures given at Cern in 1958-59)
11. Barkas, W., and Rosenfeld, A. H., *Proc. Rochester 1960*, 878¹
12. Alvarez, L. W., Eberhard, P., Good, M. L., Graziano, W., Ticho, H. K., and Wojcicki, S., *Phys. Rev. Letters*, **2**, 215 (1959)
13. Baldo Ceolin, M., and Prowse, D. J., *Phys. Rev. Letters*, **1**, 179 (1958); *Nuovo cimento*, **10**, 635 (1958)
14. Wang Kan-chang, Wang Tau-tsen, Veksler, V. I., Virgasov, N., Vrana, I., Da-tsoo Hi-in Kim, Kladnitskaya, E., Kutznetov, A., Michul, A., T-ty Nguen, Nikitin, A., and Soloviev, M., *Soviet Phys. JETP*, **38**, 1351 (1960)
15. Amaldi, E., Barbaro-Galtieri, A., Baroni, G., Castagnoli, C., Ferro-Luzzi, M., Manfredini, A., Muchnik, M., Rossi, V., and Severi, M., *Nuovo cimento*, **16**, 392 (1960)
16. Button, J., Eberhard, P., Kalbfleisch, G. R., Lannutti, J., Lynch, G. R., Maglic, B., and Lynn Stevenson, M., *Phys. Rev. Letters*, **4**, 530 (1960)
17. Ashkin, J., *Proc. Rochester 1960*, 623¹
18. Nambu, Y., *Phys. Rev.*, **106**, 1366 (1957)
- 19a. Baldin, A. M., *Nuovo cimento*, **8**, 569 (1958)
- 19b. Yamaguchi, Y., *Progr. Theoret. Phys. (Kyoto)*, **19**, 622 (1958)
20. Pontecorvo, B., *Proc. Kiev 1959*¹
21. Akimov, Yu. K., Savchenko, O. V., and Soroko, L. M., *Proc. Rochester 1960*, 49¹
22. Bernardini, C., Querzoli, R., Salvini, G., Silverman, A., and Stoppini, G., *Nuovo cimento*, **14**, 268 (1959)
23. Gomez, R., Burkhardt, H., Daybell, M., Ruderman, H., Sands, M., and Talman, R., *Phys. Rev. Letters*, **5**, 170 (1960)
24. Frisch, D. M., and Ely, R. R., *Phys. Rev. Letters*, **3**, 565 (1959)
25. Gettner, M., Holloway, L., Kraus, D., Lande, K., Leboy, E., Selove, W., and Siegel, R. T., *Phys. Rev. Letters*, **2**, 471 (1959)
- 26a. Conversi, M., Fiorini, E., Ratti, S., Rubbia, C., Succi, C., and Torelli, G., *Nuovo cimento*, **9**, 740 (1958)
- 26b. Prasad, N. O., Menon, M. G., and Sharma, O., *Nuovo cimento*, **14**, 1332 (1959)
- 26c. Keuffel, J. W., Call, R. L., Sandmann, W. H., and Larson, M. O., *Phys. Rev. Letters*, **1**, 203 (1958)
- 26d. Alikhanian, A. I., Shostakovich, N. V., Dadaian, A. T., Fedorov, V. N., and Deriagin, B. N., *Soviet Phys. JETP*, **4**, 817 (1957)
27. Steinberger, J., *Proc. Geneva 1958*, 147¹
28. Lee, T. D., and Yang, C. N., *Phys. Rev.*, **119**, 1410 (1960)
29. Yamanouchi, T., *Phys. Rev. Letters*, **3**, 480 (1959)
30. Prowse, D. J., and Evans, D., *Nuovo cimento*, **8**, 856 (1958)

¹ In this section we shall use the abbreviations:

- (a) *Proc. Geneva 1958* for *Proceedings of the 1958 Annual International Conference on High-Energy Physics at Cern* (Ferretti, B., Ed., H. Studer, Geneva)
- (b) *Proc. Kiev 1959* for *Proceedings of the 1959 Annual International Conference on High-Energy Physics in Kiev* (To be published)
- (c) *Proc. Rochester 1960* for *Proceedings of the 1960 Annual International Conference on High-Energy Physics at Rochester* (Sudarshan, E. C. G., Tinlot, H. J., and Melissinos, A. C., Eds., Interscience, New York, N. Y., 1960)

STRONG INTERACTIONS OF HEAVY MESONS AND HYPERONS 91

31. Harris, G. G., Lee, J., Orear, J., and Taylor, S., *Phys. Rev.*, **108**, 1561 (1957)
32. Prowse, D. J., *Phys. Rev. Letters*, **4**, 244 (1960)
33. Hiida, K., *Nuovo cimento*, **13**, 1117 (1959)
34. Soloviev, M. I. (Report at the Rochester Conf. 1960)¹
35. Pontecorvo, B., *Soviet Phys. JETP*, **10**, 1192 (1960)
36. Fowler, W. B., Birge, R. W., Eberhard, P., Ely, R., Good, M. L., Powell, W. M., and Ticho, H. K., *Phys. Rev. Letters*, **6**, 134 (1961)
- 37a. Muller, F., Birge, R. W., Fowler, W. B., Good, R. H., Hirsch, W., Matsen, R., Oswald, L., Powell, W. M., White, H. S., and Piccioni, O., *Phys. Rev. Letters*, **4**, 418 (539 E) 1960
- 37b. Boldt, E., Caldwell, D. O., and Pal, Y., *Phys. Rev. Letters*, **1**, 150 (1958)
38. Bransden, B., and Moorhouse, R. G., *Progr. Theoret. Phys. (Kyoto)*, **21**, 760 (1959)
39. Katsumori, H., and Shimoura, K., *Progr. Theoret. Phys. (Kyoto)*, **20**, 578 (1958)
40. Tanaka, H., *Phys. Rev.*, **119**, 1436 (1960)
41. Gasiorowicz, S., and Peterman, A., *Phys. Rev. Letters*, **1**, 457 (1958)
- 42a. Matthews, P. T., and Uretsky, J., *Phys. Rev. Letters*, **3**, 297 (1959)
- 42b. Katsumori, H., *Nuovo cimento*, **14**, 1381 (1959)
- 42c. Chou, Kuang Chao, and Ogievetskij, V. I., *Soviet Phys. JETP*, **10**, 616 (1960)
43. Bransden, B., and Moorhouse, R. G., *Phys. Rev. Letters*, **2**, 431 (1959)
44. Zimmerman, A. H., *Progr. Theoret. Phys. (Kyoto)*, **23**, 353 (1960)
45. Day, T. B., Snow, G. A., and Sucher, J., *Phys. Rev. Letters*, **3**, 61 (1959)
46. Eberhard, P., and Good, M. L., *Phys. Rev.*, **120**, 1442 (1960)
- 47a. Katsumori, H., *Progr. Theoret. Phys.*, **18**, 375 (1957)
- 47b. Okubo, S., Marshak, R. E., and Sudarshan, E. C., *Phys. Rev.*, **106**, 599 (1957)
- 47c. Nauenberg, M., *Phys. Rev.*, **109**, 2177 (1958)
48. Holladay, W., *Phys. Rev.*, **115**, 1331 (1959)
49. Treiman, S. B., *Phys. Rev.*, **113**, 355 (1958)
- 50a. Bilenky, S. M., *Nuovo cimento*, **10**, 1049 (1958)
- 50b. Bilenky, S. M., and Ryndin, R. M., *Nuovo cimento*, **12**, 106 (1959)
- 50c. Capps, R. H., *Phys. Rev.*, **115**, 736 (1959)
- 50d. Sirlin, A., and Spitzer, R., *Phys. Rev. Letters*, **3**, 110 (1959)
- 50e. Bohr, A., *Nuclear Phys.*, **10**, 486 (1959)
51. Okun, L., and Pomeranchuk, I., *Soviet Phys. JETP*, **7**, 688 (1958)
52. Block, M. M., Brucker, E. B., Hughes, I. S., Kituchi, T., Meltzer, C., Anderson, F., Pevsner, A., Harth, E. M., Leitner, J. and Cohn, H. O., *Phys. Rev. Letters*, **3**, 291 (1959)
53. Brucker, E. B., Chang, C., Gessaroli, R., Kituchi, T., Kovacs, A., Meltzer, C. M., Pevsner, A., Schlein, P., Strand, R., Cohn, H. O., Harth, E. M., Leitner, J., Monari, L., Lendinara, L., and Puppi, G., *Proc. Rochester 1960*, 419¹
54. Dalitz, R., and Downs, B., *Phys. Rev.*, **111**, 967 (1958)
55. Dalitz, R., and Liu, L., *Phys. Rev.*, **116**, 1312 (1959)
56. Sakurai, J., *Phys. Rev.*, **107**, 1119 (1957)
57. Block, M. M., Brucker, E. B., Chang, C., Kikuchi, T., Meltzer, C., Anderson, F., Pevsner, A., Cohn, H. O., Harth, E. M., Leitner, J., Brautti, G., Franzinetti, C., and Tosi, R., *Nuovo cimento*, **12**, 642 (1959)
58. Amati, D., *Phys. Rev.*, **113**, 1692 (1959)
59. Kerth, L. T., Kycia, T. F., and Baender, R. G., *Phys. Rev.*, **118**, 553 (1960)
60. Selleri, F., *Nuovo cimento*, **15**, 986 (1960)
61. Taylor, J. G., *Phys. Rev.*, **116**, 768 (1959)
62. Chew, G., *Ann. Rev. Nuclear Sci.*, **9**, 29 (1959)
63. Moravcsik, M. J., *Phys. Rev. Letters*, **2**, 352 (1959)
64. Pais, A., and Treiman, S. B., *Phys. Rev.*, **109**, 606 (1958)
65. Feldman, G., and Fulton, T., *Nuclear Phys.*, **8**, 106 (1958)
66. Sucher, J., and Snow, G. A., *Univ. Maryland Tech. Rept. 188* (1960)
67. Byers, N. (Preprint)
68. Feinberg, G., *Phys. Rev.*, **109**, 1019 (1958)
69. Meyer, P., Prentki, J., and Yama-

- guchi, Y., *Phys. Rev. Letters*, **5**, 442 (1960)
70. Baz, A., and Okun, L., *Soviet Phys. JETP*, **8**, 525 (1959); compare also Adair, R. K., *Phys. Rev.*, **111**, 632 (1958)
- 71a. Wigner, E. P., *Phys. Rev.*, **73**, 1002 (1948)
- 71b. Breit, G., *Phys. Rev.*, **107**, 1612 (1957)
- 71c. Fonda, L., *Inelastic Collisions and Threshold Effects* (Inst. for Adv. Studies Preprint, 1960)
72. Day, T. B., Snow, G. A., and Sucher, J. (To be published)
73. d'Espagnat, B., and Prentki, J., *Nuclear Phys.*, **1**, 33 (1956); *Progr. in Elementary Particle and Cosmic Ray Phys.*, **IV**, includes a detailed survey of several attempts (up to 1957) to impose high symmetries.
74. Horwitz, N., Miller, D. M., Murray, J. J., Schwartz, M., Taft, M., Dahl, O., Monara, V., and White, P. (Compare Alvarez, L. W., *Univ. Calif. Rept. UCRL 9354* (August 11, 1960))
75. Crawford, F. S., Jr., Douglass, R. L., Good, M. L., Kalbfleisch, G. R., Stevenson, M. L., and Ticho, H. K., *Phys. Rev. Letters*, **3**, 394 (1959)
76. Pais, A., *Phys. Rev.*, **110**, 574 (1958)
77. Pais, A., *Phys. Rev.*, **110**, 1480 (1958)
78. Tiomno, J., *Nuovo cimento*, **6**, 69 (1957)
79. Dallaporta, N., *Nuovo cimento*, **7**, 200 (1958)
80. Pais, A., *Phys. Rev.*, **112**, 624 (1958)
81. Pais, A., *Phys. Rev. Letters*, **1**, 418 (1958)
82. Morpurgo, G., *Nuovo cimento*, **11**, 738 (1959)
83. Sakurai, J., *Phys. Rev.*, **107**, 1119 (1957) also proposed experiments of this kind
84. Amati, D., and Vitale, B., *Nuovo cimento*, **9**, 895 (1958)
85. Gell-Mann, M., *Phys. Rev.*, **106**, 1297 (1957)
86. Sakurai, J., *Phys. Rev.*, **113**, 1679 (1959)
87. Lichtenberg, D., *Nuclear Phys.*, **8**, 13 (1958)
88. d'Espagnat, B., Martin, A., and Prentki, J., *Nuclear Phys.*, **20**, 543 (1960)
89. Dahl, O., Horwitz, N., Miller, D., Murray, J. J., and Watson, M., *Proc. Rochester 1960*, 415¹
90. Ammar, R. G., Crayton, N., Jain, K. P., Levi-Setti, R., Mott, J. E., Schlein, P. E., Shrivastava, P., and Skieggstad, O., *Proc. Rochester 1960*, 497¹
91. Dascola, G., Mora, S., Quareni, G., Quareni Vignudelli, A., and Tiegte, J., *Proc. Rochester 1960*, 438¹
92. d'Espagnat, B., and Prentki, J., *Nuovo cimento*, **15**, 130 (1960)
93. Gupta, M. L., *Nuovo cimento*, **15**, 737 (1960)
94. Kawarabayashi, K., *Progr. Theoret. Phys. (Kyoto)*, **22**, 451 (1959)
95. Capps, R. H., *Phys. Rev.*, **118**, 1097 (1960)
96. Ross, M., and Shaw, J. L., *Phys. Rev.*, **115**, 1775 (1959)
97. Treiman, S. B., *Nuovo cimento*, **15**, 916 (1960)
98. Pais, A., *Univ. Calif. Rept. UCRL 9460* (October 27, 1960)
99. Fermi, E., and Yang, C. N., *Phys. Rev.*, **76**, 1739 (1948)
100. Goldhaber, M., *Phys. Rev.*, **101**, 433 (1956)
101. Christy, R. F., *Proc. Rochester Conf.*, 7th, Sect. IX, 1 (1957)¹
102. Sakata, S., *Progr. Theoret. Phys. (Kyoto)*, **16**, 686 (1956)
103. Yamaguchi, Y., *Progr. Theoret. Phys.*, Suppl. **11**, 1 (1959)
104. Ikeda, M., Ogawa, S., and Ohnuki, Y., *Progr. Theoret. Phys.*, **22**, 715 (1959)
105. Fujii, Y., *Progr. Theoret. Phys.*, **21**, 232 (1959)
106. Sakurai, J., *Ann. Phys.*, **11**, 1 (1960)
107. Stückelberg, E. C. G., *Helv. Phys. Acta*, **11**, 225 (1938)
108. Ferretti, B. (Remarks at the 7th Annual Rochester Conf., 1957)
109. Wigner, E. P., *Proc. Natl. Acad. Sci. U.S.* **38**, 449 (1952)
110. Sakurai, J., *EFINS-60-63* (1960) (Unpublished)
111. Blin-Stoyle, R. J., *Phys. Rev.*, **120**, 181 (1960)
112. Fubini, S., and Walecka, J. D., *Phys. Rev.*, **116**, 194 (1959)
113. Feinberg, G., *Phys. Rev.*, **108**, 898 (1957)
114. Morpurgo, G., and Touschek, B. F., *Univ. Rome preprint*, 1957 [Unpublished, quoted e.g. in (6) and (112)]
115. Gupta, S. N., *Can. J. Phys.*, **35**, 1309 (1957)
116. Soloviev, V. G., *Nuclear Phys.*, **6**, 618 (E 7, 791)
117. Leitner, P. N., Jr., Rosenfeld, A. H., Solmitz, F. T., and Tripp, R. D., *Phys. Rev. Letters*, **3**, 238 (1959)

118. Block, M. M., Brucker, E. B., Gessaroli, R., Kikuchi, T., Meltzer, C., Pevsner, A., Schlein, P., Strand, R., Cohn, H. O., Harth, E. M., Leitner, J., Minguzzi-Ranzi, A., Monari, L., and Puppi, G., *Phys. Rev.*, **120**, 570 (1960)
119. Crawford, F. S., Jr., Cresti, M., Good, M. L., Solmitz, F., and Stevenson, M. L., *Phys. Rev. Letters*, **1**, 209 (1958)
120. Salmeron, R., and Zichichi, A., *Nuovo cimento*, **11**, 1461 (1959)
121. Bowen, T., Hardy, J., Jr., Reynolds, G. T., Sun, G. R., Tagliaferri, G., Werbruck, A. E., and Moore, W. M., *Phys. Rev.*, **119**, 2030 (1960)
122. Kalbfleisch, G. R., Abstr. in *Phys. Rev. Letters*, **6**, 44 (1961) (To be published)
123. Kurnetsov, E. V., Ivanovskaya, I. A., Prokesh, A., and Chuvilo, I. V., *Proc. Rochester 1960*, 384¹
124. Pais, A., *Phys. Rev. Letters*, **3**, 242 (1959)
125. Feinberg, G., and Gürsey, F., *Phys. Rev.*, **114**, 1153 (1959)
126. Ceolin, C., DeSantis, V., and Taffara, L., *Nuovo cimento*, **12**, 502 (1959)
127. Ceolin, C., and Taffara, L., *Nuovo cimento*, **6**, 425 (1957)
128. Barshay, S., *Phys. Rev. Letters*, **1**, 97 (1958)
129. Jackson, J. D., Ravenhall, D. G., and Wyld, H. W., Jr., *Nuovo cimento*, **9**, 834 (1958)
130. Dalitz, R., and Tuan, S., *Ann. Phys.*, **8**, 100 (1959)
131. Dalitz, R., and Tuan, S., *Ann. Phys.*, **10**, 307 (1960)
132. Ross, M., and Shaw, G., *Phys. Rev.*, **115**, 1773 (1959)
133. Ferrari, F., Frye, G., and Pusterla, M., *Phys. Rev. Letters*, **4**, 613 (1960)
134. Lee, B. W., *Proc. Rochester 1960*, 473
135. Alvarez, L. W., *Univ. Calif. Rept. UCRL 9354* (August 11, 1960); Rosenfeld, A. H. (Private communication, October 15, 1960)
136. Jackson, J. D., and Wyld, H., *Nuovo cimento*, **13**, 84 (1959)
137. Jackson, J. D., and Wyld, H., *Phys. Rev. Letters*, **2**, 355 (1959)
138. Compare also Matthews, P. T., and Salam, A., *Nuovo cimento*, **13**, 381 (1959) for reaction matrix formalism, in a simple form.
139. Snow, G. A., *Proc. Rochester 1960*, 407¹
- 140a. Alles, W., Biswas, N. N., Ceccarelli, M., Gessaroli, R., Quareni, G., Göing, M., Gottstein, K., Püschel, W., Tiegte, J., Zorn, G. T., Crusard, J., Hennessy, J., Dascola, G., and Mora, S., *Nuovo cimento*, **11**, 771 (1959)
- 140b. Davis, D. H., Hill, R. D., Jones, B. D., Sanjeevaiah, B., Zakrzewsky, J., and Lagnaux, G. P., *Phys. Rev. Letters*, **6**, 132 (1961)
141. Dalitz, R., and Tuan, S., *Phys. Rev. Letters*, **2**, 425 (1959)
- 142a. Day, T., Snow, G., and Sucher, J., *Nuovo cimento*, **14**, 637 (1959)
- 142b. Day, T., Snow, G., and Sucher, J., *Phys. Rev.*, **119**, 1100 (1960)
- 143a. Alston, M., Alvarez, L., Eberhard, R., Good, M. L., Graziano, W., Ticho, H. K., and Wojcicki, S., *Phys. Rev. Letters*, **5**, 520 (1960)
- 143b. Bastien, P., Berge, J. P., Ferro-Luzzi, M., Kirz, J., Murray, J., and Rosenfeld, A. H., Rosenfeld, A. H. (Private communication, October 15, 1960)
144. Morpurgo, G., *Nuovo cimento*, **9**, 564, (1958)
145. Alston, M., Alvarez, L. W., Eberhard, P., Good, M. L., Graziano, W., Ticho, H. K., and Wojcicki, S., *Phys. Rev. Letters*, **6**, 300 (1961)
- 146a. Amati, D., Stanghellini, A., and Vitale, B., *Nuovo cimento*, **13**, 1143 (1959)
- 146b. Amati, D., Stanghellini, A., and Vitale, B., *Phys. Rev. Letters*, **5**, 524 (1960)
- 146c. Bosco, B., Fubini, S., and Stanghellini, A., *Nuclear Phys.*, **10**, 663 (1959)
- 147a. Capps, R. H., *Phys. Rev.*, **119**, 1753 (1960)
- 147b. Nogami, Y., *Progr. Theoret. Phys. (Kyoto)*, **22-25** (E 468) (1959)
- 147c. Nauenberg, M., *Phys. Rev. Letters*, **2**, 351 (1959)
148. Kawaguchi, M., and Moravcsik, M. J., *Phys. Rev.*, **107**, 563 (1957)
149. Fujii, A., and Marshak, R. E., *Phys. Rev.*, **107**, 570 (1957)
150. Capps, R. H., *Phys. Rev.*, **114**, 920 (1959)
151. McDaniel, B. D., Silverman, A., Wilson, R. R., and Cortellesa, G., *Phys. Rev.*, **115**, 1039 (1959)
- 151a. Turkot, F., *Proc. Rochester 1960*, 371¹
152. Crawford, F. S., Jr., Cresti, M., Good, M. L., Gottstein, K., Lyman, E., Solmitz, F., Stevenson, M. L., and Ticho, H. K., *Proc. Geneva 1958*, 323¹
153. Goldhaber, M., *Phys. Rev.*, **101**, 433 (1956)

154. Tiomno, J., Videira, A., and Zagury, L., *Phys. Rev. Letters*, **6**, 120 (1961)
155. Warner, C., III, *Phys. Rev. Letters*, **1**, 246 (1958)
156. Ogimoto, T., and Shimizu, T., *Progr. Theoret. Phys. (Kyoto)*, **18**, 213 (1957)
157. Dallaporta, N., and Ferrari, F., *Nuovo cimento*, **9**, 842 (1958)
158. Litchtenberg, B., and Ross, M. H., *Phys. Rev.*, **107**, 1714 (1957)
159. Crawford, F. S., Cresti, M., Good, M. L., Solmitz, F. T., Stevenson, M. L., and Ticho, H. K., *Phys. Rev. Letters*, **2**, 174 (1959)
160. Russel Stannard, F., Abst., *Phys. Rev. Letters*, **6**, 43 (1961)
- 161a. Rodberg, L., and Karplus, R., *Phys. Rev.*, **115**, 1058 (1959)
- 161b. Kotani, T., and Ross, M., *Nuovo cimento*, **14**, 1282 (1959)
162. Dallaporta, N., *Interactions of K^+ mesons* (Communication at the Geneva Conf. on Nuclear Energy 15/P/1371 Session A/17, Centre national de la recherche nucléaire, 1959) (In Italian)
163. Chinowsky, W., Goldhaber, G., Goldhaber, S., Lee, W., O'Malloran, T., Stubbs, T., Slater, W. E., Stork, D. H., and Ticho, H. K., *Proc. Rochester 1960*, 451¹
164. Melkanoff, M. A., Prowse, D. J., Stork, D. H., and Ticho, H. K., *Phys. Rev. Letters*, **5**, 108 (1960)
165. Rodberg, L. S., and Thaler, R. M., *Phys. Rev. Letters*, **4**, 372 (1960)
166. Ferreira, E. M., *Phys. Rev.*, **115**, 1727 (1959)
167. Gourdin, M., and Martin, E. M., *Nuovo cimento*, **11**, 670 (1959); **14**, 722 (1959)

Note added in proof: The Proceedings of the Berkeley Conference on strong interactions have now appeared in *Reviews of Modern Physics*, **33**, 335 (1961) and should be consulted.

THEORIES OF NUCLEON-NUCLEON ELASTIC SCATTERING

BY MICHAEL J. MORAVCSIK AND H. PIERRE NOYES

*Lawrence Radiation Laboratory, University of California,
Livermore, California*

There are few problems in modern theoretical physics which have attracted more attention than that of trying to determine the fundamental interaction between two nucleons. It is also true that scarcely ever has the world of physics owed so little to so many. . . . In general, in surveying the field, one is oppressed by the unbelievable confusion and conflict that exists. It is hard to believe that many of the authors are talking about the same problem, or in fact that they know what the problem is.

M. L. GOLDBERGER (1)

TABLE OF CONTENTS

PREFACE	96
I. INTRODUCTION	97
II. PHENOMENOLOGICAL MODELS	99
1. LOW-ENERGY PARAMETERS	100
2. EARLY HIGH-ENERGY PHENOMENOLOGY	101
3. THE GAMMEL-THALER POTENTIAL	102
4. BOUNDARY CONDITION MODELS; VELOCITY-DEPENDENT AND ISOBAR MODELS	102
5. CONCLUSIONS FROM PHENOMENOLOGICAL POTENTIALS	103
III. MESON-THEORETICAL POTENTIALS	104
1. INTRODUCTION	104
2. WEAK COUPLING THEORIES	113
A. <i>Methods based on the Schroedinger equation</i>	118
(a) Perturbation theory	118
(b) Method of canonical transformations	118
(c) Expansions in the number of particles	119
(i) <i>The basic Tamm-Dancoff method</i>	119
(ii) <i>Probability interpretation of the Tamm-Dancoff method</i>	121
(iii) <i>The Brueckner-Watson method</i>	122
B. <i>Methods based on the S matrix</i>	124
C. <i>Methods based on the relativistic two-body equation</i>	126
(a) The Lévy-Klein method	126
(b) Other investigations of the Bethe-Salpeter equation	127
3. NONWEAK COUPLING THEORIES	129
A. <i>Intermediate coupling theory</i>	129
B. <i>Strong coupling theory</i>	130
C. <i>Nonlinear theories</i>	131
4. CALCULATION OF CORRECTIONS	133
A. <i>"Nonstatic" or recoil corrections</i>	133

B. Radiative corrections	136
C. Higher-order corrections	136
D. Multiple-scattering correction	137
E. Miscellaneous calculations	137
IV. COMPARISON OF THE MESON-THEORETIC POTENTIALS WITH EXPERIMENT	138
1. PROOF OF THE VALIDITY OF THE ONE-PION-EXCHANGE INTERACTION	138
2. MESON-POTENTIAL CALCULATIONS AT HIGH ENERGY	140
3. THE <i>L.S</i> CONTROVERSY	142
4. SEMIPHENOMENOLOGICAL POTENTIAL MODELS	143
V. CALCULATIONS OF NUCLEON-NUCLEON SCATTERING FROM ANALYTICITY AND UNITARITY	143
1. GENERAL THEORY OF THE MANDELSTAM REPRESENTATION	144
A. The relationship between analyticity and causality	144
B. The Mandelstam representation	145
C. The connection between nucleon-nucleon, nucleon-pion, and pion-pion scattering	151
D. Pion-pion and pion-nucleon scattering	154
2. APPLICATIONS OF DISPERSION-RELATION TECHNIQUES TO NUCLEON- NUCLEON SCATTERING	157
A. Dispersion relations in energy	157
B. Construction of the "potential"	158
C. Partial-wave dispersion relations	160
D. Calculations of the two-pion-exchange interaction	163
E. The <i>L.S</i> interaction	165
LITERATURE CITED	166

PREFACE

A review article can be written in two ways. One way is to write a didactic treatise on the important developments in the field, containing only the most important references and stressing organization, coherence, and clarity in the presentation. The other way is to write an encyclopedic summary of all developments, mostly for reference purposes, assuming either that the reader is already familiar with the field or that he is just about to investigate it and the review article will serve him only as a study outline.

The present report was supposed to fall somewhere half-way between the two extremes. No completeness is claimed, although the relatively large number of references should suffice for at least a skeletal survey of any of the subjects discussed. On the other hand, a fair amount of effort went into the organization of the quite extensive and often ambiguous subject matter.

The *Annual Review of Nuclear Science* last published a review of this field in 1953. Therefore, on the whole, it is assumed that developments before 1952 were covered in that article by Breit & Gluckstern (2). Occasionally, when continuity demands, reference is made to work prior to 1952.

The authors had the benefit of several other reviews in the field. Early work on phenomenology was discussed by Christian (3), and later work by Gammel & Thaler (4) in 1960. The two most useful reviews for meson poten-

tial theories proved to be the article by Phillips (5), published in 1959, and the *Supplement of Progress of Theoretical Physics* (6), Numbers 1 to 3, published in 1956. The survey by Hulthén & Sugawara (7) was consulted, although its subject matter did not overlap much with the present topic; the book by Bethe & De Hoffman (8) was also a valuable source. Two other reference books are the *Proceedings of the 1959 London Conference on Nuclear Forces and the Few-Nucleon Problem* (9), and the *Proceedings of the 1960 Annual International Conference on High-Energy Physics at Rochester* (10). The relevant experimental material was discussed last year in the *Annual Review* (11); that chapter will be referred to as Part I. Beyond these, however, one is forced to go to the original literature. This report is based on published literature up to about the middle of 1960.

Our article is divided into five chapters, and some of the chapters are further subdivided into sections. The individual chapters are fairly self-contained, although references are often made to relevant parts of other chapters.

We are most grateful to Drs. J. Charap, G. F. Chew, R. Cutkosky, T. Kinoshita, A. Klein, S. Machida, J. Perring, R. Phillips, C. R. Schumacher, and D. Wong for a critical reading of the manuscript and for many useful comments and suggestions. Any errors of fact or judgment are, however, strictly our own, the more particularly since several suggestions we received were mutually incompatible.

I. INTRODUCTION

The theories that have been used to predict or interpret nucleon-nucleon elastic scattering which go beyond the phase-shift analyses discussed in Part I are of three general types: phenomenological, meson theories of the static potential, and dispersion theoretic. Although some phenomenological models have used nonlocal or velocity-dependent interactions, these have rarely been pushed through to the point of making detailed quantitative predictions. Work with phenomenological static-potential models led to two general conclusions: (a) there is a short-distance repulsion present in most states, that can be adequately represented by a "hard core" of about 0.5 f; and (b) at least above 150 Mev, the data require an $L.S$ (spin-orbit) interaction in addition to central, spin-dependent, isotopic-spin-dependent, and tensor interactions. Some features of these various interactions are also indicated.

Attempts to calculate the interaction from meson theory have in general followed the program first proposed by Taketani, Nakamura & Sasaki (12) in which the researchers try to compute the outer regions of the potential from one- and two-pion exchange, while treating the shorter distances, which are certainly nonstatic, phenomenologically. The phenomenology usually takes the form of the "hard core" suggested by Jastrow (13), although a boundary condition on the wave function (14) has also been used. While all authors agree about the one-pion part of the interaction, there has been a

notable lack of agreement as to the correct treatment of two-pion exchange. We will discuss the various approaches, but we believe that Charap & Fubini (15) are correct in asserting that these difficulties usually stem from a mathematical ambiguity in taking the static limit by letting the ratio of the meson mass to the nucleon mass go to zero.

As far as agreement with experiment goes, the correctness of the one-pion-exchange interaction is now firmly established, as we will show in detail in Chapter IV. When it comes to the more sophisticated calculations, the exact means used for treating the very singular region just outside the phenomenological core is quantitatively so important that it is difficult to say whether these calculations agree with experiment or not. However, models such as those of Signell & Marshak (16, 17, 18), Bryan (19), Hamada (20, 21), & Lomon (22), which treat this region in a more phenomenological spirit but preserve the one-pion-exchange tail, are by now in better semi-quantitative agreement with experiment than are earlier purely phenomenological models. They all utilize a strong $L.S$ potential with a "range" (i.e. decreasing exponential) of half-a-pion Compton wavelength. This interaction is clearly required in $T=1$ states to explain the latest depolarization measurements at 150 Mev, and probably also at 100 Mev. Whether this interaction can be obtained from the meson theory is still under debate.

The latest approach to the problem is to use the general analyticity and unitarity requirements of quantum field theory together with the mass spectrum of strongly interacting particles to compute the covariant S matrix directly, without going through the intermediate step of computing a "potential." While these calculations have not yet been carried through to the point where a detailed comparison with experiment becomes possible, we believe that they clear up many of the ambiguities encountered in earlier calculations and offer more promise for the future. Goldberger, Nambu & Oehme (23) established a nucleon-nucleon dispersion relation in energy, but the use of this relation requires knowledge of the nucleon-antinucleon annihilation amplitude over the physically inaccessible range of energies down to two pion rest masses. The applicability of this approach is thus limited to what amounts to an effective-range treatment. However, the double spectral representation proposed by Mandelstam (24, 25), which has now been proved valid to all orders in renormalized perturbation theory (26, 26a), gives the key to the problem by showing that this annihilation amplitude can be calculated over a useful range from a knowledge of pion-pion and pion-nucleon scattering; the practical test of the method for nucleon-nucleon scattering is now waiting for the successful completion of these prior calculations. Meanwhile, a few useful partial calculations have been concluded. Charap & Fubini (15) have shown that the existence of a Mandelstam representation for potential scattering (27) allows one to go from the full relativistic amplitude at zero energy to a "potential" which, when used in the Schroedinger equation, will reproduce the relativistic amplitude for energies sufficiently below meson production threshold. This procedure gives an unambiguous definition of the "potential" in the low-energy limit which

avoids the ambiguities of the static approach, but also makes the potential less interesting because it requires a prior solution of the covariant problem to construct it. It still has not been proved that the "potential" so defined is the correct interaction to use for problems in low-energy nuclear physics, but it is a more plausible candidate than any of the earlier static models.

II. PHENOMENOLOGICAL MODELS

The most general charge-independent Lorentz-covariant nucleon-nucleon scattering matrix which is parity conserving and invariant under time reversal can be described by five independent functions of energy and momentum transfer for each of the two isotopic spin states, as was discussed in detail in Part I. Although spin is not a good quantum number in a covariant theory, the assumption of charge independence and parity conservation allows us to write the nucleon-nucleon wave function as the product of a symmetric (antisymmetric) spin function times a symmetric (antisymmetric) function of space coordinates for isotopic spin singlet states, and the reverse for isotopic triplet states. This being the case, for each value of J and I , there will be one function for the singlet spin state and a second for the triplet state with $J=L$. By parity conservation the triplet states with $J=L+1$ and $J=L-1$ cannot mix with the $J=L$ state; consequently they are described by three independent functions for the transitions $L+1 \rightarrow L+1$, $L-1 \rightarrow L-1$, and $L+1 \rightarrow L-1$. The transition amplitude $L-1 \rightarrow L+1$ is the same as for $L+1 \rightarrow L-1$ by time-reversal invariance, verifying our count of five independent functions for each value of J and I .

Feldman (28) showed that starting from the covariant S matrix, and assuming that in the nonrelativistic limit it is represented by the scattering from local static potentials in each isotopic spin state, the most general such interaction is the sum of a spin-independent, a spin-dependent, and a tensor potential. This conclusion confirms the nonrelativistic analysis of Wigner & Eisenbud (29, 30) and has the advantage of treating ordinary and exchange forces on the same footing. The general case, treated by Puzikov *et al.* (31) and Okubo & Marshak (32), allows in addition the operators $(L.S)$ and $(L.S)^2$ and shows that each of the five terms can be multiplied by arbitrary interaction functions $I(r, L^2, p^2)$ where r is the relative coordinate and p the total momentum. For elastic scattering, these reduce to functions of r and L^2 . The most general phenomenological model would therefore consist of ten such arbitrary functions (five for each isotopic spin state). Clearly this offers little advantage over specifying the S matrix directly. Even if the interaction is assumed to be "static" (i.e. independent of L^2), one still must specify ten functions of r . Note that in practice the decision whether to use an $(L.S)^2$ term, or to write $I(r, L^2) = I_0(r) + L^2 I_1(r)$ for all the other terms, is somewhat arbitrary. The chief hope of phenomenology is clearly that it will prove possible to give a quantitative description with considerably fewer than ten independent functions of r . We will find that the increasingly detailed experimental information now available has shown this hope to be illusory.

1. LOW-ENERGY PARAMETERS

Once a particular set of interaction functions has been picked, and a particular parameterization for the variation with r decided on, the phenomenologist's task consists of two rather different parts: (a) to fit the "low-energy" parameters (singlet and triplet scattering lengths and effective ranges, and the binding energy, quadrupole moment, and magnetic moment of the deuteron); (b) to refine the model further by comparison with "high-energy" differential cross section, polarization, and triple scattering experiments. Early work on part (a) is discussed in (2), and there have been numerous calculations of this type since (33 to 46). One of the most extensive numerical surveys of this type is given by Biedenharn, Blatt & Kalos (47). These surveys show that if any one particular radial form is chosen, the same parameters do not fit the singlet and triplet state. Therefore, any phenomenological model requires different singlet-central, triplet-central, and tensor potentials as a minimum. As each potential has an adjustable range and depth, there are at least six parameters even if the radial form is specified. The singlet range and depth are fixed by fitting the singlet effective-range and scattering length. The triplet scattering length and binding energy of the deuteron fix the over-all strength and range of the triplet state, while the quadrupole moment specifies the ratio of tensor to central interaction. The triplet effective range is almost completely determined by the binding energy of the deuteron and triplet scattering length, so gives no new information. Nonrelativistically, the magnetic moment of the deuteron fixes the percentage D state as 4 per cent, but this quantity is so sensitive to mesonic corrections (a factor of 2 in either direction) that in practice it does not offer much restriction. We conclude that these low-energy constants fix only five of the six range and depth parameters for the even-parity potentials and give no information about radial dependence. The effective-range expansion has a radius of convergence of 10 Mev (48) or less (49), and even proton-proton (p - p) experiments do not give the shape-dependent term in the effective-range expansion below 10 Mev (50), so shape information comes only from scattering experiments above 10 Mev (which we will call "high-energy" in this article). However, above 10 Mev we also will get scattering from the odd-parity potentials, which could bring in a minimum of another six parameters. Thus, only the sophisticated experiments discussed in Part I, which lead to unique phase shifts, will be directly interpretable, while less complete information will not distinguish clearly between effects from radial dependence and effects from differences between the even- and odd-parity potentials. The history of phenomenology given below confirms this conclusion.

Before turning to the phenomenological interpretation of high-energy experiments, we note one question of physical interest connected with effective-range calculations. Breit, Condon & Present (51) originally postulated charge independence because almost the same potential models would explain both neutron-proton (n - p) and p - p scattering in the 1S_0 state.

Schwinger (52) showed that by including the magnetic moment interaction, the residual discrepancy could be removed for a phenomenological Yukawa potential, but not for less singular potentials; a few other models share this property (53, 54). However, Salpeter (55) found that the hard core required by high-energy scattering (see below) prevented the invoking of this explanation. The situation has been clarified by Riazuddin (56) who noted that the extended magnetic moments measured in electron scattering (57) predict a very small magnetic moment correction, independent of assumptions about the nuclear potential. However, Sugie (58) and Riazuddin (59, 60) also showed that the effect of the known charged-neutral pion mass difference implies an uncertainty in the otherwise charge-independent interaction which is larger than the discrepancy. A recent dispersion-theoretic calculation by Wong & Noyes (61) shows that if the mass difference is included in single-pion exchange it is possible to maintain charge independence in this state within a priori limits set for residual charge-dependent effects in multimeson exchange. All the above calculations refer to the 1S_0 scattering length. Early attempts to discover whether the 1S_0 effective range is also charge independent are inconclusive (62, 63), but a recent analysis (64) of n - p total cross sections up to 14 Mev, using limits on higher L total cross sections estimated from one-pion exchange, is consistent with charge independence.

2. EARLY HIGH-ENERGY PHENOMENOLOGY

The earliest measurements of nucleon-nucleon scattering at energies where the effective-range approximation is clearly inadequate were 40- and 90-Mev n - p scattering and 32- and 340-Mev p - p scattering (65, 66; 67, 68; and 69, respectively). Phenomenological models constructed to fit this data have been reviewed by Christian (3) and by Breit & Gluckstern (2). Briefly, Christian & Hart (70) found that the n - p scattering could be fitted by monotonic potentials only if there were little scattering in the odd states, and even with no odd-state scattering (Serber force), the predicted total cross section was too large. Christian & Noyes (71) found that the p - p data required strong, singular, noncentral forces in the triplet odd states; taken together with the n - p analysis, this fact showed that monotonic potentials are incompatible with charge independence. Jastrow (13) attempted to save charge independence by using a hard-core model, though he found that a weak odd-state tensor force was still required. Case & Pais (72) attempted to save charge independence by using a singular L - S force.

Extension of the p - p scattering measurements to small angles at 310 and 240 Mev gave a cross section smaller than that predicted by any monotonic potential fitted to the correct effective-range and scattering length, thus establishing the hard core in singlet even states (73); similarly, the low n - p total cross sections require a hard core in triplet even states. The prediction of strong noncentral scattering in triplet odd states stimulated the measurement of p - p polarization by Oxley *et al.* (74), and it was indeed found to be

large. Calculations by Goldfarb & Feldman (75) and Swanson (76) showed that the weak tensor force of the Jastrow model gave much too small a polarization; they found that the singular noncentral force models did not give good agreement with the observed differential cross sections, but did predict polarization of the right order of magnitude. Other models have also been tried (77 to 80). The most ambitious attempt to fit both differential cross sections and polarizations was that of Gammel, Christian & Thaler (81). They used hard-core central plus tensor spin-dependent models of the Yukawa type with separately adjustable ranges and depths; even with 14 parameters at their disposal, they were unable to obtain agreement with the existing data. Clearly the phenomenological approach was being forced to abandon its original simplicity.

3. THE GAMMEL-THALER POTENTIAL

Stimulated in part by this theoretical failure, an attempt was made to determine the scattering matrix experimentally at 310 Mev. This was discussed in Part I. Wolfenstein (82) pointed out that these data and the phase-shift solutions later found by Stapp, Ypsilantis & Metropolis [(83); called SYM Solutions here] could be most easily interpreted by assuming a strong $L.S$ force as well as a tensor force. Gammel & Thaler (84, 85) included both interactions in their model; because the P -wave splitting has the $L.S$ signature of phase shifts, while the F -wave splitting has the tensor signature, their $L.S$ force is of shorter range than the tensor force. This model (based on SYM Solution 1) was the first to give semiquantitative agreement with all existing experiments. Gammel & Thaler also obtained better agreement with n - p data by using an $L.S$ potential in isotopic singlet states (86). Unfortunately, as was pointed out by Feshbach (87) and investigated in detail (88 to 91), this $L.S$ potential destroyed agreement between their model and the deuteron magnetic moment; in fact, the resulting model does not even bind the deuteron (92). This latter deficiency has now been corrected, and a number of tensor-plus $L.S$ models which fit all the low-energy parameters (but no particular value for the magnetic moment) have recently been presented in the review article by Gammel & Thaler (4).

4. BOUNDARY CONDITION MODELS; VELOCITY-DEPENDENT AND ISOBAR MODELS

A somewhat different phenomenology was suggested by Breit & Bouricius (93, 94) and by Feshbach & Lomon (14). The latter authors noted that models of the type discussed above are characterized by an interaction energy much larger than the kinetic energy localized at a finite distance of separation between the particles. The implication follows that the wave function inside this distance is much the same at all energies, which can be approximated by requiring the logarithmic derivative to have an energy-independent value at this radius. The appropriate modification of the effective-range expansion was discussed by Raphael (95). Balazs (96) showed

more generally why a formula of this type will give a reasonable representation of the average behavior of the phase shift over a broad energy region. He also showed, however, that the same parameters cannot be used at both low and high energy. Reasonable agreement with experiment was obtained by Feshbach & Lomon when they allowed some energy dependence to the 1S_0 parameters, but their phase shifts resembled SYM Solution 6 at 310 Mev. Since this solution is now experimentally excluded (cf. Part I), the simple model fails. It can be considerably improved by adding weak potential tails outside the boundary condition, as will be discussed in Chapter IV; a related model has been proposed by Moszkowski & Scott (97).

If the energy variation of the phase shift is known at all energies, and the positions and the asymptotic normalizations of the bound states are known, one can construct a unique potential for that state (98, 99). One can also use partial knowledge of the energy variation to obtain partial knowledge of the potential (100). Up to now there has not been sufficient knowledge of the phase shifts to use these methods, but we suspect they will become more important in the near future.

Other types of models have been considered for special purposes. Various authors (101 to 106) have investigated the effect of a single-nucleon excited state or isobar on the scattering; the conclusion is that such a model predicts scattering that differs widely from experiment. Separable potentials (107 to 112) have the advantage that they can be exactly solved, but the disadvantage that they give only S -wave scattering. This might have turned out to be an interesting first approximation, since SYM Solution 2 gave very small singlet D and G waves. Lee, Gammel & Thaler (113) used a nonlocal model, in which a single parameter took the interaction from the local potential to the separable potential limits, to show that SYM 2 corresponds to a nonlocal region of the order of 1 f in size. However, the latest experiments at 210 Mev (114), and the energy-dependent analyses of Breit *et al.* (115) and of Stapp *et al.* (116), proved fairly suggestive evidence that Solution 2 is spurious. A strong argument against SYM 2 given by Perring & Phillips (117) is based on the fact that this type of solution exhibits a negative 1S_0 phase at 100 Mev. Since we know this phase to be positive at low energy, and the differential cross section does not allow either a 0° or a 90° S phase anywhere between 0 and 100 Mev, it is impossible to connect this solution continuously with the low-energy region. Still another velocity-dependent model is provided by noting the mathematical similarity between tensor forces and a soluble problem in elasticity (118).

5. CONCLUSIONS FROM PHENOMENOLOGICAL POTENTIALS

In summary we note that a few reasonably firm conclusions about the kind of potential model which will reproduce the observed nucleon-nucleon scattering can be drawn from these phenomenological calculations. In the first place, there must be a short-range repulsion of the order of 0.5 f in radius in both the singlet and triplet even-parity states. Second, the singlet

even potential is both stronger and shorter-range than the simple Yukawa potential predicted by single-pion exchange using the empirical pion mass and coupling constant. Third, the triplet even-parity tensor potential required to fit the quadrupole moment of the deuteron is also evidenced in high-energy n - p scattering, and an additional L - S potential in this state can be made compatible with the low-energy requirements. Fourth, there are strong noncentral forces in the triplet odd state. A core is not clearly required, but a 3P_0 phase which changes from strong attraction at low energy to strong repulsion above about 150 Mev, together with a repulsive 3P_1 and an attractive 3P_2 state, is indicated. The easiest way to achieve this behavior is with a long-range attractive tensor force and a short-range singular L - S force which is repulsive in the 3P_0 state; higher triplet-odd phase shifts are consistent with this assumption. The singlet odd-state interaction is probably repulsive (4) and is definitely required to explain why the n - p polarization is not antisymmetric about 90° . Finally, it is possible to construct charge-independent models, but it is clear from what has just been said that they must be quite complicated; the only known departure from charge independence, the discrepancy between the 1S_0 n - p and p - p scattering lengths, is explicable in terms of charge-dependent effects known to be present.

III. MESON-THEORETICAL POTENTIALS

1. INTRODUCTION

It is appropriate for several reasons to review the status of the meson theory of nuclear forces at this time. About a quarter of a century has passed since the inception of the original Yukawa idea (119) that mesons are responsible for internucleonic forces. The particle now believed to be primarily responsible for these forces was discovered experimentally (120) about 15 years ago, and that it was pseudoscalar was established about a decade ago (121). Therefore, this multiple anniversary might indeed be a good time to review the success and shortcomings of the pion-potential theory of nuclear forces.

There is another reason which makes it particularly appropriate to review potential theories now. In the past two years a new technique of calculation, using dispersion relations, has come to the foreground, which attempts to formulate the theory directly in terms of scattering amplitudes without resorting to the use of potentials. This technique, to be discussed in a later chapter, has many advantages and is gradually replacing the conventional field-theoretical potential theories. It is likely, therefore, that the present review on meson-theoretical potentials will be one of the last ones, serving to some extent as an epitaph.

It is only fair to point out, however, that this pessimistic appraisal of the future of pion-potential theory is not shared by everybody. For instance, a recent paper by Taketani & Machida (122) announced a new work project for the Japanese theorists to calculate the fourth-order potential with all its

corrections. They claim that dispersion theory is not as complete as potential theory and, in particular, that the former is unable to distinguish between pseudoscalar and pseudovector couplings. Some initial work on this new program has already been published (123, 124). Others like to defend pion-potential theory on pragmatic grounds. They say that the problem is really to develop a useful, convergent calculational scheme for finding the properties of the two- and many-nucleon systems. To the extent that this goal can be achieved and relatively simple description can be given which checks the experimental information, it is maintained that potential theory is justified. Others state the case for the potential picture in even more modest terms. They concede that the calculation of potentials with the field-theoretical methods hitherto used is not very profitable. But they also add that the potential, defined as giving the same S matrix in the low-energy region as the full dispersion calculations, remains a simple and *anschaulich* way of describing the contribution of the "nearby singularities" in dispersion relations and as such should be used just as the optical potential is used in nuclear physics, without claiming that it has a profound interpretation.

The reasons for the decline of meson-potential theory are numerous. Its one outstanding success, a unique description of the potential at large distances, has been accomplished. At smaller distances, however, ambiguities arose which are by now recognized by many to be so fundamental to this approach as to preclude anything but a qualitative or semiquantitative calculation of the potential. The reasons for such ambiguities have been clarified throughout the past decade, and hence not much major work is left there either. Finally, the experimental information available on nucleon-nucleon scattering has widened to include data at higher energies where the potential picture is obviously incomplete. This chapter will follow the development of the meson-theoretical potentials and explain how the successes were scored and how the theory has reached its limitations.

Let us first discuss briefly why the potential concept was used in the first place. Probably the strongest motivation came from the other two forces known at the time of the birth of meson theory, namely, the electromagnetic field and gravitation. To be sure, even the complete description of the electromagnetic field requires a considerable extension of the simple potential concept as known in Newtonian gravitation theory; in fact, general relativity makes the situation somewhat complex even for gravitational forces. Nevertheless, the original idea of Yukawa was based on the analogy to photon exchange in electromagnetic interactions, and the apparent success of this analogy encouraged a belief in a close formal connection between the electromagnetic and mesonic fields. Furthermore, until relatively recently, the study of the nucleon-nucleon interaction was confined to low-energy phenomena in which the energies involved were small compared to the rest mass of the pion as well as that of the nucleon. In this limit it was hoped, and with some justification, that the potential concept would hold regardless of the complexity of the full-fledged relativistic problem. Finally, a wealth of theo-

retical techniques appeared at hand which were well suited to the potential description. This is particularly true for the Hamiltonian formalism (Schroedinger equation) where the use of a potential is most natural. For all these reasons, the meson-theoretical potentials have, until recently, enjoyed great popularity.

As the motto at the head of this article suggests, the field of meson potentials does not excel in clarity. In fact, one can hardly proceed without pausing to explain briefly the use of some of the most fundamental terms which are defined in a variety of ways in the literature.

One has to start with the concept of the potential itself. In the literature, any function or operator which appears in a Schroedinger equation-like field equation as an additive term to the free-field Hamiltonian is, at times, referred to as a potential. More careful workers (125), however, have summarized the properties that such a potential should satisfy in order to be a practically useful concept.

(a) It must be a Hermitian operator defined in the nucleon position and spin space below the threshold of pion production.

(b) It must be an energy-independent operator.

(c) The derivation from first principles must indicate precisely the Schroedinger-like equation in which it is to be inserted, together with the physical significance of the corresponding Schroedinger amplitude.

(d) The velocity dependence of the nuclear potential should be restricted so that the conventional outgoing wave boundary condition for the Schroedinger equation is enough to determine the solution uniquely. This implies that the velocity dependence of the potential can be, at most, linear in the relative momentum. If the velocity dependence is quadratic or higher, one might still obtain some soluble integrodifferential equation, but it would no longer be of the usual Schroedinger type, and hence the interpretation of the potential becomes somewhat uncertain.

In general, such a potential in the restrictive sense (which is the sense in which the word "potential" will be used here) does not exist, since it denies the use of retarded nature of the pion field mediated interactions. As a result, the potentials used in numerical evaluations are taken in some limit where these conditions can be satisfied. In this context we must discuss the use of two terms, those of the static and the adiabatic potentials.

The static potential is the easier and less ambiguous one. This is the limit when the two nucleons are taken to be strictly fixed and the potential due to the meson field is calculated. The limit can be obtained from calculations by taking only the lowest-order term in μ/M , where μ is the pion mass, and M the nucleon mass. There is still room for some confusion, however. For one thing, the μ/M limit has to be taken at the outset; taking it at the end of the calculation can be ambiguous, as shown by Charap & Fubini (15) and by Gupta (126), because of the taking of the limits in the intermediate states. Furthermore, in general, static potentials, since their sources are nailed down, are also local potentials, as point sources are usually assumed and these

nailed-down point sources define a zero region of integration. For this reason the terms "static potential" and "local potential" are often used interchangeably. In some theories, however (still in the static limit), an explicitly smeared out source is assumed, and hence a nonlocal potential is possible by integration over the finite size of the source. Thus a static potential is not always a local one, and this distinction should be kept in mind.

Much more complicated is the use of the term "adiabatic potential." The term originates in classical mechanics and quantum mechanics, where in some problems one motion is so slow compared to another that the former can be neglected during one period of the latter. How one carries this over to field theory is not always clear, however, and the prescription of going to the limit $\eta/M \rightarrow 0$, where η is the nucleon velocity, is not clear cut (15, 127, 128, 129) as used in the literature. One often encounters the description that the adiabatic approximation consists of calculating first the potential as if the motion of the nucleon could be neglected, and then taking the resulting potential to calculate this motion. This is not clear; specifically, for instance, how one neglects the nucleon motion in the intermediate states is ill defined. The taking of the $\eta/M \rightarrow 0$ limit is unambiguous only if η denotes the initial and final (but not the intermediary) nucleon velocity. Such a limit, however, is not equivalent to treating the nucleons nonrelativistically, as is sometimes assumed. Such objections are not only quibbles of a purist, but also affect practical calculations, as we shall see. In particular, it is impossible to separate unambiguously the so-called "nonadiabatic corrections" from the higher-order "adiabatic" terms. Fortunately, as mentioned above, the qualitative tangible consequences of pion theory are usually not much affected by these obscurities since the numerical potentials are customarily calculated in the static (and hence also "adiabatic") limit, sometimes with added "non-static" corrections. In the static limit these ambiguities disappear, and so the confusion is restricted to the calculations of the corrections. Unfortunately, these corrections are not always small. We will try to avoid throughout this chapter the word "adiabatic."

A few more general considerations concerning meson-theoretical potential must be listed. The original form of the Yukawa interaction potential (for neutral, scalar mesons) is $e^{-\mu r}/r$. It was recognized early that the range of such a force representing the exchange of a particle of mass μ is μ^{-1} (using $\hbar = c = 1$). From this, the three-zone picture of the nucleon-nucleon interaction has been developed (12). According to this picture, the outermost region of the interaction, from about 1.5-pion Compton wavelengths ($1.5 \mu^{-1}$) on out, is dominated by the one-pion-exchange forces. In this same region, the potential picture is also expected to be good, since the important energy range in the energy denominators involving the one-pion exchange only will be at low energies. In the second region, $0.7 \mu^{-1} < r < 1.5 \mu^{-1}$ the two-pion-exchange processes dominate. Finally, for $r < 0.7 \mu^{-1}$, three- or more pion exchanges (and perhaps strange particles) play an important role.

Three features of this picture looked particularly encouraging from the

point of view of meson theory. First, the various processes correspond to various parts of the potential, and hence one can get partial information about the interaction from a partial solution of the problem. Second, the one-pion-exchange potential which dominates the outermost region can be calculated simply and almost unambiguously. This fact represented an early success of meson potentials, thus encouraging an attack on the middle region. Third, it was found in phenomenological investigations that the innermost region was dominated by a repulsive core-type interaction, and some meson-theoretical calculations too indicated the presence of such a core (130). (For a more detailed discussion of this point, see Sect. 2 of this chapter.) This possibility meant that the higher-order pion-exchange effects might be drowned out by this repulsive core which, even if its origin is unknown, can be simply represented phenomenologically. Thus, attention was focused on the middle region; and it was believed that if only that could be calculated, the nuclear force problem would be basically solved.

These hopes have been extinguished by two circumstances. First, the above decomposition is only qualitative; and hence, for instance, three-pion-exchange effects play a role even in the two-pion-exchange region. Also, the hard repulsive core might not be so hard either, and hence the innermost region might contribute to some extent, especially at higher energies. Second, and more important, it proved impossible to carry out a quantitatively reliable calculation of the two-pion-exchange region in an unambiguous way.

To conclude these introductory remarks, we have to say a few words about the field-theoretical elements in meson-potential calculations. The various intermediate states can be described in terms of graphs. In some methods, such as covariant perturbation theory, the time-ordering of the interactions is not indicated; that is, a given graph is meant to represent the sum of all diagrams which are the same except for time-ordering. In this scheme the second-order graph (graph with two pion-nucleon vertices) is shown in Figure 1, while the fourth-order graphs are given in Figure 2. Throughout the figures we will use solid lines for nucleons and broken lines for pions. There are also fourth-order graphs in Figure 3, but they are largely renormalization contributions to the second-order graphs and hence do not have to be taken into account explicitly. Specifically, they contribute nucleon mass renormalization, meson mass renormalization, and coupling constant renormalization, respectively.

In other methods, like the Tamm-Dancoff scheme, processes are classified according to the number of intermediate particles. The one-pion intermediate state is the same as it was before (Fig. 1), plus graphs like those in Figure 4, among others, because in these graphs also no horizontal straight line cutting through the graph intersects more than one meson line. In methods like the covariant perturbation theory, graphs like those in Figure 4 would be included in the graph (a) of Figure 2 and thus would be classified as fourth-order processes. The two intermediate pion states in the Tamm-Dancoff type of theory are those in Figure 5. In the Tamm-Dancoff-type theory,

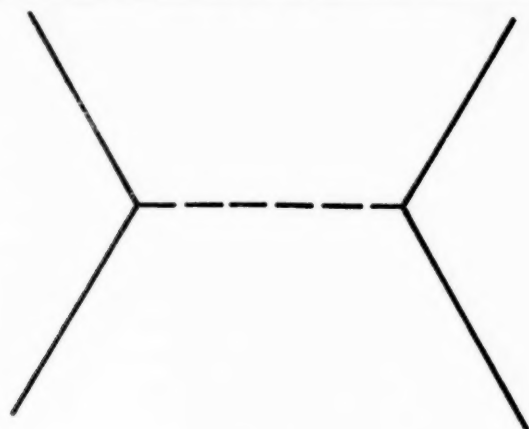
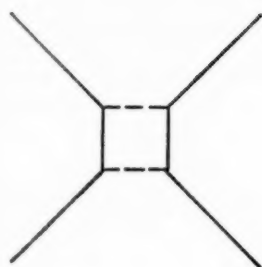
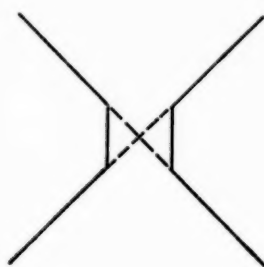


FIG. 1



(a)



(b)

FIG. 2

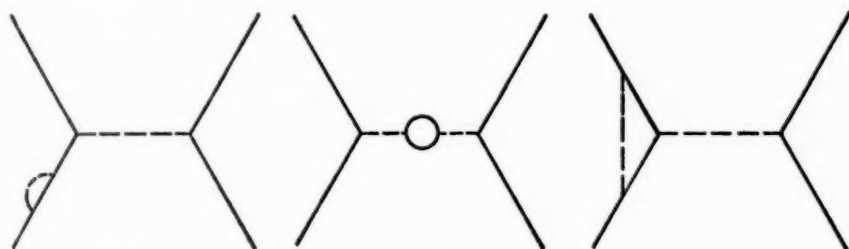


FIG. 3



FIG. 4

unlike covariant perturbation theory, one has to list separately the graphs containing antiparticle states. Thus one also has a graph for a one-pion plus one- (nucleon) -pair intermediate state, and a one-pion plus two-pair intermediate state, shown in Figure 6, both of which would be part of Figure 2 in the perturbation approach.

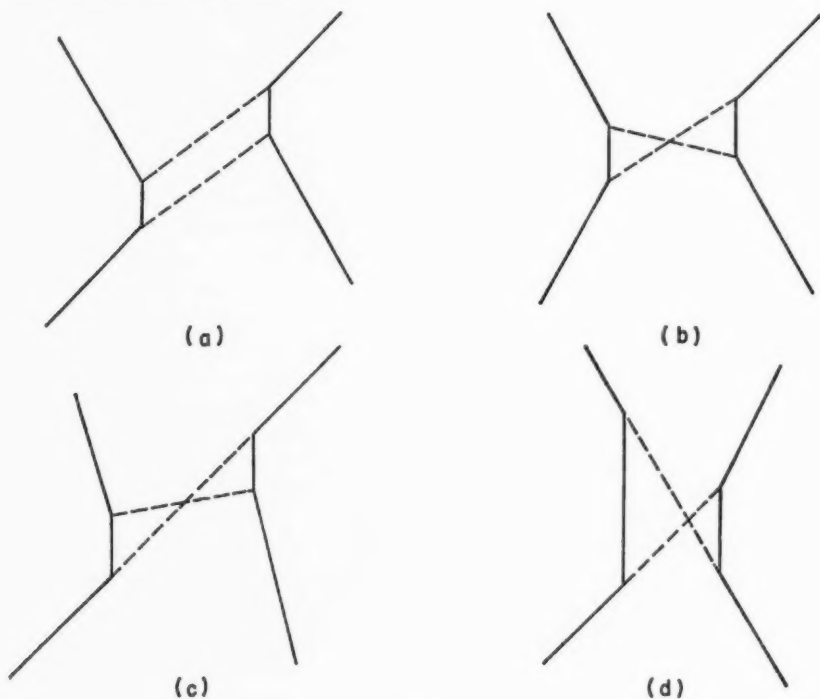


FIG. 5

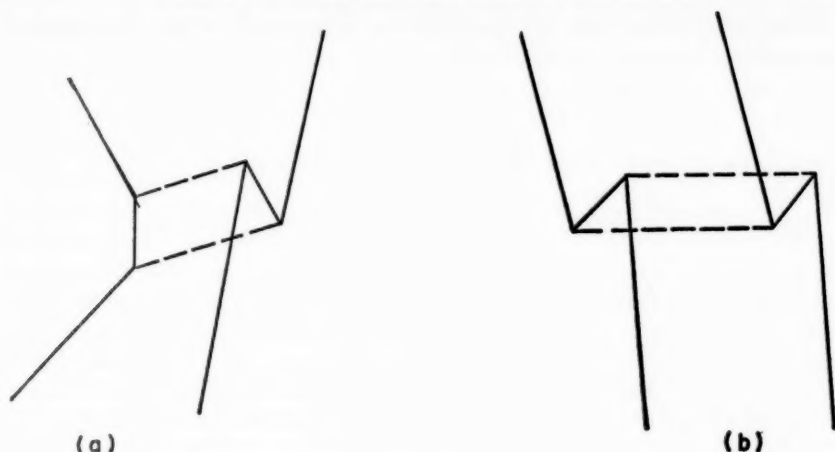


FIG. 6

The interaction between nucleons and pseudoscalar mesons can take a large number of forms. Of these, on the basis of simplicity, usually two are considered. They are the pseudoscalar coupling with an interaction Lagrangian density of

$$-ig\bar{\psi}(x)\gamma_5\psi(x)\cdot\phi(x)$$

and the pseudovector coupling with a Lagrangian density of

$$-i\frac{f}{\mu}\sum_r\bar{\psi}(x)\gamma_5\gamma_r\psi(x)\frac{\partial}{\partial x_r}\cdot\phi(x)$$

where $\psi(x)$ is the nucleon field, $\phi(x)$ the meson field (a vector in isotopic spin space), τ the isotopic spin operator, and γ_r the Dirac matrices. The coupling constants g and f are dimensionless.

The appearance of γ_5 in the pion-nucleon coupling (because the pion is pseudoscalar) has an interesting consequence concerning the relative magnitude of the terms corresponding to the various powers of the unrenormalized coupling constant (131). Since γ_5 has only off-diagonal elements, it will couple only "large" components with "small" components. Thus an odd number of applications of γ_5 is likely to result in relatively small scattering amplitudes, while it will give a large contribution if used an even number of times. For this reason the fourth-order nuclear potential is quite important next to the second-order potential, a fact that is perhaps to be regretted.

The pseudoscalar and pseudovector couplings are equivalent in several senses. First, if two nucleons interact once through either of these interactions ("Møller scattering," see Fig. 1), the resulting scattering amplitudes are identical provided one puts $g=2Mf/\mu$, where M and μ are the nucleon and pion masses, respectively. Second, one might want to compare with Hamil-

tonian densities for the two interactions. The pseudovector Hamiltonian density can be written approximately as

$$\frac{f}{\mu} \psi^* \left\{ \delta \cdot \nabla (\boldsymbol{\tau} \cdot \boldsymbol{\phi}) + \gamma_4 \frac{1}{2M} [\delta \cdot \mathbf{p}, \boldsymbol{\tau} \cdot \boldsymbol{\pi}]_+ + \gamma_4 \frac{f}{\mu} \frac{\pi^2}{2M} \right\} \psi$$

and the pseudoscalar density in a similar approximation as

$$\frac{g}{2M} \psi^* \left\{ \delta \cdot \nabla (\boldsymbol{\tau} \cdot \boldsymbol{\phi}) + \frac{\gamma_4}{2M} [\delta \cdot \mathbf{p}, \boldsymbol{\tau} \cdot \boldsymbol{\pi}]_+ + \gamma_4 g \phi^2 + \frac{g}{2M} \boldsymbol{\tau} \cdot \boldsymbol{\phi} \times \boldsymbol{\pi} \right\} \psi$$

where $\boldsymbol{\pi}$ is the canonically conjugate momentum to $\boldsymbol{\phi}$, and \mathbf{p} is the nucleon momentum. In both these expressions the components connecting negative and positive energy states have been eliminated by canonical transformations. Both these expressions give only terms up to M^{-1} in an expansion in powers of $1/M$. Also omitted are the so-called nucleon contact terms, coming from $(\psi^* \gamma_5 \boldsymbol{\tau} \psi)^2$ and representing the graph in Figure 7. These terms generate

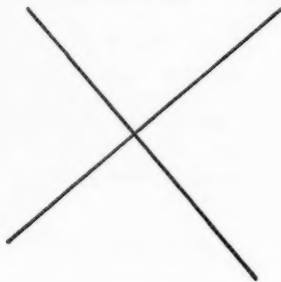


FIG. 7

zero-range potentials in the nucleon-nucleon scattering problem which are not to be taken seriously, since the innermost part of the potential must now be treated phenomenologically anyway.

We see that the pseudovector and pseudoscalar approximate Hamiltonian densities are equal as far as the first two terms are concerned. These are the terms linear in the coupling constants. The other terms come from the elimination of the nucleon-pair contributions in the terms connecting positive and negative energy states. It is evident from their form that they represent mainly S -wave nucleon-pion interaction. Since it is known empirically that the S -wave pion-nucleon interaction is small compared to what one would calculate in first-order perturbation theory, it has been conjectured that these terms are damped (pair suppression). Theoretical justification of this assumption by calculating higher orders in perturbation theory has been only partially successful (132, 133). It can be mentioned, however, that the relationship between pion-nucleon and nucleon-nucleon scatterings has strong foundations so that if one is willing to accept the empirical fact that S -wave pion-nucleon scattering is small, the consequences for nucleon-nucleon scattering follow. If these pair terms are damped, however, then the equivalence between pseudovector and pseudoscalar couplings is nearly valid.

There is a major difference between the pseudovector and pseudoscalar couplings whose practical importance is a matter of controversy. While pseudoscalar coupling can be renormalized in the conventional sense, pseudovector coupling cannot. It has been claimed, however (134, 135, 136), that the infinities arising in a theory which is unrenormalizable are caused by the particular perturbation expansion used and that it is possible to sum the infinities in other ways so that the result is finite. Furthermore, since no covariant field-theoretical calculation has been successful so far in describing the nucleon-nucleon interaction anyway, it is sometimes claimed that the criterion for the applicability of the theory should be its success in correlating data. In practice, therefore, both pseudovector and pseudoscalar couplings have been used.

In the following sections several approaches to the nucleon problem relevant to nucleon-nucleon scattering are discussed. Formalisms that have not been applied to nucleon-nucleon scattering are not included. For comparison of the potentials discussed in this chapter with experiments, see Chapter IV.

2. WEAK COUPLING THEORIES

In this section we will discuss the meson-theoretical potentials arising from the various weak coupling theories, that is, theories in which an expansion is made in terms of some parameter related to the strength of the interaction and a truncated form of this expansion is used in the calculations. There are basically three ways of obtaining a potential from such theories. First, one can use the general Schroedinger equation as the basis and from it, by expansion, elimination, or transformation, derive a Schroedinger equation which contains a potential satisfying the requirements we outlined in the previous section. Second, one can define the potential as one which gives the same nucleon-nucleon S matrix as the original interaction used in field theory. Third, one can use the relativistic two-nucleon equation (Bethe-Salpeter equation), instead of the general Schroedinger equation, as a basis and reduce from it a potential which satisfies our requirements. In practice, several of these methods may yield the same potential.

Before discussing the various approaches, we will summarize the practical results of these calculations which have led to a numerical evaluation of a potential. The most convenient description of these potentials is in terms of the nonrelativistic graphs that they include. Since no complete calculation has been carried out for higher than fourth order, only the graphs shown in Figure 8 have to be taken into account.

Graph *a* is the one-pion-exchange graph (second-order graph). Graph *b* represents those non-pair fourth-order processes which in the intermediate state never have two pions simultaneously. Graph *c* describes the fourth-order non-pair processes with two-pion intermediate states. Graphs *d* and *e* describe the two- and one-pair processes. The distinction between graphs *b* and *c* is meaningful only in formalisms which classify states in terms of the number of particles in the intermediate state (such as the Tamm-Dancoff method) and not in the power of the coupling constant. It might also be

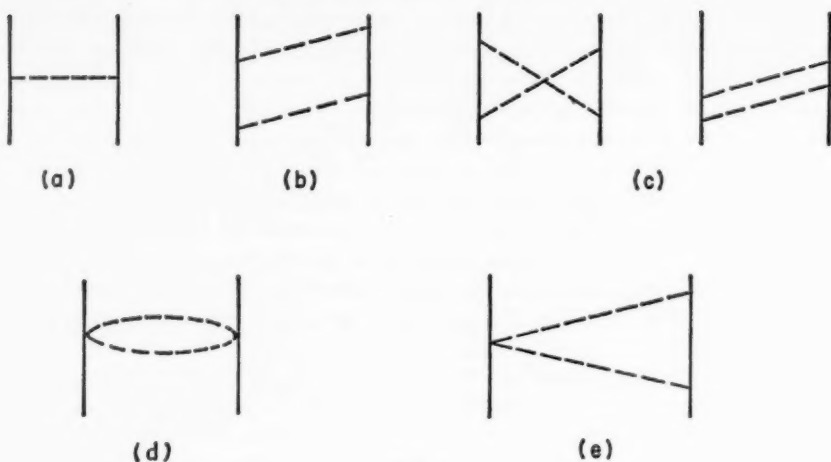


FIG. 8

noted that graphs *d* and *e* are symbolic; they represent contributions of graphs containing nucleon-antinucleon pairs. These graphs, in pseudoscalar coupling, are important because γ_5 couples "small" and "large" components, and hence also allows *S*-wave contributions, for example, which might be symbolized by the emission of a pion pair. Thus, nucleon-pair terms and pion-pair effects are related in this way.

The contributions from these graphs to the static potential are as follows.

$$\begin{aligned}
 V_a &= \frac{1}{3} \mu \boldsymbol{\tau}^{(1)} \cdot \boldsymbol{\tau}^{(2)} \frac{f^2}{4\pi} \left\{ \left[\boldsymbol{\sigma}^{(1)} \cdot \boldsymbol{\sigma}^{(2)} + S_{12} \left(1 + \frac{3}{x} + \frac{3}{x^2} \right) \right] \frac{e^{-x}}{x} - \boldsymbol{\sigma}^{(1)} \cdot \boldsymbol{\sigma}^{(2)} \delta(x) \right\} \\
 V_b &= \left(\frac{f^2}{4\pi} \right)^2 (3 - 2 \boldsymbol{\tau}^{(1)} \cdot \boldsymbol{\tau}^{(2)}) \frac{2\mu}{\pi x^3} e^{-x} \\
 &\quad \left\{ (2 + 2x + x^2) K_0(x) + (4 + 4x + x^2) \frac{K_1(x)}{x} \right. \\
 &\quad + \frac{2}{3} \boldsymbol{\sigma}^{(1)} \cdot \boldsymbol{\sigma}^{(2)} \left[(1 + x) K_0(x) + (2 + 2x + x^2) \frac{K_1(x)}{x} \right] \\
 &\quad \left. - \frac{1}{3} S_{12} \left[(1 + x) K_0(x) + (5 + 5x + x^2) \frac{K_1(x)}{x} \right] \right\} \\
 V_c &= - \left(\frac{f^2}{4\pi} \right)^2 \frac{2\mu}{\pi x^3} \\
 &\quad \left\{ \left[\frac{4 + 4x + x^2}{x} e^{-x} K_1(x) + (2 + 2x + x^2) e^{-x} K_0(x) \right] (3 - 2 \boldsymbol{\tau}^{(1)} \cdot \boldsymbol{\tau}^{(2)}) \right. \\
 &\quad + \left[(23 + 4x^2) K_0(2x) + \frac{23 + 12x^2}{x} K_1(2x) \right] \boldsymbol{\tau}^{(1)} \cdot \boldsymbol{\tau}^{(2)} \\
 &\quad \left. - 2 \left[6K_0(2x) + \frac{6 + 4x^2}{x} K_1(2x) \right] \boldsymbol{\sigma}^{(1)} \cdot \boldsymbol{\sigma}^{(2)} \right\}
 \end{aligned}$$

$$\begin{aligned}
& + \frac{2}{3} \left[K_0(x) e^{-x} (1+x) + \frac{2+2x+x^2}{x} K_1(x) e^{-x} \right] \delta^{(1)} \cdot \delta^{(2)} (3 - 2\tau^{(1)} \cdot \tau^{(2)}) \\
& + \frac{1}{3} \left[36K_0(2x) + \frac{45+12x^2}{x} K_1(2x) \right. \\
& \left. - \left((1+x)K_0(x) e^{-x} + \frac{5+5x+x^2}{x} K_1(x) e^{-x} \right) (3 - 2\tau^{(1)} \cdot \tau^{(2)}) \right] S_{12} \Big\} \\
V_d &= -6\mu \left(\frac{g^2}{4\pi} \right)^2 \left(\frac{\mu}{2M} \right)^2 \frac{K_1(2x)}{\pi x^3} \\
V_s &= 6\mu \left(\frac{g^2}{4\pi} \right)^2 \left(\frac{\mu}{2M} \right)^3 \frac{(1+x)^2}{x^4} e^{-2x}
\end{aligned}$$

There are also some higher-order graphs which contribute as follows:

$$\begin{aligned}
V_6 &= \frac{4}{3} \mu \left(\frac{g^2}{4\pi} \right)^3 \left(\frac{\mu}{2M} \right)^4 \tau^{(1)} \cdot \tau^{(2)} \frac{(1+x)^2}{x^5} e^{-2x} (\delta^{(1)} \cdot \delta^{(2)} + S_{12}) \\
V_8 &= -12\mu \left(\frac{g^2}{4\pi} \right)^4 \left(\frac{\mu}{2M} \right)^4 \frac{1}{\pi x^4} K_1(4x)
\end{aligned}$$

Finally there are "nonstatic" corrections terms appearing in some of the potentials derived so far. These are given by

$$\begin{aligned}
V_{S1} &= \frac{f^4}{(4\pi)^2} \mu \left(\frac{\mu}{M} \right) e^{-2x} \left\{ \left[\frac{3}{4x} + \frac{3}{4x^2} + \frac{6}{x^3} + \frac{21}{x^4} + \frac{27}{x^5} + \frac{27}{2x^6} \right] \right. \\
& + (\tau^{(1)} \cdot \tau^{(2)}) \left[\frac{3}{2x} + \frac{11}{2x^2} + \frac{20}{x^3} + \frac{46}{x^4} + \frac{54}{x^5} + \frac{27}{x^6} \right] \\
& - \frac{9 + 2(\tau^{(1)} \cdot \tau^{(2)})}{4} (\delta^{(1)} \cdot \delta^{(2)}) \left[\frac{4}{3x^2} + \frac{16}{3x^3} + \frac{32}{3x^4} + \frac{12}{x^5} + \frac{6}{x^6} \right] \\
& \left. + \frac{9 + 2(\tau^{(1)} \cdot \tau^{(2)})}{4} S_{12} \left[\frac{2}{3x^2} + \frac{11}{3x^3} + \frac{28}{3x^4} + \frac{12}{x^5} + \frac{6}{x^6} \right] \right\} \\
V_{S2} &= -\frac{\lambda_1^2}{(4\pi)^2} \mu \frac{6}{\pi} K_1(2x) \frac{1}{x^2} + \frac{\lambda_2^2}{(4\pi)^2} \mu (\tau^{(1)} \cdot \tau^{(2)}) \frac{2}{\pi} \left[\frac{K_0(2x)}{x^3} + \frac{K_1(2x)}{x^4} \right] \\
V_{S3} &= \frac{\lambda_1}{4\pi} \frac{f^2}{(4\pi)} \mu 6 \left(\frac{1}{x} + \frac{1}{x^2} \right)^2 e^{-2x} \\
& + \frac{\lambda_2}{4\pi} \frac{f^2}{(4\pi)} \mu \frac{8}{\mu} (\tau^{(1)} \cdot \tau^{(2)}) \left[\frac{5}{2x^3} K_0(2x) + \left(\frac{1}{x^2} + \frac{4}{2x^4} \right) K_1(2x) \right] \\
& - \frac{\lambda_1}{4\pi} \frac{f^2}{(4\pi)} \mu \frac{12}{M} \frac{1}{\pi} \left[\left(\frac{1}{x} + \frac{23}{4x^4} \right) K_0(2x) + \left(\frac{3}{x^2} + \frac{23}{4x^4} \right) K_1(2x) \right] \\
& - \frac{\lambda_2}{4\pi} \frac{f^2}{(4\pi)} \mu \frac{2}{M} 2(\tau^{(1)} \cdot \tau^{(2)}) \left[\left(\frac{1}{x^2} + \frac{4}{x^3} + \frac{10}{x^4} + \frac{12}{x^5} + \frac{6}{x^6} \right) \right. \\
& - (\delta^{(1)} \cdot \delta^{(2)}) \left(\frac{4}{3x^3} + \frac{10}{3x^4} + \frac{4}{x^5} + \frac{2}{x^6} \right) + S_{12} \left(\frac{2}{3x^3} + \frac{8}{3x^4} + \frac{4}{x^5} + \frac{2}{x^6} \right) \Big] e^{-2x} \\
& - \left\{ \frac{\lambda_1}{4\pi} \frac{f^2}{(4\pi)} \mu \frac{12}{M} \frac{2}{\pi} \left(\frac{2}{x^3} K_0(2x) + \frac{3}{x^4} K_1(2x) \right) \right. \\
& \left. + \frac{\lambda_2}{4\pi} \frac{f^2}{(4\pi)} \mu \frac{8}{M} 8(\tau^{(1)} \cdot \tau^{(2)}) \left(\frac{1}{x^2} + \frac{1}{x^3} \right)^2 e^{-2x} \right\} LS
\end{aligned}$$

$$\begin{aligned}
 V_{S4} = & \frac{f^4}{(4\pi)^2} \mu \left(\frac{\mu}{M} \right) 6 \left(\frac{1}{x} + \frac{1}{x^2} \right)^2 e^{-2x} \\
 & - \frac{f^4}{(4\pi)^2} \mu \left(\frac{\mu}{M} \right) 12 \left[\left(\frac{1}{x^2} + \frac{1}{x^3} \right) \left(\frac{1}{x} + \frac{1}{x^2} + \frac{2}{x^3} \right) \right. \\
 & \left. - \frac{\tau^{(1)} \cdot \tau^{(2)}}{3} \left(\frac{1}{x^2} + \frac{1}{x^3} \right) \left(\frac{2}{x^2} + \frac{2}{x^3} \right) \right] e^{-2x} L.S \\
 \\
 V_{S6} = & - \frac{\lambda_1}{4\pi} \frac{f^2}{4\pi} \mu \frac{\mu}{M} \frac{6}{\pi} \left[\frac{K_0(2x)}{x^3} + \left(\frac{2}{x^2} + \frac{1}{x^4} \right) K_1(2x) \right] \\
 & + \frac{\lambda_1}{4\pi} \frac{f^2}{4\pi} \mu \frac{\mu}{M} \frac{12}{\pi^2} \left[\frac{2K_0(2x)}{x^3} + \frac{3K_1(2x)}{x^4} \right] L.S
 \end{aligned}$$

The notation is as follows: g is the pion-nucleon coupling constant, x the radial coordinate in units of the inverse pion Compton wavelength, μ the pion mass, M the nucleon mass, $K(x)$ the Hankel function of imaginary argument. The δ 's refer to nucleon spin, τ to the isotopic spin; S_{12} is the usual tensorial combination, $S_{12} = 3\delta^{(1)} \cdot \mathbf{n} \delta^{(2)} \cdot \mathbf{n} - \delta^{(1)} \cdot \delta^{(2)}$, L the total orbital angular momentum, S the total spin. Sometimes f is used instead of g for the pion-nucleon coupling constant; the relationship between the two is $f = \mu g / 2M$. The λ 's are pair contribution coupling constants.

In addition to the above expressions, some potentials also contain correction terms which are the results of numerical integration and hence cannot be given in analytic forms. The various potentials compounded from these contributions are summarized in Table I.

Here we might point out the significance of the term containing $\delta(x)$ in V_a . The delta function interaction in this form would in fact have no influence on the wave function and hence was dropped in the early calculations. It was pointed out by Lévy (130), however, that the uncertainty principle demands that this delta function interaction be spread at least over a volume of radius M^{-1} . The corresponding potential will then be necessarily nonlocal, with a kernel

$$V(r, r') = - \frac{1}{3} \frac{f^2}{4\pi} \left(\frac{2M}{\mu} \right)^2 \frac{M^2}{rr'} K_1(Mr) K_1(Mr')$$

producing a strongly repulsive, short-range interaction. In all practical calculations this interaction is approximated by a repulsive hard core at a radius to be fitted to experiments. Lévy's work, however, gives at least an example of the way in which such a repulsive core might come about, even if the quantitative agreement with experiments is questionable. In this connection Schumacher (137) investigated the effects of a spread-out nucleon in the second-order potential and found that although the "extension" of the nucleon is only its Compton wavelength, 0.2 fermi, it can produce an equivalent repulsive core of almost one fermi in the central potential. The equivalent repulsive core in the tensor part of the potential, however, was found to have a much smaller radius. Several authors (138 to 141) have shown that a repulsive core is a general feature of relativistic calculations.

TABLE I
WEAK COUPLING POTENTIALS

Name	Ref.	V_a	V_b	V_c	V_d	V_e	Higher-order	Correction terms	Static?	Remarks
TMO	(143)	\times	\times	\times	\times	\times			Yes	
Lévy-Klein (1)	(149 to 153)	\times							Yes	
Lévy-Klein (2)	(149 to 153)	\times			\times		\times		Yes	
Brueckner-Watson	(184, 185)	\times		\times	Multiplied by λ^2	Multiplied by λ	V_6, V_8		Yes	λ is the pair-suppression parameter
Gartenhaus	(189)	\times		\times		\times		Yes	Yes	Cutoff, tabular form
FST	(179, 181)	\times	\times	\times		\times		Yes	Yes	Cutoff, tabular form
KMO	(201, 202)	\times	\times	\times		\times		"Radiative" correction and others $V_{S1} + V_{S2} + V_{S3} - V_d - V_e$	No	Tabular form
Sugawara-Okubo (pseudoscalar)	(182)	\times	\times	\times	\times	\times		$V_{S1} + V_{S2} + V_{S3} + V_{S4} + V_{S1} - V_d - V_e$	No	
Sugawara-Okubo (pseudovector)	(183)	\times	\times	\times	\times	\times			No	
Klein-McCormick	(200)	\times		\times	Multiplied by λ^2	Multiplied by λ		Yes, same as KMO	No	Tabular form same as in Brueckner-Watson
Gupta	(126)	\times	\times	\times	\times	\times		Yes	No	Tabular form

A. *Methods based on the Schroedinger equation.*—The Hamiltonian of the complete problem we are considering consists of three parts

$$H_{tot} \equiv H_N + H_P + H_I \equiv H_N + H'$$

where H_N represents the nucleon field, H_P the pion field, and H_I the interaction. As mentioned before, the problem is treated in practice by assuming fixed nucleons, and hence we want the solution of the equation

$$H'\psi \equiv (H_P + H_I)\psi = W\psi$$

or of its time-dependent equivalent

$$(H_P + H_I)\psi = i \frac{\partial}{\partial t} \psi$$

Let us denote the ground state of this equation by subscript zero. The next step is, then, to solve the equation for the nucleons caused by the presence of a meson field obtained from the above equation. In other words, one has to solve the equation

$$(H_N + W_0)\psi(\mathbf{r}) = E\psi(\mathbf{r})$$

where \mathbf{r} is the relative coordinate of the two nucleons, of which W_0 is a function. This $W_0(r)$ is the potential we are looking for. For a method of solving this second equation, see, for example, reference (142) which works in momentum space.

We shall discuss three methods of solving the first equation.

(a) Perturbation theory

This is the most long-standing method. One simply carries out a non-relativistic perturbation expansion using H_I as the perturbation. In practice, such an approach is not being used, since perturbation calculations are more conveniently carried out in the covariant S -matrix formalism. This will be discussed in more detail as part of the S -matrix approach.

The potential arising from such a calculation in the static limit is the same as that obtained from some other methods. In particular, the Taketani-Machida-Onuma (TMO) potential (143), to be discussed later, can also be obtained from a perturbation approach. In general, a Rayleigh-Schroedinger perturbation theory for $W_0(r)$ and canonical transformations applied to a fixed source theory are exactly identical.

(b) Method of canonical transformations

This method recognizes that one is interested only in the lowest eigenstate of the equation to be solved, and hence the diagonalization of $H_P + H_I$ has to be carried out only to the extent that the matrix elements connecting this lowest, two-nucleon state with states also containing pions must be made zero. A series of transformations leading to this partial diagonalization can be constructed so that n of these successive transformations make the non-diagonal elements proportional to g^m with $m \geq n$. The prescription is as follows.

The first transformation is

$$\psi(t) = e^{iS_1} \psi_1(t)$$

and hence

$$H_1'(t) = e^{-iS_1} H'(t) e^{iS_1}$$

where we choose S_1 such that

$$H_1 + i[H_P, S_1] = 0$$

or

$$(S_1)_{nm} = i \frac{(H_1)_{nm}}{E_n - E_m}$$

where nm refers to the matrix elements between the one-nucleon state and other states. The other elements of S_1 can be anything.

Since H_I is linear in g , and we assume S_1 also to be linear in g , in the general expression

$$\begin{aligned} e^{-iS_1} H e^{iS_1} &= H_P + i[H_P, S_1] - \frac{1}{2}[[H_P, S_1], S_1] + \dots \\ &+ H_1 + i[H_I, S] - \frac{1}{2}[[H_I, S], S_1] + \dots \end{aligned}$$

the terms proportional to g have been eliminated, and hence H' is now "diagonal" in our restricted sense up to and including terms of order g . This procedure can be repeated now on H' to transform away also the g^2 non-diagonal terms, etc.

After the n th step in this procedure one can write the resulting transformed Hamiltonian as

$$H^{(n)} = H_P + V^{(n)}$$

where $V^{(n)}$ is the Hermitian potential we are looking for, up to order g^n .

A number of authors have used this method for the calculations of potentials. Some calculations were carried out to fourth order by Nishijima (144). The results agree with the calculations of Taketani, Machida & Onuma (143), after whom this potential is named TMO potential. They used a different method, however (see Sect. 2-B of this chapter). Later Iwadare (145) also calculated a potential and agreed with the TMO potential if the expansion in μ/M was carried to the same power. Canonical transformation was also used by Lepore (146) for calculating some pair effects. For an explicit form of the TMO potential, see Table I.

Shortcomings of this method mainly arise because renormalization cannot be carried out consistently. Also, the energy range under consideration has to be cut off from above lest zero-energy denominators appear.

(c) Expansions in the number of particles

(i) *The basic Tamm-Dancoff method:* In the previous method of canonical transformation the undesirable part of the Hamiltonian was transformed away. In the Tamm-Dancoff type of scheme it will be eliminated algebraically.

Let us again consider the Schroedinger equation

$$H'\Psi = (H_P + H_I)\Psi = W\Psi$$

Let us assume now that the Ψ is written as a vector in the space which is determined by the number of particles

$$\Psi = \begin{pmatrix} \Psi_{2,0,0} \\ \Psi_{2,0,1} \\ \Psi_{3,1,0} \\ \Psi_{3,1,1} \\ \vdots \\ \vdots \end{pmatrix}$$

where the three subscripts denote the number of nucleons, antinucleons, and pions, respectively. We are interested in $\Psi_{2,0,0}$ in particular. The Hamiltonian H' can also be decomposed accordingly, resulting in

$$H' = \begin{pmatrix} H'_{2,0,0;2,0,0} & H'_{2,0,0;2,0,1} & H'_{2,0,0;3,1,0} & \cdots \\ H'_{2,0,1;2,0,0} & H'_{2,0,1;2,0,1} & H'_{2,0,1;3,1,0} & \cdots \\ H'_{3,1,0;2,0,0} & \cdots & & \\ \cdots & & & \\ \cdots & & & \end{pmatrix}$$

The Schroedinger equation can then be written as a set of coupled equations

$$(W - H'_{2,0,0;2,0,0})\Psi_{2,0,0} = H'_{2,0,0;2,0,1}\Psi_{2,0,1} + H'_{2,0,0;3,1,0}\Psi_{3,1,0} + \cdots$$

$$(W - H'_{2,0,1;2,0,1})\Psi_{2,0,1} = H'_{2,0,1;2,0,0}\Psi_{2,0,0} + H'_{2,0,1;3,1,0}\Psi_{3,1,0} + \cdots$$

This infinite set of coupled equations is made finite by the assumption that only equations up to N_1 nucleons, N_2 antinucleons, and N_3 pions are considered. Once the set is finite one can eliminate, one by one, all $\Psi_{l,m,n}$'s except $\Psi_{2,0,0}$ and hence obtain an equation for the latter. It should be noted that in this scheme, once the original mutilating assumptions are made, the rest of the problem is solved self-consistently. This is unlike perturbation theory where the effect of higher-order terms back on the lower-order terms is never considered. Since the classification of states is made here in terms of the number of particles in the intermediate state, the diagrams are different from the conventional Feynman graphs. This was discussed in Section 1 of this chapter.

The Tamm-Dancoff theory (147, 148) was used in essentially the above form by Lévy (149, 150, 151) to obtain a nucleon-nucleon potential. Some of his detailed calculations were wrong, as Klein (152, 153) pointed out. Two of the corrected versions are listed in Table I. The result obtained from the Tamm-Dancoff theory can also be obtained from the relativistic two-body equation (see Sect. 2-c of this chapter).

The literature on the interpretation of the Tamm-Dancoff scheme as related to the nucleon-nucleon scattering problem is extensive. Feldman (154) used a canonical transformation in the Tamm-Dancoff space. He emphasized that, like the Pauli reduction of the Dirac equation, the Tamm-Dancoff

scheme will be a good approximation at low energies. Baroncini (155) showed that the static second-order potential is the same as that obtained from other methods. Morpurgo & Touschek (156, 157) showed on an exactly solvable model calculation that the Tamm-Dancoff scheme gives a better approximation than the perturbation theory but is still only qualitative. Okabayashi (158) made the mathematical remark that having solved the n th order equation one can get the potential operator for the $(n+1)$ th order just by integration. The convergence of the Tamm-Dancoff expansion was investigated by Meecham (159) and was found to exist for sufficiently low cutoff.

The Tamm-Dancoff theory in the above form cannot be renormalized. Various schemes have been proposed to remedy this (160 to 172), all based on a covariant generalization of the method. These "new Tamm-Dancoff" schemes have been shown to work under special circumstances (173 to 177) but in general they are still not completely renormalizable (178).

In the static limit the Tamm-Dancoff method gives a well-defined potential just as any other method does (in this limit there is no difference between the old and new Tamm-Dancoff methods). In general, however, it gives an energy-dependent potential which is not a potential at all by our criteria. One can eliminate this energy dependence by iteration, for instance, but the resulting Hamiltonian will not be Hermitian. This is a basic objection, at least for the practical case in which the elimination is carried out nonsymmetrically. A method to remedy this situation has been given by Fukuda, Sawada & Taketani (179) and Feldman (154) and will be discussed in the next subsection.

(ii) *Probability interpretation of the Tamm-Dancoff method:* The situation is again analogous to the reduction of the Dirac equation to a nonrelativistic form: since the latter neglects the "small" components of the wave functions, the over-all normalization of the wave function has to be adjusted.

Let us start again with the Schroedinger equation

$$H'\Psi_0 = (H_P + H_I)\Psi_0 = W\Psi_0$$

where Ψ_0 represents all those states which for the free-pion field case represent the two-nucleon state (pion vacuum). Not the whole space spanned by the Ψ_0 's is, however, the two-nucleon subspace with the interaction present, but only Ψ'_0 which is related to Ψ_0 by

$$\Psi_0 = J\Psi'_0$$

that is, J^{-1} is the projection operator from the whole Ψ_0 space to the subspace spanned by the Ψ'_0 's.

Since the Ψ_0 's are normalized, we have

$$(\Psi_{01}, \Psi_{02}) = \delta_{12}$$

but

$$(\Psi'_{01}, \Psi'_{02}) \neq \delta_{12}$$

Therefore, with the use of the ψ'_0 's, probability is not conserved, and hence the corresponding Hamiltonian is non-Hermitian.

The remedy is now at hand. Defining new state vectors

$$\chi_0 = (J^+J)^{1/2}\psi'_0$$

we have

$$(\chi_{01}, \chi_{02}) = (\Psi'_{01}, J^+J\Psi'_{02}) = (\Psi_{01}, \Psi_{02}) = \delta_{12}$$

that is, the χ_0 's are normalized and one has, correspondingly, for the Schroedinger equation

$$(H_P + V)\chi_0 = W\chi_0$$

where

$$V = (J^+J)^{1/2}J^+(H_P - H_I)J(J^+J)^{1/2} - H_N$$

The interpretation of $(J^+J)^{1/2}$ is clear; it is the probability that no mesons are present.

This modified scheme is often called the renormalized Tamm-Dancoff theory, a quite misleading term indeed. We would rather call it the adjusted Tamm-Dancoff method. It has also been investigated by Okubo (180) who was able to subtract closed loops. An evaluation in the static limit was done by Inoue *et al.* (181) who found something close to the TMO potential. Their potential, called the Fukuda-Sawada-Taketani (FST) potential, uses an extended source, that is, a momentum cutoff. As a result, their "static" potential (see discussion in Sect. 1 of this chapter) cannot be expressed in terms of the expressions given in Table I and the formulae preceding it, but numerical integrations have to be carried out.

The most recent work using this method was by Sugawara & Okubo (182, 183), who calculated also some nonstatic corrections (see Sect. 4 of this chapter). In particular, they get $L.S$ terms and claim that they are unambiguous. Their work, the Sugawara-Okubo (SO) potential, calculated for both pseudoscalar and pseudovector coupling, is given in Table I.

(iii) *The Brueckner-Watson method:* This method is also based on an expansion into immediate particle states, although it is not a series in the powers of the coupling constant but a method of successive approximations.

In its original form (184, 185) the derivation of this method was based on the scattering matrix formalism. For comparison to the TMO and FST methods, however, it is more appropriate to quote Klein's derivation (186, 187).

Starting again with the Schroedinger equation we have

$$H'\psi = (H_P + H_I)\psi = W\psi$$

Let us assume for the time being that H_I is linear in meson operators and there are no pairs terms. Then

$$H_I = H_I^+ + H_I^-$$

in terms of emission and absorption operators, respectively.

Just as in the Tamm-Dancoff case, we can write ψ in terms of particle number eigenstates

$$\psi = \sum_{n=0}^{\infty} \psi_{(n)}$$

where n is the number of pions (we assumed no nucleon pairs). Then we have the following coupled equations:

$$\begin{aligned}(W - H_P)\psi_0 &= H_1^{(-)}\psi_1 \\ (W - H_P)\psi_1 &= H_1^{(-)}\psi_2 + H_1^{(+)}\psi_0 \\ &\dots \dots \dots \\ (W - H_P)\psi_n &= H_1^{(-)}\psi_{n+1} + H_1^{(+)}\psi_{n-1} \\ &\dots \dots \dots\end{aligned}$$

Now let us try to eliminate alternate components, e.g. $\psi_1, \psi_3, \dots, \psi_{2n+1}, \dots$. Using $G_P = 1/(W - H_P)$ we get the set of equations

$$\begin{aligned}(W - H_P)\psi_{2n} &= [H_1^{(-)}G_P H_1^{(+)} + H_1^{(+)}G_P H_1^{(-)}]\psi_{2n} \\ &\quad + H_1^{(-)}G_P H_1^{(-)}\psi_{2n+2} + H_1^{(+)}G_P H_1^{(+)}\psi_{2n-2} \\ &\dots \dots \dots\end{aligned}$$

Defining

$$\begin{aligned}\Delta_0 &= H_1 G_P H_1 \\ V_0 &= D(\Delta_0) \\ U_0 &= N(\Delta_0)\end{aligned}$$

where $D(\Delta_0)$ and $N(\Delta_0)$ are the diagonal and nondiagonal parts of Δ_0 in particle occupation numbers, we can rewrite

$$(W - H_P)\psi_{2n} = V_0\psi_{2n} + U^{(-)}\psi_{2n+2} + U^{(+)}\psi_{2n-2}$$

We can now eliminate from this set of equations every second component, using

$$\begin{aligned}\Delta_1 &= U_0(W - H_P - V_0)^{-1}U_0 \\ V_1 &= D(\Delta_1) \\ U_1 &= N(\Delta_1)\end{aligned}$$

etc.

The resulting $\mathcal{V} = \sum_{K=0}^{\infty} V_K$ will be the potential we are looking for satisfying

$$(W - H_P)\psi_0 = \mathcal{V}\psi_0$$

The practical results of the Brueckner-Watson method, like all others, can also be derived from a covariant approach, which will be discussed in Section 2-C-b of this chapter. In the static limit the method yields the Brueckner-Watson (BW) potential (185), as indicated in Table I. The constant λ appearing in it multiplies the pair terms they calculated; $\lambda \approx 1$ means the full pair contribution, while $\lambda = 0$ is complete suppression. The Brueckner-Watson method of eliminating every second component can also be formulated, as Tani (188) showed, in terms of a series of canonical transformations rather than in terms of algebraic elimination.

The Brueckner-Watson method was used by Gartenhaus (189), who derived a potential using a cutoff, following the Chew theory of pion interactions. Because of the cutoff, the integrations have to be carried out numeri-

cally, and hence the Gartenhaus potential cannot be expressed in terms of the analytic expressions preceding Table I.

As in most of the cases discussed, the potential calculated from the Brueckner-Watson method is useful only in the static limit. In general, the resulting \mathcal{V} is energy dependent, and the elimination of this energy dependence by iteration results in a non-Hermitian Hamiltonian.

B. *Methods based on the S matrix.*—The S -matrix method of defining the two-nucleon potential is based on choosing a potential such that it gives the same S matrix as the one we would calculate from field theory. In particular, denoting by P the time-ordered product, and $\langle \rangle$ the expectation value in pion vacuum (two-nucleon state), the definition is

$$\left\langle P \left[\exp \left(-i \int_{-\infty}^t H_1 dt \right) \right] \right\rangle = P \left[\exp \left(-i \int_{-\infty}^t \mathcal{V}(t) dt \right) \right]$$

where the operators are to be understood in the interaction representation.

It is clear that in general the "potential" thus defined will be energy dependent. Furthermore, since in the scattering formalism V is directly related to the R matrix,

$$R = V + V \frac{1}{E' - E + i\epsilon} R$$

and since the off-energy-shell components of the R matrix can be chosen arbitrarily as far as the S matrix is concerned,

$$S = \delta_{EE'} - 2\pi i \delta(E' - E) R$$

we have a great amount of arbitrariness in the definition of V . Various conventions are used.

This method was used by Watson & Lepore (190) to obtain a fourth-order potential with radiative corrections. Essentially this method was also used by Kuni (191), although he actually calculated scattering amplitudes directly from the Low-type integral equation, using several approximations.

A version of the S -matrix method was suggested by Nambu (192) who calculated the covariant fourth-order S -matrix contribution as well as the repetitions of the second-order covariant S -matrix element and then postulated that the difference between the two is the effect of the fourth-order potential. In this calculation the repetition of the second order is to be taken "with full retardation corrections," including all of its ladder diagrams. A derivation of his method is given in the original paper and will not be repeated here. It is equivalent to the canonical transformation method with full recoil. The method was used by Taketani, Machida & Onuma to calculate their TMO potential in the static limit. This potential can also be obtained by canonical transformations (see Sect. 2-A-b). The TMO potential appears in Table I. Nakabayasi & Sato (193) used the method too and included some recoil in the intermediate state. They used both pseudoscalar and pseudovector couplings, and in the former their result agrees with Lévy.

A particularly useful variant of the S -matrix method is based on the

recognition that if the diagrams in Figure 2 are bisected by a vertical line they fall into pion-nucleon scattering diagrams. Thus if one knows the pion-nucleon scattering amplitude on and off the energy shell, he can construct the S matrix also for these nucleon-nucleon diagrams. In theories which use expansions into the number of particles in the intermediate states, these diagrams (being "ladder" diagrams) are assumed to be automatically included. Henley & Ruderman (194), who used this version of the S -matrix method, pointed out, however, that such diagrams could also be construed to be "recoil" corrections to the one-pion-exchange terms and as such should be explicitly included. They used pion-nucleon scattering amplitudes as described by the fixed source (cutoff) theory. With these, the "rescattering" corrections turned out to be quite small, in contrast with later work. The spirit of this method was also dominant in Sharp's work (195); he also used the Chew cutoff theory to synthesize the nucleon-nucleon amplitude from the basic pion-nucleon amplitude. A similar approach was taken by Novozhilov and co-workers (196, 197, 198) who used explicit pion-nucleon phase shifts to express parts of the amplitudes. They found certain terms which were not included in the other potentials. An $L.S$ term can also be calculated in this way.

Similar schemes, although not in conjunction with cut-off theories, were also suggested by Miyazawa (199) and by Klein & McCormick (200). The Miyazawa version was turned into a potential by Konuma, Miyazawa & Otsuki (201, 202), while Klein & McCormick did their own calculations. These potentials are essentially the usual static potentials with various rescattering correction terms. The Konuma-Miyazawa-Otsuki (KMO) and Klein-McCormick (KMcC) potentials are tabulated in Table I. In this connection one should also remark that Klein (203) gave the first proof that the part of nuclear forces which is associated with S -wave pion-nucleon scattering (at least as represented by the isotopic nonflip combination of scattering lengths) is small because the scattering is small. The basic idea of this approach to nucleon-nucleon scattering in terms of pion-nucleon scattering was discussed by Weisskopf (204) without using field theory.

It is worth mentioning that the Miyazawa and Klein-McCormick schemes construct the nucleon-nucleon scattering amplitude from the knowledge of the pion-nucleon scattering amplitudes. Looking at it from this point of view, one can forget about the expansions and couplings and discuss the whole problem in terms of the properties and interrelationships of various scattering amplitudes. Thus these schemes form a bridge between the general approach of meson-theoretical potentials and the recent dispersion theory formalism discussed in Chapter V, where potentials are never mentioned. The two approaches differ, however, inasmuch as the Miyazawa or Klein-McCormick schemes require the knowledge of the pion-nucleon scattering amplitudes on and off the energy shell, while dispersion relations deal always with amplitudes on the energy shell, although for unphysical values of the dynamical observables.

C. *Methods based on the relativistic two-body equation.*—

(a) The Lévy-Klein method

Lévy's work (149, 150, 151) has been mentioned in connection with the Tamm-Dancoff formalism. Even in his first paper, however, Lévy mentioned that the Tamm-Dancoff amplitudes can also be obtained from the "large" components of the relativistic two-body equation, the so-called Bethe-Salpeter equation (205), when the two times of the interacting nucleons are taken to be equal. This was discussed further by Lévy in his subsequent papers, to some extent by Hamada & Sugawara (206), and perhaps most thoroughly by Klein (152, 153, 207). See also work by Macke (208, 209).

The Bethe-Salpeter equation in coordinate space can be written as

$$X(x_1, x_2) = - \int S_F^{(1)}(x_1, x_1') S_F^{(2)}(x_2, x_2') G(x_1', x_2'; x_1'', x_2'') X(x_1'', x_2'') dx_1' dx_2' dx_1'' dx_2''$$

where x_1 and x_2 are the position four-vectors of the two nucleons, S_F is the usual Dyson function, and $X(x_1, x_2)$ is the two-nucleon amplitude. The kernel of this integration equation $G(x_1', x_2'; x_1'', x_2'')$ is in practice to be expanded in terms of the coupling constant, giving

$$G = G_2 + G_4 + \dots$$

where, for instance

$$G_2(x_1', x_2'; x_1'', x_2'') = g^2 \Delta_F(x_1' - x_2') \delta(x_1', x_1'') \delta(x_2', x_2'')$$

where Δ_F is again the field-theoretical function defined by Dyson. If only G_2 is used in the expansion of G , the iteration of the integral equation will produce only iterations of the diagram in Figure 1, resulting in ladder-shaped diagrams. This is called the "ladder" approximation.

If we want to use this covariant two-time equation for the derivation of a potential, we will at least have to make the two times equal. Denoting the argument of Δ_F by $x \equiv x_1' - x_2'$ we want therefore a $\delta(x^4)$ appearing explicitly. Furthermore, the spatial part of Δ_F is replaced by

$$\int_{-\infty}^{+\infty} \Delta_F(x, x_4) dx_4$$

which, because

$$\Delta_F(x) \equiv - \frac{i}{2\pi^2} \int_0^\infty \exp\left(i\alpha x^2 - i \frac{\mu^2}{4\alpha}\right) d\alpha$$

gives just the Yukawa potential. Thus, indeed, the "nonrelativistic" reduction of the Bethe-Salpeter equation gives something familiar from nonrelativistic theories. For a full derivation of the connection with the Tamm-Dancoff amplitudes, the reader is referred to the original references already quoted by Klein and Lévy. The Lévy calculations, corrected, resulted in two alternative potentials in the static limit, depending on which graphs were considered. They are given in Table I. The Lévy-Klein reduction of the

Bethe-Salpeter equation to a Schroedinger equation with only positive energy states has been questioned by Arnowitt & Gasiorowicz (210). They obtained a closed expression for the potential which shows that the perturbation expansion is a poor one.

(b) Other investigations of the Bethe-Salpeter equation

In the previous subsection we touched upon the relationship between the Bethe-Salpeter equation and the Tamm-Dancoff method. Other investigations have also been made in this direction. In particular, Macke (208, 209) clarified the matter by deriving a nonrelativistic form of the two-nucleon operator

$$[W - (m_1^2 + \mathbf{p}^2)^{1/2} - (m_2^2 + \mathbf{p}^2)^{1/2}]a(\mathbf{p}) = -Va(\mathbf{p})$$

with W the total energy, $-V$ the interaction potential operator, and $a(\mathbf{p})$ a four-component wave function describing two nonrelativistic nucleons. Transformation of this equation can give something very close to the Tamm-Dancoff formulae. The above equation makes it easier to discuss the vacuum polarization and renormalization graphs.

The most extensive and comprehensive work on the relationship between the Bethe-Salpeter equation and the Tamm-Dancoff formalism was done by Zimmerman (211). He emphasized that the main difference between the two is in the basic amplitudes. The Tamm-Dancoff amplitude, a probability amplitude, is defined with respect to the interaction-free vacuum (bare particles), while the Bethe-Salpeter wave functions refer to the vacuum of the total energy. The article also deals extensively with the differences in the use of graphs between the two methods.

The single-time Bethe-Salpeter equation was further discussed by Macke (212) in relation to the "new" Tamm-Dancoff theory, showing that the latter is also derivable from the former. Wanders (213) showed that the nonrelativistic eigenvalue spectrum of the Bethe-Salpeter equation is identical with that of the Schroedinger equation with a Yukawa potential. An extension of the Foldy-Wouthuysen transformation to the Bethe-Salpeter equation was given by Chraplyvy (214). A generalization of the Foldy-Wouthuysen transformation by Kursunoglu (215) was applied by him to the Bethe-Salpeter equation.

The relationship of the TMO and BW potentials was discussed by Klein (187) starting from the Bethe-Salpeter equation. He concluded that in obtaining the TMO potential certain terms are neglected and that this omission is never justified. On the other hand, in the derivation of the BW potential the approximation at least has not been proved to be unapplicable.

The formal mathematical properties of the Bethe-Salpeter equation were studied by Wick (216), for bound states, by analytical extension of the momentum space amplitude on the energy variable. He showed that for two scalar massless mesons, in the ladder approximation, the problem reduces to a Sturm-Liouville problem. The latter result was extended by Sugano & Munakata (217) to a scalar-spinor interaction. The technique of analytical

continuation in the fourth component was also used by Kemmer & Salam (218) for the scattering problem. A generalization of the Wick procedure was given by Ida (219).

There are a number of other papers in addition to those mentioned above which deal with the reduction of the Bethe-Salpeter equation to a one-time equation. The Lévy (151) and Klein (153) method corresponds to taking the nonrelativistic limit after the Bethe-Salpeter equation has been iterated. Macke (209, 220, 221) laid aside at each iteration a one-time part. Symanzik (222) made his transformation on the renormalized Bethe-Salpeter equation.

There are also some attempts at a general covariant solution still in the ladder approximation. For the special case when the binding energy of the two-nucleon system is equal to their two-nucleon rest energies, Edwards (223) and Goldstein (224) obtained solutions for bound states. Green (225) also studied this question.

The scattering problem corresponds, however, to an inhomogeneous integral equation, and erudite features of the Fredholm theory have to be used to produce solutions. The solution is the ratio of two convergent powers series in the coupling constant. This was discussed by Green (226) but the results are not in such form that comparison with experiments could be made.

Nonrelativistic solutions, using also the "small" components to order η , have been obtained by Alekseev (227). Ladder approximation solutions have been given by Green & Biswas (139), Okubo & Feldman (228), Yamamoto (229), Cutkosky (230), Cutkosky & Wick (231), and Geffen & Scarf (232). The last three used the previously mentioned formalism of Wick. Cutkosky and Okubo & Feldman used an integral transform method for obtaining solutions. Gourdin (141), also using the ladder approximation, obtained the neutron-proton singlet scattering length and "verified" the presence of the hard core. Scarf & Umezawa (233) showed that some covariant solutions of the Bethe-Salpeter equation are spurious on physical grounds. Biswas (140) also obtained solutions in the ladder approximation for equal times. A general numerical solution of the Bethe-Salpeter equation for scalar particles interacting through a scalar massless particle was given by Vosko (234). He also outlined a general procedure for solving the equation, based on variational principles.

Normalization conditions for Bethe-Salpeter wave functions were discussed by Allcock (235) for bound states. Once the wave functions are normalized, Nishijima (236, 237, 238) and Mandelstam (239) have shown that the construction of normalized transition probabilities and expectation values is formally simple. See also Klein & Zemach (240).

The question of whether solutions exist at all was investigated by Mandelstam (241), who found that for $g^2/4\pi < \pi/6$ solutions always exist. More specifically he gave ranges for $g^2/4\pi$ as a function of angular momentum in which solutions exist.

The renormalization of the Bethe-Salpeter equation was discussed by

Claesson (242) who calculated the renormalization constants by a power series expansion in the coupling constant and got a finite result.

One can also use the Bethe-Salpeter equation as a basis for a nonlocal theory. This has been discussed by Jordan & Frahn (243, 244). It can be reduced to the usual local potential in the static limit.

Some general attempts have also been made to reformulate the problem. Arnowitz & Gasiorowicz (245) have given a Green's function treatment of the two-nucleon problem using a formalism by Neuman (246). Here, at least formally, no expansion into coupling constants or number of particles is needed. Glaser (247) gave another general covariant two-body equation in which the "covariant wave function" contains only one Heisenberg operator and several creation and annihilation operators for incoming and outgoing particles.

The list of papers on the Bethe-Salpeter equation given above is not meant to be complete, but to serve as a set of examples for the various aspects of the problem which have been under investigation.

The main drawback of the Bethe-Salpeter equation is that it has been, so far, unamenable to a specific reduction to a potential. Several of the potentials calculated from other methods can also be derived from it, but these use only a fraction of the power and generality of the covariant equation. Perhaps the Klein-McCormick potentials (200, 248), discussed in the subsection on the S -matrix approach, came closest. But the practical covariant treatment of the two-body problem is yet to come. The Bethe-Salpeter equation has also been used to calculate electromagnetic effects of the two-nucleon system (249, 250).

3. NONWEAK COUPLING THEORIES

A. *Intermediate coupling theory.*—The physical idea behind intermediate coupling theory is the subdivision of pions around the nucleon into two categories: the bound pions (called zero pions) and the unbound ones (the s pions). These two kinds of mesons can also be called inner and outer mesons, respectively. The zero pions are those which make a "dressed" nucleon out of the "bare" one, to use the field-theoretical language, and they participate in the processes determining the properties of the free nucleon. The s pions, on the other hand, are those occurring in dynamical processes. Thus, for instance, pion-nucleon scattering can be regarded as the conversion of an s pion to a zero pion and the subsequent reconversion.

The mathematical formulation of the intermediate coupling theory was given first by Tomonaga (251) in terms of a Ritz eigenvalue problem in a Fock space, that is, in an expansion into particle occupation numbers. For the extensive details of the derivation, the original paper should be consulted. The basic states of the formalism are made up of the bare nucleon and a certain number of (zero) pions and perhaps even nucleon-antinucleon pairs around it. Extensive calculations were carried out to determine the

properties of free nucleons and, in this connection, the number of zero pions which, on the average, make up a dressed nucleon (252, 253). This number of course depends on the coupling constant, but it was found that for reasonable values of g^2 for pseudoscalar pions, the number is quite small, which in a way "justifies" the weak coupling calculations.

The intermediate coupling formalism has also been applied to the nucleon-nucleon scattering problem. The general formulation (for scalar pions) was given by Hasegawa (254), while the application to pseudoscalar pions, with numerical calculations, was given by Nogami & Hasegawa (255). The idea is to divide the meson field into three parts: the zero pions of nucleon #1, the zero pions of nucleon #2, and the s pions. It is assumed that the individual dressed nucleons can be only in the four isobaric states with isotopic and ordinary angular momentum $\frac{1}{2}$ or $\frac{3}{2}$. It is also assumed that the transitions between these states accompanied by the emission of an s pion can be neglected. Furthermore, nucleon recoils are neglected. This last assumption is an inherent feature of intermediate coupling theory, but in practice it is not a serious limitation since, as we mentioned before, unambiguous two-nucleon potentials are always taken in the static limit anyway. Furthermore, it is assumed in these calculations by Nogami & Hasegawa that a cutoff exists, that is, that the nucleons are extended sources. This is also an inherent feature of intermediate coupling theory without which the calculations would diverge. It is, however, a more serious limitation because it turns out that the fourth-order potential, for instance, depends quite strongly on the kind of cutoff used.

The method of calculating the potential is that discussed in Section 2-A of this chapter: the potential is identified as the r -dependent eigenvalue of the Schroedinger equation. The Hamiltonian consists of terms describing the various meson fields and their interactions with (or conversion into) each other. The resulting potential is expanded into powers of e^{-x} ; thus the second-order potential gives the e^{-x} part, corresponding to the one-pion-exchange potential in weak coupling. The e^{-2x} terms correspond to the fourth-order terms in weak coupling and represent the distortion of the zero-pion clouds resulting from the presence of the other nucleon and from the excitation into isobaric states. s -Pion exchanges are neglected which might be unrealistic. The results are not unlike the weak coupling results. The second-order potential is the same as that obtained in weak coupling and is unaffected by the effects of s -pion exchange or cutoff. The fourth-order potential, however, is considerably influenced by these factors. With a reasonable cutoff of 4.1 pion masses the resulting potential is similar to the Fukuda-Sawada-Taketani potential.

B. Strong coupling theory.—In strong coupling theory the interaction is assumed to be so strong that a large number of virtual pions is present in the field. As an extreme instance, one can assume that the number of pions is so large that the quantization effects in the field can be neglected and hence the calculations can be carried out by classical field theory. Such a calculation is

reproduced in Bethe & De Hoffmann (8) and results in the same expression as that obtained for the second-order potential in weak coupling theories. The classical model is also used by Breit (256) to investigate general features of velocity-dependent effects in the two-nucleon potential (see also Sect. 4 of this chapter). In a less extreme case, one can resort to quantization. Such strong coupling theories were particularly fashionable in the decade of the forties when weak coupling theories appeared to be doomed because of the infinities. Wentzel (257) developed this theory, particularly in connection with the "pair theory" in which the basic quantum of the nucleon-nucleon field is a pair of mesons of some sort. These pair terms, however, also appear in present-day pion theories, as we have seen in Section 1 of this chapter. [See also (258, 259, 260).] The usual method used in such theory is an expansion in the inverse powers of the coupling constant. A description of the general formalism was given by Tomonaga (261). The two-nucleon problem in this formalism was discussed by Pauli (262); his result for the interaction potential is again the old familiar second-order potential known from weak coupling.

Recent work on strong coupling theory is scarce. Geilikman (263, 264, 265) has performed a series of calculations for various fields, calculating various processes including the two-nucleon potential. He improved previous calculations, for instance, by treating the spin-vector quantum mechanically also. He calculated the potential to lowest order and obtained again the familiar second-order potential. Thus, strong coupling theory so far has not yielded any practical nontrivial result for nucleon-nucleon scattering.

C. Nonlinear theories.—There is no a priori reason to assume that in meson theories the meson operator appears linearly; the assumption is usually made on the basis of simplicity. As the linear meson theories ran into numerous difficulties, an increasing amount of incentive was offered to investigate the more complicated nonlinear theories. It is worth summarizing some of the reasons which prompted such investigations (266).

(a) Linear theories gave a singular potential, regardless of the calculational methods used. (b) Linear theories had difficulty giving a finite field energy for point sources. (c) Pseudovector coupling could not be renormalized. (d) It was difficult in linear theories to get a realistic, finite repulsive core. (e) Saturation of nuclear forces was not easy to explain within linear theories. (f) Nonlinear terms arose even if basically linear theories were used. Examples are nonlinear vacuum polarization terms, pair terms from the nonrelativistic transformation, possible pion-pion interaction terms, etc. (g) Multiple production of pions in nucleon-nucleon collisions was easier to explain in nonlinear theories (267). (h) Indication of nonlinear effects in computation of the nucleon magnetic moment was obtained.

The relaxation of the linearity requirement of course opens up a multiply infinite number of possibilities, depending on the power of the meson variable involved, on the number of derivatives, etc. Moreover, these theories result in nonlinear differential (or integral) equations which have several

classes of solutions (e.g., "static" and "wave" solutions) that add to the ambiguity. Therefore, work had to be restricted to selecting, more or less randomly, a few simpler nonlinear theories and exploring their consequences.

Most of the workers in this field have used classical theories, although there have been instances of the use of quantized schemes (268). It has been argued that certain low-energy features of the two-nucleon interaction should be given fairly well by the classical theory which, if successful, can then prompt the investigation of more realistic formalisms.

Schiff investigated theories whose Lagrangian density is of the form

$$L = \frac{1}{2} \frac{\partial \phi^2}{\partial t} - \frac{1}{2} (\nabla \phi)^2 - \frac{1}{2} \phi^2 - \frac{1}{4} \alpha^2 \phi^4 + f(\mathbf{r}, t) \phi$$

where ψ is the meson function. The wave equation is therefore

$$\frac{\partial^2 \phi}{\partial t^2} = \nabla^2 \phi - \phi + \alpha^2 \phi^3 + f(\mathbf{r}, t)$$

that is, the nonlinear term is cubic. Schiff was mostly concerned with properties of nuclear matter; his most interesting result is that he automatically gets a repulsive core. Borgardt (269) gave a purely mathematical treatment of more general cubic nonlinear equations.

The most extensive work on nonlinear equations as related to nucleon-nucleon interaction has been done by Cap and collaborators (266, 270 to 274). His most successful model used the Lagrangian

$$L = \frac{1}{\alpha} \left[\sqrt{1 - \alpha \left[\left(\frac{\partial A_\lambda}{\partial x_K} \right)^2 + \mu^2 A_\lambda^2 \right]} - 1 \right]$$

where

$$\alpha = \mu/g^2$$

The "dipole" solution of the corresponding field equation is

$$A_\lambda(r, \theta) = \frac{\tau_\lambda}{\sqrt{\alpha\mu}} R(x) \cos \theta = g\tau_\lambda(\mathbf{r} \cdot \nabla) \mathcal{G}(x)$$

where $R(x)$ is a function satisfying the equation

$$R'' + \frac{2}{x} R' - \frac{2}{x^2} R - R = - \frac{R - R'/x - R/x^2}{1 - R^2} 2R'^2$$

and is such that

$$\lim_{x \rightarrow \infty} R(x) = \frac{d}{dx} \frac{e^{-x}}{x}$$

That is, the function $\mathcal{G}(x)$ has the properties of

$$\mathcal{G} = \int R(x) dx; \quad \lim_{x \rightarrow \infty} \mathcal{G}(x) = e^{-x}/x$$

This means that in the limit of large x the function goes into the Yukawa function. Correspondingly the interaction energy is

$$g^2 \mu (\tau^{(1)} \cdot \tau^{(2)}) \left\{ \delta^{(1)} \cdot \delta^{(2)} \frac{1}{x} \frac{d}{dx} + \frac{1}{3} \delta_1 \cdot \delta_2 x \frac{d}{dx} \frac{1}{x} \frac{d}{dx} + S_{12} x^2 \frac{d}{dx} \frac{1}{x} \frac{d}{dx} \right\} \mathcal{G}(x)$$

and hence, for large x , we get again the familiar second-order weak coupling potential. This is a necessary requirement for any theory, since the long-range part of the potential has been experimentally verified to a fairly high degree (see Chap. IV).

The above nonlinear theory has been quite successful in explaining the properties of the deuteron, although it has no adjustable constants beside the coupling constant. It also gives a quite isotropic differential cross section for p - p scattering at high energies, also in agreement with experiments.

4. CALCULATION OF CORRECTIONS

A. "Nonstatic" or recoil corrections.—So far, we have discussed mainly calculations of the two-nucleon potential in the static limit, that is, when only terms to the lowest order in μ/M are kept and terms containing the nucleon momentum p are neglected. Since, however, μ/M is not very small and η/M is also appreciable in most of the elastic scattering energy region, corrections to this static potential are of interest.

Calculations of these corrections can be made by any of the methods discussed in the previous sections. Let us illustrate the problem using the method based on the Schroedinger equation. Instead of first finding the lowest eigenvalue of

$$H'\psi = W\psi$$

and then solving

$$(H_N + W_0)\psi(\mathbf{r}) = E\psi(\mathbf{r})$$

as we did in Section 1, we now want to solve the exact equation

$$(H_N + H')\psi = E\psi$$

Let us denote by U the transformation which "diagonalizes" H' (in the sense of Sect. 1-A). Using

$$W \equiv U^{-1}H'U, \quad \psi = U\Phi$$

we get

$$(U^{-1}H_NU + W)\Phi = E\Phi$$

In the approximation used in Section 1-A we assumed that U and H_N commute, and thus got

$$(H_N + W)\Phi = E\Phi$$

In general, however, U and H_N do not commute. Thus the equation is, instead,

$$(H_N + W + w)\Phi \approx E\Phi$$

where w is calculated from U , and the ensuing Schroedinger equation can be solved in an expansion in μ/M , because

$$w \sim \mu/MW$$

The kind of corrections obtained from such calculations is twofold. Some are still velocity independent but give higher-order terms in μ/M . Others

give correction terms explicitly dependent on the nucleon velocity. The most common of these is the spin-orbit term. Such addition gives a potential which is different in different angular momentum states and hence is not really a potential in the sense we use in this article. The use of such $L.S$ terms is, however, quite widespread, encouraged by the success of the phenomenological Marshak-Signell and Gammel-Thaler potentials which include such an expression (see Chap. IV). Some other terms, however, are even more complicated than this. There are quadratic spin-orbit potentials (see Hamada potential, Chap. IV), perhaps still in the tolerable category although they do not satisfy the requirements given in Section 1 of this chapter. Some of the correction terms, however, contain the nucleon energy explicitly. At this point the usefulness of the potential concept becomes marginal, since it does not much simplify the description of the scattering process compared to, say, a phase-shift formalism or the knowledge of the scattering amplitudes as functions of energy. In fact, an equivalent description can be constructed in terms of dispersion relations using the spectral function on the left-hand cut in the energy plane. Such a description of the scattering amplitude (see Chap. V) has also been lately referred to as the potential. Basically, these enormous extrapolations of the potential concept simply reflect the basic failure of the simple and conventional potential to account for the two-nucleon interaction. For an extensive discussion of the kind of terms one can get in such generalized potentials, see (256) and (32).

Recoil corrections are calculated by many authors. Shindo & Nishijima (275), already quoted above, get an $L.S$ term opposite to what a shell model would require for nuclei. Extensive work was done by Nakabayasi, I. Sato (193), and I. Sato (276), who used the Nambu method. They, like most workers, made an expansion in μ/M (or η/M) and used the first few terms. They found a large correction which in some cases even changed the sign of the potential. Both velocity-independent and spin-orbit terms resulted. Some consequences of this spin-orbit term in nuclear physics were calculated by Araki (277) and also by Dresner (278); the latter found it too small for the purpose, while Sato thought it large enough. See also (279) and (280).

The terminology of "nonstatic" and "nonadiabatic" corrections is somewhat loose. As an illustration, Feldman (154) showed that the "nonadiabatic, velocity-dependent" corrections of Lévy and Klein are neither nonadiabatic nor velocity dependent, inasmuch as they already appear in the static limit, although in higher order. A similar point was also made by Sugawara & Okubo (182, 183) who showed that $g^2\eta/M$ terms can be converted into g^4 terms. They also used the Fukuda scheme and calculated "nonstatic" terms up to $g^2\eta^2/M^2$ and $g^4\eta/M$ (the two are equivalent). They obtained an $L.S$ term, but also a term of the form $[V_2(\mathbf{r}), \eta^2/2M^2]$ which, they emphasized, contributes to the long-range force and changes (although by a small amount) the usual one-pion-exchange potential. They worked with both pseudoscalar and pseudovector couplings. For a numerical evaluation of their potential see Table I.

The effect of recoil in a relativistic context was discussed by Araki (281) who found it small in the nonrelativistic limit. On a scalar model, Power (282) showed that nonstatic corrections are needed to give the right phases in a Born approximation. Eder (283) also calculated corrections starting from the Bethe-Salpeter equation; he found a strong additional attraction in the fourth order. Novozhilov & Terent'ev (198), synthesizing the potential from pion-nucleon scattering, took partial recoil into account. They expanded up to η/M , arguing that η^2/M^2 terms are equivalent to higher-order static terms. Iwadare (284, 285) also calculated nonstatic corrections and found them small beyond a pion Compton wavelength, but large inside it; he gave an explicit list of expressions for the various kinds of corrections. The method of Klein & McCormick (200, 248), which constructed the potential from pion-nucleon scattering, also calculated pion-nucleon scattering corrections, some of which are also "recoil" corrections. These calculations were extended by Tzoar, Raphael & Klein (286) to include terms that are first order in nucleon momentum. They obtained an $L.S$ term which is not wholly unlike the phenomenological Marshak-Signell potential.

A startling result was presented by Gupta (126, 287). He used an S -matrix type of method to calculate the fourth-order potential, which is listed in Table I. He also arrived at the general conclusion that the usual expansion into powers of μ/M is incorrect and can furnish misleading results. This conclusion agrees with that of Charap & Fubini (15) and has also been discussed in Section 1 of this chapter. Gupta's own calculations do not use such an expansion and hence are valid to all orders of μ/M . He does make the approximation, however, of considering the nucleon momenta squared small compared to the nucleon mass. In this "nonrelativistic" approximation he derives a potential, which is given as a numerical table. Its fourth-order contribution consists only of a central part.

A third paper of Gupta's (288) calculated the $L.S$ term resulting from a scalar ρ^0 meson with a mass about twice the pion mass and found good agreement with the phenomenological $L.S$ potential of Signell, Zinn & Marshak (18).

In summary, we see that the calculation of nonstatic corrections is not a straightforward and unambiguous process. There are some who interpret this fact simply as a practical difficulty, caused by the calculations not having been carried far enough, and by the various calculational schemes being markedly different in the approximate form in which they have been used. Others, however, claim that this complexity is an eloquent demonstration that the potential concept is not necessarily the best way to describe the nucleon-nucleon interaction beyond its crudest features. As will be shown in Chapter V, the alternative approach of the dispersion relations eliminates most of the ambiguities in principle, perhaps at the cost of making the detailed calculations more complex. Whether the practical calculations resulting from dispersion relations will be more reliable than those of potential theory is, however, yet to be seen.

B. *Radiative corrections.*—Radiative corrections consist of the effects of virtual pions emitted and reabsorbed by the same nucleon. Such correction graphs can be drawn to correspond to any of the graphs we have discussed. The radiation corrections to the graphs corresponding to the second-order potential are particularly simple to calculate. It can be shown (289) that at large distances they alter the second-order potential only inasmuch as the coupling constant has to be replaced by the renormalized coupling constant and the bare pion mass by the renormalized pion mass. Thus, formally, one gets the well-known second-order potential even if radiative corrections are included.

For the fourth-order potential the situation is different. Here the radiative corrections change the form of the potential as well as its strength. There are several calculations of the fourth-order radiative corrections. Ruderman (290), e.g., calculated them for pseudoscalar coupling and concluded that while they are large, they affect the potential mostly at small distances where higher-order effects are operative anyway. Brueckner (291) also calculated radiative corrections to demonstrate, using a Tamm-Dancoff type formalism, that they can bring about a suppression of pair effects and, hence, account for the small S state in the pion-nucleon interaction (see also Sect. 1 of this chapter).

Radiative corrections were also included in the type of calculations where the nucleon-nucleon scattering is composed of two pion-nucleon scattering diagrams (see Sect. 2-B of this chapter), but here they are submerged in many other effects so that it is difficult to estimate their magnitude [see e.g. the KMO potential (201, 202)]. For other information on radiative corrections see also (190) and (292).

C. *Higher-order corrections.*—There are good reasons for not attempting the calculation of higher than fourth-order potentials. First, the calculations become prohibitively laborious and hence only certain "representative" graphs can be treated. Second, the range of the sixth-order potential is already small enough so that the potential is mostly (but not wholly) blotted out by the repulsive core, the origin of which is unknown anyway. Finally, the difference in the ranges of the sixth- and eighth-order potentials is quite small so that the sixth-order potential would be dominant only over a very small range of r .

Accordingly, there are no available calculations aiming at a good quantitative evaluation of these higher-order potentials. The calculations are usually qualitative and are designed to exhibit either some general property of nuclear forces or the reliability of the lower-order potentials. Thus, Werle (293) concluded from his relativistic calculations that these higher-order effects always appear in conjunction with the relativistic corrections to the lower-order static potential. Henley & Ruderman (194) stated that the neglect of these higher-order terms affects the reliability of the lower-order potential also. Klein (128, 129) calculated some higher-order graphs

to study the convergence properties of the coupling constant expansion (see Sect. 1 of this chapter). Machida & Senba (294) were concerned with the range of the sixth-order potential but found it small enough so that the second- and fourth-order potentials should be reliable beyond one fermi or so.

D. *Multiple-scattering correction*.—The virtual mesons produced in the nucleon-nucleon scattering processes can be scattered by the nucleons before they are finally absorbed. Such multiple-scattering corrections have been evaluated by Brueckner & Watson (185). Sometimes the distinction between the multiple-scattering and radiation corrections is not clear, particularly when the scattering is by one of the two nucleons only. Brueckner & Watson found that multiple scattering by both nucleons is more important but is restricted to small distances, those below a fermi.

Calculations of multiple-scattering effects for a scalar pair theory have been performed by Hasegawa & Azuma (295, 296).

E. *Miscellaneous calculations*.—The effect of the pion-pion interaction on nucleon-nucleon scattering has been emphasized recently in connection with the dispersion-relation techniques; however, it was investigated to some extent long before dispersion relations became a vogue. For instance, Bonnevay (297) showed that the interaction of the two intermediate mesons in the fourth-order graph implies changes in the coupling constant of this graph. This implication tends to support Lévy, who used two different coupling constants in his fourth-order calculations. Pomeranchuk (298) investigated the effect of the meson-meson interaction on the pion-nucleon vertex function in nucleon-nucleon scattering and found it negligible.

The nucleon-nucleon potential has been discussed extensively in terms of various isobar models where the excited states of the nucleon are taken into account in some simplified way. A meson-theoretical version of such a theory was given by Matsumoto, Hamada & Sugawara (299). They introduced an additional Hamiltonian describing the spin $\frac{3}{2}$ excited state and calculated up to fourth order. They found that while the ranges do not change very much, the isobar effect adds an immense central and a minute tensor potential.

A general discussion of the velocity-dependent features of nuclear potentials was given by Breit (256), using a classical field formalism. A "static" limit is taken. In addition to the usual $L.S$ terms he also found a term proportional to $(S_{12})^2$. Velocity-dependent core radii are also a possibility. The $L.S$ term is different in even and odd states.

Pekar (300) has investigated the question whether there exist stationary quantum states of two nucleons interacting through pseudoscalar pions. The answer is in the negative for pseudovector coupling, and the proof does not depend on perturbation theory.

In all the theories discussed so far in this report, it was assumed that the nucleon-nucleon interaction is due to the direct interaction of nucleons and pions. Ferrari & Fonda (301) considered the possibility of an intermediate

boson between the nucleon and the pion. This extra leeway could account for the different core radii in singlet and triplet states. Pseudovector coupling is assumed between the nucleon and the intermediate boson, and the coupling between the intermediate boson and the pion is taken to be direct. Ferrari & Fonda use $5 m_\pi$ for the mass of the intermediary.

Among the many papers on the potential theory of nucleon-nucleon scattering, one of the remarkable ones is by Charon (302) who tried to describe the nucleon-nucleon interaction in terms of purely electrodynamic forces between charges moving almost with the velocity of light.

IV. COMPARISON OF THE MESON-THEORETIC POTENTIALS WITH EXPERIMENT

The conspicuous lack of agreement that was exposed in Chapter III as to how the "potential" should be computed from meson theory, and the uncertainty as to how these calculations are to be joined to an inner phenomenological region, make any straightforward comparison with experiment impossible. We will therefore follow the Taketani (12) program already referred to, by first establishing the validity of the one-pion-exchange part of the interaction and only then attempting to see what can be said about the inner regions.

1. PROOF OF THE VALIDITY OF THE ONE-PION-EXCHANGE INTERACTION

The success achieved in establishing the validity of the one-pion-exchange potential (OPEP) at large distances through 1956 is discussed in detail in a useful review by Iwadare, Otsuki, Tamagaki, and Watari (303). The clearest evidence comes from the sign and magnitude of the deuteron quadrupole moment and triplet effective range. That the sign of the quadrupole moment shows the pion to be a pseudoscalar rather than a vector particle had already been noted (304). Lopes & Feynman (305) failed to obtain agreement with the quadrupole moment and triplet effective range because they took their value of the coupling constant from the singlet scattering (which we shall see below is unreliable). Iwadare *et al.* (306, 307) integrated the deuteron wave function inward up to one-pion Compton wavelength using the one-pion-exchange potential and then used an arbitrary but smooth wavefunction inside. Because of the loose structure of the deuteron, Q and 3r_e are most sensitive to the outer part of the wave function; and Iwadare *et al.* found that the experimental values can be fitted only if the pion-nucleon coupling constant lies in the range $0.065 < f^2 < 0.09$, in good agreement with the value determined from pion-nucleon scattering. This result is reasonably insensitive to the magnitude or sign of the inner central part of the potential, while the wave functions which reproduce the experimental values show that the tensor potential must remain strongly attractive in the two-pion-exchange region. They noted that Lévy (130) failed to fit the quadrupole moment because he used a coupling constant of $f^2 = 0.053$, while the fits obtained by

Brueckner & Watson (185) and Gartenhaus (189) are consistent with their results.

One interesting result of this type of calculation is that the percentage D state predicted by such models is always greater than 5 per cent, in contrast to the nonrelativistic calculation of 4 per cent from the magnetic moment. Mesonic corrections could certainly accommodate a 7 per cent D state, but there is no general agreement even as to the sign of these corrections. Both the photodisintegration of the deuteron [see e.g. (308)] and the coherent photoproduction of neutral pions from deuterium (309) favor this high value. Unfortunately we have no space to discuss this interesting question here.

Having established that the one-pion-exchange potential is in agreement with the triplet even state, Iwadare *et al.* (306, 310) discuss the 1S_0 scattering length and effective range. A phenomenological Yukawa potential requires a meson mass much larger than the experimental meson mass to fit these parameters (311 to 315). If the experimental meson mass is used, the coupling constant must be 0.2, and the effective range is 50 per cent too large (305). These results are, however, consistent with the pion potentials, since all calculations agree that two-pion exchange gives a strongly attractive force in the singlet even state, which is needed to obtain agreement with the experimental 1a and 1r_e when a one-pion potential with the meson mass and $f^2=0.08$ is present. The authors noted that if there is also a short-range repulsion, the attractive region must increase in strength and decrease in range if the experimental numbers are still to be reproduced. Going to the limit indicated, they find that f^2 must be greater than 0.07, whatever happens in the multipion and phenomenological regions. Earlier work on the low-energy parameters using models with one-pion-exchange tails was done by Komoda & Sasaki (316), and by Taketani, Machida & Onuma (317); more recent calculations with such models, by Sugawara (318) and Young & Cutkosky (319). The effect of the charged-neutral mass difference on the apparent charge dependence of the 1S_0 state will be discussed in Chapter V.

The inclusion of one-pion-exchange effects in phenomenological phase-shift analyses, which was discussed in detail in Part I, has greatly increased the strength of the evidence for validity of the meson theory of the long-range part of the nuclear force. The idea arose from a study of the analytic properties of scattering amplitudes, but it seems more appropriate to discuss the results here rather than in Chapter V. In fact, Breit & Hull (320) showed that, for one-pion exchange, the appropriate relativistic modification of the calculation of scattering by the potential leads to formulae identical to those used by Czipfra *et al.* (321). Breit & Hull discussed the effective localization of the interaction in space for different angular momentum states.

The simplest application which has been made of the one-pion-exchange pole in the scattering amplitude is to determine f^2 by extrapolation of neutron-proton differential cross sections (322). All such extrapolations

(323, 324) except one (325) have given too low a value for the coupling constant as compared to the usually accepted value determined from pion-nucleon scattering. Where scattering data are sufficiently extensive to allow a phase-shift analysis, inclusion of the pole term not only gives a good value for the coupling constant, but also helps reduce ambiguities in the phase-shift analysis (321, 326, 327). An interesting variant of the method used by Signell (328) shows that the pion mass can also be measured using nucleon-nucleon elastic scattering. More detailed information is obtained by invoking the continuity of phase shifts as the energy is varied and by using all the scattering data simultaneously. By this means Breit *et al.* (115) have obtained three important results about the one-pion-exchange potential. First, they showed that the same value of G^2 fits both n - p and p - p data (329). Second, the best value of the ratio of the $\phi^{(1)} \cdot \phi^{(2)}$ term to the tensor term is that predicted by this potential. Finally (except for 1G_4 , as expected from the strong two-pion attraction already mentioned), they found that no long-range interaction can be added to this potential for $L > 4$ states without lessening the agreement with experiment (330). The statistical accuracy of these results is low, but because of the large amount of data used, these findings provided suggestive evidence for the one-pion-exchange potential.

The above survey makes it clear that a combination of experimentally independent facts shows that pion theory can quantitatively predict the longest-range part of the nuclear interaction and that the first part of the Taketani program has succeeded. The study of the intermediate region has produced no such clear-cut results, partly for experimental reasons. We still have no experimentally unique phase-shift analyses at our disposal at any energy, and before 1959 or 1960 the only reasonably complete set of experimental data available was at 310 Mev. Two quite differently motivated attacks on the problem resulted. Since the Japanese school did not believe that the potential concept could be trusted above 100 or at the most 150 Mev, they remained, in the main, content with attempting to show that existing cross-section (and later polarization) data were consistent with some of the calculations of the potential in the intermediate region. People more closely connected with the phenomenological program described in Chapter II tended to take the meson-theoretic potentials more literally and to insist that they satisfy the rigid quantitative criteria used in evaluating phenomenological models. They had to rely more strongly, therefore, on the phenomenological elements in their potentials and tended to introduce these without too much theoretical justification. We will now review the relevant calculations.

2. MESON-POTENTIAL CALCULATIONS AT HIGH ENERGY

The 3P phase shifts in proton-proton scattering below 20 Mev offer at first sight a promising quantitative test of the triplet even potential. Unfortunately, in the region below 4 Mev where these shifts can be approximated

by a single equivalent P phase (331), they are now known to be smaller than vacuum-polarization effects (332). Therefore, the original attempt to analyze them made by Otsuki & Tamagaki (333) must be disregarded. Recently, Otsuki, Taketani, Tamagaki & Watari (334) re-examined this question and showed that the 4- to 20-Mev odd-state p - p scattering does give evidence for the repulsive one-pion-exchange-potential tail. As Breit & Hull (320) emphasized, P waves are not completely shielded from the inner regions by the centrifugal barrier and cannot be used for a quantitative test of the one-pion-exchange potential at any energy. Published phase shifts (335) below 4 Mev are in significant disagreement with the "Japanese pion potential" (336). Unfortunately, the data have recently been revised for experimental reasons (337), so the whole question will have to be re-examined. Above 4 Mev, the equivalent P phase approximation is inapplicable, so we are faced with the fourfold Clementel-Villi ambiguity discussed in Part I and with a large uncertainty in the 1S_0 phase. Fortunately (see Chap. V), Riazuddin (338) has been able to prove that the particular set of P phases favored by the pion theorists in the 4- to 20-Mev range are the only ones compatible with the nucleon-nucleon dispersion relations. Consequently, the discussions of Otsuki & Fujii (339, 340), Iwadare *et al.* (341), and MacGregor (342) are still relevant, and the pion theory is again confirmed, qualitatively. We prefer not to give a quantitative discussion in the absence of the triple scattering or spin correlation experiments needed to give a good value of the 1S_0 phase in this range.

Comparison of the TMO potential with n - p and p - p differential cross sections up to 100 Mev has been given by Fujii *et al.* (343, 344) and Matsumoto & Watari (345), and with n - p polarization at 100 Mev by Iwadare *et al.* (346); similar comparisons for the Brueckner-Watson potential are given by Brueckner (347). The most charitable description of the agreement would be to call it semi-quantitative; and without comparing them to recent measurements, particularly depolarization, we can only say that these potentials are not known to be unreasonable.

Turning now to cases where more detailed calculations have been made, we can make more definite statements. The Lévy potential (in the form $V_a + \lambda V_d$ with λ adjustable) is in fair agreement with the low-energy parameters if one uses different singlet and triplet core radii, according to Jastrow (348). However, neither Blatt & Kalos (349) nor Preston & Shapiro (350) were able to obtain acceptable results when the experimental errors were taken seriously. Martin & Verlet (351) showed that the Lévy potential agrees with 18-Mev proton-proton scattering [this is consistent with the analysis of Iwadare *et al.* (341)] but already fails at as low energies as 32 Mev. Gelernter (352) and Wertheim *et al.* (353) agreed that the Lévy potential is hopeless at higher energies. Similarly, Gammel & Thaler (354) found that the Gartenhaus potential, when taken literally, bore little relation to the high-energy data, but they noted that this could well be true

because of the unrealistic calculations in the inner regions. This lack of realism is obvious when one realizes that the Gartenhaus potential predicts bound P states!

3. THE $L.S$ CONTROVERSY

The Gartenhaus potential did lead to a most interesting development when Signell & Marshak (16) found that by adding to it a purely phenomenological $L.S$ potential they could account for all proton-proton data up to 150 Mev. Both this model and that of Gammel & Thaler (84, 85, 86) provoked strong criticism (see next paragraph) on the grounds that there was no warrant in meson theory for the $L.S$ term of either this range or strength, and in the case of Signell-Marshak for the bound P states just mentioned. Signell & Marshak (17) eliminated the second objection by modifying the inner regions of the Gartenhaus potential, but this did not help the disagreement at 200 and 300 Mev (355); however, shortening the range of the $L.S$ force to an acceptable value improved the situation considerably without destroying the agreement previously obtained at lower energies (18).

The papers by Otsuki *et al.* (356), Otsuki (357), Watari (358), and Tamagaki (359), followed by the more detailed analysis of Hamada *et al.* (360, 361) in which the $L.S$ models are criticized, are of primary importance in understanding the position the meson theory of nuclear forces had reached by 1958. They emphasized in 1956 that there was already strong evidence that to arbitrarily ignore the one-pion-exchange potential in the nuclear force problem might be dangerous. The analyses of Hamada *et al.* (360, 361) are particularly interesting in their demonstration of how far it is possible to disentangle a complicated experimental situation by making full use of the leads given by the pion potential. These analyses anticipate the power that has come with the modified phase-shift analysis. These authors concluded that, within the rather large uncertainties of the intermediate region, it is unnecessary to use an $L.S$ force to explain the 90- and 150-Mev proton-proton data. However, they were aware that their conclusion depended on the depolarization (D parameter) at 150 Mev being very negative at large angles. "If it is decisively found that D is positive, it may mean something not so simple for the pion theory of nuclear forces" (361). The reason for this requirement has been clarified by Nigam (362, 363). Depolarization is particularly sensitive to the 3P_0 phase, and a large positive value of this phase shift makes the depolarization very negative at large angles. The long-range tensor force predicts a large positive 3P_0 phase, and in a P state this cannot be cut down much by any core of reasonable size. The repulsive $L.S$ force now in use is of sufficiently short range to leave 3P_0 positive at low energy but causes it to change sign a little above 150 Mev to achieve agreement with the data at 210 and 310 Mev. It has now been reported (364) that the depolarization is close to zero at large angles in 150-Mev proton-proton scattering. Therefore, the analysis of Hamada *et al.* (361) just quoted establishes

the existence of a strong spin-orbit, or at least nonstatic, effect at 150 Mev; this can also be seen at 100 Mev.

4. SEMIPHENOMENOLOGICAL POTENTIAL MODELS

Still better fits to the proton-proton data have been obtained recently by Bryan (19), and to both neutron-proton and proton-proton data by Hamada (20, 21). These models satisfy the requirement of using the one-pion-exchange potential for the long-range part and have shorter-range parts whose form, at least, is suggested by meson theory, though the parameters of this middle region are treated phenomenologically. They include, of course, an $L.S$ force; and Hamada also claimed to find some evidence for a term quadratic in L , called $Q = \frac{1}{2}[(L \cdot \sigma^{(1)})(L \cdot \sigma^{(2)}) + (L \cdot \sigma^{(2)})(L \cdot \sigma^{(1)})]$. These models tend to be very singular just outside the core; so replacing this region and the core by an energy-independent boundary condition, as Lomon (22) and more recently Saylor, Bryan & Marshak (365) did, may achieve the same results more simply. An alternative suggested by Moszkowski & Scott (97) which has advantages in nuclear structure calculations is to replace the boundary condition by a free-particle wave function inside the boundary; it is perhaps capable of similar predictions (366).

We see that the followers of the Taketani program and the semi-phenomenologists have converged to the point where the results achieved by either group will be useful to both. The remaining theoretical problems are (a) to show that those few calculations which predict a strong enough $L.S$ force [e.g. (286)] are unambiguous and (b) to show in detail that predictions for the middle region are consistent with the semi-phenomenology of this region. These are undoubtedly interesting and useful projects and probably could eventually be achieved by one or another of the methods discussed in Chapter III. We believe, however, that the approach discussed in the next chapter is clearer in principle and perhaps even easier to apply. We therefore expect that the solution will come from that direction.

V. CALCULATIONS OF NUCLEON-NUCLEON SCATTERING FROM ANALYTICITY AND UNITARITY

During the latter half of the period under review, a new approach to problems involving strong interactions has been developing. The objective of this approach is to compute the scattering matrices for any process involving strongly interacting particles directly from the analytic properties of these matrices (which are connected to causality) and from unitarity (conservation of probability), using only the general postulates of quantum field theory and a knowledge of the mass spectrum of the strongly interacting particles. This possibility was first mentioned by Gell-Mann (367) and is now becoming an actuality. Current methods use analytic properties derived (to all orders) from renormalized perturbation theory, and they could regenerate that series without ever invoking infinite quantities. But they can

probably be used where perturbation theory does not converge. Further, they can be used to construct a consistent covariant phenomenology in which the phenomenological elements can be systematically reduced as the theoretical calculations become more complete. Whether or not this approach succeeds in providing a complete dynamical theory of the strong interactions, we think it has already proved such a useful framework for discussion of these problems that future work is bound to be increasingly more often presented in this language. We therefore feel justified in presenting a reasonably complete qualitative discussion of the method, even though quantitative comparison with experiment has not yet been carried through for many interesting questions.

The general reader will find a review recently given by Mandelstam (368) a useful starting point for studying this subject. We rely in what follows on a preliminary talk given by him along these lines. Traditionally, the starting point of quantum field theories has been the quantization of the classical local Lagrangian. Because of the uncertainty principle, infinite quantities necessarily appear in the theory and have to be removed by the renormalization of the "bare" masses and coupling constants which appear in the original Lagrangian to the physically observed values. If this procedure is carried out consistently and it is required that spacelike separated operators commute (the causality requirement), the Lagrangian proves to have a unique form once the masses and quantum numbers of the particles are specified. It is therefore plausible that the finite results of the renormalized theory should be obtainable from the general postulates of quantum field theory and the mass spectrum and quantum numbers of the particles without the introduction of infinite quantities. The problem is to find a method. We note that if this general philosophy is correct, there is only one theory for pseudoscalar pions interacting with spin- $\frac{1}{2}$ nucleons; hence there is no place within this framework for a difference between pseudoscalar and pseudovector coupling.

1. GENERAL THEORY OF MANDELSTAM REPRESENTATION

A. *The relationship between analyticity and causality.*—A useful way to impose the causality requirement on the theory is by requiring the transition matrices to be boundary values of the appropriate analytic functions of the energy variables. That analyticity should be connected with causality can be seen on quite general grounds. A causal system is one in which a knowledge of its behavior over a finite (but arbitrarily small) period of time allows a prediction of its behavior at all other times. In classical theories this is accomplished by specifying the behavior in terms of differential equations, but the uncertainty principle prevents us from using such a differential description in quantum field theory. However, an analytic function is completely determined over its entire region of analyticity from a knowledge of any finite part; that this is true clearly offers an alternative mathematical method for building causality into the theory. The basic connection between

the relativistic causality requirement and analyticity originates because a signal cannot propagate faster than light. Hence, a scattering amplitude is zero up to some definite time; and when this is translated into the frequency dependence of the amplitude, one can immediately write down a dispersion relation for the real part of the scattering amplitude in terms of an integral over the total cross section (imaginary part). For light, this process leads directly to the dispersion relation of Kronig (369) and Kramers (370). That causality might imply a similar type of dispersion relation in quantum field theory was shown by Karplus & Rudermann (371) and by Goldberger (372, 373); a rigorous proof was given by Bogoliubov (374) and Symanzik (375). Since these proofs use all the postulates of field theory, it is not foolish to hope that a theory stated in terms of dispersion relations may prove sufficiently restrictive to make unique predictions.

Although the one-dimensional dispersion relations offer powerful restrictions on scattering amplitudes and their use led to much interesting work, it soon became clear that by themselves they could not provide a complete theory of the strong interactions. These dispersion relations focused attention, however, on the enormous amount of physical information which could be extracted from the realization that scattering amplitudes are analytic functions of the energy with singularities whose presence and position could be determined from a knowledge of the mass spectrum and quantum numbers of the strongly interacting particles. Since the function is completely determined, if the positions and strengths of the singularities of an analytic function are known, the problem becomes how to compute these. Further, since the behavior of an analytic function in the neighborhood of a singularity is likely to be dominated by that singularity, this approach also suggests a natural approximation scheme which starts with the nearest singularities to the region of interest and progressively refines the calculation by including more distant singularities in a systematic way.

B. The Mandelstam representation.—The most important step in this program was taken by Mandelstam (24, 25) who considered the analytic properties of two-particle scattering amplitudes. Such amplitudes are functions of only two relativistic invariants, the invariant energy and the invariant momentum transfer. The nearest singularities to the low-energy physical region are poles arising from single-particle states with the appropriate quantum numbers, and the next nearest singularities are again due to two-particle scattering states. The crucial step taken by Mandelstam was to note that the discontinuities across these two-particle singularities, the imaginary part of the two-particle scattering amplitude, are given by the unitarity condition in terms of the two-particle amplitudes. Therefore, at this level of approximation, the analyticity requirements give us integral equations for the scattering amplitudes which can be treated as dynamical equations defining them.

To bring out clearly the general features of the Mandelstam approach, we shall discuss in detail a simplified model, already used in much the same way

by Cini & Fubini (376). This useful paper is recommended to the reader for a more systematic treatment than we have space for here. We consider a spinless particle of mass m (which we will call M) which can make a (real or virtual) transition to a particle of mass r (called R) and a particle of mass v (called V) with probability G . We consider first a particular Feynman diagram related to the scattering amplitude $(MM|MM)$ and show how this diagram can be written in terms of a double spectral representation by using the unitarity condition. Then by appropriate specification of the particles we can use this general result to discuss nucleon-nucleon scattering. The diagram of interest is given in Figure 9. Here the four-momenta $P = (p_0, \mathbf{p})$ are

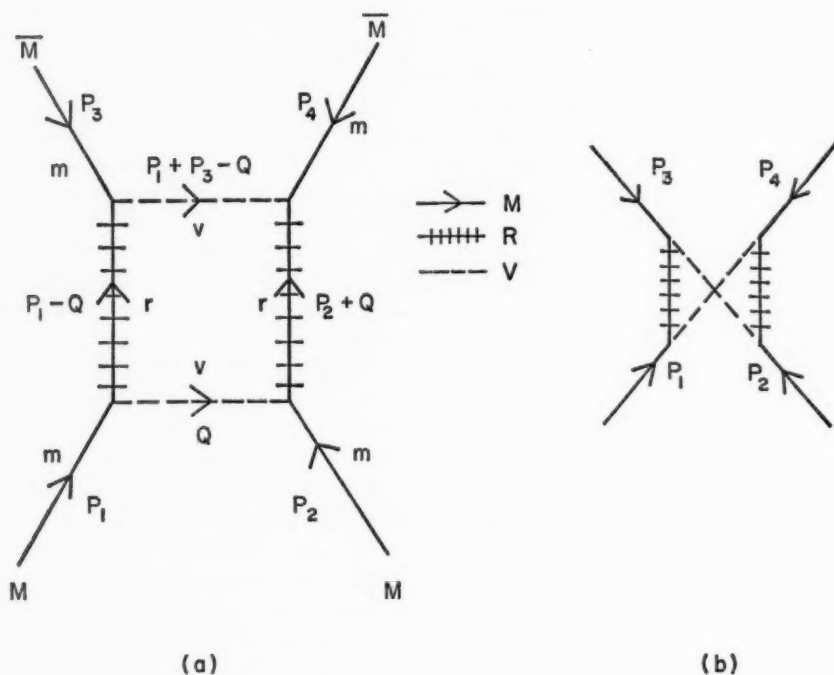


FIG. 9

defined to satisfy $P^2 = p_0^2 - \mathbf{p}^2$, and we use the Feynman rule that a particle can be changed to an antiparticle by reversing the sign of P . Over-all energy-momentum conservation gives $P_1 + P_2 + P_3 + P_4 = 0$. This single diagram then describes three scattering amplitudes:

$$MM \text{ (particle-particle) scattering } T_I = \langle M(P_1)M(P_2) | M(-P_3)M(-P_4) \rangle$$

$$M\bar{M} \text{ (particle-antiparticle) scattering } T_{II} = \langle M(P_1)\bar{M}(P_3) | M(-P_2)\bar{M}(-P_4) \rangle$$

$$\bar{M}M \text{ (particle-antiparticle) scattering } T_{III} = \langle \bar{M}(P_3)M(P_2) | \bar{M}(-P_4)M(-P_1) \rangle$$

The invariant energy variables in the three channels are defined to be

$$\text{I: } s = (P_1 + P_2)^2 = (-P_3 - P_4)^2$$

$$\text{II: } t = (P_1 + P_3)^2 = (-P_2 - P_4)^2$$

$$\text{III: } \bar{t} = (P_2 + P_3)^2 = (-P_1 - P_4)^2$$

These are not all independent because over-all energy-momentum conservation gives $s + t + \bar{t} = 4m^2$.

Consider, in particular, MM scattering in the center-of-mass system:

$$P_1 = (p_0, \mathbf{p}'), \quad P_2 = (p_0, -\mathbf{p}'), \quad P_3 = (-p_0, \mathbf{p}''), \quad P_4 = (-p_0, -\mathbf{p}'')$$

with

$$p_0^2 = \mathbf{p}^2 + m^2, \quad \mathbf{p}' \cdot \mathbf{p}'' = p^2 \cos \theta$$

Then $s = 4(p^2 + m^2)$, $t = -2p^2(1 - \cos \theta)$, $\bar{t} = -2p^2(1 + \cos \theta)$. Hence, $T_I(s, t, \bar{t}) = (MM | MM)$ describes particle-particle scattering for $s > 4m^2$ and t and \bar{t} lying between 0 and $-4p^2$. For T_{II} (or T_{III}) we find that $t(\bar{t})$ must be greater than $4m^2$ while s and $\bar{t}(t)$ must lie between 0 and $-4p^2$. Since all three processes are described by the same Feynman diagram, we can say that one function $T(s, t, \bar{t})$ describes them all for appropriate (disjoint) ranges of the variables. This apparently trivial fact about Feynman diagrams, which clearly holds to all orders in perturbation theory, is called the general substitution rule. If we boldly assert that it is also true for physical scattering amplitudes, it still seems inconsequential because the range of variables is disjoint. However, if T is an analytic function of the variables s, t, \bar{t} , and we know the location of the singularities, we can extend the function from one physical region to the other and establish a coupling between different processes. We will now show how (for this special case) the unitarity condition allows us to make this extension.

Consider first the process in channel II, and assume for the moment that the only intermediate state is that indicated in the diagram, i.e. $M\bar{M}$ annihilation into two V particles. We define the kinematical variables

$$P_1 = (E_p, \mathbf{p}'), \quad P_3 = (E_p, -\mathbf{p}'), \quad P_2 = (-E_p, \mathbf{p}''), \quad P_4 = (-E_p, -\mathbf{p}'')$$

$$Q = (\omega_q, \mathbf{q}), \quad P_1 + P_3 - Q = (\omega_q, -\mathbf{q})$$

$$E_p^2 = P^2 + m^2 = \omega_q^2 = q^2 + v^2 = \frac{1}{2}t; \quad s = -(\mathbf{p}' + \mathbf{p}'')^2$$

The unitarity condition is then simply

$$\begin{aligned} I(t, s) &= \text{Im} \langle M\bar{M}(\mathbf{p}') | M\bar{M}(\mathbf{p}'') \rangle \\ &= \frac{-1}{16\pi^4} \int d^3q \delta(E_p - \omega_q) \langle M\bar{M}(\mathbf{p}') | V(\mathbf{q})V(\mathbf{p}' - \mathbf{q}) \rangle^* \langle V(\mathbf{q})V(\mathbf{p}'' + \mathbf{q}) | M\bar{M}(\mathbf{p}'') \rangle \end{aligned}$$

In this same approximation, the amplitude for $M\bar{M}$ to VV annihilation is simply

$$\langle M\bar{M}(\mathbf{p}') | V(\mathbf{q})V(\mathbf{p}' - \mathbf{q}) \rangle = \frac{G^2}{r^2 - (P_1 - Q)^2} = \frac{G^2}{r^2 + p^2 + q^2 - 2\mathbf{p}' \cdot \mathbf{q}}$$

Hence

$$I(t, s) = -\frac{G^4}{16\pi^2 t} \int \frac{d^3 q \delta(E_p - \omega_q)}{(r^2 + p^2 + q^2 - 2\mathbf{p}' \cdot \mathbf{q})(r^2 + p^2 + q^2 + 2\mathbf{p}'' \cdot \mathbf{q})}$$

Since the process exists only if t exceeds $4v^2$, we can write down the spectral representation:

$$T_{II}(t, s) = \frac{1}{\pi} \int_{4v^2}^{\infty} \frac{I(t', s) dt'}{t' - t}$$

[The operator $\int dt'/(t' - t)$ is as usual interpreted to mean $P \int dt'/(t' - t) + i\pi \delta(t' - t)$.] To find the dependence on s , we must now carry out the integration on \mathbf{q} .

If we combine denominators by the usual Feynman trick, and carry out the integration over the magnitude of \mathbf{q} , we obtain

$$I(t, s) = -\frac{q\omega_q}{16\pi^2 t} \int_0^1 dx \frac{d\Omega_q}{D^2}$$

with

$$D = r^2 + p^2 + q^2 - 2[\mathbf{p}'x - \mathbf{p}''(1-x)] \cdot \mathbf{q}$$

Taking as our axis of integration $A(x) = \mathbf{p}'x - \mathbf{p}''(1-x)$ and noting that

$$A^2 = p^2[x^2 + (1-x)^2] - 2x(1-x)\mathbf{p}' \cdot \mathbf{p}'' = p^2 + x(1-x)s$$

the angular integration gives

$$I(t, s) = -\frac{q}{16\pi\sqrt{t}} \int_0^1 \frac{dx}{F(x)}$$

with

$$\begin{aligned} F(x) &= (r^2 + p^2 + q^2)^2 - 4p^2q^2 - 4q^2sx(1-x) \\ &= a - 4q^2sx(1-x) = 4(r^2 + v^2 + m^2)^2 + (t - 4v^2)4r^2 - (t - 4v^2)sx(1-x) \end{aligned}$$

The integration is elementary and yields

$$\begin{aligned} \int_0^1 \frac{dx}{F(x)} &= \frac{1}{2q\sqrt{s(a - q^2s)}} \tan^{-1} \frac{2q\sqrt{s(a - q^2s)}}{a - 2q^2s} \\ &= \frac{1}{2q\sqrt{s(a - q^2s)}} \left[\frac{\pi}{2} - \tan^{-1} \frac{a - 2q^2s}{2q\sqrt{s(a - q^2s)}} \right] \end{aligned}$$

We note that the first form is real and finite whether the square root is real or imaginary, but that the second develops an imaginary part when the square root is imaginary. To see which form to take, we look at $F(x)$. Since $t > 4v^2$ in the integral where we use I , a is positive definite. We conclude that $F(x)$ never vanishes when $s=0$, and hence that there is no singularity at this root of $s(a - q^2s)=0$. Therefore we can write a spectral representation for $I(t, s)$ as a function of s with a branch cut for s greater than a/q^2 . We determine the sign of the weight function by evaluating the integral for s less than a/q^2 , and find by elementary integration that

$$\int_0^1 \frac{dx}{a - 4q^2sx(1-x)} = \int_{a/q^2}^{\infty} \frac{ds'}{(s' - s)\sqrt{4q^2s'(q^2s' - a)}}$$

Therefore we can write that

$$T_{II}(t, s) = \frac{1}{\pi^2} \int_{4r^2}^{\infty} ds' \int_{4v^2}^{\infty} dt' \frac{B(s', t')}{(s' - s)(t' - t)}$$

with

$$B(s', t') = -G^4/16\sqrt{t'}([4q^2s' - a(t')])^{1/2}$$

for

$$(t' - 4v^2)(s' - 4r^2) \geq 4(r^2 + v^2 - m^2)^2$$

and $B(s', t') = 0$ otherwise.

Let us think a little about this result. If we had started out to calculate $T_I(s, t)$ instead of T_{II} , we would have had to apply the unitarity condition for the process $(MM|RR)$ instead of for $(M\bar{M}|VV)$. Hence we would have started with the spectral representation

$$T_I(s, t) = \frac{1}{\pi} \int_{4r^2}^{\infty} ds' \frac{Im \langle MM|RR \rangle ds'}{s' - s}$$

By applying the unitarity condition in an analogous way, it is clear that (since this is just the same problem with the roles of r and v , s and t reversed) we would end up with the same result. This suggests the rule [which has now been proved to all orders in perturbation theory for the processes considered in this article (26)] that the two-particle elastic scattering amplitude satisfies a double spectral representation (the Mandelstam representation) in the energy invariants for the three channels given above, with branch cuts starting at the lowest mass value consistent with the quantum numbers in that channel. If we assume that the lowest state of MM is RR , and the the lowest state of $M\bar{M}$ is VV , this rule tells us that $T(s, t, \bar{t})$ satisfies the representation

$$\begin{aligned} T(s, t, \bar{t}) = & \frac{1}{\pi^2} \int_{(2r)^2}^{\infty} ds' \int_{(2v)^2}^{\infty} dt' \frac{A_{st}(s', t')}{(s' - s)(t' - t)} \\ & + \frac{1}{\pi^2} \int_{(2r)^2}^{\infty} ds' \int_{(2v)^2}^{\infty} dt' \frac{A_{s\bar{t}}(s', \bar{t})}{(s' - s)(\bar{t}' - \bar{t})} \\ & + \frac{1}{\pi^2} \int_{(2v)^2}^{\infty} dt' \int_{(2r)^2}^{\infty} d\bar{t}' \frac{A_{t\bar{t}}(s', t')}{(t' - t)(\bar{t}' - \bar{t})} \end{aligned}$$

How is this general result related to the calculation we have just made? We see that we have calculated the first term and found that the lower limits are reached only as both s' and t' approach infinity; A_{st} is actually nonzero only inside the bounding curve given above. Since this curve depends only on kinematics, our result is generally valid (for the equal mass case). We can easily obtain the second term in the representation by noting that if we had considered \bar{t} the energy variable and s the momentum transfer, the result

would be the same with $t \rightarrow \bar{t}$ (i.e., $A_{st} = A_{s\bar{t}}$ in this case). To obtain the third term, we may consider t to be the energy variable as before but take the momentum transfer to be $\bar{t} = -(p' - p'')^2$, which is equivalent to computing the diagram in Figure 9b. For this case we see that the calculation goes through as before, but that the lower limit on the $d\bar{t}'$ integration is $(2r)^2$ rather than $(2v)^2$. Hence if $r^2 < v^2$, the Mandelstam representation as given is not valid; this is called an "anomalous threshold." However, as has been proved rigorously by Mandelstam (377), it is possible to start from the case $r^2 > v^2$ and, by making the appropriate analytic continuation in r^2 , obtain an unambiguous result for the contribution between r^2 and v^2 . We note also that if $m^2 > r^2$ or v^2 , $s = 4r^2$ or $t = 4v^2$ lies below the physical threshold for the processes $(MM|RR)$ or $(M\bar{M}|VV)$, so that the use we have made of the unitarity condition requires justification in this region; again the same proof (377) suffices. To complete our discussion of Figure 9, we rewrite the contribution of this diagram in terms of the variables appropriate to MM scattering, i.e., p^2 and $\cos \theta$.

$$\begin{aligned}
 T_{MM}(p^2, \cos \theta) = & \frac{1}{\pi^2} \int_0^\infty dp'^2 \int_{4v^2}^\infty d\bar{t}' \frac{B[4(p'^2 + m^2), t']}{(p'^2 - p^2)[t' + 2p^2(1 - \cos \theta)]} \\
 & + \frac{1}{\pi^2} \int_0^\infty dp' \int_{4v^2}^\infty d\bar{t}' \frac{B[4(p'^2 + m^2), t']}{(p'^2 - p^2)[\bar{t} + 2p^2(1 + \cos \theta)]} \\
 & + \frac{1}{\pi^2} \int_{4v^2}^\infty dt' \int_{4r^2}^\infty d\bar{t}' \frac{B(\bar{t}', t')}{[\bar{t}' + 2p^2(1 + \cos \theta)][t' + 2p^2(1 - \cos \theta)]}
 \end{aligned}$$

We have already noted that this expression will be generally valid if we replace B by the three real weight functions A_{st} , $A_{s\bar{t}}$, and $A_{t\bar{t}}$. Suppose for the moment that we know the $(M\bar{M}|VV)$ amplitude and that this is the only important intermediate state in the process. Then, as we saw above, we can immediately write down a spectral representation for the dependence of this amplitude on t and \bar{t} simply by using the unitarity condition. Hence the t and \bar{t} dependence of the A 's is known. However, we also know that the $(MM|MM)$ amplitude must satisfy a spectral representation in s , whose weight function is given by the unitarity condition in Channel I. Combining these two facts, we see that, if $Im(M\bar{M}|VV)$ is known, the Mandelstam representation gives us an integral equation for T_{MM} . Hence, insofar as we can justify the fact that the behavior of the MM system is determined primarily by known processes in the crossed channels (II and III), the Mandelstam representation does provide us with a dynamical theory for T_{MM} . We will show this in more detail a little later. If, however, as in the complete theory, we have to determine the amplitudes in all three channels simultaneously, we clearly must solve coupled integral equations subject to a complicated self-consistency requirement. Such an ambitious program (which amounts to the self-consistent determination of the A 's) is now being attempted, but the results discussed below all depend on cruder approximations.

Although the calculations reported below do not make full use even of the double spectral representation, we note that the location of singularities in an arbitrarily complicated Feynman graph has been given by Landau (378), and the strength of the singularity by Cutkosky (379, 380). The singularities under discussion occur when the Feynman denominators $A_i = m_i^2 - q_i^2$ vanish subject to the constraint $\sum x_i q_i = 0$; x_i are the usual Feynman parameters and the sums are taken around each closed loop in the graph. If the condition $A_i = 0$ holds for m lines $i \leq m$ in a Feynman graph F with N denominators, the imaginary part of F due to this singularity is given by

$$[Im F]_m = \frac{1}{2} (2\pi i)^m \int \pi \frac{(d^4 k) P(k) \delta_p(q_1^2 - m_1^2) \cdots \delta_p(q_m^2 - m_m^2)}{A_{m+1} \cdots A_N}$$

where $P(k)$ is a polynomial coming from the vertices and δ_p means that only the proper square root is to be taken in the delta-function. The interested reader can easily verify directly that this prescription leads to the result we

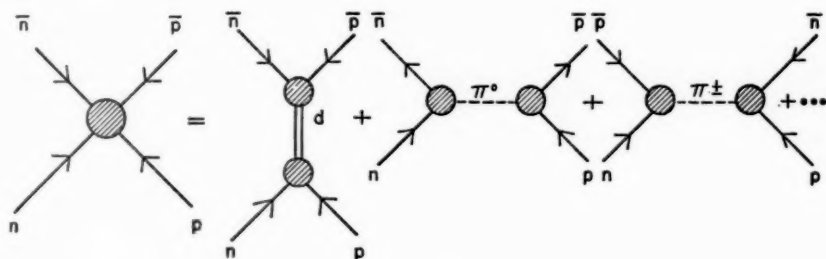


FIG. 10

computed above from unitarity for the box diagram; in fact, it is just a generalization of the unitarity condition for arbitrary groupings of particles. Hence, insofar as one believes that analytic properties proved valid to all orders in perturbation theory are to be believed, one can in principle go as far as necessary toward including inelastic amplitudes within the same framework.

C. The connection between nucleon-nucleon, nucleon-pion, and pion-pion scattering.—Let us now consider the singularities encountered in the nucleon-nucleon scattering amplitude, still ignoring complications caused by spin. Before we reach the singularities corresponding to the diagram discussed in Section B, we encounter single-particle intermediate states, which give poles rather than branch cuts. For neutron-proton scattering, these correspond to the diagrams in Figure 10. These give poles in s , t , and \bar{t} , respectively, and (for spinless nucleons and scalar pions) are given by $N^2/(M_d^2 - s)$, $-G_{op}G_{on}/(\mu^2 - t)$, and $2 G_{\pm n}G_{\pm p}/(\mu^2 - \bar{t})$. Here we have explicitly not assumed charge independence in order to emphasize that in this approach we

always deal with physical masses and coupling constants, and never need mention "renormalization." The constant N^2 in a nonrelativistic theory is just proportional to the asymptotic normalization of the bound state wave function (98). In the shape-independent approximation, which is accurate enough for most practical purposes, it can be written in terms of the triplet scattering length 3a and binding energy of the deuteron $q_0^2 = ME_b$ as $N^2 = 8(^3a) q_0^2 / (^3aq_0 - 2)M$. We will discuss below whether these two constants can be determined from the theory or must be introduced as additional parameters. The proof that the one-pion pole is actually present in the nucleon-nucleon scattering amplitude with the physical coupling constant and pion mass was given in Chapter IV.

The next nearest singularity is just the diagram we computed above (Fig. 9), if we take $m = M = r$ and $v = \mu$. This is, of course, just the fourth-order perturbation theory result, with the important distinction that we are now justified in using the physical values for the pion and nucleon masses and coupling constants and are guaranteed that these "renormalization effects" will not have to be partially cancelled against terms coming from our next approximation. We also know that we will have to do better if we are to get any agreement with experiment. But what we should do is evident, if we go back to the way the calculation was made. Clearly, the Born approximation for the $(N\bar{N}|\pi\pi)$ amplitude was used in the unitarity condition, and we can improve the calculation by improving the amplitude we use to compute our weight function. Unfortunately, as we saw above, we need this amplitude for $t > 4\mu^2$, while the physical threshold for nucleon-antinucleon annihilation is $4M^2$; so we must rely on a theoretical calculation in an unphysical region, not on experiment.

Since we need the $(N\bar{N}|\pi\pi)$ amplitude in a highly unphysical region, we must obtain a spectral representation for it in order to make the required analytical continuation. But if we write a Mandelstam representation for this amplitude, we see that the crossed channels are simply pion-nucleon scattering, so we must solve this problem before attacking the nucleon-nucleon problem. The graphs which give the nearest singularities are indicated schematically in Figure 11. The first term is the famous pole in pion-nucleon scattering, which has been used to determine the pion-nucleon coupling constant. We have seen that this gives a fourth-order term in nucleon-nucleon scattering. As is well known, this pole term gives large isotopic-spin-independent S waves in pion-nucleon scattering which are not found experimentally, so must be mainly cancelled out if our calculation is to succeed. We saw that if this term is used by itself in the unitarity condition for the $(N\bar{N}|\pi\pi)$ amplitude, it leads to the box diagram computed in Section B. Since this diagram is known to give an experimentally unacceptable nucleon-nucleon interaction, it is comforting that if we normalize the $(N\bar{N}|\pi\pi)$ amplitude to the pion-nucleon S waves, we automatically insure the necessary "pair suppression" in the nucleon-nucleon calculation. The next two

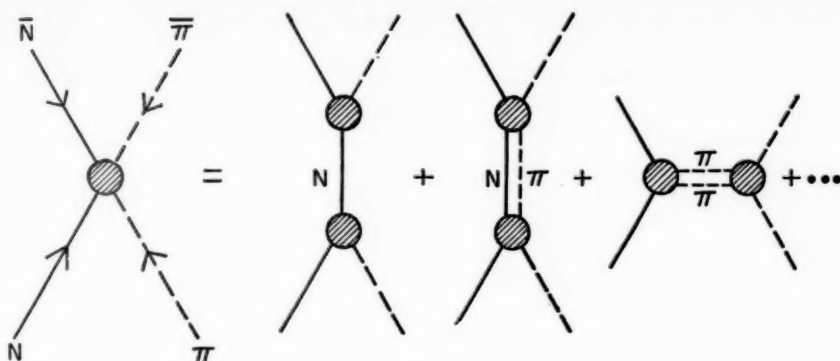


FIG. 11

diagrams will give us the weight functions for the double spectral representation, namely

$$\text{Im} \langle N\pi | N'\pi' \rangle = \int \langle N\pi | N''\pi'' \rangle \langle N''\pi'' | N'\pi' \rangle d\tau''$$

$$\text{Im} \langle N\bar{N} | \pi\pi \rangle = \int \langle N\bar{N} | \pi'\pi' \rangle \langle \pi'\pi' | \pi\pi \rangle d\tau'$$

Thus, as before, the Mandelstam representation will provide us with a non-linear integral equation for the pion-nucleon amplitude which involves a term coming from still another process, namely pion-pion scattering!

Before discussing pion-pion scattering, we wish to make a point emphasized by Cini & Fubini (376). Since the weight functions in the crossed channels are imaginary parts of scattering amplitudes, which in terms of partial waves may be written $\sum i e^{i\delta_l} \sin \delta_l (2l+1) P_l(\cos \theta)/q$, the important contribution at low energy comes only from those partial waves which are large. In particular, if a sharp resonance in one partial wave dominates the behavior, we can approximate this by a quasi-particle whose mass is equal to the total energy of the resonating system at the resonance. If only this term is kept for the 3-3 resonance in pion-nucleon scattering, one obtains the Chew-Low effective-range approximation. Taking this back into the nucleon-nucleon scattering calculation, we get an additional term like Figure 9 with the mass $r = M + w_{\text{res}}$. If this were an *S*-wave resonance, we could improve this "rescattering correction" by putting in this "particle" with a weight $A \sin^2 \delta(r)/[r^2 - \mu + M]^2$, and the calculation would still go through with *B* replaced by

$$B(s, t) = A^2 \int_{(M+\mu)^2}^{\infty} d\tau_1 \int_{(M+\mu)^2}^{\infty} d\tau_2 B_{r_1 r_2} \frac{(s, t) \sin^2 \delta(r_1) \sin^2 \delta(r_2)}{[r_1^2 - (\mu + M)^2][r_2^2 - (\mu + M)^2]}$$

Here $B_{r_1 r_2}$ is Figure 9 evaluated with unequal masses in the *R* lines. The

result is the same except that $\sqrt{s(aq^2-s)}$ has a more complicated argument (376).

We can now summarize what is needed to compute the nucleon-nucleon interaction due to one- and two-pion exchange using the Mandelstam technique. First, we must solve the pion-pion scattering problem (see below). Then we can use this amplitude to obtain a nonlinear equation for pion-nucleon scattering, which will contain a term in the weight function depending explicitly on the large pion-pion phase shifts. If this has been solved, we can then get the $(N\bar{N}|\pi\pi)$ amplitude in the region needed to compute the weight functions for nucleon-nucleon scattering. These will differ from the fourth-order perturbation theory because of terms coming from the large pion-pion and pion-nucleon phase shifts. We will show that it is then pos-

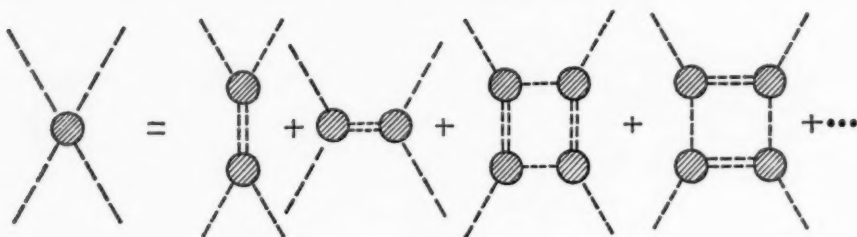


FIG. 12

sible to solve the nonlinear equation for the nucleon-nucleon partial waves. We also note that prior to a successful calculation of the pion-pion and pion-nucleon problems, it is still possible to introduce the observed resonances in a phenomenological way and make a useful preliminary calculation. As a knowledge of pion-pion and pion-nucleon scattering is required before we can compute nucleon-nucleon scattering, we now discuss the current status of these two problems.

D. Pion-pion and pion-nucleon scattering.—Because there are no pion vertices with an odd number of lines, there are no pole terms in the pion-pion amplitude. The first singularities are indicated in Figure 12. We see immediately that if we keep only the first two terms, the weight functions involve $\text{Im} \langle \pi\pi | \pi' \pi' \rangle = \int d\tau'' \langle \pi\pi | \pi'' \pi'' \rangle \langle \pi'' \pi'' | \pi' \pi' \rangle$, and we have from the Mandelstam representation an equation that involves only the pion-pion scattering amplitude. The next two diagrams contribute to the double spectral functions and can be obtained from our earlier result by putting $m = \mu = v$, $r = 2\mu$. Hence they are nonzero only for $(t - 4\mu^2)(s - 16\mu^2) \geq 16\mu^4$, and in the low-energy region t , $s \ll 16\mu^2$ will depend strongly on only one of the two variables. Recalling that in Channel I, $p^2 = \frac{1}{4}s - \mu^2$, $2p^2 \cos \theta = t + 2p^2$, we see that neglecting the dependence on t is equivalent to assuming that only S waves are large (i.e., give an appreciable imaginary part to the amplitude). Because of the symmetry of the problem, this will also be true in the

crossed channels, and the first approximation reduces to an equation in one variable [this is the essence of the Cini-Fubini (376) approach], which takes on a particularly simple form for chargeless pions. Having obtained the weight function by solving the S -wave problem, the Mandelstam representation then gives an explicit formula for all the other partial waves; consistency is checked by showing that they are in fact small.

For pseudoscalar, charge-independent pions, the pion-pion system has states of isotopic spin 0, 1, and 2. Because of Bose statistics, the $I=1$ state has only odd angular momenta, while the other two have only even angular momenta. Hence, the low-energy approximation just discussed leads to coupled equations for the $I=0, 2$ S -wave states. This system of equations, including the coupling to the $I=1$ P wave, was derived by Chew & Mandelstam (381). The pion-pion coupling constant was introduced by assigning a value to the scattering amplitude at one point, and the system was shown to possess consistent solution in which the P wave was small (382).

Unfortunately for the simplicity of the theory, there is evidence, which came first from the electromagnetic structure of the proton and neutron, that there is an $I=1$ P -state resonance in the pion-pion system. That this system gives the nearest singularity in the electromagnetic structure problem can be seen from Figure 13. The first term in Figure 13a shows us that we need to know the $(N\bar{N}|\pi\pi)$ amplitude and the pion vertex $(\pi\pi|\gamma)$, while Figure 13b shows that the pion vertex can be computed in first approximation from the $(\pi\pi|\pi'\pi')$ amplitude. By assuming an $I=1, P$ -state,

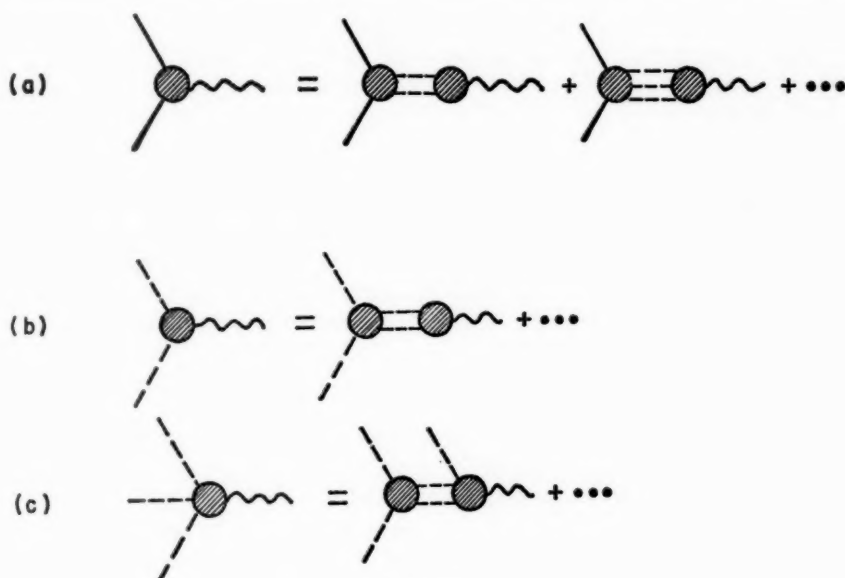


FIG. 13

pion-pion resonance, Frazer & Fulco (383, 384) succeeded in giving the first successful description of the isotopic vector part of the electromagnetic structure. The pion vertex itself has been discussed by How-Sen Wong (385) and Gourdin & Martin (386).

The difficulty in obtaining a P -state resonance from the Chew-Mandelstam equations is that the amplitude now depends strongly on t as well as on s . Since the variables change roles in the crossed channels, the integrals become divergent and a cutoff must be introduced. P -wave resonant solutions are possible (387), but since one now has two arbitrary parameters, this is not a great deal better than introducing a phenomenological resonance with adjustable position and width. By considering the inverse amplitude, Moffat (388) also obtained a two-parameter resonance. Chew & Frautschi (389) are now attempting to eliminate this arbitrariness by considering simultaneously the low momentum transfer inelastic processes at high energy and by explicitly constructing a self-consistent set of double spectral functions.

When Frautschi & Walecka (390, 391) attempted to calculate pion-nucleon scattering using the Frazer-Fulco parameters for the pion-pion resonance, they were unable to obtain agreement with experiment. A slightly less ambitious calculation by Bowcock, Cottingham & Lurie (392, 393), in which the pion-pion parameters were used to explain only the radius of the nucleon anomalous magnetic moment but not its magnitude, did succeed in fitting those parts of the pion-nucleon problem which were not used for the determination of the constants in the model. They required a higher energy for the pion-pion resonance than that used by Frazer & Fulco. Lacking a complete theory of pion-pion and pion-nucleon scattering, it is still possible to compute an empirical $(N\bar{N}|\pi\pi)$ amplitude normalized to both pion-nucleon scattering and nucleon electromagnetic structure. This has been done by Ball & Wong (394), following a method suggested by Chew, and they find that one of the Frazer-Fulco parameters is incompatible with pion-nucleon scattering. Their result should provide a quantitatively reliable method for introducing "pair suppression" into the nucleon-nucleon problem as discussed in Section C. Further experiments on the electron scattering and reanalysis in terms of pion-pion parameters (395) favor the higher resonance used by Bowcock, Cottingham & Lurie (392). These new parameters would also bring the Frautschi-Walecka (391) calculation into agreement with pion-nucleon scattering (396). Furthermore, analysis of pion production by pions in a hydrogen bubble chamber now seems to indicate a resonance at the energy required by the theoretical calculations (397). We conclude that the basic amplitudes needed to compute the two-pion-exchange part of the nucleon-nucleon interaction are now reasonably well known. Unfortunately, the latter calculation has not been reduced to numerical form as we go to press, so the specific papers on nucleon-nucleon scattering discussed in the next section refer to more limited aspects of the problem.

2. APPLICATIONS OF DISPERSION-RELATION TECHNIQUES TO NUCLEON-NUCLEON SCATTERING

Up to now we have ignored complications caused by nucleon spin. As we mentioned in Chapter II, the covariant (charge-independent) nucleon-nucleon scattering matrix is described by five independent functions of the invariant energy and momentum transfer for each isotopic spin state, but the choice of which set of five functions to use is somewhat arbitrary. At first sight, we can simply extend the above analysis by assuming that the Mandelstam representation holds separately for each of the ten independent functions. But if we then re-express the amplitude in terms of some other set, the coefficients of the transformation will in general involve factors of $E = (p^2 + M^2)^{1/2}$ and $\Delta = [2p^2(1 - \cos \theta)]^{1/2}$, which could introduce singularities at values of s , t , and \bar{t} other than those indicated by the Mandelstam representation. The correct choice of invariant amplitudes is therefore a matter of considerable practical importance. Fortunately a reasonable choice has been found and, to a considerable extent, justified (cf. Sect. 2-D).

A. *Dispersion relations in energy.*—The first attempt to face the full complexity of the covariant problem was that of Goldberger, Nambu & Oehme (23). They picked a set of ten amplitudes chosen for convenience in expressing crossing symmetry and arrived at a plausible (though not rigorously proved) set of dispersion relations in energy. These relations exhibited many of the features we have already discussed in terms of the Mandelstam representation. They obtained the deuteron pole (but explicitly exhibited the $^3S_1 - ^3D_1$ coupled state and its different contribution to each of the five $I=0$ amplitudes), the one-pion poles for pseudoscalar pions, the singularity from nucleon-nucleon scattering including the inelastic part above pion production threshold, and the singularity for $n\bar{p} \rightarrow 2\pi, 3\pi, \dots, 13\pi$. Lacking the Mandelstam representation, they did not have an explicit method for computing the neutron-antiproton ($n\bar{p}$) amplitude. However, they noted that their dispersion relation could be compared directly to that given by Khuri (398) for nonrelativistic potential scattering, and by analogy argued that the one-pion term and the $n\bar{p}$ cut correspond to the Fourier transform of the potential. Because of the one-pion pole in Δ^2 , they felt this treatment was adequate only for $\Delta^2 \leq \mu^2$ which implies that their potential has about the same range of validity as an effective-range treatment. We will see below that this range can be considerably extended. Attempts to compare their dispersion relations directly with experiment (399, 400) have been hampered by the lack of adequate phase-shift analyses at low energy. This one-dimensional dispersion-relation approach has been discussed by several authors (401 to 405).

An important application of the Goldberger-Nambu-Oehme (GNO) dispersion relations has recently been made by Riazuddin (338). Because of the Clementel-Villi ambiguity discussed in Part I, proton-proton differential cross sections below 40 Mev admit a fourfold continuum of phase-shift solutions. Riazuddin noted that two of these are ruled out by the positive polari-

zation measured at low energy (406), and he formed combinations of the GNO amplitudes which are of opposite sign for the other two. Using the analysis of MacGregor (342), he was able to show that the GNO dispersion relations can be satisfied by only one of these two choices. Since this choice depends only on the sign of certain integrals, which sign is unambiguously determined and is insensitive to the proton-antiproton contribution, the result is rigorous. Fortunately the analysis singled out the unique set predicted by meson theory and, therefore, provided a rigorous justification for previous work on the 3P states discussed in Chapter IV. He showed that the GNO relations also limit the D wave to such small values that phase-shift solutions such as those of Hull & Shapiro (407) which predicted large polarizations at low energy are also excluded. The experimental fact that the polarization is small and positive at 3.3 Mev (408) thus provides another confirmation of the meson theory of nuclear forces. This result also has the important practical consequence that the equivalent P -wave approximation can be used below 4 Mev, which greatly simplifies the analysis of proton-proton scattering experiments in this region.

The first specific application of the Mandelstam representation to nucleon-nucleon scattering was made by Cini, Fubini & Stanghellini (409). They noted that this representation gives directly a one-dimensional dispersion relation in energy if the scattering angle is held constant. For the singlet amplitude at 90° , one could therefore use experimental values of the 90° cross section to perform the integral, and extrapolate in energy to the pole term

$$\left[\frac{f^2 M}{2q^2(1 - \cos \theta) - \mu^2} + \frac{f^2 M}{2q^2(1 + \cos \theta) - \mu^2} \right]_{\cos \theta = 0}$$

to obtain the pion-nucleon coupling constant. This is clearly analogous to the similar use of an extrapolation in angle from a differential cross section at fixed energy (319). Unfortunately the experimental determination of the 90° singlet cross section requires either a phase-shift analysis or a spin correlation experiment, neither of which is available at the needed energies. Their calculation is therefore better regarded as a prediction of the 90° cross section. Similar applications of fixed-angle dispersion relations have been made by Alles & Tomasini (410, 411).

B. *Construction of the "potential."*—The problem of how to construct a potential $V(t)$ which when used in the nonrelativistic Schroedinger equation will reproduce the field-theoretic transition amplitude $T(q^2, t)$ has been discussed in a series of papers by Charap & Fubini (15, 412), and Charap & Tausner (413). They pointed out that the definition of a "potential" function which is a function of both q^2 and t offers no simplification over using the T matrix directly. If the range over which a function of t , only, works is $q^2 = \frac{1}{2}t - \mu^2 \lesssim \mu^2$, this is equivalent to an effective-range treatment. The problem is, therefore, to establish the existence of such a representation over the wider range $q^2 < q_{\text{th}}^2 = M\mu + \frac{1}{2}\mu^2 \approx 7\mu^2$, the threshold for meson production.

Imamura (414), who earlier discussed this problem from a somewhat similar point of view, did not succeed in establishing this larger range of validity.

The first paper of Charap & Fubini (15) considered the simple case of scalar nucleons interacting through a neutral scalar field, which has the advantage that there is no exchange scattering. It is then straightforward to show from the Mandelstam representation that if we drop terms of order q^2/q_{th}^2 , the field-theoretic amplitude is given to this order by the dispersion relation

$$T(q^2, t) = T_0(t) + \frac{g^2}{\pi} \int_0^\infty \frac{\text{Im } T(q'^2, t)}{q'^2(q'^2 - q^2)} dq'^2 \quad (T)$$

We have here subtracted the value of the amplitude at $q^2=0$, which we call $T_0(t)$, to insure convergence of the integral. Let the initial and final relative momenta be k_1 and k_2 , i.e. $q^2 = k_1^2 = k_2^2$, $t = -(k_2 - k_1)^2$, and introduce the notation $(k_2 | T | k_1) = T(q^2, t)$. Then, again dropping terms of order q^2/q_{th}^2 , the imaginary part of T can be computed from the elastic unitarity condition

$$i(k_2 | T^+ - T | k_1) + 2\pi \int d^3k (k_2 | T^+ | k) \frac{M}{E} \delta\left(\frac{k^2}{M^2} - \frac{k_1^2}{M^2}\right) (k | T | k_1) = 0 \quad (I)$$

Further, the subtraction term is given by the dispersion relation

$$T_0(t) = T_0(0) + \frac{t}{(2\pi)^3} \int_0^\infty \frac{F(\sigma^2) d\sigma^2}{\sigma^2(\sigma^2 - t)}$$

The constant $T_0(0)$ is just the S -wave scattering length, while the weight function $F(\sigma^2)$ is just the contribution from one-, two-, . . . meson exchange we have already discussed. Therefore, if we have succeeded in computing this weight function from pion-pion and pion-nucleon scattering, the field-theoretic amplitude to order q^2/q_{th}^2 is obtained by solving the coupled equations (T) and (I). Charap & Fubini exhibited an explicit method for doing this. The key to the construction of the potential is to note that for any potential $V(t)$ which is representable by a superposition of Yukawa potentials, the nonrelativistic amplitude $N(q^2, t) = (k_2 | N | k_1)$ has identical analyticity properties to $T(q^2, t)$ in the $q^2/q_{th}^2 \rightarrow 0$ limit [i.e. satisfies the same Mandelstam representation (27)]. Therefore, if we make the identification $N(0, t) = T_0(t)$, N satisfies equations (T) and (I), and hence is identical with $\lim_{q^2/q_{th}^2 \rightarrow 0} T(q^2, t)$. Consequently, the corresponding potential is then given explicitly by the Khuri (398) dispersion relation

$$V(t) = N(q^2, t) - \frac{1}{\pi} \int_0^\infty \frac{\text{Im } N(q'^2, t)}{q'^2 - q^2} dq'^2 = T_0(t) - \frac{1}{\pi} \int_0^\infty \frac{dq'^2}{q'^2} \text{Im } T(q'^2, t)$$

The authors then proceeded to carry through this program to order g^4 for scalar particles and exhibited explicitly the cancellation of the q^2 dependence between the fourth-order two-pion ladder diagram and the iteration of the Yukawa potential which is required by their general result. The proof nowhere made use of the static limit $(\mu/M) \rightarrow 0$; in fact, Charap & Fubini's explicit potential is not defined in a mathematical sense in this limit. That

this limit is always ambiguous has recently been shown by Goldberger & Oehme (415). See also the work of Gupta (126). We find this a convincing argument for abandoning the static (i.e. $\mu/M \rightarrow 0$) approach to the potential problem.

At first sight, the method cannot be extended to exchange forces, because these give a branch cut in the energy variable in addition to the cut in t , and this extends down to $(2\mu)^2$, whereas for neutral mesons this cut stopped at $(2M)^2$. This is a reflection of the fact that if one attempts to express an exchange potential in the Schroedinger equation by a Taylor expansion, the derivatives represent a violent velocity dependence. However, one can use the isotopic spin formalism to describe this situation by two local velocity-independent potentials (ordinary plus exchange). The same method works in field theory, as is shown by Charap & Fubini (412), and one again has a range of validity $q^2 < q_{th}^2$. The treatment of the case of physical interest (413), i.e., spin- $\frac{1}{2}$ nucleons and pseudoscalar pions, is much less satisfactory because the proof of equivalence is carried through only to fourth order in perturbation theory and not in general. The difficulty arises because no one has yet established the validity of the Mandelstam representation for (L,S) and $(L,S)^2$ potentials. Presumably this could be done with an appropriate choice of the ten basic amplitudes, and if so, the method already discussed would work. In any case, we feel that this work has been pushed far enough to show that the construction of a "potential" can be carried out, but only if one has first obtained the complete solution of the covariant problem at zero energy. The potential therefore becomes an auxiliary quantity rather than the prime object of study. Whether the potential defined by this method is the appropriate one to use in low-energy nuclear physics is an interesting question which will take further research to clarify.

C. *Partial-wave dispersion relations.*—Another way of obtaining a one-dimensional problem from the Mandelstam representation is to project out individual partial-wave amplitudes by applying the operator

$$\frac{2}{(2l+1)} \int_{-1}^1 d(\cos \theta) P_l(\cos \theta) = \frac{2}{2l+1} \int_{-t_0}^0 \frac{dt}{2q^2} P_l\left(1 - \frac{t}{2q^2}\right)$$

The one-pion-exchange pole then gives a term of the form

$$\frac{f^2 M}{4q^2} \left[A_{L,J}(q^2) \log\left(1 + \frac{4q^2}{\mu^2}\right) + B_{L,J}(q^2) \right]$$

where A and B are polynomials which depend on the particular J, L state we are considering. We see that the partial-wave amplitude as a function of q^2 will have a branch cut starting at $q^2 = -\frac{1}{2}\mu^2$ with discontinuity (twice the imaginary part) $A_{L,J}(q^2)f^2 M\pi/4q^2$. Referring to the Mandelstam representation (Sect. 1-B), we see that the double spectral function will contribute a cut starting at $q^2 = -\frac{1}{2}(2\mu)^2$ representing the interaction caused by two-pion exchange. There is an additional contribution from three-pion exchange

starting at $q^2 = -\frac{1}{4}(3\mu)^2$ and so on. Clearly, more and more negative values of q^2 correspond to the exchange of more and more massive systems, so that the Taketani separation into classical, dynamic, and phenomenological regions can be directly translated into a statement about the distance of the corresponding singularities from the physical region $q^2 \geq 0$ (416, 417). If we represent the partial-wave amplitude h_L for uncoupled states in the usual way by

$$h_L(q^2) = \frac{e^{i\delta_L} \sin \delta_L}{\sqrt{q^2}} = \frac{1}{q \cot \delta_L - i\sqrt{q^2}}$$

we see that there is also a branch cut starting at $q^2 = 0$. This is, of course, just the branch cut for nucleon-nucleon scattering starting at $s = (2M)^2$. The advantage of making the partial-wave projection is that the unitarity condition for this cut is expressed simply by requiring δ_L to be real for q^2 real and positive. Since time-reversal invariance requires $h^*(q^{2*}) = h(q^2)$, we see this is equivalent to requiring $Im[h(q^2)]^{-1} = -(q^2)^{1/2}$ on this cut.

These unitarity and analyticity requirements allow us to derive a dynamical equation for the phase shift, as we now show. Assume that we have computed the discontinuity due to one- and two-pion exchange from pion-nucleon and pion-pion scattering and have made some phenomenological assumption about the shorter-range parts of the interaction. This is equivalent to assuming that $Im h(q^2) = f^2 M \rho(q^2) \pi / 4q^2$ for $q^2 < -\frac{1}{4}$ with ρ a known function (from here on we take $\mu^2 = 1$ for convenience). Since we know the imaginary part of the inverse function for $q^2 > 0$, we follow Mandelstam's suggestion (381) and write $h(q^2) = N(q^2)/D(q^2)$. Let $N(q^2)$ have only the cut for negative q^2 and D have only the cut for positive q^2 , i.e.

$$Im N(q^2) = \frac{f^2 M \rho(q^2) \pi}{4q^2} D(q^2), \quad q^2 < -\frac{1}{4}; \quad Im D(q^2) = -\sqrt{q^2} N(q^2), \quad q^2 > 0$$

Then we can immediately write down a dispersion relation for N in terms of D and D in terms of N ; making use of our taking a ratio to set $D(0) = 1$, substituting one equation into the other, and making the indicated change of variable, we obtain the remarkably simple result

$$D\left(-\frac{1}{4x}\right) = E(x) = 1 + \frac{1}{2} f^2 M \int_0^1 \frac{dy R(y) E(y)}{\sqrt{x} + \sqrt{y}}; \quad R(y) = \rho\left(-\frac{1}{4y}\right)$$

If we solve this integral equation to obtain $E(x)$, the phase shift is then given simply by

$$q \cot \delta = \frac{1 + 2q^2 f^2 M \int_0^1 \frac{\sqrt{x} E(x) R(x)}{1 + 4q^2 x} dx}{f^2 M \int_0^1 \frac{E(x) R(x)}{1 + 4q^2 x} dx}$$

[The relativistic generalization is easy, but obscures the simplicity of the result; cf. (416).] We wish to emphasize that if we had simply considered the

inverse amplitude, we could obtain spurious poles from zeros in h ; the N/D method, however, has been shown by Chew & Froissart to give essentially unique results, even when there are bound states (418). Thus the theoretical problem lies entirely in the computation of the interaction function $R(y)$. Further, since even in the phenomenological region ($0 \leq y \leq 1/9$), we can make numerical estimates of the value of $R(y)$ from production cross sections, we can test the sensitivity of the calculation to phenomenological assumptions. This approach also can be used to improve the accuracy of the determination of nucleon-nucleon phase shifts from scattering experiments by allowing experiments at different energies to be analyzed simultaneously (416).

The first application of the partial-wave nucleon-nucleon dispersion relations was made by Wong (419). He described the 3S_1 - 3D_1 coupled state by using the one-pion-exchange cut and a phenomenological pole to represent the bound state. The position and residue of this pole in the 3S_1 state are fixed by the binding energy of the deuteron and the triplet scattering length, but the residue of the pole in the coupling amplitude can be determined from the requirement that the (Stapp) coupling parameter \bar{e}_1 vanish like q^3 as $q \rightarrow 0$. This predicts an S - D asymptotic ratio of 0.029 in the deuteron, in good agreement with the range 0.027-0.032 obtained from phenomenological models which fit the low-energy parameters. The result therefore gives another quantitative verification of the presence of the one-pion-exchange interaction in the outer part of the deuteron.

Noyes & Wong (48) made a similar calculation of the 1S_0 phase, using the effective-range and scattering length as phenomenological parameters describing the effect of multipion exchange. Since for $T_{lab} = 10$ Mev, $q^2 = +\frac{1}{4}$, and as we saw above the one-pion cut starts at $q^2 = -\frac{1}{4}$, the usual effective-range expansion has a radius of convergence of 10 Mev. In this calculation, the one-pion cut is exactly included, so the radius of convergence is extended to 40 Mev. That the one-pion-exchange interaction is so weak in this state compared to shorter-range forces makes it dubious whether the calculation using only two phenomenological parameters can actually be trusted to so high an energy. The calculation of Cini, Fubini & Stanghellini (409), considered as a prediction of the 1S_0 phase, is equivalent to replacing the one-pion cut by a single pole. It is an excellent numerical approximation to the solution of the integral equation given by Noyes & Wong over the range of interest. Both predictions give a deviation from the shape-independent approximation of opposite sign to that predicted by conventional hard-core models such as that of Gammel & Thaler. However, it is possible to construct hard-core models which fit all the relevant quantities and still have the same behavior as the dispersion-relation prediction (420, 421), so measurement of the 1S_0 phase at low energy will not necessarily discriminate between the two types of model. This is made even clearer by Martin (422), who showed that, given the discontinuity $R(y)$ in an S -wave amplitude, the weight function for the superposition of exponential (or Yukawa) potentials which reproduce the same phase shift can be explicitly constructed.

To make a comparison between dispersion-theoretic predictions of the proton-proton 1S_0 phase and experiment possible, it is necessary to include the long-range electrostatic effect in the calculation. Wong & Noyes (61) pointed out that at low energy and large distance, the proton-proton wave function can be expected to approach the nonrelativistic wave function given by the Schroedinger equation for a Coulomb potential plus a nuclear potential with the one-pion-exchange Yukawa tail. They showed that the amplitude

$$e^{i\delta} \sin \delta / \mathcal{C}^2 q; \quad \mathcal{C}^2 = \frac{2\pi n}{\exp(2\pi n) - 1}; \quad n = \frac{e^2}{\hbar v} = \frac{Me^2}{2q}$$

is free of singularities for $-\frac{1}{4} < q^2 < 0$, and that the cut in this function for $-1 < q^2 < -\frac{1}{4}$ is the same as that in the absence of the electrostatic interaction, except for a factor which goes to unity as $e^2 \rightarrow 0$. By using the fact that the usual function (51, 312)

$$\mathcal{C}^2 q \cot \delta + Me^2 [\frac{1}{2}\psi(in) + \frac{1}{2}\psi(-in) - \ln n]$$

is regular at $q^2=0$, they were able to determine this quantity in terms of the solution of an integral equation which reduces to the equation given above for $q \cot \delta$ as $e^2 \rightarrow 0$. Beyond $q^2 = -1$ the electrostatic modification of the cut is less than ~ 3 per cent, and there will be additional electrodynamic modifications because of meson mass differences, etc., which they did not know how to compute and which are of the same order. The hypothesis of charge independence stated in this language is therefore that for $q^2 < 1$; the same singularities should predict both neutron-proton and proton-proton scattering. Quantitatively, they found that if the entire interaction is represented by a single pole, the n - p and p - p scattering lengths (which differ by a factor of 3 experimentally) are reproduced to about 10 per cent. If the one-pion cuts, including the $\pi^\pm - \pi^0$ mass difference, are treated exactly, and the coupling constants for this interaction are assumed to be the same for the n - p and p - p systems, the experimental scattering lengths can be reproduced by a phenomenological multimeson-exchange term which is the same to within $\sim 3\frac{1}{2}$ per cent, confirming the charge-independence hypothesis to the expected accuracy. Wong & Noyes also predicted a neutron-neutron scattering length of $-29 \pm 3f$, assuming exact charge symmetry.

D. *Calculations of the two-pion-exchange interaction.*—The Cini-Fubini (376) method has been applied to nucleon-nucleon scattering by Amati, Leader & Vitale (423, 424, 425). As noted above, one of the major problems in any realistic approach is the choice of the ten relativistic invariant amplitudes. They picked a set with simple symmetries under the $t \leftrightarrow \bar{t}$ interchange and showed that if this set has only the Mandelstam singularities, then the set which has convenient symmetries for particle-antiparticle exchange also has only the Mandelstam singularities. Further, they showed explicitly that this set has only the Mandelstam singularities in fourth-order perturbation theory. The Cini-Fubini method was then applied and the connection to

pion-nucleon and pion-pion scattering explicitly exhibited. Formulae are given for the full two-pion-exchange contribution for $L \geq 2$, and for the left cut in the partial-wave amplitudes for S and P states. Numerical calculations using the same parameters that proved successful in pion-nucleon scattering (392) are under way, and the results are eagerly awaited.

Cziffra (426), using the choice of amplitudes discussed in the next paragraph, has computed the entire contribution from the fourth-order diagram to each of the ten invariant amplitudes. He also gave the partial-wave projections of each of these, and the method by which the Frazer-Fulco amplitudes for $(N\bar{N}|\pi\pi)$ are to be introduced to take account of the normalization to pion-nucleon and pion-pion scattering. Hence his result can be used directly for those partial waves in which three-pion exchange is unimportant. Grashin & Kobsarev (427) have performed a similar calculation, but without including the necessary "pair suppression."

Goldberger, Grisaru, MacDowell & Wong (428) discussed the choice of invariant amplitudes from another point of view. They note that for any order of the perturbation theory expansion, the transition matrix differs from that of the scalar problem only by a polynomial of the momentum components. Since the Hall-Wightman theorem (429) states that the domain of analyticity of a function of the relativistic invariants is at least as broad as a function of their individual components, Goldberger *et al.* could then show that their choice of invariant functions (which is the same as in Amati *et al.*) has only the Mandelstam singularities. They gave explicit formulae for the nucleon-antinucleon as well as the nucleon-nucleon amplitudes and wrote down the absorptive part of the $N\bar{N} \rightarrow 2\pi$ amplitude in the notation of Frazer & Fulco. They discussed the partial-wave dispersion relations, including a matrix N/D method for coupled states and a variational method for approximating the integral equations. They found that the helicity amplitudes of Jacob & Wick (430) are more convenient to use for the partial-wave decomposition than the Stapp (83) amplitudes.

Goldberger and associates also discussed the question we have ignored up to now of whether the masses and coupling constants completely determine the theory or whether additional phenomenological parameters are needed. At first sight, subtractions, which would introduce two arbitrary constants, are needed to make the S -wave dispersion relations convergent. However, there proves to be a relationship between the five amplitudes at $q^2 = -M^2$ (i.e. $E^2 = 0$). This relationship, together with the threshold condition at $q^2 = 0$, can be used, in principle, to determine these two constants. Therefore, if we were good enough mathematicians to give a complete solution, no new constant would enter the theory. In particular, the solution for the 3S_1 denominator function should develop a zero at the binding energy of the deuteron, and the residue of that pole should be N^2 . In practice, we note that the value $q^2 = -M^2$ is well beyond the point where the approximation of using only elastic scattering amplitudes is reliable, so the S -wave

scattering lengths will have to be taken from experiment for a long time to come. How many additional phenomenological constants will be needed to fit experiment will provide a quantitative criterion for the success of the theory. The normalization of the $N\bar{N} \rightarrow 2\pi$ amplitude to pion-nucleon scattering (which we have noted is the analogue of "pair suppression" in this approach) was carried out by Ball & Wong (394) including a determination of the pion-pion constants from electromagnetic structure. Numerical work is in progress and again the results are eagerly awaited.

E. *The $L.S$ interaction.*—These numerical programs will have to be completed before we know whether two-pion exchange provides a sufficiently strong $L.S$ force to explain the effects attributed to this interaction phenomenologically. Although Tzoar, Raphael & Klein (286) did succeed in getting a strong $L.S$ force of the right sign, there is by no means agreement among the meson-potential theorists that it is actually present, and it may well not appear with the newer approaches either. The situation would be profoundly altered if there were strong $J=1$ resonances at low energy in the two- and three-pion systems. Sakurai (431) recently pointed out that vector mesons strongly decaying into two or three pions can be used to give a unified picture of the strong interactions. These, or the resonances just mentioned which would be hard to distinguish from them, would provide (a) a spin-orbit force of the right sign and magnitude, (b) a short-range repulsion or "core" in the nucleon-nucleon system, and (c) a strong attraction in the nucleon-anti-nucleon system which would explain the large annihilation cross sections found in the multi-Bev region. Sakurai showed in particular (432) that the Wolfenstein C parameter at 310 Mev, which has a large imaginary part, could be reproduced both in magnitude and angular variation by the pole term corresponding to a vector meson of about three pion masses. The relationship between a possible vector meson and the nuclear force problem, including, of course, the $L.S$ force and the short-distance repulsion, had earlier been investigated in detail by Breit (433). He criticized (434) the calculation by Sakurai, remarking that keeping only the pole term corresponds to Born approximation in a potential calculation and that calculations with potential models do not reproduce Sakurai's result. While we agree that Sakurai's fit is suggestive rather than quantitative, we believe that the pole approximation could be a better first guess at 310 Mev than a Schroedinger equation calculation. Finally, there is some evidence from the energy spectrum of H^3 and He^3 produced in proton-deuteron collision around 700 Mev as measured by Abashian, Booth & Crowe (435) that there is a very sharp resonance or bound state in the $I=0$ pion system at about 2.3 pion masses. If such "particles" should prove to exist, the calculations described in this section would have to be started over practically from the beginning. However, the techniques discussed above would still be applicable.

In summary, therefore, we can say the following about the application of nucleon-nucleon dispersion relations to nucleon-nucleon scattering. Just

as in the meson-potential calculations, there is no ambiguity about the one-pion-exchange contribution. As far as two-pion-exchange contributions go, dispersion relations eliminate most of the ambiguities we encountered in the potential calculations and show clearly and unambiguously how in principle the nucleon-nucleon amplitude is connected to pion-nucleon and pion-pion scattering. More complicated exchanges require a knowledge of meson production amplitudes, and although Cutkosky has given a general method for including these as well, in practice the calculations required are so complicated that they are unlikely to be attempted soon. However, the approach through analyticity and unitarity allows us to give a covariant phenomenology for the effect of this region on the nucleon-nucleon scattering, and the sensitivity of the theory to the phenomenological elements can be studied quantitatively. During the next five years we will undoubtedly learn whether a knowledge of pion-pion and pion-nucleon scattering sufficient to compute the two-pion-exchange interaction suffices to explain most of the features of nucleon-nucleon elastic scattering, or whether novel features such as $J=1$ "particles" or resonances must also be invoked.

LITERATURE CITED

- Goldberger, M. L., *Proc. Midwest Conf. Theoret. Phys.*, 50-63 (Purdue Univ., Lafayette, Ind., April 1960)
- Breit, G., and Gluckstern, R., *Ann. Rev. Nuclear Sci.*, 2, 365 (1953)
- Christian, R. S., *Repts. Progr. in Phys.*, 15, 68 (1952)
- Gammel, J. L., and Thaler, R. M., *Progr. in Cosmic Ray Phys.*, 5, 99 (1960)
- Phillips, R. J. N., *Repts. Progr. in Phys.*, 22, 562 (1959)
- Progr. Theoret. Phys. (Kyoto)*, Suppl. 3 (1956)
- Hulthén, L., and Sugawara, M., *Encyclopedia Phys.*, 39, 1 (1957)
- Bethe, H. A., and De Hoffmann, F., *Mesons and Fields, II* (Row, Peterson and Co., Evanston, Ill., 1955)
- Proc. Conf. Nuclear Forces and the Few-Nucleon Problem, London, 1959* (Pergamon Press, London, Engl., 1960)
- Proc. Ann. Intern. Conf. High-Energy Phys., Rochester, 1960* (Interscience, New York, N. Y., 1960)
- MacGregor, M. H., Moravcsik, M. J., and Stapp, H. P., *Ann. Rev. Nuclear Sci.*, 10, 291 (1960)
- Taketani, M., Nakamura, S., and Sasaki, M., *Progr. Theoret. Phys. (Kyoto)*, 6, 581 (1951)
- Jastrow, R., *Phys. Rev.*, 81, 165 (1951)
- Feshbach, H., and Lomon, E., *Phys. Rev.*, 102, 891 (1956)
- Charap, J. M., and Fubini, S. P., *Nuovo cimento*, (10)14, 540 (1959)
- Signell, P. S., and Marshak, R. E., *Phys. Rev.*, 106, 832 L (1957)
- Signell, P. S., and Marshak, R. E., *Phys. Rev.*, 108, 1229 (1958)
- Signell, P. S., Zinn, R., and Marshak, R. E., *Phys. Rev. Letters*, 1, 416 (1958)
- Bryan, R. A., *Nuovo cimento*, 16, 895 (1960)
- Hamada, T., *Progr. Theoret. Phys. (Kyoto)*, 24, 1033 (1960)
- Hamada, T., *Progr. Theoret. Phys.*, 25, 246 (1961)
- Lomon, E. L., *Proc. Conf. Nuclear Forces and the Few-Nucleon Problem, London, 1959*, 83 (Pergamon Press, London, Engl., 1960)
- Goldberger, M. L., Nambu, Y., and Oehme, R., *Ann. phys.*, 2, 226 (1957)
- Mandelstam, S., *Phys. Rev.*, 115, 1741 (1959)
- Mandelstam, S., *Phys. Rev.*, 115, 1752 (1959)
- Eden, R. J., *Phys. Rev.*, 121, 1567 (1961). See, however, Eden, R. J., Landshoff, P. V., Polkinghorne, J. C., and Taylor, J. C. (to be published) for situations in which the Mandelstam representation does not hold.

- 26a. Landshoff, P. V., Polkinghorne, J. C., and Taylor, J. C., *Nuovo cimento*, **19**, 939 (1961) (In press). See, however, Eden, R. J., Landshoff, P. V., Polkinghorne, J. C., and Taylor, J. C. (to be published) for situations in which the Mandelstam representation does not hold.
27. Blankenbecler, R., Goldberger, M. L., Khuri, N. M., and Treiman, S. B., *Ann. Phys.*, **10**, 62 (1960)
28. Feldman, D., *Phys. Rev.*, **92**, 824 (1953)
29. Wigner, E. P., *Phys. Rev.*, **51**, 106 (1937)
30. Wigner, E. P., and Eisenbud, L., *Proc. Natl. Acad. Sci. U.S.*, **27**, 281 (1941)
31. Puzikov, L. D., Ryndin, R., and Smorodinskii, Ya. A., *J. Exptl. Theoret. Phys. (USSR)*, **5**, 489 (1957)
32. Okubo, S., and Marshak, R. E., *Ann. phys.*, **4**, 166 (1958)
33. Hall, H. H., and Powell, J. L., *Phys. Rev.*, **90**, 912 (1953)
34. Überall, H., *Acta Phys. Austriaca*, **6**, 119 (1952)
35. Salpeter, E. E., and Goldstein, J. S., *Phys. Rev.*, **90**, 983 (1953)
36. Fogel, K. G., *Arkiv Fysik*, **4**, 573 (1952)
37. Hulthén, L., and Skavlem, S., *Phys. Rev.*, **87**, 297 (1952)
38. Turner, J. S., *Proc. Phys. Soc. (London)*, **A 67**, 111 (1954)
39. Gustavi, S. G. M., *Arkiv Fysik*, **11**, 437 (1956)
40. Laurikainen, K. V., and Lyytikäinen, S., *Nuclear Phys.*, **8**, 416 (1958)
41. Hamada, T., *Progr. Theoret. Phys. (Kyoto)*, **20**, 114 (1958)
42. Keller, A., *Proc. Phys. Soc. (London)*, **68**, 930 (1955)
43. Skavlem, S., and Espe, L., *Arkiv Fysik*, **10**, 89 (1960)
44. Bird, J. R., and Preston, M. A., *Can. J. Phys.*, **33**, 399 (1955)
45. Preston, R. L., and Preston, M. A., *Can. J. Phys.*, **36**, 579 (1958)
46. Kalos, M. H., Biedenharn, L. C., and Blatt, J. M., *Nuclear Phys.*, **1**, 233 (1956)
47. Biedenharn, L. C., Blatt, J. M., and Kalos, M. H., *Nuclear Phys.*, **6**, 359 (1957)
48. Noyes, H. P., and Wong, D. Y., *Phys. Rev. Letters*, **3**, 191 (1959)
49. Roth, B., *Phys. Rev.*, **92**, 1250 (1953)
50. Heller, L., *Phys. Rev.*, **120**, 627 (1960)
51. Breit, G., Condon, E. U., and Present, R. D., *Phys. Rev.*, **50**, 825 (1936)
52. Schwinger, J., *Phys. Rev.*, **78**, 135 (1950)
53. Shapiro, J., and Preston, M. A., *Can. J. Phys.*, **34**, 451 (1956)
54. Preston, M. A., and Shapiro, J., *Phys. Rev.*, **96**, 813 L (1954)
55. Salpeter, E. E., *Phys. Rev.*, **91**, 994 (1953)
56. Riazuddin, *Nuclear Phys.*, **7**, 217 (1958) [Erratum **10**, 96 (1959)]
57. Hofstadter, R., *Revs. Mod. Phys.*, **28**, 214 (1956)
58. Sugie, A., *Progr. Theoret. Phys. (Kyoto)*, **11**, 333 (1954)
59. Riazuddin, *Nuclear Phys.*, **2**, 188 (1956)
60. Riazuddin, *Nuclear Phys.*, **7**, 223 (1958) [Erratum **10**, 96 (1959)]
61. Wong, D. Y., and Noyes, H. P., *Phys. Rev.* (To be submitted)
62. Snow, G., *Phys. Rev.*, **87**, 21 (1952)
63. Hafner, E. M., Hornyak, W. F., Falk, C. E., Snow, G., and Coor, T., *Phys. Rev.*, **89**, 204 (1953)
64. *Proc. Ann. Intern. Conf. High-Energy Phys., Rochester, 1960*, 107 (Interscience, New York, N. Y., 1960)
65. Hadley, J., Kelly, E., Segrè, E., Wiegand, C., and York, H., *Phys. Rev.*, **75**, 351 (1949)
66. Brueckner, K., Hartsough, W., Hayward, E., and Powell, W. M., *Phys. Rev.*, **75**, 555 (1959)
67. Cork, B., Johnson, L., and Richman, C., *Phys. Rev.*, **79**, 71 (1950)
68. Panofsky, W. K. H., and Fillmore, F. L., *Phys. Rev.*, **79**, 57 (1950)
69. Chamberlain, O., and Wiegand, C., *Phys. Rev.*, **79**, 81 (1950)
70. Christian, R. S., and Hart, E. W., *Phys. Rev.*, **77**, 441 (1950)
71. Christian, R. S., and Noyes, H. P., *Phys. Rev.*, **79**, 85 (1950)
72. Case, K. M., and Pais, A., *Phys. Rev.*, **80**, 203 (1950)
73. Noyes, H. P., and Camnitz, H. G., *Phys. Rev.*, **88**, 1206 L (1952)
74. Oxley, C. L., Cartwright, W. F., and Rouvina, J., *Phys. Rev.*, **93**, 806 (1954)
75. Goldfarb, L. J. B., and Feldman, D., *Phys. Rev.*, **88**, 1099 (1952)
76. Swanson, D., *Phys. Rev.*, **89**, 749 (1953)
77. Matsumoto, M., and Watari, W., *Progr. Theoret. Phys. (Kyoto)*, **11**, 63 (1957)
78. Noyes, H. P., and Pandya, S. P., *Phys. Rev.*, **102**, 269 (1956)

79. Bhatia, A. B., and Shah, S. M., *Progr. Theoret. Phys. (Kyoto)*, **17**, 561 (1957)
80. Clementel, E., and Villi, C., *Nuovo cimento*, (10)**4**, 935 (1956)
81. Gammel, J., Christian, R., and Thaler, R., *Phys. Rev.*, **105**, 311 (1957)
82. Wolfenstein, L., *Bull. Am. Phys. Soc.*, **1**, 36 (1956)
83. Stapp, H. P., Ypsilantis, T., and Metropolis, N., *Phys. Rev.*, **105**, 302 (1957)
84. Gammel, J. L., and Thaler, R. M., *Phys. Rev.*, **107**, 291 (1957)
85. Gammel, J. L., and Thaler, R. M., *Phys. Rev.*, **108**, 163 L (1957)
86. Gammel, J. L., and Thaler, R. M., *Phys. Rev.*, **107**, 1337 (1957)
87. Feshbach, H., *Phys. Rev.*, **107**, 1626 (1957)
88. Laurikainen, K. V., *Nuclear Phys.*, **8**, (1958) [Erratum **10**, 96 (1959)]
89. Laurikainen, K. V., and Varho, O., *Nuclear Phys.*, **12**, 606 (1959)
90. Newton, R. G., and Schofield, J. H., *Phys. Rev.*, **110**, 785 L (1958)
91. Sessler, A. M., and Foley, H. M., *Phys. Rev.*, **110**, 995 L (1958)
92. *Proc. Conf. Nuclear Forces and the Few-Nucleon Problem*, London, 1959, 396 (Pergamon Press, London, Engl., 1960)
93. Breit, G., and Bouricius, W., *Phys. Rev.*, **75**, 1029 (1949)
94. Saperstein, A. M., and Durand, L., III, *Phys. Rev.*, **104**, 1102 (1956)
95. Raphael, R. B., *Phys. Rev.*, **102**, 905 (1956)
96. Balazs, L., *Phys. Rev.* (To be submitted)
97. Moszkowski, S. A., and Scott, B. L., *Phys. Rev. Letters*, **1**, 298 (1958)
98. Jost, R., and Kohn, W., *Phys. Rev.*, **87**, 977 (1952)
99. Newton, R. G., and Fulton, T., *Phys. Rev.*, **107**, 1103 (1957)
100. Raphael, R. B., *Phys. Rev.*, **107**, 1135 (1957)
101. Solmitz, F. T., *Phys. Rev.*, **89**, 1295 L (1953)
102. Iwadare, J., *Progr. Theoret. Phys. (Kyoto)*, **9**, 94 (1943)
103. Kikuta, T., *Progr. Theoret. Phys.*, **11**, 118 (1954)
104. Thaler, R. M., Bengston, J., and Breit, G., *Phys. Rev.*, **94**, 683 (1954)
105. Solmitz, F. T., *Phys. Rev.*, **92**, 164 (1953)
106. Zharkov, G. F., *Soviet Phys. JETP*, **7**, 837 [34, 1211 (1958)]
107. Yamaguchi, Y., *Phys. Rev.*, **95**, 1628 (1954)
108. Yamaguchi, Y., and Yamaguchi, Y., *Phys. Rev.*, **95**, 1635 (1954)
109. Gourdin, M., and Martin, A., *Nuovo cimento*, (10)**6**, 757 (1957)
110. Gourdin, M., and Martin, A., *Compt. rend.*, **244**, 1469 (1957)
111. Gourdin, M., and Martin, A., *Compt. rend.*, **244**, 1329 (1957)
112. Gourdin, M., and Martin, A., *Compt. rend.*, **244**, 1153 (1957)
113. *Proc. Conf. Nuclear Forces and the Few-Nucleon Problem*, London, 1959, 43 (Pergamon Press, London, Engl., 1960)
114. *Proc. Ann. Intern. Conf. High-Energy Phys., Rochester, 1960*, **11**, 117 (Interscience, New York, N. Y., 1960)
115. Breit, G., Hull, M. H., Jr., Lassila, K., and Pyatt, K. D., Jr., *Phys. Rev.*, **120**, 2227 (1960)
116. Stapp, H. P., Moravcsik, M. J., and Noyes, H. P., *Phys. Rev.* (To be submitted)
117. Perring, J. K., and Phillips, R. J. N. (Private communication)
118. Moshinsky, M., *J. phys., radium*, **15**, 725 (1954)
119. Yukawa, H., *Proc. Phys. Math. Soc. Japan*, **17**, 48 (1935)
120. Lattes, C. M. G., Occhialini, G. P. S., and Powell, C. F., *Nature*, **160**, 453 (1947)
121. Aamodt, R. L., Hadley, J., and Panofsky, W. K. H., *Phys. Rev.*, **81**, 565 (1951)
122. Taketani, M., and Machida, S., *Progr. Theoret. Phys. (Kyoto)*, **24**, 1317 (1960)
123. Hoshizaki, N., and Machida, S., *Progr. Theoret. Phys.*, **24**, 1325 (1960)
124. Goto, J., and Machida, S., *Progr. Theoret. Phys.*, **25**, 64 (1961)
125. Nishijima, K., *Progr. Theoret. Phys., Suppl.* **3**, 138 (1956)
126. Gupta, S. N., *Phys. Rev.*, **117**, 1146 (1960)
127. Machida, S., and Nishijima, K., *Progr. Theoret. Phys.*, **7**, 57 (1952)
128. Klein, A., *Phys. Rev.*, **91**, 740 (1953)
129. Klein, A., *Phys. Rev.*, **92**, 1017 (1952)
130. Lévy, M. M., *Phys. Rev.*, **88**, 725 (1952)
131. Bethe, H. A., *Phys. Rev.*, **76**, 191 (1949)
132. Hamada, T., and Shono, Y., *Progr. Theoret. Phys. (Kyoto)*, **13**, 102 (1955)

133. Brueckner, K. A., Gell-Mann, M., and Goldberger, M., *Phys. Rev.*, **90**, 476 (1953)
134. Arnowitz, R., and Deser, S., *Phys. Rev.*, **100**, 349 (1955)
135. Cooper, L. N., *Phys. Rev.*, **100**, 362 (1955)
136. Green, H. S., *Nuclear Phys.*, **1**, 360 (1956)
137. Schumacher, C. R. (Private communication)
138. Werle, J., *Nuovo cimento*, (10)1, 537 (1955)
139. Green, H. S., and Biswas, S. N., *Progr. Theoret. Phys. (Kyoto)*, **18**, 121 (1957)
140. Biswas, S. N., *Progr. Theoret. Phys.*, **19**, 725 (1958)
141. Gourdin, M., *Nuovo cimento*, (10) 7, 338 (1958)
142. Signell, P., *Progr. Theoret. Phys.*, **22**, 492 (1959)
143. Taketani, M., Machida, S., and Onuma, S., *Progr. Theoret. Phys.*, **7**, 45 (1952)
144. Nishijima, K., *Progr. Theoret. Phys.*, **5**, 815, 911 (1951)
145. Iwadare, J., *Progr. Theoret. Phys.*, **13**, 189 (1955)
146. Lepore, J. V., *Phys. Rev.*, **88**, 750 (1952)
147. Tamm, I., *J. Phys. USSR*, **9**, 449 (1945)
148. Dancoff, S. M., *Phys. Rev.*, **78**, 382 (1950)
149. Lévy, M. M., *Phys. Rev.*, **86**, 806 (1952)
150. Lévy, M. M., *Phys. Rev.*, **88**, 725 (1952)
151. Lévy, M. M., *Phys. Rev.*, **88**, 72 (1952)
152. Klein, A., *Phys. Rev.*, **89**, 1158 (1953)
153. Klein, A., *Phys. Rev.*, **90**, 1101 (1953)
154. Feldman, D., *Phys. Rev.*, **98**, 1456 (1955)
155. Baroncini, D., *Nuovo cimento*, (9)9, 642 (1952)
156. Morpurgo, G., and Touschek, B. F., *Nuovo cimento*, (9)10, 1681 (1953)
157. Morpurgo, G., *Nuovo cimento*, (9) 103 (1954)
158. Okabayashi, T., *Progr. Theoret. Phys. (Kyoto)*, **12**, 545 (1954)
159. Meecham, W. C., *Phys. Rev.*, **104**, 828 (1956)
160. Dyson, F. J., *Phys. Rev.*, **90**, 994 (1953)
161. Dyson, F. J., *Phys. Rev.*, **91**, 421 (1953)
162. Dyson, F. J., *Phys. Rev.*, **91**, 1543 (1953)
163. Kursunoglu, B., *Phys. Rev.*, **92** 1069 (1953)
164. Cini, M., *Nuovo cimento*, (9)10, 526 (1953)
165. Cini, M., *Nuovo cimento*, (9)10, 614 (1953)
166. Fubini, S., *Nuovo cimento*, (9)10, 851 (1953)
167. Cini, M., and Fubini, S., *Nuovo cimento*, (9)10, 1695 (1953)
168. Itabashi, K., *Progr. Theoret. Phys. (Kyoto)*, **12**, 494 (1954)
169. Itabashi, K., *Progr. Theoret. Phys.*, **12**, 585 (1954)
170. Schweber, S. S., *Phys. Rev.*, **94**, 1089 (1954)
171. Kursunoglu, B., *Phys. Rev.*, **96**, 1690 (1954)
172. Rukhadze, A. A., *Soviet Phys. JETP*, **2**, 570 (1956) [29, 709 (1955)]
173. Cini, M., Morpurgo, G., and Touschek, B., *Nuovo cimento*, (9)11, 316 (1954)
174. Okubo, S., *Progr. Theoret. Phys. (Kyoto)*, **12**, 603 (1954)
175. Klein, A., *Phys. Rev.*, **95**, 1676 (1955)
176. Taylor, J. C., *Phys. Rev.*, **95**, 1313 (1955)
177. Taylor, J. C., *Phys. Rev.*, **96**, 1438 (1954)
178. Lehmann, H., *Z. Naturforsch.*, **8a**, 579 (1953)
179. Fukuda, N., Sawada, K., and Taketani, M., *Progr. Theoret. Phys. (Kyoto)*, **12**, 156 (1954)
180. Okubo, S., *Progr. Theoret. Phys.*, **12**, 603 (1954)
181. Inoue, K., Machida, S., Taketani, M., and Toyoda, T., *Progr. Theoret. Phys.*, **15**, 122 (1956)
182. Sugawara, M., and Okubo, S., *Phys. Rev.*, **117**, 605 (1960)
183. Sugawara, M., and Okubo, S., *Phys. Rev.*, **117**, 611 (1960)
184. Brueckner, K. A., and Watson, K. M., *Phys. Rev.*, **90**, 699 (1953)
185. Brueckner, K. A., and Watson, K. M., *Phys. Rev.*, **92**, 1023 (1953)
186. Klein, A., *Phys. Rev.*, **91**, 1285 (1953)
187. Klein, A., *Progr. Theoret. Phys. (Kyoto)*, **20**, 257 (1958)
188. Tani, S., *Progr. Theoret. Phys.*, **12**, 104 (1954)
189. Gartenhaus, S., *Phys. Rev.*, **100**, 900 (1955)
190. Watson, K. M., and Lepore, J. V., *Phys. Rev.*, **76**, 1157 (1949)
191. Kuni, F. M., *Soviet Phys. JETP*, **7**, 113 (1958) [33, 163 (1958)]
192. Nambu, Y., *Progr. Theoret. Phys. (Kyoto)*, **5**, 614 (1950)

193. Nakabayasi, K., and Sato, I., *Phys. Rev.*, **88**, 144 (1952)
194. Henley, E. M., and Ruderman, M. A., *Phys. Rev.*, **92**, 1036 (1953)
195. Sharp, R. T., *Nuovo cimento*, **9**, 23 (1958)
196. Novozhilov, I. V., *Soviet Phys. JETP*, **5**, 1030 (1957) [**32**, 1262 (1957)]
197. Novozhilov, I. V., *Soviet Phys. JETP*, **6**, 692 (1957) [**33**, 901 (1957)]
198. Novozhilov, I. V., and Terent'ev, I. A., *Soviet Phys. JETP*, **9**, 89 (1959) [**36**, 129 (1959)]
199. Miyazawa, H., *Phys. Rev.*, **104**, 1741 (1957)
200. Klein, A., and McCormick, B. H., *Phys. Rev.*, **104**, 1747 (1956)
201. Konuma, M., Miyazawa, H., and Otsuki, S., *Phys. Rev.*, **107**, 320 (1957)
202. Konuma, M., Miyazawa, H., and Otsuki, S., *Progr. Theoret. Phys. (Kyoto)*, **19**, 17 (1958)
203. Klein, A., *Phys. Rev.*, **95**, 1061 (1955)
204. Weisskopf, V. F., *Phys. Rev.*, **116**, 1615 (1959)
205. Salpeter, E. E., and Bethe, H. A., *Phys. Rev.*, **84**, 1232 (1951)
206. Hamada, T., and Sugawara, M., *Progr. Theoret. Phys.*, **9**, 555 (1953)
207. Klein, A., *Phys. Rev.*, **94**, 195 (1954)
208. Macke, W., *Z. Naturforsch.*, **8a**, 599, 615 (1953)
209. Macke, W., *Phys. Rev.*, **91**, 195 (1953)
210. Arnowitz, R., and Gasiorowicz, S., *Phys. Rev.*, **94**, 1057 (1954)
211. Zimmerman, W., *Nuovo cimento*, **11**, 43 (1954)
212. Macke, W., *Phys. Rev.*, **92**, 1072 (1953)
213. Wanders, G., *Phys. Rev.*, **104**, 1782 (1956)
214. Chraplyvy, Z. V., *Phys. Rev.*, **92**, 1310 (1953)
215. Kursunoglu, B., *Phys. Rev.*, **101**, 1419 (1956)
216. Wick, G. C., *Phys. Rev.*, **96**, 1124 (1954)
217. Sugano, R., and Munakata, Y., *Progr. Theoret. Phys. (Kyoto)*, **16**, 532 (1956)
218. Kemmer, N., and Salam, A., *Proc. Roy. Soc. (London)*, **230**, 266 (1955)
219. Ida, M., *Progr. Theoret. Phys.*, **23**, 1151 (1960)
220. Macke, W., *Nuovo cimento*, (9)**10**, 1198 (1953)
221. Macke, W., *Z. Naturforsch.*, **8a**, 599 (1953)
222. Symanzik, K., *Nuovo cimento*, **11**, 88 (1954)
223. Edwards, S. F., *Phys. Rev.*, **90**, 284 (1953)
224. Goldstein, J. S., *Phys. Rev.*, **91**, 1516 (1953)
225. Green, H. S., *Phys. Rev.*, **97**, 540 (1955)
226. Green, H. S., *Proc. Phys. Soc. (London)*, **A68**, 577 (1955)
227. Alekseev, A. I., *Soviet Phys. JETP*, **9**, 1020 (1959) [**36**, 1435 (1959)]
228. Okubo, S., and Feldman, D., *Phys. Rev.*, **117**, 292 (1960)
229. Yamamoto, H., *Progr. Theoret. Phys. (Kyoto)*, **22**, 73 (1959)
230. Cutkosky, R. E., *Phys. Rev.*, **96**, 1135 (1954)
231. Cutkosky, R. E., and Wick, G. C., *Phys. Rev.*, **101**, 1830 (1956)
232. Geffen, D. A., and Scarf, F. L., *Phys. Rev.*, **101**, 1829 (1956)
233. Scarf, F. L., and Umezawa, H., *Phys. Rev.*, **109**, 1848 (1958)
234. Vosko, S. H., *J. Math. Phys.*, **1**, 505 (1960)
235. Allcock, G. R., *Phys. Rev.*, **104**, 1799 (1956)
236. Nishijima, K., *Progr. Theoret. Phys. (Kyoto)*, **10**, 549 (1953)
237. Nishijima, K., *Progr. Theoret. Phys.*, **12**, 279 (1954)
238. Nishijima, K., *Progr. Theoret. Phys.*, **14**, 203 (1955)
239. Mandelstam, S., *Proc. Roy. Soc. (London)*, **A233**, 248 (1955)
240. Klein, A., and Zemach, A., *Phys. Rev.*, **108**, 126 (1958)
241. Mandelstam, S., *Proc. Roy. Soc. (London)*, **A237**, 496 (1956)
242. Claesson, A., *Arkiv Fysik*, **7**, 565 (1952)
243. Jordan, J. L., and Frahn, W. E., *Z. Naturforsch.*, **8a**, 620 (1953)
244. Jordan, J. L., and Frahn, W. E., *Z. Naturforsch.*, **9a**, 572 (1954)
245. Arnowitz, R., and Gasiorowicz, S., *Phys. Rev.*, **95**, 538 (1955)
246. Neuman, M., *Phys. Rev.*, **92**, 1021 (1953)
247. Glaser, V., *Phys. Rev.*, **98**, 840 (1955)
248. Klein, A., and McCormick, B. H., *Progr. Theoret. Phys. (Kyoto)*, **20**, 876 (1958)
249. Deser, S., *Phys. Rev.*, **92**, 1542 (1953)
250. Pearlstein, L. D., and Klein, A., *Phys. Rev.*, **118**, 193 (1960)
251. Tomonaga, S., *Progr. Theoret. Phys. (Kyoto)*, **2**, 6 (1947)
252. Matthews, P. T., and Salam, A., *Phys. Rev.*, **86**, 715 (1952)
253. Jean, M., *J. phys., radium*, **15**, 694 (1954)

254. Hasegawa, H., *Progr. Theoret. Phys. (Kyoto)*, **13**, 47 (1955)
255. Nogami, Y., and Hasegawa, H., *Progr. Theoret. Phys.*, **15**, 137 (1956)
256. Breit, G., *Phys. Rev.*, **111**, 652 (1958)
257. Wentzel, G., *Helv. Phys. Acta*, **15**, 111 (1942)
258. Wentzel, G., *Phys. Rev.*, **86**, 802 (1952)
259. Lomsadze, I. M., *Soviet Phys. "Doklady"*, **1**, 571 (1956)
260. Arnous, E., *J. phys., radium*, **17**, 107 (1956)
261. Tomonaga, S., *Progr. Theoret. Phys. (Kyoto)*, **1**, 109 (1946)
262. Pauli, W., *Meson Theory of Nuclear Forces* (Interscience, New York, N. Y., 1946)
263. Geilikman, B. T., *Soviet Phys. JETP*, **2**, 451 (1956) [29, 572 (1955)]
264. Geilikman, B. T., *Soviet Phys. JETP*, **2**, 509 (1956) [29, 417 (1955)]
265. Geilikman, B. T., *Soviet Phys. JETP*, **2**, 601 (1956) [29, 430 (1955)]
266. Cap, F., *Nuovo cimento*, (10) **4**, Suppl., 807 (1956)
267. Heisenberg, W., *Z. Physik*, **126**, 569 (1949)
268. Schiff, L. I., *Phys. Rev.*, **86**, 856 (1952)
269. Borgardt, A. A., *Soviet Phys. JETP*, **6**, 43 (1957) [33, 60 (1957)]
270. Cap, F., *Phys. Rev.*, **95**, 287 (1954)
271. Cap, F., *Progr. Theoret. Phys. (Kyoto)*, **13**, 62 (1955)
272. Cap, F., and Grobner, W., *Nuovo cimento*, (10) **1**, 1211 (1955)
273. Cap, F., *Nuovo cimento*, (9) **10**, 1347 (1953)
274. Cap, F., *Final Rept. on AF61 511-666-C Contract, 1955* (US Air Force Research Development Command)
275. Shindo, M., and Nishijima, K., *Progr. Theoret. Phys. (Kyoto)*, **13**, 103 (1955)
276. Sato, I., *Progr. Theoret. Phys.*, **10**, 323 (1953)
277. Araki, G., *Progr. Theoret. Phys.*, **13**, 13 (1955)
278. Dresner, L., *Phys. Rev.*, **91**, 201 (1953)
279. Sato, S., *Progr. Theoret. Phys.*, **13**, 457 (1955)
280. Sato, I., Itabashi, K., and Sato, S., *Progr. Theoret. Phys.*, **14**, 303 (1955)
281. Araki, G., *Progr. Theoret. Phys.*, **6**, 379 (1951)
282. Power, E. A., *Nuovo cimento*, (9) **12**, 323 (1954)
283. Eder, G., *Z. Naturforsch.*, **9a**, 565 (1954)
284. Iwadare, J., *Progr. Theoret. Phys. (Kyoto)*, **14**, 16 (1955)
285. Iwadare, J., *Progr. Theoret. Phys.*, **13**, 218 (1955)
286. Tzoar, N., Raphael, R., and Klein, A., *Phys. Rev. Letters*, **2**, 433 (1959) [Erratum: **3**, 145 (1959)]
287. Gupta, S. N., *Nuovo cimento*, **18**, 823 (1960)
288. Gupta, S. N., *Phys. Rev. Letters*, **2**, 124 (1959)
289. Hiida, K., Iwadare, J., and Machida, S., *Progr. Theoret. Phys. (Kyoto)*, **15**, 189 (1956)
290. Ruderman, M., *Phys. Rev.*, **90**, 183 (1953)
291. Brueckner, K. A., *Phys. Rev.*, **91**, 761 (1953)
292. Zharkov, G. F., *Soviet Phys. JETP*, **2**, 55 (1956) [29, 85 (1955)]
293. Werle, J., *Phys. Rev.*, **89**, 527 (1953)
294. Machida, S., and Senba, K., *Progr. Theoret. Phys. (Kyoto)*, **13**, 389 (1955)
295. Hasegawa, K., and Azuma, S., *Progr. Theoret. Phys.*, **12**, 546 (1954)
296. Hasegawa, K., and Azuma, S., *Progr. Theoret. Phys.*, **13**, 360 (1955)
297. Bonnevey, G., *Compt. rend.*, **238**, 164 (1954)
298. Pomeranchuk, I. I., *Soviet Phys. JETP*, **2**, 739 (1956) [29, 869 (1955)]
299. Matsumoto, T., Hamada, T., and Sugawara, M., *Progr. Theoret. Phys. (Kyoto)*, **10**, 199 (1953)
300. Pekar, S. I., *Soviet Phys. JETP*, **2**, 462 (1956) [29, 599 (1955)]
301. Ferrari, F., and Fonda, L., *Nuovo cimento*, **6**, 1510 (1957)
302. Charon, J., *J. phys., radium*, **17**, 887 (1956)
303. *Progr. Theoret. Phys. (Kyoto)*, Suppl. **3**, 32-105 (1956)
304. Taketani, M., Ohnuma, S. and Koide, S., *Progr. Theoret. Phys. (Kyoto)*, **6**, 635 (1951)
305. Lopes, J. L. and Feynman, R. P., *Symposium on Nuclear Research Techniques in Physics* (July 1952)
306. Iwadare, J., Otsuki, S., and Watari, W., *Progr. Theoret. Phys.*, **15**, 86 (1956)
307. Iwadare, J., Otsuki, S., Tamagaki, R., and Watari, W., *Progr. Theoret. Phys.*, **16**, 455 (1956)
308. de Swart, J. J., and Marshak, R. E., *Phys. Rev.*, **111**, 272 (1958)
309. Hadjionnou, F. T., *Bull. Phys. Am. Soc.*, **5**, 504 (1960)
310. Iwadare, J., Otsuki, S., Tamagaki, R., and Watari, W., *Progr. Theoret. Phys. (Kyoto)*, **16**, 472 (1956)

311. Blatt, J. M., and Jackson, J. D., *Phys. Rev.*, **76**, 18 (1949)
312. Jackson, J. D., and Blatt, J. M., *Revs. Mod. Phys.*, **22**, 77 (1950)
313. Hart, H. E., and Hatcher, R. D., *Phys. Rev.*, **87**, 375 L (1952)
314. Yovits, M. C., Smith, R. L., Jr., Hull, M. H., Jr., Bengston, J., and Breit, G., *Phys. Rev.*, **85**, 540 (1952)
315. Hull, M. H., Jr., and Herschman, A., *Phys. Rev.*, **90**, 482 (1953)
316. Komoda, T., and Sasaki, M., *Progr. Theoret. Phys. (Kyoto)*, **9**, 468 (1953)
317. Taketani, M., Machida, S., and Onuma, S., *Progr. Theoret. Phys.*, **7**, 45 (1952)
318. Sugawara, M., *Phys. Rev.*, **117**, 614 (1960)
319. Young, H. D., and Cutkosky, R. E., *Phys. Rev.*, **117**, 595 (1960)
320. Breit, G., and Hull, M. H., Jr., *Nuclear Phys.*, **15**, 216 (1960)
321. Cziifra, P., MacGregor, M. H., Moravcsik, M. J., and Stapp, H. P., *Phys. Rev.*, **114**, 880 (1959)
322. Cziifra, P., and Moravcsik, M. J., *Phys. Rev.*, **116**, 226 (1959)
323. Larsen, R. R., *Lawrence Radiation Lab. Preprint UCRL-9292* (1961)
324. *Proc. Ann. Intern. Conf. High-Energy Phys., Rochester, 1960*, 64 (Interscience, New York, N. Y., 1960)
325. *Proc. Ann. Intern. Conf. High-Energy Phys., Rochester, 1960*, 69 (Interscience, New York, N. Y., 1960)
326. MacGregor, M. H., Moravcsik, M. J., and Stapp, H. P., *Phys. Rev.*, **116**, 1248 (1959)
327. MacGregor, M. H., and Moravcsik, M. J., *Phys. Rev. Letters*, **4**, 524 (1960)
328. Signell, P., *Phys. Rev. Letters*, **5**, 574 (1960)
329. Breit, G., Hull, M. H., Jr., Lassila, K., and Pyatt, K. D., Jr., *Phys. Rev. Letters*, **4**, 79 (1960)
330. Breit, G., Hull, M. H., Jr., Lassila, K., and Ruppel, H. M., *Phys. Rev. Letters*, **5**, 274 (1960)
331. Breit, G., *Univ. of Penn. Bicentennial Conf.*, 1940, 10 (1941)
332. Durand, L. III, *Phys. Rev.*, **108**, 1597 (1957)
333. Otsuki, S., and Tamagaki, R., *Progr. Theoret. Phys. (Kyoto)*, **12**, 806 (1954)
334. Otsuki, S., Taketani, M., Tamagaki, R., and Watari, W., *Progr. Theoret. Phys.* (In press)
335. Knecht, D. J., Messelt, S., Berners, E. D., and Northcliffe, L. C., *Phys. Rev.*, **114**, 550 (1959)
336. Iwadare, J., *Proc. Phys. Soc. (London)* (In press)
337. Knecht, D. (Private communication)
338. Riazuddin, *Phys. Rev.*, **121**, 1509 (1961)
339. Otsuki, S., and Fujii, S., *Progr. Theoret. Phys. (Kyoto)*, **12**, 521 (1954)
340. Otsuki, S., and Tamagaki, R., *Progr. Theoret. Phys.*, **14**, 52 (1955)
341. Iwadare, J., Otsuki, S., Tamagaki, R., and Watari, W., *Progr. Theoret. Phys.*, **16**, 604 (1956)
342. MacGregor, M. H., *Phys. Rev.*, **113**, 1559 (1959)
343. Fujii, S., Iwadare, J., Otsuki, S., Taketani, M., Tani, S., and Watari, W., *Progr. Theoret. Phys.*, **10**, 478 (1953)
344. Fujii, S., Iwadare, J., Otsuki, S., Taketani, M., Tani, S., and Watari, W., *Progr. Theoret. Phys.*, **11**, 11 (1954)
345. Matsumoto, M., and Watari, W., *Progr. Theoret. Phys.*, **12**, 503 (1954)
346. Iwadare, J., Otsuki, S., Tamagaki, R., and Watari, W., *Nuovo cimento*, (10)**4**, 1204 (1956)
347. Brueckner, K. A., *Phys. Rev.*, **96**, 508 (1954)
348. Jastrow, R., *Phys. Rev.*, **91**, 749 (1953)
349. Blatt, J. M., and Kalos, M. H., *Phys. Rev.*, **92**, 1563 (1953)
350. Preston, M. A., and Shapiro, J., *Can. J. Phys.*, **35**, 451 (1957)
351. Martin, A., and Verlet, L., *Nuovo cimento*, (9)**12**, 463 (1954)
352. Gelernter, H., *Phys. Rev.*, **105**, 1068 (1957)
353. Wertheim, M. S., Hull, M. H., Jr., and Saperstein, A. M., *Phys. Rev.*, **104**, 764 (1956)
354. Gammel, J. L., and Thaler, R. M., *Phys. Rev.*, **103**, 1874 (1956)
355. Hull, M. H., Jr., Pyatt, K. D., Jr., Fischer, C. R., and Breit, G., *Phys. Rev. Letters*, **2**, 264 (1959)
356. Otsuki, S., Tamagaki, R., and Watari, W., *Progr. Theoret. Phys. (Kyoto)*, **19**, 217 (1958)
357. Otsuki, S., *Progr. Theoret. Phys.*, **20**, 171 (1958)
358. Watari, W., *Progr. Theoret. Phys.*, **20**, 181 (1958)
359. Tamagaki, R., *Progr. Theoret. Phys.*, **20**, 505 (1958)
360. Hamada, T., Iwadare, J., Otsuki, S.,

- Tamagaki, R., and Watari, W., *Progr. Theoret. Phys.*, **22**, 566 (1959)
361. Hamada, T., Iwadare, J., Otsuki, S., Tamagaki, R., and Watari, W., *Progr. Theoret. Phys.*, **23**, 366 (1960)
362. Nigam, B. P., *Progr. Theoret. Phys.*, **23**, 61 (1960)
363. *Proc. Conf. Nuclear Forces and the Few-Nucleon Problem, London, 1959* 14 (Pergamon Press, London, Engl., 1960)
364. *Proc. Ann. Intern. Conf. High-Energy Phys., Rochester, 1960*, 100, 107 (Interscience, New York, N. Y., 1960)
365. Saylor, D. P., Bryan, R. A., and Marshak, R. E., *Phys. Rev. Letters*, **5**, 266 (1960)
366. MacGregor, M. H., *Phys. Rev. Letters*, **2**, 106 (1959)
367. Gell-Mann, M., *Phys. Rev.*, **100**, 1795 (T) (1955)
368. Mandelstam, S., *Repts. Progr. in Phys.* (In press)
369. Kronig, R., *J. Opt. Soc. Am.*, **12**, 546 (1926)
370. Kramers, H. A., *Atti Congr. intern. fis., Como*, **2**, 545 (1927)
371. Karplus, R., and Ruderman, M. A., *Phys. Rev.*, **98**, 771 (1955)
372. Goldberger, M. L., *Phys. Rev.*, **97**, 508 (1955)
373. Goldberger, M. L., *Phys. Rev.*, **99**, 979 (1959)
374. Bogoliubov, N. N., *Rept. Intern. Conf. Theoret. Phys., Seattle* (1956)
375. Symanzik, K., *Phys. Rev.*, **105**, 743 (1957)
376. Cini, M., and Fubini, S., *Ann. phys.*, **10**, 352 (1960)
377. Mandelstam, S., *Phys. Rev. Letters*, **4**, 84 (1960)
378. Landau, L. D., *Nuclear Phys.*, **13**, 181 (1959)
379. Cutkosky, R. E., *Phys. Rev. Letters*, **4**, 624 (1960)
380. Cutkosky, R. E., *J. Math. Phys.*, **1**, 429 (1960)
381. Chew, G. F., and Mandelstam, S., *Phys. Rev.*, **119**, 467 (1960)
382. Chew, G. F., Mandelstam, S. and Noyes, H. P., *Phys. Rev.*, **119**, 478 (1960)
383. Frazer, W. R., and Fulco, J. R., *Phys. Rev.*, **117**, 1603 (1960)
384. Frazer, W. R., and Fulco, J. R., *Phys. Rev.*, **117**, 1609 (1960)
385. Wong, H. S., *Phys. Rev. Letters*, **5**, 70 (1960)
386. Gourdin, M., and Martin, A., *Nuovo cimento*, **16**, 78 (1960)
387. Chew, G. F., and Mandelstam, S., *Nuovo cimento* (In press)
388. Moffat, J. W., *Phys. Rev.*, **121**, 926 (1961)
389. Chew, G. F., and Frautschi, S. C., *Phys. Rev. Letters*, **5**, 580 (1960)
390. Frautschi, S. C., *Phys. Rev. Letters*, **5**, 159 (1960)
391. Frautschi, S. C., and Walecka, J. D., *Phys. Rev.*, **120**, 1486 (1960)
392. Bowcock, J., Cottingham, W. N., and Lurie, D., *Nuovo cimento*, **16**, 918 (1960)
393. Bowcock, J., Cottingham, W. N., and Lurie, D., *Phys. Rev. Letters*, **5**, 386 (1960)
394. Ball, J., and Wong, D. Y., *Phys. Rev. Letters*, **6**, 29 (1961)
395. Herman, R., and Hofstadter, R., *Phys. Rev. Letters*, **6**, 293 (1961)
396. Chew, G. F. (Private communication)
397. Anderson, J. A., Bang, V. X., Burke, P. G., Carmony, D. D., and Schmitz, N., *Phys. Rev. Letters* (April 1961); *Revs. Mod. Phys.* (July 1961)
398. Khuri, N. N., *Phys. Rev.*, **107**, 1148 (1957)
399. *Proc. Conf. Nuclear Forces and the Few-Nucleon Problem, London, 1959*, 171 (Pergamon Press, London, Engl., 1960)
400. Blank, V. Z., and Isaev, P. S., *Soviet Phys. "Doklady"*, **2**, 532 (1957) [117, 785 (1957)]
401. Natsuyama, S., and Miyazawa, H., *Progr. Theoret. Phys. (Kyoto)*, **18**, 328 (1957)
402. Matsuyama, S., and Miyazawa, H., *Progr. Theoret. Phys.*, **19**, 517 (1958)
403. Kuni, F. M., *Soviet Phys. "Doklady"*, **1**, 686 (1956) [111, 571 (1956)]
404. Grisaru, M. T., *Phys. Rev.*, **111**, 1719 (1958)
405. Hamilton, J., *Phys. Rev.*, **114**, 1170 (1959)
406. Blanpied, W. A., *Phys. Rev.*, **116**, 738 (1959)
407. Hull, M. H., Jr., and Shapiro, J., *Phys. Rev.*, **109**, 846 (1958)
408. Alexeff, I., and Haeberli, W., *Nuclear Phys.*, **15**, 609 (1960)
409. Cini, M., Fubini, S., and Stanghellini, A., *Phys. Rev.*, **114**, 1633 (1959)
410. Alles, W., and Tomasini, A., *Nuovo cimento*, **13**, 1265 L (1959)

411. Alles, W., and Tomasini, A., *Nuovo cimento*, **13**, 1273 L (1959)
412. Charap, J. M., and Fubini, S. P., *Nuovo cimento*, (10) **15**, 73 (1960)
413. Charap, J. M., and Tausner, M. J., *Nuovo cimento*, (10) **18**, 316 (1960)
414. Imamura, T., *Progr. Theoret. Phys. (Kyoto)*, **13**, 183 (1955)
415. Goldberger, M. L., and Oehme, R., *Ann. phys.*, **10**, 153 (1960)
416. Noyes, H. P., *Phys. Rev.*, **119**, 1736 (1960)
417. Furuichi, S., and Machida, S., *Nuovo cimento*, **19**, 396 (1961)
418. Chew, G. F., *Double Dispersion Relations and Unitarity As the Basis For a Dynamical Theory of Strong Interactions (UCRL-9289, 1960)*; Revised (1961)
419. Wong, D. Y., *Phys. Rev. Letters*, **2**, 406 (1959)
420. Perring, J., and Phillips, P., *Nuclear Phys.* (In press)
421. Signell, P., and Yoder, R., *Phys. Rev.* (In press)
422. Martin, A., *Nuovo cimento*, **19**, 1257 (1961)
423. Amati, D., Leader, E., and Vitale, B., *Nuovo cimento*, **17**, 68 (1960)
424. Amati, D., Leader, E., and Vitale, B., *Nuovo cimento*, **18**, 409 (1960)
425. Amati, D., Leader, E., and Vitale, B., *Nuovo cimento*, **18**, 458 (1960)
426. Cziifra, P., *The Two-Pion-Exchange Contribution to the Higher Partial Waves of Nucleon-Nucleon Scattering (UCRL-9249, Doctoral thesis, Univ. Calif., Berkeley, Calif., 1960)*
427. Grashin, A. F., and Kobsarev, I. Yu., *Nuclear Phys.*, **17**, 218 (1960)
428. Goldberger, M. L., Grisaru, M. T., MacDowell, S. W., and Wong, D. Y., *Phys. Rev.*, **120**, 2250 (1960)
429. Hall, D., and Wightman, A. S., *Kgl. Danske Videnskab. Selskab, Mat.-fys. Medd.*, **31**, No. 5 (1957)
430. Jacob, M., and Wick, G. C., *Ann. phys.*, **7**, 404 (1959)
431. Sakurai, J. J., *Ann. phys.*, **11**, 1 (1960)
432. Sakurai, J. J., *Phys. Rev.*, **119**, 1784 (1960)
433. Breit, G., *Phys. Rev.*, **51**, 248 (1936); Share, S., and G. Breit, *Phys. Rev.*, **52**, 546, (1957); Breit, G., *Phys. Rev.*, **53**, 153 (1938); Breit, G., and Stehn, J. R., *Phys. Rev.*, **53**, 459 (1938); Breit, *Proc. Natl. Acad. Sci. US*, **46**, 746 (1960)
434. Breit, G., *Phys. Rev.*, **120**, 287 (1960)
435. Abashian, A., Booth, N. E., and Crowe, K. M., *Phys. Rev. Letters*, **5**, 258 (1960)

NUCLEAR ORIENTATION¹

BY LOUIS D. ROBERTS AND J. W. T. DABBS

Oak Ridge National Laboratory, Oak Ridge, Tennessee

INTRODUCTION

Nuclear spin orientation studies were first suggested by Kurti & Simon (1) and by Gorter (2) in connection with the early development of the magnetic cooling process. In an electron magnetic cooling experiment a paramagnetic salt is subjected isothermally to a magnetic field H_i , for example 20 koe, at a temperature T_i near, say, 1°K. The result is a polarization G_1 (or magnetization $\langle M_z \rangle$) of the electron spin system with a corresponding reduction of the spin-system entropy. When the magnetic field is then decreased to zero adiabatically, the temperature of the salt falls to a value T_f such that the entropy or degree of ordering of the spin system due to internal spin-spin and spin-lattice interactions has the same value it had at (H_i, T_i) . The weaker these internal interactions are, the lower T_f will be. Thus it was realized that the lowest temperature would be obtained by performing this magnetic cycle on a nuclear spin system where the spin interactions are much weaker than for the electron spin case. As was indicated above, the first stage in this nuclear cooling cycle is the polarization of the nuclear spin system. For the purpose of thermodynamic discussion this polarization is adequately described by $\langle M_z \rangle$.

The orientation of nuclei is also of interest in nuclear physics. Usually, a more general definition (3, 4, 5) of nuclear orientation which reflects the nuclear physics of the problem is needed here. By nuclear orientation we mean that the $2I+1$ substates m_I of a nucleus of spin I do not all have the same population. Equal population of the substates implies a spatially isotropic system, whereas an unequal population of these substates corresponds to an anisotropy and to the introduction of a preferred direction in space. The emission or absorption of radiation by such an oriented spin system will display an anisotropy relative to this preferred direction. A measurement of this radiation anisotropy will yield information about the population distribution of the system over the substates m_I , information relative to the preferred direction, and information about the angular momentum changes and matrix elements associated with the emission or absorption of the radiation. The anisotropy will often, although not always, be spatial in character. For example, in the interaction of polarized s -wave neutrons with polarized nuclei, the cross section for the process may be modified by the polarization while the spatial angular distribution of the reaction remains isotropic. However, gamma emission from oriented nuclei will usually display an angular anisotropy of intensity.

¹ The survey of literature pertaining to this review was concluded in April 1961.

The angular distribution $W(\theta)$ of radiation emitted or absorbed by a system of oriented nuclei may be precisely and simply described in terms of angular momentum theory. For example, in a frequently adequate formulation the angular distribution of the intensity has the form

$$W(\theta) = \sum B_\nu G_\nu P_\nu(\cos \theta)$$

Here the B_ν are constants containing all of the nuclear information, $P_\nu(\cos \theta)$ is a Legendre polynomial of order ν , and the G_ν are parameters describing the nuclear orientation. The maximum value of ν is set by angular momentum considerations, and in general only a few terms in this sum are required for an exact description of $W(\theta)$. Perhaps the basic reasons that nuclear orientation experiments have some usefulness in nuclear and in solid state physics are, first, that an exact theoretical framework is available for the interpretation of experimental results and, second, that within this framework, the nuclear physics and the solid state physics enter in separate, well-defined parameters.

There have been a number of excellent reviews of the field of nuclear orientation, two of these being quite recent (6, 7). Well over a dozen methods of nuclear orientation have been proposed which have yielded some useful nuclear orientation; most of these have been thoroughly discussed in these recent reviews. Thus, for older work we refer the reader to the earlier papers and will restrict this discussion to those aspects of the field which are currently most active. This current work covers a wide diversity of experimental and theoretical material.

GENERAL CONSIDERATIONS

As was indicated above, nuclear orientation consists in producing a non-uniform population of the $2I+1$ substates of the nuclear spin I . The possibility of doing this, of course, implies that these substates have been in some way distinguished by interaction with their surroundings. Over the past 15 years, a considerably body of information has been obtained about these hyperfine-structure nuclear electric and magnetic interactions in solids using resonance methods (8, 9, 10). For quite dilute paramagnetic materials, the spin-system energy levels are precisely describable in terms of an "effective" spin Hamiltonian \mathcal{H} . For example, for a simple case with axial symmetry,

$$\begin{aligned} \mathcal{H} = & g_{\parallel}\beta H_z S_z' + g_{\perp}\beta(H_x S_x' + H_y S_y') + A I_z S_z' + B(I_x S_x' + I_y S_y') \\ & + P(I_z^2 - \frac{1}{3}I(I+1)) - g_n \beta_n \mathbf{H} \cdot \mathbf{I} \end{aligned} \quad 2.$$

Here H is an externally applied magnetic field, S' is the "effective" electron spin operator, g_{\parallel} and g_{\perp} are the spectroscopic splitting factors, β and β_n are the electron and nuclear Bohr magneton numbers, g_n is the nuclear gyromagnetic ratio, and A , B , and P are coupling constants (8).

The "effective" electron spin S' appears rather than the actual spin S of the free ion because of crystalline electric field effects. For example, for

Ce^{+++} the free ion is in a $^2F_{5/2}$ state with an electron angular momentum J of $5/2$. In a suitable salt, for example, $\text{Ce}_2\text{Mg}_3(\text{NO}_3)_{12} \cdot 24\text{H}_2\text{O}$, the water molecules which surround the Ce^{+++} ion produce an anisotropic electric field in the region of motion of the single magnetic electron. Correspondingly, some orbital states are of lower energy than others. Thus the crystalline field separates the $2J+1=6$ substates into three doublets. The spacing of the lower pair of doublets is 26 cm^{-1} which is equivalent to approximately 38°K (11). Nuclear alignment and electron paramagnetic resonance experiments are usually performed at temperatures in the liquid helium region or below, i.e., less than 4.2°K . Here only the lowest doublet will be appreciably populated and S' is thus one-half, reflecting the degeneracy of the doublet state. The anisotropy of the electron g factor tensor expressed in terms of g_{\parallel} and g_{\perp} then predominantly reflects the "crystal field" wave functions (8) of this lowest doublet. This anisotropy is very large with $g_{\parallel} < 0.03$ and with $g_{\perp} = 1.84$ (9, 34). An effective spin $S' = \frac{1}{2}$ is fairly typical, an exception being ions with half-filled electron shells such as Mn^{++} or Gd^{+++} .

The Hamiltonian Equation 2 is for magnetically dilute materials; the degree of magnetic dilution is, of course, relative. There will always be terms in \mathcal{H} involving the interaction between electron spins on different atoms. For resonance or other magnetic studies near 4°K , these terms are very small in $\text{Ce}_2\text{Mg}_3(\text{NO}_3)_{12} \cdot 24\text{H}_2\text{O}$ relative to the interaction of the electron spin with an external magnetic field of, say, a few thousand oersteds. Yet it is terms of this type (including the magnetic interaction of the Ce^{+++} ion with the proton moments of the water of hydration) which limit the temperature decrease in the magnetic cooling of this salt to $\sim 0.003^\circ\text{K}$. As will be seen in the course of this review, $\text{Ce}_2\text{Mg}_3(\text{NO}_3)_{12} \cdot 24\text{H}_2\text{O}$ has been perhaps the most useful of the materials so far investigated in the production and measurement of millidegree temperatures and in the production of nuclear orientation. This usefulness comes from the characteristics mentioned above, i.e., the high degree of magnetic dilution, the large anisotropy of the g tensor, and the large number of water molecules of crystallization.

For more concentrated magnetic materials, for example $\text{CuCl}_2 \cdot 4\text{H}_2\text{O}$, the electron spin-spin interaction is rather stronger and this salt becomes antiferromagnetic at 4.2°K (12). Here the spin-spin interaction terms clearly may not be neglected in Equation 2. In antiferromagnetic materials, the electron spin system often orders itself in a complex superlattice, and time-dependent effects in the electron spin system which can provide a nuclear spin-lattice relaxation are not yet well understood. Thus, nuclear orientation experiments involving dense antiferromagnetic materials tend to be more a study of antiferromagnetism, including correlation time effects, than of nuclear physics.

The situation is somewhat better from the nuclear physics viewpoint in the case of metallic ferromagnetic materials. Here the electron spin correlation times, at temperatures low compared to the ferromagnetic Curie temperature T_c , will in general be long relative to the lifetimes of nuclear states.

The ferromagnetic interaction, of course, does not affect the nucleus directly but acts effectively to suppress the off-diagonal elements of the hyperfine structure coupling. Thus Equation 2 becomes, for example, in an approximation useful for ferromagnetic metals at temperatures well below T_c ,

$$\mathcal{H} \cong g\beta H_z S_z' + A I_z S_z' + P(I_z^2 - \frac{1}{3}I(I+1)) - g_n \beta_n H_z I_z \quad 3.$$

Of course, in an arbitrary ferromagnetic material, one would not necessarily expect all the tensors describing the interactions in \mathcal{H} to have the same axis. This model has been used for the interpretation of some interesting experiments on nuclear orientation in ferromagnets which, again, have thus far yielded primarily solid state information relative to the magnitude of the constant A .

We wish to note that the spin Hamiltonian will often be more complex than in Equations 2 or 3. In addition to the terms discussed above, the crystal field may introduce in \mathcal{H} a variety of terms in the electron spin (8), for example, of the form $D[S_z'^2 - \frac{1}{3}S'(S'+1)]$.

Assuming the electron and nuclear total and projection angular momentum quantum numbers S , m_s , I , m_I , nuclear orientation is describable (3, 4, 5) in terms of the $(2S'+1)(2I+1)$ states of \mathcal{H} . One would expect that suitable parameters for the description of the nuclear results of nuclear orientation experiments for situations with axial symmetry would be of the form of $\langle I_z \rangle$, $\langle I_z^2 \rangle$, etc., and this is indeed the case. The particular form of these averages which arises naturally in angular momentum theory is the function G_ν (or f_ν , which is proportional to G_ν). In axial symmetry G_ν has the form

$$G_\nu = \frac{\sum_i \langle i | T_{\nu 0} | i \rangle P_i}{\sum_i P_i} \quad 4.$$

where i designates the set of wave functions for which \mathcal{H} is diagonal and P_i is the population of the i th state. The set of operators $T_{\nu 0}$ have, for example, the form

$$T_{00} = (2I+1)^{-1} \quad 5a.$$

$$T_{10} = \left[\frac{3}{I(I+1)(2I+1)} \right]^{1/2} I_z \quad 5b.$$

$$T_{20} = \left[\frac{180(2I-2)!}{(2I+3)!} \right]^{1/2} [I_z^2 - \frac{1}{3}I(I+1)] \quad 5c.$$

where I_z is an operator. There are a number of other convenient forms for the G_ν . If \mathcal{H} happens to be diagonal in the S , m_s , I , m_I representation, the $\langle i | T_{\nu 0} | i \rangle$ are Clebsch-Gordan coefficients (cf. Eq. 17). Experimental situations may of course arise where one does not have axial symmetry. The relevant tensors have been discussed by Fano & Racah (13).

We now consider the several ways of producing population variations over the states i . In most of the nuclear orientation work done thus far in

which nuclear results were obtained, these variations have been produced by lowering the temperature of the spin system to a value such that kT becomes of the order of one or more of the coupling constants A , B , or P in Equation 2. In a few instances $T \sim 1^\circ\text{K}$ will suffice, but usually temperatures in the millidegree region are required. Nuclear orientations approaching 100 per cent may sometimes be achieved. This essentially thermodynamic procedure is generally called the static method. Here it is usually convenient to write

$$G_\nu = \frac{\text{Tr}[T_{\nu 0} \exp(-\mathcal{H}/kT)]}{\text{Tr} \exp(-\mathcal{H}/kT)} \quad 6.$$

In a diagonal representation the populations are, of course,

$$P_i = \frac{\exp(-E_i/kT)}{\sum_i \exp(-E_i/kT)} \quad 7.$$

A dynamic method for nuclear orientation has become important in the past few years. Here one applies a magnetic field of the order 10 koe to a suitable paramagnetic sample at a temperature so low that the electron spin system is strongly magnetized. The needed temperature of about 1°K is much more easily achieved than the millidegree requirements of the static method. Then—as will be described below—by saturating certain transitions between the levels of \mathcal{H} , one may force a nonuniform population of the $(2S'+1)(2I+1)$ levels of the system. The nuclear orientation parameters G_ν , as defined in Equation 4, also apply here. A nuclear polarization comparable to the electron spin magnetization of the system may in principle be expected, and quite large nuclear polarizations have been obtained.

One often hears the terms "nuclear polarization" and "nuclear alignment." Usage seems to have given these terms the following meaning. In general, polarization is associated with nonzero values for the G_ν of odd ν , whereas alignment is associated with nonzero values of the G_ν of even ν . All of the G_ν except G_0 , which is related to the intensity, become zero in the absence of nuclear orientation. It is interesting that if the system is polarized it will often also be aligned, but not vice versa. For small G_1 , G_2 is of the order of G_1^2 ; but as G_1 approaches saturation, G_2 may also.

The following material is classified according to the procedure used to produce the nuclear orientation.

DYNAMIC METHODS

Dynamic methods of nuclear orientation have given a number of interesting results in nuclear and solid state physics (6, 14). For example, in nuclear physics, the angular distribution of gamma emission from a number of oriented nuclear species has been observed and magnetic moments of excited nuclear states have been measured. In solid state physics, the magnitude and sign of hyperfine structure coupling constants have been determined with precision, and the electron and nuclear spin relaxation times associated

with the dynamic nuclear orientation process have been obtained. Quite recently, dynamic proton polarization experiments have yielded a polarization near 20 per cent (15, 25), and even higher values may be expected from reasonable extensions of the techniques. These proton polarization results may be of much value in particle scattering experiments. Because of their potential usefulness in nucleon interaction studies, we shall direct our attention in this section primarily toward these recent proton polarization experiments, including some discussion of studies leading up to them.

ORIENTATION USING A RELAXATION PROCESS

The method used in this proton orientation work is an outgrowth of a suggestion by Overhauser (16) that the nuclei of a sample of metal might be oriented by a combination of the selective excitation of a particular electron resonance followed by the de-excitation of this state through a process in which a nuclear spin is flipped. In particular, he discussed the case of a metal sample in an external magnetic field. Here, the field produces a Zeeman splitting ΔE of the conduction electron spin states. These states will then have different populations at thermal equilibrium. If an rf field of frequency $\nu = \Delta E/h$ is suitably applied to the sample, transitions between the electron spin states are induced, and with increasing rf power the populations of the two states may be made to approach equality, i.e., the spin system may be made to approach saturation. In a steady state situation the number of spins entering the higher-energy state through the rf excitation will of course equal the number leaving it through various de-exciting mechanisms. One expected relaxation mechanism will be the scattering of the excited state conduction electrons on nuclei. If these nuclei have spin, the scattering operator will involve spin-orbit coupling of the conduction electron angular momentum with that of the nucleus.

$$\mathcal{H}_{s.o.} \sim I_z S_z + (I_+ S_- + I_- S_+)/2 \quad 8.$$

Terms of the form $I_+ S_-$ or $I_- S_+$ will de-excite the higher-energy electron spin-state and flip a nuclear spin in the process. Because of the rf excitation, there will be a preferred relaxation flow of electron spin-state population from, say, $m_s = +\frac{1}{2}$ to $m_s = -\frac{1}{2}$ with a corresponding flow of nuclear spin-state population in the opposite direction toward higher projection quantum number. If all nuclear spin relaxation processes tending to destroy the above dynamically produced orientation were slow relative to the above rate of dynamic nuclear orientation, the degree of nuclear polarization would be of the order $\beta H/kT = 0.67 \times 10^{-4} H/T$. For $H \sim 10^4$ oe and $T \sim 1^\circ K$, it is found that $\beta H/kT = 0.67$, corresponding to a respectable degree of nuclear polarization. The maximum value of H is set by the maximum frequency at which adequate rf power is available to saturate the electron spin system. At present, for the most favorable systems, this is in the neighborhood of 30,000 mc/sec which is equivalent to fields in the vicinity of 10^4 oe. A temperature near $1^\circ K$ is quite easily attainable through the application of usual

liquid helium techniques. Also, well-engineered refrigeration methods are being developed for the attainment of temperatures near 0.3° to 0.4°K with a substantial heat load using a gas-liquid helium-3 cycle. Lower temperatures at substantially lower heat load capacities are, of course, available through a magnetic cooling refrigeration cycle of the kind described in the introduction. The point here is that, potentially at least, large dynamic nuclear polarizations would seem to be available at values of magnetic field and temperature that are relatively convenient to attain.

The above nuclear polarization ideas were quickly verified by Carver & Slichter (17) using metallic lithium and sodium and also a solution of sodium in anhydrous liquid ammonia. Relatively low magnetic fields in the range 12 to 44 oe were used. The experiments were performed at room temperature. The nuclear polarization was measured by observing the nuclear magnetic resonance of the lithium, sodium, or hydrogen (in the ammonia) nuclei, the amplitude of this resonance being approximately proportional to the polarization. The nuclear polarization was enhanced by a large factor by the Overhauser process, but it was rather less than that theoretically predicted for the lithium and sodium metals. In the case of lithium this was attributed to a competing nuclear spin relaxation process destructive to the nuclear orientation and in the case of sodium to a very short conduction electron spin relaxation time which did not permit a saturation of the sodium electron spin resonance with the available rf power. For protons in the sodium-anhydrous liquid NH_3 solution, a full effect was observed, but the nuclear polarization obtained was still very small because of the high temperatures and low magnetic fields.

This first experiment succeeded in part because it was performed at low magnetic fields and frequencies and at relatively high temperatures. The extrapolation of this first work to lower temperatures and higher fields and thus to larger nuclear polarizations presented a number of practical difficulties. Among these was the fact that at, say, 30,000 mc/sec and 1°K the rf skin depth in a metal would be exceedingly small, making it difficult to attain a sample thickness adequate for most nuclear physics applications. This difficulty may be alleviated through the use of an insulator or semiconductor sample material, and such experiments have been done successfully. Another problem arises because the conduction electron spin-lattice relaxation time for metals is expected in general to be very short, as with sodium, above, with the result that high rf power levels would be required at these high frequencies to saturate the electron spin resonance. A third disadvantage of the Overhauser process is that the polarization is built up in the sample through a relaxation process for which the relaxation time may be quite long.

SATURATION OF PARTIALLY FORBIDDEN TRANSITIONS

With the success of the Carver-Slichter experiments, a number of authors (14, 18, 19) pointed out that the method was not restricted to the saturation of the electron spin resonance in metals but was a technique which should be

quite widely applicable to paramagnetic materials exhibiting a hyperfine structure coupling and having suitable spin relaxation times. It was pointed out that this hyperfine structure interaction could be of a quite general type, for example, dipole-dipole coupling. Of especial importance was the recognition by Jeffries (19) that nuclear polarization could be produced through the saturation of the partially forbidden transitions in which electron and nuclear spins simultaneously undergo a change of projection quantum number. Here the reorientation of the nuclear spin is directly forced by the applied radiofrequency power, and the polarization may be expected to build up quickly. This is in contrast to the Overhauser process in which the polarization builds up with relative slowness through a relaxation process.

Jeffries first applied his ideas in an experiment for the dynamic polarization of cobalt 60, the magnitude of the polarization being measured through the anisotropy of gamma emission from the oriented nuclear spin system (20). A nuclear polarization G_1 of the order of 10 per cent, equivalent to an alignment G_2 of about 1 per cent, was obtained. This was about half the theoretically expected value. The sample used was a crystal of $\text{La}_2\text{Mg}_3(\text{NO}_3)_{12} \cdot 24\text{D}_2\text{O}$ in which 1 mc of Co^{60} and a very small amount of Co^{59} replaced a portion of the Mg. Although the gamma anisotropy was relatively small, about 1 per cent, it was precisely observable because of a relatively high level of gamma activity.

In the above experiment, the resonant electron spin and the nucleus being oriented belonged to the same atom and were coupled by a hyperfine structure coupling of sufficient magnitude to be resolved readily in an electron paramagnetic resonance experiment. It is then possible to saturate particular transitions of the system selectively. An external magnetic field large relative to the hyperfine structure coupling was applied to the sample, largely decoupling the electron and nuclear spins and giving spin wave functions of the general form $|m_s, m_I > +\alpha |m_s - 1, m_I + 1 >$. The important terms in the static Hamiltonian are then the hyperfine structure coupling and the interaction of the electron spin with the external field, the direct interaction of this external field with the nuclear spin being negligible here. The partially forbidden transitions were excited by placing the oscillating rf magnetic field parallel to the dc field H , the transitions taking place by way of the small term in $\alpha \sim B/H$ in the wave function. The magnitude of the polarization was expected to be $\sim (2I+1)^{-1} (h\nu/kT)$ if only one of the $2I$ partially forbidden electron resonances were saturated. Other things being equal, a larger polarization evidently results with smaller nuclear spin. This procedure has been applied (6) to Mn^{54} , Mn^{52} , Sb^{123} , and As^{76} as well as to Co^{60} , above. The gamma-ray anisotropies were observed and the nuclear moments were determined.

The next significant advance in dynamic nuclear orientation studies came as follows. As was pointed out in the above work on Co^{60} , the electron and nuclear spins entering the process both belonged to the same atom.

Erb, Motchane & Ubersfeld (21), Abragam & Proctor (22), and Abraham, McCausland & Robinson (23) found that the saturation of "forbidden" electron resonances of paramagnetic impurity atoms in various substances could induce the polarization of nuclei of the host material in the volume surrounding the impurity atom. This process has been further investigated by Leifson & Jeffries (24), by Borghini & Abragam (25), and by Khutsishvili (26). A considerable number of nuclei have been polarized in some degree (6, 14), and it was by this procedure that proton polarizations near 20 per cent have been obtained (25). The paramagnetic impurity may be introduced, for example, as a small amount of paramagnetic Ce^{+++} replacing the La^{+++} in $\text{La}_2\text{Mg}_3(\text{NO}_3)_{12} \cdot 24\text{H}_2\text{O}$ which itself has no electron paramagnetism, or as F centers or free radicals produced by radiation damage in a plastic or other dielectric material. For a sufficient paramagnetic impurity atom density, this polarization could extend throughout the entire volume of the sample. In common with the method of Jeffries, this process depends on the saturation of partially forbidden transitions. The terms in \mathcal{H} , however, have a somewhat different order of importance.

In a simple model (14, 24), we consider a crystal lattice consisting of relatively few electron spins S_k (i.e., paramagnetic ions) and many nuclear spins I_i in atoms in the vicinity of the paramagnetic ion. Let S_k be the k th electron spin, I_i be the i th nuclear spin, and let the sample be subject to a magnetic field H . For convenience we assume the electron spectroscopic splitting factor g to be isotropic. We have then

$$\mathcal{H} = g\beta \sum_k \mathbf{H} \cdot \mathbf{S}_k - g_n\beta_n \sum_i \mathbf{H} \cdot \mathbf{I}_i + \sum_{i,k} \mathbf{D}_{ik} + \sum_{ij} U_{ij} + \mathcal{H}_{\text{relax}} + \mathcal{H}_{\text{rf}} \quad 9.$$

for the spin Hamiltonian for the crystal, omitting any terms which do not directly contribute to the dynamic nuclear orientation. The interaction between the k th electron and the i th nucleus is given by \mathbf{D}_{ik} . This interaction is predominantly dipole-dipole in character but may include a contribution from terms of the form $\mathbf{S}_k \cdot \mathbf{I}_i$ arising indirectly from an overlap of the wave function of \mathbf{S}_k with the wave functions of the i th atom. The term $\mathcal{H}_{\text{relax}}$ represents the operators leading to spin-spin and spin-lattice relaxation, and \mathcal{H}_{rf} represents the term leading to the absorption of the rf signal in the sample. The Zeeman splitting of the electron spin levels will correspond to a frequency $\nu_e \sim 10^3$ times greater than the equivalent nuclear frequency ν_n of the nuclear levels. These terms would be entirely independent except for the term in \mathbf{D}_{ik} which slightly mixes the electron and nuclear states. This mixing leads to resonances at $\nu_e \pm \nu_n$ as well as at ν_e . Figure 1 illustrates these energy levels for assumed electron and nuclear spins $S = I = \frac{1}{2}$. The states are designated by m_S and m_I , the quantum numbers of the decoupled system. In the absence of the \mathbf{D}_{ik} term, only the allowed transition Q (or the equivalent nuclear transitions) could occur; but with the \mathbf{D}_{ik} coupling, the so-called forbidden transitions R and S may also be induced.

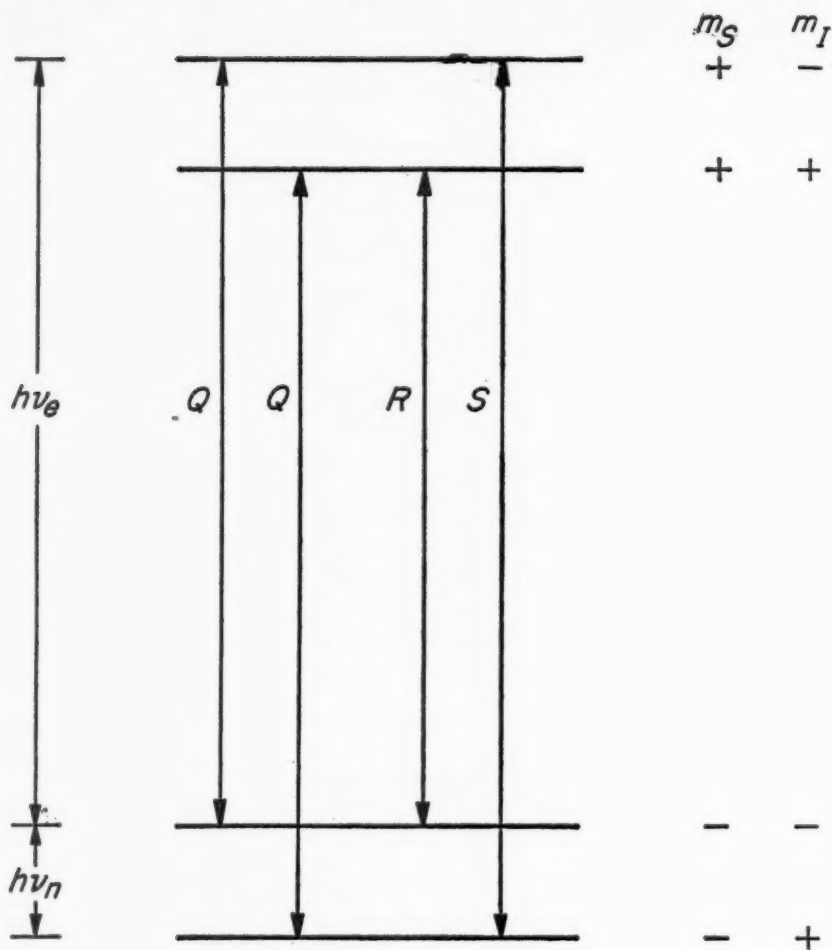


FIG. 1. Energy levels of a system with $S=\frac{1}{2}$, $I=\frac{1}{2}$ in a strong magnetic field.

The probability of the R and S transitions will depend on the degree of mixing of the electron and nuclear wave functions, and in turn this degree of mixing will reflect a coefficient of the form $\langle |D_{ik}| \rangle / (g\beta H)$. Thus, at large distances from the paramagnetic impurity where the dipole-dipole interaction $\langle |D_{ik}| \rangle$ is small, the rate of direct dynamic nuclear orientation will be weak.

The term U_{ij} in Equation 9 represents the dipole-dipole interaction between the i th and j th nuclear spins. It has been shown by Bloembergen (27), Jeffries (24), and others that the nuclear orientation may diffuse through the

nuclear spin system by way of this spin-spin coupling of neighboring nuclei, tending to give a uniform density of nuclear polarization even though the paramagnetic impurity density may be small. This diffusion of the polarization P (not to be confused with P in Eq. 2) has been described in terms of a diffusion equation

$$\partial P / \partial t = D \nabla^2 P \quad 10.$$

where t is the time and D the diffusion coefficient. Thus it is found that $P \propto \exp(-Dt^2)$. Jeffries *et al.* (24) estimate $D \sim 3 \times 10^{-12} \text{ cm}^2/\text{sec}$. Polarization initially confined to a volume near a paramagnetic ion would diffuse through a sphere of 10^{-6} -cm radius in one second.

Leifson & Jeffries (24) have made an extensive study of the thermal relaxation and dynamic orientation of protons in single crystals of $\text{La}_2\text{Mg}_3(\text{NO}_3)_{12} \cdot 24\text{H}_2\text{O}$ in which a small portion of the La^{+++} has been replaced by paramagnetic Ce^{+++} . This work was performed at temperatures in the range 1.6° to 4.2°K with Ce^{+++} ion concentrations in the range 0.05 to 5 per cent of the La^{+++} . The partially forbidden electron paramagnetic resonance was strongly induced at 9400 mc/sec, and the degree of proton polarization was measured simultaneously by observing the proton nuclear magnetic resonance at 16 mc/sec. For a 1 per cent Ce^{+++} ion concentration at a temperature of 1.6°K , the proton polarization was enhanced by a factor of 140 above the thermal equilibrium value in the applied magnetic field of about 3700 oe. Because of the relatively small value of this field, the proton hyperfine structure was not resolved, i.e., $\langle |g_n \beta_n I_z H| \rangle$ was comparable to the electron resonance line width.

If one calculates the expected polarization enhancement on the basis of a simple model which neglects nuclear spin relaxation effects destructive to the induced polarization, a value of 605 is obtained, somewhat more than four times that observed. This fact of course shows that competing relaxation effects are important. The observed polarization enhancement of 140 is equivalent to an actual polarization $P = 0.03$.

The proton spin-lattice relaxation time T_{1n} was found to vary with the absolute temperature as T^{-7} at constant Ce^{+++} ion concentration in the temperature range 1.6°K to 4.2°K . At fixed temperature, the inverse relaxation time T_{1n}^{-1} was found to be roughly proportional to the square of the Ce^{+++} ion concentration. The electron spin-lattice relaxation time of the Ce^{+++} ion T_{1e} was found to be independent of the Ce^{+++} ion concentration in the concentration range studied, and to depend on the temperature as T^{-14} in the temperature range 1.9° to 2.6°K .

In these studies evidence for a diffusion of proton polarization is obtained from the observation of the time required for the polarization to build up after the rf power is turned on. It was concluded that both the direct polarization of the protons which are near neighbors to the Ce^{+++} and the polarization of more distant protons through diffusion are important mechanisms.

Similar measurements have been made by Borghini & Abragam (25) at a higher frequency of 34,000 mc/sec in the temperature range of 1.5° to 2.1°K. Again the substance studied was $\text{La}_2\text{Mg}_3(\text{NO}_3)_{12} \cdot 24\text{H}_2\text{O}$ in which a small fraction of the La^{+++} was replaced with Ce^{+++} . The concentration of Ce^{+++} ion was in the range 0.1 to 20 per cent. Here, at the higher field value of 13,500 oe, the proton hyperfine structure was clearly resolved, i.e., the partially forbidden transitions *R* and *S* could be well resolved from the allowed transition *Q*, Figure 1. Results of relaxation time measurements at this higher frequency were in agreement with those of Jefferies *et al.* (24) in the lower-frequency range. A crystal with 0.5 per cent Ce^{+++} ion concentration was investigated most extensively, and at the lower temperatures polarization enhancements of over 200 were obtained. At 1.5°K this enhancement corresponded to $P=0.19$. This magnitude for P should be useful in nuclear physics investigations. High-energy proton-proton scattering experiments are being set up both at Saclay (30) and Harwell (31), using the above method to produce a polarized proton target.

It may be reasonably objected that the partial polarization of but a fraction of the nuclides in a complex salt such as the $\text{La}_2\text{Mg}_3(\text{NO}_3)_{12} \cdot 24\text{H}_2\text{O}$ does not provide a very satisfactory polarized target for scattering experiments, and in general this is true. The molecular weight of this salt is 1530; thus only about 3 per cent of the nucleons present, i.e., the protons of the $24\text{H}_2\text{O}$, may be polarized. To improve the situation Robinson (28) and Hwang & Sanders (29) have investigated the possible use of polyethylene or of high-molecular-weight paraffins of general formula $\text{C}_n\text{H}_{2n+2}$ where n is large. Here roughly one nucleon in 7 (or 14 per cent of the nucleons) is a proton which potentially may be polarized. These compounds are normally nonmagnetic with regard to electron paramagnetism. They may, however, be subjected to radiation damage, which breaks a small fraction of the chemical bonds producing free radicals with an electron spin paramagnetism. Once more, by strongly inducing the "forbidden" transitions an appreciable proton polarization has been obtained which, however, has not been as large as with the $\text{La}_2\text{Mg}_3(\text{NO}_3)_{12} \cdot 24\text{H}_2\text{O}$. A polarization P of 1.2 per cent has been reported by Hwang & Sanders (29). As the hydrocarbon has a much more favorable ratio of protons to total nucleons than the lanthanum salt, the 1.2 per cent polarization in the paraffin may be comparably as useful as the 20 per cent in the lanthanum salt, for some experiments.

The hydrocarbon work is only in its initial stages, and the processes involved are not yet completely understood. In some respects, the lanthanum salt seems more ideal. Here, the frequencies of the two partially forbidden transitions *R* and *S* are defined effectively by the interactions of the electrons and protons directly with the external field. The dipole-dipole interaction D_{ik} weakly mixes the electron and proton spin states but has little effect on the energy of the transitions ν_e and $\nu_e \pm \nu_n$. Thus, in a sense, all of the protons are equivalent. In the radiation-damaged paraffins, one seems

to have a different and somewhat less simple situation. The C_nH_{2n+2} consists of long chain molecules. In the radiation damage the chain is broken and the two electrons which were involved in the now broken bond are free to move, one in each of the fragments. There are many protons in each fragment which are individually coupled through a contact-type interaction to the one itinerant electron. This leads to a complex hyperfine structure with a broad band of partially forbidden transitions. The lack of sharpness leads to difficulty in saturating the *R* or *S* transitions. This work is thus giving interesting solid state information and it holds much promise for nuclear applications.

The high degree of dilution of the protons in the lanthanum salt renders the use of this material as a polarized proton target difficult though not impossible. In a proton-proton scattering experiment, if one measures the energy and angle of both emergent protons, the scattering from the polarized protons may be differentiated from scattering by unpolarized nucleons bound in other nuclei. Development work toward such experiments is currently being considered both at Harwell (31) and at Saclay (30). To obtain the higher polarization of about 20 per cent, the apparatus is being designed for temperatures near 1°K and frequencies near 34,000 mc/sec, corresponding to wavelengths near one centimeter. With present methods, this short wavelength restricts the size of the sample to roughly a square centimeter area by about a one-tenth-centimeter thickness. These dimensions appear to be useful for the measurements contemplated.

For scattering experiments in the very-high-energy region much thicker targets will be most desirable. The problem here is one of rf technique—that of obtaining a uniform, adequately intense rf field in the millimeter wavelength region over a sample whose dimensions are a number of rf wavelengths. This development does not seem to have been attempted seriously as yet.

Returning once more to the present development of nuclear polarization in the lanthanum salt, there seem to be a number of useful—if selective—applications. For example, it should be possible to prepare the lanthanum salt with heavy water and obtain a high degree of deuteron polarization. This target could be conveniently used to measure the neutron-deuteron scattering lengths for polarized thermal neutrons, for example. We are not aware of any work thus far on the dynamic polarization of deuterons.

STATIC METHODS

THE "BRUTE FORCE" METHOD OF POLARIZATION

The first method for nuclear spin orientation proposed (1, 2) was direct orientation through the application of a large external magnetic field to the system at very low temperatures. Here G_1 is proportional to the nuclear magnetization, or polarization P .

$$P = Tr I_z \exp(-\mathcal{H}/kT) / [Tr \exp(-\mathcal{H}/kT)] \quad 11.$$

With $\mathcal{H} = -\mu_n \cdot H$ and for all presently accessible values of H and T

$$P = (I + 1)g_n\beta_n H / (3kT) = 1.22 \times 10^{-8}(I + 1)\mu_n H / (IT) \quad 12.$$

Thus a large P is favored by a large μ_n and a small I . In principle, the method may be applied to any nucleus with a magnetic moment. As will be discussed later, the practical lower limit to T seems to be about 0.01°K and the upper limit of H at present seems to be of the order of 10^8 oe with $H/T \sim 10^7$. Thus for μ_n and I each of the order of one, a polarization of 24 per cent should be obtainable. Thus far, the maximum H/T which has actually been obtained (32) is about 3×10^6 oe/deg corresponding to a field of 30,000 oe at a temperature of 0.01°K .

The principal application of the "brute force" procedure is in the orientation of nuclei which have negligible hyperfine structure coupling to their surroundings and in which the sample of oriented nuclei must be dense and must contain only a single nuclear species. A serious experimental difficulty immediately becomes apparent; the strong magnetic field must be maintained at the sample simultaneously with the very low temperature. Since such temperatures can only be reached by adiabatic demagnetization at present, it is clear that the nuclear sample must be maintained in the strong field while the magnetic interaction of the cooling agent (paramagnetic salt) with this strong field is reduced to a near zero value in the magnetic cooling cycle. This has been accomplished in two ways: by using the indirect cooling process in which there is a spatial separation of the nuclear sample and the cooling salt so that the field requirements can be met; or by using a magnetic cooling salt which also includes the nuclei to be oriented and which has a highly anisotropic spectroscopic splitting factor g , for example $\text{Ce}_2\text{Mg}_3(\text{NO}_3)_{12} \cdot 24\text{H}_2\text{O}$. In the latter case, cooling may be obtained by rotating the salt crystal relative to the field (33) from the direction of the large g factor to the direction of the small g factor while maintaining the magnetic field at full or high value. This latter approach has been widely used for the orientation of nuclei in ions having a hyperfine structure coupling, as will be discussed below, and has been used for "brute force" polarization in the case of protons (34, 35). In the former "indirect" cooling method, a separation of less than ~ 10 cm between the high and low field regions is difficult to obtain; thus a "heat transfer link" of considerable length is involved. The thermal conductivity of copper or silver has been adequate for this purpose down to temperatures in the vicinity of 0.01°K .

Among the heats to be transferred from the nuclear sample to the cooling salt are the heat of magnetization given off when the nuclei of the sample make transitions to the lower Zeeman levels as they become polarized, the heat arising from eddy currents due to fluctuations of the strong field or arising when this field is applied, and the heat generated by the detection or measurement process.

The process of heat conduction has fundamental limitations as virtually

all materials have thermal conductivities which decrease with temperature.² Thus for a given geometry and heat input at the nuclear sample, there is little to be gained by lowering the temperature of the coolant salt to a value small compared to the temperature drop along the conducting material and into the cooling salt. With $\text{Ce}_2\text{Mg}_3(\text{NO}_3)_{12} \cdot 24\text{H}_2\text{O}$, temperatures as low as 0.003°K may be obtained within the salt; but because of these temperature drops within the cooling link, it has not proved feasible to cool samples external to the cooling salt to so low a temperature. Using presently available indirect cooling techniques, temperatures near 0.05° to 0.10°K may be readily obtained at the nuclear sample, but the attainment of a temperature of 0.01° to 0.02°K by heat transfer methods requires that every aspect of the thermal isolation of the sample and of the heat transfer process be optimized (32). The subject has recently been well discussed by Miedema (37). The coolant salts which have proved most useful are $\text{Mn}(\text{NH}_4)_2(\text{SO}_4)_2 \cdot 6\text{H}_2\text{O}$ down to about 0.15°K , $\text{FeNH}_4(\text{SO}_4)_2 \cdot 12\text{H}_2\text{O}$ down to about 0.04°K , and $\text{CrK}(\text{SO}_4)_2 \cdot 12\text{H}_2\text{O}$ down to about 0.01°K (38).

On the basis of heat transfer considerations, the transient times for cooling to temperatures near 0.01°K may become quite long. Times of the order of hours were involved in the helium-3 thermal conductivity measurements (36). In addition, another time enters the problem in the orientation of nuclei; this is the time required for transitions to occur among the nuclear Zeeman levels of the oriented sample. Little is precisely known about this nuclear spin-lattice relaxation time for paramagnetic salts at $H/T \sim 10^7$. For metals such as copper or silver at small fields, the time should be of the order of $1/T$ in seconds down to $T \sim 0.01^\circ\text{K}$. Fields up to 30,000 oe do not seem to lengthen the time excessively compared to the small field value (32).

The first application of the "brute force" method was in the first determination of μ_n for protons by a direct measurement of their magnetization in solid H_2 by Laserew & Schubnikow (39). At the temperature used (2°K), the nuclear magnetization was of course quite small. Thus far, there have been two other applications of nuclear polarizations of the "brute force" type; the attainment of exceedingly low temperatures in the range 10^{-5} to 10^{-6}°K by nuclear demagnetization (32), and the study of the spin dependence of nuclear interactions. Rose (3) suggested the use of polarized neutron beams for the latter purpose.

When polarized slow neutrons are captured or scattered by nuclei whose spins are randomly oriented, the cross section is independent of neutron polarization. If both neutron and nuclear spins are polarized, a change in effective cross section may occur (3), reflecting the spin-dependence of the interaction. If the neutron energy is assumed to be near a resonance of a

² An exception is worthy of note: liquid helium 3 at temperatures below about 0.2°K exhibits a thermal conductivity of $(50/T)$ ergs/cm sec (36). However, boundary resistances play a large role in practical cases.

compound nucleus of angular momentum $J_+ = I + \frac{1}{2}$ or $J_- = I - \frac{1}{2}$, the polarization-dependent cross sections are given for s -wave neutrons by

$$\sigma_+ = \sigma_0 \left(1 + \frac{I}{I + \frac{1}{2}} f_n P \right) \quad 13a.$$

and

$$\sigma_- = \sigma_0 (1 - f_n P) \quad 13b.$$

where f_n is the neutron polarization, given by $(N \uparrow - N \downarrow) / (N \uparrow + N \downarrow)$, and P is the nuclear polarization defined by Equation 12. Thus, by a simple reversal of the direction (hence sign) of either f_n or P , the observation of the direction of the change in σ_+ or σ_- enables one to judge immediately whether J_+ or J_- is the angular momentum associated with the compound state.

This approach was first used in a demonstration of "brute force" polarization at the Oak Ridge National Laboratory by Dabbs, Roberts & Bernstein (40); In^{115} metal was cooled to 0.04°K by heat conduction to a paramagnetic salt which was thermally connected to the indium metal sample. The "heat link" consisted of 20 thin silver wires soldered to the 20 thin indium plates which comprised the sample. A field of 11,000 oe was applied in the indium but not to the salt approximately 12 cm away. The 2.1 per cent nuclear polarization was observed by a 7 per cent change in the transmitted intensity of a polarized neutron beam when the neutron polarization was reversed relative to the polarization of the nuclei. The experiment established that the angular momentum of the compound state in In^{116} for 1.458-ev neutrons was $J = I + \frac{1}{2} = 5$.

An important extension of this work using similar experimental techniques has recently been carried out at the Naval Research Laboratory by Stolovy (41). In these measurements, the earlier work was verified and, in addition, J values for the 3.86-ev and 9.10-ev neutron capture resonances in In^{115} were found to be 4 and 5, respectively.

More recently, an experimental cryostat designed for general use in this field has been developed at Brookhaven National Laboratory (42). Although no "brute force" polarizations have as yet been performed, several studies using (ferromagnetic) Ho^{166} metal as the nuclear sample and Ho^{166} in the ethylsulfate have been made, utilizing the hyperfine structure couplings present in these substances.

To date, the most refined application of the "brute force" method has been the production of temperatures near 10^{-6}°K by Kurti and his collaborators (32). A nuclear polarization was produced at about 0.01°K with applied fields up to 30,000 oe. The nuclear sample was Cu metal, and consisted of about 1500 fine Cu wires. One end of each wire was in thermal contact with a paramagnetic salt, $\text{CrK}(\text{SO}_4)_2 \cdot 12\text{H}_2\text{O}$, and the other end was folded into a bundle with the other wires to make a massive compact nuclear specimen. The arrangement is shown in Figure 2. After the ordinary electronic cooling

of the copper specimen to 0.01°K , a nuclear demagnetization was performed, starting from 0.01°K and 30,000 oe. This gave a final temperature roughly 10^3 times lower than any previously achieved with electronic demagnetization, for the reasons discussed at the beginning of this article. Temperatures of 10^{-5}°K or below were measured from the bulk magnetic susceptibility of the nuclear sample. In these susceptibility measurements Curie's law holds and the temperatures can be determined to a few per cent. No attempt to isolate the copper nuclear sample thermally from the $\text{CrK}(\text{SO}_4)_2 \cdot 12\text{H}_2\text{O}$ cooling salt before nuclear demagnetization has yet been made. However, there is the natural (and rather poor) isolation afforded by the nuclear spin-lattice relaxation time. An effort to effect this thermal isolation may be anticipated. This should further open the possibility of the study of nuclear spin cooperative effects in solids.

With the continued development of very-low-temperature and high magnetic-field technology, a more widespread use of the "brute force" method as a tool of nuclear physics as well as solid state physics seems probable. The current development of superconductors such as NbZr and Nb₃Sn alloys (43) which remain superconducting in fields near 10^6 oe presents interesting possibilities.

Again, for nuclear reaction physics investigations with polarized particles, a restriction presently exists in the energy ranges in which polarized neutrons can be obtained. At present, polarized neutron beams are available only in the 0- to 10-ev range, approximately, and in certain higher-energy ranges where nuclear scattering reactions provide a polarization mechanism. There are, nevertheless, many neutron resonances which can be studied with available techniques.

In addition to work in neutron physics there is the possibility of investigating the interaction of polarized protons in the Mev-energy range with polarized targets. Little work has been done along this line.

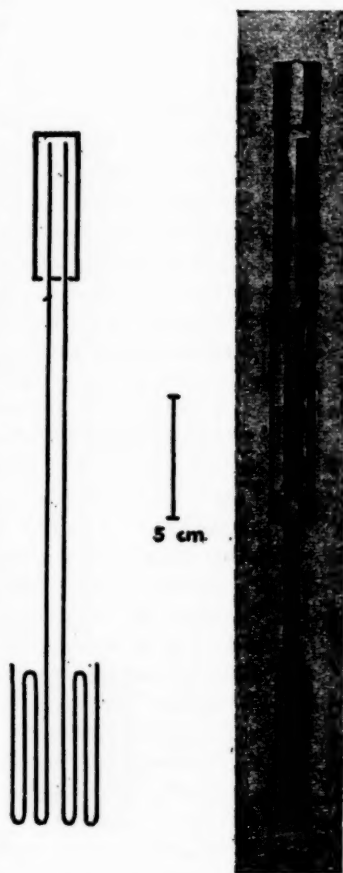


FIG. 2. Nuclear demagnetization assembly.

ORIENTATION OF NUCLEI INCLUDED IN FERROMAGNETIC OR ANTIFERROMAGNETIC MATERIALS

In ferromagnetic and antiferromagnetic materials, one often finds immense "effective" magnetic fields at the nucleus of the magnetic atom. This effective field may be as large as 10^5 to 10^6 oe. Since the magnetic induction in ferromagnets is only of the order of 2×10^4 oe or less and is zero in antiferromagnets, this effective field clearly is more a property of the individual atoms than of their collective magnetic behavior. A detailed theory of the effective field which correctly gives its sign and magnitude has not yet been developed. One can, however, say that it probably arises from a polarization of inner-shell s electrons. The polarization presumably comes from an electrostatic or exchange interaction between the inner s states and the outer d or f shells responsible for the bulk magnetic properties. In any case, the effective field is parallel to the direction of orientation of the atomic angular momentum and thus is parallel to the bulk magnetization in a saturated ferromagnet or to the sublattice magnetization in an antiferromagnetic material.³ Thus this effective field may be suitable for nuclear orientation experiments. This field H_{eff} is proportional to the constant A of the spin Hamiltonian, Equation 3, and is given by $AS'/(g_n\beta_n)$.

There is an interesting point about nuclear spin-lattice relaxation times. For metallic materials, in which at low temperatures the conduction electrons provide the relaxation mechanism, one may expect this time to be fairly short—of the order of $1/T$ in seconds. For nonmetallic antiferromagnetics, on the other hand, the nuclear relaxation presumably must be by way of antiferromagnetic spin waves. Indications are that the antiferromagnetic relaxation times for magnetically dense materials may be expected to be hours to days at temperatures below 0.1°K or so. Thus metallic materials, and preferably metallic ferromagnetic substances, will tend to be more useful for nuclear orientation studies than nonmetallic antiferromagnetics. As a useful magnetic cooling cycle can only be performed on paramagnetic materials, ferromagnetic or antiferromagnetic substances can be cooled effectively only by direct methods such as those discussed in connection with the "brute force" method.

The pioneering experiments on the orientation of nuclei in ferromagnetic materials were performed by Kurti and co-workers (44, 45, 46). They observed the angular distribution of gamma rays from nuclei oriented in cobalt

³ Quite recently information about the sign and magnitude of these effective fields has been obtained by the Mössbauer method. Hanna *et al.* have measured an effective field of -333 koe in metallic iron (43a). The negative sign of this field, which had not been anticipated theoretically, has been discussed theoretically by Goodings & Heine (43b). Similarly, H_{eff} has been measured for tin 119 dissolved in ferromagnetic metals by Boyle *et al.* (43c), and for gold 197 in a number of ferromagnetic alloys by Roberts & Thomson (43d).

metal and in alloys of iron and cobalt. Because the Co^{60} decay scheme was understood, this work gave information about the magnetic hyperfine structure coupling constant A . Details of the alloy work have not been published. More recently, Samoilov *et al.* have performed some interesting nuclear orientation studies on the nuclei of diamagnetic atoms such as gold dissolved in a ferromagnetic material (47). They discovered that the gold electrons took part in the ferromagnetism of the host and that quite large effective magnetic fields occurred at the nuclei of the solute atoms.

The method has been applied for polarizing gold, antimony, and indium nuclei using alloys of these elements in iron. The degree of orientation was determined from the anisotropy of gamma rays emitted by radioactive Au^{198} , Sb^{122} , and In^{114m} nuclei. The active isotopes either were obtained by thermal-neutron irradiation of the sample or were introduced into it in the process of preparation of the alloy. The specimen, in the shape of a thin disk, was soldered to the upper end of a copper rod, the lower end of which was brazed to copper fins pressed in a cooling pill of potassium chrome alum (the contact area being about 50 cm^2). There was a small electromagnet inside the helium Dewar flask which magnetized the specimen. The gamma rays emitted by the radioactive nuclei were detected by two scintillation counters. The activity of the specimen used in the experiments was 5 to $10 \mu\text{c}$. The salt was demagnetized starting with an initial field of about 20 koe and a temperature of 1.05 to 1.10°K . The time dependence of the gamma-ray counting rates along and at right angles to the applied field [$W(0)$ and $W(\pi/2)$, respectively], as well as the "magnetic" temperature of the salt, was measured. It was discovered that the thermal equilibrium between the specimen and the salt was normally reached in 30 to 40 minutes after the time of demagnetization (by this time the salt had usually heated up to $\sim 0.03^\circ\text{K}$). This relaxation time was probably primarily the time for heat transfer from the copper fins into the cooling salt. Defining the gamma-ray anisotropy as $\epsilon = [W(\pi/2) - W(0)]/W(\pi/2)$, at 0.03°K an anisotropy of 0.06 was obtained for gold, 0.08 for antimony, and 0.28 for indium. The corresponding effective magnetic fields calculated from ϵ , the decay scheme, and the temperature were 1×10^6 , 2.8×10^5 , and 2.5×10^5 oe.

As was indicated earlier, Sailor and co-workers have used these methods to investigate the interaction of polarized neutrons with polarized holmium nuclei (42, 48). A polycrystalline sample of holmium ethylsulfate was cooled down to 1.0°K . The Ho^{165} nuclei (spin $7/2$) were polarized with the aid of an external magnetic field. The spin Hamiltonian proposed by Bleaney and Baker was used for calculating the degree of nuclear polarization along the direction of the applied magnetic field. The nuclear polarization for the polycrystalline sample at 1.0°K was 0.15. The nuclei were expected to be polarized in the hemisphere of the positive direction of the applied magnetic field, because of the positive value of A . To reduce possible interactions between the Ho^{+++} ions, the applied magnetic field was made large, e.g., 10.4 koe.

The relative difference $(T^+ - T^-)/(T^+ + T^-)$ in transmission with the neutrons polarized parallel (T^+) or polarized antiparallel (T^-) with respect to the applied magnetic field was measured for the 3.96-ev resonance to be 2.9 ± 0.1 per cent. Hence the spin of the compound nucleus at the 3.96-ev resonance is $I + \frac{1}{2} = 4$. Preliminary measurements for the 12.8-ev resonance indicated spin 4 for this resonance also. Similar measurements were also made with holmium metal, which is ferromagnetic: the polarization found was somewhat less than for the salt, but other results such as the compound nucleus spin values were in agreement.

Similar measurements to the above have been made by Stolovy on gadolinium 155 and 157 using ferromagnetic gadolinium metal (49). The measurements were made in the vicinity of 0.1°K. The spin states associated with resonances in gadolinium were studied by observing the interaction of polarized resonance neutrons with a polarized target. The resonances in Gd^{156} at 2.10 ev and 2.57 ev were found to have different spin states in spite of their similar radiation widths. In view of the small magnetic moments of the gadolinium isotopes, the size of the effects observed indicated strong hyperfine coupling, with an effective field at the nucleus of about 1.4×10^6 oe. The direction of the field relative to the bulk magnetization direction has not been established, but within available information it is negative. This would make $J=1$ for the 2.01-ev level and $J=2$ for the 2.57-ev level. Data taken at 0.09 ev indicate that the 0.031-ev resonance in Gd^{157} , which predominates, has the same spin state as the 2.01-ev resonance in Gd^{155} .

Nuclear orientation in antiferromagnetic single crystals has been investigated at some length by Daniels and co-workers (50). The idea here is that the antiferromagnetic interaction would orient the electron spins parallel to the magnetic sublattice axis and that at lower temperatures, the nuclei would orient parallel to this axis also. Nuclear orientation has been observed through an anisotropy of gamma-ray emission from Mn^{54} and Co^{60} in the following salts: $MnCl_2 \cdot 4H_2O$; $MnBr_2 \cdot 4H_2O$; $CoCl_2 \cdot 6H_2O$; $Co(NH_4)_2(SO_4)_2 \cdot 6H_2O$; and $MnSiF_6 \cdot 6H_2O$. Single crystals of each of these salts were placed in contact with $CrK(SO_4)_2 \cdot 12H_2O$ where the latter served as a magnetic cooling substance to lower the temperature of the composite to about 0.05 K. As nuclear orientation experiments have been previously performed with Mn^{54} and Co^{60} , the information gained primarily concerned relaxation times and the orientation of the magnetic sublattices. This work constitutes one of the few investigations of dense antiferromagnetic materials below 1°K.

NUCLEAR ORIENTATION THROUGH HYPERFINE STRUCTURE COUPLING IN DILUTE PARAMAGNETIC SALTS

There are a number of paramagnetic salts (8, 9, 10, 38) suitable for magnetic cooling in which the nuclei to be oriented may be directly incorporated. Since the electron spin system responsible for the magnetic cooling and the nuclear spin system to be oriented are now within the same

lattice, heat transfer may be quite rapid between the two. Thus, whereas it has been possible at best to cool a nuclear sample to about 0.01°K in "brute force"-type experiments, it is relatively easy to orient nuclei at 0.01° to 0.02°K by the present method, and temperatures near 0.003°K may sometimes be approached. In the Hamiltonian \mathcal{H} Equation 2, nuclear orientation may arise from electric quadrupole coupling [Pound alignment (51)], from magnetic hyperfine structure coupling if $A \neq B$ [Bleaney alignment (52)], and from magnetic hyperfine structure coupling plus an externally applied magnetic field [Rose-Gorter polarization (53, 54)]. For the Pound- and Bleaney-type alignments it is virtually essential and for the Rose-Gorter polarization it is desirable that all of the nuclei being oriented should be at crystallographically equivalent sites, i.e., that the same \mathcal{H} , Equation 2, with equivalent principal axes should apply at all of the sites.

The method of this section is thus far the one most widely used in nuclear orientation studies. Because A/k , B/k , or P/k may sometimes be large relative to 0.01°K , the nuclear orientation may then approach saturation. When the lowest possible temperature near 0.003°K is required or if the nuclei are to be polarized, the best host cooling substance is the versatile salt $\text{Ce}_2\text{Mg}_9(\text{NO}_3)_{12} \cdot 24\text{H}_2\text{O}$. Rare-earth nuclei may be oriented by substituting some of the desired isotope for a portion of the cerium. Nuclei of the first transition series elements may be oriented by substituting some of the latter for a portion of the magnesium. Here the Ce^{+++} ion is the cooling agent; this ion has a highly anisotropic g factor and may be cooled magnetically by rotating the direction of an applied magnetic field from the axis of large g to that of small g (33). By thus cooling the salt in a strong field a Rose-Gorter polarization may be produced. If the magnetic field is removed, a Bleaney-type alignment may result. These procedures work well for the rare earths since all of the Ce^{+++} (or other rare-earth) sites are equivalent. There are, however, two nonequivalent sites for the Mg^{++} ion (or a first transition-series element), and this leads to some difficulty in interpreting data taken at small magnetic fields. For large fields where one has a Rose-Gorter polarization, experiments can apparently be adequately interpreted.

If a Bleaney-type alignment is desired, the ethylsulfate is a suitable salt for the rare-earth metals (8, 9, 10), and a mixed fluosilicate of nickel and zinc works well for the first transition series (55, 56). Both of these salt series are uniaxial with all of the metal sites crystallographically equivalent. Temperatures near 0.01° to 0.02°K may be obtained with the latter two salts.

Although there are many possible applications of the above methods, it is still unfortunately true that they are limited to only a small portion of the periodic table. Even in cases where nuclei may be oriented by these methods, a large radioactive heating rate may make experimental working times at the lowest temperatures unacceptably short. Another somewhat difficult problem arises when the specific heat due to the hyperfine structure coupling terms in \mathcal{H} , Equation 2, of the nuclear spin system to be oriented is comparable to the cooling capacity of the coolant electron spin system. In these

latter circumstances a measurement using magnetically dilute salts may sometimes be possible by resort to the indirect cooling methods described in Sections on the Brute Force Method of Polarization and on Orientation of Nuclei Included in Ferromagnetic or Antiferromagnetic Materials (57).

In the remainder of this section we present examples typical of recent work along the above lines.

Parity nonconservation.—Perhaps the most useful application of nuclear orientation methods to date has been in the famous experiments first demonstrating the nonconservation of parity. This earlier work, principally by Wu, Ambler, Hayward, Hoppes, and Hudson, has been reviewed definitively by Ambler (6). More recently a refined study of the angular distribution of beta particles from cerium-141 nuclei has been made by Hoppes, Hayward & Ambler at the National Bureau of Standards (58, 59).

According to the present theory of the beta interaction, the investigation of the angular distribution of beta particles with respect to the nuclear spin direction $W(\theta) = \sum_n a_n f_n P_n(\cos \theta)$ provides information on the nuclear matrix elements involved in the first forbidden decay. Theoretical discussions by Morita & Morita (59a) and others provide the basis for an analysis of the experimental results. The various terms of the angular distribution function depend in general on complicated combinations of the six possible reduced nuclear matrix elements which are of the next higher order than that "allowed" in the beta interaction. The first two matrix elements result from operators of tensor rank zero, the next three from operators of rank one, and the final from one of rank two. In contrast to the allowed case, all demand a change of parity of the nuclear states, a circumstance often found in the rare-earth region. A considerable simplification results if approximations are made. The "ξ" approximation, recently discussed by Kotani (59b), should apply to cerium 141. Within the framework of this approximation, the coefficient a_1 can be expressed by considering operators of the same tensor rank as a group; thus higher orders must be used to distinguish the individual matrix elements. In the coefficient a_2 only the matrix elements $M(r)$, $M(\mathbf{r} \times \mathbf{r})$, and $M(B_{ij})$ appear, so that a measurement of the beta anisotropy from aligned nuclei gives direct information on this particular combination.

The nuclide cerium 141 provides an interesting subject for such investigations. The decay scheme

$$\frac{7}{2} \beta_1 \rightarrow \frac{7}{2} \gamma \rightarrow \frac{5}{2} \quad \text{and} \quad \frac{7}{2} \beta_2 \rightarrow \frac{5}{2}$$

has been established, while a known Ce^{141} ground-state magnetic moment and established spin-Hamiltonian constants permit a calculation of the orientation parameters for a crystal of Ce^{141} -neodymium ethylsulfate. The 70 per cent $\Delta J=0$, β_1 branch can involve all six matrix elements, while the $\Delta J=1$, β_2 branch will depend only on those of tensor rank one or two. The gamma-ray anisotropy provides a measure of the effective temperature of the crystalline surface layer in which the source is incorporated.

The experimental apparatus is much the same as that used in studies on the nature of the beta interaction (6). A large single crystal of neodymium ethylsulfate is mounted with the c axis vertical in the demagnetization apparatus. An anthracene scintillator located vertically above the thin disk of activity grown on the uppermost surface of the crystal provides the input to a 100-channel analyzer for analysis of the beta spectrum. To separate the distribution for the 438-kev inner beta branch from that for the 580-kev ground-state transition, three $2'' \times 2''$ NaI equatorial gamma counters are used to measure coincidences by means of a fast-slow coincidence system. A $2'' \times 2''$ polar counter also monitors the gamma-ray distribution.

The polarization measurements are made by applying a vertical magnetic field of 200 oe, having cooled the sample by demagnetization from a horizontal field of 23 koe at 0.9°K . According to unpublished measurements by Hudson & Kaeser, the bulk of the crystal should attain a temperature of about 0.03°K under these circumstances. Depending on the direction of the magnetic field, the beta detector takes a sampling of the electrons emitted at an angle of about 0° to 180° with respect to the nuclear spin direction. Counting was continued for alternate polarizing field directions for periods up to one hour, during which time the uncorrected up-down asymmetry at the high end of the beta spectrum remained larger than 0.21. Since the normalization for the gamma-ray anisotropy depended on a reliable "warm" count, the sample was raised to the helium bath temperature after this period of time.

The alignment runs were made under similar conditions. The uncorrected value for the fractional change in the polar high-energy beta counting rate upon demagnetizing was about 0.07, indicating that this $a_2f_2P_2$ -term contribution would be a small correction to the $a_1f_1P_1$ term at the higher temperatures of the polarization experiments.

The energy and angular distributions of beta particles from oriented Ce^{141} allow one, in principle, to determine the relative values of the four contributing first-forbidden (real) nuclear matrix elements. In practice, however, the insensitiveness of the energy dependence allows a determination of the relative values only after one ratio has been fixed by theory. By taking into account all possible shell-model configurations for Ce^{141} and praseodymium 141, one finds that two ratios can be fixed uniquely and independently of any details of the radial wave functions. This method of analysis yields the ratios $M(i\mathbf{r})/M(\mathbf{d} \times \mathbf{r}) = -1$, $M(i\mathbf{B}_{ij})/M(\mathbf{d} \times \mathbf{r}) = -1.9$, and $M(\alpha)/M(\mathbf{d} \times \mathbf{r}) = -37 \pm 1.5$. These values are based on the use of lepton wave functions expanded in powers of $\alpha Z/(2R)$.

Nuclear alignment of iodine 131 by electric quadrupole coupling.—The coupling between the nuclear electric quadrupole moment and the local electric field gradient in a crystal should produce appreciable nuclear alignment at very low temperatures ($\sim 0.01^\circ\text{K}$) (51). To determine whether pure quadrupole relaxation times in nonmagnetic atoms in crystals become very long at temperatures of the order of 0.01°K , an experiment was made by

Johnson, Schooley, Shirley & Rasmussen (60) using a single crystal of copper *p*-iodobenzenesulfonate containing a few microcuries of iodine 131. In this crystal all the carbon-iodine bonds lie at a small angle from the *a* axis, which is thus nearly the axis of alignment. Preliminary experiments demonstrated that adiabatic demagnetization of this salt from 18 koe and 1.1°K resulted in its cooling to about 0.03°K. A crystal containing I^{131} was cooled by adiabatic demagnetization, and the intensities of the two most prominent gamma rays in the radioactive decay were measured at several temperatures as a function of the angle θ between the direction of emission and the *a* axis. The results could be fitted to $W(\theta) = 1 + (0.0007 \pm 0.0001)P_2(\cos \theta)/T^*$ for the 364-keV gamma ray and to the expression $W(\theta) = 1 - (0.0013 \pm 0.0003)P_2(\cos \theta)/T^*$ for the 637-keV gamma ray. Thus the iodine nuclei have been aligned, and the nuclear spin-lattice relaxation time must be shorter than a few seconds down to 0.03°K. The 637-keV gamma ray is believed to be pure *E2*, and the magnitude of its anisotropy gave the spin of the 637-keV state in xenon 131 as 5/2. This gave a value of -950 ± 190 mc for the quadrupole coupling parameter eQq/h which is consistent with the results of quadrupole resonance measurements on stable iodine. The anisotropy of the 364-keV gamma ray yields the multipolarity assignment 97.8 per cent *E2*, 2.2 per cent *M1* for this gamma ray.

Beta and gamma emission from oriented holmium 166(m).—Experiments on the anisotropy and linear polarization of gamma rays emitted from aligned Ho^{166m} nuclei incorporated in a single crystal of neodymium ethylsulfate have been carried out by Postma, Huiskamp, Miedema, and Eversdijk Smulders (61, 62). At the lowest temperatures obtained, $T = 0.025^\circ K$, the orientation is nearly complete. The hyperfine structure splitting of the ground state (non-Kramers doublet), neglecting small terms, is given by the spin Hamiltonian:

$$\mathcal{H} = g\beta H_z S_z + \Delta_x S_x + \Delta_y S_y + AS_z I_z \quad 14.$$

where

$$\Delta/k = (\Delta_x^2 + \Delta_y^2)^{1/2}/k \approx 0.09^\circ K$$

Thus, *A* is very large. Neglecting Δ and assuming a spin of Ho^{166m} $I_0 = 6$, it was calculated from the temperature-dependence of the gamma anisotropy that $A/k = 0.27 \pm 0.03^\circ K$ and that $\mu_n = 3.2 \pm 0.5$ nm. The 817- and 706-keV radiations are *M1*+*E2* and *E1* transitions, respectively. The final state of the main beta decay was assigned as 6^- . Observed reduction of orientation of this 6^- state in Er^{166} relative to the initial concentration of the Ho^{166m} due to beta decay is simply understood by a beta transition with $\Delta I = 0$ proceeding only by matrix elements with $J = 1$.

The directional distribution of beta particles emitted from oriented nuclei of spin I_0 may generally be expressed by

$$W^\theta(\theta) = S_{(n)} \left\{ 1 + \sum_k B_k [f_k(I_0)/f_{km}(I_0)] P_k(\cos \theta) \right\} \quad 15.$$

where S_n is the shape factor of the β spectrum and $f_{km}(I_0)$ are the values of the orientation parameters for complete orientation (5). The parameters B_k depend on nuclear matrix elements. It is found that for allowed decays $k=1$ and for once-forbidden decays $k=1, 2, 3$.

Measurements were performed on the beta emission from polarized and aligned $\text{Ho}^{166\text{m}}$ nuclei incorporated in thin layers of single crystals of neodymium ethylsulfate. For the upper half of the beta spectrum an asymmetry $\alpha = (W \uparrow - W \downarrow) / (W \uparrow + W \downarrow) = -0.14 \pm 0.03$ $f_1 v/c$ was measured, where $W \uparrow$ and $W \downarrow$ are intensities of beta emission parallel and antiparallel to the polarizing field. A positive nuclear magnetic moment is assumed; i.e., the nuclear spin is parallel to the magnetic field. Measurements showed that the beta emission from aligned holmium-166 nuclei is isotropic within 4 per cent. From this it was concluded that $|B_2| < 0.07$. The measurements on the beta emission are easily understood, postulating a beta decay with $\Delta I = 0$, proceeding only by matrix elements with $J = 1$. Thus one has $I_0 = I' = 6$, where I' is the spin of erbium 166. When $\Delta I = 0$, B_2 is usually zero and $\alpha = B_1 f_1(I_0)$, where $B_1 = -(1/7)v/c$. An assignment 7^+ for $\text{Ho}^{166\text{m}}$ necessitates a mixing of matrix elements; 7^- and 8^+ are definitely rejected by experiment, while 6^+ is rejected on the basis of the decay scheme. It seems that a 6^- assignment is most likely, but 7^+ cannot be rejected completely.

Nuclear alignment of promethium isotopes.—Nuclear orientation studies of promethium isotopes have been made recently by Grace *et al.* for Pm^{149} and Pm^{151} (63), and by Shirley and co-workers for Pm^{144} (64). Paramagnetic resonance had been looked for in the case of long-lived Pm^{147} but none was observed. This lack was attributed to the smallness of the ionic g factor. Thus the information presently available about the spin Hamiltonian comes predominantly from nuclear alignment work.

In the studies by Grace and co-workers (63) the nuclei were aligned both in the ethylsulfate and in cerium magnesium nitrate lattices. In the course of this work, the decay scheme of Pm^{149} was also further investigated, with results indicating that the spin of this isotope must be $5/2^+$, $7/2^+$, or $9/2^+$, with $7/2^+$ most probable. A single 285-kev gamma ray was observed. In the alignment studies using the double nitrate, about $5 \mu\text{c}$ of Pm^{149} were grown into a 4-g single crystal and this crystal was cooled by the magnetic cooling procedure to a temperature near 0.003°K . At the lowest temperatures an anisotropy of the 285-kev gamma $[W(\pi/2) - W(0)] / W(\pi/2) = +0.096 \pm 0.005$ was observed. In the similar experiment in which the Pm^{149} was grown into neodymium ethylsulfate as the cooling agent, a small anisotropy of the opposite sign was observed. At the lowest temperature of 0.018°K this was -0.057 ± 0.005 for the 285-kev gamma ray.

It seems probable that the alignment in the ethylsulfate is "axial." The negative sign of the anisotropy of the Pm^{149} gamma radiation in this lattice indicates that the transition cannot be pure $E2$ of the $3/2 \rightarrow 7/2$ or $11/2 \rightarrow 7/2$ type since both would produce positive anisotropies when aligned axially. This leaves $5/2$ or $7/2$ or $9/2 \rightarrow 7/2$ as possible transitions and each of these

three will, in general, contain $M1$ radiation. Since the daughter nucleus samarium 149 with 87 neutrons lies below the region of strongly deformed nuclei, it is to be expected that the $E2$ enhancement will be weak and hence the transition will be largely $M1$.

This expectation is supported by two experimental observations. First, the K/L conversion ratio of 8 ± 2.5 measured by Rutledge *et al.* is consistent with the transition's being largely $M1$. The theoretical value is 8.2 for a pure $M1$ and 5.0 for a pure $E2$ transition. Second, no Coulomb excitation of this level of Sm^{149} could be detected by Heydenburg and Temmer. This absence shows that the partial $E2$ half life must be greater than about 10^{-9} sec. The single-particle value is 3×10^{-9} sec, in accord with the expected lack of $E2$ enhancement. The single-particle model predicts a value for the $M1$ half life of 10^{-12} sec which implies that the $E2$ constituent is less than 10^{-8} and the dominant part of the transition must be $M1$.

The angular distribution may be expressed as $W(\theta) = 1 + U_2 F_2 G_2 P_2(\cos \theta)$ where U_2 and F_2 are coupling coefficients for the beta-ray and gamma-ray transitions. The largest observed gamma-ray anisotropy ($+0.093$ for the double nitrate) combined with the maximum possible value for $|G_2|$ sets a lower limit to the quantity $U_2 F_2$. Since F_2 is rather sensitive to δ , the $E2/M1$ amplitude mixing ratio, it was possible to set some limits on δ . If the gamma ray is emitted in a transition between states both of spin $7/2$, then δ must be less than -0.6 . This large $E2$ admixture (at least 25 per cent) is incompatible with a predominantly $M1$ transition, and hence it was concluded that the 285-kev state could not be of spin $7/2$. For a $5/2$ to $7/2$ transition, δ must be greater than -0.05 and, for a $9/2$ to $7/2$ transition, δ must be less than $+0.13$. Both are consistent with a largely $M1$ transition. It was not possible to distinguish between these choices. The best fit to the data was obtained by taking the spin of Pm^{149} to be $7/2$. This corresponds to a δ of -0.04 if the transition is $5/2$ to $7/2$ and $+0.12$ if it is $9/2$ to $7/2$. These experiments thus limit the spin of the 285-kev state to $5/2$ or $9/2$.

The difference in signs of the gamma-ray anisotropies for the two lattices shows that in one case the alignment must be "axial" and in the other "planar." It is probable that the lowest state in the ethylsulfate is a doublet with a reasonably large value for A (See Eq. 2). Since the electric quadrupole hyperfine structure is predicted to be small with P about $3 \times 10^{-6} \text{ cm}^{-1}$, promethium must be aligned in an "axial" sense in the ethylsulfate. Hence the double nitrate must produce the "planar alignment." Since the low-lying doublet in the double nitrate must have $B=0$ and should have a large A , it was concluded that the singlet must lie lowest and that the hyperfine structure is quadrupole-like. Assuming that the "pseudo-quadrupole" effect is responsible for the hyperfine structure in the double-nitrate lattice and that g_n is about 1, a value for E , the singlet-doublet energy separation for Pm^{+++} , was obtained, showing E to be about 1 cm^{-1} .

Nuclear orientation of manganese isotopes.—Experiments by several groups have shown that manganese isotopes incorporated in the lattice of

paramagnetic cooling salts can be oriented. This technique (Rose-Gorter method) was used to produce nuclear polarization of Mn^{54} by Grace and co-workers (65), of 5.7-day Mn^{56} by Huiskamp and collaborators (66), and of the relatively short-lived 2.6 hr Mn^{56} by Bauer & Deutsch (67); all used cerium magnesium nitrate with an external field of several hundred oersteds. Recently Dagley *et al.* (68) worked with nickel fluosilicate to align Mn^{56} using the internal crystalline field to produce nuclear orientation (Bleaney method).

Quite recently this work has been extended by Bauer *et al.* to Mn^{52m} by the magnetic hyperfine structure orientation method. Further work on Mn^{54} was also done (69). In these studies the manganese isotopes were incorporated either in the lattice of cerium magnesium nitrate or that of nickel fluosilicate. Since the short lifetime of Mn^{52m} (21 min) made it impractical to incorporate it directly into the coolant crystals, the fact that this nuclide can be derived by radioactive decay from an 8-hr parent, Fe^{52} , was used. The Fe^{52} was incorporated in the cooling salt. The measurement of the angular distribution of the gamma rays from Mn^{54} indicated its spin to be 3 or 2; in the latter case, the beta decay must be predominantly of the Fermi type with an upper limit of 10 per cent of a possible Gamow-Teller admixture. From a simultaneous measurement of the angular distribution of the gamma rays from Mn^{54} and 5.7-day Mn^{52} , the ratio of the nuclear g values of the two isotopes was found, which gave a magnetic moment for Mn^{54} of 2.55 ± 0.21 nm (for spin 3) or 2.16 ± 0.26 nm (for spin 2). The circular polarization measurements of the gamma rays from Mn^{54} determine this moment to be positive. Similar angular distribution experiments on Mn^{52m} , assuming spin 2, yielded a magnetic moment of 1.04 ± 0.16 nm if the beta decay is predominantly a Gamow-Teller transition, or 0.72 ± 0.16 nm if it is a pure Fermi transition. These results indicate that the nuclear g values of the 21-min and the 5.7-day states of Mn^{52} are about the same.

Nuclear orientation experiments with uranium and neptunium isotopes.—In 1953 Hill *et al.* suggested that the spheroidal shape found for many of the heavy nuclei should have a marked effect on the character of alpha-particle emission (70). For example, they pointed out that for a nucleus with a positive quadrupole moment, the barrier against alpha emission should be weaker in the polar region of the nuclear surface and that, correspondingly, there may be preferred alpha emission along the nuclear symmetry axis. For an odd-mass nucleus of positive quadrupole moment in its ground state, one may expect the angular momentum vector to be along the symmetry axis also. Thus it is predicted that the preferred alpha emission should be along the nuclear angular momentum vector. It was suggested by Bohr in 1955 that the spheroidal deformation of heavy nuclei should also have a marked effect on the character of the nuclear fission process (71). For example, for a nucleus of positive quadrupole moment undergoing thermal-neutron fission, it was proposed that fragment emission would be predominantly perpendicular to the nuclear angular momentum vector.

The mechanism of the above example may be understood as follows. It was assumed that the most probable fission process would be the mode which had the maximum energy in the specific nuclear motion leading to fission, and thus the mode which had the minimum energy in other aspects of the nuclear motion required to conserve angular momentum and parity. Generally speaking, the type of nuclear motion requiring the least energy for a given amount of angular momentum is a state which is entirely or predominantly rotational in character. For such a rotational state, the symmetry axis is approximately perpendicular to the angular momentum vector. Then, assuming that fission occurs from a rotational state and that the fragments are emitted along this symmetry axis, the fragment intensity would be greatest perpendicular to the angular momentum vector. In terms of the symmetric top wave function of the Bohr model, D_{MK}^I , this picture implies that fission predominantly occurs from states with K equal to or near zero.

From the above discussion it appears that if one orients spatially the angular momentum vector of a system of nuclei such as uranium, for example, one should expect alpha emission predominantly along this vector and fission-fragment emission predominantly perpendicular to it. Obviously, one should also expect alpha emission and fission to be predominantly perpendicular to each other. Bleaney- and Pound-type nuclear orientation experiments of the above type have been performed with U^{233} , U^{235} , and Np^{237} nuclei (72 to 75). The actinide elements are particularly favorable for Bleaney and Pound nuclear orientation procedures. The expectation value of r^{-3} for the valence electrons of these high- Z elements tends to be quite large. Since the nuclear quadrupole moments and the magnetic moments especially of the odd proton nuclei are also quite large (76), the hyperfine structure couplings in some of the actinide compounds are among the largest that have been observed. This makes nuclear orientation experiments with certain of these elements possible at easily attainable temperatures.

The chemical compounds which have been used for actinide nuclear orientation work are of a type unique to the elements U, Np, Pu, and Am, i.e., those containing the linear MO_2^{++} group. For UO_2^{++} and NpO_2^{++} , usefully large quadrupole couplings (9, 77) have been observed; and for NpO_2^{++} and PuO_2^{++} , similarly large magnetic couplings have also been measured. The electric coupling in UO_2^{++} or PuO_2^{++} and the electric and magnetic couplings for AmO_2^{++} have not been measured thus far, but these also may be expected to be conveniently large for nuclear orientation studies. The rhombohedral compound $MO_2Rb(NO_3)_3$, in which all of the MO_2^{++} groups are crystallographically equivalent and parallel to the crystalline c axis, has been found particularly suitable for nuclear orientation work. In this compound the effective spin Hamiltonian is generally of the form given in Equation 2. Table I lists the available information about the coupling constants. Using these parameters, it may be seen that the over-all splitting of the hyperfine structure multiplet for NpO_2^{++} , for example, is of the order of 0.65°K, and thus an appreciable degree of nuclear orientation may be expected near 1°K.

TABLE I
COUPLING CONSTANTS OF THE EFFECTIVE SPIN HAMILTONIAN (EQ. 2)
(for the MO_3^{++} group)

	A (cm^{-1})	$ B $ (cm^{-1})	P (cm^{-1})
$\text{U}^{233}\text{O}_3^{++}$	0	0	~ 0.03 (est.)
$\text{U}^{235}\text{O}_3^{++}$	0	0	~ 0.015 (est.)
$\text{Np}^{237}\text{O}_3^{++}$	-0.16547	0.01782	+0.03015
$\text{Pu}^{241}\text{O}_3^{++}$	0.0609	—	—

The first experiments (72, 73) on the emission of alpha particles from oriented nuclei were for neptunium-237 nuclei aligned in $\text{NpO}_2\text{Rb}(\text{NO}_3)_3$. Early microwave results by Bleaney *et al.* demonstrated that A and P are of opposite sign. From theoretical considerations, these results gave $A > 0$, $P < 0$ (77). Corresponding to this, the nuclear spin state of least energy in the hyperfine structure multiplet would be $I_z = I = 5/2$; i.e., at low temperatures, the nuclear angular momentum vector would tend to orient parallel to the crystalline c axis. The nuclear orientation results demonstrated, however, that as the nuclei became oriented, the predominant alpha emission was perpendicular to this c axis and, if the above signs (77) of A and P are assumed, perpendicular to the nuclear angular momentum vector as well. Thus either the above signs of A and P or the predictions of the theory of alpha emission were in error.

The absolute signs of the constants of the spin Hamiltonian have been determined experimentally only for a relatively small number of cases (9). With the NpO_3^{++} ion it proves possible to determine these signs from a nuclear orientation experiment (78, 79). Following the angular momentum formalism given by Rose (3), the angular distribution $W(\theta)$ of alpha particles emitted by a system of oriented nuclei may be described by a specialization of Equation 1.

$$W(\theta) = \sum_{LL'} C_{LL'} C(LL'; 00) W(IILL'; \nu I') G_\nu P_\nu(\cos \theta) \quad 16.$$

with

$$G_\nu = \sum_m (-)^{I-m} C(II\nu; m, -m) P(m) \quad 17.$$

where the $C_{LL'}$ are intensity parameters, $C(LL'; 00)$ and $C(II\nu; m, -m)$ are Clebsch-Gordan coefficients, $W(IILL'; \nu I')$ is a Racah coefficient, and $P_\nu(\cos \theta)$ is a Legendre polynomial. Here, I is the angular momentum of the nucleus before alpha emission with m as the projection quantum number on the axis of nuclear orientation; L and L' are the angular momenta of the alpha-particle partial waves, and I' is the angular momentum of the daughter nucleus. The quantity $P(m)$ is the population of the m th substate; it is a function of \mathcal{H} and the absolute temperature T . The angle θ is measured from the axis of nuclear orientation, the c axis for $\text{NpO}_2\text{Rb}(\text{NO}_3)_3$. The summation

index ν takes even values (parity conservation) between 0 and $2I$. For Np^{237} with $I=5/2$, ν may take the values 0, 2, 4; but only the values 0 and 2 have been experimentally observed to be important. Expanding G_2 , Equation 15, in terms of $1/T$ and using the spin Hamiltonian of Equation 2 at zero magnetic field, one obtains

$$G_2 = \frac{1}{2I+1} \sqrt{\frac{(2I+3)!}{180(2I-2)!}} \left\{ -\frac{P}{kT} + \left(\frac{4I(I+1)-15}{42} \right) \frac{P^2}{k^2 T^2} + \frac{(A^2 - B^2)}{8k^2 T^2} \right\} \quad 18.$$

and

$$W(\theta) \sim 1 + b_2 F(T) P_2(\cos \theta) \quad 19.$$

The point which should be emphasized is that A first enters $W(\theta)$ as A^2 whereas P first enters linearly. Thus, depending on the sign of P , the magnetic coupling will tend to reinforce or weaken the nuclear alignment produced by the quadrupole coupling. Physically, the magnetic coupling always tends to orient the nuclei with $I_z = I$ for either sign of A . If $P < 0$, quadrupole coupling tends to orient the nuclei with $I_z = I$ also, and the electric and magnetic coupling terms reinforce each other. However, if $P > 0$, the quadrupole coupling tends to orient the nuclei in the $I_z = \pm \frac{1}{2}$ state which opposes the magnetic coupling effect. Near 1°K the nuclear alignment is predominantly due to the quadrupole coupling (P term), but at lower temperatures near 0.2°K both electric and magnetic coupling terms are important and the above interference effect may be seen clearly. Thus the sign of P may be determined from the temperature-dependence of the coefficient of $P_2(\cos \theta)$, Equations 16 to 19, in a nuclear orientation experiment.

Figure 3 shows schematically the apparatus which was used for this experiment (78, 79). The alpha-emitting sample was prepared in the following way. A single crystal of $\text{UO}_2\text{Rb}(\text{NO}_3)_3$ weighing 1.4 g was grown. An additional layer of ~ 0.002 g of $\text{NpO}_2\text{Rb}(\text{NO}_3)_3$ was grown onto the surface of this base crystal. This sample was held in a ball-bearing mount contained in a copper enclosure which could be cooled to temperatures down to $\sim 0.2^\circ\text{K}$ by adiabatic demagnetization of a thermally attached mass of $\text{Mn}(\text{NH}_4)_2(\text{SO}_4)_2 \cdot 6\text{H}_2\text{O}$. The mass was so large (187 g) and the heat leaks to the sample so small that no appreciable temperature drifts were observable during the course of the experiments. Heat transfer from the neptunium sample to the copper enclosure was accomplished by the use of He^3 gas which still has an appreciable vapor pressure and heat conductivity at 0.2°K . The alpha particles were counted by a germanium surface barrier counter (80) which was found to function splendidly at these low temperatures. As is seen from Figure 3, a small bar magnet was also attached to the ball-bearing sample mount; and through the agency of a small magnetic field applied from outside the cryostat, it was possible to turn this bar magnet and thus the $\text{NpO}_2\text{Rb}(\text{NO}_3)_3$ sample crystal axis relative to the germanium counter. Thus $W(\theta)$, the intensity of alpha emission, could be measured as a function of θ and T down to $\sim 0.2^\circ\text{K}$.

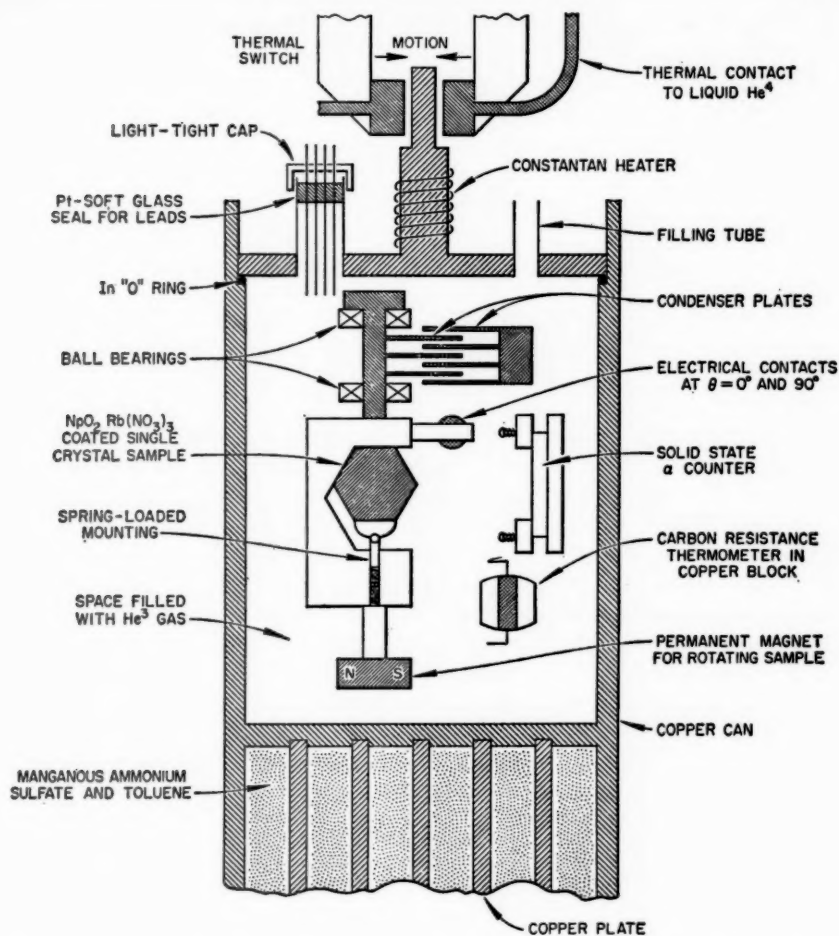


FIG. 3. Apparatus for the study of the angular distribution of alpha particles emitted from neptunium nuclei oriented at temperatures down to 0.2°K .

The results of these measurements are shown in Figure 4 compared with the two theoretical curves for G_2 , Equation 17, one for $A < 0$, $P > 0$ and the other for $A > 0$, $P < 0$. It is clearly seen that $A < 0$, $P > 0$ is the correct result. There was no evidence for any appreciable amount of $\nu=4$, i.e., $P_4(\cos \theta)$. We note that the anisotropy of alpha emission at the lowest temperatures is quite large. It is seen that the alpha emission is enhanced at $\theta=90^{\circ}$, i.e., perpendicular to the c axis by the nuclear orientation. That P is positive means in this temperature region the Np^{237} spins also tend to orient perpendicular to the c axis; that is, I_z tends toward $\pm \frac{1}{2}$. Thus the alpha particles

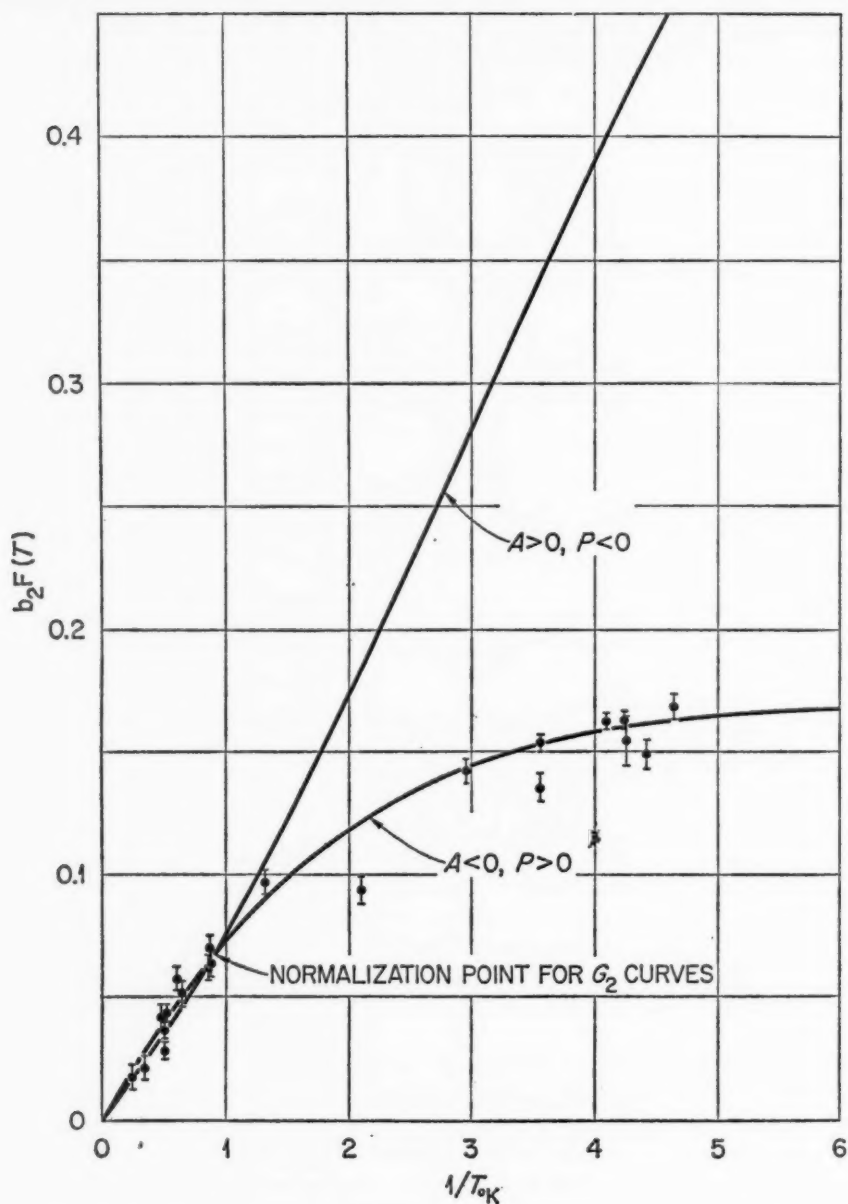


FIG. 4. Amplitude of measured alpha-particle anisotropy compared with the theoretical curves for $A > 0, P < 0$ and for $A < 0, P > 0$ (Eq. 2).

are emitted predominantly along the nuclear angular momentum vector in agreement with the predictions of nuclear theory.

This experiment does not determine the sign of the nuclear quadrupole moment. In the early work of Bleaney (77, 81) the theoretical result $P < 0$ was obtained through the assumption, in agreement with the expectations of nuclear systematics (76), that the quadrupole moment of Np^{237} is positive and that the electron charge cloud of the covalent bond in NpO_2^{++} is also "cigar" shaped (81). Here the lowest-energy state would indeed be with the major axis of the nucleus parallel to the major axis of the NpO_2^{++} bond, i.e., $P < 0$. The experimental result $P > 0$ means that either Np^{237} has a negative quadrupole moment or that the NpO_2^{++} bonding charge distribution is "toroidally" shaped. Either conclusion is unexpected.

In a recent paper, Pryce revised earlier calculations of A and P , and these recent theoretical results give $A < 0$, $P > 0$ in agreement with the measurements (82). He retains the picture that the NpO_2^{++} bonding charge distribution is essentially "cigar" shaped and correspondingly suggests that the quadrupole moment of Np^{237} is negative. Shell-model expectations would predict a positive value for Q for Np^{237} .

The character of the angular distribution of alpha emission from uranium 233 and 235 oriented in $\text{UO}_2\text{Rb}(\text{NO}_3)_3$ is similar to the above result for Np^{237} . As the temperature is lowered, alpha emission is enhanced perpendicular to the crystalline c axis. Here the sign of the nuclear quadrupole moment of each nucleus is given from spectroscopic studies as positive (76), but the sign of the quadrupole coupling constant P has not been determined. If alpha emission here is predominantly along the nuclear angular momentum vector as with Np^{237} , the results would require $P > 0$. However, for P to be positive, the UO_2^{++} bonding charge distribution would again have to be characterized by a "toroid" rather than a "cigar" shape, as seen from the nucleus.

Because U^{234} is an even-even nucleus with I equal to zero, no nuclear alignment can occur. The alpha-particle angular distribution for $\text{U}^{234}\text{O}_2\text{Rb}(\text{NO}_3)_3$ should be isotropic and temperature independent; this expectation was confirmed experimentally.

A preliminary study (75) has been made of the thermal-neutron fission of oriented uranium nuclei. In these experiments, a base crystal of $\text{UO}_2\text{Rb}(\text{NO}_3)_3$ (normal uranium) coated with a thin layer of either the U^{235} or U^{233} salt was mounted in a cryostat that could be cooled to $\sim 1^\circ\text{K}$. The cryostat was mounted at the Oak Ridge National Laboratory graphite reactor so that the above crystal could be irradiated with a neutron beam. Germanium solid state counters were used to count the fission fragments in these studies. The counter was thermally isolated from the sample crystal and operated at liquid nitrogen temperatures while the sample could be held at temperatures down to $\sim 1^\circ\text{K}$. As with the Np^{237} alpha experiment described above, it was possible to rotate the sample crystalline c axis relative to the counter. The experiment consisted of measuring the emission rate of alpha particles and

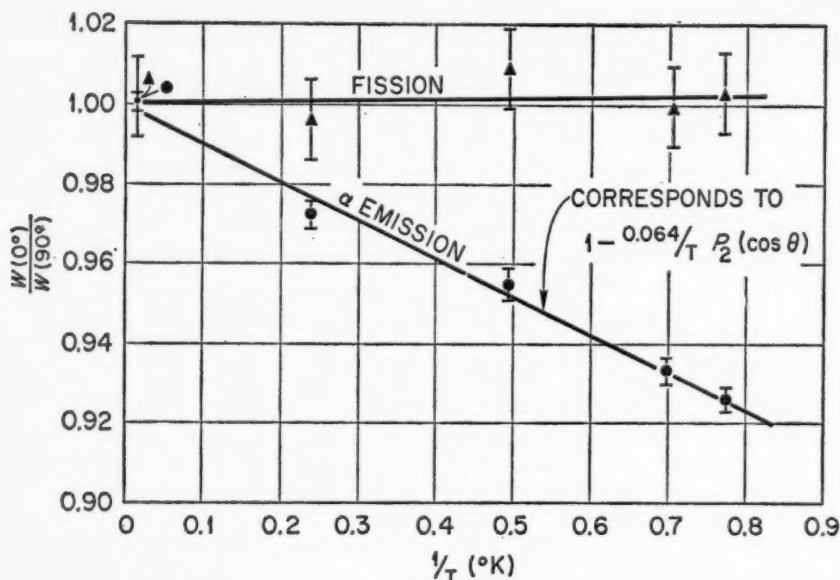


FIG. 5. Anisotropy of thermal-neutron fission and of alpha-particle emission from aligned uranium-233 nuclei.

of the fragments from thermal-neutron fission both parallel, $W(0)$, and perpendicular, $W(\pi/2)$, to the c axis. The results of these experiments are plotted as $W(0)/W(\pi/2)$ versus $1/T$ in Figure 5 for U^{233} and in Figure 6 for U^{235} .

For U^{233} , it was found that the fission-fragment emission remained isotropic as the temperature was decreased and thus was independent of the nuclear orientation. A small anisotropy of fission fragment emission was found for U^{235} , however, and it is interesting to note that this anisotropy is of opposite sign to that observed for the U^{235} alpha emission. This is in qualitative agreement with the idea presented above that the predominant intensities of alpha emission and of fission should tend to be perpendicular to one another (70, 71).

A quantitative formulation (83) of the Bohr picture (71) for the thermal fission of oriented nuclei has been given. The expression for the angular distribution of fission fragments $W(\theta)$ is

$$\dot{W}(\theta) = \sum (-)^{j-1/2-K-\nu} C(II\nu; K, -K) W(jIjI; 1/2\nu) G_\nu P_\nu(\cos \theta) \quad 20.$$

In this expression j is the spin of the target nucleus, I is the total angular momentum of the compound state after s -wave neutron capture, and K is the projection of I on the nuclear symmetry axis; G_ν is the nuclear alignment parameter associated with the target nucleus, the same G_ν given by Equation 16. The C and W are Clebsch-Gordan and Racah coefficients, respectively,

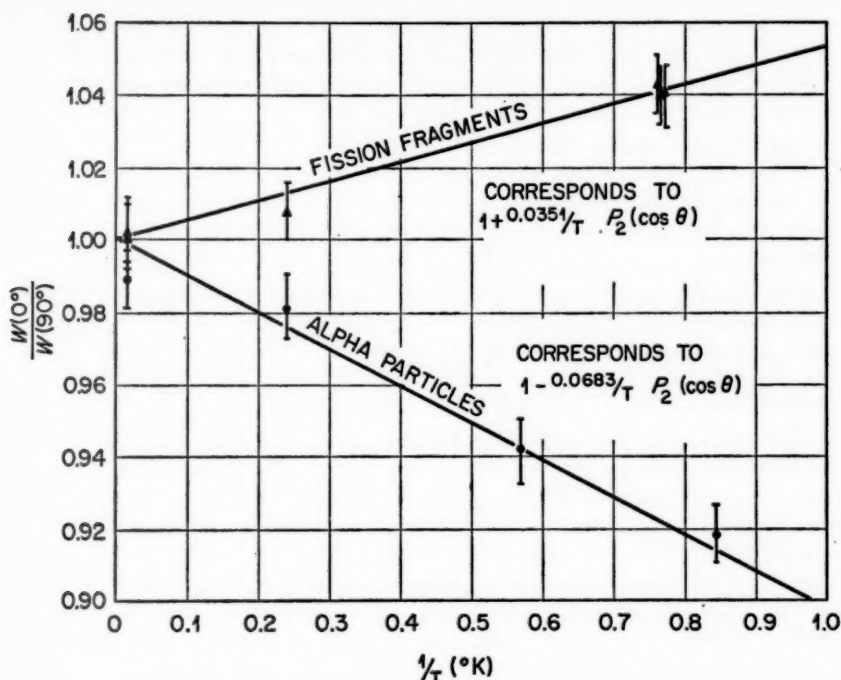


FIG. 6. Anisotropy of thermal-neutron fission and of alpha-particle emission from aligned uranium-235 nuclei.

and P , is a Legendre polynomial. In this picture the fission channel is characterized by I and K . The nuclear alignment is brought about here through electric quadrupole coupling with $\mathcal{H} = P[I_s^2 - I(I+1)/3]$.

For U^{233} , $j=5/2^+$, and to terms in $P_2(\cos \theta)$, one obtains

$$W(\theta) = 1 - \frac{4}{9} (3K^2 - 6) \frac{P}{kT} P_2(\cos \theta) \quad \text{for } I = 2^+ \quad 21a.$$

$$W(\theta) = 1 - \frac{1}{3} (3K^2 - 12) \frac{P}{kT} P_2(\cos \theta) \quad \text{for } I = 3^+ \quad 21b.$$

For U^{235} , $j=7/2^-$,

$$W(\theta) = 1 - \frac{5}{12} (3K^2 - 12) \frac{P}{kT} P_2(\cos \theta) \quad \text{for } I = 3^- \quad 22a.$$

$$W(\theta) = 1 - \frac{1}{4} (3K^2 - 20) \frac{P}{kT} P_2(\cos \theta) \quad \text{for } I = 4^- \quad 22b.$$

The essence of Bohr's suggestion that the fission state should be predominantly rotational in character is expressed here by a zero or small K value. For U^{233} , Equation 21 predicts a large anisotropy for $K=0$ or 1, where-

as the experiments give an anisotropy quite close to zero. Within this picture of the fission process, a small anisotropy could come from the channel $I=3^+$, $K=2$. Except for this possibility, it seems clear that more than one channel would be involved and that the channels of smallest possible K , in any case, do not strongly predominate. For U^{235} , the observed anisotropy of fission is positive, i.e., $W(0)/W(\pi/2) > 1$. This result seems to correspond to the lower K values under the assumption of a positive value for P , but again it seems clear from the rather small size of $[W(0)/W(\pi/2) - 1]$ even at the lowest temperature that the lowest K value is not the only K value involved. These results, then, support the current view that several channels are of importance in the fission process (85). The assumption $P < 0$ would reverse the predicted anisotropies and, thus, require a predominance of the $K \cong I$ channels. This seems unlikely in view of Bohr's idea that the most probable fission modes correspond to the lower K values.

The magnitude of the anisotropy of alpha emission in the above experiments enables one to estimate the value of $|P|$ as $\sim 0.03 \text{ cm}^{-1}$ for U^{233} . If it were assumed that the bonding in UO_2^{++} should be predominantly ionic, the value for $\langle |r^{-3}| \rangle$ for two negative charges on each oxygen would be $\sim 4/(1.6)^3 \times 10^{24}$ or $\sim 10^{24} \text{ cm}^{-3}$. The bond length is $\sim 1.6 \text{ \AA}$. This $\langle |r^{-3}| \rangle$ value is more than an order of magnitude too small to account for the above value of P assuming a nuclear quadrupole moment of $\sim 10 \text{ b}$. This demonstrates conclusively that P arises from an anisotropic charge configuration on the uranium.

The above discussion has shown that $P > 0$ is required if the α emission and fission results are to be consistent with the expectations of nuclear theory. Since U^{233} and U^{235} have positive quadrupole moments, $P > 0$ requires that

$$\langle |P_2(\cos \theta)/r^3| \rangle > < 0$$

for the MO_2^{++} bonding charge distribution. Because of the chemical behavior and especially the quite short bond length of $\sim 1.6 \text{ \AA}$, one concludes that the UO_2^{++} bond is strongly covalent. This is consistent with the earlier observation as to the magnitude of P . For a strongly covalent UO_2^{++} bond one would normally expect that all of the available charge would be in σ states (81, 82) to maximize the overlap integral of the uranium wave functions with those of the oxygen atoms. If one has $P > 0$, this cannot be the case.

The quadrupole coupling which may arise from all of the possible configurations on the uranium has been estimated (84), using $5f$, $6d$, $7s$, and $7p$ relativistic Hartree wave functions for U^{5+} which have been calculated using an IBM-704 code prepared by S. Cohen. On the basis of these calculations $P > 0$ may be understood if one assumes that the UO_2^{++} or NpO_2^{++} bond has a substantial contribution of $P-\pi$ character.

LITERATURE CITED

1. Kurti, N., and Simon, F., *Proc. Roy. Soc. (London)*, **A**, 149, 152 (1935)
2. Gorter, C. J.; cf. Debye, P., *Physik. Z.*, **35**, 928 (1934)
3. Rose, M. E., *Elementary Theory of Angular Momentum* (John Wiley & Sons, New York, N. Y., 1957)
4. Blin-Stoyle, R. J., and Grace, M. A., *Handbuch der Physik*, **42**, 555 (Springer, Berlin, Germany, 1957)
5. Steenland, M. J., and Tolhoek, H. A., *Progr. in Low Temp. Phys.*, **2**, 292 (1957)
6. Ambler, E., *Progr. in Cryogenics*, **2**, 1 (1960)
7. Huiskamp, W. J., and Tolhoek, H. A., *Progr. in Low Temp. Phys.*, **3**, 333 (1961)
8. Bleaney, B., and Stevens, K. W. H., *Repts. Progr. Phys.*, **16**, 108 (1953)
9. Bowers, K. D., and Owen, J., *Repts. Progr. Phys.*, **18**, 304 (1955)
10. Bagguley, D. M. S., and Owen, J., *Repts. Progr. Phys.*, **20**, 304 (1957)
11. Finn, C. B. P., Orbach, R., and Wolf, W. P., *Proc. Intern. Conf. Low Temp. Phys.*, 7th, 54 (1961)
12. Poulis, N. J., and Gorter, C. J., *Progr. in Low Temp. Phys.*, **1**, 245 (1955)
13. Fano, U., and Racah, G., *Irreducible Tensorial Sets* (Academic Press, New York, N. Y., 1959)
14. Jeffries, C. D., *Progr. in Cryogenics* (To be published, 1961)
15. Borghini, M., and Abragam, A., *Compt. rend.*, **248**, 1903 (1959)
16. Overhauser, A. W., *Phys. Rev.*, **92**, 411 (1953)
17. Carver, T. R., and Slichter, C. P., *Phys. Rev.*, **102**, 975 (1956)
18. Brovetto, P., and Ferroni, S., *Nuovo cimento*, **12**, 190 (1954)
19. Jeffries, C. D., *Phys. Rev.*, **106**, 164 (1957)
20. Abraham, M., Kedzie, R. W., and Jeffries, C. D., *Phys. Rev.*, **106**, 165 (1957)
21. Erb, E., Motchane, J. L., and Ubersfeld, J., *Compt. rend.*, **246**, 2121, 3051 (1958)
22. Abragam, A., and Proctor, W. G., *Compt. rend.*, **246**, 2253 (1958)
23. Abraham, M., McCausland, M. A. H., and Robinson, F. N. H., *Phys. Rev. Letters*, **2**, 449 (1959)
24. Leifson, O. S., and Jeffries, C. D., *Phys. Rev.* (To be published)
25. Borghini, M., and Abragam, A. (To be published)
26. Khutsishvili, G. R., *Soviet Phys. JETP*, **11**, 679 (1960)
27. Bloembergen, N., *Physica*, **15**, 386 (1949)
28. Robinson, F. N. H. (Private communication)
29. Hwang, C., and Sanders, T. M., *Proc. Intern. Conf. Low Temp. Phys.*, 7th, 148 (1960)
30. Abragam, A. (Private communication)
31. Rose, B. (Private communication)
32. Kurti, N., Robinson, F. N. H., Simon, F., and Spohr, D. A., *Nature*, **178**, 451 (1956); and Hobden, M. V., and Kurti, N., *Phil. Mag.*, **4**, 1092 (1959)
33. Ambler, E., Grace, M. A., Halban, H., Kurti, N., Durand, H., Johnson, C. E., and Lemmer, H. R., *Phil. Mag.*, **44**, 216 (1953)
34. Estle, T. L., Hart, H. R., Jr., and Wheatley, J. C., *Phys. Rev.*, **112**, 1576 (1958)
35. Dabbs, J. W. T., and Roberts, L. D., *Phys. Rev.*, **95**, 307 (1954)
36. Anderson, A. C., Salinger, G. L., Steyert, W. A., and Wheatley, J. C., *Phys. Rev. Letters*, **6**, 331 (1961)
37. Miedema, A. R., *Some Experiments on Heat Transfer and Magnetism Below 1°K* (Doctoral thesis, Univ. Leiden, Leiden, Netherlands, 1960)
38. Garrett, C. G. B., *Magnetic Cooling* (Harvard Press and John Wiley & Sons, New York, N. Y., 1954)
39. Laserew, B., and Schubnikow, L., *Physik. Z. Sowjetunion*, **11**, 445 (1937)
40. Dabbs, J. W. T., Roberts, L. D., and Bernstein, S., *Phys. Rev.*, **98**, 1512 (1955)
41. Stolovy, A., *Phys. Rev.*, **118**, 211 (1960)
42. Sailor, V. L. (Private communication)
43. Kunzler, J. E., Buehler, E., Hsu, F. S. L., and Wernick, J. H., *Phys. Rev. Letters*, **6**, 89 (1961)
- 43a. Hanna, S. S., Heberle, J., Perlow, G. J., Preston, R. S., and Vincent, D. H., *Phys. Rev. Letters*, **4**, 513 (1960)
- 43b. Goodings, D. A., and Heine, V., *Phys. Rev. Letters*, **5**, 370 (1960)
- 43c. Boyle, A. J. F., Bunbury, D. St. P., and Edwards, C., *Phys. Rev. Letters*, **5**, 553 (1960)
- 43d. Roberts, L. D., and Thomson, J. O., *Bull. Am. Phys. Soc.*, **6**, 75 (1961)
44. Kurti, N. (Private communication)
45. Grace, M. A., Johnson, C. E., Kurti, N., Scurlock, R. G., and Taylor, R. T., *Phil. Mag.*, **4**, 948 (1959)
46. Baldock, D., *Some Applications of Nuclear Orientation* (Doctoral thesis, Oxford Univ., Oxford, Engl., 1950)

47. Samoilov, B. N., Sklyarevskii, V. V., and Stepanov, E. P., *J. Exptl. Theoret. Phys. (USSR)*, **38**, 359 (1960)
48. Postma, H., Marshak, H., Sailor, V. L., Shore, F. J., and Reynolds, C. A., *Bull. Am. Phys. Soc.*, **6**, 275 (1961)
49. Stolovy, A., *Bull. Am. Phys. Soc.*, **6**, 275 (1960)
50. Daniels, J. M., Giles, J. C., and LeBlanc, M. A. R., *Can. J. Phys.*, **39**, 53 (1961)
51. Pound, R. V., *Phys. Rev.*, **76**, 1410 (1949)
52. Bleaney, B., *Proc. Phys. Soc. (London)*, **A**, **64**, 315, (1951)
53. Rose, M. E., *Phys. Rev.*, **75**, 213 (1949)
54. Gorter, C. J., *Physica*, **14**, 504 (1948)
55. Cooke, A. H. (Private communication)
56. Dagley, P., Grace, M. A., Hill, J. S., and Sowter, C. V., *Phil. Mag.*, **3**, 489 (1958)
57. Roberts, L. D., Bernstein, S., Dabbs, J. W. T., and Stanford, C. P., *Phys. Rev.*, **95**, 105 (1954)
58. Hayward, R. W., Ambler, E., and Hoppes, D. D., *Bull. Am. Phys. Soc.*, **6**, 71 (1961)
59. Hoppes, D. D., *Proc. Intern. Conf. Low Temp. Phys.*, **7th**, 186 (1961)
- 59a. Morita, M., and Morita, R. S., *Phys. Rev.*, **110**, 461 (1958)
- 59b. Kotani, T., *Phys. Rev.*, **114**, 795 (1959)
60. Schooley, J. F., Shirley, D. A., and Rasmussen, J. O., *Proc. Intern. Conf. Low Temp. Phys.*, **7th**, 191 (1961)
61. Postma, H., and Huiskamp, W. J., *Proc. Intern. Conf. Low Temp. Phys.*, **7th**, 180 (1961)
62. Postma, H., Miedema, A. R., and Eversdijk Smulders, M. C., *Physica*, **25**, 671 (1959)
63. Chapman, C. J. S., Grace, M. A., Gregory, J. M., and Sowter, C. V., *Proc. Roy. Soc. (London)*, **A**, **259**, 377 (1960)
64. Schooley, J. F., Shirley, D. A., and Rasmussen, J. O., *Proc. Intern. Conf. Low Temp. Phys.*, **7th**, 174 (1961)
65. Grace, M. A., Johnson, C. E., Kurti, N., Lemmer, H. R., and Robinson, F. N. H., *Phil. Mag.*, **45**, 1192 (1954)
66. Huiskamp, W. J., Steenland, M. J., Miedema, A. R., Tolhoek, H. A., and Gorter, C. J., *Physica*, **22**, 587 (1956)
67. Bauer, R. W., and Deutsch, M., *Phys. Rev.*, **117**, 519 (1960)
68. Dagley, P., Grace, M. A., Gregory, J. M., and Hill, J. S., *Proc. Roy. Soc. (London)*, **A**, **250**, 550 (1959)
69. Bauer, R. W., Deutsch, M., Mutchler, G. S., and Simons, D. G., *Phys. Rev.*, **120**, 946 (1960)
70. Hill, D. L., and Wheeler, J. A., *Phys. Rev.*, **89**, 1102 (1953)
71. Bohr, A., *Proc. Intern. Conf. Peaceful Uses Atomic Energy, Geneva, 1955*, **2**, 151 (1956)
72. Dabbs, J. W. T., Roberts, L. D., and Parker, G. W., *Physica*, **24**, 69 (1958)
73. Roberts, L. D., Dabbs, J. W. T., and Parker, G. W., *Proc. Intern. Conf. Peaceful Uses Atomic Energy, 2nd*, **15**, 322 (1958)
74. Dabbs, J. W. T., Hanauer, S. H., Roberts, L. D., Walter, F. J., and Parker, G. W., *Proc. Intern. Conf. Low Temp. Phys.*, **7th**, 177 (1961)
75. Roberts, L. D., and Dabbs, J. W. T., *Proc. Kingston Intern. Conf. Nuclear Structure*, 884 (Univ. Toronto Press, Toronto, Canada, 1960)
76. Hill, D. L., *Handbuch der Physik*, **39**, 178 (1957)
77. Bleaney, B., Llewellyn, P. M., Pryce, M. H. L., and Hall, G. R., *Phil. Mag.*, **45**, 992 (1954)
78. Hanauer, S., *The Angular Distribution of Alpha Particles Emitted by Oriented Neptunium-237 Nuclei* (Doctoral thesis, Univ. Tennessee, Knoxville, Tenn., 1960)
79. Hanauer, S., Dabbs, J. W. T., Roberts, L. D., and Parker, G. W. (To be published)
80. Walter, F. J., Dabbs, J. W. T., and Roberts, L. D., *Rev. Sci. Instr.*, **31**, 756 (1960)
81. Eisenstein, J. C., and Pryce, M. H. L., *Proc. Roy. Soc. (London)*, **A**, **229**, 20 (1955)
82. Pryce, M. H. L., *Phys. Rev. Letters*, **3**, 375 (1959)
83. Roberts, L. D., Dabbs, J. W. T., and Parker, G. W., *Oak Ridge Natl. Lab. Rept.* 2430, 51 (1957)
84. Roberts, L. D., and Dabbs, J. W. T., *Oak Ridge Natl. Lab. Rept.* 2910, 62 (1960); *Bull. Am. Phys. Soc.*, **II**, **5**, 22 (1960)
85. Halpern, I., and Strutinski, V. M., *Proc. Intern. Conf. Peaceful Uses Atomic Energy, Geneva, 1958*, **15**, 408 (1958)

SHIELDING OF HIGH-ENERGY ACCELERATORS^{1,2}

BY S. J. LINDENBAUM

Brookhaven National Laboratory, Upton, Long Island, New York

INTRODUCTION

Background.—At the beginning of the last decade (1950) the shielding of a high-energy accelerator was quite often considered as an afterthought or last-minute addition to the early experimental-program requirements. The rapid increase of beam energies, machine sizes, and beam intensities, coupled with the severe lowering of both biologic radiation tolerances and what are considered acceptable experimental background fluxes, have all contributed to the rapid growth of the magnitude of the shielding problems encountered. With several high-energy accelerators for which adequate original shielding designs were not made, the required additions have been found expensive, time consuming, inconvenient, and not necessarily satisfactory.

It is now generally realized that the shielding design must be considered as a very important and expensive part of the original design because the usefulness, quality, and intensity of the particle beams obtained from an accelerator are considerably affected by the details of the shield. Furthermore, foundation requirements and the usefulness of the arrangement of an experimental area are greatly affected by the particular choice of a shield design.

Although shielding design has not yet reached the simple handbook formula stage, it is nevertheless possible to make reasonably precise designs in many instances and to allow for an adequate range of designs in many other cases.

Biological requirements and shielding.—The general biological requirements of shielding have been extensively discussed in previous articles by Moyer (1) and by Rossi (2). However, the basic radiation concepts required for shielding design will be briefly treated here. The biologic exposure to radiation is believed, on the basis of many investigations, to be best expressed as a product of the ionization loss per gram of exposed tissue multiplied by the relative biologic effectiveness (RBE) of the particular radiation sample. The unit generally used for measuring exposure of tissue to ionizing radiation is the rad, which is that exposure to ionization which leads to an absorption of 100 ergs/g of tissue or equivalently 6×10^5 Mev/g of tissue. The relative biological effectiveness of a particular type of radiation is defined relative to X-ray, gamma radiation, or beta radiation, all of which by definition are assumed to have an RBE of 1. The biologic exposure (product

¹ The survey of literature pertaining to this review was concluded in January 1960.

² Among the abbreviations used in this chapter are: AGS (alternating-gradient synchrotron); CERN (European Council for Nuclear Research); FM (frequency-modulated); and RBE (relative biological effectiveness).

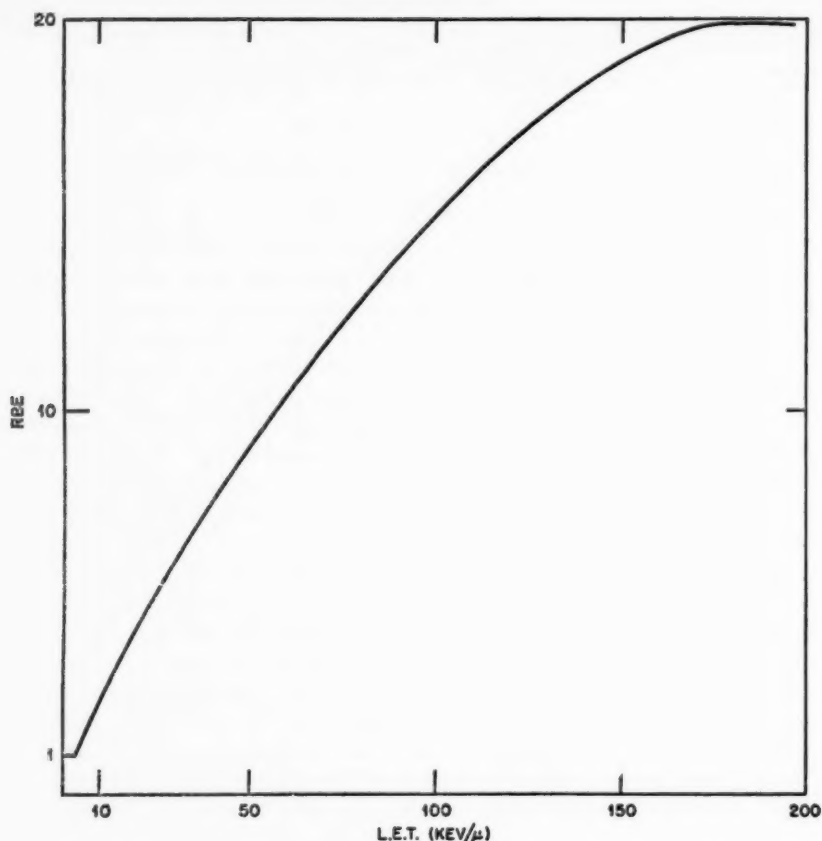


FIG. 1. Correlation of relative biological effectiveness with linear energy transfer from Rossi (2).

of ionization loss and RBE) is sometimes expressed in terms of a unit called the rem (roentgen equivalent in man; $1 \text{ rem} = 1 \text{ rad} \times \text{RBE}$).

The most fundamental definition of RBE for a particular type of radiation (e.g. *R* radiation) would be to select a particular radiation effect and then experimentally determine the dose of X or gamma radiation and the dose of *R* radiation which produced the same effect. The ratio of the first to the second quantity would then give the RBE of the *R* radiation for the particular effect desired. Of course, for another effect there might well be another RBE. The results of many experiments have shown that RBE is always greater than or equal to 1 and that there is an almost unique relationship between RBE and the density of ionization loss such that the minimum or near-minimum ionizing particles have an RBE of 1 and such that, as the energy loss per unit length of an ionizing particle increases, the RBE also increases. Figure 1 shows (2) how the RBE varies with the linear energy

TABLE I
RBE AS A FUNCTION OF NEUTRON ENERGY*

Neutron energy, Mev	RBE
Thermal	3
0.0001	2
0.005	2.5
0.02	5
0.1	8
0.5	10
1.0	10.5
2.5	8
5.0	7
7.5	7
10	6.5

* Reprinted from Rossi (2, p. 152).

transfer (LET) in kev/μ of water.³ The minimum value of ionization is $0.2 \text{ kev}/\mu$ of water, and the RBE remains 1 from minimum ionization till a linear energy transfer of $3.5 \text{ kev}/\mu$ of water. The curve then rises to a value of approximately 20 at $175 \text{ kev}/\mu$ of water which represents the maximum linear energy transfer of the alpha particle.

The most common secondary radiation component from a high-energy accelerator with an RBE of >1 is the neutron (see Table I). The average RBE of neutrons approaches 10 in the energy region of a few Mev, which is an important component of the secondary radiation in many high-energy accelerators. One should keep in mind that the high-energy particles (charged as well as neutral) which interact with nuclei by the strong-interaction nuclear cross section can make stars, etc., and that incomplete data have been gathered on their relative biological effectiveness. Furthermore, charged secondary beams of low energy can deliver high doses to certain areas of the body if they have a well-defined range which ends in the interior of the body [see e.g. (1)] and thereby deliver a much higher dose to a portion of the body than one would measure, for example, with a standard tissue-equivalent chamber. Also, the question of RBE for eye cataract is not completely settled yet.

For all these reasons it has become a conservative custom in high-energy accelerator shielding work, where neutrons and other particles which strongly interact with nuclei predominate, to use a tissue-equivalent ionization chamber (an ionization chamber that indicates the dose which would be absorbed by human tissues) to measure a dose in rads and use an over-all RBE of 10 or at least 5 to determine the dose in rem. It is the author's opinion that the over-all assumption of an average RBE of 10 in these cases is justifiable, in view of the many uncertainties involved. The present practice regarding

³ Note that $1 \text{ kev}/\mu$ of water = $10 \text{ Mev}/\text{cm}$ of water.

maximum permissible radiation dose which is approved by the Atomic Energy Commission⁴ and generally used in high-energy accelerator installations is based on the 1957 recommendations of the National Committee for Radiation Protection (3) and the May 13, 1960, Staff Report of the Federal Radiation Council (4). These dose limits can be summarized as follows:

Occupational personnel.—The personnel involved in a high-energy accelerator operation includes physicists, accelerator-operating and maintenance engineers, technicians, physicians, and nurses. Radiation exposure indicators or film badge control should be used on occupational personnel. The maximum dose is 3 rem per quarter of a year (i.e., ~ 231 mrem/week averaged over a quarter), but the maximum accumulated exposure is less than or equal to 5 ($A-18$) rem where A is the age in years. This formula means that age 18 should be the earliest exposure date and that the accumulated average should not exceed 5 rem/year. However, of course, an older man starting his exposure at age 30 could be exposed to 12 rem/year for 8 years until the formula would require his exposure to be reduced to the order of 5 rem/year.

Nonoccupational (including background and medical) exposures.—The maximum dose is 14 rem in 30 years averaged over large groups of population. The practical recommendation (2) for unmonitored personnel around an accelerator is about 500 mrem/year.

It is of practical interest in shielding design to convert the biologic radiation dose in mrem/hr approximately into fluxes of particles/sq cm/sec. One usually assumes that for particles producing minimum ionization the RBE is unity; because of possible star effects, this assumption is questionable for those particles (pions and protons) which have strong nuclear interaction, but it is well justified for muons or electrons, for example. On this assumption, ~ 9 minimum ionization particles per sq cm/sec produce 1 mrem/hr. Figure 2 shows the relation between neutrons/sq cm/sec and mrem/hr, and Table I shows the RBE as a function of neutron energy. In the energy region of 1 to 10 Mev, about 7 neutrons/sq cm/sec are equivalent to 1 mrem/hr.

The level of radiation exposure at which the weekly (usually 40 hr) accumulated dose would exceed the maximum permissible radiation dose is generally referred to as a tolerance dose. In the present work we shall simply define 6 mrem/hr as the tolerance level for radiation workers although it is obvious that for young personnel and others whose maximum average weekly exposure (footnote 4) must be kept to 100 mrem, the corresponding true tolerance dose (for a 40-hr week) would be 2.5 mrem/hr; a different true tolerance dose would apply for nonradiation workers or

⁴ The AEC regulations for maximum radiation exposure levels for personnel since Jan. 1, 1961 are described in this paragraph and are embodied in amendments to Title 10, Chapter 1, part 20, of the Code of Federal Regulations entitled *Standards for Protection Against Radiation*.

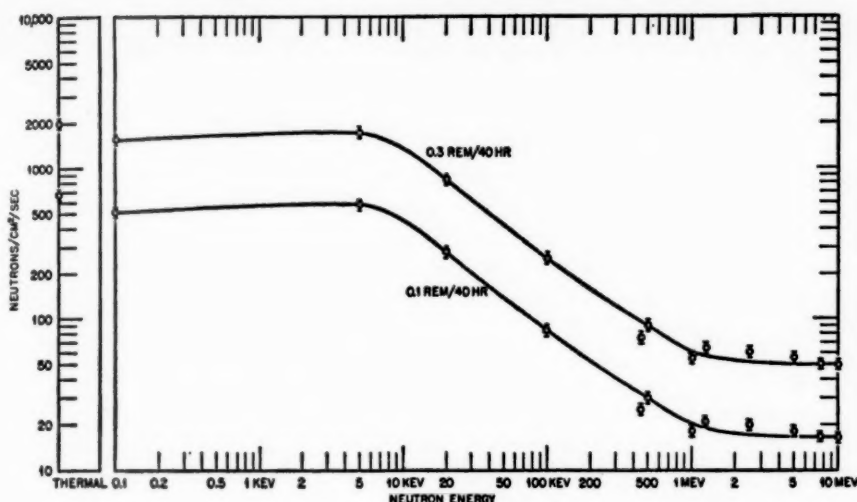


FIG. 2. Flux of neutrons to deliver the stated dose as a function of neutron energy [Rossi (2, p. 153)].

radiation workers working other than a 40-hr week. Henceforth, the mere statement "tolerance level" or "tolerance" will mean 6.0 mrem/hr unless otherwise specified. Those readers who are familiar with bubble chamber and low-rate counter experiments will quickly recognize from the above figures that 1/10 to 1/100 tolerance or less may in many instances be required for experimental purposes.

BASIC SHIELDING PROBLEM FOR PROTON ACCELERATORS IN THE SEVERAL-HUNDRED-MEV TO SEVERAL-BEV ENERGY RANGE

General considerations.—Let us consider a source of protons of intensity N_0 per sec and energy E_0 incident upon and interacting with a small (essentially point) target consisting of various commonly used target materials, including beryllium, carbon, polyethylene, iron, copper, and lead. It will be convenient for shielding purposes to consider, in addition to light targets, moderately heavy targets such as iron or copper since the shield itself if it contains heavy concrete, iron, or lead, etc., will develop a nucleonic cascade characteristic of a moderately heavy target, even if the target is a light element. The results of the interactions of a high-energy proton with nuclei in the region of several hundred Mev to several Bev have been reasonably well investigated, and it is well known (5 to 10) that the nucleonic cascade generated in a target nucleus by a high-energy nucleon contains high-energy neutrons and protons, low-energy neutrons and protons, heavier nuclear fragments, pi mesons, and K mesons, etc., if the energy is high enough. The

reader is particularly referred to the review articles by Miller & Hudis (8) and by the author which review the subject of nucleonic cascades (9).

Typical intensities of primary beams in frequency-modulated (FM) cyclotrons and high-intensity proton synchrotrons are of the order of magnitude $\geq 10^{11}$ to 10^{12} beam particles/sec. (Some FM cyclotrons approach 10^{13} beam particles/sec.) Allowing a typical multiplication of nuclear particles by the order of 10 in a heavy target, one has particle fluxes of the order of 10^{12} to 10^{13} /sec to contend with.

Let us now consider what is the required shielding attenuation to reduce the flux to the radiation tolerance level (6.0 mrem/hr) at a typical working distance of ~ 30 ft from the target. We will consider the equivalent isotropic case, although in all practical cases there will be relatively more flux near the forward direction and relatively less flux at large angles.

At 30 ft the fractional solid angle subtended by 1 sq cm $(d\omega)/4\pi$ is 0.95×10^{-7} . Therefore a typical secondary particle intensity (allowing for multiplication) is, for 10^{11} primary beam particles/sec, of the order of 10^6 nuclear particles/sq cm/sec at 30 ft. For 10^{12} primary beam particles/sec it is about 10^6 nuclear particles/sq cm/sec at 30 ft. As we recall, the tolerance dose corresponds to ≤ 48 nuclear particles/sq cm/sec (the exact number depending on particle type). Therefore, shielding attenuations⁵ of ≥ 2000 to 20,000 will in this average isotropic case be required to approach radiation tolerance.

Let us now consider surrounding the target with a concrete shield (ordinary or heavy concrete) since this is the most generally used practical shielding material. The nucleonic cascade started in the target nucleus will be continued by the energetic secondary nucleons, pi mesons, etc., in the shield nuclei. As we shall see, the most penetrating component is the high-energy neutron flux, and the attenuation characteristics of the high-energy neutron component generally determine the required shield thickness. The mean free path for removal from the beam of high-energy neutrons of kinetic energy $E > 100$ –150 Mev is estimated to be ~ 20 in. in ordinary concrete and ~ 12.3 in. in Ilmenite (a widely used heavy concrete). Therefore, to attain attenuations of at least several thousand for the high-energy neutrons, the practical shield we are considering must have a thickness of more than seven or eight mean free paths for removal. It is obvious that all charged particles issuing directly from the target will be stopped by ionization loss in such a shield unless they, via nuclear interactions or decay, transform into a neutral particle or a cascade of neutral particles which can emerge from the shield or interact near the outer edge of the shield to locally produce charged particles of sufficient range to leave the shield.

One-dimensional infinite slab problem.—Consider for example a parallel beam of radiation of one monoenergetic neutron component of effectively

⁵ Further buildup of the nucleonic cascade in the beginning of the shield has been neglected but is roughly included in the particle multiplication number.

infinite transverse extent incident upon a perpendicular plane shield of effectively infinite width and depth. The flux of primary neutrons of energy E_0 , $n(E_0/\text{sq cm/sec})$ would obviously attenuate with depth in the shield according to the formula:

$$\Phi_x = \Phi_0 e^{-x/\lambda_p} \quad 1.$$

where λ_p is the mean free path for effective removal of the primary component. Naturally, the meaning of "effective removal of the primary component" depends somewhat on the exact definition of removal. In the case of nuclear interactions of the primary neutron, it would obviously be effectively removed if it is transformed into charged particles, especially those which have a limited range (i.e., much less than λ_p). However, if one or more secondary neutrons are emitted in the interaction, the primary can or cannot be considered effectively removed depending on one's exact definition of removal. In the present work unless otherwise stated we shall, for convenience, consider the primary removed by any inelastic nuclear interaction, and those elastic scatterings which for the purpose of radiation shielding substantially change the energy or direction of the primary. The nuclear cascades which remove the primary will build up secondary components as one proceeds through the shield, and this will contribute to a definite ionization loss per unit volume per unit time as function of x which can, for any arbitrary case, be represented by

$$I(x) = B(x)e^{-x/\lambda_p} \quad 2.$$

provided $B(x)$ is arbitrary. $B(x)$ will obviously be 0 for $x \leq 0$ for a neutron primary if we neglect the possibility of back-scattering.

Let us now consider three particular cases of general interest:

(a) Case 1.—If all secondaries generated by the nuclear interactions have a limited range (low-energy charged particles) or are neutrons, etc., which satisfy $\lambda_s \ll \lambda_p$ (where the subscripts denote secondaries and primaries), then $B(x)$ will attain a peak value in a distance equal to a few times the characteristic forward transport distance of the longest mean-free-path secondary component. Thereafter $B(x)$ will remain approximately constant.

$$I(x) = B_s e^{-x/\lambda_p} \quad \text{for } x \gg \lambda_s \quad 3.$$

For unit primary flux, $B(x)$ is usually defined as the ionization buildup factor and will be denoted by $b(x)$. One can also define a buildup factor for particle flux due to a unit primary particle flux which can be referred to as $\beta(x)$. For $\lambda_s \ll \lambda_p$, $\beta(x)$ will also saturate for large enough x .

(b) Case 2.—Another case of interest arises when one of the secondary components has a much longer mean free path for collision than the primary component and other secondary components. For example, when a high-energy electron or photon beam is incident on a concrete shield, the high-energy secondary neutrons generated by the photons or electrons have a

much longer mean free path (λ_s) than the mean free path (radiation length) of the primary (λ_p). In this case after a sufficient transition distance the secondary component of long mean free path obviously predominates over the primary, and the asymptotic form of $I(x)$ becomes:

$$I(x) \rightarrow e^{-x/\lambda_s} \quad \text{for } x \gg \lambda_s \quad 4.$$

(c) Case 3.—Another simple case of some general interest is the situation where a high-energy primary, for example a neutron of $E_0 > \text{several hundred Mev}$, can, after a collision, either continue to propagate near its original direction at reduced energy with about the same mean free path as the primary or generate one or more energetic secondaries near the same direction with about the same mean free path until a sufficient number of cascades have degraded the primary energy to a point where the process no longer propagates. The mean free path for collision of a neutron in concrete shields is relatively constant for $E \geq 150$ Mev and rapidly decreases with decreasing energy thereafter. Hence a situation having characteristics similar to the above is actually encountered in high-energy neutron beams. There obviously will be a distribution function for the number of cascade collisions required to reduce a primary and its generated secondaries to low enough energy (say $E \lesssim 50$ Mev) so that they are effectively removed from the beam in the early part of a thick shield, and this distribution function will depend on the dynamic characteristics of the inelastic interactions which take place. However, for simplicity in illustration, let us consider that a particular number of inelastic interactions are required to remove a particle effectively from the beam, and that the mean free path of the secondary particle of reduced energy is equal to that of the primary particle until the n th interaction when it is reduced in energy sufficiently to have a relatively short mean free path thereafter and can therefore be considered effectively removed. Then it can be shown that, if $N(x)$ is the total number of particles per second passing through a plane perpendicular to x at distance x , the character of $N(x)$ as a function of x is representable by:

$$N_n(x) = N_0(x)\beta_n(x/\lambda_p)e^{-x/\lambda_p} \quad 5.$$

When

$$n = 1, \quad N_1(x) = N_0(x)e^{-x/\lambda_p} \quad 6.$$

When

$$n = 2, \quad N_2(x) = N_0(x)(1 + x/\lambda)e^{-x/\lambda_p} \quad 7.$$

When

$$n = 3, \quad N_3(x) = N_0(x)(1 + x/\lambda + x^2/2\lambda^2)e^{-x/\lambda_p} \quad 8.$$

where β is obviously the particle buildup factor. Therefore it is clear from the above that for $n > 1$ the buildup factor does not saturate and indeed is a

monotonically increasing function of x .⁶ However, when x/λ is much greater than n , approximately exponential absorption occurs with a very slightly longer mean free path than λ_p , the difference ($\Delta\lambda_p \sim n\lambda/x$) becoming smaller as x/λ increases. Therefore, to measure the equilibrium mean free path for exponential removal it will be necessary to use a rather thick shield. In those cases where extensive cascading is important, a series of different exponentials may be required to fit the over-all behavior of a thick shield from the beginning to the end. When the ionization buildup factor is approximately saturated, the observed effective mean free path for removal will be referred to as λ_r and defined as the distance in which the ionization density loss is reduced by $1/e$.

If $\lambda_r \rightarrow \lambda_{\text{collision}}$, then it is safe to assume that cascading is no longer important, although it is also true that equilibrium exponential absorption with a well-defined λ_r may still occur approximately, even if λ_r is considerably larger than $\lambda_{\text{collision}}$ (i.e., electron showers, etc.).

Neutron attenuation.—In all high-intensity accelerators with initial beam energy of less than a few Bev, the thickness of the required shielding is primarily controlled by the attenuation characteristics of the high-energy neutron flux. Therefore let us now consider the quantitative behavior of the neutron inelastic cross sections (11 to 15), as a function of energy, which are depicted for various elements in Figures 3 and 4. It is clear from Figures 3 and 4 that for neutron energies between ~ 100 Mev and ~ 150 Mev the inelastic cross sections are approximately constant; and to the extent that information exists at higher energies, one can conclude that the inelastic cross sections do not change appreciably at higher energies.

Figure 5 shows the proton-proton and neutron-proton total and inelastic cross sections (6) as a function of energy. From these and other data one can conclude, by use of the optical model (which is a reasonable approximation), that the neutron inelastic cross sections probably do not change substantially at least up to ~ 25 Bev; and it is likely that this is true at higher energies also. One can also conclude from these general arguments and experiments that the high-energy proton-nucleon inelastic cross sections are probably very close in value to the neutron inelastic cross sections. Below 100 Mev the neutron inelastic cross section increases rapidly with decreasing energy until $E < 25$ Mev where in most cases the neutron inelastic cross sections level off and then decrease suddenly as shown in Figure 3 and in more detail in Figure 4. The increasing inelastic neutron cross section with decreasing energy in the region $25 \text{ Mev} \leq E_n \lesssim 100 \text{ Mev}$ means that neutron secondaries of high-energy primaries in this energy range reach an equilibrium buildup factor relative to the long-range primary component which

* This increase of buildup factor with x will be even faster if more than one secondary is generated per collision. For example, if s secondaries are generated per collision and $N=2$, we have: $N_2(x) = (1 + sx/\lambda)e^{-x/\lambda}$.

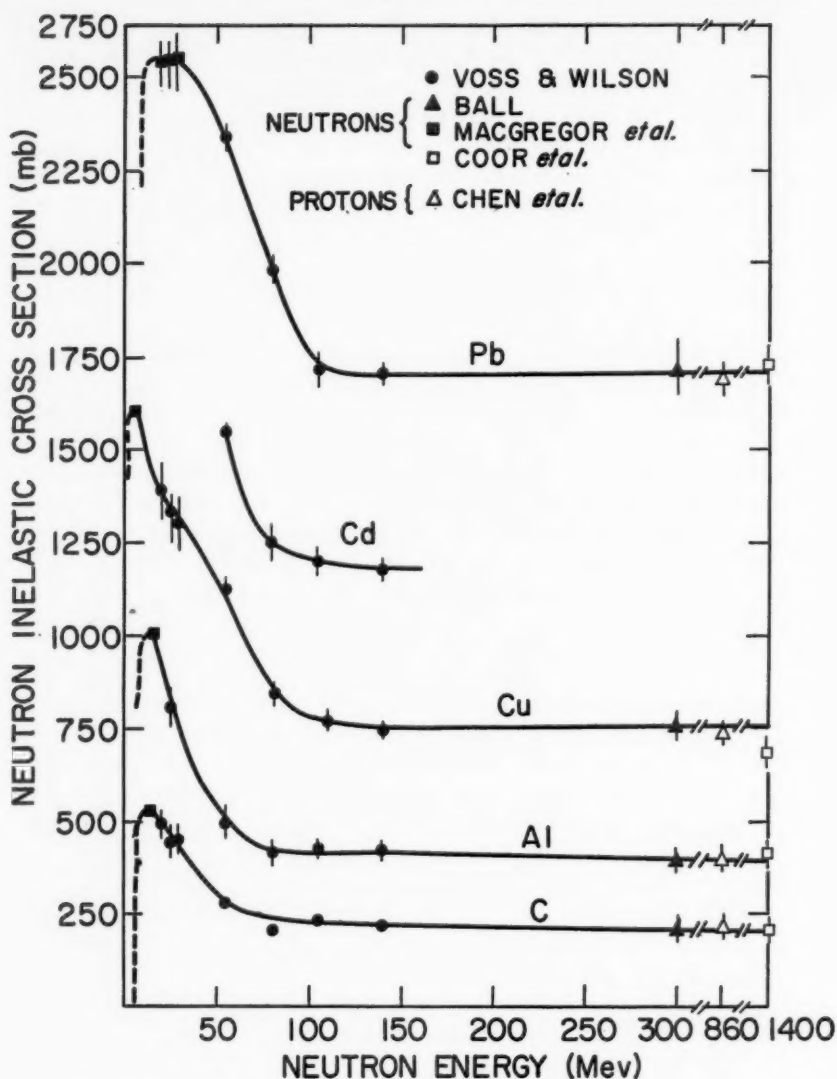


FIG. 3. Inelastic neutron cross sections as a function of energy (0 to 1.4 Bev). The data are from (11 to 14).

controls the attenuation. For $E > 100$ Mev the secondary neutrons may still have an effectively shorter mean free path than a higher-energy secondary, even though the inelastic cross sections are about the same, because of the increasing angular divergence with decreasing energy of the secondaries. It is these facts which tend to make high-energy ($E < \text{several hundred Mev}$ to several Bev) nucleon beams attenuate approximately exponentially (after

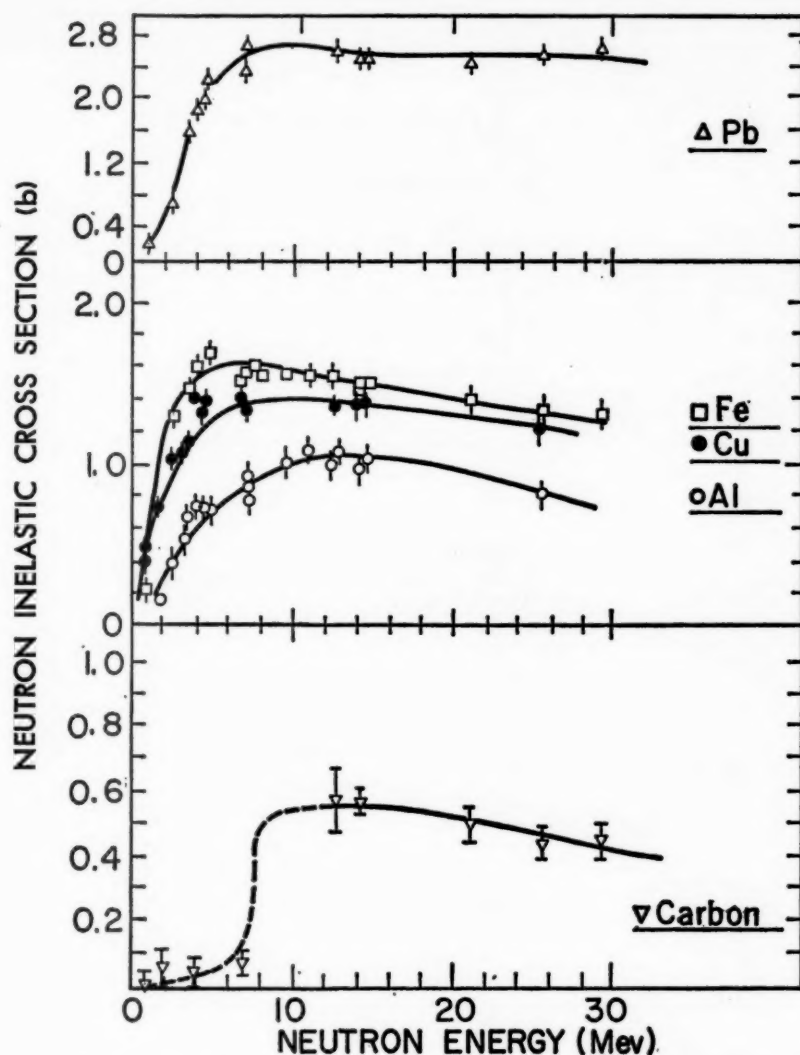


FIG. 4. Inelastic neutron cross sections as a function of energy at low energies (0 to 30 Mev). The data are from a review of the field by MacGregor *et al.* (15).

a sufficient transition region) with a mean free path which is not very sensitive to the initial energy and is not much longer than the geometric mean free path calculated from the inelastic cross sections of the elements in the shield. Of course, the existence of deep enough "holes" in the inelastic cross sections below 25 Mev could, in certain cases, vitiate the above arguments. However, these holes are usually taken care of by a sufficient hydrogen (i.e.,

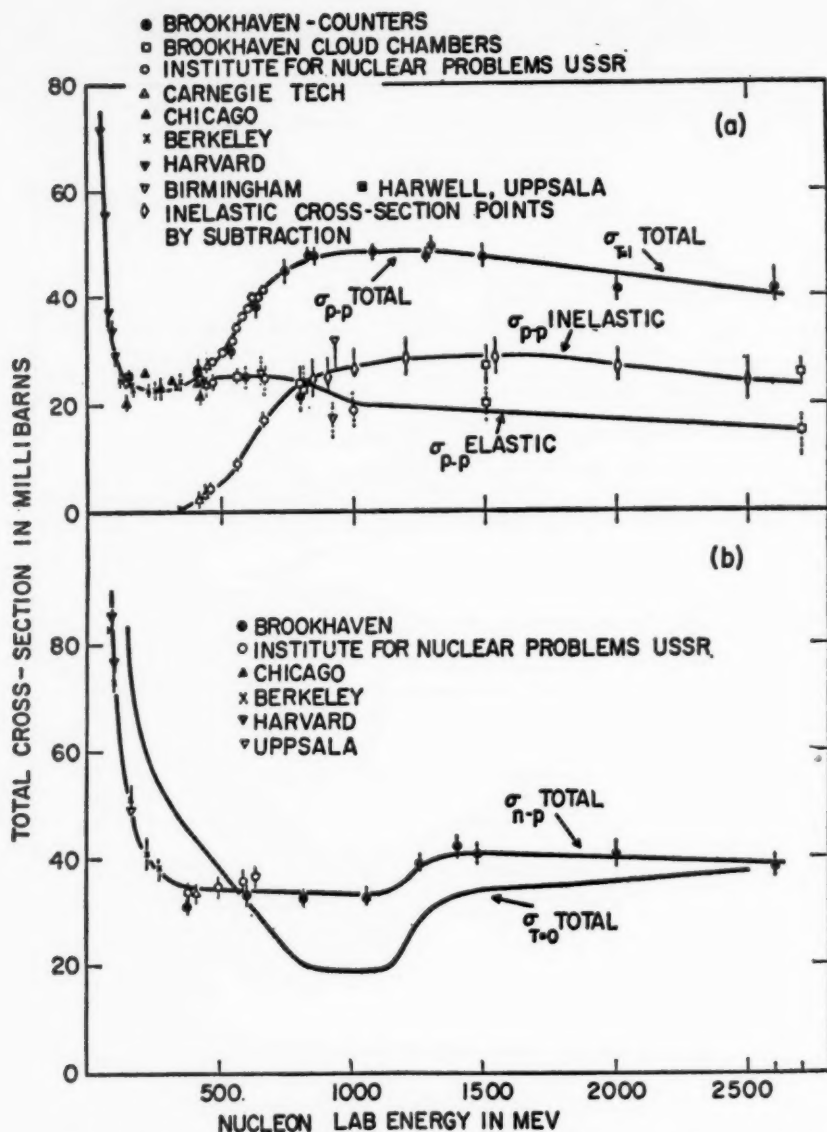


FIG. 5a. The total, elastic, and inelastic cross sections for $p-p$ interactions as a function of energy. All curves shown are empirical. The open diamond points have been obtained by a subtraction of the elastic cross section from the total cross-section curve, and estimated errors are attached. In the region beyond 300 to 400 Mev, the errors on elastic points have been made by broken lines so that they may be distinguished from inelastic or total cross sections. Since $p-p$ interactions occur only via the isotopic spin 1 ($T=1$) state, the cross sections are equal to the corresponding ones for the $T=1$ state.

FIG. 5b. The total neutron-proton cross section is shown as a function of energy. The $T=0$ total cross section deduced from the total $p-p$ and $n-p$ cross sections is also shown. All curves are empirical—from Lindenbaum (9, p. 331).

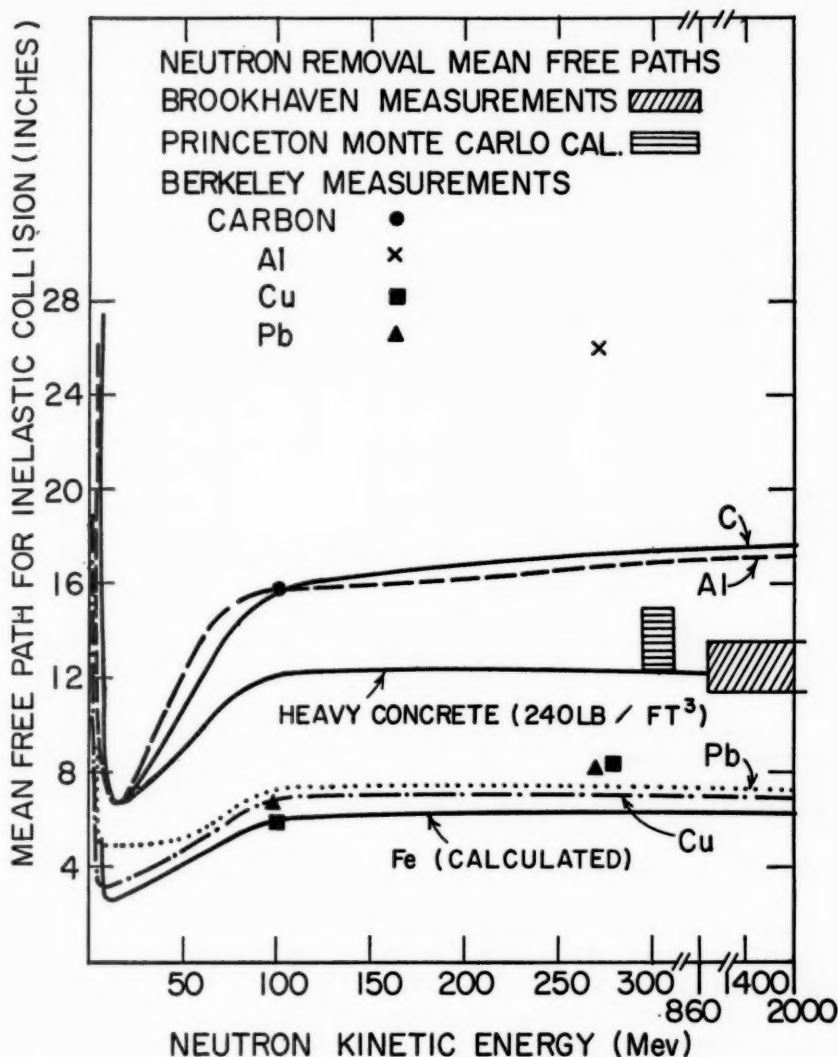


FIG. 6. The calculated mean free path for inelastic collisions of high-energy neutrons.

water) content in a well-designed shield, since the rapid increase of the neutron-proton cross section at low energy, followed finally by neutron capture, can effectively compensate for these holes. For high-energy shields about 1 to 2 per cent water content is adequate for this purpose, whereas in reactor shields approximately 4 per cent water is recommended [see (16) for reactor shields]. The calculated mean free path for removal of high-energy neutrons by inelastic collision is given in Figure 6 as a function of neutron energy for various elements and concrete, etc.

Berkeley shielding measurements.—A series of measurements of the removal half-value thickness⁷ of various materials at various energies has been made by several groups, notably Moyer and co-workers (17, 18) at Berkeley using the neutron beams of the large FM cyclotron. Although the details of the geometry corrections, the transition effects, and the basic accuracy of the measurements all impart a considerable degree of uncertainty to many of these results, their nominal values are of definite interest. Since monochromatic neutron beams were never available, the associated neutron energies are only representative of the average values in the neighborhood of the high-energy peak of the spectrum. The general characteristics of the test setup are shown in Figure 7. These data are shown in

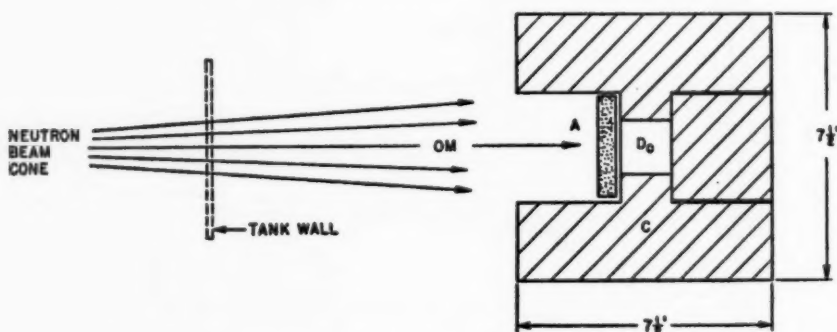


FIG. 7. Arrangement for testing shielding properties of concrete (median plane section) from Moyer (17) and Patterson (18). A, slab under test (dimensions: 3×3 ft by thickness). C, concrete "igloo." D, detector in 1.5 in. cubical cavity. M, beam monitor.

Table IIa and also Figure 6. A quote from the original article (17) follows: "This geometry was chosen because although it fulfilled the requirements for neither 'good' nor 'poor' geometry, it represented the configuration existing in a thick shield." Therefore, one should be somewhat circumspect in relating these values to idealized removal mean free paths.

Typical values of the mean free path for removal of high-energy nucleons determined by shielding experiments at Brookhaven National Laboratory (19, 20) are shown in Table IIb and also in Figure 6. It is clear from Figure 6 and Table IIb that the mean free path for neutron removal is close to the mean free path for collisions at energies below 1 to 2 Bev and appears to increase with energy thereafter. One exception seems to be in the region of about 300 Mev where the mean free path for neutron removal appears to

⁷ The half-value thickness for removal ($d_{1/2}$) is that thickness which reduces the radiation parameter measured to one-half its value. The mean free path for removal λ_r is related to the half-value thickness by: $\lambda_r = d_{1/2}/0.69$. Values of $d_{1/2}$ and λ_r for various substances are shown in Table II.

TABLE IIA

BISMUTH FISSION-CHAMBER MEASUREMENTS OF HALF-VALUE THICKNESSES
OF VARIOUS MATERIALS FOR NEUTRONS DETERMINED AT BERKELEY*

Material	Average neutron energy, 90 Mev		Average neutron energy, 270 Mev	
	Half-value thickness (inches)	Calculated removal mean free path (inches)	Half-value thickness (inches)	Calculated removal mean free path (inches)
Pb	4.7	6.8	5.8	8.4
Cu	4.2	6.1	5.7	8.3
Al	10.7	15.7	18.0	26.0
C	15.1	22.0		
Concrete (ordinary)	9.5	13.8	18.0	26.0

* References (17) and (18).

TABLE IIB

MEASUREMENTS OF HALF-VALUE THICKNESS OF ($\rho \sim 4.0-4.3$) HEAVY CONCRETE
FOR HIGH-ENERGY NUCLEONS DETERMINED AT BROOKHAVEN*

Estimated nucleon energy (Bev)	Half-value thickness for effective removal (inches)	Effective removal mean free path (inches)
$\sim 1-2$	$8.5^{+1.0}_{-0.5}$	$12.3^{+1.5}_{-0.8}$
$\sim 2-3$	11 ± 2	16 ± 3

* References (19) and (20).

exceed that for collision considerably. However, it is probable that the lack of a well-defined geometry, etc., in the experiments is to a large extent responsible for this discrepancy.

Brookhaven shielding measurements.—Brookhaven shielding measurements have been used as an important element in several recent designs of multi-Bev proton accelerator shields; therefore the experiments and their analysis (19, 20) will be briefly described.

The 3.0-Bev external beam of the Brookhaven Cosmotron was allowed to strike a wall of heavy concrete ($\rho \approx 4.0-4.3$) at normal incidence. Most of the beam was included in a 6×6 in. square, and its estimated average divergence was less than about 3° . The wall thickness was varied from 34 in. to 13.5 ft, and measurements were made of ionization density (using Health

Physics monitoring equipment) and also of the number of penetrating particles per unit area ($E_p > 50$ Mev, $E_{pion} > 25$ Mev) as a function both of wall thickness and distance from beam center. The measurements of penetrating particles exhibited a sharply peaked behavior around the beam center, which over the range of the thickness starting from 6 to $8\frac{1}{2}$ ft and ending at 13 ft appeared to be consistent with the compound effects of multiple nuclear scattering and multiple Coulomb scattering which were estimated by the author (20) to spread the beam by $\sim 15^\circ$ full half width. The ionization density measurements exhibited similar types of peaked patterns near the beam center which were broader and also had considerably larger tails. The sharply peaked patterns observed are attributable to the propagation through the shield of the primary proton component which by ionization loss is continually decreasing in energy by ~ 200 Mev per ft. Therefore, over the range of 6 to 13 ft the energy of the primary proton component decreases continuously from about 1800 Mev to about 400 Mev. The data were analyzed to determine the appropriate half-attenuation thickness⁸ along the beam direction for the following: (a) the primary component, (b) the ionization loss per unit volume, (c) the health dose, and (d) the total ionization loss per unit length.

It is clear from the previously published analysis (20) that the controlling element in the behavior of (a), (b), (c) in the latter part of the shield (i.e., after the first 6 to $8\frac{1}{2}$ ft) is the progress of the primary radiation through the shield. In fact, along the beam center, (a), (b), and (c) are all representable by an exponential of the form $N_0 e^{-x/\lambda}$ for shielding thickness in the range 6 to 13 ft, and all have the same nominal half-attenuation value of $8\frac{1}{2}$ in. over this range of shielding thicknesses.

As already pointed out (20), the geometry is poor enough after 6 to $8\frac{1}{2}$ ft so that a measurement of the behavior for (a), (b), and (c) near beam center essentially gives the appropriate half-attenuation thickness with only small geometry errors. Therefore it appears that over the shield-thickness range of 6 to 13 ft (i.e., primary proton component energy in the range of 1800 to 400 Mev), the half-attenuation thickness of the primary component is approximately independent of energy. In regard to (d), an integration over the shield area normal to the beam was required. Although this is a more inaccurate determination since the shapes of the radiation patterns varied rapidly over the intervals used, the result for the latter part of the shield (beyond 8 ft) also yielded⁹ a half-attenuation thickness of the order of $8\frac{1}{2}$ in. This of course is further support for the interpretation that the primary component controls the radiation pattern, and makes it clear that this half-attenuation thickness is appropriate for use in shielding calculations concerned with dose rates.

⁸ Half-attenuation thickness and half-value thickness (see footnote 7) are used interchangeably.

⁹ There was an erroneous value listed for this length in the original report (19). The value now stated is the correct one determined from the data.

A consideration of all sources of error including monitoring, geometry, and dimensional uncertainties results in an error estimate of $-\frac{1}{2}$ in. and $+1$ in. where the asymmetry is introduced by the fact that geometry corrections can only increase the values in the poor-geometry measurements. The resultant half-attenuation thickness is $8\frac{1}{2}$ in. $+\frac{1}{2}$ in. $-\frac{1}{2}$ in.

In the first 6 to 8 ft the half-attenuation length is not easy to determine. Transition effects and the rapid spreading of the beam in the first few feet of concrete make the estimates rather uncertain. However, one can estimate from (a), (b), (c), and (d) that a half-attenuation thickness of $11 \text{ in.} \pm 2 \text{ in.}$ is consistent with the data. Considering that the various nuclei in the shield (except hydrogen) are composed of approximately equal numbers of neutrons and protons and that the differences in n - p and p - p total cross sections are not too large over the energy interval ~ 400 to 2500 Mev, one can conclude that the half-attenuation lengths for neutrons in this energy range will be essentially the same as those for protons. Hence the values obtained above apply for nucleons in this energy range.

Buildup factors.—Moyer and his collaborators have extensively studied buildup factors (17, 21, 22) at the FM cyclotron at Berkeley. The following is a quote from the article "Build-up Factors" by Moyer (21):

We make estimates from known relative intensities of components outside a well shielded synchrocyclotron. We are accustomed to find slow neutron flux densities about 10 times larger than those of fast neutrons in the Mev region, and gamma produced ionization which measures in mr/hour about 1/10 the fast neutron flux density.

Thus, relative component measurements such as 100 slow neutrons per sq cm/sec, 10 fast neutrons/sq cm/sec (mean energy about 1 Mev), and 1 mrem/hr gamma-produced radiation are quite typical. Using Figure 2 or Table I, we conclude for the ratios of the various doses that if the fast-neutron dose corresponds to ~ 1.4 mrem/hr, the slow-neutron dose corresponds approximately to ~ 1 mrem/hr compared to ~ 1 mr/hr gamma-produced radiation. The contributions to the dose due to the protons and pi-mesons are small in an FM cyclotron of a few hundred Mev. Therefore about 40 per cent of the health dose is due to fast neutrons, about 30 per cent of the dose is due to slow neutrons, and about 30 per cent of the dose is due to gamma-produced radiation. Since the radiation length in ordinary concrete shields is ~ 25 g/sq cm while the neutron removal mean free path is 125 g/sq cm or more, it is obvious that the gamma-produced ionization outside the shield does not come directly from the target but is produced locally by nuclear processes such as capture gammas, nuclear de-excitation gammas, and a small number of locally produced π^0 gammas. One should note that electrons are produced by Compton scattering, photoelectric effect, and pair production by gammas. In a heavy-concrete shield ($\rho \sim 4.0$) the radiation length is ~ 17 g/sq cm and hence the proportion of gamma-produced radiation will be smaller. Several years ago, Moyer kindly supplied the author with some data on fast-neutron buildup factors for a thick ordinary concrete shield determined from measurements with the FM cyclotron at

Berkeley (22). For neutron primaries of 100 to 300 Mev the fast-neutron buildup factor is estimated to be ~ 10 . If one wishes for convenience in calculating health doses to incorporate the slow-neutron dose into an equivalent fast-neutron buildup factor $\bar{\beta}_{fn}$ which gives the same health dose as the actual neutron radiation, the foregoing data on ratios give $\bar{\beta}_{fn} \approx 17 \pm 5$ where the error estimate is rather uncertain.

Figure 8 depicts the estimated approximate average numbers of cascade neutrons and evaporation neutrons and also total neutrons produced per collision based on the work of Metropolis *et al.* (10), and is from the work of Tsao, Curtis, Harrison & O'Neill (23, 24). It is clear that in comparing these numbers to the buildup factor estimates by Moyer, one has to consider the following effects. The evaporation neutrons have a much smaller mean free path for removal than the neutron primaries. Therefore, they essentially come from an effective depth ~ 25 to 40 g/sq cm (transport mean free path) while the cascade neutrons come from depths ~ 125 g/sq cm. Hence the relative contribution of evaporation neutrons at the surface of the shield is about one-third to one-fifth of those produced per collision. On the other hand, each high-energy neutron primary of ~ 300 -Mev incident energy can, because of the nature of the nucleonic cascade, be accompanied on the average by perhaps as much as one or at least a fraction of one energetic neutron secondary which contributes to the over-all buildup of the so-called fast-neutron flux; this flux tends to peak between 1 Mev and a few Mev and is composed of both evaporation nucleons and cascade nucleons of degraded energy. When all of this and the uncertainties in the measurements are considered, it appears that the order of magnitude of the Berkeley observations can probably be reasonably explained theoretically. One can also see from Figure 8 that the variation of buildup factor with energy will be relatively slow.

The interactions of nucleons (about equal numbers of protons and neutrons) of about 300 Bev with lithium hydride have been studied by Dobrotin & Slovatsky (25) using a "calorimetric" method which consists of a series of ionization chamber trays separated by slabs of dense absorber totaling 5.3 units of nuclear interaction. The arrangement is shown in Figure 9. The upper cloud chamber determined whether the shower particles were charged or neutral while the lower cloud chamber enabled the authors to determine the number, emission angles, and momenta of the overwhelming majority of charged secondaries. By this method the authors were able to relate the total energy of the shower to the measured ionization with a stated accuracy of 30 per cent and hence were able to determine the individual primary nucleon energies directly. The average number of charged shower particles per shower at this energy is found to be 8 ± 1 . The average multiplicity at 10 Bev was determined by experiments at the Dubna accelerator to be 3.0 ± 0.1 . This demonstrates that the average multiplicity of shower particles in a nucleon-nucleon collision increases only slowly with energy. Of course the buildup factors to be used for shielding purposes will increase considerably faster with energy than the basic shower multiplicity because

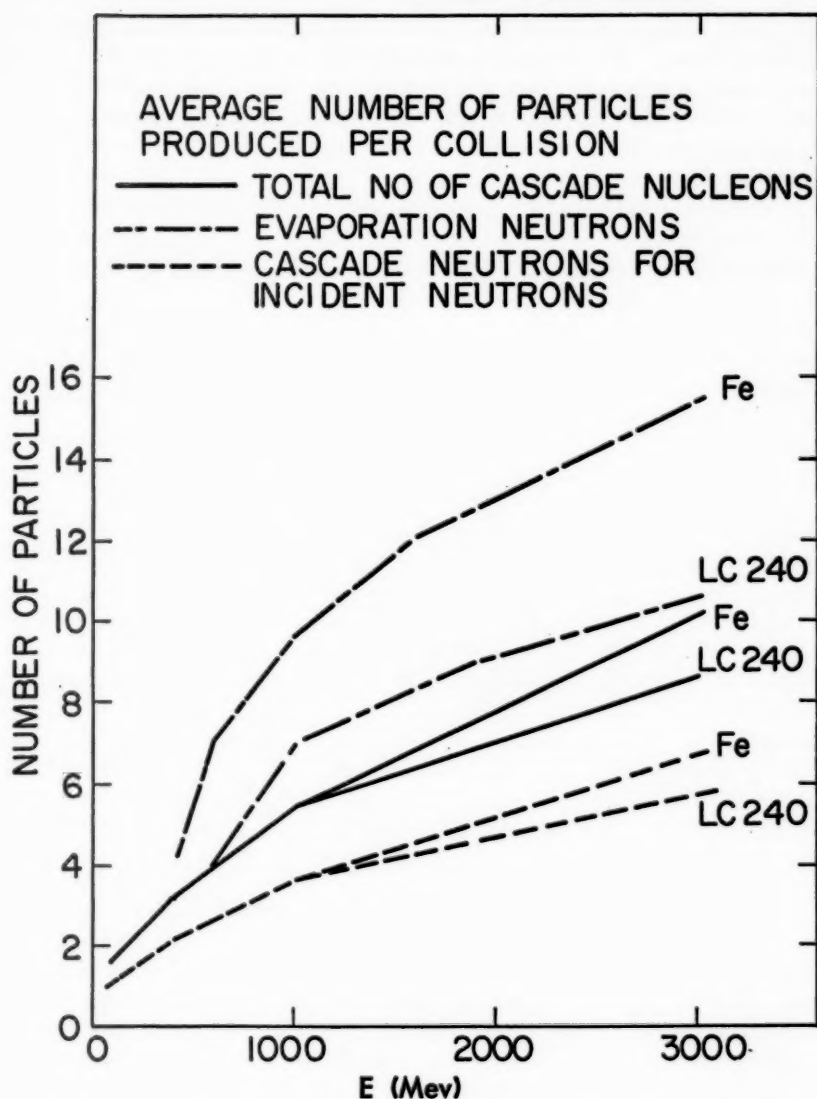


FIG. 8. Average number of particles produced per collision for various materials as a function of incident nucleon energy (23, 24).

the shower particles produced by high-energy primaries contain more energy and hence can themselves produce other showers. In this regard it appears that the average inelasticity of these high-energy events is one-third. Therefore, several interactions will be required to degrade a high-energy nucleon to 1 Bev or less. Nevertheless, from considerations like these one can crudely estimate that the over-all shielding buildup factor will probably go up con-

siderably more slowly with energy than linearly, and a guess might be a buildup factor $\sim E^{1/n}$ where n is probably at least 2. Naturally, as indicated previously the buildup factor will probably only have a near-saturated value when $\bar{n}x/\lambda \gg 1$, where \bar{n} is the average number of collisions required to degrade the primary nucleon into secondary nucleons of energy of a few hundred Mev.

Nucleonic cascades and Monte Carlo calculations.—The characteristics of the inelastic interactions of nucleons with nuclei have been reasonably well explained via a nucleonic cascade composed of single nucleon-nucleon en-

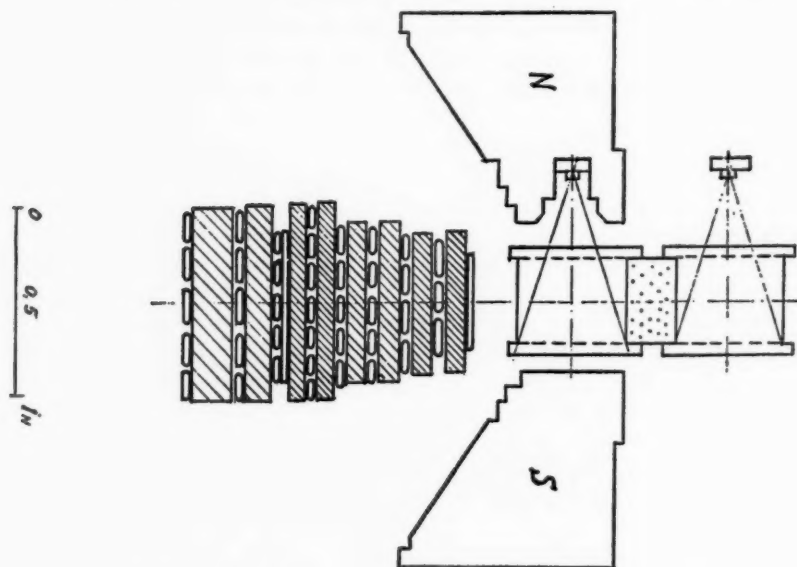


FIG. 9. Experimental arrangement of ionization calorimeter (25).

counters in a Fermi gas nucleus. Several authors (5, 6, 7, 10) have, over the last decade, applied the Monte Carlo method to the treatment of these nucleonic cascades. The results agree reasonably well with experiments as regards both mean values and the large fluctuations inherent in these stochastic processes. An extensive series of nuclear cascade calculations has been recently carried out by Metropolis *et al.* (10), using the MANIAC electronic computer. Cascades of nucleon-nucleon collisions including pion production and reabsorption were considered. The number, kind, energy, and direction of emitted particles of each cascade as well as the nature and value of the excitation of the residual nucleus were tabulated. Incident nucleons from 46 to 1830 Mev were treated. In addition, cascades initiated by incident pions from 0 to 1500 Mev were considered for various target nuclei which include aluminum, copper, ruthenium, cerium, bismuth, and uranium.

About 1000 cascades were calculated for each incident energy and target nucleus. These authors have made extensive comparisons of their calculations to available experimental data and have found a generally good agreement of the characteristics of the nucleons. The discrepancies which do appear mainly in the pion spectra are primarily due to the particular simplifying assumptions made for the characteristics of pion production. Therefore the Monte Carlo calculations serve as an excellent source for shielding calculations.

Tsao, Curtis, Harrison & O'Neill (23, 24) have applied the Monte Carlo method to calculations¹⁰ of the shielding for the Princeton-Pennsylvania 3-Bev proton synchrotron which is under construction. These authors have used the Metropolis *et al.* Monte Carlo cascade calculations as a starting point and have traced subsequent neutron and proton cascades through heavy (Ilmenite) concrete of density 240 lb/cu ft (composition by weight: iron 38 per cent, oxygen 32 per cent, calcium 22 per cent, and silicon 8 per cent). Pions and gamma rays are neglected and several simplifying assumptions have been made. Furthermore, in order to save computer time and obtain reasonable statistics, the particle flux has been doubled a sufficient number of times so that, even after a thick shield, a few particles emerge per entering particle. This latter technique can and does introduce large fluctuations in some of the results.

A typical result of general interest is the normal incidence of 300-Mev neutrons on a flat slab of heavy concrete ($\rho \sim 240$ lbs/cu ft). Although fluctuations of the points made the results somewhat uncertain, these authors have found that between 11- and 15-ft shield thickness the half-attenuation thickness is ~ 10 in. with an error which the author estimates to be $\sim \pm 1$ in. For this case the calculated collision mean free path is ~ 8.3 in. From a plot of the particle buildup factor from 2 to 16 ft, it appears that the assumption that two collisions are required to remove the primary fits the data very well. The particles leaving the shield are practically all neutrons. A typical energy distribution at 170 in. is given in Table III.

Therefore, the buildup factor per primary neutron (kinetic energy > 250 Mev) appears to be ~ 45 , but cascade fluctuations make the error considerable. If one computes the buildup factor for neutrons below 100 Mev relative to those above 100 Mev, one obtains ~ 3.2 . Hence Moyer's estimate which is intermediate between these two is reasonably consistent with the results of these calculations.

When the secondary particles from the target which is hit by 3.0-Bev protons are allowed to be incident on the 15-ft thick shield, the energy spectrum of the particles on the outside of the shield is given in Table IV. The apparent fluctuations are attributable to statistics and the stochastic fluctuations.

¹⁰ Some of the early results of the Monte Carlo type of calculation were reported by O'Neill (24). However, it is the author's understanding that the inelastic neutron cross sections used at intermediate energies (~ 300 Mev) were too low and therefore these results are superseded by those reported in (23).

TABLE III

A TYPICAL CALCULATED (23) ENERGY DISTRIBUTION OF THE PARTICLES*
AT 170-IN. SHIELD THICKNESS† FOR 300-MEV INCIDENT NEUTRONS‡

Energy range (Mev)	No. of particles
0- 5	146
5- 10	12
10- 20	31
20- 30	13
30- 40	15
40- 50	10
50- 60	13
60- 70	9
70- 80	9
80- 90	21
90-100	13
100-200	125
250-500	9

* Practically all of these particles are neutrons.

† This shield is heavy concrete.

‡ Reference (24).

TABLE IV

CALCULATED (23) ENERGY SPECTRUM OF THE PARTICLES ON THE OUTSIDE OF A
15-FT. THICK HEAVY CONCRETE SHIELD WHEN 3.0-BEV PROTONS
ARE THE PRIMARY RADIATION

Energy range (Mev)	Fraction of particles in the energy range
0- 5	0.324
5- 10	0.052
10- 20	0.075
20- 30	0.043
30- 40	0.042
40- 50	0.029
50- 60	0.030
60- 70	0.017
70- 80	0.028
80- 90	0.029
90-100	0.039
100-200	0.249
250-500	0.044

tuations due to particle splitting. One should note that the general character of this particle energy spectrum is similar to that for incident neutrons of 300 Mev. The fast-neutron buildup factor computed relative to neutrons of 250 to 500 Mev is ~ 22 . The fast-neutron buildup factor computed relative to neutrons > 100 Mev is 3.3.

Phenomenological shielding calculations.—As pointed out earlier, the fact that the high-energy neutrons control the particle cascade in proton accelerators of a few hundred Mev to a few Bev energy and the additional fact that the mean free path for neutron removal is relatively independent of energy above 100 Mev¹¹ and decreasing with decreasing energy thereafter make the treatment of shielding problems by the phenomenological method previously developed (see p. 218 to 21) quite feasible. The present case is a mixture of Case 1 and Case 3 of the section entitled "One-Dimensional Infinite Slab Problem" (see p. 218 to 21). Since the target is generally the center of the most intense source of radiation, we shall for simplicity at present treat the target as the only source of radiation. Then, if the target is surrounded by a homogeneous spherical shield separated by a distance r_0 from the target, we can generalize the previous one-dimensional treatment in the following manner.

Let us define $n(r, \theta)$ as the total flux of neutrons and other health dose particles/sq cm/sec at a distance r from the target and at a polar angle θ to the beam direction at the target. Let us define $i(r, \theta)$ as the ionization loss per unit volume per unit time. Then the appropriate formulae become

$$n(r, \theta) = \frac{N(r_0, \theta)\beta(r, \theta)e^{-(r-r_0)/\lambda_r}}{4\pi r^2} \quad 9.$$

$$i(r, \theta) = N(r_0, \theta)b(r, \theta)\frac{e^{-(r-r_0)/\lambda_r}}{4\pi r^2} \quad 10.$$

where the dependence on θ has been introduced to take account of the angular dependence of the various quantities.

The relations of our previous one-dimensional quantities to the present ones are given by:

$$\oint \frac{N(r, \theta)}{4\pi} d\Omega = N(r) \quad 11.$$

$$\oint \frac{\beta(r, \theta)N(r, \theta)}{4\pi} d\Omega = \beta(r)N(r) \quad 12.$$

$$\oint \frac{b(r, \theta)N(r, \theta)}{4\pi} d\Omega = b(r)N(r) \quad 13.$$

In practice, provided the shield is thick enough and the conditions assumed are met, approximately exponential attenuation with a well-defined λ_r will occur and the apparent r dependence of both β and b will be small over a few mean free paths. Although there will still be a considerable angular

¹¹ There is some evidence for an increase in the mean free path for neutron removal at ~ 300 Mev (see Fig. 6).

dependence due to the forward peaking of high-energy nucleons from a target, $\beta(r, \theta)/b(r, \theta)$ will tend to be approximately a constant relatively independent of r and θ .

In practice, an equivalent $N(r)$ can be used in terms of neutrons only, which gives the same dose as the actual particle mixture. This calculational procedure can then be used with empirical or phenomenologically estimated mean free paths for neutron removal and empirical or estimated effective buildup factors. Of course, experimental measurements under known conditions can be used to calibrate effective buildup factors.

The same treatment can be reasonably well applied to cylindrical pillbox shields. However, one must remember that in this case r_0 varies and that estimated corrections must be made for oblique incidence on the shield wall where the departure from normal incidence is appreciable. These techniques can also be modified for other odd-shaped shields. In the case where the radiation source is not concentrated at a point, the radiation dose through the shield can be estimated by a rough integration of the effects of a distribution of point sources. The author has used variations of simple techniques such as these to design the new basic shielding for the Brookhaven Cosmotron (20) and has found them quite successful in the sense that actual performance matched design within a factor of ~ 2 which is smaller than the estimated errors in the calculations. Figures 11a and 11b show the Brookhaven Cosmotron shielding. The point to remember is that in most practical shielding situations the shield is far enough removed from the target and is large enough so that the treatment of the shield can be broken down into the separate treatment of various subsections which interact with each other only to a small extent, and then the total radiation flux can be estimated as the sum of the fluxes due to each subsection of the shield.

Barrier shielding and sky shine.—The term "sky shine" generally refers to the indirect radiation from a source which originally proceeds upward from the surface of the earth and is then scattered back to a point near the surface of the earth by one or many collisions with air nuclei, which may be elastic or inelastic. Some scattering and absorption by the earth will also be involved. A high-energy accelerator without a roof shield or with an inadequate roof shield will be a prolific source of sky shine. The use of local shielding barrier walls to block off the direct radiation issuing from an accelerator and the omission of a roof shield or the inclusion of an inadequate roof shield have been chronic conditions in many of the larger accelerators, as for example the Bevatron and early versions of the shielding for the Cosmotron and the FM cyclotron at Berkeley. This neglect of roof shielding was caused partly by a lack of early realization of the enormous magnitude of the sky shine radiation, and partly by a reluctance to incur the high cost and mechanical support difficulties involved in completely enclosing the accelerators with a shield. Furthermore, the present high-intensity levels of operation were not foreseen in many cases. Adequate attention to roof shielding becomes of extreme importance in high-intensity, high-energy

accelerators, since as we shall soon see, barrier shielding is already inadequate at intensity levels $\sim 10^{10}$ protons/sec.

The author has investigated (26) the sky shine problem for high-energy proton accelerators, and the following will be a summary and discussion of this article. In general the sky shine radiation is dominated by low-energy neutrons from 1 Mev to about 10 or a few tens of Mev. The reason is that, if there is an effective thick target or a thin target followed by shielding material in the path of the secondaries from the target, the buildup of secondary low-energy neutrons (~ 1 –10 Mev) corresponds as we have seen to ≥ 10 per energetic primary. The mean free path for scattering of these secondary neutrons by the air nuclei has been shown to be ~ 450 ft. The mean free path for scattering of the high-energy neutrons ($E \geq 100$ Mev) is ~ 2000 to 3000 ft. For distances less than about one mean free path the sky shine flux is, crudely speaking, inversely proportional to the incident mean free path for scattering and directly proportional to the flux from the target. This implies that the number of ~ 1 - to 10-Mev neutrons¹² will be ~ 50 times that of the higher-energy sky shine neutrons ($E \geq 100$ Mev). The author assumed isotropic scattering in the center-of-mass system and an average total and inelastic cross section for neutrons in the low-energy range. These assumptions are not expected to alter substantially the conclusions reached. The simplest problem treated is that of a point neutron source in an infinite isotropic scattering medium with absorption. The methods of transport theory (27) were used.

A scalar flux $\phi(r, t) = \rho(r, t)v$ was defined which is the product of the density of neutrons $\rho(r, t)$ (i.e., number of neutrons/cu cm) and the absolute value of the neutron velocity in cm/sec. The scalar flux is the appropriate unit for dose fluxes. Then the general solution to the steady state problem of an isotropic point neutron source emitting q neutrons/sec in an infinite isotropic scattering medium with absorption is:

$$\phi(r) = \frac{qe^{-\Sigma_t r}}{4\pi r^2} [\epsilon(c, r)] + \frac{qK\epsilon^{-k_0 r}}{4\pi Dr} \quad 14.$$

where $\Sigma_t = N\bar{\sigma}_t$ is the total macroscopic cross section in cm^{-1} , N is the number of nuclei/cu cm, $\bar{\sigma}_t$ is the average total cross section, and $c = \Sigma_s/\Sigma_t = \bar{\sigma}_s/\bar{\sigma}_t$ is the ratio of the total elastic scattering cross section to the total cross section. Here $c \approx 0.97$ for air. However, when the effects of the ground are taken into account, it is shown that $c \approx 0.8$ to 0.9 is more appropriate. We shall here consider the case $c \approx 0.9$:

$$\text{For } |c - 1| \ll 1, \quad k_0 \approx \sqrt{3\Sigma_a\Sigma_t(1 - 2/3A)} \quad 15.$$

$$D = \frac{1}{3\Sigma_t(1 - 2/3A) \left(1 - \frac{4\Sigma_a}{5\Sigma_t} + \frac{2/3A}{1 - 2/3A} \cdot \frac{\Sigma_a}{\Sigma_t} \right)} \quad 16.$$

¹² Reference (26) treats 1- to 5-Mev neutrons for simplicity. However, the basic conclusions will be the same.

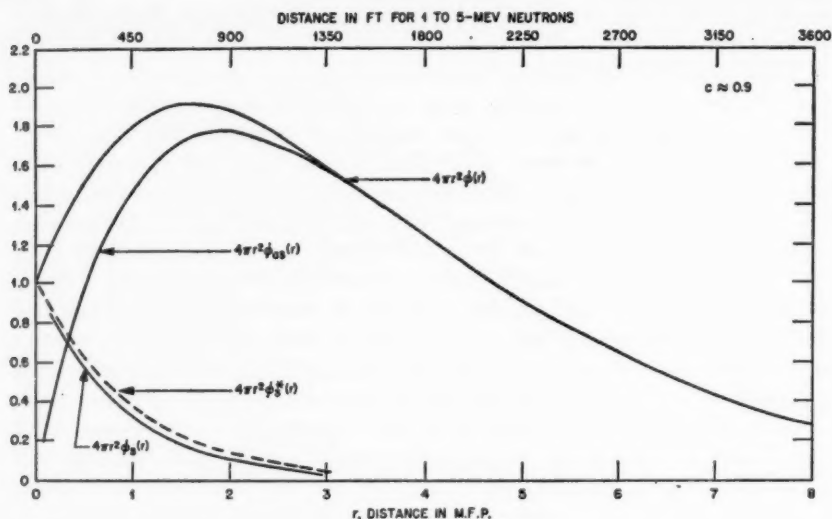


FIG. 10. Plot of Equation 18 with $q=1$ and $c \approx 0.9$.

where Σ_a is the macroscopic absorption cross section and A is the average atomic number. For $c \sim 1$, $\epsilon(c, r)$ is unity at $r=0$ and decreases very slowly and monotonically from unity at $r=0$ to 0.31 at $r=20$ mean free paths.¹³ The symbol K represents the fraction of all neutrons present in the second term, i.e., the $1/r$ term [K is a function of c and is plotted on p. 62 of (27)]. For $c \approx 0.9$, $K \approx 0.9$. For air with $\bar{\sigma} \approx 1.5$ barns, and $c \approx 0.9$, one mean free path ($1/\Sigma_t$) is about 450 ft $\approx 1.33 \times 10^4$ cm.

$$1/k_0 \approx 830 \text{ ft} \approx 2108 \text{ cm} \quad 17a.$$

$$D \approx 0.5 \times 10^4 \text{ cm} \approx 170 \text{ ft} \quad 17b.$$

The first term in Equation 14 represents the source term and is defined as $\phi_s(r)$. If $\epsilon(c, r)$ were exactly unity, the first term in Equation 14 would at all distances represent the flux from the source which arrived at point r without a nuclear scattering or interaction in the air. Let us define this latter quantity as $\phi_s^*(r)$. The first term of Equation 14 will become negligible in comparison to the second term at large enough distances since $1/r \gg 1/r^2$ and also $e^{-\Sigma_a r} \ll e^{-k_0 r}$ for $\Sigma_a < \Sigma_t$. Therefore the $e^{-k_0 r}/r$ term, which represents the sky shine, is the asymptotic solution (ϕ_{as}) for large r . A convenient form for plotting Equation 14 is obtained by multiplying $\phi(r)$ by $4\pi r^2$:

$$4\pi r^2 \phi(r) = q e^{-\Sigma_a r} \epsilon(c, r) + \frac{q K r e^{-k_0 r}}{D} \quad 18.$$

Figure 10 is a plot of Equation 18 with $q=1$ and $c \approx 0.9$. Distances are plotted in mean free path units and are also shown in feet using the mean free path

¹³ The quantity $\epsilon(c, r)$ is tabulated on p. 91 and plotted on p. 97 of (27).

of 450 ft deduced for 1- to 5-Mev neutrons. For $r \gtrsim 0.3$ mean free path (≈ 150 ft), $\phi_{as}(r)$ becomes larger than either $\phi_s(r)$ or $\phi_s^*(r)$. For a neutron source in vacuum, $4\pi r^2 \phi(r) = 1$ for all r . It is clear from Figure 10 that $4\pi r^2 \phi_{as} > 1$ for $0.5 < r < 4.7$. If one locally blocked off or ignored the direct radiation from the source which had not interacted with air nuclei, the resultant indirect radiation which we will call sky shine would have a scalar flux ϕ_{ss} given by $\phi_{ss} = \phi_{as} - (\phi_s^* + \phi_s) \approx \phi_{as}$. For reasons previously given, the high-energy components will contribute only a few per cent to $\phi(r)$ at distances near the source. However, after several thousand feet the high-energy components may dominate because of the long mean free path. The long-distance behavior of $\phi(r)$ from a shield can probably be approximately represented empirically by the following formula:

$$\phi(r) = \frac{\alpha_1}{r} e^{-k_0 r} + \frac{f(\theta, r) \alpha_2 e^{-k_0' r}}{r}$$

where the first term represents the low-energy fast-neutron component and the second term the higher-energy components which in general will have a scalar flux which is a function of angle. It is probable that $f(\theta, r)$ is mainly a function of θ only and in general $\alpha_1 \gg \alpha_2$ and $k_0 \gg k_0'$. In general, several terms might replace each exponential if a more exact solution were desired.

The low-energy fast-neutron scalar flux due to the radiation issuing from the roof of a shield (the order of 2π solid angle opening) was evaluated to be:

$$\phi_{ss} \sim \frac{0.47 \times 10^{-4} q^*}{r} e^{-r/630} \text{ with } r \text{ in ft}$$

Here the effective neutron source strength in neutrons/sec is denoted by $q^* = [\alpha N_p \beta(\gamma\Omega)]/4\pi S$ where N_p represents the number of protons or other high-energy primaries incident per second on the target area, α represents the fraction of the incident beam that is converted in the effective target area, β represents the buildup factor for low-energy fast neutrons escaping per interacting primary, Ω represents the solid-angle opening for escaping neutrons, and γ is a correction factor for anisotropic sources which appropriately modifies the original source strength so that the effective isotropic source strength is obtained. S is the factor by which the escaping low-energy neutrons are attenuated by whatever roof shielding exists, and S can be less than 1 if the roof shield is thin enough to act as a converter.

Observations of sky shine at the Brookhaven Cosmotron as a function of distance from about 100 to 800 ft at various angles ranging from about 10° from the forward beam direction to angles near the backward direction have revealed a more or less constant sky shine radiation dose which does not differ by more than a factor ~ 2 from the forward to the backward direction and which decreases approximately as $1/r$, the decrease becoming noticeably faster after 500 ft. The absolute monitoring and relative accuracy of these

measurements are probably not known better than within a factor of 2; therefore, we have not been able to determine the exponential term accurately. However, one can say that an exponential decay distance of 1000 to 2000 ft is not inconsistent with the data. Furthermore, reasonable agreement (within a factor ~ 2) was found between the measurements and theoretical estimates from the above theory.

The shielding attenuation factor of even an infinitely effective barrier with an open roof is limited to the ratio of the sky shine to direct flux. For distances less than 100 ft we can neglect the exponentials, and therefore this ratio is approximately $\Omega K r / 4\pi D \approx r / 400$ for low-energy fast neutrons.

To obtain the above we assumed $\Omega / 4\pi \sim 1/2$ (i.e. open upper half plane). Hence at small distances from the source (~ 25 to 50 ft), at the Cosmotron the sky shine is ~ 6 to 12 per cent of the direct unshielded radiation when the target does not have a roof. Hence at ~ 25 to 50 ft from a target (typical distances at the Brookhaven Cosmotron and other accelerators), an infinite shielding barrier reduces the low-energy fast-neutron component by only 88 to 94 per cent. For high-energy particles greater than about 100 to 500 Mev, the mean free path is ~ 7 to 10 times larger than for low-energy neutrons; hence the effective value of D is decreased by about an order of magnitude and we have sky shine/direct flux $\approx r / 4000$, with r in ft.

At the Brookhaven Cosmotron before the new roof shielding was installed (1958), the estimated sky shine radiation level at distances of 50 ft from a standard beryllium target (in which one-third of the beam interacts) was ~ 3 mrem/hr for an average intensity $\sim 2 \times 10^9$ protons/sec (energy 3.0 Bev). In a 40-hr week this level will result in exposure of 120 mrem which is greater than the maximum permissible average integrated dose from age 18 onward (100 mrem/week). For heavy-element targets the sky shine increases by another factor of 5. Similar difficulties with sky shine have been observed (28) at the Bevatron. Therefore since both the Cosmotron and the Bevatron are capable of operating at proton fluxes 4×10^{10} /sec and are expected eventually to attain intensity levels at least 3 to 5 times higher than this, eventually it is evident that roof shielding is required from the sky-shine point of view. Relatively little roof shielding would be required for a low-energy neutron source because of the short mean free path. However, in practical cases involving high-energy accelerators (one to several Bev), there is a considerable high-energy radiation component upward from the target. When a roof shield is added, these high-energy particles attenuate with rather long mean free paths and build up an equilibrium component of several low-energy neutrons per high-energy nucleon which emerge from the end of the roof shield. This means that rather thick roof shields will be required at the high-intensity machines. As a matter of fact, to the extent that the effective mean free path for removal of the high-energy nucleons striking the roof is the same as for those striking other parts of the shield, it is easy to show that in a well-designed shield which is not to be sky-shine-limited, there will be approximately constant differences of a few feet of

heavy concrete between side walls and roof for an accelerator like the Cosmotron, for example. Therefore, if a thick side wall shield is contemplated, the roof shielding required becomes almost comparable.

A problem similar to sky shine is leakage under a shield when a concrete (especially heavy concrete) or iron shield is placed around an accelerator at or near ground level and the shield extends upward from the ground level only. Then there obviously is a leakage path downward from the accelerator through the less dense earth¹⁴ and then upward again at the outside of the shield. For any given accelerator shield the leakage-path geometry results in a sizable effective attenuation; however, the effectiveness of the above-ground relative to the below-ground shielding increases both with increasing shield thickness and, for a given shielding attenuation, with the density of the above-ground shielding material. The net result is that for a specific accelerator geometry and a given choice of above-ground shield material, there is a critical above-ground shield attenuation beyond which further increases will be less effective because of ground leakage. If a less dense shield were used, the critical attenuation would obviously be accordingly greater. Actually, in cases where this problem becomes important, building a deep concrete foundation for the shield into the ground will solve the problem. Also if advantage can be taken of rock foundations, the problem will be alleviated. One should note that the choice of density of the shield material should also be considered in terms of the projected intensity of the accelerator design and the resultant possibility of difficulties caused by the ground leakage. This problem has to be taken into account also in the design of experimental block houses of high shielding attenuation in external beam areas of accelerators.

SPECIAL SHIELDING CONSIDERATIONS FOR FM CYCLOTRONS

Since a major share of shielding measurements for the FM cyclotron range was made at Berkeley, we will treat this cyclotron as a typical case. The shielding measurements connected with the original operation of the Berkeley FM cyclotron up to a deuteron energy of 200 Mev (17, 18) showed that the 200-Mev deuterons gave rise to a conical spray of fast neutrons with an upper limit of neutron energy somewhat above 100 Mev when a target of high atomic number was used. The angle of the cone from the peak intensity per sterad at beam axis to the half intensity value was about 5.5° . These neutrons, due primarily to the stripping reaction, had an energy spectrum peaking somewhat below 100 Mev. Later, when the Berkeley FM cyclotron was converted to 340-Mev proton operation, the forward beam cone of neutrons had a mean energy ≈ 270 Mev, and Moyer (22) found that the relative yield per unit solid angle of neutrons over 50 Mev had a peak at 0° and fell to half value at $\approx 25^\circ$ and to ~ 1 per cent ± 1 per cent at 85° .

¹⁴ The earth has a density $\rho \sim 100$ lb/cu ft, while ordinary concrete has $\rho \sim 150$ lb/cu ft, heavy concrete (Ilmenite) $\rho \sim 250$ lb/cu ft, and iron $\rho \sim 500$ lb/cu ft.

Hence this forward cone from a target is a general characteristic of FM cyclotrons and requires special attention in shielding designs.

The roof shielding problem.—As reported (18), three separate courses of shielding finally placed in total a 15-ft wall of ordinary concrete around the Berkeley FM cyclotron plus a 7.5-ft concrete cube in the forward direction to reduce the radiation levels in this forward beam. Although the highest radiation levels existed in the forward direction of the beam, moderately high levels existed in the backward direction because of circulating protons striking part of the Dee structure. For this and other reasons the actual shielding design adopted placed 15 ft of ordinary concrete walls around the machine. One must remember here that once a well-balanced shielding design for a particular setup has been obtained, increased requirements of shielding attenuation generally necessitate the addition of about equal amounts of shielding material to the radiation path lengths of the high-energy, cascade-controlling neutrons in the various parts of the machine. This means that approximately fixed differences rather than ratios tend to exist between various parts of the shield which are exposed to high-energy neutron secondaries. The roof on the Berkeley FM cyclotron was for the previously described design only ~ 4 ft of ordinary concrete. This fact led some time ago to some general speculation in the shielding field that the ratio of roof shielding to side shielding should be ~ 1 to 4. One must remember here that in an FM cyclotron the high-energy particles issuing upwards from an internal target are particularly well shielded by the huge mass of iron in the yoke and magnet pole tips. This of course reduces the apparent shielding requirements on the roof. Observations of this effect have been made at the University of Chicago synchrocyclotron (29) where ten times tolerance level was observed above a 5-ft concrete roof over an external cyclotron beam area even though the beam intensity was only 10^{10} protons/sec, i.e. $\sim 1/60$ the normal peak internal intensities which are of the order of $0.1 \mu\text{a}$ and are thus comparable to Berkeley FM cyclotron intensities.

The shielding characteristics and experiences of the FM cyclotrons at the University of Chicago, Columbia University, Harvard University, University of Rochester, and Carnegie Institute of Technology are described in (29 to 33).

SPECIAL SHIELDING CONSIDERATIONS FOR WEAK- FOCUSING PROTON SYNCHROTRONS

The previous shielding experience (as of 1957) at the Brookhaven Cosmotron, a 3.0-Bev (weak-focusing) proton synchrotron, and that of the Berkeley 6.0-Bev Bevatron (also a weak-focusing proton synchrotron) are described in (20) and (28), respectively. Both proton synchrotrons experienced early serious trouble from lack of roof shielding, and it became clear that even for internal intensity levels of a few times 10^9 protons/sec serious health-hazard and experimental background problems existed without roof shields. At the Brookhaven Cosmotron an extensive experimental study

and a theoretical analysis were made to determine the characteristics of the radiation sources around the machine ring under various conditions (19, 20). The standard internal target for counter experiments is a beryllium target of 2×2 in. cross section perpendicular to the beam and 6 in. along the beam, and it is usually placed in the east straight section of the Cosmotron. About $\frac{1}{3}$ of the beam interacted in the target. Since for most targets used the thickness is ≤ 1 mean free path, $\geq \frac{1}{3}$ of the primary beam does not interact with the target but loses energy in it, and also some of the beam scatters via shadow scattering and multiple Coulomb scattering. The energy loss introduces a change of mean radius of the noninteracting beam which depends on the thickness of the target. For the standard ($2 \times 2 \times 6$ in.) beryllium target at a 350-in. radius (normal inside target position) this results in a sizable portion of the noninteracting primary beam striking the inner wall of the Cosmotron at a mean azimuthal angle $\phi \sim 75^\circ$ downstream of the target position. The Landau effect in energy loss and the radial oscillations of the beam lead to an azimuthal distribution of this secondary target hot spot over a range of ± 5 to 10 ft around its main position on the inner magnet wall. Perhaps $\sim \frac{1}{3}$ of the initial beam is dumped into this well-defined secondary target area. In addition the shadow- and Coulomb-scattered primary beam which went through the target will be spread over a much wider area and much of it will strike the vacuum chamber and magnet steel above and below the median plane, and a good fraction will spill outward radially from the machine. For most practical target situations including practical backup target techniques, ϕ will be in the range of ~ 30 to 120° downstream from the target. The secondaries from these hot spots will also spread the effective source size by interacting, themselves, with the magnet steel. In addition, as previously mentioned there will be a comparable amount of primary beam distributed around a larger area of the machine. From plots of the radiation intensities in the median plane resulting from the standard $2 \times 2 \times 6$ in. beryllium target, one can clearly deduce that for $\phi \sim 90^\circ$ downstream from the target the radiation level is $\sim \frac{1}{2}$ the level near the target. On the other hand for $120^\circ \leq \phi \leq 340^\circ$, the radiation level is $\lesssim 1/7$ to $1/20$ that near the target. Measurements inside the *C* magnet ring give levels $< 1/10$ to $1/50$ those measured outside the ring, and hence it is clear that high levels outside the ring away from the target ($\phi \geq 90^\circ$) are not caused by indirect radiation proceeding from the target but rather by primary and secondary beams spread around the machine. Since it was decided to restrict most high-intensity targeting operations to the south and east straight sections, it was possible in view of the above considerations to break up the design for the recently (1958) installed basic machine shield into a thicker half and a thinner half differing in shielding attenuation by a factor ~ 20 . The Brookhaven Cosmotron shielding is shown in Figures 11a and 11b.

Although the secondary beams emanating from the target in the forward direction require much more shielding material along their path than the wide-angle beams from the target, it turns out that shieldings calculated

for the wide-angle beams incident nearly normally on the circumferential shield are adequate for the forward beams which are incident very obliquely. The radiation and general characteristics of the Cosmotron shielding were designed¹⁵ by the author (20) and the mechanical and structural designs made by M. Karelitz, L. Smith, and J. Lancaster (34). The roof thickness was chosen not only to prevent excessive sky shine but also to protect personnel on the balconies around the machine from direct radiation. This latter requirement is the dominant one. Provision has been made for replacing some of the concrete over the south and east straight sections with steel when the machine intensity approaches $\sim 10^{13}$ protons/pulse (i.e. 2×10^{11} protons/sec). The Cosmotron shielding was designed (20) to keep outside radiation levels to ~ 7.5 mrem/hr, and measurements to date indicate that its performance is as expected.

One important characteristic of the Cosmotron is the external beam ejection system which allows $\sim \frac{1}{3}$ to $\frac{1}{2}$ the internal circulating beam to be ejected externally into a well-defined focused beam $\lesssim 1$ in. diameter and delivered by a beam transport system to various targets in the new experimental-area building extension as shown in Figure 11a. Three external beams I, II, and III have been extracted from the machine. The basic technique consists of using a beam jump target which by ionization loss causes a radial oscillation whose maximum inward excursion is ~ 3 in. and occurs $\sim 180^\circ$ radially or $\sim 360^\circ$ azimuthally, at which point (i.e. location of jump target) it enters a deflecting magnet located radially inward from the jump target and via a pulsed field applied to the ejection magnet causes an outward bend in the particle trajectory sufficient to make it leave the machine through a magnetic-shim-corrected exit in the fringing field, which is located in a pump hole $\sim 90^\circ$ downstream from the ejection magnet. As shown in Figure 11a these external-beam areas involve vast complexes of shielding in addition to the basic machine shield. Furthermore, practically all scheduling at the Cosmotron is for external-beam experiments. The shielding of the external-beam areas is not a fixed installation but is, of course, dictated by the precise requirements of the beam and experimental detection characteristics in each area, and designs for each area are tailored to requests by individual experimental groups. Some general characteristics which are common to all these external-beam problems are:

(a) Most of the external beams use vacuum piping to lead the proton beam from the Cosmotron to the external target area. This is necessary to reduce increases of beam size due to air scattering, general background radiation due to interaction of the beam with air nuclei (mean free path of beam ~ 2500 ft in air), and also the resultant attenuation of beam intensity.

(b) The shielding between the Cosmotron and the final high-intensity

¹⁵ Radiation level and other Health Physics measurements and control were performed by Cowan, Faust, Bishop, and other members of the Brookhaven Health Physics Group, and the author wishes to acknowledge the cooperation of the Brookhaven Health Physics Group in AGS measurements to be reported later.

THE
JOURNAL
OF
JAMES
M. SMITH
1846
TO
1854
BY
JAMES M. SMITH
NEW YORK
PUBLISHED BY
J. B. LIPPINCOTT & CO.
1854

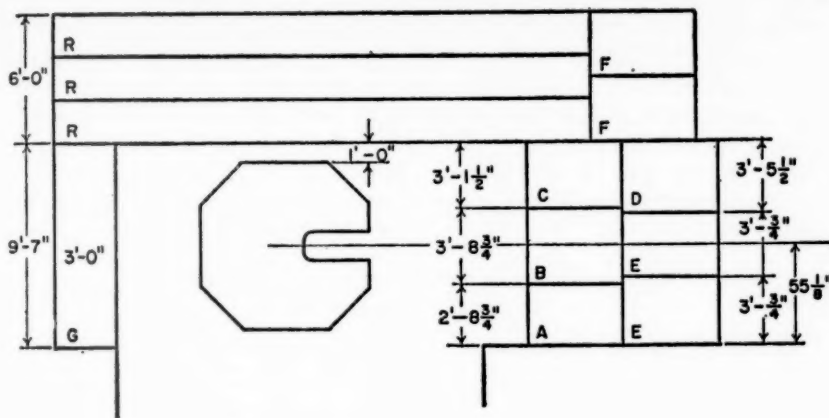


FIG. 11b. Cosmotron shielding (cross section of the main shield—thicker half).

beam target areas need only be sufficient to contain radiation scattering from secondary centers and back scattering from the main target areas, and also to provide protection against accidental movement of beams because of magnet current changes. All beam paths including those in transit areas are roofed over.

(c) The high-intensity target areas are usually characterized by a shielding block house which contains a rather thick shield (≥ 18 mean free paths) in the forward direction to dispose of the high-energy primary protons which do not interact in the target, less heavy side walls comparable with side walls of the main Cosmotron shielding, and shielding roofs again comparable with the main Cosmotron shielding roof. These rather substantial shielding requirements in the external beam are easy to understand when one remembers that $\sim \frac{1}{3}$ to $\frac{1}{2}$ of the internal beam is ejected and that the high-energy primary and secondary radiation in the forward direction requires more shielding than the wide-angle secondaries. One should note that practically all final primary and forward secondary beam disposal is handled in the individual beam blockhouses, as indicated above. The author's philosophy has always been that for high-intensity external beam operations this is the practical and economical solution in most cases. In the early history of our external beam operations, final disposal of the forward primary and secondary beams was in most cases left to an external earthen beam catcher erected in the back yard. [See (20) for details of this.]

The shielding of the 6-Bev Berkeley Bevatron is described by Moyer (28). The major part of the concrete wall has a thickness of 5 ft and is about 15 ft high. Except for the center section of the wall around the median plane, which is concrete of density 3.5 g/cu cm, the rest is ordinary structural concrete of density 2.4 g/cu cm. In the vicinity of the west tangent tank which is the principal target region, the shield wall is 10 ft thick. There is no roof,

and radiation measurements have shown this to be the major deficiency of the shield. The same general characteristics of secondary hot spots which were observed at the Cosmotron were also observed at the Bevatron. Some experiments with clipper targets placed to intercept the particle flux proceeding toward these hot spots were also recorded.

For descriptions of the shielding designs of the Princeton 3.0-Bev and the Argonne 12.5-Bev proton synchrotrons, which are under construction, see (35, 36).

SHIELDING CONSIDERATIONS FOR STRONG-FOCUSING PROTON SYNCHROTRONS

Two high-energy, strong-focusing alternate-gradient proton synchrotrons (AGS) have come into operation recently. First the CERN 28-Bev proton synchrotron (1959) and shortly thereafter the Brookhaven 33-Bev AGS (1960). These machines represent unique shielding problems both because of their size and their energy. The Brookhaven AGS has a circumference ~ 2600 ft, and its very size necessitates burial of the machine to provide the bulk of the shielding (37) for other than explicit target areas.

In the Cosmotron and Bevatron the radial betatron wavelength is about twice the circumference of the machine; therefore, depending on target thickness, the beam that has been scattered or degraded in energy in a target can be intercepted by a clipper target (or inside walls) located downstream $\sim 90^\circ$ to 180° of radial phase or $\sim 180^\circ$ to 360° of machine azimuthal phase (\geq half the machine). Only a fraction of the beam will be stopped by a clipper target. Hence, as we have previously seen, at least the first half of the circumference is a source of high radiation intensity, and even the second half contains ~ 10 per cent of the source strength. Fortunately, in the case of the AGS machines, the betatron wavelength is a small fraction of the circum-

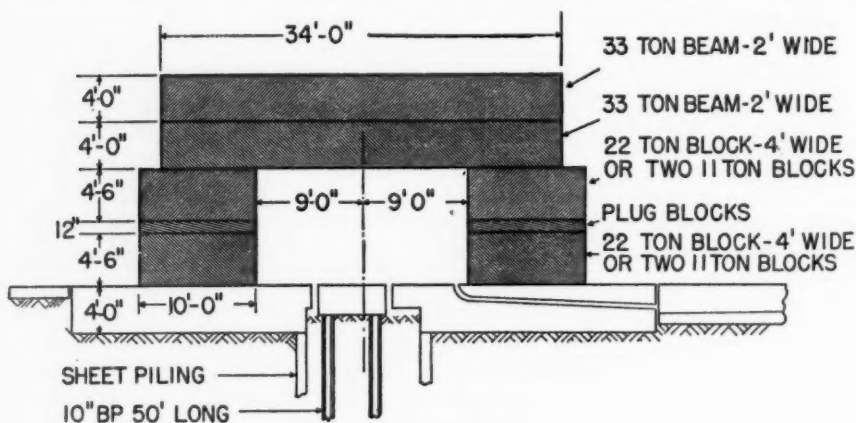


FIG. 12a. Shielding layout at Brookhaven AGS. Cross section of shield in target building.

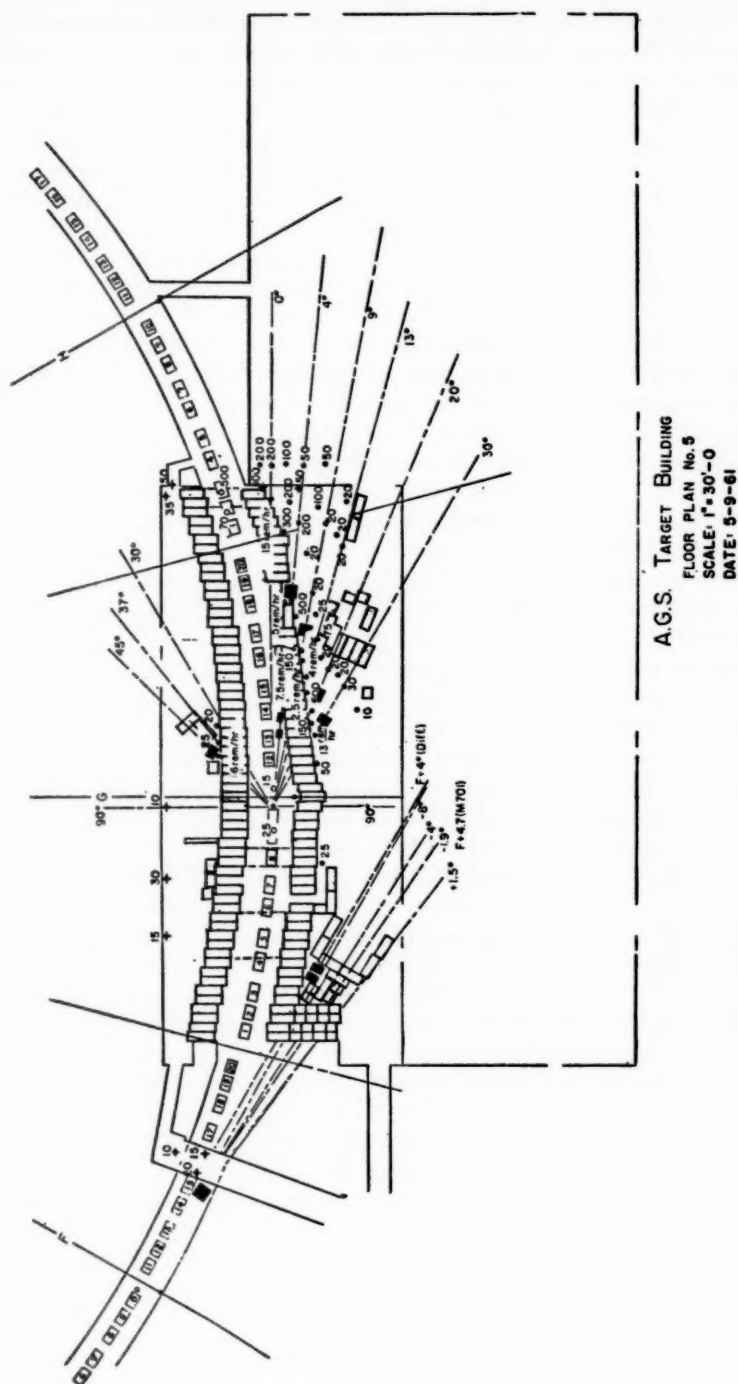


FIG. 12b. Shielding layout at Brookhaven AGS. Top view of experimental area.

ference [$\sim 1/9$ in the Brookhaven machine (37)]. Therefore, by arranging clipper targets to clean up the beam issuing from a target within a betatron wavelength or at most two, one can dispose of the beam locally; a localized shielding arrangement can then be built. The striking success of the phase-lock radiofrequency system both at CERN and Brookhaven has made it possible to think in terms of accelerating practically all of the initially captured beam without appreciable loss until it is delivered onto a target. This, of course, makes it easier to apply clean-up-target techniques in a well-shielded area. The first shielding layout of the target building at the Brookhaven AGS is shown in Figure 12. The CERN shielding is generally similar in principle.

Although there is still considerable uncertainty about the mean free paths for removal of high-energy nuclear particles and about the buildup factors to be used in this high-energy region, one striking fact that has been established at both Brookhaven and CERN is that the muon shielding problem is a dominant one in all cases where forward-direction beams are incident normally on the shielding walls (i.e. the "L"-shaped section of the shield at AGS). Hence, for the first time, nuclear particles do not necessarily control the ionization attenuation with distance. Obviously, the muon problem will become even worse at still higher energies and, unfortunately, is expected to be the most difficult shielding problem even in the high-energy electron accelerator proposed by Stanford.

The interaction of the primary protons ($E \sim 30$ Bev) in a target leads to a number of high-energy neutrons, protons, and pions which in the forward direction have typical energies of a few Bev to ~ 20 Bev. Since the ionization range of these high-energy nuclear particles is very large (~ 4 to 5 ft of heavy concrete per Bev), it is no longer true that the neutrons alone control the nucleonic cascade except in the case of exceedingly thick shields. Hence the nucleonic cascade within the shield is fed by a mixture of nucleons and pions. The pions which are created in the target decay in the drift space between the target and the beginning of the shield with a mean free path for decay of $\sim 180 \eta$ ft, where η is lab momentum in Bev/c. Once the pions enter the shield wall they still continue to decay but they are interacting with a nuclear cross section and they are being removed from the beam or degraded in energy with a mean free path of 1 to $1\frac{1}{2}$ ft in heavy concrete. Hence, the effective distance for decay of pions to muons inside a shield is contained within the first few feet. In general, therefore, the major contribution to muons comes from the generally large drift spaces between target and shielding. The muon problem can be enormously improved and in some cases solved by the appropriate placing of shielding material right near sources to attenuate the pions by nuclear interactions before they can decay. However, for various practical reasons this solution is in many cases only partly applicable. At least some qualitative consideration of the muon problem is therefore necessary.

Let us arbitrarily assume that as a result of the geometry of the drift space in which the muons decay and the properties of the pion spectrum, 10^{-3} of the beam particles incident on the beginning of the shield make muons of kinetic energy $\gtrsim 5$ Bev. These muons will be stopped almost exclusively by ionization loss. Therefore, they will have a path length through the shield of $\gtrsim 20$ ft of heavy concrete. Such a shield would represent $\gtrsim 14$ mean paths for attenuation of nuclear particles (assuming $\lambda_r \approx 1$ to $1\frac{1}{2}$ ft). Since e^{-14} is $\approx 10^{-6}$, it is obvious that, even if a few mean free paths are allowed for transition and buildup effects at the beginning of the shield, the subsequent exponential decrease in ionization due to nuclear attenuation will bring the flux of nuclear particles below the level of the muon flux in such a shield. Thereafter, with increasing shield thickness there will be only a slow decrease of ionization density with distance due to the stopping of the slower muons. At this point the muon flux is large compared to the nuclear-particle flux and this condition will persist until the thickness of shield is sufficient to stop enough muons so that once again the nuclear particles (now mostly neutrons) begin to predominate. Thereafter, depending on the exact muon spectrum, there will generally be a huge drop in ionization density in the region where the muons are stopped since one will go from the ionization density associated with the muon numbers to the nuclear particle ionization density associated with the tail of the nucleonic cascade. At the Brookhaven AGS the muon problem has dominated the ionization density in the 16-ft heavy concrete wall (see Fig. 12) placed so that the forward beams from the target enter it at nearly normal angles; originally it led to high radiation levels and undesirable experimental background. Yet, only a 10-ft heavy concrete wall which is tangential to the machine and which the forward beams from the target enter nearly tangentially has eliminated troublesome radiation or background levels. This demonstrates the importance of shield geometry where muons are a problem. One should note here that the secondary particle beams from ~ 30 -Bev protons are very markedly peaked forward in angular distribution and also that the energy spectrum is a rapidly decreasing function of angle. Therefore, long shields parallel to the machine circumference are strikingly more efficient for the same thickness than shields normal to the forward beam.

Citron, Gentner & Sittkus (38) have analyzed the shielding problem in the early phases of the CERN proton synchrotron design study. They used as a basis cosmic ray data plus various simplifying assumptions for convenience. Their analysis is of considerable interest and contains many useful points. However, it appears in the light of more recent information to be deficient in the following major respects: (a) underestimate of the muon problem; (b) use of what is very probably a substantially too long mean free path for removal (λ_r of 220 g/sq cm was used); (c) the angular distribution of the penetrating particles which appears from experiments at Brookhaven and CERN to be more peaked forward than was assumed.

SHIELDING OF ELECTRON ACCELERATORS

Because of the space limitations on this article the treatment of electron accelerators will necessarily be brief and restricted to the most important features. We shall, in particular, review the shielding problems connected with the newer types of higher-energy electron accelerators such as the Cambridge 6-Bev electron synchrotron which is under construction and the proposed 45-Bev Stanford linear accelerator. When the primary electron beam in an electron accelerator is incident on the target, it creates the well-known continuous spectrum of bremsstrahlung which extends up to the initial energy of the electrons. The typically sharp forward collimation of the higher-energy portion of the bremsstrahlung is such that at the Cambridge electron accelerator ~ 90 per cent or more will be contained within a cone about the beam direction of about 4×10^{-4} radians (0.02°) half-angle. The intensity of the X-ray beam depends on target thickness and material. Livingston points out (39) that the maximum that has been achieved in practice with synchrotrons is ~ 20 per cent electron beam power converted to gamma radiation.

Although one might offhand think the shielding problem for electron accelerators is vastly different from that for proton accelerators, it turns out there is an intimate relationship between them. This comes about because the radiation lengths and effective attenuation lengths for the electron-photon showers are much smaller than the neutron attenuation lengths for practical shielding materials including earth, concrete, iron, and other metals. Therefore, since neutrons (and other nuclear particles) are produced by gamma radiation with a cross section which can be crudely characterized by $\sim 1/137$ the nuclear cross section, it is clear that neutrons (and perhaps other nuclear particles) will dominate the shielding problem. Livingston (39) has discussed several analyses by Williams (40) and various other considerations of the shielding problem for the 6-Bev Cambridge electron accelerator which is under construction. The most probable process in the target and the shield walls of this accelerator is star formation which, in heavy nuclei, leads to the emission of neutrons, protons, pions, and other nuclear fragments. Williams has used a three-group treatment to treat the nucleonic cascade developed by the gamma radiation. These groups are:

(a) low-energy neutrons similar to cyclotron-produced neutrons which have a peak in energy at ~ 2 to 3 Mev;

(b) high-energy neutrons ranging from 40 to 300 Mev with the characteristic energy ~ 100 Mev;

(c) neutrons, protons, and pi mesons with an energy of about $\gtrsim 1$ Bev. The rate of production of low-energy neutrons is estimated to be about $2E$ neutrons per electron where E is the electron energy in Bev. The angular distribution is assumed to be isotropic. For high-energy neutrons the estimated production rate is $1.7 \times 10^{-3} E$ /electron. The angular distribution is nearly isotropic with a forward maximum such that 50 per cent are centered within a forward cone of about 25° half angle.

Group (c), the nucleonic type of radiation in the Bev region, originates primarily through photoproduction of pi mesons. The estimated intensity of this group is about an order of magnitude less than that of the high-energy neutron component. The interaction of the high-energy pions with matter produces more nucleons as well as degraded-energy pions. The final conclusion is that shielding thicknesses needed for proper attenuation of the neutrons are more than sufficient to contain the gamma-ray radiation. For the details the reader is referred to (39, 40). However, one point might be worth noting here, namely, that the accelerator is located in an underground shielded tunnel near the Harvard cyclotron.

The shielding problems and design for the Stanford two-mile linear electron accelerator which Panofsky (41) has reported will be summarized. The extensive showers generated when a 45-Bev electron interacts with matter are a combination of soft and penetrating components. Panofsky and co-workers divide the processes into the following categories: (a) production of low-energy photoneutrons in the 10- to 80-Mev region by gamma rays in the photon-electron (i.e. soft) showers, (b) production of photoneutrons of energy >80 Mev, (c) photomeson and associated nucleon production, (d) muons from pion decay, (e) penetration of the soft electron showers, (f) penetration of the nucleonic cascade, and (g) neutron air scattering.

The low-energy photoneutron production is calculated by shower theory, with due regard for the fact that the "giant resonance" cross section peaks sharply at a photon energy ~ 20 Mev. The resulting estimates are 34 neutrons/electron in concrete (or earth), 25 neutrons/electron in iron, 18 neutrons/electron in lead.

The high-energy neutrons of $E > 80$ Mev are produced by the direct photo effect and their production is calculated by an effective-deuteron model. The calculated results for the various groups of neutrons in the total neutron flux per incident electron as a function of depth in concrete are shown in Figure 13. For a primary electron beam of 2×10^{13} electrons/sec $\approx 3 \mu\text{a}$, Panofsky concludes that the shielding requirements transverse to the beam are determined primarily by the neutron flux and are ~ 22 ft of ordinary concrete, or 29 ft of earth, or 15.5 ft of ferrite concrete, or 8 ft of iron.

Even in the calculations for the "in line" forward direction shielding, the nucleonic component requires considerably more shielding than the photon-electron cascade. The estimated required thicknesses which are considerably greater than for the transverse component are 35 ft of ordinary concrete, or 45 ft of earth, or 25 ft of ferrite concrete, or 12.3 ft of iron.

The muons from the decay of photo-produced pions will, according to Panofsky's estimates, require considerably more in-line shielding than the nucleons; Fermi's theory of multiple pion production was used and a drift space of only 3 ft was assumed before the beginning of an iron absorber placed close to the target to absorb pions before they decay. Panofsky finds that if one wishes the safe side of the shield to be ~ 50 to 100 ft from the target, ~ 20 to 40 ft of iron (depending on the exact assumptions made) in

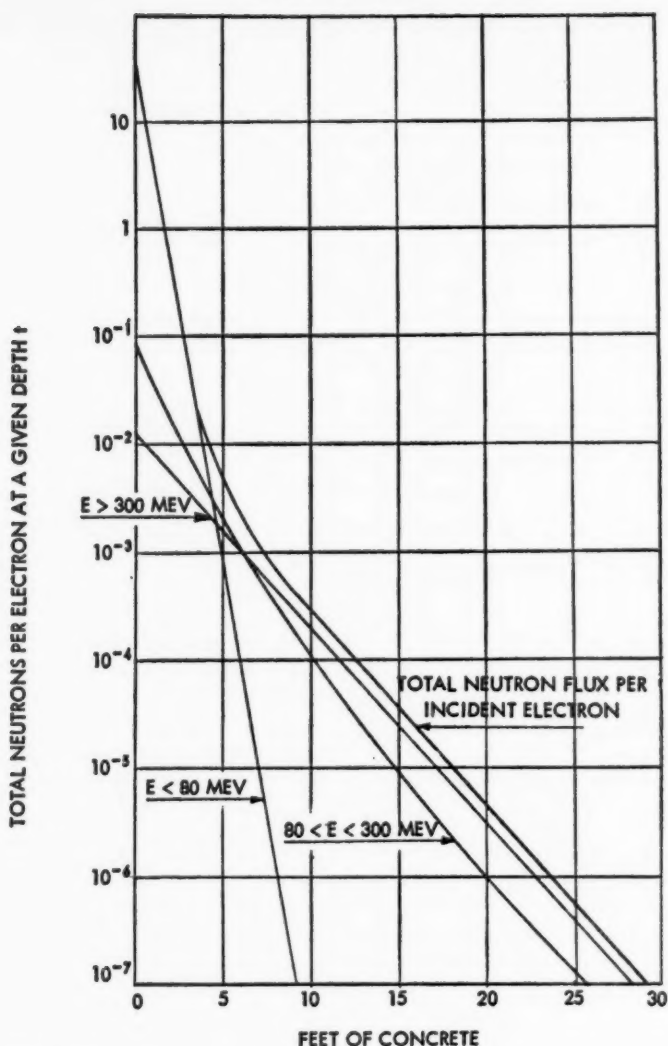


FIG. 13. Total number of neutrons per incident electron surviving at a depth (in ft) in concrete. Includes neutrons of all energies to be considered for shielding requirements transverse to the beam—from Panofsky (41).

addition to a basic 15-ft shield wall of ferrite concrete (density 3.2) are required. However, since the high-energy muons are expected to come out in a cone with a half angle of 7° to 15° depending on the energy, Panofsky has estimated that the additional iron required for the muons can probably be fabricated in a cylinder with a base diameter of 6 ft which can precede the ferrite wall.

A general summary of shielding experiences and designs in several other existing electron accelerators can be found in references (42 to 47). At this point the author would like to express his regrets for not having been able to discuss all existing accelerator shieldings. Selections obviously had to be made on the basis of space limitations of this article, general applicability of the material, and the availability of detailed information to the author.

SHIELDING MATERIALS

The specific choice of a shielding material depends on many factors including:

(a) The macroscopic inelastic cross section $\Sigma_i = N\sigma_i$ where Σ_i is in cm^{-1} , N is the number of nuclei/cu cm and σ_i is the inelastic cross section per nucleus. If σ_i is proportional to $A^{2/3}$ then $\Sigma_i \propto \rho/A^{1/3}$ (where ρ is the density and A is the atomic number) is a figure of merit for removal of high-energy neutrons in a thick shield (i.e. λ_r is of the order of $1/\Sigma_i$). The above relationship is almost literally true for neutrons of sufficiently low energy, i.e., <100 Mev over the range of nuclei where the range of transparency effects is small. In these cases the existence of additional nucleons in the nucleus, which are shadowed by the first nucleons which are struck, does not add to the shielding effectiveness since one collision is sufficient for effective removal of a primary. Of course, at high enough energies, where many collisions may be necessary to remove a primary effectively, especially in the part of the shield which is near the source side, this simple relationship does not hold. Berkeley data illustrating this type of behavior are plotted in Figure 14.

It is clear that the combination of high density and low atomic number is desirable for shields. For this reason and also because of the relatively lower cost, iron is the most popular of the metals for high-energy nucleon shielding.

(b) Radiation length.—In shielding for electron and photon sources of radiation, $\lambda_r \sim$ radiation length. Hence lead is a very popular material from this point of view. However, as one can see by comparison of Table V with Table II, almost all practical shielding materials have radiation lengths considerably less than their mean free paths for removal of high-energy neutrons; also, we have seen previously that the shield thicknesses, where large shielding attenuations are required, are determined by the neutron attenuation characteristics. It therefore is clear that the radiation length characteristic is not so important in these cases.

(c) Engineering convenience, availability, and cost.—These are the most decisive criteria in the selection of a shield material when large quantities are involved. They, in combination with requirements (a) and (b), generally speaking make concrete and earth the most generally used shielding materials.

Davis (48) has extensively discussed and summarized the properties and costs of many commonly used concretes. Three of his points that are particularly worth noting for the present purposes are:

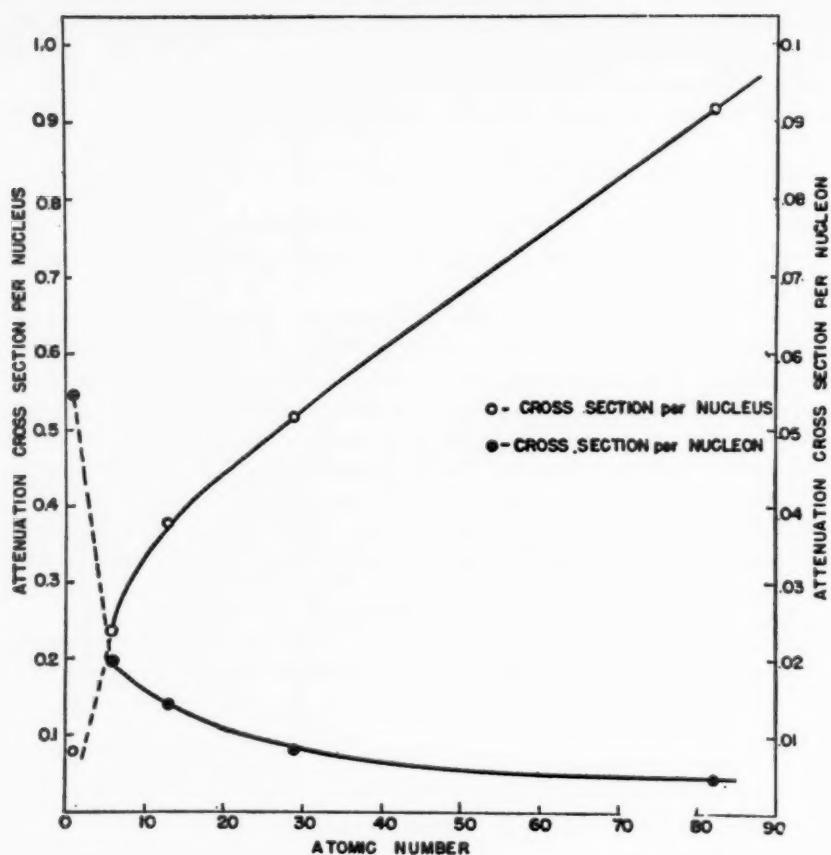


FIG. 14. Cross sections for reduction of neutron beam intensity vs. atomic number (ionization chamber detectors)—from Patterson (18).

TABLE V
RADIATION LENGTH VERSUS MATERIAL

Material	Density		Radiation length	
	g/cu cm	lb/cu ft	g/sq cm	ft
Ordinary concrete	2.3	145	25	0.36
Ferrite concrete	3.2	200	19	0.19
Ferrite loaded concrete	4.25	265	17	0.13
Earth	1.8	112	25	0.45
Iron	7.8	490	14.4	0.060
Lead	11.3	700	5.9	0.019

(i) Radiation damage limit on the lifetime.—Experiments demonstrate that concrete will have a life of at least ten years in a flux of $\sim 10^{11}$ neutrons/sq cm/sec. This corresponds to a minimum integrated flux of $\sim 3 \times 10^{10}$ neutrons/sq cm.

(ii) High-temperature damage.—High-temperature damage occurs when excessive temperature rises or gradients occur in the shield. Lane (49) has concluded that the maximum tolerable heat flux on the inside of a concrete shield is about 100 Btu/hr/sq ft or 2×10^{11} Mev/sq cm/sec. This gives about a 50°F rise in the shield.

(iii) Water content.—As previously noted, about 4 per cent by weight of water content is required in concrete shields to obtain the minimum mean free path for removal of low-energy fast neutrons. The author has already estimated that water contents ~ 1 –2 per cent are adequate for high-energy shields. Davis points out that only part of the water added initially to a concrete mix is fixed or chemically bound in the hardened cement paste, and part is evaporable. Actually, ten or twenty years may be required for all the evaporable water to diffuse through a thick shielding wall at low temperature and considerably less time when the shield is exposed to high temperatures. A complete analysis of the water content variation is presented by Davis.

Lancaster (50) has extensively analyzed the cost and other properties of various types of concrete in conjunction with a design study for the Brook-

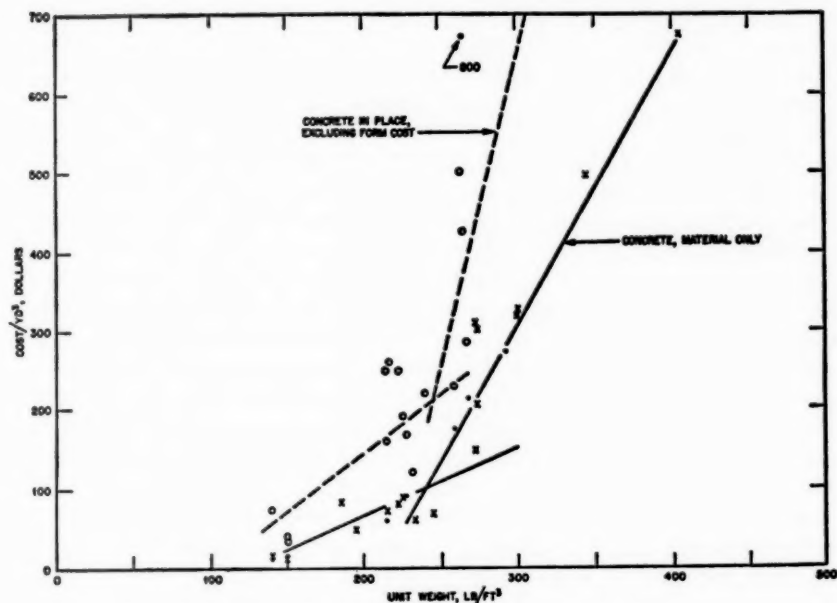


FIG. 15. Cost vs. density for high-density concrete shielding.

haven AGS. Figure 15 depicts cost in dollars/cu yd versus density in lb/cu ft based on published data. He concluded that the most advantageous density considering cost and volume was in the range of 240 to 250 lb/cu ft. This point is graphically illustrated in Figure 15. He also pointed out the competitive status of Canadian Ilmenite ore ($\rho \gtrsim 4.7$) for use in the north-eastern United States. For several high-energy accelerator shields, advantage has been taken of this. Lancaster and others have pointed out the reductions in cost that would be made possible by relaxing dimensional tolerances. Exact detailed engineering design of a shield is of course a complicated problem which cannot be treated here.

The factors involved in the choice of a location for an accelerator and also other general factors connected with shielding design have been discussed by a panel with Haworth (51) as moderator.

SHIELD BLOCK DESIGN, CRACKS, AND COLLIMATOR

Although some or even many parts of a shield can be constructed of a fixed, nonremovable wall, it is generally common in high-energy accelerator shields to have at least a considerable portion of the shield constructed of removable blocks. Exact prescriptions for designing blocks do not exist, and the individual designer usually relies on various rules of thumb based both on analysis and experience. Since concrete is the most generally used shielding material, let us consider some of the most common factors in concrete block design for high-intensity accelerators.

(a) The basic block weight is, where possible, usually chosen to equal the crane capacity available, in order to minimize assembly and de-assembly time. Of course, in many cases, considerably less than crane capacity is chosen for some or even all of the blocks if smaller sizes are required for other reasons.

(b) The block design should allow for a sufficient number of separate blocks in the wall thickness, placed so that the cracks are not in line with each other. In the author's opinion it is generally more satisfactory to limit block thickness to $\lesssim 3$ to 5 mean free paths when the more or less standard block tolerances $\sim \frac{1}{8}$ in. to $\frac{1}{4}$ in. are used. If the individual block thickness is allowed to become too large, the crack leakage can lead to serious local hot spots and can also considerably reduce the calculated attenuation of the block. It is also considered by the author to be good practice to choose the cross-sectional area of a block such that the circumference (in a plane normal to the thickness dimension) multiplied by the average crack dimension (i.e. the crack area) is at most a few per cent of the block cross-sectional area. Then if the cracks are staggered so that they are not in line by at least a few inches, a reasonable block design for general purposes will in the author's opinion be obtained. Most of us are aware that beam channels through the shielding will lead to high-intensity radiation levels in line with the beam direction. What is perhaps not so generally realized is that in a high-intensity accelerator, beam channels can also lead to high radiation levels in the gen-

eral area surrounding the accelerator which is not in line with the beams. The mechanism for this spreading of the radiation is both via air scattering (i.e. sky shine) and scattering from other materials such as walls and roofs. One technique which can reduce these effects when only narrow momentum intervals of charged beam are required externally is to analyze the beams magnetically inside of the shield so that a straight-through channel looking at the target is avoided. Double magnetic deflection will help even further. However, even with analyzed charged beams, if the beam intensity is high enough, the whole beam area may have to be treated as a new source of radiation and enclosed with additional shielding. Techniques similar to those which were used to estimate sky shine effects can also be used for estimating the scattered radiation from the beam channels.

LITERATURE CITED

1. Moyer, B. J., *Ann. Rev. Nuclear Sci.*, **8**, 327 (1958)
2. Rossi, H. H., *Conf. Shielding High-Energy Accelerators, Oak Ridge, TID7545*, 150 (1957)
3. *National Committee on Radiation Protection Recommendations* (AEC in the Federal Register, May 2, 1959)
4. *Staff Report of the Federal Radiation Council, Rept. No. 1* (Background material for the development of Radiation Protection Standards, May 13, 1960)
5. Bernardini, G., Booth, E. T., and Lindenbaum, S. J., *Phys. Rev.*, **83**, 669 (1951); *Phys. Rev.*, **88**, 1017 (1952)
6. Morrison, G. C., Muirhead, H., and Rosser, W. G. V., *Phil. Mag.*, **44**, 1326 (1953)
7. Goldberger, M. L., *Phys. Rev.*, **74**, 1269 (1948)
8. Miller, J. M., and Hudis, J., *Ann. Rev. Nuclear Sci.*, **9**, 159 (1961)
9. Lindenbaum, S. J., *Ann. Rev. Nuclear Sci.*, **7**, 317 (1957)
10. Metropolis, N., Bivins, R., Storm, M., Miller, J. M., Friedlander, G., and Turkevich, A., *Phys. Rev.*, **110**, 185, 204 (1958)
11. Voss, R. G. P., and Wilson, R., *Proc. Roy. Soc. (London)*, **A**, **236**, 41 (1956)
12. Ball, W. P., *Univ. Calif., Radiation Lab., Rept. UCRL-1938* (1952)
13. Coor, T., Hill, D. A., Hornyak, W., Smith, L., and Snow, G., *Phys. Rev.*, **98**, 1369 (1955)
14. Chen, F. F., Leavitt, C. P., and Shapiro, A., *Phys. Rev.*, **99**, 857 (1955)
5. MacGregor, M. H., Ball, W. P., and Booth, R., *Phys. Rev.*, **111**, 1155 (1958)
16. Blizzard, E. P., *Ann. Rev. Nuclear Sci.*, **5**, 73 (1955)
17. Moyer, B. J., Hildebrand, R., Parmley, T. J., and York, H., *U. S. Atomic Energy Comm. Document, AECD-2149* (1947)
18. Patterson, H. W., *Conf. Shielding High-Energy Accelerators, Oak Ridge, TID7545*, 3 (1957)
19. Beebe, L., Cumming, J., Moore, W., and Swartz, C., *Shielding Measurements* (Cosmotron Internal Rept., Brookhaven Natl. Lab., Upton, N. Y., 10/1/56)
20. Lindenbaum, S. J., *Conf. Shielding High-Energy Accelerators, Oak Ridge, TID7545*, 28 (1957); (Internal Brookhaven reports and private communications)
21. Moyer, B. J., *Conf. Shielding High-Energy Accelerators, Oak Ridge, TID7545*, 96 (1957)
22. Moyer, B. J. (Private communications)
23. Tsao, C. J., Curtis, R. B., Harrison, B. K., and O'Neill, G. K., *Monte Carlo Calculations of the Shielding of the Princeton-Pennsylvania 3 Bev Proton Synchrotron* (To be published); (Private communications)
24. O'Neill, G. K., *Conf. Shielding High-Energy Accelerators, Oak Ridge, TID7545*, 87 (1957)
25. Dobrotin, N. A., and Slovatsinsky, S. A., *Proc. Ann. Rochester Internat. Conf. High-Energy Phys.*, **819** (1960)
26. Lindenbaum, S. J., *Conf. Shielding High-Energy Accelerators, Oak Ridge, TID7545*, 101 (1957)
27. Case, K. M., De Hoffman, F., and Placzek, G., *Introduction to the Theory of Neutron Diffusion*, **I**

- (Los Alamos Sci. Lab., Los Alamos, N. M., 1953)
28. Moyer, B. J., *Conf. Shielding High-Energy Accelerators, Oak Ridge, TID7545*, 38 (1951)
 29. Marshall, J., *Conf. Shielding High-Energy Accelerators, Oak Ridge, TID7545*, 14 (1957)
 30. Goodell, W. F., Jr., *Conf. Shielding High-Energy Accelerators, Oak Ridge, TID7545*, 20 (1957)
 31. Preston, W. M., *Conf. Shielding High-Energy Accelerators, Oak Ridge, TID7545*, 25 (1957)
 32. Barnes, S. W., *Conf. Shielding High-Energy Accelerators, Oak Ridge, TID7545*, 27 (1957)
 33. Hinman, C. W., *Conf. Shielding High-Energy Accelerators, Oak Ridge, TID7545*, 8 (1957)
 34. Karelitz, M., *Conf. Shielding High-Energy Accelerators, Oak Ridge, TID7545*, 197 (1957)
 35. White, M. G., *Conf. Shielding High-Energy Accelerators, Oak Ridge, TID7545*, 187 (1957)
 36. Crosbie, E., *Conf. Shielding High-Energy Accelerators, Oak Ridge, TID7545*, 167 (1957)
 37. Green, G. K., *Conf. Shielding High-Energy Accelerators, Oak Ridge, TID7545*, 193 (1957)
 38. Citron, A., Gentner, W., and Sittkus, A., *CERN PS/WG1* (1952) and *CERN PS/WG3* (1953) [European Council for Nuclear Research (CERN), Geneva, Switzerland]
 39. Livingston, M. S. (Presented by R. W. Williams), *Conf. Shielding High-Energy Accelerators, Oak Ridge, TID7545*, 171 (1957)
 40. Williams, R. W., *Cambridge Accelerator Project Documents, CAP-6* (June 23, 1955); *CAP-23* (Mar. 20, 1956); *CEA-10* (Aug. 31, 1956) (Cambridge, Engl.)
 41. Panofsky, W. K. H., *Conf. Shielding High-Energy Accelerators, Oak Ridge, TID7545*, 199 (1957)
 42. Walker, R. L., *Conf. Shielding High-Energy Accelerators, Oak Ridge, TID7545*, 45 (1957)
 43. Livingston, M. S., *Conf. Shielding High-Energy Accelerators, Oak Ridge, TID7545*, 49 (1957)
 44. Leiss, J. E., *Conf. Shielding High-Energy Accelerators, Oak Ridge, TID7545*, 50 (1957)
 45. Palfrey, T. R., Jr., *Conf. Shielding High-Energy Accelerators, Oak Ridge, TID7545*, 53 (1957)
 46. Littauer, R., *Conf. Shielding High-Energy Accelerators, Oak Ridge, TID7545*, 54 (1957)
 47. Panofsky, W. K. H., *Conf. Shielding High-Energy Accelerators, Oak Ridge, TID7545*, 55 (1957)
 48. Davis, H. S., *Conf. Shielding High-Energy Accelerators, Oak Ridge, TID7545*, 67 (1957)
 49. Lane, J. A., *Nucleonics*, 13, No. 6, 56-58 (1955)
 50. Lancaster, T. H., *Conf. Shielding High-Energy Accelerators, Oak Ridge, TID7545*, 212 (1957)
 51. Haworth, L. J. (Moderator—Panel Discussion), *Conf. Shielding High-Energy Accelerators, Oak Ridge, TID7545*, 58 (1957)

NEUTRON CAPTURE GAMMA RAYS¹

By G. A. BARTHOLOMEW

Neutron Physics Branch, Chalk River Project, Atomic Energy of Canada Limited

I. INTRODUCTION

Studies of neutron capture γ rays have contributed to our knowledge of neutron separation energies, γ -ray transition probabilities, decay schemes, and properties of nuclear energy levels and have shed light on a number of other aspects of the broad problem of nuclear structure. However, for various technical reasons certain areas of the field have received much more attention than others and our knowledge of the γ radiations is still far from complete.

A glimpse of the present development of these studies and some insight into the technical problems may be obtained from a consideration of the use that experimenters in the field have made of various techniques of γ -ray spectroscopy. As we shall see below, various types of precision spectrometer have been employed and a large amount of data concerning energies and intensities has been accumulated. On the other hand, only moderate use has been made of techniques for measuring γ - γ coincidences and angular correlations, γ -ray circular polarization, and internal conversion coefficients. Little or no use has been made so far of methods for detecting directional polarization correlations, electron pair correlations, delayed coincidences, resonance fluorescence, or neutron-gamma-ray angular distributions. In this review I shall attempt to account for this pattern of development, to give a résumé of the experimental results obtained with each of the various techniques and, wherever possible, to indicate the types of experiment which will probably receive concentrated attention in the near future.

In surveying the results of neutron capture γ -ray measurements it is necessary to recognize two categories: (a) General nuclear data such as neutron cross sections, reaction Q values, and spins and parities of energy levels. The present development of the art of making such measurements will be outlined, but no attempt will be made to relate such data to current theories of nuclear structure. (b) Information on the spectral distributions of capture γ rays, transition probabilities of primary neutron capture γ rays, and the mechanism of neutron capture. These data are more specific to the neutron-gamma (n, γ) process itself and concern matters about which studies in other fields may have had less to say. In these areas experimental results will be compared with theory.

The field of neutron capture γ rays naturally divides into two distinct areas depending on whether the neutrons have thermal (≤ 0.025 eV) or epithermal energies. In the former area most of the information obtained pertains to the properties of the bound levels of the nucleus and to the properties

¹ The survey of literature pertaining to this review was concluded in February 1961.

of the "capturing state" which is formed at the neutron separation energy; in the latter most of the information so far obtained concerns the properties of the unbound levels. These areas will be discussed in Sections II and III, respectively. The theory and experimental results directly concerned with the nature of the neutron capture process itself will be discussed in Section IV.

For earlier surveys of the field the reader is referred to reviews by Kinsey (1, 2) and Bartholomew (3) and to the Geneva paper by Groshev *et al.* (4). Compilations of neutron capture γ rays have been published by Mittelman & Liedtke (5), Bartholomew & Higgs (6), and Groshev and co-workers (7). These publications together contain exhaustive bibliographies of work published before June 1958 approximately.

II. THERMAL-NEUTRON CAPTURE

A. SUMMARY OF TECHNIQUES

Thermal-neutron capture γ rays are usually studied in one of two fundamentally different experimental arrangements. In the first arrangement the target is placed in a region of high thermal-neutron flux and the capture γ rays pass as a beam through a hole in a shielding wall to the experimental apparatus. In the second, the element under study is bombarded with a beam of neutrons, and the γ rays emitted are detected in spectrometers placed near the target. Although the thermal neutrons are usually provided by a reactor, some experiments have used suitably moderated neutrons from a neutron source (8, 9) or an accelerator (10).

The γ -ray beam method is ideally suited for study of energies and intensities of capture γ rays since sources of extreme intensity can be produced. The lateral dimension of the source is limited only by the size of the experimental hole in the pile shield, and the thickness of the source is limited by the self-absorption of γ rays in the sample material. Such large sources permit the use of spectrometers of very high resolution and high precision, and consequently energy and intensity measurements have received much attention in past investigations in this field.

The neutron beam method is essential for experiments in which the source of capture γ rays is required to be situated very near the detector. Such experiments include internal conversion measurements and coincidence and angular correlation measurements between successive γ rays.

An excellent review of the various techniques for studying neutron capture γ rays has been given by Bäckström (11).

1. *Energy and intensity measurements.*—Many techniques have been used for studying energies and intensities of capture γ rays by the γ -ray beam method. Several methods with relatively poor resolution, among them absorption techniques (12), emulsions (13), and ion chambers (14), have been useful for determining the over-all spectral distributions averaged over many γ rays and for obtaining rough estimates of the upper energy limit of the spectrum.

Methods involving various arrangements of scintillation spectrometers

are particularly suited for applications where high counting efficiency is required, e.g., where low neutron fluxes are available or where the capture cross section is very low. Single-crystal NaI scintillation spectrometers have been used by various workers (9, 10, 15 to 21) for detection of low-energy capture γ rays. Because of the low resolution (~ 5 per cent) and the inherently complicated line shape, it is difficult to resolve any but the more intense γ rays by this technique. A two-crystal Compton spectrometer was used originally by Braid (22) and later by others (8, 23) to resolve low-energy γ rays in some of the light elements. For energies above about 3 Mev the inability to discriminate between Compton and pair events, together with a decreased counting efficiency, limits the usefulness of this method. A three-crystal pair spectrometer has been employed by Segel (24) and Treado & Chagnon (25) to resolve γ rays at the high-energy end of the spectrum. The resolution of this instrument is typically 4 per cent at 6 Mev. It is particularly useful when combined with a single-crystal spectrometer in a coincidence arrangement for detecting cascade transitions (see Sect. IIA3). Single-crystal scintillation spectrometers with anticoincidence mantles have been used by Monahan *et al.* (26) and by Draper & Bostrom (27). Resolutions of about 9 per cent at 0.662 Mev and 3 per cent at 6 Mev have been obtained with peak efficiencies comparable to that of a single-crystal NaI spectrometer and with at least a twofold reduction in the low-energy tail.

The best resolution and precision have been obtained with magnetic spectrometers and crystal diffraction spectrometers of various kinds. For full details of these instruments the reader is referred to the original papers and to a review by Bartholomew, Knowles & Lee Whiting (28). Only the salient features of their performance will be outlined here.

The 180° magnetic pair spectrometer, originally devised by Walker *et al.* (29), has been used extensively for (n, γ) studies by the Chalk River group (6), by the Zurich group (30, 31), and by Burgov & Danilian (32). The transmission of this instrument increases rapidly with energy, changing by a factor of 100 between 2.75 and 10 Mev; at 5 Mev and ~ 1 per cent resolution the efficiency is about 3×10^{-8} counts/ γ -ray incident on the radiator (33, 34). Greater efficiencies can be obtained by employing several detectors on each side of the radiator (31, 32). Although, in principle, this instrument can function at energies as low as 1.02 Mev, the rapidly decreasing efficiency has made it ineffective below about 2.7 Mev. An example of the spectra obtained with this instrument at 1 per cent resolution is shown in Figure 1b.

A thin-lens β spectrometer has been used by Motz (35) as a Compton spectrometer for detection of γ rays from Cd^{114} . Background radiation was suppressed by recording coincidences between the Compton electron and the scattered photon detected in small NaI crystals placed near the radiator. The resolution was about 5 per cent.

A flat Compton spectrometer first used for (n, γ) work by Groshev *et al.* (36, 37) has an energy range which covers essentially the entire range of neutron capture γ rays from about 0.1 to 12 Mev (see Fig. 5 for examples of

the spectra obtained). The early instruments of this type had a resolution of about 2.3 per cent from 0.3 to 12 Mev and rather poorer resolution at lower energies. Their efficiencies were about 7×10^{-7} counts per incident photon at 5 Mev. A later version also built by Groshev *et al.* (38) employs two magnets, the first serving to focus the forward-scattered Compton electron beam onto the entrance slit of the second which is an analysing magnet of $\pi\sqrt{2}$ type. This instrument has a resolution of 0.3 per cent above 2 Mev and an efficiency of about 7×10^{-8} counts per incident photon at 5 Mev. A sample spectrum is shown in Figure 1c. To reduce background effects, the Compton spectrometers devised by Groshev *et al.* use two thin-walled counters placed one behind each slit and connected in coincidence.

A similar Compton instrument employing a single $\pi\sqrt{2}$ focusing magnet has been built by Motz & Carter (39). In this instrument, sodium iodide crystals are arranged to detect the back-scattered γ quanta, and a count is registered only when the electron and γ -ray detectors count in coincidence. A multiple counting arrangement is used in which coincidences between either of two γ -ray detectors and any one of four electron detectors may be recorded. In typical experiments this instrument has been operated at a resolution of about 0.5 per cent. An example of the spectra obtained is shown in Figure 1d.

Crystal diffraction spectrometers of three types have been used for neutron capture studies. Each has unique features which suit it to a certain type of measurement.

The Argonne bent-crystal spectrometer (41) is a line-source transmission instrument which makes use of a thin, edge-on, target placed in an experimental hole of the reactor. Resolutions up to 0.3 per cent at 300 kev have been achieved. This instrument is ideally suited for experiments involving small quantities of source material, e.g. for separated isotopes. However, its efficiency decreases rapidly with energy and it does not appear to have been used above about 2 Mev.

The Cauchois spectrometer is optically a back-to-front line-source transmission spectrometer in which γ rays are detected by a photographic emulsion placed to coincide with the focusing circle. An instrument with a 2-m radius of curvature has been used by Chupp *et al.* (42) for measurement of γ -ray energies up to 2.23 Mev, and an instrument with a 6-m radius has been built by Kazi *et al.* (43). The 2-m instrument has an energy resolution of 0.1 per cent at 60 kev. Attractive features of this instrument are its mechanical simplicity and the ability to record large portions of the spectrum at the same time. In contrast to the line-source transmission instrument, the Cauchois spectrometer requires large sources for efficient operation.

The flat-crystal diffraction spectrometer devised by Knowles (44) may be used with a single diffracting crystal or with two diffracting crystals. In the single-crystal spectrometer a Soller slit defines the resolution of the instrument. This arrangement is useful where high transmission is required and relatively low resolution can be tolerated. In the double-crystal arrange-

ment the γ -ray collimating function is supplied by the first diffracting crystal, the Soller slit serving only as a baffle to eliminate the direct beam. The resolution of the instrument is then determined by the mosaic width of the diffracting crystals. Since the crystals are not distorted by a bending process, the mosaic width is preserved at its natural value, about ten times smaller than that achieved in the bent-crystal spectrometer. Many different crystals with different atomic spacings, mosaic resolutions, absorption properties, and reflecting powers can be easily introduced as desired. This instrument has been used over the energy range from 65 keV to 5 MeV, and further extension of range is quite feasible (44). The energy resolution used in most experiments with the double-crystal spectrometer is ~ 0.5 per cent over a wide energy range, 0.5 to 5 MeV; below 2 MeV it has been used occasionally with a resolution of 0.2 per cent. This instrument is clearly useful for studying a wide energy range but requires high intensity sources of large area. An example of the spectrum obtained with this instrument is shown in Figure 1a.

Only one experiment has been reported in which photoelectric external conversion has been applied to the study of neutron capture γ rays [Motz (35)]. In this work a thin-lens spectrometer with a resolution of 2 to 5 per cent was used to measure γ rays below 4 MeV in Cd^{114} . Background from the Compton effect and other sources was suppressed by counting only those electrons which were in coincidence with K X-rays from the converter.

2. *Internal conversion measurements.*—Internal conversion electrons following neutron capture may be studied if the element of interest is placed at the source position of a β spectrometer and is bombarded by a beam of thermal neutrons. Experiments of this type have been carried out by Hibdon & Muehlhause (45) and Church & Goldhaber (46) using 180° β -ray spectrographs. Thin-lens spectrometers have been used by Bell & Elliott (47) for measuring the $\text{H}^1(n, \gamma)\text{H}^2$ 2.23-MeV γ ray and by Motz (35) for the study of the Cd^{114} spectrum. Groshev, Demidov & Naidenov (48) adapted the flat Compton spectrometer described above, for detecting conversion lines from Cd, Sm, Dy, Gd, and Hg. They report a resolution of 1.6 per cent at 150 keV, but much better results appear to have been achieved with a later instrument (49).

The requirement of a very thin source (to avoid electron scattering) conflicts with the need for obtaining a high counting rate. For this reason the study of internal conversion electrons using an external neutron beam seems to be limited to elements with capture cross section greater than about 100 b. A promising and novel approach has been described by Maier-Leibnitz (50) in which the target is placed near the core of a reactor and the conversion electrons are allowed to pass through a magnetically shielded tube to a double focusing spectrometer placed outside the shield. The narrow acceptance angle of the arrangement is compensated by the high neutron flux and a relatively large source area.

Several of the above authors (45, 48, 49) were able to determine K/L ratios or conversion coefficients for some of the radiations detected and were

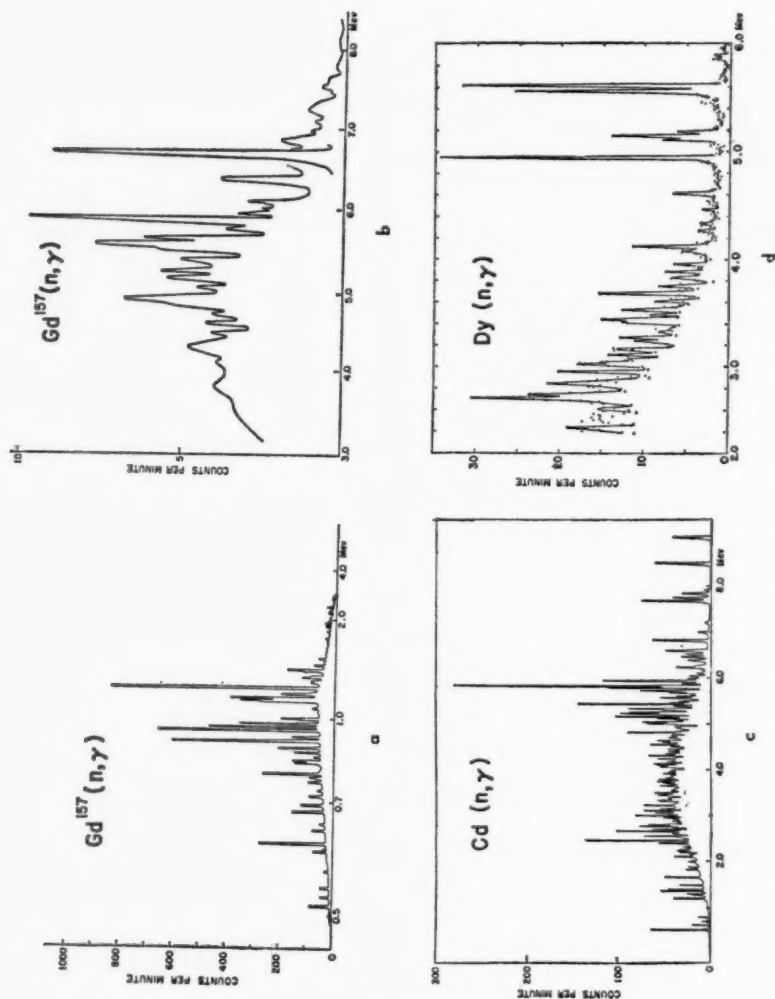


FIG. 1. Heavy element capture γ -ray spectra as observed with various high resolution spectrometers. (a) Low-energy spectrum from $Gd^{157}(n, \gamma)$ obtained with a flat-crystal diffraction spectrometer, resolution $\sim 0.5\%$ [Knowles *et al.* (40)]. (b) High-energy spectrum from $Gd^{157}(n, \gamma)$ obtained with a pair spectrometer, resolution $\sim 1\%$ (40). (c) Spectrum from $Cd(n, \gamma)$ obtained with a Compton spectrometer, resolution $\sim 0.3\%$ [Groshev (49)]. (d) Partial spectrum from $Dy(n, \gamma)$ obtained with a Compton spectrometer, resolution $\sim 0.5\%$ [Motz & Carter (39)].

therefore able to make multipolarity assignments. No experiments have yet been performed in which internal pair conversion was used for the study of neutron capture γ rays. However, a spectrometer with good resolution in which the angular correlation of internal pair electrons may be measured seems feasible (51) and may find a use in such studies.

3. *Coincidence and angular correlation measurements.*—Various experiments to study coincidences and angular correlations between cascading pairs of neutron capture γ rays have been carried out (20, 24, 53, 54, 55). In these experiments the target to be bombarded by a neutron beam is placed between a pair of NaI crystal detectors. In the usual arrangement the detectors are connected to a fast-slow coincidence circuit (56), and the spectrum of pulses in coincidence with pulses falling in a selected energy channel is recorded on a multichannel pulse-height analyser. A few coincidence measurements have been made for γ rays following capture of epithermal neutrons (57); these will be discussed in Section III.

To resolve complex spectra by coincidence techniques it is desirable to use methods which provide a better resolution than the single-NaI-crystal spectrometer without seriously reducing the over-all efficiency. One method successfully employed by Segel (24) is to use a three-crystal pair spectrometer for detection of high-energy γ rays and a single NaI crystal for low-energy γ rays. Although the efficiency of the pair spectrometer (excluding the solid angle subtended at the source) is less than 1 per cent of that of a single NaI crystal (58), it is possible to compensate for this loss by moving the detectors close to the target and thus increasing the solid angle. Cascade transitions with intensities as low as 1 per cent per capture have been studied, and much information concerning the decay schemes of Hg^{200} (24), Cl^{36} (59), and Fe^{67} (60) has been acquired with this equipment. However, the very large solid angles and the restricted freedom of motion of the detectors caused by placing the detectors near the target exclude the use of the instrument for angular correlation measurements.

A second technique that seems ideally suited for the study of neutron capture γ rays in cascade is the sum coincidence method of Hoogenboom (61). This method uses a coincidence circuit which demands that, in order to be recorded, coincidences between the two scintillators must be produced by pulses whose sum is approximately equal to the total energy available in the cascade. The method, therefore, automatically ensures that only one peak, that is the full energy peak, of the NaI response curve corresponding to each γ ray will be recorded. The application of this technique to (n, γ) experiments has been described by Schwäger (62) and by Draper & Fleischer (63), and excellent results have been obtained by these workers for vanadium (64) and chlorine (65), by Vervier (66, 67) for samarium and mercury, and by Burmistrov (68) for chlorine and sulphur. The method can be applied directly to the study of angular correlations, although much longer counting times are required with this method than with the ordinary technique to accumulate the same statistics for a particular pair of γ rays. This disadvan-

tage is offset because the angular correlations of all two-step cascades from the capture state may be measured at the same time.

Only one experiment has been reported in which delayed coincidence techniques have been used to determine the lifetimes of excited states fed by neutron capture γ rays [D'Angelo (69)]. The levels at 26, 109, and 210 keV in Mn^{56} were found to have lifetimes of 10.7^{+2}_{-3} , 4.9 ± 0.6 , and ≤ 0.5 μsec , respectively. This technique will undoubtedly be exploited to a much greater extent.

More complicated coincidence experiments than those already considered, such as triple coincidence and correlation measurements (all three radiations observed) and linear polarization directional correlations, have lower over-all efficiencies than the simple NaI-crystal arrangements. Such techniques are feasible at present only for very strong cascades, and no experiments of this sort have so far been reported.

4. *Circular polarization measurements.*—The possibility of detecting circular polarization of γ rays after capture of polarized neutrons and of using such measurements for spin determinations was discussed originally by Halpern (70) and by Biedenharn, Rose & Arfken (71). The theoretical expressions relevant to an experimental investigation of such effects have been summarized by Trumpy (53, 72) whose notation will be followed here. The emission probability for a γ ray following capture of a polarized thermal neutron is:

$$W = 1 + pP_n R \cos \theta \quad 1.$$

where p has the value ± 1 depending on whether the radiation is left or right circularly polarized; θ is the angle between the γ ray and the neutron-spin direction; P_n is the neutron polarization; and R is a coefficient depending on the spins of the target nucleus J_i , the compound nucleus J_c , and the state formed by γ emission J_f , and on the multipole order of the γ ray L . For the case of pure multipole radiation, R is given by:

$$R = \frac{2(J_c - J_i)}{2J_i + 1} \frac{L(L+1) + J_c(J_c+1) - J_f(J_f+1)}{L(L+1)} \quad 2.$$

A more complete expression for R which includes multipole mixing is given by Trumpy (53). For all practical cases the limits of R are $1 \geq R \geq -\frac{1}{2}$.

The circular polarization of the γ ray is defined as the ratio of the difference to the sum of the intensities for left and right circular polarization. From Equation 1 we obtain:

$$P_\gamma = \frac{W^+ - W^-}{W^+ + W^-} = P_n R \cos \theta \quad 3.$$

The circular polarization of neutron capture γ rays was first detected by Trumpy (72). In this experiment the neutron beam was polarized by passing it through magnetized iron, giving $P_n = 0.19$. In a similar experiment Vervier

(73) used a neutron beam polarized to 90 per cent by Bragg diffraction from a magnetized CoFe crystal. In both experiments the degree of circular polarization was determined by measuring the transmission of the γ rays through a magnetized iron analyser in a direction such that $\cos \theta = \pm 1$. The intensities of left and right circularly polarized radiation were obtained by making measurements with the magnetic field of the analyser parallel and antiparallel to the neutron polarization. Different methods of reversing the relative directions of these vectors were used in the two experiments. Trumpy used a fixed neutron orientation and switched the field direction in the analysing magnet. In this method two analysing magnets mounted on opposite sides of the target permitted simultaneous measurement of the transmission for two different polarizations at the same time. Vervier used one analysing magnet which was maintained with fixed polarity; he reversed the relative direction of the neutron polarization and magnetic field by flipping the neutron spin. The latter operation was accomplished by passing the neutrons through a suitable radio frequency field. Trumpy's method has the advantage that the neutron polarization remains constant during the experiment, while in Vervier's method it is necessary to monitor the degree of polarization of the neutrons for both the spin-up and spin-down beams. On the other hand, Vervier's method avoids troublesome variations in the photomultiplier response caused by changing the magnetic field.

The asymmetry observed in an experiment in which a monoenergetic γ ray is detected is:

$$Q = \frac{N_i' - N_i''}{N_i' + N_i''} \quad 4.$$

where N_i' and N_i'' are the total counting rates of γ rays reaching the detector (both as transmitted and scattered radiation) under conditions in which the magnetic field is parallel and antiparallel to the neutron polarization respectively. The asymmetry Q is related to P_n , R , and to P_a , the polarization sensitivity of the detector, by:

$$Q = P_n P_a R \beta \gamma \quad 5.$$

where β is a correction factor for depolarization of the neutrons scattered in the target and γ measures the fraction of the total γ rays detected which are transmitted without scattering through the analysing magnet. Equation 5 is used to determine the constant R which, with the aid of Equation 2, may be used to obtain information concerning the spins of the levels or the multipolarity of the γ ray.

Because of the small values of P_n (19 per cent) and of P_a (1.96 per cent), very small asymmetries (in the neighborhood of 10^{-4}) were observed in Trumpy's experiments. These small values of Q , together with a relatively low neutron beam intensity, necessitated counting times of the order of weeks or months. The superior neutron polarizations and higher beam intensities in Vervier's experiments permitted counting times of the order of hours or days to be used.

The spectrum of γ rays from titanium shown in Figure 2 is a good example of the results obtained in Vervier's circular polarization measurements. The upper curve shows the sum spectrum $N_i' + N_i''$, and the lower curve the difference spectrum $N_i' - N_i''$. The curves clearly show that the strong γ rays at 6.77 and 6.41 Mev have asymmetries of opposite sign. This result is interpreted as showing conclusively that the spins of the 1.39- and 1.75-Mev levels in Ti^{49} are $\frac{3}{2}$ and $\frac{1}{2}$ respectively (73).

Circular polarization experiments have been carried out successfully for only a limited number of well-chosen nuclei, such as Ti^{49} , where one or two intense well-isolated γ rays are present at the high-energy limit of the spectrum. The study of γ rays of lower energy is extremely difficult not only because of the inherently poor line width of the total absorption peak obtained with NaI detectors, but also because γ rays of lower energy are always superimposed on the "tails" of γ rays of higher energy. As an additional complication, the tail corresponding to a particular γ ray does not show as large an asymmetry as the total absorption peak since quanta which have been Compton-scattered in the analysing magnet contribute to the tail and such scattered radiation exhibits an asymmetry opposite to that of the transmitted quanta [Vervier (73)].

Grechukhin (74) has shown that the circular polarization averaged over the cascade spectrum of γ rays following capture of polarized thermal neutrons can, in principle, be used to discriminate between the two possible spins of the capturing state $J_c = J_i \pm \frac{1}{2}$, and also can give the magnitude of the parameter σ in the expression (75) for the spin dependence of the level density:

$$\rho(J) = \text{const } (2J + 1) e^{-(J+1/2)^2 / (2\sigma^2)} \quad 6.$$

The average circular polarization, assuming dipole radiation only, is given by:

$$\bar{P}_{J_c}(\theta) \sim A \xi_1(J_c) \cos \theta \quad 7.$$

where A is a constant which depends on σ , on J_c , and on the details of the cascade, θ is the angle between the γ quantum and the neutron polarization direction, and $\xi_1(J_c)$ is a function of J_i , J_c , and P_n .

Values of $\bar{P}_{J_c}(\theta)$ calculated with the parameters $P_n = 1$, $\theta = 0^\circ$, $J_c = 3$ or 4, and $\sigma \approx 3$ approach 10 per cent in absolute value. The determination of the sign of \bar{P}_{J_c} is sufficient to distinguish between the two alternative values of J_c . Attempts to detect these effects have not yet been reported. Such experiments would perhaps be complicated by multipole mixing, which was not taken into account in the theory. Furthermore, if circular polarization analysers of the type used by Trumpy and Vervier were used, the observed asymmetry would be at most 0.2 per cent and probably rather less than this since (unlike the situation in experiments involving only the γ ray of highest energy) there is no obvious way of discriminating against degraded radiation scattered into the detector by the analyser.

Another experiment that should perhaps be mentioned here is the at-

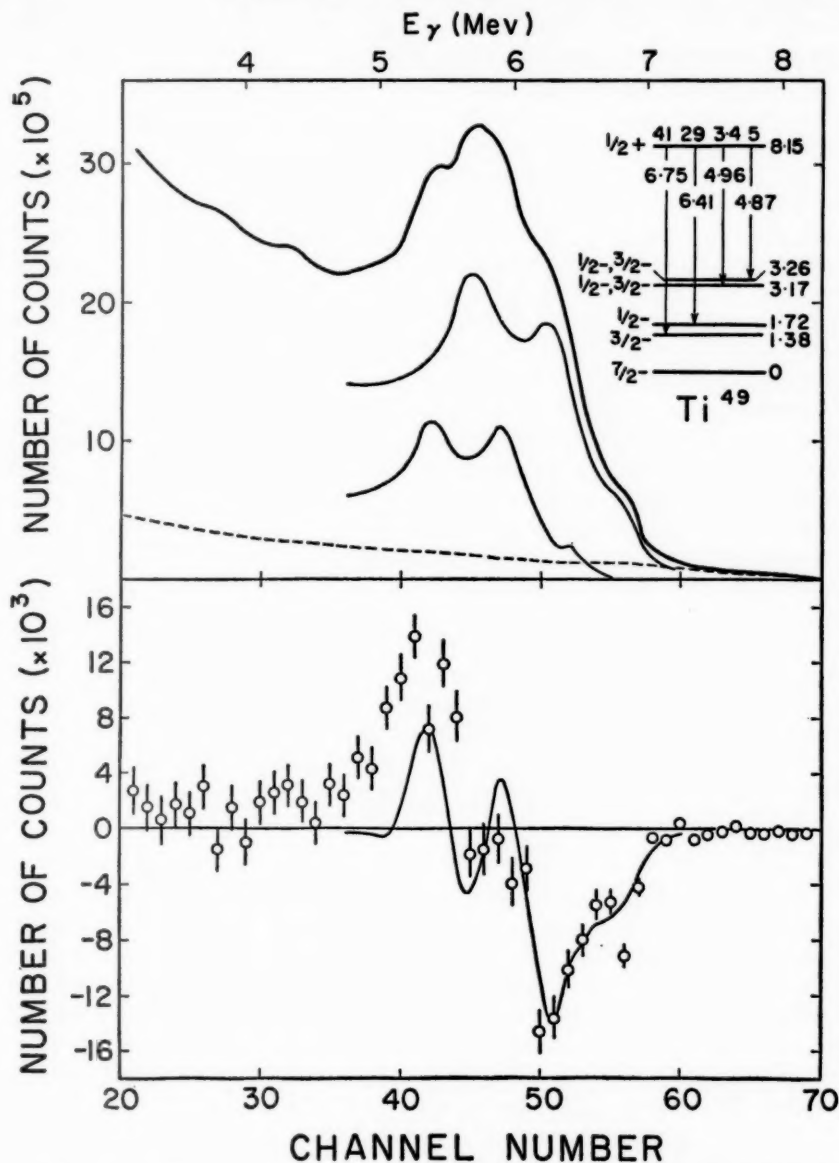


FIG. 2. Measurements of the circular polarization of the 6.75- and 6.41-Mev γ rays following capture of polarized neutrons in Ti^{48} [Vervier (73)]. The upper diagram shows the sum spectrum $N'_1 + N''_1$ obtained by adding the data recorded with the two orientations of neutron spin. The separate γ -ray lines and the background (dotted) are also shown. The lower diagram shows the difference spectrum $N'_1 - N''_1$. The full curve is the theoretical spectrum calculated with the assumption that the spin of 1.38-Mev level is $3/2$ and that of the 1.72-Mev level $1/2$.

tempt by Haas, Leipuner & Adair (76) to measure the magnitude of the parity nonconserving part of nuclear forces using γ rays following the capture of polarized neutrons by Cd^{113} . Since this investigation lies rather outside the field of interest for neutron capture γ -ray spectroscopy, the reader is referred to the original article for details.

5. *Other techniques.*—Among other techniques that have only begun to be exploited in the study of neutron capture γ rays, resonance fluorescence and neutron capture by oriented nuclei should be mentioned. The latter is discussed by Roberts elsewhere in this review (77); I shall restrict myself to a few remarks concerning the former.

The central problem in resonance absorption of γ rays is to devise a method of compensating for the loss of γ -ray energy caused by recoil of both the emitting and absorbing nuclei. Various methods used to restore this energy are outlined in a recent review by Devons (78). Two approaches may be applicable to the study of resonance fluorescence in levels of nuclei formed in the (n, γ) process: (a) the use of the decay γ ray from the same level with recoil motion supplied by a previous γ ray or (b) the use of an external source of γ radiation whose energy spans the level energy. One experiment of the latter type recently performed by Reibel & Mann (79) is of special interest in neutron capture since it casts some light on the properties of levels in the neighborhood of the neutron separation energy. The 6.92- and 7.12-Mev γ rays obtained from the reaction $\text{F}^{19}(p, \alpha\gamma)\text{O}^{16}$ at a proton energy of 2.05 Mev were used as the fluorescing radiation. These γ rays have widths of about 130 kev and therefore were capable of exciting several resonances near 7 Mev in the nuclei studied. The experiments lead to estimates of average total and average partial radiation widths and average level spacings for levels near the neutron separation energy in Cu, Ag, Sn, Hg, Pb, and Bi.

B. SUMMARY OF RESULTS

The shape of the capture γ -ray spectrum is determined in detail by the energies, spins, and parities of the levels between the capturing state at energy E_0 and the ground state, and by the γ -ray transition probabilities which depend not only on energy and multipolarity but also on the detailed structure of the states. The states whose properties are most easily studied are the capturing state itself and certain levels near the ground state (excitation energy $E < \sim 3$ Mev) which have a high probability of being excited by cascade transitions. Individual levels nearer the capturing state ($E > \sim 4$ Mev) have a low probability of being excited in most nuclei. Although in principle the capture spectra contain information about these levels the experimental difficulties in extracting it are formidable. However, the over-all shape of the spectrum is largely determined by the energy distribution of these higher energy levels and their modes of decay. In summarizing the data derived from studies of thermal-neutron capture γ rays we shall be concerned, therefore, with detailed properties of the capturing state and of indi-

vidual low-energy states, and with certain statistical properties of the levels up to the neutron separation energy.

1. *Properties of the capturing state.*—This heading will cover neutron separation energies, thermal-neutron capture cross sections, and partial radiation widths. Occasionally, also, the spin of the capturing state has been determined by γ -ray angular correlation methods, but it will be convenient to discuss these results, together with the spin determinations for bound levels, in the next section.

The neutron separation energy of a particular nucleus may be obtained directly from the energy of the ground state γ ray, or from the sum of the energies of the γ rays in a competing cascade, provided the usual corrections are applied for nuclear recoil. Additional information in the form of a less accurate estimate of the separation energy and some knowledge of the low-energy levels is usually necessary to prove that the γ ray of highest energy or a particular cascade of γ rays actually feeds the ground state and not a nearby excited state. The obvious method of testing for the ground-state γ ray by searching for γ rays in coincidence with the γ ray of highest energy is not reliable since it might fail to detect very-low-energy, highly converted, or long-lived transitions. On the other hand, as pointed out by Schwäger (64), the sum coincidence method using two detectors is a promising way of determining the neutron separation energy from the capture spectrum alone (at least in nuclei for which the over-all spin change is not so great as to preclude all two-step cascades).

Values for neutron separation energies determined from the (n, γ) reaction are complementary to those obtained from mass differences and from the (γ, n) , deuteron-proton (d, p) , and other reactions. Compilations of reaction Q values have been published by Van Patter & Whaling (80) and by Gove (81). A unified mass table using all available data has been constructed by Everling *et al.* (82). Among the more important Q values which can be determined with great accuracy by the (n, γ) reaction is the deuteron binding energy. A comparison of various determinations of this quantity is given in Table I.

The absolute intensity I_γ (in photons per capture) of a capture γ ray may be determined if the radiative capture cross section σ_A of the target nucleus A is known, and conversely. These quantities are related by the expression:

$$I_\gamma \sigma_A = k C_\gamma / (N_A e_\gamma) \quad 8.$$

where the counting rate C_γ , the detector efficiency e_γ , and the number of target atoms N_A are known or measurable quantities. The constant k is easily evaluated by a comparison experiment, the details of which are discussed elsewhere (33). In general, σ_A is known whereas the absolute γ -ray intensities remain to be determined. In a few nuclides, absolute intensities have been deduced independently from a knowledge of the decay scheme and it has then been possible to use the above method to measure σ_A . The results of such determinations are summarized in Table II.

TABLE I
VARIOUS DETERMINATIONS OF DEUTERON BINDING ENERGY

Reaction	Instrument	Reference calibration energy	Energy (kev)	Ref
$H^1(n, \gamma)H^2$	Thin-lens spectrometer	ThC'' 2.615 kev	2230 ± 7	(47)
$H^1(n, \gamma)H^2$	Cauchois spectrometer	Au ¹⁹⁸ 411.77 kev	2225 ± 3	(83)
$H^1(n, \gamma)H^2$	Total-absorption scintillator	Na ²⁴ , Cs ¹³⁷	2226 ± 3	(84)
$H^1(n, \gamma)H^2$	Compton spectrometer	Na ²⁴ 2753.3 kev	2224.3 ± 1.0	(85)
$H^1(n, \gamma)H^2$	Double-crystal diffraction spectrometer	annihilation 510.976 kev	2224.29 ± 0.24	(86)
$H^2(\gamma, n)H^1$	Variable X-ray source	Li ⁷ (p, n) threshold 1.881 Mev	2226 ± 3	(87)
Mass data least-squares fit			2224.71 ± 0.40	(82)

The partial radiation width Γ_γ' of a primary γ ray emitted when capture is dominated by a single resonance may be computed directly from the product of the total radiation width (92, 93) of the resonance Γ_γ and the absolute intensity of the γ ray. When no resonance is present at thermal energies, it is incorrect to talk about partial widths for the observed γ rays in the sense that this implies that they are emitted by a single level. Nevertheless, there are two situations where useful representative values of Γ_γ' may be obtained from such γ rays (94): (a) Both spin states $J_c = J_i \pm \frac{1}{2}$, ($J_i \neq 0$) may decay to a given final state with emission of radiation of the same multipolarity. (b) The target nucleus may have zero spin so that only

TABLE II
ISOTOPIC CAPTURE CROSS SECTIONS

Isotope	$\sigma(n, \gamma)$	Ref
Li ⁶	28 \pm 8 mb	(88)
B ¹⁰	0.5 \pm 0.2 b	(88)
C ¹³	0.8 \pm 0.2 mb	(89)
N ¹⁴	0.08 \pm 0.02 b	(88)
V ⁵⁰	250 \pm 200 b	(90)
Pb ^{206, 207}	$\sigma(207)/\sigma(206) \leq 13$	(91)

compound states with $J_c = \frac{1}{2}$ are formed. In either case, the product of the observed absolute intensity of a particular γ ray and the mean total radiation width for nearby resonances represents an order-of-magnitude value for the partial widths for that γ ray averaged over all contributing s -wave resonances (neglecting possible interference effects). When the γ ray in question is allowed for one value of J_c but not the other, the same calculation yields a lower limit for the partial width. Comparisons of experimental partial radiation widths with theoretical predictions have been discussed at length in past publications (1, 3, 94, 95), and only a brief summary will be given here.

The radiative widths for $E1$, $M1$, and $E2$ γ rays of energy ϵ emitted in transitions from the capturing state may be written in the following approximate forms which are derived from expressions given by Blatt & Weisskopf (96):

$$\Gamma_\gamma'(E1) = 0.11\epsilon^3 A^{2/3} D / D_0 \quad 9.$$

$$\Gamma_\gamma'(M1) = 0.021\epsilon^3 D / D_0 \quad 10.$$

$$\Gamma_\gamma'(E2) = 1.2 \times 10^{-7} \epsilon^5 A^{4/3} D / D_0 \quad 11.$$

where D is the spacing at the separation energy of levels with the same spin and parity as the capturing state, D_0 is the single-particle level spacing for states of the same spin and parity, and A is the mass number. The quantities ϵ , D , and D_0 are in Mev, and Γ_γ' in ev. The numerical constants in Equations 9 and 11 depend on the nuclear radius, which is here assumed to be $1.5 \times 10^{-13} A^{1/3}$ cm.

The ratios of partial widths of competing primary γ rays of different multipolarity have been determined experimentally in a few light nuclei ($A \approx 30$). In these nuclei the ratio $\Gamma_\gamma'(E1)/\Gamma_\gamma'(M1)$ is found to be in rough agreement with the prediction of Equations 9 and 10 (3). The few $E2$ primary γ rays that have been detected are found to be between 10 and 100 times weaker (at 7 Mev) than competing $M1$ γ rays, also in rough agreement with the theory.

Observed partial radiation widths for $E1$ and $M1$ γ rays emitted in different nuclei may be scrutinized by plotting the reduced widths:²

$$k_{E1} = \frac{\Gamma_\gamma'(E1)_{\text{obs}}}{\epsilon^3 A^{2/3} D}, \quad k_{M1} = \frac{\Gamma_\gamma'(M1)_{\text{obs}}}{\epsilon^3 D} \quad 12.$$

as a function of mass number (95). The quantities k are, of course, the experimental equivalent of C/D_0 where C is the numerical constant in Equations 9 and 10.

Values of k_{E1} and k_{M1} for all known $E1$ and $M1$ primary neutron capture γ rays emitted in both resonant and nonresonant capture are summarized in Figure 3. The total radiation widths used in plotting these points were taken from the compilations of Levin & Hughes (92), Stolovy & Harvey (93), and Hughes & Schwartz (97), when measured values were available, and from

² These might also be called radiation strengths since they are analogous to the strength function for particles.

Cameron's estimated values (98) in all other cases. The level spacings were taken from Hughes & Schwartz (97) in all cases except Ca^{41} , Ti^{48} , Ti^{49} , Fe^{56} , Cr^{54} , Zn^{69} , Ga^{70} , and Sr^{87} where spacings estimated by Cameron (99) were used.³ The absolute γ -ray intensities were taken from Bartholomew & Higgs (6), Groshev *et al.* (7), and Knoepfel *et al.* (31). Gamma rays emitted by capturing states whose spins are ambiguous (both spins contributing) are shown as lower limits if there is a possibility that the γ ray may be forbidden for one spin value. Upper limits are shown for γ rays which are expected to be present from a knowledge of the spins and parities of the levels concerned but which were too weak to be observed. To facilitate intercomparison of the energy-reduced radiation widths Γ_γ'/e^2 , for $E1$ and $M1$ γ rays, the k_{M1} have been normalized with respect to the k_{E1} by shifting the k_{M1} axis by an amount corresponding to a mean mass number factor, $A^{-2/3} \equiv 130^{-2/3}$. The theoretical k values from Equations 9 and 10 are shown for a single-particle level spacing D_0 of 15 Mev; they fall satisfactorily close to the medians of the experimental values, $k_{E1} \simeq 3 \times 10^{-3}$ and $k_{M1} \simeq 4 \times 10^{-3}$.

Figure 3 shows that although there is a wide distribution in the matrix elements, the median values are essentially independent of A , a result which confirms the predicted (96) dependence of the radiation width on D .⁴ The figure also shows that although the matrix elements for the $E1$ and $M1$ transitions largely overlap, the strongest $E1$ transitions are about an order of magnitude stronger than the strongest $M1$ transitions. Therefore, these diagrams are sometimes useful for testing whether a particularly strong γ ray of known radiation width but of unknown multipolarity is of $E1$ type or not. Gamma rays whose multiplicities are unknown but which have k larger than that of a known $E1$ γ ray in the same spectrum are shown by open circles.⁵ The reduced widths derived from the resonance fluorescence measurements of Reibel & Mann (79) are also shown (as crosses) on the $E1$ graph. For Cu, Ag, and Bi, points corresponding to different possible values of the excited-state spin are connected by vertical bars. The overlap of these data with the capture γ -ray reduced widths is at first sight rather surprising in view of the order-of-magnitude larger γ -ray partial widths obtained in the resonance fluorescence experiments. However, Reibel & Mann point out that these experiments select just those levels which have large dipole matrix elements and such levels must occur with a correspondingly larger spacing.

It will be seen that the largest values of k_{E1} tend to occur near mass num-

³ From level spacings observed in charged particle experiments, it now appears that the formula used here may give level spacings near the neutron separation energy which are too small by as much as an order of magnitude for nuclei in the region $A < 70$. (A. G. W. Cameron, private communication, 1961.)

⁴ Strictly speaking, D_0 should vary as $A^{-1/3}$ which may partly explain a noticeable tendency for the median values of k_{E1} and k_{M1} to increase slowly with A .

⁵ One γ ray of special interest for the resonance capture experiments to be discussed later is the 4.06-Mev γ ray in U^{239} (100). This γ ray is shown as an open circle at $A = 239$ in the $E1$ diagram. There would appear to be little doubt that it is of $E1$ type.

bers 90, 150, and 180. In such nuclei, which lie near the 50, 82, and 126 neutron shells, the γ rays corresponding to these values of k_{E1} are a prominent feature of the high-energy spectrum, as first noticed by Kinsey & Bartholomew (94). On the other hand, in the region $40 < A < 70$, where γ rays of even greater absolute intensity are observed, the values of k_{E1} in Figure 3 are relatively small (and perhaps should be even smaller if too-small level spacings have been used in Eq. 12, see footnote 3). In consideration of this anomaly it must be noted that for nuclei in the range $A < 70$, radiation widths have been determined only for resonances in product nuclei Na^{24} , Cl^{36} , Mn^{56} , Co^{60} , and Zn^{69} (92, 93) and that none are known for any of the even- Z product nuclei such as Ti^{49} , Fe^{67} , and Ni^{59} whose spectra each contain two or three γ rays of exceptional intensity. Although the radiation widths given by Cameron's formula (98) for nuclei in the range $A > 70$ are usually correct to within a factor of 2, it is conceivable that the statistical methods used in such a calculation are subject to large errors for the light masses $A < 70$ and that the true widths in these even- Z nuclei are actually an order of magnitude larger than predicted. It is also possible that these intense γ rays are not a resonance phenomenon and that the above analysis which uses parameters of local resonances is not appropriate (see Sect. IV).

2. *Properties of bound levels.*—The properties of the low-energy excited states which have been studied in greatest detail by means of the (n, γ) reaction are excitation energies and spins of levels and γ -ray branching ratios.

Level diagrams and decay schemes constructed from neutron capture γ -ray information alone always contain an element of ambiguity since alternatives are usually possible for the order of emission of the γ rays and the positions of energy levels. The construction of a consistent decay scheme is greatly facilitated if additional information from other reactions is available. In many cases data from (d, p) reactions or β decay, and data from (n, γ) reactions are mutually corroborative and complementary [see, e.g., Paris *et al.* (101) and Bockelman & Buechner (102)].

With present techniques, spin determinations by angular correlation measurements can seldom be carried out for more than one or two strong cascades in any given nucleus. If one of the levels involved is the capturing state, complications in interpretation may arise unless thermal capture is overwhelmingly dominated by one resonance. (This difficulty is not present in the particular case when the target nucleus has spin zero.) In many cases, capturing state spins determined by γ - γ correlations can be checked by circular polarization measurements (Sect. IIA4).

In Table III are summarized all spin determinations that have been reported to date from angular correlation and circular polarization measurements of neutron capture γ rays. Other data on multipole mixtures or capturing state spin mixtures have also been obtained and will be found in the references cited.

A procedure by which neutron capture γ -ray intensities in odd-odd nu-

TABLE III
SPINS OF BOUND LEVELS AND CAPTURING STATES
DETERMINED IN (n, γ) EXPERIMENTS

Product nucleus	Level (Mev)	J		Product nucleus	Level (Mev)	J	
		Angular correlations	Circular polarization			Angular correlations	Circular polarization
N ¹⁵	6.33	$> 1/2^a$					
Mg ²⁵	3.41	$3/2^b$		Cu ⁶⁴	0.60	$\begin{Bmatrix} 3^c \\ 1, 2^a \end{Bmatrix}$	
Si ²⁹	4.93	$3/2^b$			7.91*		(1) ^d
	6.38	$1/2^b$		Zn ⁶⁵	0.0?		$3/2^c$
P ³²	1.15	1^b		Y ⁹⁰	0.202	$3?^h$	
	3.26	2^b			0.777	$2?^h$	2^d
S ³³	3.22	$3/2^b$	$3/2^d$	Zr ⁹²	2.34	3^a	
Ca ⁴¹	1.95		$3/2^e$		8.66*	2^a	
Ti ⁴⁹	1.38	$3/2^{f,g}$	$3/2^{d,e}$	Te ¹²⁴	9.400*	1^i	
	1.72	$1/2^{f,g}$	$1/2^d$	Nd ¹⁴⁴	1.560	3^i	
Cr ⁵⁴	9.72*	1^e			7.814*	3^i	
	0.83	$1, 2^e$	2^e				
Fe ⁵⁷	0.364	$3/2^a$		Gd ¹⁵⁸	1.182	2^i	
Ni ⁵⁹	0.0	$3/2^e$	$3/2^{d,e}$		7.923*	2^i	
	0.45	$3/2^e$	$1/2^d$	W ¹⁸³	0.0		$1/2^e$
		$\begin{Bmatrix} 0^e \\ 1, 2^a \end{Bmatrix}$	$\begin{Bmatrix} 0, 3^e \\ 2^d \end{Bmatrix}$	Hg ²⁰⁰	1.59	1^a	
Cu ⁶⁴	0.28				8.401*	0^a	

* Capturing state.

^a See (103).^d See (73).^e See (104).^b See (54).^e See (72).^h See (105).^c See (53).^f See (20).ⁱ See (106).

clei may be used for predicting the spins J of the various levels of the multiplet formed by coupling the odd proton (spin j_p) to the odd neutron (spin j_n) has been pointed out by Varshalovich (107). It is assumed that the nucleus is well represented by the shell model and that residual interactions which split the multiplet are small compared to single-particle excitation energies. Assuming that γ -ray transitions from the capturing state J_c to a level of the multiplet involve only the single-neutron jump $j_{n1} \rightarrow j_{n2}$, the ratio of reduced transition probabilities for γ rays feeding any two members of the multiplet may be written:

$$\frac{B(L, J_c \rightarrow J_1)}{B(L, J_c \rightarrow J_2)} = \frac{(2J_1 + 1)W^2(j_{n1}J_cj_{n2}J_1, j_pL)}{(2J_2 + 1)W^2(j_{n1}J_cj_{n2}J_2, j_pL)} \quad 13.$$

where the W 's are Racah coefficients. Applying this analysis to P³², Varshalovich shows that the primary γ -ray intensities are consistent with spin

assignments of 0, 1, and 2 for the levels at 0.51, 1.15, and 3.26 Mev, respectively. Comparison with Table III will show that these predictions concerning the 1.15 and 3.26 Mev levels are confirmed by angular correlation measurements. Unfortunately this method of predicting spins, which depends on the absence of appreciable configuration mixing, does not appear to have a large area of applicability.

The decay schemes of Cl^{36} and Y^{90} in Figure 4 are presented to illustrate the effectiveness of current techniques for obtaining energy level and decay scheme information from neutron capture γ -ray spectra. These diagrams are self explanatory.

3. *The spectral distribution.*—Early measurements of heavy element spectra by a pair spectrometer (94) covered only the energy range from the top of the spectrum down to about 2.7 Mev, a region containing of the order of one-quarter of the total energy radiated. These measurements demonstrated that the center of gravity of the spectra changed with mass number in a way that correlated with the reduction of level density in the neighborhood of closed neutron shells (94, 111). For elements near Pb (126 neutrons), and to a lesser degree for elements near Pr (82 neutrons) and Zr (50 neutrons), the amount of radiation in the upper end of the spectrum was greater than for nuclei farther removed from the shells. This fact was demonstrated in a more quantitative way by Groshev (112) who plotted the fraction of the total energy radiated which appeared as γ rays with energies greater than one-half the neutron separation energy.

The greater energy range of the Compton spectrometer (36) has made it possible to obtain, in one experiment, an essentially complete spectral distribution from below 1 Mev to the top of the spectrum. These distributions have been extensively studied by Groshev and co-workers (113) who have pointed out many important features which were not revealed by the earlier work with the more limited energy range.

The general features of the spectra of even-even and odd-odd nuclei in the nonspherical region are typified by the spectra of Gd^{158} and Ho^{166} , Figure 5. The intensity $\nu(\epsilon)$ (γ rays per capture per unit energy interval at energy ϵ) increases rapidly with decreasing energy, beginning (for nuclei in the region $100 < A < 200$) at about 6.4 Mev in both even-even and odd-odd types. This energy corresponds to transitions to states near zero excitation in the odd-odd nucleus and near 1.2 Mev in the even-even nucleus. This phenomenon, first noted by Kinsey (2) and discussed in detail by Groshev *et al.* (4), is in accord with the suggestion of Hurwitz & Bethe (114) that the level distributions of the two types of nuclei are statistically similar if they are measured from a characteristic energy which varies smoothly with mass number. In Ho^{166} the spectral intensity continues to increase monotonically with decreasing energy, with a slight bulge appearing just below 3 Mev, while in Gd^{158} the spectrum reaches a peak at this energy. It is characteristic that the unresolved continuum in the spectrum for the even-even nucleus tends

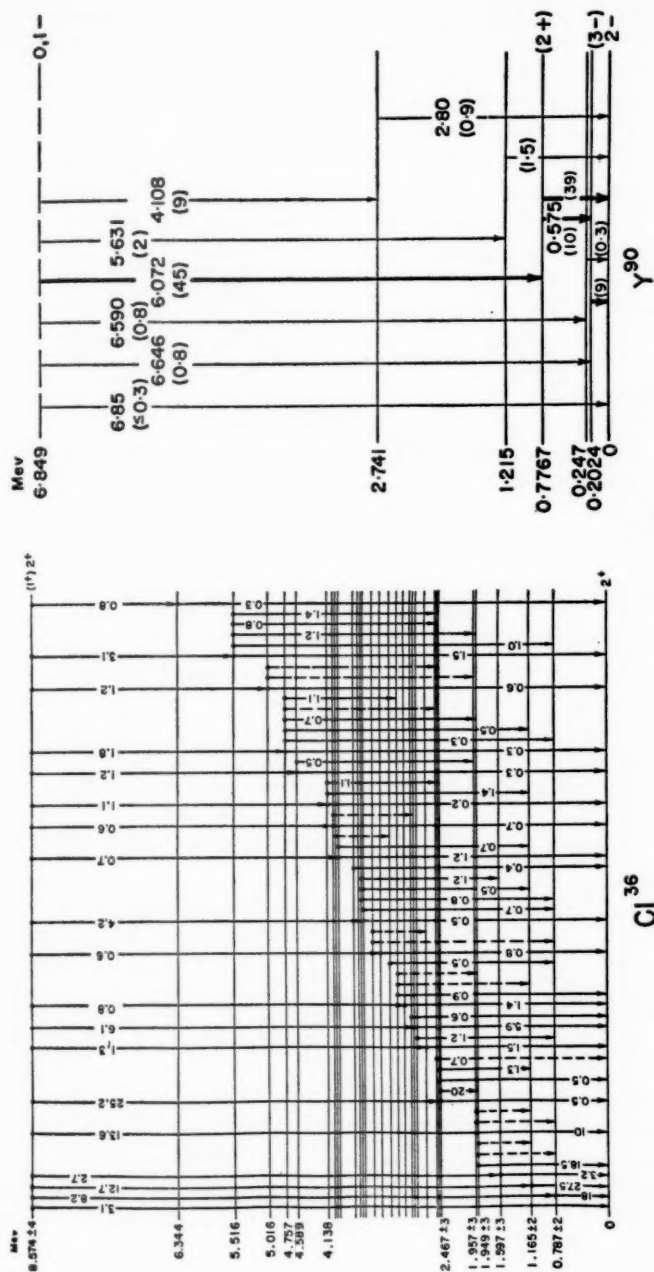


FIG. 4. Examples of decay schemes based on (n, γ) data. In Cl^{36} the γ -ray decay scheme is that of Groshev *et al.* (108) who report the level energies shown. The γ -ray intensities are given on the arrows. The levels below 4.138 MeV, with the exception of that at 1.949 MeV, were observed in the (d, p) reaction by Prais *et al.* (101) who gave the level energies shown. The existence of the 1.949-MeV level is deduced from the observed γ rays. The (d, p) stripping l_n values for many of the lower levels have been determined by Teplov (109). Various authors (52, 53, 59, 65, 68) have carried out γ - γ coincidence experiments which confirm many of the γ -ray assignments. As yet it has not been possible to make unambiguous spin assignments for any of the levels.

In γ^{90} , the γ -ray energies and intensities (105) are shown on the arrows; the level energies from the (n, γ) reaction are given on the left. Only one level, at 1.17 MeV, has been observed in the (d, p) reaction [Wall (110)]. The capture γ -ray spectrum contains remarkably few strong lines, a state of affairs which facilitated the angular correlation (105), and polarization correlation measurements (73), which form the basis for the spin assignments for the 0.2024- and 0.7767-MeV levels.

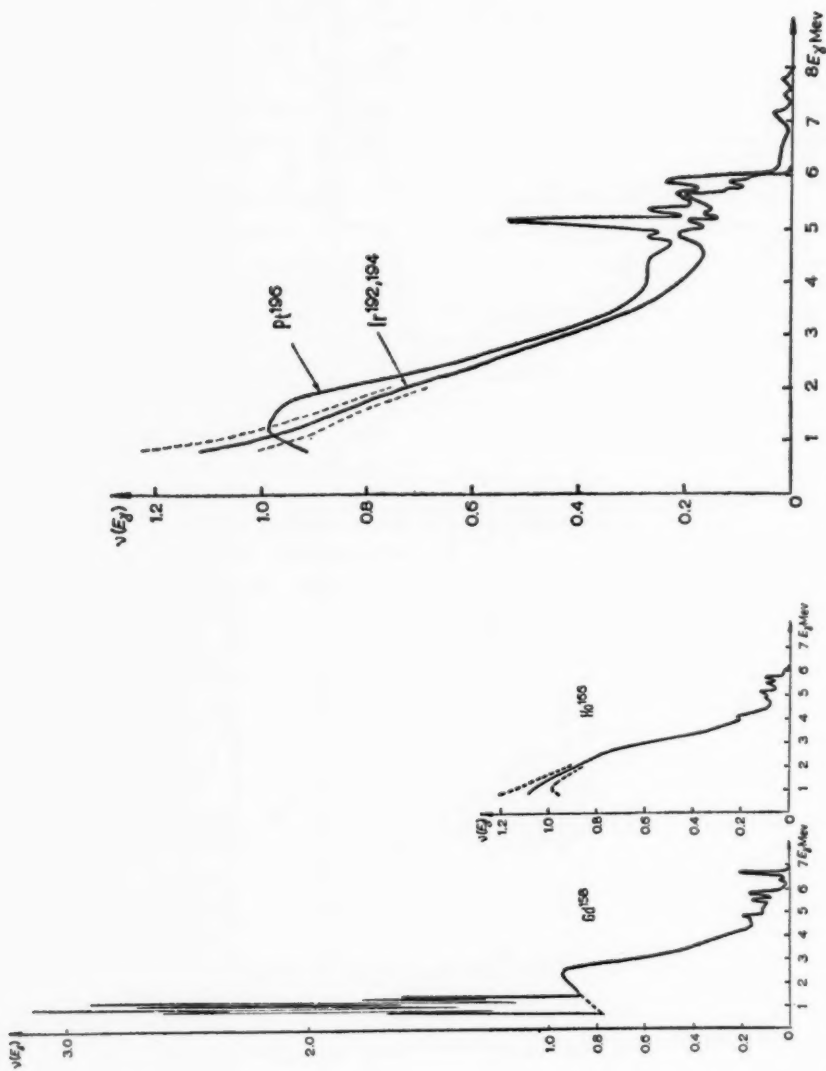


FIG. 5. Typical spectra of even-even and odd-odd nuclei in the region $100 < A < 200$ as measured by Groshev *et al.* (113). The ordinate gives the number of γ rays per capture per unit energy interval.

to contain rather more radiation between 2 and 4 Mev than the odd-odd spectrum whereas the reverse is true below 2 Mev. Near 1 Mev, the spectra of nonspherical even-even nuclei are characterized by a most remarkable group of intense γ rays standing out well above the general continuum. This feature was not observed in odd-odd or even-odd nuclei (115) and is much less prominent or entirely absent in spherical even-even nuclei. The spectra of Pt^{196} and $\text{Ir}^{192,194}$, also shown in Figure 5, demonstrate that the similarities between the spectra of the two types of nuclei persist at higher A . These spectra also provide examples of the unusual predominance of high-energy radiation in elements near the 126-neutron shell mentioned earlier. The spectra of spherical odd-odd nuclei with $A \simeq 110$ closely resemble those of the distorted odd-odd nuclei such as Ho^{166} except that the bulge at 3 Mev is absent [Groshev *et al.* (113)].

The spectrum shape may be calculated if the energy dependence of the γ -ray transition probability and the level density distribution are accurately known. By an elaboration of a statistical expression given originally by Blatt & Weisskopf (96), we may write for the spectrum emitted in the decay of a level of excitation energy E :

$$\nu(\epsilon, E) = C(E) \sum_L k_L(\epsilon, E) \epsilon^{2L+1} \rho_L(E - \epsilon) \quad 14.$$

where $\nu(\epsilon, E)$ is the number of γ rays per capture per unit energy interval at ϵ , $2L$ is the γ -ray multipolarity, and $k_L(\epsilon, E)$ is a mean reduced width for transitions of multipolarity $2L$ between the level at E and combining levels at the energy $(E - \epsilon)$. The quantity $\rho_L(E - \epsilon)$ is the density of levels at $(E - \epsilon)$ to which transitions of multipolarity $2L$ are allowed. It is assumed that ρ_L varies continuously with energy and that there is no irregular distribution of parities with energy. The constant $C(E)$ is a normalizing constant such that

$$\int_0^E \nu(\epsilon, E) d\epsilon = p(E) \quad 15.$$

where $p(E)$ is the population acquired by the level at E by transitions from higher levels in the cascade; $p(E)$ has the value unity for the capturing state.

The spectral distribution in the total spectrum is given by

$$\nu(\epsilon) = \int_{\epsilon}^{E_0} \nu(\epsilon, E) dE \quad 16.$$

where E_0 is the neutron separation energy. The integration may be carried out numerically by a step-by-step procedure beginning with the capturing state if suitable expressions for $k_L(\epsilon, E)$ and $\rho_L(E - \epsilon)$ are assumed.

The γ -ray reduced widths discussed earlier show that the decay of the capturing state proceeds predominantly by dipole radiation. There is evidence from a study of the isotopic capture cross sections by Huizenga &

Vandenbosch (116) that dipole radiation also plays a major part throughout the remainder of the cascade. Thus, although it is recognized that electric quadrupole transitions may play a significant part in the decay of low-energy rotational states in some nuclei, it would appear to be sufficiently accurate for the statistical calculations of spectrum shape to include only the term with $L=1$ in Equation 14.

A detailed analysis of the capture γ -ray spectra from even-even and odd-odd product nuclei in the region $100 < A < 200$ has been carried out by Groshev *et al.* (113) and Strutinski *et al.* (117). In this analysis an attempt is made to determine the form of the level density distribution which best reproduces the observed spectra and to account for the differences between the spectra of even-even and odd-odd nuclei and for the prominent group of lines near 1 Mev in the spectra of distorted even-even nuclei. Of central importance in this analysis is the recognition of the part played by the pairing energy gap Δ (118, 119) in determining the shape of the even-even spectra. The total spectrum is divided into three parts: $\nu(\epsilon, E_0)$, the primary spectrum of transitions to levels above the energy gap; ν_a , the spectrum of cascade transitions feeding levels above the gap (called *a*-type transitions); and ν_b , the spectrum of transitions from levels above the gap to the ground state (*b*-type transitions). It is assumed that the matrix elements for transitions of type-*b* may be different from those of type-*a*. Primary transitions from the capturing state to the ground state are neglected, and for simplicity all levels of the ground state band are assumed to have zero energy. Equation 16 is therefore written:

$$\nu(\epsilon) = \nu(\epsilon, E_0) + \nu_a + \nu_b \quad 17.$$

where

$$\nu(\epsilon, E_0) = C(E_0)\epsilon^2\rho(E_0 - \epsilon) \quad (E_0 - \epsilon) > \Delta \quad 18.$$

$$\nu_a = \int_{\epsilon}^{E_0 - \Delta} C(v)\epsilon^2\rho(v - \epsilon)dv \quad v = E - \Delta \quad 19.$$

and

$$\nu_b = \alpha C(\epsilon)\epsilon^2 \quad \epsilon \geq \Delta \quad 20.$$

The quantity $\alpha = k_{E1_b}[k_{E1_a}\rho(0)]^{-1}$ allows for a possible difference between the matrix element of *a*- and *b*-type transitions and for the fact that only a single final state is involved for *b*-type transitions.

Equation 17 was used to fit the observed average spectral distributions assuming $\Delta = 1.2$ Mev for even-even nuclei and $\Delta = \alpha = 0$ for odd-odd nuclei. The calculations were carried out for a range of values of the parameter α and for various values of the parameters τ and a -for two alternative level density expressions (for levels above Δ):

$$\rho(v) = e^{v/\tau} \quad 21.$$

and

$$\rho(v) = e^{\sqrt{av}} \quad 22.$$

It was found that although Equation 22 with $a = 15 \text{ Mev}^{-1}$ gave the best fit for spherical odd-odd nuclei, it gave a relatively poor fit for even-even nuclei. On the other hand, Equation 21 with $\tau = 0.8 \text{ Mev}$ best reproduced the spectra of nonspherical odd-odd nuclei (including the 3-Mev bulge) and also, with the parameter α equal to 0.5 Mev, gave the best fit to the general shape of the spectra of the even-even nuclei (ignoring the group of intense lines at 1 Mev).

To best reproduce the lines near 1 Mev with $\tau = 0.8 \text{ Mev}$ and at the same time preserve the high-energy fit, it was necessary to divide the ν_0 contribution, Equation 20, into two parts with $\alpha = 0.0025 \text{ Mev}$ for $\nu < 0.4 \text{ Mev}$ and $\alpha = 0.5 \text{ Mev}$ for $\nu > 0.4 \text{ Mev}$. The last result implies that, for a region of about 0.5 Mev above the gap, transitions to the ground state are strongly inhibited compared to those from levels at higher energies. As suggested by Strutinski *et al.* such an effect could be understood as a consequence of the K -selection rule (120) if there were a paucity of states with K equal to 0 or 1 in this energy region. In a supplementary calculation, in which it was assumed that b -type transitions were of quadrupole type, Strutinski *et al.* (117) found it was impossible to fit the data for any values of the adjustable parameters. This analysis of spectral shapes is not sufficiently definitive to permit a clear choice to be made between Equations 21 and 22; both expressions give similar results. However, the analysis does show that in the region just above the pairing energy the level density increases more slowly than is implied by Equation 22 (117). It is also noteworthy, as Strutinski and co-workers point out, that their fitted value $a = 15 \text{ Mev}^{-1}$, which corresponds to $a' = 3.8 \text{ Mev}$ in the usual exponential expression $e^{2\sqrt{a'}\nu}$, is not in good agreement with determinations of this quantity from other reactions. For example, recent unpublished data of D. B. Thompson from the (n, n') reaction reviewed by Ericson (121) show $a' \simeq 15 \text{ Mev}$ for A near 180, a value in good agreement with that obtained from the spacing of neutron resonances near the separation energy.

A more satisfactory fit of the spectrum shape might perhaps result if the more realistic form $\nu^{-2}e^{2\sqrt{a'}\nu}$ had been used for the level density. It is pointed out by Strutinski *et al.* that this expression leads to some improvement in the a' discrepancy. A more elaborate theory might also take into account the enhancement of the transition probability for primary transitions to final states which contain a large-neutron single-particle p -state admixture (see Sect. IV). The preponderance of high-energy γ rays in the spectra of Pt and Ir in Figure 5 is no doubt due to such an enhancement, and it seems possible that the 3-Mev bulge in odd-odd nuclei at $A \simeq 170$, which is absent at $A \simeq 110$, might be a remnant of this effect persisting at lower mass numbers.

An alternative approach in analysing the spectral distribution is to begin by assuming a particular form for the level density distribution which is adjusted to fit the known density at the neutron separation energy for each individual nucleus. In one such calculation (95, 98), Newton's level density expression (118), modified by Cameron (99), was used to compute the spec-

tral distributions, Equation 16, for nuclei in the region $30 < A < 208$. Newton's level density formula takes account of the effects of shell structure and pairing energy on the level density. The transition probabilities were assumed proportional to ϵ^3 with a constant average reduced radiation width. Although, as mentioned above, the exponential form for the level density, which forms the basis of Newton's formula, might not be realistic for the low-energy levels, such an approach might be expected to reproduce reasonably well the spectrum shape for γ rays feeding levels above, say, 2Δ and should reflect the effects of shell structure on the γ -ray distribution. Some confirmation of the validity of this approach, at least for nuclei above $A = 70$, is supplied by the success of the same procedure in accounting for the dependence of total radiation width on mass number (see later discussion). The theoretical spectral distributions obtained in this way were used to calculate F , the fraction of the total energy radiated which appears in the spectrum as γ rays with energies greater than one-half the effective excitation energy ($E_0 - \Delta$) (95). A comparison of these theoretical values of F with those obtained from the observed spectra showed satisfactory agreement in the region $70 < A < 160$, although the experimental points showed considerable scatter. However, in the mass region $170 < A < 208$ the values of F obtained theoretically were too small by as much as a factor of 2. There was also a suggestion of a similar but smaller discrepancy for some nuclei in the region $A \approx 60$. Since the Newton-Cameron level density expression (98, 118) is based on the assumption (now somewhat in doubt) that the exponential increase of level density begins just above the gap, it probably results in an overestimation of the level density at low energies and, consequently, an overestimation of F . If this is indeed the case, the disagreement in the values of F must be even greater than observed. The discrepancy may be interpreted as showing that a statistical description of the spectrum shape (which takes account of shell structure and uses a constant average k_{B1}) cannot account for the observed shape at all mass numbers and that it is therefore necessary to assume an enhancement of the transition probabilities for certain primary γ rays feeding low-energy levels of nuclei in the range $170 < A < 208$ and possibly also for A near 60. This question will be discussed further in Section IV.

Other quantities directly related to the statistical problem of the γ -ray cascade are the multiplicity, the ratio of the yields of isomeric states following neutron capture, and the total radiative width of neutron resonances. Although the latter two quantities are not directly determined from the γ -ray spectrum itself, a review of the agreement between experimental and theoretical values for these quantities is relevant here since it gives an indication of the validity of the assumptions on which the statistical description is based.

The multiplicity is defined by the equation

$$\bar{N} = \int_0^{E_0} \nu(\epsilon) d\epsilon \quad 23.$$

This quantity has been determined for many nuclei by a coincidence method by Muehlhause (122), by a direct counting technique in which the number of γ rays per capture was compared with that from a known standard by Springer & Draper (123), and by direct application of Equation 23 to the observed spectrum by Groshev *et al.* (4). The value of \bar{N} changes little from nucleus to nucleus; it varies from ~ 2 for nuclei near Al to ~ 6 for Sm with most nuclei having a value near 4.

The ratios of the cross sections for the formation of the two members of a pair of isomeric states have been discussed in terms of a statistical model of the γ -ray cascade by Huizenga & Vandenbosch (116). With the assumption of a continuous level distribution and no irregularities in the distribution of parity, the estimation of the relative populations of levels of various spins after a given number of steps in cascade have occurred may be carried out by a simple step-by-step calculation. The calculation is independent of the form of the level density distribution with energy but depends on the spins assumed for the initial and final states and on the distribution of levels as a function of spin. It was assumed that the distribution of levels with spin followed Equation 6. By using both σ and the multiplicity \bar{N} as variable parameters, it was possible to fit most of the observed ratios (for cases where the spins were known) with $3 \leq \bar{N} \leq 4$ and $3 < \sigma \leq 6$. This value of \bar{N} is in accord with the results of direct measurement discussed above. The consistency of the calculated results indicates that isomeric cross section ratios may provide a reliable method for making spin assignments for the capturing state.

The total radiation widths are observed to decrease slowly with mass number from ~ 500 mv near $A = 50$ to ~ 30 mv near $A = 240$ with distinct peaks occurring for nuclei just preceding closed shells (92, 93). Various attempts to account for this trend have been made (92, 93, 98, 124). The total radiation width may be computed by summing the partial widths of all γ rays in the primary spectrum. The most detailed approach has been that of Cameron (98) who used the following expression derived from the theory of Blatt & Weisskopf (96):

$$\Gamma_{\gamma} = \langle k_{E1} \rangle A^{2/3} D(E_0) \int_0^{E_0 - \Delta} e^{\rho'(E_0 - \epsilon)} d\epsilon \quad 24.$$

where Γ_{γ} is in ev and D , ϵ , and E_0 are in Mev. The density ρ' is the density of all levels at $(E_0 - \epsilon)$ which are fed by $E1$ transitions from the capturing state. Radiation widths computed in this way, with ρ' given by a modified version (98) of Newton's formula (118) and with $\langle k_{E1} \rangle$ as an adjustable parameter, closely reproduced the variation of Γ_{γ} with A for nuclei in the range $A > 70$. There remained a small tendency for the ratio Γ_{γ} (observed)/ Γ_{γ} (calculated) to form a maximum in the region $150 < A < 180$. The value of $\langle k_{E1} \rangle$ corresponding to this fit, 3.3×10^{-4} ev/Mev,⁴ is plotted in Figure 3 where it is seen to be much lower than the k_{E1} values for the individual primary γ rays; it corresponds to a D_0 of 330 Mev. This low value of $\langle k_{E1} \rangle$ may be accounted

for in part if, as mentioned above, the Newton-Cameron level density expression introduces too many levels at low excitation energies, for then Γ_γ would be shared between too many γ rays.

III. EPITHERMAL NEUTRON CAPTURE

The capture γ -ray experiments reviewed in this section are concerned with the detailed study of the spectra from different resonances. The principal objects of these experiments have been: (a) to identify which isotopes in a natural target are responsible for various resonances, (b) to determine the distribution of the partial radiation widths for primary γ -ray transitions to a given final state from resonances of the same spin, and (c) to determine the spins of resonances.

Experiments in which capture γ rays serve only as a convenient tool for determining various other nuclear properties will not be discussed in detail. Notable experiments of this type are the pulsed beam, self-indication transmission measurements carried out at the Nevis synchrocyclotron (125, 126) and resonance capture cross-section measurements at Harwell (127, 128). The object of these experiments is to obtain the energies, spacings, neutron widths, total radiation widths, and spins of energy levels. In the same category are various experiments to determine radiative capture cross sections with the aid of pulsed neutron beams and neutron capture gamma-ray total absorption detectors (129, 130, 131). Recently, neutron capture γ rays have also been used to determine photonuclear cross sections and thresholds in a number of heavy nuclei (132).

Nearly all measurements of the γ -ray spectra from individual resonances have been limited to neutron energies below approximately 2 kev, with most attention concentrated in the region below 300 ev. From elementary barrier considerations one expects that resonances in heavy nuclei at neutron energies less than, say, 500 ev are almost certain to be of s -wave type. However, relatively strong p -wave resonances may be encountered in nuclei situated near a maximum in the p -wave strength function, and in these special cases it may not be safe to assume that all resonances observed at these energies are s -wave resonances. The magnitude and the dependence on mass number of the p -wave strength function are not nearly so well known as for the s -wave strength function, but this function does appear to have a maximum or maxima near A equal to 100 (133, 134) and another is expected near A equal to 200. Indeed, the frequent occurrence of resonances with unusually small neutron reduced widths in neutron cross-section experiments of Saplakoglu *et al.* (135) in $\text{Nb}^{93}+n$; Desjardins *et al.* (126) in $\text{Ag}^{107,109}+n$; and Bollinger *et al.* (136) and Rosen *et al.* (125) in $\text{U}^{238}+n$ have been interpreted as showing that weak p -wave resonances are being detected at energies even below 100 ev. Unfortunately the study of individual γ rays in the spectra from these weak resonances would be difficult; and neutron-gamma angular distribution experiments, which would give spin information if the

levels are indeed produced by p -wave capture, seem rather beyond the range of present techniques.

Only one experiment to study the γ -ray spectra following capture of fast neutrons has been reported [Bergqvist & Starfeldt (137)]. The object of this experiment was to measure the spectra following capture of 125-keV neutrons in various elements and to compare these with the thermal spectra in order to determine changes in the spectra caused by p -wave capture, and to throw light on the role played by "direct" capture at different neutron energies (Sect. IV).

A. SUMMARY OF TECHNIQUES

All resonance neutron capture γ -ray measurements involve time-of-flight methods for selecting neutrons of the desired energy from a heterogeneous beam. Both pulsed neutron beams from accelerators or mechanical velocity selectors (fast choppers) using neutrons from reactors have been used as sources. The first capture γ -ray experiments of this type were carried out at Yale University (138) using a 6-MeV electron linear accelerator. More powerful linear accelerators have been used at Harwell (139 to 142) and at Saclay (143, 144). A pulsed beam from a cyclotron has been employed by Galanina *et al.* (145). Fast choppers have been used for capture γ -ray measurements at the Argonne reactor (57, 146, 147) and at the Brookhaven and Chalk River reactors (148, 149, 150). In all of these experiments the problem of obtaining a satisfactory γ -ray counting rate is of paramount concern. Flight paths consistent with adequate neutron energy resolution and which, at the same time, permit reasonable γ -ray counting rates with targets of manageable size (of the order of 200 cm² in area), range between 3.1 m (138) and 53.8 m (144).

The fast-neutron source used by Bergqvist & Starfeldt (137) was obtained from the $H^3(p, n)He^3$ reaction at a bombarding energy of 1.3 MeV. Neutrons striking the target (at 75° to the proton beam) had energies in the range 125 ± 35 keV. The proton beam was pulsed and a time gate was used to discriminate against background radiation reaching the γ -ray detector later than the γ rays of interest.

Because of the low neutron beam intensities all measurements of epithermal neutron capture γ -ray spectra have been made with large NaI scintillators. These are used as single crystals (140, 144) or in clusters to increase the detector efficiency (151). The Argonne group has reported some experiments (57, 147) in which two detectors have been used for detection of coincidences between pairs of capture γ rays. Various methods of time and pulse-height analysis have been used to maximize the efficiency of data recording (57, 152, 153).

B. SUMMARY OF RESULTS

Gamma rays in different parts of the spectrum present different advantages for attacking the three types of problem alluded to earlier, isotope iden-

tification, measurement of partial radiation width distributions, and spin determination. It is to be expected that since the low-energy levels in a heavy nucleus are fed by many different cascade channels they would reach nearly the same populations for all resonances of the same spin and that these populations would not differ greatly for resonances of adjacent spin. Therefore, the intensities of the strong low-energy γ rays emitted in the decay of these levels should also vary little for resonances of adjacent spin. In spite of the statistical smoothing process, however, such small differences as may be observed in certain nuclei may give information about the initial spin (154). Furthermore, since each product nucleus usually has a distinctive level scheme, these spectra provide a reliable way of distinguishing between resonances belonging to different isotopes. The intensities of the high-energy primary γ rays, on the other hand, are subject to no statistical smoothing, and the strengths of primary transitions to a given final state may be expected to be strongly dependent not only on the spin but also on other individual properties of the resonances. These γ rays are therefore found to be useful not only for spin identification but also for studying the fluctuations of radiation widths. They are also used occasionally for isotopic identification of resonances; for example, they may be used to pick out resonances associated with the product nucleus with the greatest neutron separation energy.

1. *Isotopic identification.*—Isotopic identifications of resonances have been made in neodymium by Draper & Hickok (155), in erbium by Fenstermacher *et al.* (156), in platinum by Bird & Waters (141), and in mercury by Carpenter & Bollinger (57). In some cases, the assignments may be compared to those deduced from transmission measurements using separated isotopes. For example, in Nd and Pt several resonances have been identified in transmission measurements by Stolovy & Harvey (93), and the isotopic assignments in mercury were verified in a similar manner by Carpenter & Bollinger (57). The excellent agreement of the isotopic assignments by the two methods attests to the reliability of the γ -ray methods.

2. *Fluctuations of primary gamma-ray partial radiation widths.*—The determination of the distribution of partial radiation widths of γ rays emitted in transitions to the same final state from different resonances of the same spin is of interest not only theoretically, for the light it may cast on the problem of radiative transitions from complicated initial states, but also for the "practical" purpose of determining the spins of resonances. It is well established that, in general, radiation widths of primary neutron capture γ rays of a given multipolarity conform to broad distributions ranging over several orders of magnitude (Sect. IIB1). It is also known from charged particle reactions in light elements that partial radiation widths for transitions to a given final state from highly excited (unbound) states of the same spin fluctuate by at least an order of magnitude [see Table XV in the review by Lane (157)]. It is of interest to determine whether large fluctuations of the latter type also occur in neutron resonances in heavy nuclei or whether some

averaging process, perhaps associated with the complex nature of such resonances, operates to narrow the distribution. It is customary to measure such fluctuations by assuming that the partial widths follow a χ^2 distribution with ν degrees of freedom [Porter & Thomas (158)]. This distribution for variable x is

$$P(x, \rho)dx = \Gamma(\rho)^{-1}(\rho x)^{\rho-1}e^{-\rho x}\rho dx \quad 25.$$

where $\nu = 2\rho$ and $\Gamma(\rho)$ is the gamma function. Quantitatively, then, the question is whether the partial radiation widths follow a one-channel distribution ($\nu = 1$), as do the neutron widths, a many-channel distribution as do the total γ -ray widths ($\nu > 50$ for $U^{238} + n$), or something in between as do the fission widths $2 < \nu < 4$ [see Harvey (159)].

Present-day detection techniques using NaI scintillators preclude the possibility of studying the intensities of any primary γ rays except those feeding the ground state and one or two of the low-lying excited states. Even for these, the task of obtaining reliable intensity data is very difficult. Not only are the problems of low counting rate and relatively high background formidable, but also the poor inherent resolution necessitates the use of troublesome unfolding procedures to extract individual line intensities from the combined spectrum. In addition, the high-energy tails of many intense low-energy lines may make a significant contribution in the energy region of interest, and ultimately the intensity of the sum peak caused by simultaneous detection in one detector of two cascading γ rays imposes a lower limit on the intensities that can be measured. The quantity usually considered to be proportional to the partial radiation width is, in these experiments, the ratio of the number of counts in an energy interval which includes the γ -ray total absorption peak to the total number of counts within a wide energy interval which includes most of the spectrum. It is assumed that the counting rate from the latter channel is proportional to the total number of captures and that the total radiation width remains constant from resonance to resonance. The error in this method of estimating relative partial radiation widths is of the order of the variations of \bar{N} from resonance to resonance which have been found by Springer & Draper (123) to be usually less than 25 per cent.

Various attempts to determine ν (Eq. 25) have been reported. Wide fluctuations of an order of magnitude or more have been observed for the intensities of individual high-energy γ rays in product nuclei W^{184} (140, 146, 160), Pt^{196} (140, 141, 150, 160, 161), and Hg^{200} (140, 142, 161). Bollinger and co-workers estimate that there is an 80 per cent probability that ν falls in the range $0.7 \leq \nu \leq 2.0$ from their Pt^{196} results and in the range $0.3 \leq \nu \leq 1.9$ from their Hg^{200} results (161). Chrien and co-workers estimate $\nu \approx 1$ for single γ rays in Pt (150). Contrasting with these results is the observation by Hughes *et al.* (162) of small fluctuations of the intensity of a γ -ray peak at 4.06 Mev over ten resonances in $U^{238} + n$. Unfortunately little is known about

the origin of the 4.06-Mev radiation in the U^{239} decay scheme or about the number of γ rays of about the same energy that may be present in the spectrum. Thermal-neutron capture measurements at 1 per cent resolution (100) show that, in addition to the strong apparently monoenergetic line at 4.06 Mev, at least one weak γ ray may be present within the 240-kev resolution used by Hughes *et al.*, and it seems likely that others may also be present. That a large number of γ rays may not be necessary to give the observed effect is suggested by recent observations of Chrien *et al.* (150). They found that when the intensities of the three γ rays feeding the ground state and first two excited states in Pt^{196} are summed, the fluctuations of the total intensity correspond to a ν of ~ 11 and not 3 as expected if the transitions were independent and each followed a χ^2 distribution with $\nu = 1$. The possibility that the W^{184} γ rays may show the same effect was pointed out by Bollinger *et al.* (146). Correlations of this sort could account for the U^{239} results, but at the same time would call into question the applicability of the χ^2 distribution, since a basic assumption justifying the use of this distribution is that the partial widths be independent (158).

(3) *Spin assignments.*—It is clear that the large fluctuations in $\Gamma_{\gamma'}$ preclude any universal method of distinguishing between alternative J_c values based on the observation of primary γ -ray intensities alone. However, a critical test is still possible in special cases where a transition is allowed for a resonance with spin J_1 but forbidden for the alternative spin J_2 . Observation of this "critical" γ ray then definitely establishes the spin as J_1 although failure to observe it does not prove that the spin is J_2 . These conditions apply ideally when the final state has spin 0 and the resonances are either 0 or 1, although situations in which the γ ray is $M2$ for one spin and $E1$ for the other are, for all practical purposes, equally reliable. Both conditions apply when the target nucleus is $\frac{1}{2}^-$. In the first experiment of this type [Landon & Rae (139)] it was shown that the 34-ev resonance in $Hg^{199} + n$ decayed by the emission of a ground state γ ray and therefore could be assigned $J_c = 1$. In more recent experiments similar measurements have been made at other resonances in Hg^{199} and in other nuclei with the same spin and parity. The most extensive work has been that of the Saclay group who have identified over two dozen $J_c = 1$ resonances in both $W^{183} + n$ and $Pt^{196} + n$ (143, 144).

Two coincidence methods have been investigated by the Argonne group in an effort to improve the resolution for detecting individual primary transitions and to find a reliable method for making J_c assignments for a wider range of target spins. In $Mn^{55} + n$ the capture spectra at thermal energies and at three resonances of known spin at 337, 1080, and 2360 ev were studied by observing the low-energy γ rays in one detector in coincidence with γ rays of high energy accepted by an energy channel associated with a second detector (147). It was found that the coincidence intensity ratios for the low-energy γ rays were markedly different for the two 3^- resonances at 1080 and

2360 ev and that, contrary to expectations, the thermal neutron capture γ -ray spectrum was not the same as that of the nearest 2^- resonance at 337 ev. The second coincidence method (163, 164) consisted of measuring the combined counting rate of all two-step cascades whose total energy was equal to the binding energy. This quantity, when normalized for the resonance cross section, may be expected to depend on the spin of the initial state. Measurements with $\text{Cd}^{111}+n$, $\text{Cd}^{113}+n$, and $\text{Hg}^{199}+n$ resonances confirm that large differences in the coincidence rate occur from resonance to resonance and that in $\text{Hg}^{199}+n$ the differences are correlated, as expected, with the known resonance spins.

TABLE IV
RESONANCE SPINS DETERMINED BY CAPTURE γ -RAY METHODS

Target	Resonance ev	<i>J</i> by γ -ray methods						<i>J</i> by other methods (166)
		Argonne (146)	Brookhaven (150, 165)	Harwell (141)	Saclay (144)	USSR (145)	Yale (160)	
Pt^{195}	11.8	1	1			1		1
	19.4	1	1			[0]	[1]	1
	68.9	1	1	1	1	1		1
	113.0		1	1*	[1]			1
	120.5		1	1*	1			1
	140		1	1*	1			1
	151		[1]	—	1			1
	155		[1, 0]	—	1			[0]
	189		1	1*	1			
	203		0	[0]				
	223		1	1*	1			
	252		[0]	—	[1]			
		Argonne (57)	Brookhaven (152)	Harwell (139, 140, 142, 153)				(57, 103, 142)
Hg^{199}	-2	0		[0]				0
	34	1	1	1				[1]
	130	0		[0]				[0]
	173	1		1				1

* These spin assignments are not actually stated in (141) but may be inferred from the γ -ray intensity information presented.

The results of various laboratories for the spins of resonances in $\text{Pt}^{195}+n$ and $\text{Hg}^{199}+n$ are compared in Table IV. The lists are limited to a few of the lower-energy resonances in each nucleus where the results of more than one group are available. Doubtful assignments are shown in brackets. Wherever possible, spin determinations by other methods are also shown. The spin determinations by the γ -ray methods are for the most part in good agreement with each other and with the other methods. However, as expected, the re-

sults reflect an uncertainty in discriminating between levels with spin 0 and levels with spin 1 but which emit abnormally weak ground state γ rays.

Investigations of the strong low-energy γ rays and their possible application in determining the resonance spin have been carried out largely by the Yale group (138, 154, 156). Others reporting similar measurements are Bird *et al.* (142) and Vogt (167). Significant fluctuations have been found in $\text{In}^{115}+n$ (154, 167) and in $\text{Hf}^{177}+n$ (156). The extent to which such fluctuations reflect the spins of the capturing resonances is not well established since not all of the resonances for which fluctuations have been observed have known spins. A positive correlation does appear to be present in the γ rays from the 1.5-, 3.9-, and 9.1-ev resonances in $\text{In}^{115}+n$ (167).

The question of the spin dependence of the isomeric capture cross section ratio and the multiplicity \bar{N} is obviously closely related to that of the spin dependence of the intensities of low-energy γ rays. Both the isotopic capture cross-section ratio (168) and \bar{N} (123) have been measured for the In^{115} resonances already mentioned; and the fluctuations, like those of the intensities of the low-energy γ rays, are found to be correlated with the known resonance spins (169). A similar correlation of isotopic capture ratio (170) and spin is observed in $\text{Eu}^{151}+n$ (171, see also 116); the accuracy of the measurements of \bar{N} (123) is not, however, great enough to show whether or not this quantity also varies for the resonances concerned. In $\text{Hf}^{177}+n$, differences in the intensities of low-energy γ rays (156) do not appear to be accompanied by very large differences of \bar{N} . In sum, the available experimental evidence seems to support the belief that these various quantities may provide reliable methods of determining the resonance spin.

The total radiation widths in some nuclei also show significant fluctuations from resonance to resonance, and this raises the possibility that Γ_γ may provide a means of identifying J_c . However, as pointed out by Brink (124), assuming a $(2J+1)$ statistical spin dependence of the level density,⁶ Equation 24 should be independent of spin. Fluctuations of Γ_γ have been observed in neutron capture in In^{115} and Eu^{151} by Landon & Sailor (172), in Hf^{177} by Igo & Sailor (173), in Au^{197} by Desjardins *et al.* (126), and in Hg^{201} by Carpenter & Bollinger (57) and by Bolotin *et al.* (174). In both In^{115} and Eu^{151} the fluctuations of Γ_γ appear to be correlated with J_c . On the other hand, in silver the values of Γ_γ for levels with J_c equal to 0 and 1 are the same to an accuracy of 10 per cent [Rae *et al.* (128)], and in Au^{197} resonances of the same J_c have Γ_γ differing by almost a factor of 2. In Hg^{201} where, unfortunately, only two of seven resonances studied have known spins, fluctuations of Γ_γ of the order of a factor of 2 are also observed (57). Although the Hg^{201} data are consistent with the possibility of a spin dependence, the fluctuations are of such strength that there appears to be no obvious division of the values of Γ_γ into two distinct groups. Moreover, the fluctuations may be accounted for entirely by fluctuations of Γ_γ' of a few individual primary γ

⁶ This spin dependence is a good approximation to Equation 6 for $\sigma > 3$.

rays (57). Finally, we note that theoretical analysis by Vogt (175) of the neutron cross section in U^{235} shows that the first two resonances have the same spin and Γ_γ differing by almost a factor of 2. The present evidence, therefore, indicates that the total radiation width may not provide a reliable method for determining the resonance spin.

The above pattern is not inconsistent with the statistical model. The relative intensities of transitions between low-energy states, the isotopic capture cross-section ratios, the multiplicity, and the intensities of two-step cascades are similar in that they all depend on the spin difference between J_c and the J of a particular level or levels such as the ground state or other low-lying states and are all statistical quantities depending on an averaging process involving many cascade routes. In the limit of a perfectly "statistical" decay scheme (constant average reduced radiative width and smoothly varying level distribution with high level density), each of these quantities would remain constant for levels of the same J_c but would be expected to be somewhat different for levels with different J_c . For less than perfectly statistical level systems, where transitions to a few favored levels may dominate the cascade, the above quantities will reflect the random fluctuations of Γ_γ' for these few strong transitions. Depending on the prominence of individual primary γ rays, these fluctuations may be large enough to obscure the J_c dependence. On the other hand, following Brink (124), Γ_γ must be constant and independent of J_c in the completely statistical level system. For less than perfectly statistical level systems Γ_γ will also fluctuate in a manner depending on the contributing partial widths. In the special case of a "non-statistical" decay scheme, wherein the level spacing is low and one or two critical γ rays are predominant for $J_c = I \pm \frac{1}{2}$ but spin forbidden for the alternative value of J_c , all of the quantities considered above, including Γ_γ , may show a dependence on J_c which reflects that of the critical γ rays. These considerations indicated that the low-energy γ -ray intensities, the intensities of two-step cascades, the multiplicity, or the isomeric cross-section ratio in very complex spectra should provide a reliable index for J_c , provided it can be shown to be improbable that random fluctuations of the Γ_γ' could cause the fluctuations observed. It may be possible to deduce this from examinations of the primary spectrum at each resonance. One is also led to believe that the total radiation width does not, in general, provide a trustworthy method of determining J_c and, at best, can provide no better means of spin discrimination than could be obtained from observing the intensities of critical primary γ rays (if any) in the same spectrum.

IV. CAPTURE MECHANISM

Several phenomena suggest that neutron capture does not completely conform to the predictions of the strong interaction or "black nucleus" model. On the basis of this model no correlations between the final state particle configuration and the transition probability for γ rays of given multipolarity are predicted. That contributions to the capture cross section

from external parts of the wave function may be significant was recognized by Breit & Yost (176), and a mechanism of this sort has been invoked by Thomas (177, 178) and Griffiths (179) to account for anomalous capture cross sections in light elements. An attempt will be made here to summarize the evidence against complete adherence to the black nucleus picture for neutron capture and briefly sketch the conclusions of the recent, detailed theoretical description of low-energy neutron capture given by Lane & Lynn (180, 181).

One piece of evidence against strict adherence to the black nucleus picture has been mentioned several times above, viz., the discrepancy between the amount of radiation observed experimentally in the high-energy spectrum of certain nuclei and the theoretical predictions. This enhancement of the high-energy spectrum is very apparent in the nuclei $170 < A < 208$, where a connection with the presence of the $3p$ shell-model orbital in states near the ground state has been recognized (4, 94). A similar predominance of isolated γ rays feeding states with a large p -wave admixture is very obvious from inspection of the spectra of nuclei in the mass range $24 < A < 70$ (94) although, as we have seen, there is no evidence in Figure 3 for unusually large transition probabilities for these γ rays. The involvement of the p -wave neutron orbital in the region $170 < A < 208$ is further indicated because the energy of the group of strong γ rays varies with A in a manner which corresponds to the change of binding energy of the p state in the nuclear well [Groshev *et al.* (4)]. A similar effect is noticeable for $A < 70$ (180). It is also relevant, as pointed out by Groshev & Demidov (182), that there is a superficial similarity between the spectra of neighboring even-odd and odd-odd isotopes in the region $A < 60$ insofar as the one or two anomalously strong γ rays in the even-odd nucleus are matched by a group of outstanding γ rays in the odd-odd nucleus. This effect suggests that the neutron p state in the odd-odd nucleus is shared among the multiplet states formed by coupling the odd neutron and proton.

A dependence of the γ -ray transition probability on the shell-model configuration of the final state is also apparent from a comparison of competing transitions in certain nuclei. For example, Zaretskii (183) has shown that the relative probabilities for primary transitions to the $2p_{1/2}$ and $2p_{3/2}$ neutron levels in Si^{28} , S^{32} , Ca^{41} , and Ni^{59} may be calculated with satisfactory accuracy using a single-particle model. As another example, it has been pointed out by Lane & Lynn (181) that the $E1$ γ rays in K^{40} feeding the ground state multiplet $[(d_{3/2})^{-1}, f_{7/2}]$ have matrix elements almost an order of magnitude smaller than those feeding the excited state multiplet $[(d_{3/2})^{-1}, p_{3/2}]$. A similar inhibition for transitions which involve a single-particle $s \rightarrow f$ neutron jump would explain the relative weakness of the ground state transitions in K^{42} and Sc^{46} (3). In Pb^{207} , the capture transition of the $p_{1/2}$ ground state is at least 25 times (91) stronger than the transition of the $\frac{3}{2}^-$ level at 0.87 Mev which presumably has a configuration that cannot be formed by a

single-particle transition from the initial state formed by adding an *s*-wave neutron to the Pb^{206} core (181, 184, 185).

Strong evidence for single-particle effects in neutron capture is also provided by the similarity between the intensities of neutron capture γ rays and proton groups in the corresponding (*d*, *p*) stripping reaction. This similarity was noticed in early investigations of both reactions in Si^{29} , S^{32} (186), P^{32} (187), Al^{28} (188), and Ca^{41} (102). Later experimental evidence has been thoroughly reviewed by Groshev *et al.* (4). An explanation of this effect has been suggested by Lane & Wilkinson (189) who pointed out that the matrix elements of both reactions contain a parentage overlap factor which, in the extreme case of a unique (target nucleus) parent for the radiating state in the (*n*, γ) reaction, could give rise to a correlation between the intensities of corresponding γ rays and proton groups. The unique parent concept is of course not consistent with the usual compound nucleus picture. This hypothesis has been examined quantitatively by Bockelman (190) with the aid of data from the mass range $A \leq 41$. In this investigation certain quantities *r*, proportional to the quotient $\gamma_{n\gamma}^2/\gamma_{dp}^2$ of matrix elements for the two reactions, were computed from the relative reduced widths in the (*d*, *p*) reaction and the γ -ray absolute intensities in the (*n*, γ) reaction. Ratios of the quantities *r* for transitions involving *E1* radiation (or pure *M1* radiation) were found to be confined within rather narrow limits predicted by the theory for the product nuclei Li^7 , Mg^{25} , Al^{28} , Si^{29} , S^{32} , and Ca^{41} as well as in a number of other cases for which the test was, however, rather less definitive. In B^{11} , C^{13} , and N^{15} the rule was not obeyed for reasons which may be connected with capture in specific resonances (190).

Various calculations to explain some of the neutron capture γ -ray intensity anomalies have been carried out by different authors (178, 184, 190). However, the most complete description of the capture mechanism was given recently by Lane & Lynn (180, 181) and in the following we shall devote our attention largely to their findings. These authors began with basic dispersion theory and derived a formulation for the complete capture cross section in the resonance region in terms of three parts: (a) the familiar compound nucleus (resonance internal) part, (b) a contribution from capture in the entrance channel caused by modifications in the wave function produced by nearby resonances, and (c) the contribution from hard-sphere potential scattering together with its modification by the "direct" capture induced by distant resonances. Both the potential and "channel resonance" cross sections depend on the strength of single-particle *p*-wave configurations in the final states and can give rise to strong radiative transitions when the *p*-wave admixture is large. Moreover, Lane & Lynn established the important result that even the resonance internal part may give rise to enhanced transitions to pure single-particle *p* states if the initial-state neutron reduced width is large. It is necessary to assume a nuclear model in order to estimate the potential capture cross section and thus arrive at realistic estimates of the rela-

tive importance of the various cross sections for elements of different A . Lane & Lynn based their calculations on two models: (a) the strong coupling model with the assumption of relatively pure single-particle final states and (b) the intermediate coupling model with a diffuse complex potential (ignoring spin-orbit coupling) with the assumption of a pure single-neutron p state for the final state. The calculated cross sections were compared with the fraction of the observed capture cross section which corresponds to the emission of γ rays of anomalously high intensity in the mass regions $A < 70$ and $170 < A < 208$ where p states occur near the ground state. It was found that potential capture could make a significant contribution to the anomalous cross section in lead, and also for some nuclei above $A = 60$ and below $A = 45$ for which this cross section amounted to a few tenths of a barn. In some of the lighter nuclei and particularly between Sc^{46} and Co^{59} , where the complex potential gave rise to a minimum in the potential cross section, the "channel resonance" cross section was sufficient to account for the anomalous intensity. For most of the nuclei in the range $170 < A < 208$ the enhanced transitions could not be accounted for by either potential or channel resonance capture. On the other hand, the mean reduced radiation width for a transition to a pure p state from a resonance with a large neutron-reduced width was found to be comparable to the observed values in Figure 3 in the region $140 < A < 180$ from the complex potential-well calculation. A plot of the reduced radiation widths as a function of mass number reached a maximum near mass number 160. A similar calculation showed that exceptionally strong γ rays feeding final p -wave states could follow capture in resonances with large neutron widths in the region $40 < A < 70$.

The conclusion of Lane & Lynn that an appreciable part of resonance capture occurs through coupling a single s -wave neutron to a number of low-lying excited states of the target, in the initial state, and coupling of a single p -wave neutron to the same target states in the final state of the compound nucleus appears to account at least qualitatively for many of the observed intensity anomalies. The same mechanism was suggested by Cameron (98) to explain the maximum he found in the total radiation width for nuclei near mass number 160, after correction for level density effects had been made. Such an increased total width would be expected to coincide with the maximum in the partial radiative width for transitions to states with a large p -wave admixture following resonance capture in these nuclei. As pointed out by Bartholomew (106), a similar explanation may account for the large differences in intensity, of the order of a factor of 100, between competing $E1$ transitions to low-lying levels for a number of nuclei in the same mass region, viz., Nd^{144} , Gd^{156} , Gd^{158} , Hf^{178} , and W^{183} . It seems possible that the failure of γ rays in the region $A < 70$ to show k_{E1} values as large as those of heavier nuclei (Fig. 3) may be connected with the fact that the former may be produced by potential capture while the latter are a resonance phenomenon. On the other hand, there are some intensity anomalies which do not appear to fall within the framework of the Lane-Lynn theory. In par-

ticular, the exceptionally large values of k_{E1} for γ rays in nuclei near mass numbers 90 (and 240) in Figure 3 cannot be explained by the complex potential-well calculation since these nuclei occur at minima in the s -wave strength function where enhanced radiation widths are not predicted.

The implications of these anomalous capture effects for the question of the fluctuations of the intensities of primary γ rays from resonance to resonance are not entirely clear. However, the partial width for an "enhanced" transition to a single-particle p state following resonance capture as given in the Lane-Lynn theory is proportional to the reduced neutron width of the resonance, and therefore the radiation widths for such γ rays would be expected to conform to the χ^2 distribution with $\nu = 1$ obeyed by the neutron widths. Much remains to be done in investigating anomalous capture effects as a function of neutron energy both at resonances and between resonances. A beginning in this direction has been made at high neutron energies by Bergqvist & Starfeldt (137).

ACKNOWLEDGMENT

The author is deeply indebted to B. N. Brockhouse, A. G. W. Cameron, R. E. Chrien, L. G. Elliott, J. W. Knowles, and E. Vogt for many helpful suggestions concerning the contents of this review and to J. Vervier for making the results of his measurements available prior to publication.

LITERATURE CITED

1. Kinsey, B. B., *Beta and Gamma Ray Spectroscopy* (Siegbahn, K., Ed., Interscience Publishers, New York, N. Y., 959 pp., 1955)
2. Kinsey, B. B., *Handbuch der Physik, XL* (Springer-Verlag, Berlin, Germany, 553 pp., 1957)
3. Bartholomew, G. A., *Nuclear Spectroscopy, Part A*, 304 (Ajzenberg-Selove, F., Ed., Academic Press, Inc., New York, N. Y., 621 pp., 1960)
4. Groshev, L. V., Demidov, A. M., Lutsenko, V. N., and Pelekhov, V. I., *Proc. Intern. Conf. Peaceful Uses Atomic Energy*, 2nd, Geneva, 15, 138 (1958)
5. Mittelman, P. S., and Liedtke, R. A., *Nucleonics*, 31, 537 (1953)
6. Bartholomew, G. A., and Higgs, L. A., *Compilation of Thermal Neutron Capture Gamma Rays* (Atomic Energy of Can. Ltd., Chalk River Project, Rept. No. A.E.C.L., 669, 1958)
7. Groshev, L. V., Demidov, A. M., Lutsenko, V. N., and Pelekhov, V. I., *Atlas of γ -Ray Spectra from Radiative Capture of Thermal Neutrons*, 198 pp. (Principal Commission on Utilization of Atomic Energy, USSR, Council of Ministers, Moscow, 1958; Engl. ed., Pergamon Press, London, 1959)
8. Reardon, W. A., Krone, R. W., and Stump, R., *Phys. Rev.*, 91, 334 (1953)
9. Pringle, R. W., Taylor, H. W., and Roulston, K. I., *Phys. Rev.*, 87, 1016 (1952)
10. Draper, J. E., *Phys. Rev.*, 114, 268 (1959)
11. Bäckström, G., *Nuclear Instr. & Methods*, 4, 5 (1959)
12. Kubitschek, H. E., and Dancoff, S. M., *Phys. Rev.*, 76, 531 (1949)
13. Hamermesh, B., *Phys. Rev.*, 80, 415 (1950)
14. Wilson, R., *Phys. Rev.*, 80, 90 (1950)
15. Hamermesh, B., and Hummel, V., *Phys. Rev.*, 88, 916 (1952)
16. Estulin, I. V., Kalinkin, L. F., and Melioranskii, A. S., *Nuclear Phys.*, 4, 91 (1957)
17. Skliarevskii, V. V., Stepanov, E. P., and Obiniakov, B. A., *Atomnaya Energ.*, 4, 22 (1958); *Soviet J. Atomic Energy*, 4, 19 (1958)
18. Urbanec, J., Kajfosz, J., and Kopecký, J., *Czechoslov. J. Phys.*, 9, 544 (1959); 10, 275 (1960)
19. Dragomirescu, D., Mateiciuc, V., and Cristu, M., *Intern. Atomic Energy Agency Symposium on Pile Neutron Research in Physics, Vienna*, Paper PNR/8 (1960)
20. Kardon, B., Kiss, D., Lovas, I., and Zamori, Z., *Intern. Atomic Energy Agency Symposium on Pile Neutron Research in Physics, Vienna*, Paper PNR/24 (1960)
21. Patronis, E. T., and Marshak, H., *Phys. Rev.*, 115, 1287 (1959)
22. Braid, T. H., *Phys. Rev.*, 102, 1109 (1956)
23. Reier, M., and Shamos, M. H., *Phys. Rev.*, 100, 1302 (1955)
24. Segel, R. E., *Phys. Rev.*, 111, 1620 (1958)
25. Treado, P. A., and Chagnon, P. R., *Bull. Am. Phys. Soc.* [II], 5, 369 (1960)
26. Monahan, J., Raboy, S., Ringo, G. R., and Trail, C. C., *Intern. Atomic Energy Agency Symposium on Pile Neutron Research in Physics, Vienna*, Paper PNR/40 (1960)
27. Draper, J. E., and Bostrom, C. O., *Bull. Am. Phys. Soc.* [II], 5, 17 (1960); Draper, J. E. (Private communication, 1960)
28. Bartholomew, G. A., Knowles, J. W., and Lee Whiting, G. E., *Repts. Progr. in Phys.* 23, 453 (1960)
29. Walker, R. L., and McDaniel, B. D., *Phys. Rev.*, 74, 315 (1948)
30. Balzer, R., Knoepfel, H., Stoll, H., and Wölfl, W., *Helv. Phys. Acta*, 31, 328 (1958)
31. Knoepfel, H., Scherrer, P., and Stoll, P., *Z. Physik*, 156, 293 (1959)
32. Burgov, N. A., and Danilian, G. V., *Izvest. Akad. Nauk SSSR, Ser. Fiz.*, 20, 941 (1956); *Bull. Acad. Sci. USSR, Phys. Ser.*, 20, 852 (1957)
33. Kinsey, B. B., and Bartholomew, G. A., *Can. J. Phys.*, 31, 537 (1953)
34. Bartholomew, G. A., Campion, P. J., and Robinson, K., *Can. J. Phys.*, 38, 194 (1960)
35. Motz, H. T., *Phys. Rev.*, 104, 1353 (1956)
36. Groshev, L. V., Adyasevich, B. P., and Demidov, A. M., *Proc. Intern. Conf. Peaceful Uses Atomic Energy, Geneva*, 1955, 2, 39 (1955)
37. Groshev, L. V., Gavrilov, B. I., and Demidov, A. M., *Atomnaya Energ.*, 6, 281 (1960); *Soviet J. Atomic Energy*, 6, 170 (1960)
38. Groshev, L. V., Demidov, A. M.,

- Lutsenko, V. N., and Malov, A. F., *Izvest. Akad. Nauk SSSR*, **24**, 791 (1960)
39. Motz, H. T., and Carter, R. E., *Proc. Intern. Conf. Nuclidic Masses, Hamilton, 1960*, 299 (Univ. Toronto Press, Toronto, Can., 539 pp., 1960)
 40. Knowles, J. W., Manning, G., Bartholomew, G. A., and Campion, P. J., *Nuclear Phys.* (To be published)
 41. Rose, D., Ostrander, H., and Hamermesh, B., *Rev. Sci. Instr.*, **28**, 233 (1957)
 42. Chupp, E. L., DuMond, J. W. M., and Mark, H., *Rev. Sci. Instr.*, **29**, 1153 (1958)
 43. Kazi, A. H., Rasmussen, N. C., and Mark, H., *Rev. Sci. Instr.*, **31**, 983 (1960)
 44. Knowles, J. W., *Can. J. Phys.*, **37**, 203 (1959)
 45. Hibdon, C. T., and Muehlhause, C. O., *Phys. Rev.*, **88**, 943 (1952)
 46. Church, E. L., and Goldhaber, M., *Phys. Rev.*, **95**, 626 (1954)
 47. Bell, R. E., and Elliott, L. G., *Phys. Rev.*, **79**, 282 (1950)
 48. Groshev, L. V., Demidov, A. M., and Naidenov, V. A., *Izvest. Akad. Nauk SSSR, Ser. Fiz.*, **21**, 1619 (1957); *Bull. Acad. Sci. USSR, Phys. Ser. (Engl. transl.)*, **21**, 1606 (1958)
 49. Groshev, L. V., *Proc. Intern. Conf. Nuclear Structure, Kingston, Canada, 1960*, 568 (Bromley, D. A., and Vogt, E. W., Eds., Univ. Toronto Press, Toronto, Can., 990 pp., 1960)
 50. Maier-Leibnitz, H., *Intern. Atomic Energy Agency Symposium on Pile Neutron Research in Physics, Vienna, Paper PNR/15* (1960)
 51. Bartholomew, G. A., *Can. J. Phys.*, **38**, 871 (1960)
 52. Recksiedler, A. L., and Hamermesh, B., *Phys. Rev.*, **96**, 109 (1954)
 53. Trumpy, G., *Joint Establishment for Nuclear Energy Research, Rept. J.E.N.E.R., No. 13*, 81 pp. (1957)
 54. Manning, G., and Bartholomew, G. A., *Phys. Rev.*, **115**, 401 (1959)
 55. Melioranskii, A. S., Éstulin, I. V., Kalinkin, L. F., and Kudinov, B. S., *Zhur. Ekspl. i Teoret. Fiz.*, **38**, 758 (1960); *Soviet Phys JETP*, **11**, 548 (1960)
 56. Bell, R. E., *Ann. Rev. Nuclear Sci.*, **4**, 93 (1954)
 57. Carpenter, R. T., and Bollinger, L. M., *Nuclear Phys.*, **21**, 66 (1960)
 58. Sample, J. T., Neilson, G. C., Chadwick, G. B., and Warren, J. B., *Can. J. Phys.*, **33**, 828 (1955)
 59. Segel, R. E., *Phys. Rev.*, **113**, 844 (1959)
 60. Segel, R. E., and Kane, W. R., *Bull. Am. Phys. Soc. [II]*, **5**, 240 (1960)
 61. Hoogenboom, A. M., *Nuclear Instr.*, **3**, 57 (1958)
 62. Schwäger, J. E., *Univ. Calif., Lawrence Rad. Lab. Rept. UCRL 5975* (Livermore, Calif., 32 pp., 1960)
 63. Draper, J. E., and Fleischer, A. A., *Nuclear Instr.*, **9**, 67 (1960)
 64. Schwäger, J. E., *Phys. Rev.*, **121**, 562 (1961); **121**, 569 (1961)
 65. Draper, J. E., and Fleischer, A. A., *Bull. Am. Phys. Soc. [II]*, **4**, 476 (1959); Draper, J. E. (Private communication)
 66. Vervier, J. F., *Bull. Am. Phys. Soc. [II]*, **4**, 476 (1959)
 67. Fettweis, P., and Vervier, J., *Intern. Atomic Energy Agency Symposium on Pile Neutron Research in Physics, Vienna, Paper PNR/26* (1960)
 68. Burmistrov, V. R., *Izvest. Akad. Nauk SSSR, Ser. Fiz.*, **23**, 898 (1959); *Bull. Acad. Sci. USSR, Phys. Ser. (Engl. transl.)*, **23**, 886 (1959)
 69. D'Angelo, N., *Phys. Rev.*, **117**, 510 (1960)
 70. Halpern, O., *Phys. Rev.*, **82**, 753 (1951)
 71. Biedenharn, L. C., Rose, M. E., and Arfken, G. B., *Phys. Rev.*, **83**, 683 (1951)
 72. Trumpy, G., *Nuclear Phys.*, **2**, 664 (1956)
 73. Vervier, J. F., *Nuclear Phys.* (To be published)
 74. Grechukhin, D. P., *J. Exptl. Theoret. Phys. (USSR)*, **38**, 621 (1960); *Soviet Phys. JETP*, **11**, 446 (1960)
 75. Bloch, C., *Phys. Rev.*, **93**, 1094 (1954)
 76. Haas, R., Leipuner, L. B., and Adair, R. K., *Phys. Rev.*, **116**, 1221 (1959)
 77. Roberts, L. D., and Dobbs, J. W. T., *Ann. Rev. Nuclear Sci.*, **11**, 175 (1961)
 78. Devons, S., *Nuclear Spectroscopy, Part A* (Ajzenberg-Selove, F., Ed., Academic Press, New York, N. Y., 621 pp., 1960)
 79. Reibel, K., and Mann, A. K., *Phys. Rev.*, **118**, 701 (1960)
 80. Van Patter, D. M., and Whaling, W., *Revs. Mod. Phys.*, **26**, 402 (1954); **29**, 757 (1957)
 81. Gove, N. B., *1959 Nuclear Data Tables* (Way, K., Ed., Nuclear Data Project, Natl. Acad. Sci.—Natl. Research Council, US Govt. Printing Office, Washington, D. C., 1959)

82. Everling, F., König, L. A., Mattauach, J. H. E., and Wapstra, A. H., *Nuclear Phys.*, **18**, 529 (1960)
83. Jewell, R. W., and John, W., *Univ. Calif., Lawrence Rad. Lab. Rept. UCRL 6095* (Livermore, Calif., 6 pp., 1960)
84. Raboy, S., and Trail, C., *Bull. Am. Phys. Soc.* [II], **4**, 218 (1959)
85. Motz, H. T., Carter, R. E., and Fisher, P. C., *Bull. Am. Phys. Soc.* [II], **4**, 477 (1959); Motz, H. T. (Private communication, 1960)
86. Knowles, J. W. (Private communication)
87. Mobley, R. C., and Laubenstein, R. A., *Phys. Rev.*, **80**, 309 (1950)
88. Bartholomew, G. A., and Campion, P. J., *Can. J. Phys.*, **35**, 1347 (1957)
89. Bartholomew, G. A., and Campion, P. J. (To be published)
90. Bartholomew, G. A., and Kinsey, B. B., *Phys. Rev.*, **89**, 386 (1953); **93**, 1434 (1954)
91. Journey, E. T., Carter, R. E., and Motz, H. T., *Bull. Am. Phys. Soc.* [II], **6**, 62 (1961)
92. Levin, J. S., and Hughes, D. J., *Phys. Rev.*, **101**, 1328 (1956)
93. Stolovy, A., and Harvey, J. A., *Phys. Rev.*, **108**, 353 (1957)
94. Kinsey, B. B., and Bartholomew, G. A., *Phys. Rev.*, **93**, 1260 (1954)
95. Bartholomew, G. A., Campion, P. J., Knowles, J. W., and Manning, G., *Proc. Intern. Conf. Neutron Interactions with the Nucleus, Columbia Univ., New York, 1957*, 252 (US Atomic Energy Comm., Tech. Inf. Serv., Oak Ridge, Tenn. *Rept. TID-7547*, 1957)
96. Blatt, J. M., and Weisskopf, V. F., *Theoretical Nuclear Physics* (John Wiley & Sons, New York, N. Y., 864 pp., 1952)
97. Hughes, D. J., and Schwartz, R. B., "Neutron Cross Sections," 2nd ed. *Brookhaven Natl. Lab. Rept. BNL 325* (1958); Hughes, D. J., Magurno, B. A., and Brussel, M. K., *Ibid.*, Suppl. 1 (1960)
98. Cameron, A. G. W., *Can. J. Phys.*, **37**, 322 (1959)
99. Cameron, A. G. W., *Can. J. Phys.*, **36**, 1040 (1958)
100. Campion, P. J., Knowles, J. W., Manning, G., and Bartholomew, G. A., *Can. J. Phys.*, **37**, 377 (1959)
101. Paris, C. H., Buechner, W. W., and Endt, P. M., *Phys. Rev.*, **100**, 1317 (1955)
102. Bockelman, C. K., and Buechner, W. W., *Phys. Rev.*, **107**, 1366 (1957)
103. Bartholomew, G. A., and Vervier, J. F., *Nuclear Phys.* (To be published)
104. Knowles, J. W., Manning, G., Bartholomew, G. A., and Campion, P. J., *Phys. Rev.*, **114**, 1065 (1959)
105. Bartholomew, G. A., Campion, P. J., Knowles, J. W., and Manning, G., *Nuclear Phys.*, **10**, 590 (1959)
106. Bartholomew, G. A., *Proc. Intern. Conf. Nuclear Structure, Kingston, Canada, 1960*, 573 (Bromley, D. A., and Vogt, E. W., Eds., Univ. Toronto Press, Toronto, Can., 990 pp., 1960)
107. Varshalovich, D. A., *J. Exptl. Theoret. Phys. (USSR)*, **38**, 172 (1960); *Soviet Phys. JETP*, **11**, 125 (1960)
108. Groshev, L. V., Demidov, A. M., and Lutsenko, V. N., *Izvest. Akad. Nauk SSSR, Ser. Fiz.*, **24**, 833 (1960)
109. Teplov, I. B., *Zhur. Eksptl. i Teoret. Fiz.*, **31**, 25 (1956); *Soviet Phys. JETP*, **4**, 31 (1957)
110. Wall, N. S., *Phys. Rev.*, **96**, 664 (1954); **96**, 670 (1954)
111. Jackson, J. D., and Kinsey, B. B., *Phys. Rev.*, **82**, 345 (1951)
112. Groshev, L. V., *Doklady Akad. Nauk SSSR*, **100**, 651 (1955) (Engl. transl., Assoc. Tech. Services, East Orange, N. J., *Rept. A.T.S. RJ-442*)
113. Groshev, L. V., Demidov, A. M., and Pelekhov, V. I., *Nuclear Phys.*, **16**, 645 (1960)
114. Hurwitz, H., and Bethe, H. A., *Phys. Rev.*, **81**, 898 (1951)
115. Groshev, L. V., Demidov, A. M., Lutsenko, V. N., and Pelekhov, V. I., *Proc. Intern. Conf. Neutron Interactions with the Nucleus, Columbia Univ., New York, 1957*, 261 (US Atomic Energy Comm. Tech. Inf. Serv., Oak Ridge, Tenn., *Rept. TID-7547*, 1957)
116. Huizenga, J. R., and Vandenbosch, R., *Phys. Rev.*, **120**, 1305 (1960)
117. Strutinski, V. M., Groshev, L. V., and Akimova, M. K., *Nuclear Phys.*, **16**, 657 (1960)
118. Newton, T. D., *Can. J. Phys.*, **34**, 804 (1956)
119. Bohr, A., Mottelson, B. R., and Pines, D., *Phys. Rev.*, **110**, 936 (1958)
120. Alaga, G., Alder, K., Bohr, A., and Mottelson, B. R., *Kgl. Danske Videnskab. Selskab, Mat.-fys. Medd.*, **29**, No. 9 (1955)

121. Ericson, T., *Proc. Intern. Conf. Nuclear Structure, Kingston, Canada, 1960*, 697 (Bromley, D. A., and Vogt, E. W., Eds., Univ. Toronto Press, Toronto, Can., 990 pp., 1960)
122. Muehlhause, C. O., *Phys. Rev.*, **79**, 277 (1950)
123. Springer, T. E., and Draper, J. E., *Bull. Am. Phys. Soc.* [II], **4**, 35 (1959); and to be published.
124. Brink, D. M., Doctoral thesis, Oxford Univ., 1955, quoted by Kinsey, B. B., *Handbuch der Physik*, **XL**, 316 (1957)
125. Rosen, J., Desjardins, J. S., Rainwater, L. J., and Havens, W. W., *Phys. Rev.*, **118**, 687 (1960)
126. Desjardins, J. S., Rosen, J., Havens, W. W., and Rainwater, L. J., *Phys. Rev.*, **120**, 2214 (1960)
127. Poole, M. J., and Wiblin, E. R., *Proc. Intern. Conf. Peaceful Uses Atomic Energy*, 2nd, Geneva, **14**, 266 (1958)
128. Rae, E. R., Collins, E. R., Kinsey, B. B., Lynn, J. E., and Wiblin, E. R., *Nuclear Phys.*, **5**, 89 (1958)
129. Diven, B. C., Terrell, J., and Hemmendinger, A., *Phys. Rev.*, **120**, 556 (1960)
130. Neiler, J. H., Gibbons, J. H., Macklin, R. L., and Miller, P. D., *Bull. Am. Phys. Soc.* [II], **4**, 474 (1959)
131. Block, R. C., *Bull. Am. Phys. Soc.* [II], **4**, 474 (1959)
132. Welsh, R. E., and Donahue, D. J., *Phys. Rev.*, **121**, 880 (1961)
133. Seth, K., *Proc. Intern. Conf. Nuclear Optical Model, Florida State Univ. Studies*, No. 32, 172 (Florida State Univ., Tallahassee, Fla., 1959)
134. Krueger, T. K., *Bull. Am. Phys. Soc.* [II], **6**, 94 (1961)
135. Saplakoglu, A., Bollinger, L. M., and Coté, R. E., *Phys. Rev.*, **109**, 1258 (1958)
136. Bollinger, L. M., Coté, R. E., Dahlberg, D. A., and Thomas, G. E., *Phys. Rev.*, **105**, 661 (1957)
137. Bergqvist, I., and Starfeldt, N., *Nuclear Phys.*, **22**, 513 (1961)
138. Fenstermacher, C. A., Bennett, R. G., Walters, A. E., Bockelman, C. K., and Schultz, H. L., *Phys. Rev.*, **107**, 1650 (1957)
139. Landon, H. H., and Rae, E. R., *Phys. Rev.*, **107**, 1333 (1957)
140. Bird, J. R., *Proc. Intern. Conf. Peaceful Uses Atomic Energy*, 2nd, Geneva, **14**, 294 (1958)
141. Bird, J. R., and Waters, J. R., *Nuclear Phys.*, **14**, 212 (1959)
142. Bird, J. R., Moxon, M. C., and Firk, F. W. K., *Nuclear Phys.*, **13**, 525 (1959)
143. Huynh, V. D., Julien, J., Corge, C., Netter, F., and Simic, J., *Compt. rend.*, **248**, 2330 (1959)
144. Corge, C., Huynh, V. D., Julien, J., Mirza, S., Netter, F., and Simic, J., *Compt. rend.*, **249**, 413 (1959)
145. Galinina, N. D., Shvartsman, B. F., and Diamant, A. Ya., *Zhur. Ekspl. i Teoret. Fiz.*, **38**, 1446 (1960); *Soviet Phys. JETP*, **11**, 1045 (1960)
146. Bollinger, L. M., Coté, R. E., and Kennett, T. J., *Phys. Rev. Letters*, **3**, 376 (1959)
147. Kennett, T. J., Bollinger, L. M., and Carpenter, R. T., *Phys. Rev. Letters*, **1**, 76 (1958)
148. Hughes, D. J., Brussel, M. K., Fox, J. D., and Zimmerman, R. L., *Phys. Rev. Letters*, **2**, 505 (1959)
149. Fox, J. D., Zimmerman, R. L., Hughes, D. J., Palevsky, H., Brussel, M. K., and Chrien, R. E., *Phys. Rev.*, **110**, 1472 (1958)
150. Chrien, R. E., Bolotin, H. H., and Palevsky, H., *Bull. Am. Phys. Soc.* [II], **6**, 69 (1961); Chrien, R. E. (Private communication, 1961)
151. Palevsky, H., and Fox, J., *Bull. Am. Phys. Soc.* [II], **4**, 472 (1959)
152. Brussel, M. K., and Fox, J. D., *Bull. Am. Phys. Soc.* [II], **4**, 34 (1959)
153. Rae, E. R., and Firk, F. W. K., *Nuclear Instr.*, **1**, 227 (1957)
154. Draper, J. E., Fenstermacher, C. A., and Schultz, H. L., *Phys. Rev.*, **111**, 906 (1958)
155. Draper, J. E., and Hickok, R. L., *Nuclear Phys.*, **19**, 436 (1960)
156. Fenstermacher, C. A., Draper, J. E., and Bockelman, C. K., *Nuclear Phys.*, **10**, 386 (1959)
157. Lane, A. M., *Revs. Mod. Phys.*, **32**, 519 (1960)
158. Porter, C. E., and Thomas, R. G., *Phys. Rev.*, **104**, 483 (1956)
159. Harvey, J. A., *Proc. Intern. Conf. Nuclear Structure, Kingston, Canada, 1960*, 659 (Bromley, D. A., and Vogt, E. W., Eds., Univ. Toronto Press, Toronto, Can., 990 pp., 1960)
160. Draper, J. E., and Bostrom, C. O., *Nuclear Phys.*, **14**, 693 (1959)
161. Bollinger, L. M., as quoted in Harvey, J. A., *Proc. Intern. Conf. Nuclear Structure, Kingston, Canada, 1960* (Univ. Toronto Press, Toronto,

- Can., 1960); see also Carpenter, R. T., and Bollinger, L. M., *Nuclear Phys.*, **21**, 66 (1960)
162. Hughes, D. J., Palevsky, H., Bolotin, H., and Chrien, R., *Proc. Intern. Conf. Nuclear Structure, Kingston, Canada, 1960*, 771 (Bromley, D. A., and Vogt, E. W., Eds., Univ. of Toronto Press, Toronto, Can., 990 pp., 1960)
 163. Bollinger, L. M., and Coté, R. E., *Bull. Am. Phys. Soc.* [II], **5**, 294 (1960)
 164. Bollinger, L. M., and Coté, R. E., *Argonne Natl. Lab., Phys. Div. Summary, Rept. ANL 6146*, 1 (1960)
 165. Brussel, M. K., and Zimmerman, R. L., *Bull. Am. Phys. Soc.* [II], **4**, 472 (1959)
 166. Harvey, J. A., *Bull. Am. Phys. Soc.* [II], **4**, 473 (1959)
 167. Vogt, R. H., *Bull. Am. Phys. Soc.* [II], **5**, 295 (1960)
 168. Domanic, F., and Sailor, V. L., *Phys. Rev.*, **119**, 208 (1960)
 169. Stolovy, A., see Vogt, R. H., *Bull. Am. Phys. Soc.* [II], **5**, 295 (1960)
 170. Wood, R. E., *Phys. Rev.*, **95**, 453 (1954)
 171. Stolovy, A., *Bull. Am. Phys. Soc.* [II], **5**, 294 (1960)
 172. Landon, H. H., and Sailor, V. L., *Phys. Rev.*, **98**, 1267 (1955)
 173. Igo, G., and Landon, H. H., *Phys. Rev.*, **101**, 726 (1956)
 174. Bolotin, H. H., Chrien, R. E., and Jain, A. P., *Bull. Am. Phys. Soc.* [II], **4**, 473 (1959)
 175. Vogt, E., *Phys. Rev.*, **112**, 203 (1958) and remarks in discussion *Proc. Intern. Conf. Nuclear Structure, Kingston, Canada, 1960*, 674 (Bromley, D. A., and Vogt, E. W., Eds., Univ. Toronto Press, Toronto, Can., 990 pp., 1960)
 176. Breit, G., and Yost, F. L., *Phys. Rev.*, **48**, 203 (1935)
 177. Thomas, R. G., *Phys. Rev.*, **84**, 1061 (1951)
 178. Thomas, R. G., *Phys. Rev.*, **88**, 1109 (1952)
 179. Griffiths, G. M., *Compt. rend. congr. intern. phys. nucléaire, Paris*, 447 (Dunod, Paris, France, 1959)
 180. Lane, A. M., and Lynn, J. E., *Nuclear Phys.*, **17**, 563 (1960)
 181. Lane, A. M., and Lynn, J. E., *Nuclear Phys.*, **17**, 586 (1960)
 182. Groshev, L. V., and Demidov, A. M., *Atomnaya Energ.*, **3**, No. 8, 91 (1957); *Nuclear Energy*, **11**, 8, 103 (1958)
 183. Zaretskii, D. F., *J. Exptl. Theoret. Phys. (USSR)*, **37**, 1084 (1959); *Soviet Phys. JETP*, **37**, 772 (1960)
 184. Peker, L. K., *J. Exptl. Theoret. Phys. (USSR)*, **29**, 865 (1955); *Soviet Phys. JETP*, **2**, 753 (1956)
 185. Shut'ko, A. V., and Zaretskii, D. F., *J. Exptl. Theoret. Phys. (USSR)*, **29**, 866 (1955); *Soviet Phys. JETP*, **2**, 769 (1956)
 186. Kinsey, B. B., Bartholomew, G. A., and Walker, W. H., *Phys. Rev.*, **85**, 1012 (1952)
 187. Van Patter, D. M., Endt, P. M., Sperduto, A., and Buechner, W. W., *Phys. Rev.*, **86**, 502 (1952)
 188. Enge, H. A., Buechner, W. W., and Sperduto, A., *Phys. Rev.*, **88**, 963 (1952)
 189. Lane, A. M., and Wilkinson, D. H., *Phys. Rev.*, **97**, 1199 (1955)
 190. Bockelman, C. K., *Nuclear Phys.*, **13**, 205 (1959)

NEUTRON DIFFRACTION¹

BY M. K. WILKINSON, E. O. WOLLAN, AND W. C. KOEHLER

Oak Ridge National Laboratory, Oak Ridge, Tennessee

INTRODUCTION

The words "neutron diffraction" are taken to encompass all the scattering phenomena associated with the passage of thermal neutrons through matter. These scattering processes are most readily understood in terms of the wave properties of the neutron, and the word "diffraction" emphasizes the interference effects which are associated with most scattering phenomena.

Although the wave properties of material particles were known when the neutron was discovered in 1932, neutron diffraction became a practical technique in a real sense only after intense neutron beams were available from nuclear reactors about ten years later. In the succeeding few years it was found that beams of neutrons could be diffracted by crystals and that they could be totally reflected at grazing angles by mirrors in much the same way as a beam of X rays. It was also found that neutrons could be spin polarized by reflection from magnetized mirrors or by Bragg reflection from magnetized crystals. These and other technical achievements opened up many possibilities for a large range of previously impossible neutron experiments. These experiments include studies in nuclear physics, crystal structure determinations, and crystal dynamics, and investigations of magnetism at the atomic level.

In its applications to solid state problems, neutron diffraction is similar in theory and experiment to X-ray diffraction, but its importance arises from the significant differences in the scattering of these two types of radiation. The scattering of X rays by atoms results from a scattering interaction with the atomic electrons, and the scattering amplitudes are approximately proportional to the atomic number of the scatterer. Since the electrons are distributed within the atom at distances comparable to X-ray wavelengths, interference effects occur which produce an angular distribution of the scattering (usually referred to as a form-factor) that is descriptive of the spatial distribution of the electrons. In the scattering of neutrons by atoms, there are two important interactions. One is the short-range nuclear interaction of the neutron with the atomic nucleus, and the other involves the interaction of the magnetic moment of the neutron with the spin and orbital magnetic moments of the atom. The nuclear interaction produces isotropic scattering, and there is no regular variation of scattering amplitudes with atomic number. The magnetic interaction depends on the size and orientation of the atomic magnetic moment, and the intensity of scattering has a form-factor angular dependence that is representative of the magnetic electrons.

¹ The survey of literature pertaining to this review was concluded in March 1961.

An attempt will be made in this article to give an over-all view of the research that has been and is being done in the various fields involved with neutron diffraction techniques. It is impossible to include specific details of the investigations or exhaustive coverage. Additional information can be found in review articles by Bacon (1), Shull & Wollan (2), and Ringo (3).

THEORETICAL CONSIDERATIONS

WAVE PROPERTIES

The behavior of neutrons, as well as that of other material particles, is well described by the equations of quantum mechanics. Associated with such particles is a de Broglie wave of wavelength $\lambda = h/mv = h/(2mE)^{1/2}$, where m is the mass, v the velocity, and E the kinetic energy of the particle. The amplitude and phase of the associated wave at a given point in space and time are represented by a wave function $\Psi(x, y, z, t)$, and the quantity $\Psi\Psi^*d\tau$ gives the probability of finding the particle in question in a volume element $d\tau$ at a time t . The wave equation representing the interaction of a neutron with an atom is

$$\nabla^2\Psi + k'^2\Psi = 0 \quad 1.$$

in which $k' = [2m(E - V)/\hbar^2]^{1/2}$ is the wave number inside the atom where the interaction potential is $V(r)$.

SCATTERING BY AN ATOM

Nuclear scattering.—The interaction of neutrons with isolated nuclei may be formulated in terms of the Breit-Wigner resonance theory [see e.g. (4)]. According to this theory, nuclear processes occur through the formation of a compound nucleus which comprises the neutron and the target nucleus. Since the scattering of thermal neutrons by nuclei involves only s -wave neutrons with a spin of $\frac{1}{2}$, the compound nucleus can only have spins of $I + \frac{1}{2}$ and $I - \frac{1}{2}$, where I is the spin of the target nucleus. The scattering cross section and its dependence on the energy of the incident particles are given by the Breit-Wigner one-level formula which has the form

$$\sigma_s = 4\pi\beta \left[\frac{\lambda_0\Gamma_n/2}{(E - E_0) + i\Gamma/2} + a_{p1} \right]^2 + 4\pi(1 - \beta)a_{p2}^2 \quad 2.$$

where $\beta = \frac{1}{2}[1 \pm 1/(2I + 1)]$. In this expression, λ_0 is the wavelength at resonance divided by 2π , Γ_n the neutron width at resonance, Γ the total width, E the energy of the incident neutrons, E_0 the energy of the resonance, a_{p1} the potential-scattering amplitude for the combination of neutron and target spins involved in the resonance, a_{p2} the potential-scattering amplitude for the other possible combination of spins, and β a weighting factor that depends on the spin of that state in the compound nucleus showing the resonance (if the resonance state is $I + \frac{1}{2}$, the sign is positive, and if it is $I - \frac{1}{2}$, the sign is negative).

When there are no resonances near thermal energy, the cross section corresponds only to the potential scattering, and the scattering amplitude is

real and positive. Potential scattering can be represented as the scattering by an impenetrable sphere of radius a_p , and the cross section is given by $4\pi a_p^2$. There is a regular variation of this cross section with mass number A , since $a_p \approx 1.5 \times 10^{-13} A^{1/3}$ cm.

When the energy is close to a scattering resonance, large deviations from potential scattering may be observed. The scattering amplitude can have imaginary components of appreciable size and can also be negative in sign when the interference effects between resonance and potential scattering result in a phase change on scattering opposite to that in potential scattering. Since potential scattering corresponds to scattering by an impenetrable sphere, the outgoing wave must be exactly out of phase with the incident wave; in other words, a phase change of 180° must occur in the scattering process. This phase change has been verified experimentally (5) in studies made on the reflection of slow neutrons from mirrors containing nuclei with no nearby resonances. A similar phase relationship exists for scattering in which the potential term is dominant and for those scattering processes where the neutron energy is larger than the resonance energy. However, when $E < E_0$, the phase change on scattering will be 0° under certain conditions, and the corresponding scattering amplitude will be negative.

Magnetic scattering.—In addition to the interaction of neutrons with atomic nuclei, there is a strong interaction between the magnetic moment of the neutron and the magnetic moment of an atom, for which the basic scattering theory was developed by Bloch (6) and by Schwinger (7). The interaction involves a potential of the form, $V = -\int \mathbf{y}_n \cdot \mathbf{H}_A d\tau$, where \mathbf{y}_n is the magnetic moment of the neutron, \mathbf{H}_A is the magnetic field arising from the spin and orbital moments of the atom, and the integration is performed over the volumes of the neutron and atom. The basic magnetic-scattering theory has been placed in convenient form by Halpern & Johnson (8) for magnetic atoms in which the magnetic moment is due entirely to the electron spin. Later theoretical investigations (9, 10, 11) have extended the theory to include the scattering of neutrons by atoms in which there is also a contribution to the magnetic moment from the orbital currents.

In the Born approximation, the scattered wave resulting from the magnetic interaction between a neutron and a magnetic atom is determined by evaluating the matrix elements for the interaction. If the atom has a magnetic moment resulting only from the electron spins, then the differential scattering cross section is given by

$$\frac{d\sigma}{d\Omega} = A^2 g^2 f^2(k) \left| \langle \chi_N' \chi_S' | \mathbf{S}_N \cdot \mathbf{S} - (\mathbf{S}_N \cdot \mathbf{e})(\mathbf{e} \cdot \mathbf{S}) | \chi_N \chi_S \rangle \right|^2 \quad 3.$$

where A is a constant equal to $e\gamma/2mc^2$, γ is the magnetic moment of the neutron, g is the gyromagnetic ratio, $f(k)$ is the form-factor for the magnetic electrons, χ_S and χ_N are the spin parts of the wave functions of the initial states of the atom and neutron, χ_S' and χ_N' have the same significance for the final states, \mathbf{S}_N and \mathbf{S} are the spin operators for the neutron and atom,

and e is the unit scattering vector given by $(\mathbf{k} - \mathbf{k}')/|\mathbf{k} - \mathbf{k}'|$, where \mathbf{k} and \mathbf{k}' are the incident and scattered wave vectors.

The total magnetic scattering includes interactions in which the spin of the atom is flipped in the scattering process as well as interactions in which the atomic spin is not changed. These two types of interactions produce different diffraction effects when neutrons are scattered by a crystal, and these effects are discussed in a later section.

NUCLEAR SCATTERING EFFECTS

Nuclear-spin dependence.—The Breit-Wigner relationship of Equation 2 indicates that when the scattering nucleus has a spin I , there will be two scattering amplitudes corresponding to the two spin states of the compound nucleus. In this particular expression, it is assumed that there is a resonance in only one of the states, and it should be emphasized that regardless of the resonance conditions, there are always two scattering amplitudes (corresponding to the $I + \frac{1}{2}$ and $I - \frac{1}{2}$ spin states of the compound nucleus) unless the target nucleus has zero spin. Furthermore, the cross sections for the scattering by these two spin states cannot be observed separately, except for aligned nuclear spins, and the observed cross section represents a weighted average of the two individual cross sections. If the amplitude for scattering by a free nucleus is designated by a , then the total scattering cross section for a single nucleus of spin I is given by

$$\sigma_s^f = 4\pi \left[\frac{I+1}{2I+1} a_{I+1/2}^2 + \frac{I}{2I+1} a_{I-1/2}^2 \right] \quad 4.$$

where the superscript f indicates scattering by a nucleus which is free to recoil, such as an atom in a gas. The cross section contributions of the spin states are weighted according to the probability that these states would exist in the compound nucleus.

Chemical binding.—There is a difference in the cross section for neutron scattering by an atom which is free to recoil and by one which is bound to a particular position, such as an atom in a crystal lattice. The scattering amplitude b for a rigidly bound nucleus is related to the amplitude a for a free nucleus by $b = [(1+A)/A]a$, where A is the mass number of the scattering nucleus. Consequently, for a bound nucleus with a spin I , the expression for the total scattering cross section given in Equation 4 must be changed to

$$\sigma_s^b = 4\pi \left[\frac{I+1}{2I+1} b_{I+1/2}^2 + \frac{I}{2I+1} b_{I-1/2}^2 \right] \quad 5.$$

The difference between b and a is insignificant for heavy nuclei, but for light nuclei it can be appreciable, and, of course, $b = 2a$ for hydrogen. All coherent-scattering effects between distant neighbors in a crystal must be associated with the bound scattering amplitudes, because recoil effects would destroy the coherence. However, in diffuse scattering from a crystal, the effective cross section can vary between the bound and free limits, since various amounts of recoil energy can be given to vibrational modes of the crystal.

Isotopic effects.—When scattering measurements are made on an element that contains more than one isotope, conditions are similar to those resulting from nuclear spin dependence. Each isotope has a specific scattering amplitude, and the observed nuclear scattering cross section corresponds to a weighted average of the cross sections for the various isotopes. If the measurements are made with bound nuclei and all isotopes have zero nuclear spin, the total scattering cross section per nucleus will be

$$\sigma_s^b = 4\pi \sum_n p_n b_n^2 \quad 6.$$

where p_n is the fractional abundance of the n th isotope which has a scattering amplitude b_n .

If each isotope has a nuclear spin I_n , then the two effects must be combined and the expression becomes

$$\sigma_s^b = 4\pi \left\{ \sum_n p_n \left[\frac{I_n + 1}{2I_n + 1} b_{I_n+1/2}^2 + \frac{I_n}{2I_n + 1} b_{I_n-1/2}^2 \right] \right\} \quad 7.$$

SCATTERING BY A CRYSTAL

All of the equations for scattering cross sections given in the previous sections represent total scattering cross sections for various types of atoms. If the scattering atoms are arranged with a definite periodicity such as that of the atoms in a crystal lattice, interference effects between the scattered waves cause part of this scattering to be found in discrete reflections. The rest of the scattering is incoherent and merely adds to the diffuse scattering by the crystal.

Coherent scattering.—The coherent scattering of radiation by a crystal can be treated classically as the summation of amplitudes of the scattered waves over the crystal lattice. Therefore, the coherent scattering cross section always involves the square of the weighted average of the scattering amplitudes associated with the atoms in the crystal. For a crystal containing atoms with a single nuclide with a nuclear spin I , the total nuclear scattering cross section is given by Equation 5, but the coherent nuclear scattering cross section is

$$\sigma_{coh} = 4\pi \left[\frac{I + 1}{2I + 1} b_{I+1/2} + \frac{I}{2I + 1} b_{I-1/2} \right]^2 \quad 8.$$

In fact, since this spin dependence in the scattering always exists except for zero-spin nuclei, the effective nuclear coherent scattering amplitude is the quantity measured in an experiment and it corresponds to $b = \pm (\sigma_{coh}/4\pi)^{1/2}$. A similar expression can be obtained for the effective nuclear coherent scattering cross section of an element which contains more than one isotope; and when the experimental values of σ_{coh} and σ_s^b are equal, it is evident that the individual nuclear scattering amplitudes for the major isotopic constituents must be nearly the same.

The theory for the coherent scattering of neutrons is closely related to the theory which was developed for X-ray scattering, and the equations contain

only minor modifications. These scattering equations always involve the scattering amplitude per unit cell for the crystal under investigation. Proper coherent scattering amplitudes must be introduced; and if the scattering specimen contains magnetic atoms, both nuclear and magnetic scattering amplitudes must be included. The effective amplitude for the coherent scattering of a neutron, which has its spin polarized along a unit vector λ , by an atom with a nuclear coherent scattering amplitude b and a spin-only magnetic moment parallel to a unit vector κ , may be written

$$b\lambda + pq \quad 9.$$

where $p = A S f(k)$ is the magnetic coherent scattering amplitude with the terms defined for Equation 3 and $q = \kappa - e(e \cdot \kappa)$. Therefore, the expression for the scattering amplitude per unit cell for a reflection with Miller indices of h, k, l can be written

$$F_{hkl} = \sum_j (b_j \lambda + p_j q_j) R_j \quad 10.$$

where $(b_j \lambda + p_j q_j)$ is the total scattering amplitude of the j th atom, $R_j = e^{2\pi i(hx_j + ky_j + lz_j)}$ is the usual geometrical factor, and the summation is taken over all atoms in the unit cell.

The integrated intensity in a Bragg reflection is proportional to F_{hkl}^2 , and if there is only one type of atom in the crystal, this quantity becomes

$$F_{hkl}^2 = (b^2 + 2bpq \cdot \lambda + q^2 p^2)_{hkl} R_{hkl}^2 \quad 11.$$

where $R_{hkl} = \sum_j R_j$ and $q^2 = 1 - (e \cdot \kappa)^2$. It is evident from this expression that for unpolarized neutrons the cross-term will average to zero and the total intensity is actually the sum of the nuclear and magnetic intensities. For polarized neutrons and aligned atomic magnetic moments, the cross-term is very important and these conditions will be discussed in a later section.

Incoherent scattering.—There are no interference effects in incoherent scattering processes, and it is necessary to combine only the intensities of the scattered radiation rather than the amplitudes of the scattered waves. Incoherent scattering is always present when the total scattering is larger than the coherent scattering, and the cross section for this incoherent part is merely the difference between σ_s and σ_{coh} . For example, the cross section for nuclear-spin incoherent scattering from a crystal containing atoms of a single nuclide with a nuclear spin I is obtained by subtracting Equation 8 from Equation 5 to give

$$\sigma_{spin \text{ incoh}} = 4\pi \frac{I(I+1)}{(2I+1)^2} (b_{I+1/2} - b_{I-1/2})^2 \quad 12.$$

It is seen from this equation that the spin incoherent scattering will be zero when the scattering amplitudes for parallel and antiparallel nuclear spins are equal, and this is certainly the case for a target nucleus with zero spin. Similar expressions can be calculated to give the incoherent scattering by a crystal which contains an element with more than one isotope or one which exhibits a randomness in the distribution of the nuclei.

In the scattering from magnetic materials, incoherent scattering always arises from those interactions in which the atomic moments are flipped. This scattering depends on experimental conditions such as the neutron energy, the coupling energy between magnetic moments, and the short-range magnetic correlations in the sample. When the neutron energy is large compared to the coupling energy, the differential cross section per atom for spin-flip scattering from an ordered system of spin-only magnetic moments can be expressed (12)

$$\frac{d\sigma}{d\Omega} = \frac{1}{2} A^2 g^2 S f^2(k) [1 + (\mathbf{e} \cdot \mathbf{k})^2] \quad 13.$$

If there is a randomness in the distribution of magnetic moments throughout the crystal, additional incoherent magnetic scattering will occur from those scattering processes in which the atomic moments are not flipped. Consequently, for a paramagnetic material with completely independent magnetic moments, all magnetic scattering is incoherent. The differential cross section per atom for paramagnetic scattering from a magnetic substance with spin-only moments is given by

$$\frac{d\sigma}{d\Omega} = \frac{2}{3} A^2 g^2 S(S+1) f^2(k) \quad 14.$$

Short-range correlations among neighboring atoms cause scattering processes in which the scattering is not truly coherent or incoherent. These processes can be either elastic or inelastic, and they occur in both nuclear and magnetic scattering. The diffraction effects result in angular distributions which contain broad maxima similar to those observed in liquid scattering; and when these effects occur, the simple pictures given for coherent and incoherent scattering become more complex. A detailed consideration of this scattering will not be included in this article, but references to many papers which involve the inelastic scattering processes are given in the last section.

EXPERIMENTAL PROCEDURES

EQUIPMENT

Neutron sources.—Nuclear reactors now provide the best sources for the thermal neutrons required in neutron diffraction experiments, and it appears unlikely that other machines will be able to compete with reactors for this purpose. The exact energy distribution of the neutrons depends on the reactor construction, but in general it is almost Maxwellian with the maximum near 0.07 eV, and this neutron energy corresponds to a neutron wavelength of about 1 Å. Most of the new research reactors provide a thermal-neutron flux in excess of 10^{13} neutrons/cm²/sec, and some have been constructed in which the value is about 5×10^{14} neutrons/cm²/sec. The neutron beam is obtained from the reactor merely by constructing a hole of the desired geometry through the reactor shield and reflector; and if the hole is tangential to the reactor core, undesirable fast neutrons and gamma rays can be minimized. Removable plugs are usually inserted into the hole to provide the desired collimation.

Monochromators.—Most techniques that have been used in neutron diffraction experiments require monochromatic radiation. Since the thermal neutrons from a reactor have a continuous energy distribution, the monochromatic beams must be obtained by isolating a narrow slice of the neutron spectrum. This process is usually accomplished by diffraction from large single crystals, and many substances have been used for this purpose. Crystals of materials which have large coherent scattering cross sections, small incoherent scattering cross sections, and small absorption cross sections are obviously preferable; but the mosaic spread of the crystal (13) is also important in the selection of a monochromator. In general, it is best to match the mosaic spread to the geometrical angular spread of the collimating system (14) since this condition allows the collimating system to be more completely filled with radiation. This arrangement may result in reduced wavelength resolution, but such a compromise is usually necessary to provide optimum neutron intensities. Since most present-day instruments have collimating systems with an angular spread of perhaps one-half degree to a degree, metallic crystals are preferable as monochromators, and single crystals of Be, Cu, and Pb have been widely used.

When extremely good resolution is necessary, more perfect crystals such as NaCl, CaCO_3 , or MgO would be preferable. Polarized neutrons are frequently required in certain investigations of magnetic materials, and, as discussed in a later section, such a beam can be obtained in the monochromating process from single crystals of an FeCo alloy or of magnetite.

Filters and velocity selectors can also be used for monochromatization. Filters are usually used to obtain a rather rough wavelength selection of long-wavelength neutrons, and velocity selectors have had limited use since they sacrifice a large percentage of the available neutron intensities when the rotors are closed. However, a recent article by Lowde (15) indicates that the intensity loss with velocity selectors can be offset by other advantages, and it is likely that more instruments of this type will be used in the future at research reactors with high neutron fluxes.

Neutron detectors.—The detection of the thermal neutrons in neutron diffraction experiments is usually accomplished by a proportional counter filled with BF_3 gas in which the boron is enriched in boron 10. These counters are satisfactory from a performance point of view, and the main disadvantage is their size. In order to obtain a good counting efficiency at reasonable gas pressures, these proportional counters are usually made about 18 inches long. Since a large amount of shielding is required around the counter to reduce the neutron background, the complete detector is a large instrument and its motion is usually restricted to a single plane.

A great reduction in the counter size can be obtained by using scintillation materials such as LiI crystals activated with europium (16, 17). However, the over-all size of the detector cannot be reduced by the same amount because the shielding must surround the photomultiplier tube as well as the crystal.

TECHNIQUES

Although the intensities of thermal-neutron beams from nuclear reactors are lower than those obtained from good X-ray tubes, most of the X-ray diffraction methods can be used with neutrons. Furthermore, since the neutron absorption for many materials is small, diffraction effects can also be investigated by measuring the transmission of neutrons through a sample; and some of the early investigations (18 to 21) made use of this method. However, the majority of neutron diffraction investigations involving crystalline materials have been accomplished by the Debye-Scherrer-Hull powder method of analysis and by the method of Bragg scattering from single crystals.

The basic equipment which is necessary for these two techniques is similar and, with minor modifications, the same diffractometer can be used for both types of experiments. All diffractometers in existence are similar in principle to the one used in the early investigations by Wollan & Shull (22). The reactor neutrons are incident on a single crystal for monochromatization, and the monochromatic beam is collimated and passes over the diffractometer table where the scattering specimen is mounted. The neutron detector is rotated around the scattering specimen to determine the angular distribution of the scattered neutrons, and a second neutron detector monitors the primary monochromatic beam to allow normalization of the data for changes in the power level of the reactor. In some diffractometers the positions of the collimating slits in the monochromator shield can be varied to alter the wavelengths of the neutron beams, but in those with fixed slit systems, the crystal planes used for monochromatization must be changed to provide neutrons of different wavelengths.

Powder method.—The majority of structural investigations which have been made by neutron diffraction have used the powder method of analysis. This method is generally used when exact absolute intensity measurements are desired, and it must be used when single crystals of a material are not available. The polycrystalline sample, in the form of a powder or filings, is placed in either a flat or cylindrical cell depending on the type of experiment and the amount of material available. The optimum sample size is governed by the total cross section of the sample; but in general, flat cells have cross-sectional dimensions of about 2 inches by 2 inches and a thickness of about $\frac{3}{8}$ inch, while the cylindrical cells are about 2 inches high with a $\frac{3}{8}$ -inch diameter. Cells are usually made from vanadium or aluminum, because the low cross sections of these elements for coherent scattering of neutrons make the scattering contribution from the cell small. Cells and windows can also be fabricated (23) from alloy systems in which elements with positive and negative scattering amplitudes are mixed in the proper proportions to give no coherent scattering.

The powder diffraction pattern is analyzed in terms of the scattering amplitudes of atoms in the scattering specimen with the use of equations

that have been adapted from corresponding expressions applicable to X-ray diffraction [see e.g. (24)]. For a flat sample

$$P_{hkl} = P_0 \frac{\lambda^3 z h \rho' e^{-\mu h} \sec \theta}{4\pi r \rho \sin^2 2\theta} N^2 j_{hkl}^2 F_{hkl}^2 e^{-2W} \quad 15.$$

where P_{hkl} is the total power in an (hkl) reflection as measured through a counter slit opening of height z at a distance r from the sample, P_0 the beam power in the primary monochromatic beam, λ the neutron wavelength, ρ' the measured density of the powder which would have a density ρ in the solid crystal, μ the linear attenuation coefficient, h the thickness of the specimen, θ the Bragg angle of reflection, j_{hkl} the number of planes which contribute to the scattering at this angle, N the number of unit cells per cm^3 of crystal, F_{hkl} the scattering amplitude per unit cell for the particular crystal structure, and e^{-2W} the Debye-Waller temperature factor. Equation 10 gives F_{hkl} , and

$$W = \frac{6h^2}{mk_B\Theta} \left(\frac{\varphi(x)}{x} + \frac{1}{4} \right) \frac{\sin^2 \theta}{\lambda^2} \quad 16.$$

where Θ is the Debye temperature of the crystal, $\varphi(x)$ is the Debye function with $x = \Theta/T$, and the other terms have their usual meaning. For the case of a cylindrical sample, a similar expression is used, in which the geometrical terms in Equation 15 are modified.

While the intensities of the reflections in X-ray analyses are usually determined on a relative basis, it has been valuable to make absolute determinations in neutron diffraction. However, the direct measurement of the power P_0 in the monochromatic incident beam is a difficult problem. Hence, the value of P_0 and the other quantities in Equation 15 which are constant for a given arrangement are obtained by comparison with the diffracted intensities from a sample of known coherent scattering cross section. For a monoisotopic element with zero nuclear spin, the coherent scattering cross section and the total scattering cross section are identical, and the latter can be obtained from a transmission experiment. In practice, nickel powder is usually taken as the standard, because its scattering properties (25) have been well determined.

Single-crystal method.—The single-crystal technique provides a much better resolution of the diffraction peaks, and this method is required for the study of complicated structures. However, the effects of extinction and crystal distortion make absolute intensity measurements somewhat more difficult. The conditions for extinction were first treated for neutron radiation by Bacon & Lowde (26), and Hamilton (27) has recently considered extinction effects in crystals which produce both nuclear and magnetic scattering. To prevent this effect from being a serious problem in single-crystal analyses, it is necessary that the crystals have dimensions of the order of one millimeter. However, even though the crystal is quite small, the intensities in the Bragg reflections will usually be larger than those in powder patterns, because the whole volume of the crystal contributes to a reflection when it

is set in the proper orientation. The smaller size also has the advantage of reducing the diffuse scattering relative to the coherent scattering in the reflections. Peterson & Levy (28) have pioneered in the single-crystal method, and they have shown that the data can be interpreted by application of the following equation which is adapted from a similar X-ray expression:

$$E_{hkl} = \frac{I_0 \lambda^3 N^2 V F_{hkl}^2 A_{hkl} e^{-2W}}{\omega \sin 2\theta} \quad 17.$$

In this equation, E_{hkl} is the integrated intensity in an (hkl) reflection, I_0 the incident neutron intensity, ω the angular velocity of rotation of the crystal, V the volume of the scattering specimen, A_{hkl} the absorption correction; and the other terms were defined for Equation 15. For crystals of arbitrary shape, the determination of A_{hkl} can be difficult, but procedures (29) have been established for using an electronic computer in this calculation.

Absolute determinations of the intensities of the reflections have been necessary in the single-crystal technique also, and the value of I_0 is established by comparison with similar measurements on a standard single crystal. This standard crystal must be one which is known not to have any extinction effects, and it must be carefully calibrated against a powdered sample of a material with a known coherent scattering cross section.

Photographic techniques.—Although photographic techniques have played an important role in X-ray diffraction, these techniques have not yet been applied to neutron diffraction investigations. Wollan, Shull & Marney (30) showed that Laue photographs can be obtained with neutrons, and patterns were obtained for a number of substances such as NaCl, quartz, calcite, and LiF, but prolonged exposure times were required. This requirement resulted from the low neutron intensity available and from the difficulty in photographing the scattered neutrons. Since photographic film is quite insensitive to neutrons, it is necessary to use a neutron-sensitive screen in conjunction with the film; and in these early experiments, β particles resulting from neutron capture in a thin sheet of indium produced the photographic effect.

The larger neutron intensities available from new research reactors and the development of better sensitive screens make photographic techniques quite possible in future neutron diffraction experiments. Sun & Wollan (31) have shown that a screen containing ZnS(Ag) phosphor and boron plastic can be used with photographic film to give exposure times comparable with those obtained in X-ray diffraction, and new glass scintillators containing lithium 6 also show considerable promise (32, 33) for neutron photography.

AUXILIARY EQUIPMENT

The basic neutron diffractometer is, in principle, a rather simple instrument, and it can also be simple in construction. However, the applications of the technique to specific problems frequently require a large amount of auxiliary apparatus for controlling the conditions of the samples. In most solid state investigations, it is necessary to change the sample temperatures,

and low-temperature cryostats have been developed (34, 35) for experiments down to 1.25°K , while furnaces have maintained sample temperatures (36) up to 1250°K . Unlike the equipment in X-ray diffraction experiments, the design of this auxiliary equipment presents no particular problems, because vacuum jackets and radiation shields can be readily fabricated from materials with low neutron cross sections, such as aluminum. In the investigation of magnetic materials, it is frequently necessary to place the samples in an external magnetic field, and electromagnets have been constructed for use with many diffractometers.

Because of the particular sample conditions required, it may become desirable to make the auxiliary equipment an integral part of the diffractometer; and the low-temperature magnet unit at the Oak Ridge National Laboratory is a good example of such an instrument. A photograph of this diffractometer, which was designed specifically for the study of magnetic materials at low temperatures, is shown in Figure 1. Both single crystals and powdered specimens can be investigated, and the samples can be maintained at temperatures down to 1.3°K in magnetic fields up to 21.5 kilo-oersteds applied at variable angles with respect to the sample.

NUCLEAR STUDIES

Although the scattering of slow neutrons is generally considered a tool for the study of solid state phenomena, many investigations have been per-

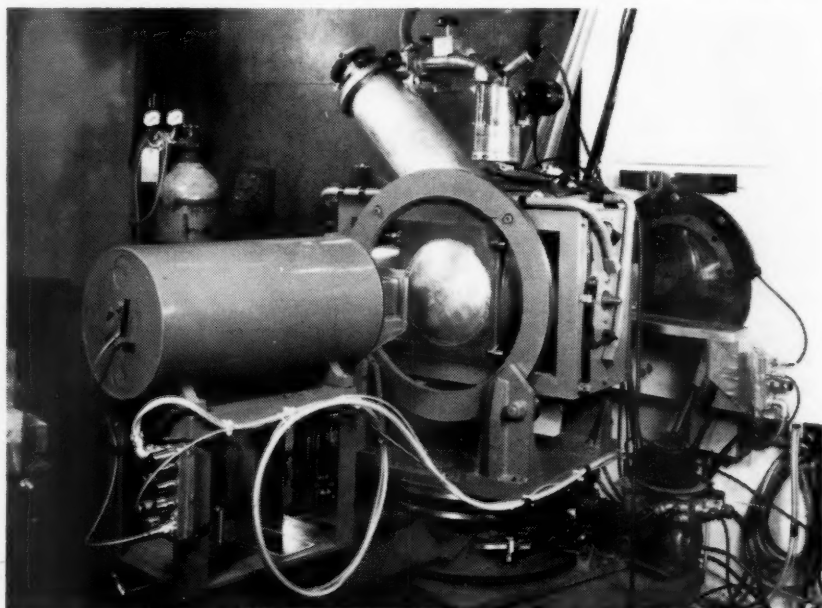


FIG. 1. Low-temperature magnet diffractometer at the Oak Ridge National Laboratory.

formed to obtain information necessary for the understanding of nuclear processes. Diffraction techniques have been employed primarily to measure numerous coherent scattering amplitudes under special conditions, and these determinations have provided details on potential scattering, resonance effects, and the neutron-proton interaction.

NUCLEAR SCATTERING AMPLITUDES

Coherent nuclear scattering properties for a large number of elements and isotopes were obtained in the early powder diffraction experiments of Shull & Wollan (37). Additional results have been obtained by various other workers in the field, and the present status of these measurements is given in Table I. This table shows that wide variations exist in scattering cross sections from isotope to isotope and that negative scattering amplitudes occur much less frequently than the positive amplitudes. The differences between the total scattering cross sections and coherent scattering cross sections indicate the presence of incoherent nuclear scattering processes. As mentioned previously neutron diffraction techniques measure relative values of the coherent scattering amplitudes which must be compared to a standard. Most of these values in Table I were obtained with nickel as the standard for comparison, and the scattering cross section of nickel was established relative to nickel 58 and carbon.

If the diffraction experiment is performed on a sample which contains only one nuclide, a direct determination of the coherent scattering amplitude can be made when the temperature correction factors are known. Data on elastic constants or Debye characteristic temperatures are usually available to permit determination of these correction terms, but they can also be obtained from the diffraction data for a series of reflections. As shown in Equation 16, the Debye-Waller factor varies exponentially with $\sin^2\theta/\lambda^2$ and becomes unity at a scattering angle of zero. Consequently, extrapolation of the data for several reflections to a zero scattering angle will give the magnitude of the scattering amplitude directly. In an experiment with a single nuclide, no information is obtained on the sign of the scattering amplitude, since the intensity in the Bragg reflections depends on the square of the amplitude. However, additional measurements made on chemical compounds can determine this sign. For compounds, the scattering amplitudes of the constituent nuclides are combined in various ways to give different values of F_{hkl} for the various reflections, so that intensity measurements give the interference effects between the different nuclides. Thermal correction factors must also be applied in these analyses; and if the masses of the nuclides are not equal, different correction terms are necessary to account for the thermal motions. It should be emphasized that only relative phases of scattering are obtained in these measurements, and absolute phases must be determined directly by critical reflection of neutrons from mirrors. A positive scattering amplitude corresponds to a phase change of 180° on scattering, while a negative amplitude means that the phase change is 0° .

TABLE I
 NEUTRON SCATTERING DATA FOR ELEMENTS AND ISOTOPES

Element or isotope	b (10^{-12} cm)	σ_{coh} (barns)	$\sigma_a b$ (barns)	Element or isotope	b (10^{-12} cm)	σ_{coh} (barns)	$\sigma_a b$ (barns)
H	-0.378	1.79	81.5	Rb	0.55	3.8	5.5
D	0.65	5.4	7.6	Sr	0.57	4.1	10
He	0.30	1.1	1.1	Zr	0.70	6.2	6.3
Li	-0.18	0.4	1.2	Nb	0.69	6.0	6.6
Li ⁶	0.16	0.3		Mo	0.67	5.6	6.1
Li ⁷	-0.21	0.55	1.4	Ru	0.73	6.7	6.8
Be	0.774	7.53	7.54	Rh	0.60	4.5	5.6
B			4.4	Pd	0.60	4.5	4.8
C	0.66	5.50	5.51	Ag	0.61	4.6	6.5
C ¹³	0.60	4.5	5.5	Ag ¹⁰⁷	0.83	8.7	10
N	0.94	11.0	11.4	Ag ¹⁰⁹	0.43	2.3	6
O	0.58	4.2	4.24	*Cd	0.38+0.12i	2.0	
F	0.53	3.5	4.0	*Cd ¹¹³	-0.80+0.75i	15.1	
Ne			2.9	In	0.36	1.6	1.6
Na	0.35	1.55	3.4	Sn	0.61	4.6	4.9
Mg	0.54	3.6	3.7	Sb	0.54	3.7	4.2
Al	0.35	1.5	1.5	Te	0.56	4.0	4.5
Si	0.40	2.0	2.4	Te ¹²⁰	0.52	3.4	
P	0.53	3.5	3.6	Te ¹²³	0.57	4.2	
S	0.31	1.2	1.2	Te ¹²⁴	0.55	3.9	
Cl	0.98	12.1	15	Te ¹²⁵	0.56	4.0	
A	0.20	0.5	0.9	I	0.52	3.4	3.8
K	0.35	1.5	2.2	Cs	0.49	3.0	7
Ca	0.49	3.0	3.2	Ba	0.53	3.5	6
Ca ⁴⁰	0.49	3.0	3.1	La	0.83	8.7	9.3
Ca ⁴⁴	0.18	0.4		Ce	0.47	2.8	2.8
Sc	1.18	17.5	24	Ce ¹⁴⁰	0.48	2.9	2.9
Ti	-0.34	1.45	4.0	Ce ¹⁴²	0.46	2.7	2.7
Ti ⁴⁶	0.48	2.9		Pr	0.44	2.4	4.0
Ti ⁴⁷	0.33	1.4		Nd	0.72	6.5	16
Ti ⁴⁸	-0.58	4.2		Nd ¹⁴²	0.77	7.5	7.5
Ti ⁴⁹	0.08	0.08		Nd ¹⁴⁴	0.28	1.0	1.0
Ti ⁵⁰	0.55	3.8		Nd ¹⁴⁶	0.87	9.5	9.5
V	-0.050	0.032	5.1	Sm ¹⁵²	-0.5	3	
Cr	0.35	1.6	4.1	Sm ¹⁵⁴	0.8	8	
Cr ⁵²	0.49	3.0		Tb	0.75	7.1	
Mn	-0.37	1.7	2.0	Ho	0.85	9.1	13
Fe	0.96	11.4	11.8	Dy	1.69	35.9	
Fe ⁵⁴	0.42	2.2	2.5	Er	0.79	7.8	15
Fe ⁵⁶	1.01	12.8	12.8	Tm	0.55	3.8	
Fe ⁵⁷	0.23	0.64	2	Yb	1.27	20.5	
Co	0.25	0.8	6	Lu	0.73	6.7	
Ni	1.025	13.2	18.0	Hf	0.88	9.7	
Ni ⁵⁸	1.44	25.9		Ta	0.70	6.1	6
Ni ⁶⁰	0.30	1.1		W	0.47	2.7	5.7
Ni ⁶²	-0.87	9.5		Re	0.92	10.6	
Cu	0.79	7.8	8.0	Os	1.08	14.7	14.9
Cu ⁶³	0.67	5.7		Ir	0.36	1.6	1.7
Cu ⁶⁵	1.11	15.5		Pt	0.95	11.2	12
Zn	0.61	4.7	4.2	Au	0.76	7.3	
Ga			7.5	Hg	1.3	22	
Ge	0.84	8.8	9.0	Tl	0.89	10.0	10.1
As	0.73	6.7	8	Pb	0.96	11.5	11.4
Se	0.89	10.0		Bi	0.864	9.35	9.37
Br	0.67	5.7	6.1	Th	1.01	12.8	12.6
Kr	0.76	7.2	7.7	U	0.85	9.0	

* Values for $\lambda = 1.075$ Å.

An experimental observation of the imaginary component of the scattering amplitude has recently been made by Peterson & Smith (38) in investigations on α cadmium sulfide at a series of neutron energies near the resonance of the cadmium-113 isotope. Since the phase of scattered radiation is not directly observable, the effect of the imaginary component can be made apparent only through intensity differences caused by interference. In the Bragg scattering of neutrons from a noncentrosymmetric crystal such as

α -CdS, the imaginary component from a resonant nucleus can be detected through interference with a real component which is in phase because it originated from nuclei at appropriately displaced sites. Such interference results in a failure of Friedel's law [see e.g. (39)] and $I_{hkl} \neq I_{\bar{h}\bar{k}\bar{l}}$. This effect is shown in Figure 2(a) where the diffraction patterns of the $(00\bar{2})$ and (002) reflections from α -CdS are plotted for a wavelength of 0.87 Å. The ratio of $I_{00\bar{2}}/I_{002}$ as a function of wavelength is given in Figure 2(b), and the strong energy-dependence of this ratio is the result of the variation of the complex scattering amplitude of cadmium. The smooth curve through the data is based on the Breit-Wigner formulation.

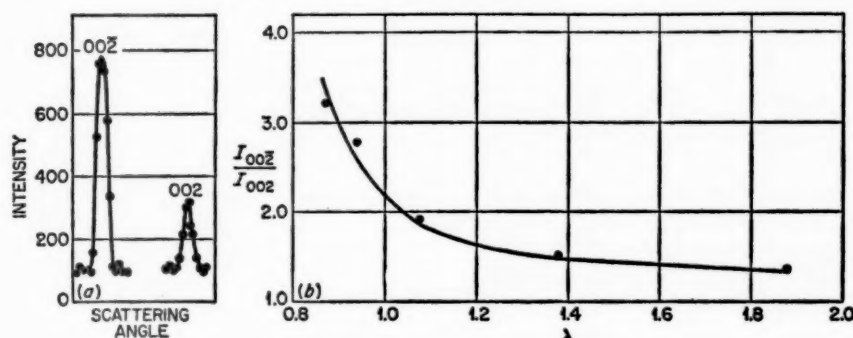


FIG. 2(a). Intensities of the $(00\bar{2})$ and (002) reflections from α -CdS at $\lambda = 0.87$ Å. (b). Wavelength dependence of the $(00\bar{2})/(002)$ intensity ratio from α -CdS in the cadmium resonance region. The smooth curve through the experimental points is based on the Breit-Wigner formulation.

NEUTRON-PROTON INTERACTION

One of the most important nuclear investigations that has used the scattering of slow neutrons is the determination of the neutron-proton scattering amplitudes for parallel and antiparallel spins, corresponding to the triplet and singlet states. Since this is a two-body problem it is amenable to theoretical analysis, and this measurement gives information on the nuclear-spin dependence of neutron-proton scattering and on the properties of the deuteron. Three types of investigations have been performed and the results are summarized in Table II. Calculations (40) based on the most accurate results give an effective range for the neutron-proton interaction in the singlet state that is in good agreement with the range for the proton-proton singlet interaction.

The first studies followed a suggestion by Schwinger & Teller (41) and involved the transmission of neutrons through ortho- and para-hydrogen, which are the two forms of the hydrogen molecule in which the protons are parallel and antiparallel, respectively. When measurements are made on samples with different ortho- and para-concentrations, the results permit a

determination of the individual singlet and triplet scattering amplitudes. Since the measured cross section depends on the square of the average scattering amplitudes, there is a sign ambiguity in the result; but this can be eliminated because it is known that the triplet state corresponds to the bound state of the deuteron for which the amplitude is positive. There are many complications associated with these experiments and particularly with the determination of the exact concentration of ortho- and para-hydrogen. Consequently, the early experiments (42, 43) were not precise, but they did show very clearly the strong nuclear-spin dependence of the scattering. Recent measurements (44) made by this method have given much more accurate results.

TABLE II
RESULTS OF NEUTRON-PROTON SCATTERING AMPLITUDES
OBTAINED BY VARIOUS METHODS*

Method	b_H (10^{-12} cm)	a_T (10^{-12} cm)	a_S (10^{-12} cm)	Ref.
Ortho-para hydrogen	-0.380 ± 0.005			(44)
NaH	-0.41 ± 0.02			(37, 45)
Liquid hydrocarbons	-0.378 ± 0.002	0.5377 ± 0.0023	-2.369 ± 0.006	(47)

* A comparison is made of the bound scattering amplitude for hydrogen, and the corresponding free coherent scattering amplitudes for the triplet and singlet states are listed only for the most accurate value.

Neutron diffraction investigations on NaH by Shull *et al.* (45) provided the second determination of the neutron-proton scattering amplitude. Powdered NaH was used and the coherent scattering amplitude of hydrogen was obtained relative to that of Na by measuring the intensities of the Bragg reflections. From the values of the coherent scattering amplitude and the free-proton scattering cross section (46), the individual singlet and triplet amplitudes were obtained. The first results did not include a careful correction for the effects of thermal motion, and the value given in the table includes refinements (37) in these correction terms. The discrepancy with the other results is greater than would be expected on the basis of known experimental errors and is not understood.

The most accurate determination of the nuclear coherent scattering amplitude of hydrogen was made by Burgy, Ringo & Hughes (47), who used the total reflection of slow neutrons from liquid hydrocarbons. The composition of the samples was so chosen that the total negative scattering amplitude of the hydrogen nuclei was slightly more than compensated by the positive scattering amplitude of the carbon nuclei. Therefore, the samples exhibited small net positive nuclear scattering amplitudes, and a neutron beam in air experienced external reflection at critical angles which could be

measured with reasonable accuracy. The coherent scattering amplitude of hydrogen was measured relative to that of carbon; and with corrections for the small carbon-13 content, the latter was accurately determined by transmission measurements. As in the neutron diffraction investigation of NaH, the value of the coherent scattering cross section for hydrogen was combined with the free-proton scattering cross section to obtain the singlet and triplet scattering amplitudes.

CRYSTALLOGRAPHY AND CHEMICAL BONDING

INTRODUCTION

In the field of chemical crystallography, the technique of neutron diffraction naturally has been developed around the problems for which other types of diffraction techniques cannot give as much information. These problems involve particularly those studies in which the uniform variation of coherent scattering amplitudes with atomic number, as observed in both X-ray and electron diffraction, is a serious disadvantage. Neutron diffraction is also frequently applied to problems in which the isotropic neutron scattering furnishes significant information at large angles which could not be obtained with the other types of radiation because of the form-factor dependence of the scattering.

Even when the scattering amplitudes of the elements within a compound are not favorable for an investigation, it is frequently possible to substitute an enriched isotope which has scattering characteristics that are markedly different from those of the element. This effect is illustrated in Figure 3 where portions of the diffraction patterns (25) for samples of NiO enriched in Ni^{58} , Ni^{60} , and Ni^{62} are compared with normal NiO. Since the coherent neutron scattering amplitudes are quite different for the nickel isotopes, there is little similarity between the diffraction patterns. Of course, such an effect would not be observed in X-ray diffraction since the scattering involves an interaction with the atomic electrons. Isotopic substitution can also be used in neutron diffraction experiments to minimize incoherent scattering and neutron absorption.

COMPOSITE CRYSTALS WITH HEAVY AND LIGHT ATOMS

The most significant application of neutron diffraction in chemical crystallography is the structure determination of composite crystals which contain both heavy and light atoms. In X-ray and electron diffraction, the intensities observed in the diffraction peaks contain such a tremendous contribution from the heavy atoms that little or no information on the light atoms can be obtained.

Hydrogen-containing substances.—By far the most important compounds that fall into this general classification are the hydrogen-containing substances, and over 50 of them have now been analyzed by neutron crystallographic techniques. These compounds have included a variety of different

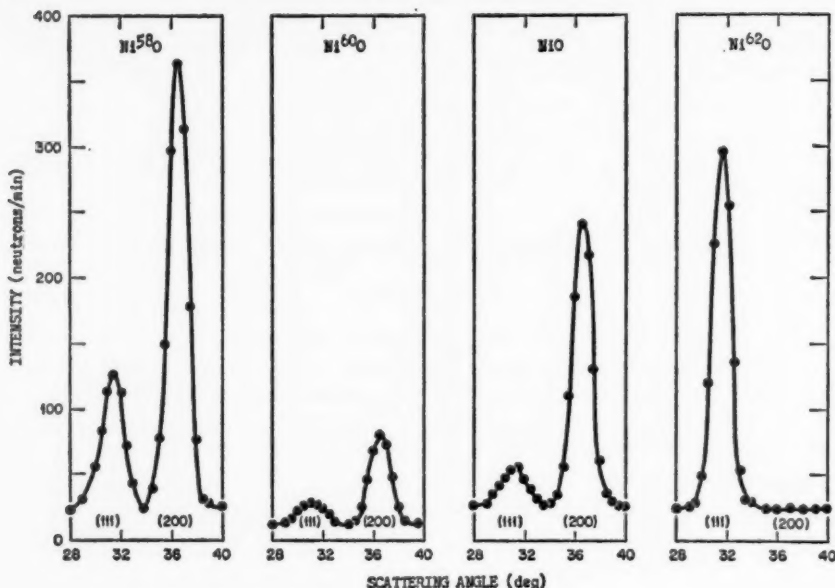


FIG. 3. Portions of neutron diffraction powder patterns for isotopically enriched samples of NiO.

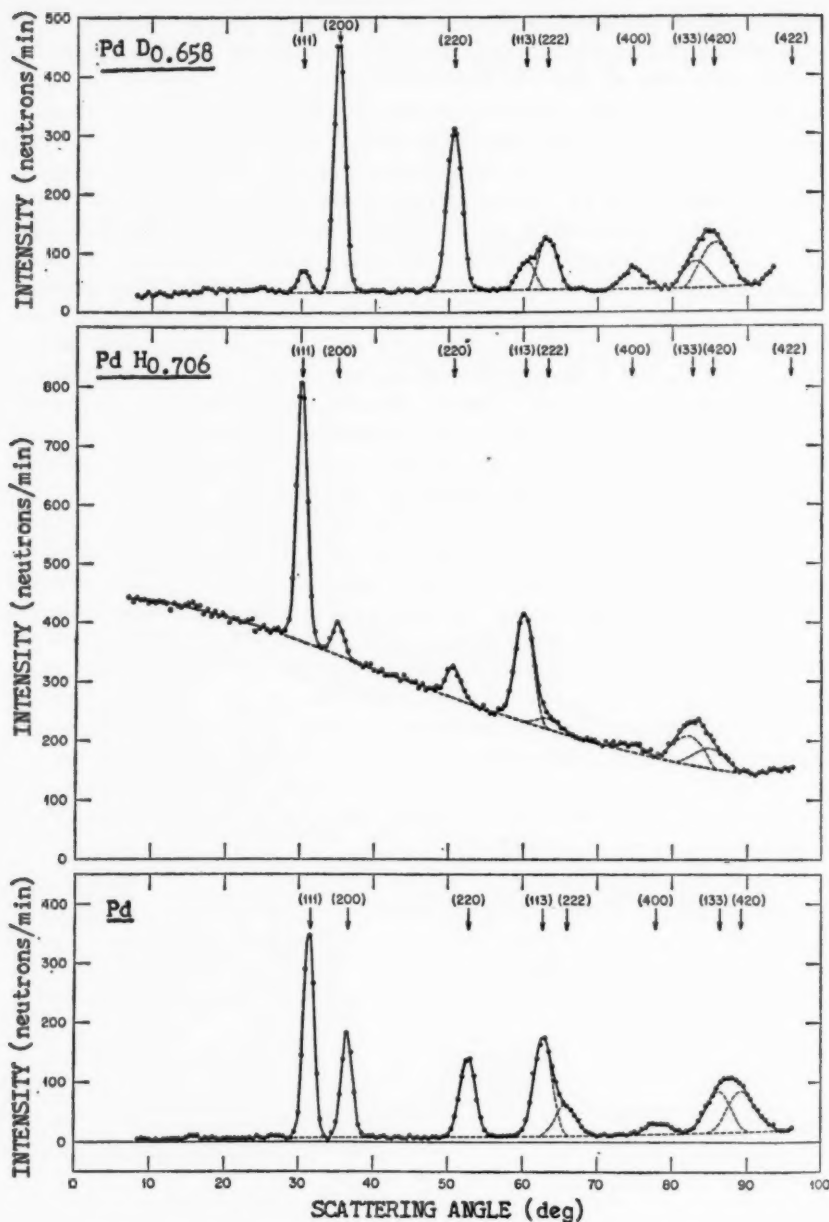
types of substances, and recent reports by Levy & Peterson (48) and by Bacon (49) have summarized most of the results.

The neutron diffraction investigation of the palladium-hydrogen system provides a good illustration of neutron scattering from hydrogen and deuterium atoms in a crystal lattice, and typical diffraction patterns (50) are shown in Figure 4. The pattern from palladium powder is compared with similar patterns from the identical powder after it was loaded with hydrogen and deuterium gases to the indicated atomic compositions. The crystal structure is not changed with the addition of the gas, and there is merely an expansion of the lattice which displaces the reflections to slightly smaller angles. Therefore, the effect of hydrogen and deuterium scattering can be easily observed by comparing relative intensities of two reflections such as the (111) and (200) reflections in the three patterns. Not only do the relative intensities change with the addition of the gas atoms, but the changes in intensity for the deuteride are opposite to those for the hydride, which is the condition to be expected since deuterium and hydrogen have coherent nuclear scattering amplitudes with opposite signs. The intense diffuse scattering in the $\text{PdH}_{0.706}$ pattern is a consequence of the nuclear spin-dependent incoherent scattering from hydrogen, and this diffuse scattering has an angular variation since the hydrogen atoms in the lattice were not rigidly bound relative to the energy of the incident neutrons. The palladium-hydrogen sys-

tem has been of considerable interest for many years because of the unusual diffusion characteristics of the gas in the metal, and the neutron diffraction investigation showed that the gas atoms are actually located in the octahedral positions of the palladium lattice and do not exist in an extensive "rift network" as had been postulated (51). A more complete single-crystal neutron investigation (52) on electrolytically loaded palladium hydride has recently confirmed these results and given interesting information on the proton vibrations within the crystal lattice. Investigations (53) have also been made on hafnium and titanium hydrides, and these experiments have located the hydrogen positions in the different crystal phases that exist for various amounts of hydrogen taken up by the metals. An interesting technique (54) is possible with the titanium compounds, since titanium 48 has a negative coherent scattering amplitude. It is possible to mix various isotopes with titanium 48 and obtain a titanium metal which has an effective coherent scattering amplitude of zero. Diffraction patterns obtained when hydrogen is placed in such a "full-matrix" would give reflections which are representative of only the hydrogen atoms in the lattice.

Although some investigations have been performed with polycrystalline samples, most of the studies on compounds containing hydrogen have been made with single crystals, because the single-crystal technique is necessary for detailed structural analysis. The first hydrogen-bonded compound to be studied by single-crystal methods was KHF_2 in which Peterson & Levy (55) showed that the $\text{F}-\text{H}-\text{F}$ bond is symmetrical with no detectable departure from spherical symmetry in the vibration of the proton. This investigation was also the first attempt to determine Fourier projections of scattering density from neutron scattering data. These methods have now been extended to investigations of more complex inorganic compounds such as calcium hypophosphite (56) and chromium potassium alum (57) and to studies of organic structures such as hexamethylene tetramine (58), alpha-resorcinol (59), and potassium hydrogen bis-phenylacetate (60). Furthermore, the techniques used in this work are sufficiently accurate to allow detailed structure refinements. Complete least-squares analyses have yielded parameters with a high degree of precision, and procedures have been established for obtaining previously unavailable information on the thermal vibrations in crystals (61).

One particularly interesting problem which has been investigated by neutron diffraction is the structure of ice, and there have been numerous reports in the literature on this compound. Although it had been shown in 1922 by W. H. Bragg that the oxygen atoms are arranged in a loose-packed hexagonal network of interconnected oxygen tetrahedra, there was much speculation concerning the possible locations of the hydrogen atoms. The first neutron diffraction experiments on ice were made by Wollan, Davidson & Shull (62) on polycrystalline D_2O . Although the intensities and resolution were limited, the results were in agreement with a model proposed by Pauling in which the hydrogen positions were of a resonating type. In this

FIG. 4. Neutron diffraction patterns of Pd, PdH_{0.706}, and PdD_{0.658}.

structure, two hydrogen atoms would be associated with a particular oxygen atom, but each hydrogen atom would divide its time between two positions along the oxygen linkages. This "half-hydrogen" model has now been confirmed by the single-crystal neutron diffraction results of Peterson & Levy (63), and their Fourier projection of the neutron scattering density in D_2O is shown in Figure 5. The deuterium scattering lies along a line joining two oxygen atoms, and, as indicated by the level of the scattering density, there are two semi-stable positions for the deuterium atoms along this linkage. Precise information was also obtained from this investigation concerning the orientation and magnitudes of the thermal distributions. These results are important in accounting for some of the physical properties of ice and suggest that the hydrogen-oxygen bonding must be of an exchange type rather than an electrostatic type. Several crystalline hydrates have also been examined recently to determine the bonding properties of the water molecules. In $Na_2CO_3 \cdot NaHCO_3 \cdot 2H_2O$, the water hydrogen atoms are involved in strong hydrogen bonds (64) comparable to those in ice, whereas in cuprous chloride dihydrate (65) and oxalic acid dihydrate (66), the hydrogen bonds are fairly weak and the water molecules have dimensions comparable to those in steam. Other hydrates that have been studied have shown bonding properties of the water molecules between these two apparent extremes.

All of the investigations performed on hydrogen-containing compounds have made important contributions to our understanding of hydrogen bonds in crystals. Most of the analyses have been based on two-dimensional projections of neutron scattering density, so that the choice of compounds has been influenced by the feasibility of obtaining significant information from such a projection. However, the most important considerations have involved the inherent interest in the materials and the ability to obtain single crystals for the investigations which required them.

Ferroelectric compounds.—In recent years there has been considerable interest in certain materials which exhibit spontaneous electric polarization and are consequently called ferroelectrics. This effect is caused by ionic displacements which occur below the ferroelectric Curie temperature and produce an electric dipole moment per unit cell. Since the displacements are the same in all unit cells within a ferroelectric domain, the material has a macroscopic electric polarization.

Many of these compounds have required neutron diffraction investigations to determine the ionic displacements which are responsible for the ferroelectric behavior. In KH_2PO_4 , for example, the use of neutron scattering has been necessary in establishing the role of the hydrogen atoms, and there have been extensive investigations (67, 68, 69) of this compound. The hydrogen atoms in this structure form connecting bonds between the oxygen ions of the PO_4 groups, and Figure 6 shows a two-dimensional projection obtained from single-crystal measurements by Bacon & Pease of the O—O linkage at temperatures above and below the ferroelectric Curie point of $123^\circ K$. In the high-temperature results, the proton appears as an elongated

shape between the oxygen ions, and this distribution can be interpreted as a centrally-located proton with very anisotropic motion or, more probably, as a disordered distribution of the protons between two possible positions on each side of the mid-point in the O—O linkage. In the low-temperature ferroelectric state, the hydrogen atom has taken a preferred position near one of the oxygen ions. To obtain this low-temperature projection it was necessary to order the entire crystal as a single ferroelectric domain, and this was accomplished by applying an electric field of about 8000 v per cm

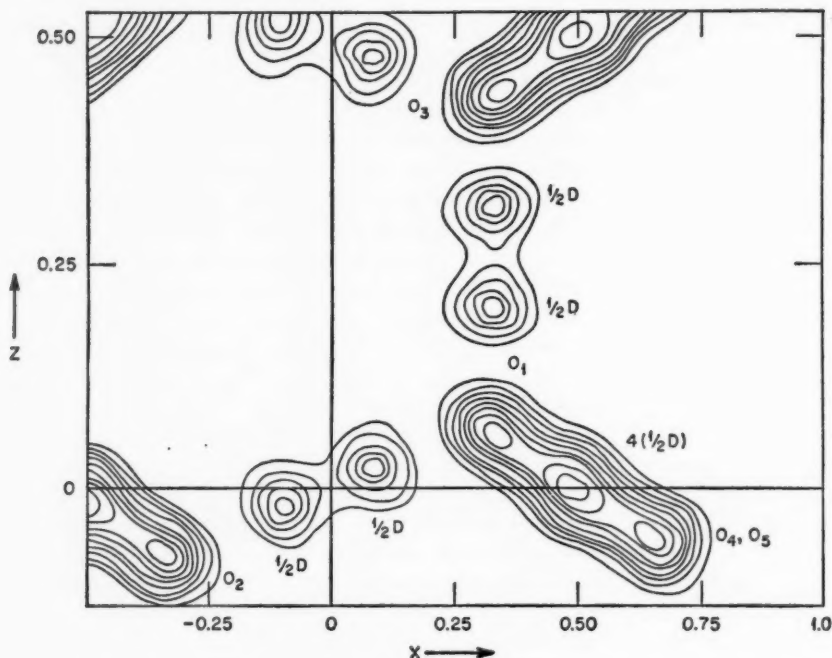


FIG. 5. Fourier projection of the neutron scattering density in heavy ice showing two semistable positions for the deuterium atoms along the oxygen linkages.

along the c axis. A reversed electric field caused the protons to move to the opposite side of the mid-point in the O—O linkage and changed the intensities of many reflections. It is not clear how the proton distribution can produce an electric dipole moment, and the electric polarization at low temperatures is believed to be associated with small displacements of the potassium and phosphorus atoms which also occur below the Curie point.

Neutron diffraction investigations have also determined the structure changes that occur in BaTiO_3 and PbTiO_3 when these compounds become ferroelectric. Both compounds have the cubic perovskite-type structure at high temperatures, and a tetragonal distortion occurs below the ferroelectric

Curie point. The distortion in PbTiO_3 was large enough to allow the application of powder diffraction techniques (70) but in BaTiO_3 a single-crystal analysis (71) was required. In both compounds, there is a displacement of the positive ions relative to the negative oxygen ions to produce net electric dipole moments.

Other compounds.—In addition to compounds involving hydrogen-bonding and ferroelectricity, neutron diffraction techniques have been used to investigate many other compounds with special chemical or magnetic

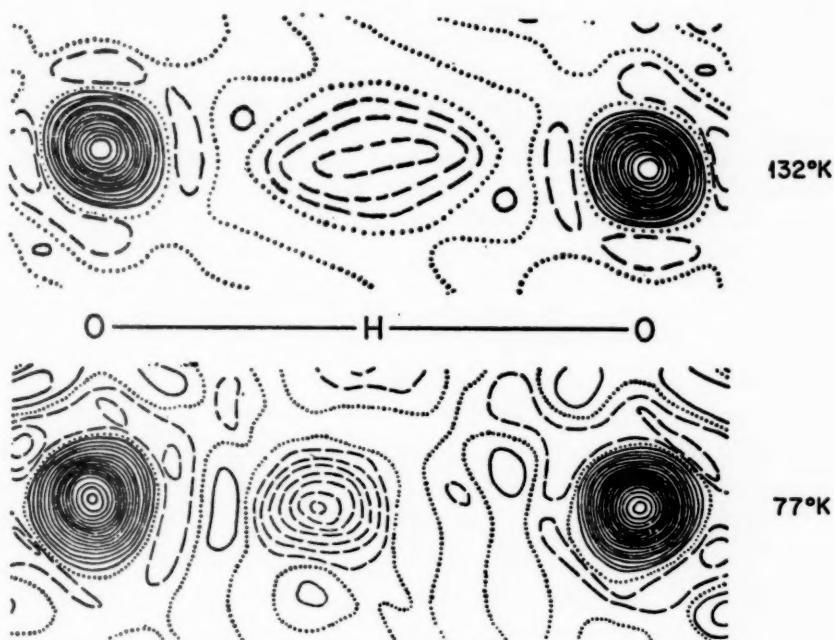


FIG. 6. Fourier projections of the neutron scattering density of a typical O-H-O linkage in KH_2PO_4 above and below the ferroelectric Curie point.

properties. Recent investigations of lead nitrate (72), barium nitrate (73), and potassium cobalticyanide (74) can be classified in the former group. The investigations of $\text{Pb}(\text{NO}_3)_2$ and $\text{Ba}(\text{NO}_3)_2$ were undertaken to determine any significant rotation of the nitrate group about its symmetry axis, and none was observed. Neutron techniques were applied to $\text{K}_3\text{Co}(\text{CN})_6$ to determine the relative positions of the carbon and nitrogen atoms within the cyanide complex, and it was found that the carbon atoms are adjacent to the cobalt ions. In the investigations of magnetic materials, the determination of specific parameters of the anions in certain compounds has been of great importance in accounting for the magnetic properties of the materials. These investiga-

tions include ferrites (75, 76) with the spinel structure and the sesquioxides of rare-earth elements (77). Neutron diffraction has also been applied recently (78) to nonstoichiometric FeO in an attempt to determine the role of cation vacancies in the magnetic behavior of this compound.

ORDER-DISORDER PHENOMENA IN ALLOY SYSTEMS

With appropriate heating procedures, many binary alloy systems form ordered solid solutions in which one atomic species becomes located preferentially with respect to the other. Diffraction patterns of these ordered structures show additional reflections, and their intensities depend on the degree of order and on the difference between the coherent scattering amplitudes of the two atoms. In alloys which contain atoms with almost the same atomic number, the regular variation of X-ray scattering amplitudes makes the determination of the degree of order difficult; and in many of these cases (79), neutron diffraction investigations can give the result easily. Order-disorder phenomena in alloys containing transition elements are particularly important in solid state investigations, since many physical and magnetic properties of these materials are quite sensitive to the degree of order in the sample. Neutron diffraction work on binary alloys has included investigations of the atomic magnetic moments in several transition metal alloys (80) and a recent study (81) of the dynamics of the ordering process in Ni_3Mn .

LIQUIDS AND AMORPHOUS MATERIALS

The investigation of liquid structures by diffraction techniques provides information on the local arrangement of atoms within the liquid, and it is frequently of interest to compare this arrangement with that in the crystalline solid of the same composition. While many liquids have been studied by X-ray diffraction, neutron radiation provides definite advantages in these investigations. The relatively low neutron absorption allows the use of large samples, and the isotropic neutron scattering provides additional information at large scattering angles which is significant for the structure determination. Furthermore, the neutron analysis is somewhat easier since the intensity at large angles approaches a constant value instead of a rapidly decreasing form-factor curve which may not be accurately known.

A neutron diffraction investigation was recently (82) performed on all the alkali metals in the liquid state, and Figure 7(a) shows diffraction patterns which were obtained just above the melting temperatures. For both lithium and sodium, there was a decrease in the scattered intensity at large angles, since the atoms were not tightly bound in the liquid; and the curves for these two liquids have been corrected for the free-atom recoil. No correction of this type was necessary for the patterns obtained on the liquids with heavier atoms. The neutron data were analyzed by the usual method (83, 84), and Figure 7(b) shows the atomic distribution functions that were obtained from the Fourier inversions. The smooth curves represent the uniform

density distributions, and the actual scattering densities fluctuate with respect to these curves. All five distribution functions are similar in their general features; and, within experimental error, the areas of all of the first peaks correspond to about nine nearest neighbors. Since there are twelve nearest neighbors in a close-packed solid, these liquids can be described as loose structures; the peak widths in the distribution curves suggest that the nearest neighbors are not discrete or permanent.

The liquid structures of a number of other elements have also been determined from neutron diffraction investigations. These include sulfur (85), lead (85, 86), bismuth (85, 86), mercury (87), helium (88), neon (89), argon (90, 91), and krypton (92). In the latter investigation, it was necessary to have a sample cell capable of withstanding pressures of the order of 100 atmospheres. In order to meet this requirement with a cell that would not produce an intense or complex diffraction pattern, the cell (93) was fabricated from a single crystal of aluminum and oriented so that it gave negligible scattering at the angles of interest.

MAGNETIC INVESTIGATIONS

The interaction of the magnetic moment of the neutron with the orbital and spin moments in magnetic atoms makes neutron scattering a unique tool for the study of magnetic phenomena at the atomic level. It is important for magnetic investigations not only that there is such an interaction but that the cross section is large and that the interaction depends on the orientation of the spin of the neutron relative to the scattering vector and to the atomic moments with which the neutron interacts. Neutron scattering is used as a tool to investigate a wide variety of magnetic phenomena.

PARAMAGNETISM

In the paramagnetic state of a solid, there are atoms which possess a permanent magnetic moment, and the orientation of these moments is effectively random. In most solids with a high density of magnetic atoms, magnetic forces between the moments on nearby atoms lead to an ordered moment arrangement at a sufficiently low temperature, but at higher temperatures these solids behave as paramagnets. Many facts about the paramagnetic state can be obtained from magnetic susceptibility measurements, but additional important information can be obtained from neutron diffraction investigations. As indicated in Equation 14, the magnetic scattering of neutrons by paramagnetic atoms is incoherent, and the differential cross section of this scattering is proportional to $\mu_p^2 f^2$ where μ_p is the effective moment per atom in the paramagnetic state [equal to $2\sqrt{S(S+1)}$ for a spin-only moment] and f is the form-factor of the magnetic electrons. This form-factor, which can be obtained from the angular dependence of the scattering, is frequently of considerable importance since it contains information on the spin and orbital contributions to the moment and can be analyzed to give the radial distribution of the magnetic electrons.

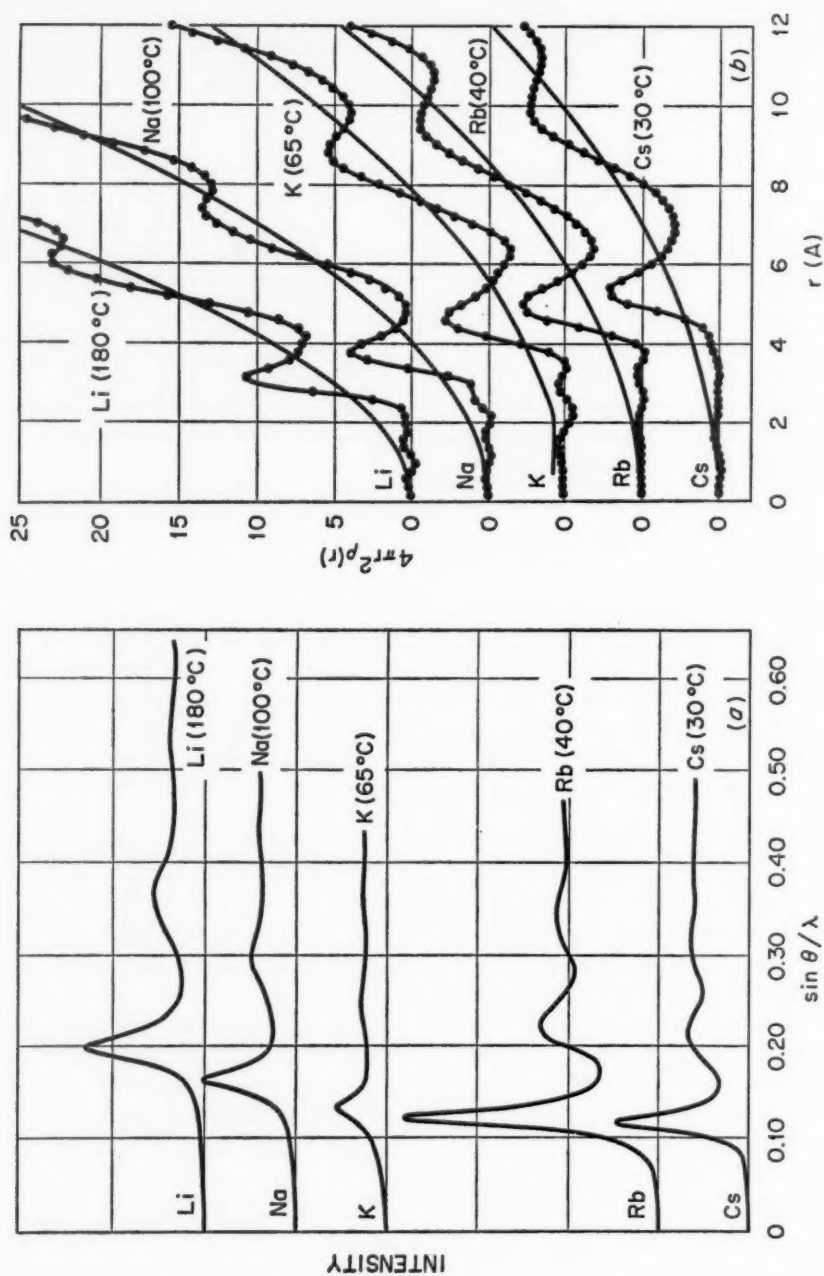


FIG. 7. Studies of liquid alkali metals near the melting temperatures. (a). Neutron diffraction patterns. (b). Atomic distributions.

The scattering by a paramagnetic substance will consist of nuclear Bragg scattering and a number of contributions to the diffuse background scattering. The latter may contain nuclear incoherent effects, thermal diffuse scattering, and multiple scattering in addition to the paramagnetic scattering. Although good corrections can usually be applied to account for thermal diffuse scattering, corrections for the other effects are not always reliable, and an accurate determination of the paramagnetic scattering can be made only when the extraneous effects are small. However, for paramagnetic systems which undergo magnetic ordering at lower temperatures, a second method of analysis can be used; this method utilizes the difference in diffuse scattering at temperatures well above and well below the ordering transition. If experimental conditions do not permit a significant change in the "spin-flip" incoherent scattering between the two temperatures, the difference represents that part of the paramagnetic scattering which becomes ordered at low temperatures. Consequently, it is proportional to $\mu^2 f^2$ where μ is the average atomic magnetic moment in the ordered magnetic lattice (equal to $2S$ for a spin-only moment). This difference method has the advantage of eliminating any background effects and nuclear scattering effects which are independent of temperature. It is also useful in determining the value of the magnetic moment that exists in the ordered magnetic lattice at low temperatures, because a knowledge of the exact magnetic structure is not required.

The first neutron diffraction investigations on paramagnetic materials were made by Shull, Strauser & Wollan (94) on a series of salts containing divalent manganese. These experiments confirmed the theory of paramagnetic scattering given by Halpern & Johnson (8) and provided a determination of the Mn^{++} form-factor. Fourier inversion of this form-factor was performed and the radial distribution of electron density in the $3d$ shell of Mn^{++} was obtained. Although form-factor determinations from paramagnetic scattering do not reveal detailed anisotropic effects, they provide information at small scattering angles which cannot usually be obtained from coherent magnetic scattering. Investigations of this type have been performed on many iron group substances (95, 96), on rare-earth compounds (97, 98), and on molybdenum trifluoride (99) in the $4d$ -transition series. A recent paramagnetic scattering experiment on metallic cerium (100) was helpful in clarifying the anomalous behavior observed in specific-heat and magnetic-susceptibility measurements. These results showed that the interesting magnetic behavior could be correlated with the three crystallographic phases present in the samples and that there is a change in the electronic configuration of the cerium atoms when the collapsed face-centered cubic phase is formed.

For substances which become magnetically ordered, there is a temperature region near the ordering transition in which the angular dependence of the diffuse scattering is strongly influenced by magnetic short-range order. The angular variation which results from these short-range correlations has been calculated (101), and the experimental observations provide informa-

tion on the strength of the exchange interactions. The room temperature pattern of MnO in Figure 8, which shows an attenuation of the paramagnetic scattering at small angles and a broad maximum near the position where antiferromagnetic reflections develop, illustrates the effects of antiferromagnetic short-range order. The diffraction pattern from a substance that possesses strong ferromagnetic short-range correlations has enhanced scattering at small angles and broad maxima near the nuclear reflections.

FERROMAGNETISM

In a ferromagnetic substance, the atomic magnetic moments are spontaneously aligned below a Curie temperature T_C to give a net magnetization within crystal domains which are large compared to atomic dimensions. A simple ferromagnet such as iron contains atoms of the same type, and all atoms have the same moment value. Coherent magnetic neutron scattering is observed from such a ferromagnet, and it occurs at the same angular positions as the nuclear reflections with an intensity corresponding to the value of F_{hkl}^2 given in Equation 11. Therefore, to analyze the magnetic scattering, it is necessary to separate the nuclear and magnetic contributions to the Bragg reflections. If the temperature range is convenient, perhaps the easiest method of separation is to determine the difference in diffraction patterns obtained at temperatures above and below T_C . However, appropriate corrections must be applied to account for any changes in the nuclear scattering with temperature. It is also possible to obtain the magnetic scattering in the reflections by plotting the experimentally determined differential scattering cross sections as a function of the scattering angle. The angularly dependent part represents the magnetic contribution, while the isotropic portion is due to nuclear scattering. However, the most flexible method for studying ferromagnets involves the use of an external magnetic field. If the crystalline anisotropy is sufficiently small, a moderate external field can align all atomic moments in the field direction; and as seen from the definition of q (cf. p. 308), the magnetic scattering depends on the moment orientation relative to the scattering vector. The usual method involves a comparison of the total Bragg scattering in zero field to that with the field applied parallel to the scattering vector. If the moments are aligned in the field direction, there is no magnetic contribution since q is zero, and a difference between the two results gives a direct measurement of the magnetic scattering in the unmagnetized condition.

The magnetic moments of a simple ferromagnet can usually be obtained from saturation magnetization experiments. Consequently, after the original neutron diffraction investigations on ferromagnets by Shull, Wollan & Koehler (102), the primary importance of neutron experiments on these substances has been the determination of accurate magnetic form-factors. Most of this work has been done with the use of polarized neutron beams and will be discussed in a later section.

In addition to the simple ferromagnets, there are substances such as ferro-

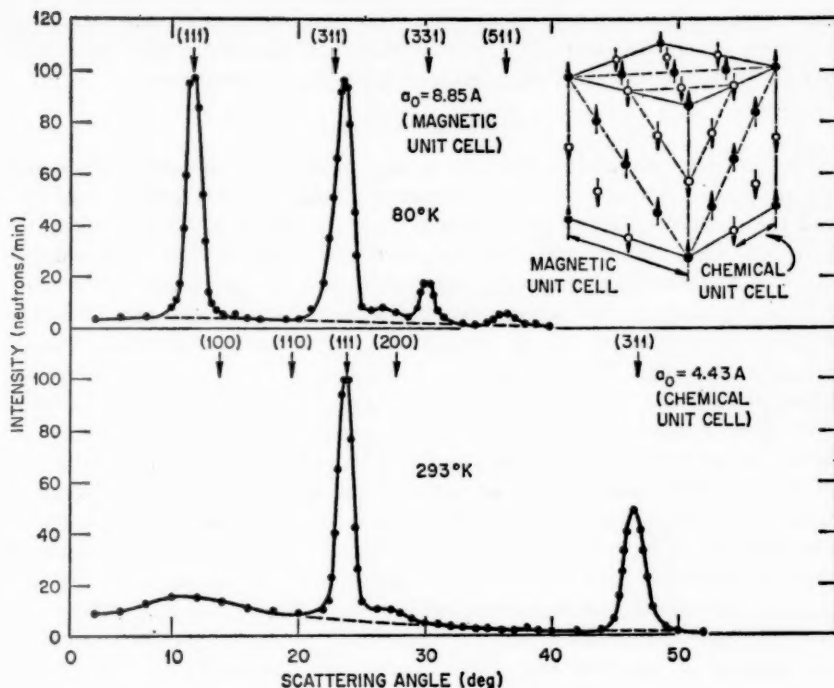


FIG. 8. Neutron diffraction patterns from polycrystalline MnO at temperatures above and below the Néel temperature of 122°K. The atomic magnetic moments in the antiferromagnetic structure are directed along a magnetic axis within the (111) planes.

magnetic alloys, in which the moments are in parallel alignment, but different types of atoms have different moment values. Since magnetic measurements can give only the average moment of the alloy, the determination of the individual magnetic moments of the constituent atoms has been one of the important aspects of the neutron diffraction technique. The first studies of this type were made by Shull & Wilkinson (103) on a number of binary alloys which included both ordered and disordered arrangements of the atoms. In an ordered alloy such as Ni_3Fe , the magnetic contribution to the reflections at nuclear positions depends on the sum of the moments of the constituents, and there are magnetic superlattice reflections in which the magnetic intensity depends on the difference between the moments. A solution of the two expressions gives the individual moment values; but there is a sign ambiguity if unpolarized neutrons are used, and this results in two possible sets of solutions. In the disordered alloys, a similar situation exists except that the expression involving the difference in moment values of the constituent atoms is obtained from ferromagnetic disorder scattering rather

than from superlattice reflections. It is often possible to eliminate one set of solutions on the basis of other information, and the ambiguity can be removed experimentally by experiments with polarized neutrons.

ANTIFERROMAGNETISM

An antiferromagnetic substance is one in which the magnetic moments of the atoms become ordered spontaneously below a Néel temperature T_N , and the ordered arrangement produces no net moment within the magnetic unit cell. This type of magnetic state was proposed by Néel (104) on the basis of macroscopic magnetic properties, and it was possible to show directly by neutron diffraction that such a state does indeed exist. The first neutron investigations on an antiferromagnet were performed by Shull, Strauser & Wollan (94) on MnO, and diffraction patterns which were obtained above and below the Néel temperature of 122°K are shown in Figure 8. The room temperature pattern contains only nuclear reflections; and at 80°K the additional reflections, occurring at angles that are different from the nuclear positions, are characteristic of the scattering from an antiferromagnetic lattice. The ordered arrangement of moments shown in the figure was determined from these results, and later experiments (105, 106) showed that the moments were oriented in a direction parallel to the (111) planes.

The investigation of antiferromagnetic substances is one of the most important applications of the neutron diffraction technique, because detailed information on the size and orientation of the atomic moments in these systems cannot be obtained by other methods. Over 100 antiferromagnetic structures have now been investigated, and a compilation of some of their most important properties has recently been made by Corliss & Hastings (107). As it is impossible to discuss all of these structures here, only a brief survey of the characteristic types and their relationship to other properties of the systems will be given.

One of the major objectives in undertaking these studies is to gain a better understanding of the fundamental nature of the magnetic coupling responsible for the development of magnetic structures. In the pure metals the magnetic coupling interactions must arise in some way by direct overlap of the wave functions of the metal atoms, but the magnetic cations in compounds may be coupled by interactions through the surrounding anions. The early work on MnO showed that the antiferromagnetic coupling between moments of the manganese atoms must be of an indirect type via the oxygen atoms. Furthermore, the similar compounds MnO, FeO, CoO, and NiO have been found (94, 105) to have the same magnetic structures, but the spin directions relative to the crystal are different. In these compounds the predominant magnetic coupling occurs between next-nearest neighbors, and theoretical considerations show that this is a favorable direction for coupling through the p orbitals of the intermediate oxygen atoms. The basis of the theory for such indirect interactions, which have been referred to as super-

exchange, was first developed by Kramers (108) and has been extended by Anderson (109) and others (110, 111). Since MnS exists in three simple polymorphic forms, it provides a convenient system for studying the role of the nonmagnetic ion in magnetic coupling. Corliss, Elliott & Hastings (106) have determined the magnetic structures of these three substances, and the first-neighbor relations of the ordering are shown in Figures 9(g), 9(h), and 9(i). All three magnetic structures can be interpreted in terms of an indirect magnetic coupling of the manganese magnetic moments through the neighboring sulfur ions.

Probably the simplest compounds for a consideration of indirect magnetic interactions are the trifluorides and the perovskites of transition group elements. In these compounds the metal ions occupy the corners of a cube (which may be distorted), and they are separated by anions which lie along the cube edges. In the perovskites there is also an ion located at the center of the cube; but if this ion is not magnetic, it merely establishes the valence state of the magnetic cation and is not directly involved in the magnetic properties of the system. Consequently, only indirect nearest-neighbor magnetic interactions through the intervening anions are important in these compounds, and these interactions cause two simple types of magnetic structures, which have been designated the *G* type and *A* type (112) and are shown in Figures 9(a) and 9(b). The *G*-type structure has been observed (99, 112 to 115) for the 3*d* compounds LaCrO₃, LaFeO₃, CaMnO₃, CrF₃, FeF₃, CoF₃, KMnF₃, KFeF₃, KCoF₃, and KNiF₃ and for the 4*d* compound MoF₃. In these structures the coupling of the metal-ion moments is antiferromagnetic to all six of the nearest neighbors. The *A*-type structure has been determined (112, 114, 115) for LaMnO₃, MnF₃, and KCrF₃ and involves ferromagnetic coupling to four nearest neighbors and antiferromagnetic coupling to the other two. The first satisfactory explanation of the magnetic coupling in systems of this type was made by Goodenough (116) on the basis of a hybrid-orbital approach similar to that which had been applied (117) to spinel-type crystals. It was later shown (114, 118) that a better interpretation could be obtained by considering the properties of the orbitals which result from the splitting of the *d* levels by the crystalline field. The magnetic coupling in all of these compounds can be explained on the basis of the spatial properties, the type of energy splitting, and the electron occupation of these orbitals.

Except for these simple magnetic structures, the nature of the magnetic coupling in compounds is difficult to determine even on a phenomenological basis. However, neutron diffraction experiments have provided specific coupling information on many different types of magnetic compounds. One particularly interesting class of compounds that was investigated recently (119) includes the anhydrous dibromides and dichlorides of iron and cobalt. These compounds, which are hexagonal layer-type structures consisting of layers of metal atoms separated by two layers of halide atoms, were given the

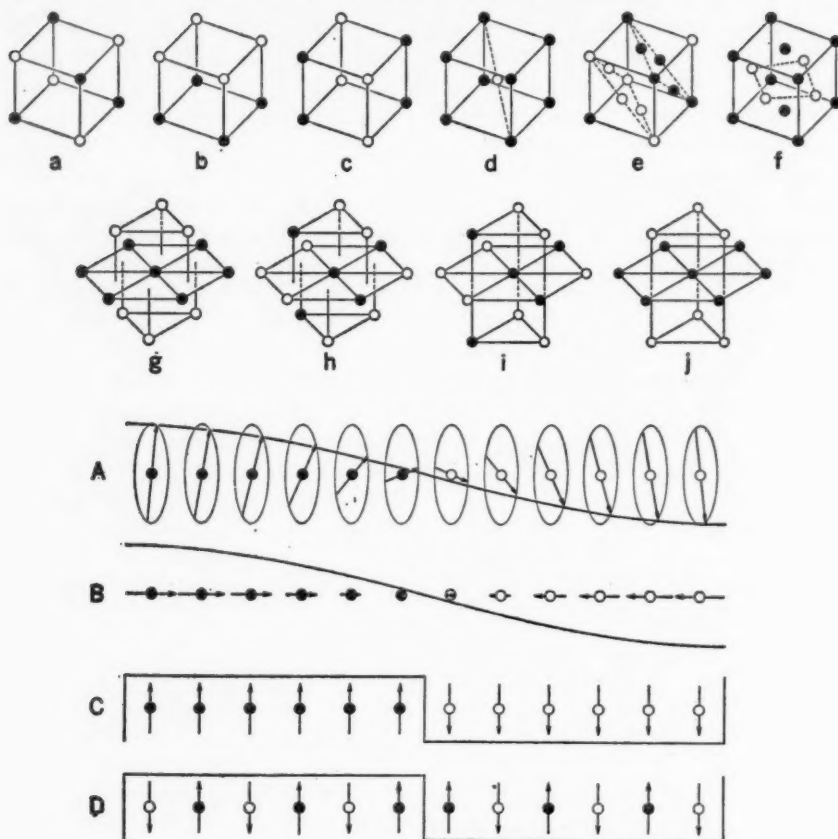


FIG. 9. Various antiferromagnetic systems studied by neutron diffraction. In structures (a) through (j) there is a single magnetic axis with the atomic moments at the open circles antiparallel to those at the solid circles. Figures (A) through (D) indicate various types of antiferromagnetism with a long-range modulation of the moment distribution.

designation "metamagnetics," since their unusual magnetic properties suggested both ferromagnetic and antiferromagnetic behavior. The neutron diffraction studies showed that the compounds are antiferromagnetic at low temperatures with the magnetic moments within a metal layer arranged in ferromagnetic sheets and adjacent sheets arrayed in antiparallel alignment. The ferromagnetic coupling between moments within a layer is much stronger than the antiferromagnetic coupling between atoms in adjacent layers, and the unusual magnetic behavior arises from the ease with which the antiferromagnetic forces can be overcome by an external magnetic field to place all the moments in parallel alignment. Neutron diffraction studies

(35, 120) of the similar compounds containing manganese have shown that these compounds are not metamagnetic and have more complicated antiferromagnetic structures.

The results of neutron diffraction investigations have also been prominent in determining the antiferromagnetic properties of some of the transition metals and their alloys. In fact, the first direct evidence for magnetic order in the nonferromagnetic iron group metals was obtained by the neutron diffraction experiments of Shull & Wilkinson (121) which showed chromium and α -manganese to be antiferromagnetic at low temperatures. Superlattice reflections from polycrystalline chromium were observed and were consistent with the simple body-centered antiferromagnetic structure shown in Figure 9(d) with a magnetic moment per atom about $0.4 \mu_B$. However, as discussed later, recent single-crystal investigations have shown that there is a long-range modulation superimposed on this simple structure. The antiferromagnetic structure of α -Mn has been found (122) to be intricate, and this is probably the result of its unusual crystal structure. More recently, several investigations have been performed on alloy systems which contain the iron group metals in simple crystal structures. Results obtained by Meneghetti & Sidhu (123) and by Bacon *et al.* (124) on MnCu alloys with a small amount of Cu have indicated that face-centered manganese has the antiferromagnetic structure shown in Figure 9(f). Alloys of manganese with nickel (125) and with chromium (126) have also been studied, and the magnetic structures and moment values have been determined. In spite of the large number and variety of experiments performed on the $3d$ metals, their magnetic properties are not well understood from a theoretical point of view. New approaches to this problem have recently been developed by Wollan (118) and by Goodenough (127), which appear to lead to a clearer understanding of many of the distinct features of the metals and their alloys.

In most antiferromagnetic substances the magnetic moments are found in truly antiparallel arrays, but more complicated systems have been encountered recently. In the antiferromagnetic structures of CrSe (128) and some rare-earth orthoferrites (129), the magnetic moments are canted with respect to each other, and several systems have been found in which there is a long-range modulation of the moment distribution. The single-crystal investigations of Corliss, Hastings & Weiss (130) on metallic chromium provided the first direct evidence for a long-range periodicity and showed that the antiferromagnetic reflections observed in the early work actually consisted of small groups of reflections. They have tentatively identified this structure as an antiphase domain type similar to that shown in Figure 9(D). In this model the simple antiparallel arrangement would be predominant, but there would be "mistakes" occurring at regular distances where adjacent moments would be parallel. The single-crystal investigations of chromium also showed a spin-flip transition at low temperatures and a Néel temperature of 308°K compared to the value of 475°K observed in the experiments on powders. Additional investigations (131 to 134) have been performed in an attempt

to understand these effects and to establish definitely the details associated with this type of structure. Other types of long-range modulations observed in magnetic structures include helical and related arrangements of the atomic magnetic moments. Yoshimori (135) was first to determine that a helical system is stable for certain exchange interactions, and he showed that unexplained data (136) on MnO_2 could be accounted for on this basis. Similar theoretical arguments for helical structures were developed independently by Villain (137) at about the same time as an explanation of neutron diffraction results (138) on the MnAu_2 system and by Kaplan (139) as a possible explanation of Cr. More recently, single-crystal investigations by the Oak Ridge group have shown that the unusual magnetic behavior exhibited by the heavy rare-earth metals is caused by magnetic ordering processes of this type. All of these metals have the simple hexagonal close-packed crystal structure, and most of them order antiferromagnetically first and then become ferromagnetic at lower temperatures. Dysprosium (140) has an antiferromagnetic transition at 179°K to nearly the pure helical structure indicated in Figure 9(A), and then it becomes ferromagnetic at 85°K. Holmium (141) also has primarily the helical structure below 131°K, but there appear to be small perturbations superimposed on the true helix. Furthermore, only the component of the moment parallel to the c axis becomes ferromagnetic spontaneously at 20°K. Erbium (142) originally orders antiferromagnetically at 80°K with moments along the c axis only, and the amplitudes of these moments are modulated sinusoidally as shown in Figure 9(B). At about 52°K, the moment components perpendicular to the c axis order in a helical arrangement, and the components parallel to the c axis tend to develop the square-wave properties (except for moment orientation) shown in Figure 9(C). In the ferromagnetic region below 20°K, the c axis components go into parallel alignment, and the structure is similar to that of ferromagnetic holmium.

The neutron diffraction patterns obtained from these systems with a long-range modulation of the moment distribution are similar, and the observed reflections can be considered satellites of the nuclear reflections. These reflections correspond to the satellites observed in a grating when a periodic error is imposed on the normal line spacings. The positions of the nuclear reflections represent the atomic spacings in the crystal, and the superposed long-range modulation of magnetic scattering power causes coherent reflections on both sides of the nuclear reflections. The spacings of the satellites are a direct measurement of the wavelength of the modulation, and the intensities are related to the moment distribution.

FERRIMAGNETISM

The term "ferrimagnetism" has been applied to magnetic substances in which the atomic moments are oriented with antiparallel components but still possess a net ferromagnetic moment. This type of structure was first suggested by Guillaud (143) to explain his magnetic measurements on

Mn_2Sb , and the development of the basic concepts of ferrimagnetism has been evolved principally by Néel (144). Since these substances have both ferromagnetic and antiferromagnetic components, their neutron diffraction patterns have the characteristics of both types and show magnetic reflections at the nuclear and other positions.

Most experiments involving ferrimagnetic materials have been made on a class of compounds with the general formula $X^{+2}Y_2^{+3}\text{O}_4$ which crystallize in the spinel structure. This structure is essentially cubic and contains *A* sites in which the metal ions are tetrahedrally coordinated to four oxygen neighbors and *B* sites in which there is octahedral coordination to six oxygen neighbors. In the normal form, the divalent metal ions occupy the *A* sites and the trivalent ions the *B* sites, while in the inverted form the *A* sites are filled with trivalent ions and the *B* sites are equally divided between divalent and trivalent ions. Magnetite, which is a basic example of these structures, was one of the early compounds investigated by means of neutron diffraction (102), and the results of this investigation confirmed the magnetic structure proposed by Néel on the basis of magnetic measurements. It was found to be inverted and hence has the form $(\text{Fe}^{+3})_A(\text{Fe}^{+2}\text{Fe}^{+3})_B\text{O}_4$. The moments in the *A* and *B* sites were found to be antiparallel so that the net magnetic moment is due only to the Fe^{+2} ions. Extensive neutron diffraction studies have been made by Hastings & Corliss (76, 145) and their colleagues (146, 147) on compounds of this type, including Ni, Mn, Mg, and Zn ferrites. The nickel-iron chromite and manganese-iron chromite systems (148) have also been studied recently with neutron diffraction. All of these experiments, together with conventional magnetic measurements on these compounds, have furnished fundamental information on the degree of crystallographic inversion and on the corresponding magnetic coupling in such systems.

Most of the spinels studied have the magnetic coupling properties proposed by Néel. He predicted large antiferromagnetic (*A-B*) interactions and small antiferromagnetic (*A-A*) and (*B-B*) interactions which would result in a magnetic structure with moments on the *A* and *B* sites antiparallel. Yafet & Kittel (149) have shown that when the three interactions are comparable a triangular arrangement of the moments may be produced. Neutron diffraction experiments by Prince (150) have shown that such a triangular network of moments exists in copper chromite, giving the first experimental verification that ordered magnetic structures are not restricted to a single axis of magnetization. A similar structure has recently been suggested for Mn_2O_4 on the basis of both magnetic measurements (151) and neutron diffraction investigations (152). However, although the concept of canted spins in this compound appears to be correct, there are discrepancies (153) with respect to the Yafet-Kittel model.

The rare-earth garnets belong to another class of ferrimagnetic compounds that possess interesting and unusual magnetic properties. In most of these garnets the spontaneous magnetization is large at low temperatures, decreases rapidly as the temperature is raised, vanishes at a compensation

temperature, reappears at higher temperatures, and finally vanishes at a Curie point of approximately 560°K. This behavior is associated with the development of magnetic order in the iron sublattices at the Curie temperature and with the ordering of the moments of the rare-earth ions at a lower temperature. Extensive measurements have been made on the crystal chemistry (154) and magnetic properties (155) of many of these compounds, and the low-temperature magnetic structure of holmium garnet ($5\text{Fe}_2\text{O}_3 \cdot 3\text{Ho}_2\text{O}_3$) has recently been determined from neutron diffraction investigations on polycrystalline samples by Herpin, Koehler & Mériel (156).

MAGNETIC TRANSITIONS

The neutron diffraction technique has made it possible to study the details of magnetic transitions in all types of magnetic structures merely by measuring the temperature variation of the magnetic reflections. This is of particular importance in antiferromagnetic systems, for which the usual magnetic measurements provide no information, and in ferrimagnetic systems, in which the different types of moments can be observed separately.

In most magnetic substances the magnetic ordering is a second-order transition and the magnetic intensities follow a Brillouin-type dependence (95). However, in a few cases, notably for MnBr_2 and MnI_2 , a sharp first-order type of magnetic transition between the paramagnetic and the antiferromagnetic states has been observed (35, 157). The temperature dependence associated with magnetic ordering in these compounds is much like that found for positional ordering of the atoms in an A_2B type of binary alloy.

Magnetic transitions can also involve a change from one state of magnetic order to another, and various types of order-order transitions have been studied with neutron diffraction techniques. These studies include changes in the moment orientation of an ordered magnetic structure (94, 158, 159), changes from one type of antiferromagnetic order to another (120), and transitions between antiferromagnetism and ferromagnetism or ferrimagnetism (140, 141, 142, 160).

MAGNETIC FIELD EFFECTS

A variety of changes can be produced in the neutron diffraction patterns from magnetic crystals by application of magnetic fields sufficiently strong to change the orientation of the atomic moments and the corresponding value of q in Equation 9. Without regard to the actual magnitude of the magnetic field itself, field effects can be classified as weak or strong relative to the magnetic-exchange coupling in the crystal. There are the usual weak field effects which are involved with the orientation of the domain structure in a ferromagnetic or ferrimagnetic substance; and these domain effects, which have also been observed in certain antiferromagnetic compounds, are related to the anisotropy resulting from the crystal field or to anisotropic-

exchange effects. The strong field effects provide additional information on the nature and strength of the magnetic interactions that exist in the magnetic structures.

In ferromagnetic materials, as discussed in a previous section, an external magnetic field is useful in separating the magnetic coherent scattering from the nuclear scattering. It is also possible to obtain information on the domain size in a ferromagnetic material from neutron scattering effects. Small-angle magnetic scattering is produced by a distribution of small magnetic domains with different magnetic axes, and this scattering can be made to disappear by aligning the domains in an external magnetic field. However, extremely good resolution must be employed by experiments of this type because, as shown in investigations on iron (161), small-angle scattering from ferromagnetic domains of normal size is found at angles of only a few minutes.

The neutron diffraction technique has been very valuable in studying the domain properties of antiferromagnetic crystals, and two distinct types of domains have been observed. One type is the counterpart of the usual ferromagnetic domain in which only the moment direction changes at a domain boundary, and a single domain can be formed merely by orienting the moments along a common axis. In more complicated antiferromagnetic systems such as manganese bromide and chloride, the magnetic structure is formed (35, 120) at random along equivalent crystal directions, but there is a structural orientation associated with the specific direction. Such domains, which have been referred to as structural domains, must be separated by small regions of disorder; and they can be brought into coincidence throughout the crystal only by a breakdown of the structure and a subsequent formation along some chosen domain direction. Both types of domains can be transformed into a single domain by relatively weak magnetic fields, and in some cases the single-domain structures are almost completely preserved when the field is removed. In complex magnetic systems, the development of single domains has been found almost essential in determining specific details of the magnetic structures.

Although most of the applications of external magnetic fields in neutron diffraction involve domain transformations, interesting information on the magnetic interactions is also obtained when exchange forces can be overcome. In metamagnetic cobalt chloride and iron chloride, which have weak antiferromagnetic forces between metal layers, moderate magnetic fields applied in the proper direction were able to bring all moments into parallel alignment, and the details of these processes were determined from diffraction experiments (119). The rare-earth metals also have a metamagnetic type of behavior in which strong ferromagnetic interactions and weak antiferromagnetic interactions produce the helical structures in the antiferromagnetic states (140, 141, 142). Consequently, the antiferromagnetic to ferromagnetic transitions in these metals can be strongly influenced by a magnetic field, and the corresponding magnetic structure changes have been observed.

NEUTRON POLARIZATION

Although most neutron diffraction experiments are performed with unpolarized neutrons, polarized neutron beams are required for certain types of investigations. Enhanced sensitivity is obtained with polarized neutrons in the determination of magnetic scattering from ferromagnetic and ferrimagnetic substances, and this technique also provides an accurate method for separating the magnetic and nuclear contributions. Consequently, small magnetic cross sections, which are encountered for small moment values or at large scattering angles where the magnetic form-factor is small, can be measured accurately in these substances with the polarized beam technique only.

Highly polarized beams of neutrons can be obtained by total reflection from magnetized mirrors (162) and by Bragg reflection from magnetic crystals. The latter method is most frequently used in diffraction work because intense beams of polarized neutrons can be obtained by this method in the monochromating process. As indicated in Equation 11, the polarization of a neutron beam has its source in the interference effects between the nuclear and magnetic scattering. If the magnetic moments within a crystal are aligned by a magnetic field in a direction perpendicular to the scattering vector, a beam of unpolarized neutrons diffracted by this crystal will be resolved into two components which have spin vectors parallel and antiparallel to the moment direction. Under these conditions $|q|$ becomes unity and $(q \cdot \lambda) = \pm 1$, so that the values of F_{hkl}^2 for the two spin states will be:

$$F_{hkl(+)}^2 = (b + p)_{hkl}^2 R_{hkl}^2$$

and

$$F_{hkl(-)}^2 = (b - p)_{hkl}^2 R_{hkl}^2 \quad 18.$$

where the (+) and (-) refer to the scattering processes in which the neutron spins and atomic moments are either parallel or antiparallel to each other. If the magnetic amplitude p and the nuclear amplitude b are equal for a reflection from a crystal, it is evident that the scattering will be zero for one spin state and that the diffracted beam will be completely polarized. This condition is nearly satisfied for the (220) reflection from magnetite, and this crystal was used to produce the first highly polarized neutron beams obtained (102) by Bragg reflection. Nathans, Shull, and their collaborators (163, 164) have developed the use of polarized beams in recent years and have shown that single crystals of a CoFe alloy containing 92 atomic per cent cobalt have a great polarizing efficiency in the (111) reflection. Since the neutron reflectivity for this reflection is greater than that for the (220) magnetite reflection and since there is also less second-order contamination in the reflected beam, CoFe crystals are used as monochromating crystals in most polarized-beam diffractometers.

These diffractometers are modified double-crystal units in which the second crystal is either a polarization analyzer (usually also a CoFe crystal)

or a specimen crystal and there is some method of flipping the neutron spins in the incident monochromatic beam from one polarization state to the other. If a ferromagnetic or ferrimagnetic scattering specimen is magnetized with the moments perpendicular to the scattering vector, the magnetic scattering amplitude in an (hkl) reflection can be determined from measurements of the scattered intensities for the (+) and (-) polarization states. As the two expressions in Equation 18 show, the ratio of these intensities provides a value of p_{hkl}/b_{hkl} , so that the magnetic scattering amplitude is determined in terms of the nuclear scattering amplitude when appropriate corrections have been made for extinction and depolarization. The sensitivity of this method results from a comparison of p with b instead of p^2 with b^2 , and the procedure normalizes the results in terms of a quantity which can be accurately measured. This technique has been used in structure determinations (165) and in measurements of accurate magnetic form-factors.

MAGNETIC FORM-FACTORS

The spatial distribution of unpaired electrons in magnetic atoms gives rise to a form-factor dependence of magnetic neutron scattering, and consequently the magnetic cross section decreases with scattering angle. Determinations of magnetic form-factors can be made from neutron diffraction measurements of magnetic intensities in the coherent reflections and from measurements of the paramagnetic scattering. Such measurements, when accurately made over a large range of $\sin \theta/\lambda$, give valuable information about the wave-function properties of the magnetic electrons in crystalline solids. Furthermore, this information is specifically related to the unpaired electrons in the particular shell responsible for the magnetic properties of the atoms involved. For example, Fe^{3+} and Mn^{2+} ions have five unpaired $3d$ electrons, and the form-factor measurements on crystalline compounds provide a direct determination of the spatial distribution of these electrons in their surroundings.

The form-factor for the Mn^{2+} ion has been determined from the angular dependence of antiferromagnetic reflections from several chemical compounds (166), and the results are shown in Figure 10(a). Similar data for the $4d$ electrons in a Mo^{3+} ion, as determined by analyses (99) of the paramagnetic scattering and the antiferromagnetic reflections from MoF_3 , are shown by the lower curve in this figure. The best form-factor results for ferromagnetic and ferrimagnetic substances have been obtained by the polarized-neutron technique, described in the previous section. This technique has been used by Nathans, Shull, and others (164, 167) for investigations of the $3d$ metals iron, cobalt, and nickel, and the results for iron and nickel are shown by the upper two curves in Figure 10(a). Comparison of the general shape of these curves has shown that the variation from element to element is consistent with the differences in their respective nuclear charges. Furthermore, the accurate results at large scattering angles have demonstrated asymmetries that exist in the unpaired-electron densities.

In the $3d$ metals and their compounds, the atomic moments are usually associated almost wholly with the electron spins, the effects of the orbital currents being in most cases completely quenched. Since the moment associated with the spin resides on the electrons themselves, the form-factor dependence of the magnetic scattering in such cases will be directly associated with the spatial distribution of these electrons.

The rare-earth elements, which possess unpaired electrons in the $4f$ shell, have a strong Russell-Saunders coupling between the electron spins and their orbital angular momenta; and the orbital currents are not quenched. The angular dependence of the neutron scattering for the rare-earth metals and their compounds is thus not a direct measurement of the distribution of the magnetic electrons; it depends also on the magnetic-moment distribution arising from the orbital currents. In a classical picture, the orbital currents can be considered as magnetically equivalent to a sheet of magnetic moments bounded by the current loops. These moments are thus more centrally distributed within the atom than the moments associated with the moving electrons which produce them, and the corresponding form-factors must decrease less rapidly with scattering angle than those associated with the electron spins.

A simple illustration of the effects of the orbital contributions was obtained by a neutron study of the Nd^{3+} and Er^{3+} ions in the oxides (97). These rare-earth ions have the same values of L and S with J_{Nd} equal to $L-S$ and J_{Er} equal to $L+S$. It was shown that the orbital and spin parts of the scattering amplitudes for these similar ions can be qualitatively represented as the sum and difference of the measured amplitudes for each ion. The relative total magnetic scattering amplitudes for Nd^{3+} and Er^{3+} are shown as the solid curves in Figure 10(b), and the approximate orbital and spin contributions to the magnetic scattering for both ions are shown by the dashed curves. The complicated unraveling of the spin and orbital effects was placed on more fundamental grounds by Trammell (9), and recent studies by Odier & Saint-James (11) have extended these calculations.

INELASTIC SCATTERING

In addition to investigations using the elastic scattering of thermal neutrons, important solid state information can also be obtained from inelastic scattering experiments. These experiments fall into the broad scope of neutron diffraction, but they are basically different from those usually associated with this technique. Therefore, the purpose of this section is merely to mention the types of inelastic neutron scattering investigations without indicating their over-all importance.

The diffraction effects caused by inelastic neutron scattering are more pronounced than those observed in X-ray scattering because of the different momentum-energy ratios. Moreover, with thermal neutrons the energy changes can be caused either by an interaction with the lattice vibrations or by a magnetic interaction with the atomic moments. The first theoretical

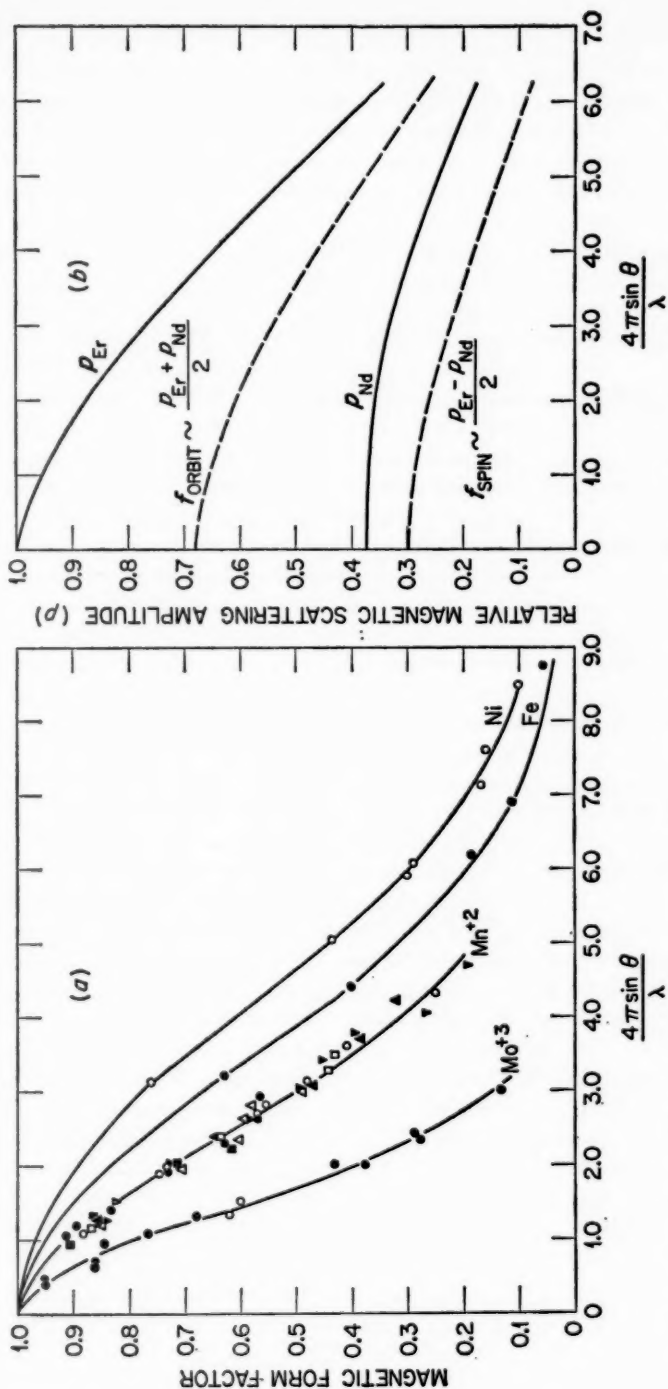


Fig. 10(a). Magnetic form-factors for certain atoms and ions with spin-only atomic magnetic moments. (b). Relative magnetic scattering amplitudes and corresponding approximate magnetic form-factors for trivalent erbium and neodymium.

treatment, by Weinstock (168), of the inelastic effects associated with neutron scattering by crystals was similar to that for the corresponding X-ray effects (169), in which temperature motions in the lattice were considered in terms of the amplitudes of a set of plane-polarized standing waves. The energy transfers between the neutron and crystal were represented by quantized frequency changes, and the term "phonon" was used to describe the energy quantum involved. Both absorption and emission of phonons are possible depending on the energy conditions, and although one-phonon processes are more probable, multiple-phonon processes (170, 171) frequently must be considered. Several theoretical investigations (172 to 179) have added to the original theory for the interaction of thermal neutrons with lattice vibrations, and the inelastic processes which result from magnetic interactions have also been considered (180 to 184). In the latter case, the term "magnon" is often used to represent the energy quantum associated with changes in the magnetic order of a system, and scattering processes can cause both magnon emission and magnon absorption in direct similarity to the phonon picture.

The first experiments involving inelastic scattering were transmission experiments (185, 186) using neutrons with wavelengths above the cutoff for Bragg scattering and were performed primarily to test certain aspects of the theory. In recent years two other methods have been used in investigations of this type. The most direct method (187) is one in which the energy spectrum of the scattered neutrons is measured with an additional crystal spectrometer or a neutron velocity selector. Brockhouse & Stewart have used this technique in investigations of aluminum (188) and vanadium (189), and they have shown that the results can be interpreted directly in terms of the dispersion relations of the normal modes of the crystal without the large corrections necessary in similar X-ray investigations. The magnetic inelastic scattering from magnetite has also been studied by this method (190), and results of this investigation are consistent with the magnetic spin-wave theory within the limits of analysis. The major disadvantage of this type of experiment is the requirement of intense neutron beams which can be obtained only at high-flux reactors, and the second method used in these investigations does not have this restriction. This method, originally discussed by Moorhouse (180), requires single-crystal samples and involves the measurement of the widths of inelastic scattering peaks as the crystal is rotated away from the position for Bragg reflection. The experimental details of this technique were developed by Lowde (191), and he has obtained important information concerning the magnetic properties of iron (192) from experiments of this type. Riste, Blinowski & Janik (193) have recently applied the same method to investigations of magnetite, and these observations indicate that magnetic inelastic neutron scattering from this substance is well described by spin-wave theory over a wide temperature range.

LITERATURE CITED

1. Bacon, G. E., *Neutron Diffraction* (Clarendon Press, Oxford, Engl., 1955)
2. Shull, C. G., and Wollan, E. O., *Solid State Physics*, II, 137 (Seitz, F., and Turnbull, D., Eds., Academic Press, New York, N. Y., 1956)
3. Ringo, G. R., *Handbuch der Physik*, XXXII, 552 (Flugge, S., Ed., Springer-Verlag, Berlin, Gottingen, Heidelberg, 1957)
4. Blatt, J. M., and Weisskopf, V. F., *Theoretical Nuclear Physics*, Chap. VIII (John Wiley & Sons, New York, N. Y., 1952)
5. Fermi, E., and Marshall, L., *Phys. Rev.*, **70**, 103 (1946); *Phys. Rev.*, **71**, 666 (1947)
6. Bloch, F., *Phys. Rev.*, **50**, 259 (1936); *Phys. Rev.*, **51**, 994 (1937)
7. Schwinger, J., *Phys. Rev.*, **51**, 544 (1937)
8. Halpern, O., and Johnson, M. H., *Phys. Rev.*, **55**, 898 (1939)
9. Trammell, G. T., *Phys. Rev.*, **92**, 1387 (1953)
10. Kleiner, W. H., *Phys. Rev.*, **90**, 168 (1953)
11. Odier, S., and Saint-James, D., *Phys. and Chem. Solids*, **17**, 117 (1960)
12. Trammell, G. T. (Private communication)
13. Weiss, R. J., Hastings, J. M., and Corliss, L. M., *Phys. Rev.*, **83**, 863 (1951)
14. Caglioti, G., Paoletti, A., and Ricci, F. P., *Nuclear Instr.*, **3**, 223 (1958)
15. Lowde, R. D., *J. Nuclear Energy, Part A, Reactor Science*, **11**, 69 (1960)
16. Schenck, J., *Nature*, **171**, 518 (1953)
17. Schenck, J., and Neiler, J. H., *Nuclear Science*, **12**, 28 (1954)
18. Halpern, O., Hammermesh, M., and Johnson, M. H., *Phys. Rev.*, **59**, 981 (1941)
19. Fermi, E., Sturm, W. J., and Sachs, R. G., *Phys. Rev.*, **71**, 589 (1947)
20. Fermi, E., and Marshall, L., *Phys. Rev.*, **72**, 408 (1947)
21. Wu, C. S., Rainwater, L. J., and Havens, W. W., *Phys. Rev.*, **71**, 174 (1947)
22. Wollan, E. O., and Shull, C. G., *Phys. Rev.*, **73**, 830 (1948)
23. Sidhu, S. S., Heaton, L., Zaubers, D. D., and Campos, F. P., *J. Appl. Phys.*, **27**, 1040 (1956)
24. Compton, A. H., and Allison, S. K., *X-Rays in Theory and Experiment*, 415 (D. Van Nostrand Co., Inc., New York, N. Y., 1946)
25. Koehler, W. C., Wollan, E. O., and Shull, C. G., *Phys. Rev.*, **79**, 395 (1950)
26. Bacon, G. E., and Lowde, R. D., *Acta Cryst.*, **1**, 303 (1948)
27. Hamilton, W. C., *Acta Cryst.*, **10**, 629 (1957); *Acta Cryst.*, **11**, 585 (1958)
28. Peterson, S. W., and Levy, H. A., *J. Chem. Phys.*, **19**, 1416 (1951)
29. Busing, W. R., and Levy, H. A., *Acta Cryst.*, **10**, 180 (1957)
30. Wollan, E. O., Shull, C. G., and Marney, M. C., *Phys. Rev.*, **73**, 527 (1948)
31. Sun, K. H., and Wollan, E. O. (Unpublished)
32. Ginther, R. J., *IRE, Trans. NS-7*, No. 2-3, 28 (1960)
33. Slaughter, G. G., Firk, F. W. K., and Ginther, R. J., *Bull. Am. Phys. Soc.*, **6**, 275 (1961)
34. Erickson, R. A., *Phys. Rev.*, **90**, 779 (1953)
35. Wollan, E. O., Koehler, W. C., and Wilkinson, M. K., *Phys. Rev.*, **110**, 638 (1958)
36. Wilkinson, M. K., and Shull, C. G., *Phys. Rev.*, **103**, 516 (1956)
37. Shull, C. G., and Wollan, E. O., *Phys. Rev.*, **81**, 527 (1951)
38. Peterson, S. W., and Smith, H. G., *Phys. Rev. Letters*, **6**, 7 (1961)
39. James, R. W., *The Optical Principles of the Diffraction of X-Rays*, 33 (Bell and Sons Ltd., London, Engl., 1954)
40. Salpeter, E. E., *Phys. Rev.*, **82**, 60 (1951)
41. Schwinger, J., and Teller, E., *Phys. Rev.*, **52**, 286 (1937)
42. Halpern, J., Esterman, I., Simpson, O. C., and Stern, O., *Phys. Rev.*, **52**, 142 (1937)
43. Brickwedde, F. G., Dunning, J. R., Hoge, H. J., and Manley, J. H., *Phys. Rev.*, **54**, 266 (1938)
44. Squires, G. L., and Stewart, A. T., *Proc. Roy. Soc. (London)*, **A**, **230**, 19 (1955); *J. Chem. Phys.*, **22**, 754 (1954)
45. Shull, C. G., Wollan, E. O., Morton, G. A., and Davidson, W. L., *Phys. Rev.*, **73**, 842 (1948)
46. Melkonian, E., *Phys. Rev.*, **76**, 1744 (1949)
47. Burgoyne, M. T., Ringo, G. R., and Hughes, D. J., *Phys. Rev.*, **84**, 1160 (1951)
48. Levy, H. A., and Peterson, S. W., *Revs. Mod. Phys.*, **30**, 101 (1958)

49. Bacon, G. E., *Revs. Mod. Phys.*, **30**, 94 (1958)
50. Worsham, J. E., Wilkinson, M. K., and Shull, C. G., *Phys. and Chem. Solids*, **3**, 303 (1957)
51. Smith, D. P., *Hydrogen in Metals* (University Press, Univ. Chicago, Ill., 1948)
52. Bergsma, J., and Goedkoop, J. A., *Physica*, **26**, 744 (1960)
53. Sidhu, S. S., Heaton, L., and Zauberis, D. D., *Acta Cryst.*, **9**, 607 (1956)
54. Sidhu, S. S., Heaton, L., and Mueller, M. H., *J. Appl. Phys.*, **9**, 1323 (1959)
55. Peterson, S. W., and Levy, H. A., *J. Chem. Phys.*, **20**, 704 (1952)
56. Loopstra, L. H. (Doctoral thesis, Univ. Amsterdam, Amsterdam, Netherlands, 1958)
57. Bacon, G. E., and Gardner, W. E., *Proc. Roy. Soc. (London)*, **246**, 78 (1958)
58. Andresen, A. F., *Acta Cryst.*, **10**, 107 (1957)
59. Bacon, G. E., and Curry, N. A., *Proc. Roy. Soc. (London)*, **235**, 552 (1956)
60. Bacon, G. E., and Curry, N. A., *Acta Cryst.*, **10**, 524 (1957); *Acta Cryst.*, **13**, 717 (1960)
61. Busing, W. R., and Levy, H. A., *Proc. Symposium on Computer Methods* (Glasgow, Scotland, 1960); *Acta Cryst.*, **11**, 450 (1958)
62. Wollan, E. O., Davidson, W. L., and Shull, C. G., *Phys. Rev.*, **75**, 1348 (1949)
63. Peterson, S. W., and Levy, H. A., *Acta Cryst.*, **10**, 70 (1957)
64. Bacon, G. E., and Curry, N. A., *Acta Cryst.*, **9**, 82 (1956)
65. Peterson, S. W., and Levy, H. A., *J. Chem. Phys.*, **26**, 220 (1957)
66. Garrett, B. S., Doctoral thesis, *Oak Ridge Natl. Lab. Rept. 1745* (1954)
67. Levy, H. A., Peterson, S. W., and Simonsen, S. H., *Phys. Rev.*, **93**, 1120 (1954)
68. Pepinsky, R., and Frazer, B. C., *Science*, **117**, 1 (1953)
69. Bacon, G. E., and Pease, R. S., *Proc. Roy. Soc. (London)*, **A**, 220, 397 (1953); *Proc. Roy. Soc. (London)*, **A**, 230, 359 (1955)
70. Shirane, G., Pepinsky, R., and Frazer, B. C., *Acta Cryst.*, **9**, 131 (1956)
71. Frazer, B. C., Danner, H. R., and Pepinsky, R., *Phys. Rev.*, **100**, 745L (1955)
72. Hamilton, W. C., *Acta Cryst.*, **10**, 103 (1959)
73. Dachs, H. (Private communication)
74. Curry, N. A., and Runciman, W. A., *Acta Cryst.*, **12**, 674 (1959)
75. Bacon, G. E., and Roberts, F. F., *Acta Cryst.*, **6**, 57 (1953)
76. Hastings, J. M., and Corliss, L. M., *Revs. Mod. Phys.*, **25**, 114 (1953)
77. Koehler, W. C., and Wollan, E. O., *Acta Cryst.*, **6**, 741 (1953)
78. Roth, W. L., *Acta Cryst.*, **13**, 140 (1960)
79. Shull, C. G., and Siegel, S., *Phys. Rev.*, **75**, 1008 (1949)
80. Shull, C. G., and Wilkinson, M. K., *Phys. Rev.*, **97**, 304 (1955)
81. Marcinkowski, M. J., and Brown, N., *J. Appl. Phys.*, **32**, 375 (1961)
82. Gingrich, N. S., and Heaton, L., *J. Chem. Phys.*, **34**, 873 (1961)
83. Zernike, F., and Prins, J. A., *Z. Physik*, **41**, 184 (1927)
84. Debye, P., and Menke, H., *Ergebnisse der Technische Röntgenkunde*, **II**, 1 (Akad. Verlagsgesellschaft, Leipzig, Germany, 1931)
85. Chamberlain, O., *Phys. Rev.*, **77**, 305 (1950)
86. Sharrah, P. C., and Smith, G. P., *J. Chem. Phys.*, **21**, 228 (1953)
87. Vineyard, G. H., *J. Chem. Phys.*, **22**, 1665 (1954)
88. Hurst, D. G., and Henshaw, D. G., *Phys. Rev.*, **100**, 994 (1955)
89. Henshaw, D. G., *Phys. Rev.*, **111**, 1470 (1958)
90. Henshaw, D. G., Hurst, D. G., and Pope, N. K., *Phys. Rev.*, **92**, 1229 (1953)
91. Henshaw, D. G., *Phys. Rev.*, **105**, 976 (1957)
92. Clayton, G. T., and Heaton, L., *Phys. Rev.* (To be published)
93. Clayton, G. T., and Heaton, L., *Rev. Sci. Instr.*, **31**, 1355 (1960)
94. Shull, C. G., Strauser, W. A., and Wollan, E. O., *Phys. Rev.*, **83**, 333 (1951)
95. Erickson, R. A., *Phys. Rev.*, **90**, 779 (1953)
96. Cable, J. W., Wilkinson, M. K., and Wollan, E. O., *Phys. Rev.*, **118**, 950 (1960)
97. Koehler, W. C., and Wollan, E. O., *Phys. Rev.*, **92**, 1380 (1953)
98. Koehler, W. C., Wollan, E. O., and Wilkinson, M. K., *Phys. Rev.*, **110**, 37 (1958)
99. Wilkinson, M. K., Wollan, E. O., Child, H. R., and Cable, J. W., *Phys. Rev.*, **121**, 74 (1961)
100. Wilkinson, M. K., Child, H. R., McHargue, C. J., Koehler, W. C.,

- and Wollan, E. O., *Phys. Rev.*, **122**, 1409 (1961)
101. Slotnick, M., *Phys. Rev.*, **83**, 1226 (1951)
102. Shull, C. G., Wollan, E. O., and Koehler, W. C., *Phys. Rev.*, **84**, 912 (1951)
103. Shull, C. G., and Wilkinson, M. K., *Phys. Rev.*, **97**, 304 (1955)
104. Néel, L., *Ann. phys.*, **18**, 5 (1932); *Ann. phys.*, **5**, 232 (1936)
105. Roth, W. L., *Phys. Rev.*, **110**, 1333 (1958)
106. Corliss, L. M., Elliott, N., and Hastings, J. M., *Phys. Rev.*, **104**, 924 (1956)
107. Corliss, L. M., and Hastings, J. M., *Am. Inst. Phys. Handbook* (To be published)
108. Kramers, H. A., *Physica*, **1**, 182 (1934)
109. Anderson, P. W., *Phys. Rev.*, **79**, 350 (1950); *Phys. Rev.*, **115**, 2 (1959)
110. Pratt, G. W., Jr., *Phys. Rev.*, **97**, 926 (1955)
111. Nesbitt, R. K., *Ann. phys.*, **4**, 87 (1958)
112. Wollan, E. O., and Koehler, W. C., *Phys. Rev.*, **100**, 545 (1955)
113. Koehler, W. C., and Wollan, E. O., *Phys. and Chem. Solids*, **2**, 100 (1957)
114. Wollan, E. O., Child, H. R., Koehler, W. C., and Wilkinson, M. K., *Phys. Rev.*, **112**, 1132 (1958)
115. Scatturin, V., Corliss, L. M., Elliott, N., and Hastings, J. M., *Acta Cryst.*, **14**, 19 (1961)
116. Goodenough, J. B., *Phys. Rev.*, **100**, 564 (1955)
117. Goodenough, J. B., and Loeb, A. L., *Phys. Rev.*, **98**, 391 (1955)
118. Wollan, E. O., *Phys. Rev.*, **117**, 387 (1960)
119. Wilkinson, M. K., Cable, J. W., Wollan, E. O., and Koehler, W. C., *Phys. Rev.*, **113**, 497 (1959)
120. Wilkinson, M. K., Cable, J. W., Wollan, E. O., and Koehler, W. C., *Oak Ridge Natl. Lab. Rept.* **2430**, 65 (1957)
121. Shull, C. G., and Wilkinson, M. K., *Revs. Mod. Phys.*, **25**, 100 (1953)
122. Kasper, J. S., and Roberts, B. W., *Phys. Rev.*, **101**, 537 (1956)
123. Meneghetti, D., and Sidhu, S. S., *Phys. Rev.*, **105**, 130 (1957)
124. Bacon, G. E., Dunmur, I. W., Smith, J. H., and Street, R., *Proc. Roy. Soc. (London)*, **A**, **241**, 223 (1957)
125. Kasper, J. S., and Kouvel, J. S., *Phys. and Chem. Solids*, **11**, 231 (1959)
126. Kasper, J. S., and Waterstrat, R. M., *Phys. Rev.*, **109**, 1551 (1958)
127. Goodenough, J. B., *Phys. Rev.*, **120**, 67 (1960)
128. Corliss, L. M., Elliott, N., and Hastings, J. M., *Phys. Rev.* (To be published)
129. Koehler, W. C., Wollan, E. O., and Wilkinson, M. K., *Phys. Rev.*, **118**, 58 (1960)
130. Corliss, L., Hastings, J., and Weiss, R., *Phys. Rev. Letters*, **3**, 211 (1959)
131. Bykov, V. N., Golovkin, V. S., Ageev, N. V., Levдик, V. A., and Vinogradov, S. I., *Soviet Phys. "Doklady"*, **4**, 1070 (1960)
132. Hastings, J. M., *Bull. Am. Phys. Soc.*, **5**, 455 (1960)
133. Bacon, G. E., *Bull. Am. Phys. Soc.*, **5**, 455 (1960)
134. Wilkinson, M. K., Wollan, E. O., and Koehler, W. C., *Bull. Am. Phys. Soc.*, **5**, 456 (1960)
135. Yoshimori, A., *J. Phys. Soc. Japan*, **14**, 807 (1959)
136. Erickson, R. A. (Unpublished)
137. Villain, J., *Chem. and Phys. Solids*, **11**, 303 (1959)
138. Herpin, A., Mériel, P., and Villain, J., *Compt. rend.*, **249**, 1334 (1959)
139. Kaplan, T. A., *Phys. Rev.*, **116**, 888 (1959)
140. Wilkinson, M. K., Koehler, W. C., Wollan, E. O., and Cable, J. W., *J. Appl. Phys.*, **32**, 48S (1961)
141. Koehler, W. C., Cable, J. W., Wollan, E. O., and Wilkinson, M. K., *Proc. Rare Earth Seminar* (Lake Arrowhead, Calif., 1960)
142. Cable, J. W., Wollan, E. O., Koehler, W. C., and Wilkinson, M. K., *J. Appl. Phys.*, **32**, 49S (1961)
143. Guillaud, C. (Doctoral thesis, Univ. Strasbourg, Strasbourg, France, 1943)
144. Néel, L., *Ann. phys.*, **3**, 137 (1948)
145. Hastings, J. M., and Corliss, L. M., *Phys. Rev.*, **102**, 1460 (1956); *Phys. Rev.*, **104**, 328 (1956)
146. Brockhouse, B. N., Corliss, L. M., and Hastings, J. M., *Phys. Rev.*, **98**, 1721 (1955)
147. Corliss, L. M., Hastings, J. M., and Brockman, F. G., *Phys. Rev.*, **90**, 1013 (1953)
148. Pickart, S. J., and Nathans, R., *Bull. Am. Phys. Soc.*, **3**, 231 (1958); *Phys. Rev.*, **116**, 317 (1959)
149. Yafet, Y., and Kittel, C., *Phys. Rev.*, **87**, 290 (1952)
150. Prince, E., *Acta Cryst.*, **10**, 554 (1957)
151. Jacobs, I. S., *Phys. and Chem. Solids*, **11**, 1 (1959)

152. Kasper, J. S., *Bull. Am. Phys. Soc.*, **4**, 178 (1959)
153. Dwight, K., and Menyuk, N., *Phys. Rev.*, **119**, 1470 (1960)
154. Geller, S., *J. Appl. Phys.*, **31**, 30S (1960)
155. Pauthenet, R., *J. Appl. Phys.*, **30**, 290S (1959)
156. Herpin, A., Koehler, W. C., and Mériel, P., *Compt. rend.*, **251**, 1359 (1960)
157. Cable, J. W., Wilkinson, M. K., Wollan, E. O., and Koehler, W. C., *Phys. Rev.* (To be published)
158. Corliss, L. M., Hastings, J. M., and Goldman, J. E., *Phys. Rev.*, **93**, 893 (1954)
159. Wilkinson, M. K., Gingrich, N. S., and Shull, C. G., *Phys. and Chem. Solids*, **2**, 289 (1957)
160. Cloud, W. H., Jarrett, H. S., Austin, A. E., and Adelson, E., *Phys. Rev.*, **120**, 1969 (1960)
161. Hughes, D. J., Burgy, M. T., Heller, R. B., and Wallace, J. W., *Phys. Rev.*, **75**, 565 (1949)
162. Hughes, D. J., and Burgy, M. T., *Phys. Rev.*, **81**, 498 (1951)
163. McReynolds, A. W., Nathans, R., and Shull, C. G., *Proc. Am. Cryst. Assoc. Meeting* (French Lick, Ind., 1956)
164. Nathans, R., Shull, C. G., Shirane, G., and Andresen, A., *Phys. and Chem. Solids*, **10**, 138 (1959)
165. Nathans, R., Pigott, M. T., and Shull, C. G., *Phys. and Chem. Solids*, **6**, 38 (1958)
166. Hastings, J. M., Elliott, N., and Corliss, L. M., *Phys. Rev.*, **115**, 13 (1959)
167. Nathans, R., and Paoletti, A., *Phys. Rev. Letters*, **2**, 254 (1959)
168. Weinstock, R., *Phys. Rev.*, **65**, 1 (1944)
169. Zachariasen, W. H., *Phys. Rev.*, **57**, 597 (1940)
170. Finkelstein, R. J., *Phys. Rev.*, **72**, 907 (1947)
171. Squires, G. L., *Proc. Roy. Soc. (London)*, **A**, 212, 192 (1952)
172. Cassels, J. M., *Progr. in Nuclear Phys.*, **1**, 185 (1950)
173. Placzek, G., *Phys. Rev.*, **86**, 377 (1952)
174. Wick, G. C., *Phys. Rev.*, **94**, 1228 (1954)
175. Van Hove, L., *Phys. Rev.*, **95**, 249 (1954)
176. Placzek, G., and Van Hove, L., *Nuovo cimento*, **1**, 233 (1955)
177. Waller, I., and Froman, P. O., *Arkiv Fysik*, **4**, 183 (1952)
178. Froman, P. O., *Arkiv Fysik*, **4**, 191 (1952); *Arkiv Fysik*, **5**, 53 (1952)
179. Glauber, R. J., *Phys. Rev.*, **98**, 1692 (1955)
180. Moorhouse, R. G., *Proc. Phys. Soc. (London)*, **A**, 64, 1097 (1951)
181. Elliott, R. J., and Lowde, R. D., *Proc. Roy. Soc. (London)*, **A**, 230, 46 (1955)
182. Maleev, C. V., *Zhur. Ekspl. i. Teoret. Fiz.*, **33**, 1010 (1957)
183. Van Hove, L., *Phys. Rev.*, **95**, 1374 (1954)
184. Elliott, R. J., and Marshall, W., *Revs. Mod. Phys.*, **30**, 75 (1958)
185. Cassels, J. M., *Proc. Roy. Soc. (London)*, **A**, 208, 527 (1951)
186. Hughes, D. J., and Palevsky, H., *Phys. Rev.*, **92**, 1206 (1953)
187. Brockhouse, B. N., *Phys. Rev.*, **98**, 1171A (1955)
188. Brockhouse, B. N., and Stewart, A. T., *Revs. Mod. Phys.*, **30**, 236 (1958)
189. Stewart, A. T., and Brockhouse, B. N., *Revs. Mod. Phys.*, **30**, 250 (1958)
190. Brockhouse, B. N., *Phys. Rev.*, **106**, 859 (1957); *Phys. Rev.*, **111**, 1273 (1958)
191. Lowde, R. D., *Proc. Roy. Soc. (London)*, **A**, 221, 206 (1954)
192. Lowde, R. D., *Proc. Roy. Soc. (London)*, **A**, 235, 305 (1956)
193. Riste, T., Blinowski, K., and Janik, J., *Phys. and Chem. Solids*, **9**, 153 (1959)

NUCLEAR EFFECTS OF COSMIC RAYS IN METEORITES¹

BY JAMES R. ARNOLD

*School of Science and Engineering, University of California, San Diego
La Jolla, California*

INTRODUCTION

Meteorites are fragments of rock and metal which reach the earth's surface from outer space. They carry within them, among other treasures, a record of the bombardment by cosmic rays which they have undergone. This record is in the form of radioactive and stable nuclei produced by transmutation. Because of the chemical and physical stability of meteorites, the information generally is well preserved. By studying it we can hope to learn much about the meteorites. We may try to discover, for example, how they were formed as small objects and put into the orbits from which the earth has captured them. To do this we need first to know the duration of the bombardment, to fix the time of the original event. Another question concerns the size and shape of meteorites before their passage through the earth's atmosphere, during which they suffer extensive ablation and often break into many pieces. This may be answered by sufficiently detailed study of the variation with depth in the meteorite of the abundance of certain bombardment products.

Much can also be learned about the cosmic rays. Particularly important is the question of possible variations of the intensity of the radiation with time over long periods of the past. No other data exist on this point. Since the orbits of at least some meteorites extend far beyond that of Mars, one may study the variation in intensity with distance from the sun.

It is well known that cosmic rays produce effects in the earth's atmosphere similar to those in meteorites. The first and most important application of this fact is carbon-14 dating, developed by Libby (1). Many other product species have since been discovered and used in various ways. The general subject has been reviewed by Lal & Peters (2).

The field of the present review was last covered in print by Geiss (3) in 1957. An unpublished lecture by Eberhardt & Geiss (4) gives a more recent account. The reader may also find useful some references on the general subjects of meteorites (5, 6, 7) and cosmic rays (8, 9, 10).

GLOSSARY

It will be helpful first to define a few terms concerning meteorites:

- "fall" A meteorite whose fall has been observed and recorded.
"find" Any meteorite which is not a "fall."

¹ The survey of literature pertaining to this review was concluded in May 1961.

- iron** A meteorite composed almost entirely of iron-nickel alloy. The nickel concentration is typically around 8 per cent but varies widely. Small inclusions occur containing sulfides, phosphides, graphite, iron (II) chloride (lawrencite), and other substances.
- stony-iron** A meteorite composed of a mixture of iron-nickel and silicate in comparable amounts. Iron is usually the external phase.
- stone** A meteorite consisting mainly of silicate minerals. Stones are classified as chondrites or achondrites.
- chondrite** A meteorite containing a complex assemblage of minerals, including characteristic small round structures called chondrules. Chondrites usually contain a substantial fraction of iron metal (of the order of 10 per cent). The most abundant elements in order are O, Si, Mg, Fe, Ca, S, Ni, and Na. The chondrite is by far the commonest type of meteorite among "falls."
- achondrite** Any stone which is not a chondrite. This category includes some stones closely similar in composition to chondrites, along with a variety of others.

HISTORY

The history of the subject begins with the researches of Paneth (11, 12) on rare gases in meteorites. Paneth attempted to measure ages of meteorites (since solidification) by the uranium-helium method. The results were discordant. Bauer (13, 14) pointed out the existence of a negative correlation between meteorite mass and helium content. This led him to suggest that the observed helium was produced by cosmic ray bombardment rather than by the decay of uranium. As a test of this hypothesis, he proposed that the ratio of helium 3 to helium 4, in the meteoritic helium, should be of the order of 0.1 to 0.5, as among spallation fragments, as compared to a much lower value for terrestrial or solar helium (15). A similar suggestion was made independently by Huntley (16). Paneth, Reasbeck & Mayne (17) measured this ratio in several small iron meteorites and found a value of 0.3. A decrease in helium content with depth was looked for in the small meteorite Treysa but was not found. Calculations of depth effects and of absolute rates of production were made by Singer (18) and Martin (19). Other rare gases were later measured (20, 21); their isotopic ratios also deviated widely from terrestrial values and were consistent with production by high-energy bombardment.

The first measurements of a radioactive species (hydrogen 3) in iron and stone meteorites were made by Fireman & Schwarzer (22), and Begemann, Geiss & Hess (23). These authors introduced the calculation of cosmic ray bombardment ages without recourse to difficult calculations of absolute production rates. If for example, the ratio of hydrogen 3 to helium 3 at production is known, the ratio observed in a "fall" can be used directly to give a ratio of the total bombardment to the present-day bombardment intensity. If the flux is assumed constant, an age or bombardment time can be given. Later workers have developed both experimental methods and theory much further.

EXPERIMENTAL METHODS

The amounts of radioactive and stable cosmogenic nuclides in meteorites are small. The fraction of the atoms in a meteorite which are transmuted is at most of the order of 10^{-7} of the total, while some interesting species are produced in yields below 10^{-3} per interaction. Measurements are difficult to make and require quite special techniques.

The concentration of stable rare-gas nuclides is measured by mass spectrometry. The sample is melted, or even vaporized, in a thoroughly out-gassed system. After purification from reactive gases, the extracted noble gas is admitted to the spectrometer. It is usually measured under static conditions, that is, with the system closed off, to increase sensitivity. The blank corrections and absolute calibrations must be made with great care. The technique is described in detail by Signer & Nier (24). Figure 1 taken from their paper shows an especially clean spectrum of cosmogenic argon. Hoffman & Nier (25), Schaeffer & Zähringer (26), and Eberhardt & Eberhardt (27) should also be consulted.

In the nature of mass spectrometric methods, isotope ratios in a sample can be measured directly with high accuracy. The measurement of absolute amounts and ratios of different elements, however, requires a number of corrections and auxiliary measurements. It is in such measurements that disagreements between laboratories have most often occurred.

Another problem is the correction for terrestrial contamination and primordial gas. The former is now well understood, although errors may sometimes be underestimated. The latter, representing gas incorporated early in the meteorite's history, is more difficult to correct for, because of uncertainty in the isotopic composition. This problem is carefully treated by Stauffer (28).

Fireman (29) has measured the concentration of helium 3 in iron meteorites by activation analysis, using the reaction $\text{He}^3 (n, p) \text{H}^3$. This reaction is especially useful because of its high cross section (5400 barns). The competing reaction $\text{Li}^6 (n, \alpha) \text{H}^3$ ($\sigma = 945$ barns) does not seem to interfere seriously in irons.

Wänke (30) has measured stable cosmogenic scandium 45 in iron meteorites by activation analysis using the reaction $\text{Sc}^{45} (n, \gamma) \text{Sc}^{46}$. The latter is an 84-day β^- emitter. Amounts of the order of 10^{-10} g/g were easily measured.

Stauffer & Honda (31) have measured vanadium 50 and a number of stable calcium isotopes in the iron phase of meteorites, using solid-source mass spectrometry. Each element must first be separated chemically. Measurements of chemical yield and natural contamination are made by isotope dilution. A remarkable achievement in this area is the measurement of K^{40} and K^{41} by Voshage & Hintenberger (74).

Radioactive species with $Z \leq 28$ emit beta, gamma, or X radiation or sometimes more than one of these. Gamma radiation is emitted by species such as aluminum 26, manganese 54, and the cobalt isotopes. Measurements

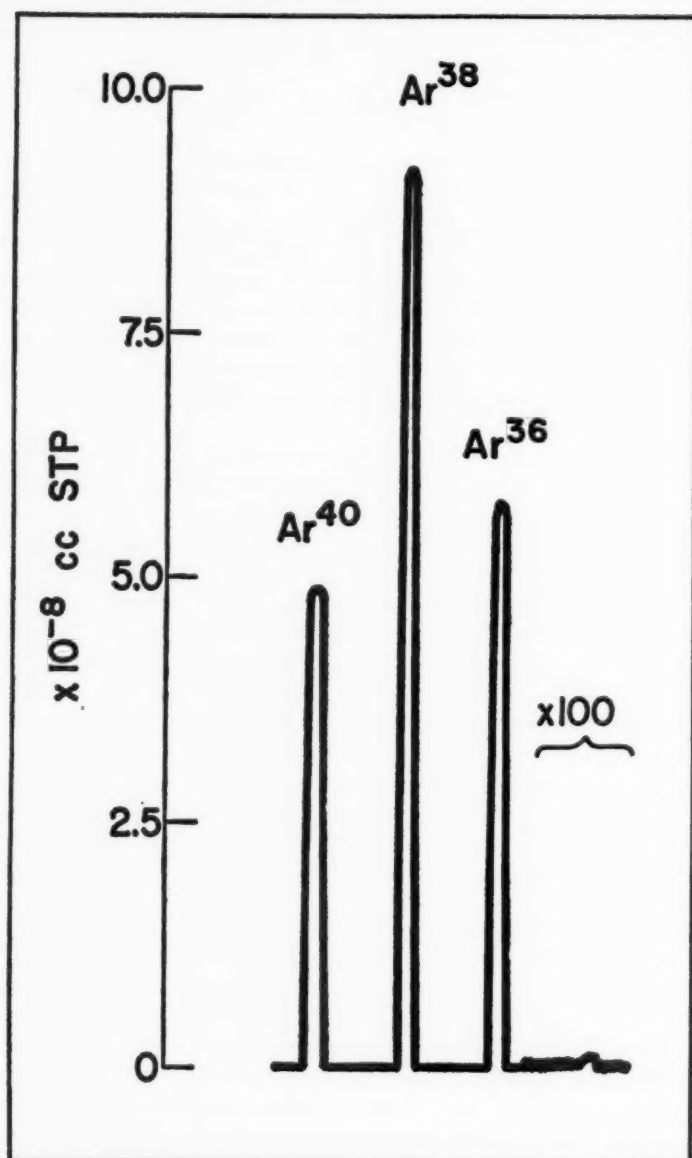


FIG. 1. Argon spectrum, sample 56 b of Grant.
Note background peak at mass 34 (24).

can be made using the intact meteorite, thanks to the great penetration of this radiation (32, 33).

Beta radiation is best measured in an anticoincidence arrangement of the type developed by Libby and co-workers for carbon-14 dating (1). The external shield, which removes local gamma radiation, is generally of steel. The anticoincidence counters may be a cluster of cosmic-ray tubes (1), a large annular multiwire counter (35), or a flat, multiwire tray (36). The working counter may assume a variety of forms (35 to 38) depending on the species to be counted.

The *K-X* radiation emitted by radioactive nuclides in the region of iron may be measured by means of Geiger (39) or proportional (34, 40) counters filled with gas mixtures based on argon. The use of a proportional counter with pulse height selection permits positive identification of the X rays of each element, achieving at the same time a substantial reduction in background.

When several isotopic species occur at once, they may be distinguished by their half lives or characteristic radiations, and by use of other special techniques (34, 38). The extraction of each element in chemically and radiochemically pure form is the most difficult part of the experiment. Radioactive argon isotopes are extracted by the same techniques used for the stable ones. The methods of wet chemistry must be employed for most other elements. Much use is made of ion exchange and solvent extraction methods, since they minimize chemical losses and can be made highly specific. The details cannot be given here; the reader is referred to examples (34, 35, 39). A good procedure must meet the criteria of high and precisely measurable chemical yield and of demonstrable radiochemical purity of the product. The former requires that all chemical forms of the element, including added carrier if any, must be brought into exchange equilibrium at the start of the procedure. An example of difficulty in this is chromium, whose complex ions are numerous and stable toward exchange and chemical reaction. The accepted method here is to oxidize to chromate as soon as possible. The introduction of significant amounts of the element in the laboratory is sometimes hard to avoid, especially for common elements such as potassium, calcium, and aluminum. The use of plastic, platinum, and quartz ware, along with careful choice of reagents (for example, HCl and ammonia as gases), is often necessary. Large amounts of carrier are helpful where they can be tolerated in the later measurement. Losses may be much greater at microgram levels and below.

Radiochemical purity requires the use of activity-free carriers and reagents. The final procedure should be specific to the element desired. However, experience shows that unexpected interferences occur in most if not all procedures (41, 42). The best available safeguard is to repurify the counting samples at least twice, using each time a completely different chemical procedure. Finally the half life and other properties of the radiation must be checked as completely as possible, given the low level of activity. The method

of milking daughter activities is used wherever possible. Much has been made of the necessity to conserve meteoritic material, but it must be emphasized that small samples yielding marginal quantities of radioactivity may be completely wasted, because the checks just discussed cannot be carried out.

The case of tritium in iron meteorites deserves special mention. The early finding (22) of activity in about the expected amount has not been verified. Surprisingly, iron meteorites show little or no hydrogen 3 (43) while a positive result has been reported for the iron phase of a chondrite (44). The observed ratio of helium 3 to helium 4 is difficult to reconcile with the loss of tritium in space. Apparently it is lost under terrestrial conditions, but the situation is still obscure.

COSMIC RAY AGE

The cosmic ray age, or bombardment age, can be defined as the ratio of the total accumulated concentration of a nuclide divided by its production rate at the present time. It may be interpreted directly as elapsed time if the flux bombarding the individual sample used for measurement has been constant throughout the bombardment.

In principle this age can be calculated from the concentrations of any two nuclides, of which one is short lived compared to the observed age (and thus in secular equilibrium) and the other is not. The latter is usually a stable species. The data required are the decay rate of the radioactive nuclide A_i corrected to the time of fall of the meteorite, the concentration of the stable species C_j expressed in compatible units, and the ratio of the production rates R_i/R_j . Then the bombardment age T_{ij} is given by

$$T_{ij} = \frac{R_i C_j}{R_j A_i} \quad 1.$$

The ratio R_i/R_j would be exactly known (and equal to one) if the stable species j were produced entirely by decay of the radioactive species i . The closest approach to this is the pair Cl^{36} and Ar^{36} in iron meteorites. About 80 per cent of Ar^{36} is formed by decay of Cl^{36} (45). Other isobaric pairs are also useful if the ratio has been measured. This is made easier because ratios of production rates of isobars in high-energy reactions are usually insensitive to the energy of the bombarding radiation (59). The ratio is thus insensitive to the spectrum of bombarding particles and to depth in the meteorite. It may be determined by a measurement of the cross-section ratio at an appropriate energy. Possible examples are Cl^{36} — Ar^{36} , H^3 — He^3 , Na^{22} — Ne^{22} , and Ca^{46} — Sc^{46} . The pair at mass 3 is subject to difficulties because of apparent H^3 loss (see above).

The next best case is that of pairs of closely similar mass numbers, produced by high-energy reactions. Depth effects are still small in this case. The best-known example is Ar^{39} — Ar^{38} (in iron meteorites). Laboratory cross sections are still useful. Other possibilities are V^{49} — V^{50} — Cr^{51} , Sc^{46} — Sc^{46} , and Na^{22} — Ne^{21} .

Now that the ratios of production rates are understood, at least for "small" iron meteorites (see below) any convenient pair may be used for an estimate of the bombardment age, accurate to a factor of two or better.

Finally, since the production rates of most species are rather insensitive to depth and size in small meteorites (see below), and since most meteorites appear to be in this category, a crude estimate may be made of the age using stable-nuclide data on a meteorite together with a production rate calculated from well-studied meteorites. Such an estimate may be substantially too low, if the meteorite is a fragment of a larger mass, but will usually be correct to a factor of two or three.

In the use of Equation 1 the time of fall is assumed known. Some "finds" apparently have substantial terrestrial ages (see below).

Cosmic ray ages of meteorites are always much shorter than their ages of about 4.5×10^9 years determined from decay of natural radioactivities. The idea that this results from a lower primary cosmic ray intensity in the past is eliminated by the undoubted fact that different meteorites have different cosmic ray ages. The great majority of irons show ages of hundreds of millions of years, with few if any above a billion. The ages of chondrites, on the other hand, appear to be less than about thirty million years in all cases studied so far.

A simple interpretation of these facts is given by Eberhardt (46). Meteorites, in this picture, were originally part of larger asteroid bodies, and thus shielded from the cosmic radiation. A depth of three to ten meters would be sufficient for shielding. At some time in the past two such bodies collided, and the meteorite began its history of exposure. Rates of collision in the asteroid belt have been calculated by Öpik (47) and shown to be sufficient. There is an apparent difficulty in imparting sufficient velocity relative to the colliding bodies (which presumably move in closely similar orbits and thus at rather small speed relative to each other). However, it has been shown (48) that small fragments can be "sprayed out" at high velocity relative to bodies colliding at velocities of a few kilometers per second.

The effect of successive collisions on the production of cosmogenic nuclides depends on meteorite size (see below). Since production in small meteorites shows little depth or size variation, successive collisions would produce small effects, detectable only if the pre-atmospheric size and shape were known. If, however, the mass of a meteorite is in the region of tons, successive collisions may expose more or less "fresh" surfaces. Such meteorites would show different cosmic ray ages in different portions. Vilcsek & Wänke have pointed out the apparent existence of this effect in the large iron meteorite Sikhote-Alin (83). Evidence of violent collisions is frequently seen in iron meteorites; a striking example is the Japanese meteorite Shirahagi (50).

On this model the difference between the bombardment age of a typical chondrite, $\sim 2 \times 10^7$ years, and that of a typical iron meteorite, $\sim 5 \times 10^8$ years, is explained by a difference in durability. The meteorites, in highly eccentric orbits, must suffer many more collisions than the original bodies.

Durable pieces, the irons, survive while the soft, friable chondrites are quickly destroyed, that is, reduced to a size too small to penetrate the earth's atmosphere. A difficulty with this model is the low apparent bombardment age of several low-nickel iron meteorites (49). One achondrite, Norton County, appears to have a bombardment age of 2×10^8 years (23).

There is an apparent tendency of cosmic ray ages of meteorites to cluster around certain typical values. Geiss, Oeschger & Signer (51) have suggested that most or all chondrites have the same true cosmic ray age, 2.2×10^7 years, assuming that He^3 and H^3 are produced at equal rates. They explain the lower values observed in some chondrites by rare-gas leakage. Even if there is no gas loss, a visible clustering remains. It is possible that most irons have a single age of around 5×10^8 years. If so, the obvious conclusion is that most members of each class were born in a single major collision. This would have far-reaching consequences; for example, it would cast doubt on the frequently used assumption that the chemical composition of chondrites represents that of average undifferentiated matter of the solar system. No final conclusion can be drawn at present.

Another model attributes the short ages to slow, uniform erosion of larger bodies by dust particles (52). On this assumption the differences in age are caused by the differing rates of erosion of hard and soft bodies. Serious objections have been raised to this model in its pure form (46, 53), but such effects have not been ruled out as contributing factors. There is no sharp division between the notions of erosion and of successive collisions when the number of the latter grows large.

TERRESTRIAL AGE OF METEORITES

The terrestrial ages of "falls" are of course well known. The age of a "find" can be calculated from activity data under certain conditions. The best case is that in which the activities of such comparatively long-lived species as beryllium 10 and manganese 53 in an unknown can be compared with those in a "fall." If both these species, which represent extremes in terms of the mean energies of the bombarding particles, show the same activity, this should also be true of intermediate species. Sometimes comparisons of closer pairs are possible. The ratio of the activity of a short-lived species to the value expected from these considerations must be $e^{-\lambda\tau}$ where τ is the terrestrial age.

The only cases of measured terrestrial age known presently to the writer are the irons Williamstown (39) and Keen Mountain (49). The former shows virtually the same Be^{10} and Mn^{53} as the "fall" Aroos but about 3.5 dpm/kg Cl^{36} (39, 55) as against 14–18 for Aroos (34, 49, 54, 56). Thus the terrestrial age appears to be of the order of 6×10^5 years, an unexpectedly high figure for the time of survival of an iron meteorite in a wet climate. The age is supported by the absence of Ni^{59} ($t_{1/2} = 8 \times 10^4$ years) (54) and Ar^{39} ($t_{1/2} = 325$ years) (57). The neutron-capture species nickel 59 cannot easily be used,

however, to determine ages, since its production rate varies greatly from one meteorite to another.

Many measurements of argon 39 in "finds" have been made by Wänke (49) and Fireman & de Felice (38). Only one definite positive value has been reported, that for Keen Mountain (49) whose terrestrial age, computed with chlorine 36 as a standard, is about 1000 years. All others are older than 1500 years. From the limited data we can conclude that typical ages for iron "finds" may be in the region of 10^4 to 10^6 years.

TYPES OF NUCLEAR REACTIONS

Nuclear reactions of all possible kinds take place when cosmic rays bombard meteorites. The primary particles produce an abundance of secondaries, which cause most of the transmutations. Neutrons, protons, and π^\pm mesons are the most important of these secondaries. In the Bev region all three components are of comparable abundance. At lower energies the yield of mesons is not very large compared with that of nucleons. Also, at lower energies, charged particles are frequently brought to rest by ionization without undergoing nuclear reaction. Below 100 Mev, only the flux of neutrons need be considered (58).

The term "spallation," originally used to describe the removal of many individual particles from a target nucleus struck by a high-energy particle, has been extended in current usage to include all high-energy reactions except fission. The course of a spallation reaction is usually described (59) as consisting of two phases: a knock-on and an evaporation phase. In the first phase a collision occurs between the bombarding particle and an individual nucleon. This may be followed by one or more further high-energy collisions. Mesons may be created in this step. At the end one or more fast particles emerge from the nucleus. The next stage, when no high-energy particles remain, is characterized by a short nuclear mean free path and a rapid distribution of the residual energy among the nucleons. The final result is the loss of energy by the evaporation of more nucleons, this time of low energy. The remaining energy after the knock-on stage determines the number of emitted nucleons. For a given bombarding energy, these residual or deposition energies have broad distributions, but mean values may range from perhaps 30 Mev for proton bombardment at 100 Mev to 200 Mev at 2 Bev (59). For a given mass number (A) in the low-mass region ($A \lesssim 70$), the distribution of products tends to cluster around the atomic number (Z) values of stable isobars. As the energy of the bombarding particle increases, the distribution of A becomes broader, until in the Bev region all values are represented in similar yield. Figure 2, which shows the calculated distribution of products from bombardment of iron (58, 60) at different energies, gives a picture of this behavior.

The dependence of cross section on the A and Z of target and residual nuclei, and on the energy of the bombarding particle, has been analyzed

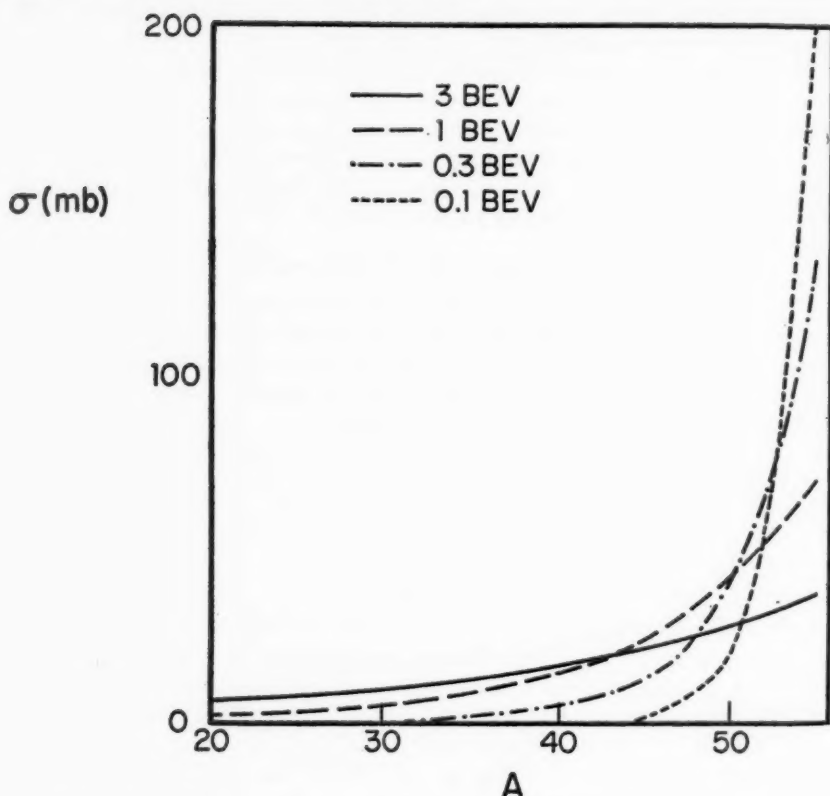


FIG. 2. Calculated dependence of the total production cross section for each mass number on A , for bombardment of Fe^{56} by protons of various energies (58, 60).

semi-empirically by Rudstam (60) and later workers (61). For a given target the cross section varies smoothly with product A . For each A the logarithm of the cross section, plotted against Z , is a parabola. Only a few nuclei of a given A are produced in high yield.

The variation of production cross section for each product nuclide with energy (E , in Bev) may be represented approximately by

$$\ln \sigma(E, A, Z) = \ln P - P\Delta A + C(A, Z) \quad 2.$$

Here $P = 0.11E^{-0.64}$ (58) and $C(A, Z)$ is a constant for each product nuclide. The shape of the curve is roughly sigmoid, the cross section rising rather steeply for an interval above an effective threshold, then increasing or decreasing slowly. The greater ΔA , the higher the effective threshold. It is about 1 Bev for neon isotopes produced in iron.

Nuclei close to the target are produced also by neutrons below 100 Mev. For these species production rates may not vary smoothly with A and Z . At low energies the cross section for reactions such as $(n, 2n)$ may vary by a factor of three or more from one element to the next. Emission of α particles is important for light target nuclei.

Small product nuclei are a special case. In general they are emitted fragments rather than residual nuclei. Those up to and including helium 4 are emitted in evaporation at all energies. Species such as beryllium 7 are emitted only at high energies. The rise in their production cross sections continues into the Bev region (62).

For the study of depth effects it would be most convenient to possess products which would serve as "markers" for particles of particular energies. This would require that the excitation function of each show a sharp peak, preferably dropping off to very small values at high energy. The best case would be a nuclide produced by the (n, p) reaction. The cross section of this reaction usually reaches several hundred millibarns at an energy around 10 Mev; it drops to about a millibarn at several hundred Mev. Unfortunately most (n, p) products in meteorites are too short lived for measurement. Favorable examples are $\text{Ni}^{58}(n, p)\text{Co}^{58}$ and $\text{S}^{32}(n, p)\text{P}^{32}$, although both products are also made in other ways. The $(n, 2n)$ and (n, pn) reactions also show high peaks at low energy, and production at these energies is much larger than at higher energies (where the cross section levels off at some tens of millibarns). Some good examples are Co^{57} from Ni^{58} , and Fe^{56} from Fe^{56} . In a chondrite, Al^{26} and Na^{22} are made by this and similar low-energy reactions.

In general, because the differential flux spectrum inside a meteorite decreases monotonically with energy (see below), each spallation product is produced mainly near the "knee" of its excitation function.

There is a characteristic difference between irons and stones in the average energy of particles producing a particular species. In iron, for a species like sodium 22, $\Delta A = 34$ and the production is caused by particles in the Bev region. In a stone, Na^{22} is made chiefly from magnesium and silicon isotopes, and ΔA is small. Neutrons below 100 Mev are the active particles. A species like scandium 46, with $\Delta A = 10$ relative to iron, is made in nearly the same way in stones as in irons, because of the low abundance of elements between iron and calcium in the stones. But by comparison with other species it is classed as a "high-energy product" in stone and a "low-energy product" in iron.

The neutron capture reaction is especially interesting. Low-energy neutrons must be produced by moderation. This requires many collisions, especially in an iron.

VARIATIONS WITH DEPTH AND SIZE

Early experimental studies on changes of helium concentration with depth in iron meteorites (17) have been followed by more detailed measurements on this and other rare gases. The best-studied meteorites are Grant

(24, 25, 63) and Carbo (29, 64). Grant is a 440-kg, roughly spherical individual. Figures 3 and 4, taken from Signer & Nier (24), show some of the results obtained on samples from a slice through the center of this specimen. Results on Carbo demonstrate that it is a piece of a larger object. No experimental studies exist of depth effects in stones.

The most striking fact about the depth effects in Grant is that they are small. The largest depth effect is observed for neon. The radius of Grant corresponds to a path of 200 g/cm², while the interaction mean free path for high-energy protons in iron is about 100 g/cm². A collimated beam would be attenuated by a factor of e^2 in this interval. Three major factors account for the observed slow variation: (a) production by high-energy secondary particles, (b) the fact that the beam is isotropic, and (c) atmospheric ablation, which removes a layer of undetermined thickness from the surface. Little progress has been made in measuring ablation independently of cosmic ray effects, but Maringer & Manning (65) have estimated 2 to 6 cm in the case of Grant. Another effect, important for lower-energy products, is the angular spread of the secondary particles relative to the incident primary.

The calculation of depth effects was first carried out by Martin (19) using cascade theory. Later calculations on this model are those of Ebert & Wänke (66), Hoffman & Nier (25), and Signer & Nier (24). The theoretical model traces the development of the cascade, starting with assumed 3-Bev primaries, each of which generates three secondaries of 300 Mev. The model is semiquantitative for the rare gases in irons, but not sufficiently realistic to be used for species near the target (and thus for rare gases in stones). Realistic *a priori* cascade calculations, using energy distributions of primary and secondary particles, have so far not been attempted because of their mathematical complexity and the inadequacy of some of the basic data.

Estimates of ablation in Grant, based on this model, are in the region of 12 cm (24, 25). In their calculation, Signer & Nier treat the relative production cross sections as free parameters. The values determined agree well with experiment except for the ratio $\sigma_{\text{He}^3}/\sigma_{\text{He}^4}$ at high energy for which the observed values are all in the region of 0.3, while the calculated one is 0.67.

The effect of meteorite mass on the production rate of most species is also rather small so long as the mass is in the region between a few and a few hundred kg. This may be seen from the experimental data on radioactive species given in Table I (34, 39, 67). It should be noted that not more than one ton of any chondrite has been recovered.

The small magnitude of size and depth effects in small meteorites is a great convenience in studies of cosmic ray ages and variations in time. Conversely it limits the accuracy of calculated values of ablation. A promising approach, not yet carried out, is to use the depth effects on concentration of low-energy products such as manganese 53 and iron 55. Their production should increase by a factor of about 1.5 from edge to center of Grant in the absence of ablation, because of the rapid growth in the number of secondaries of 10 to 20 Mev with depth (58).

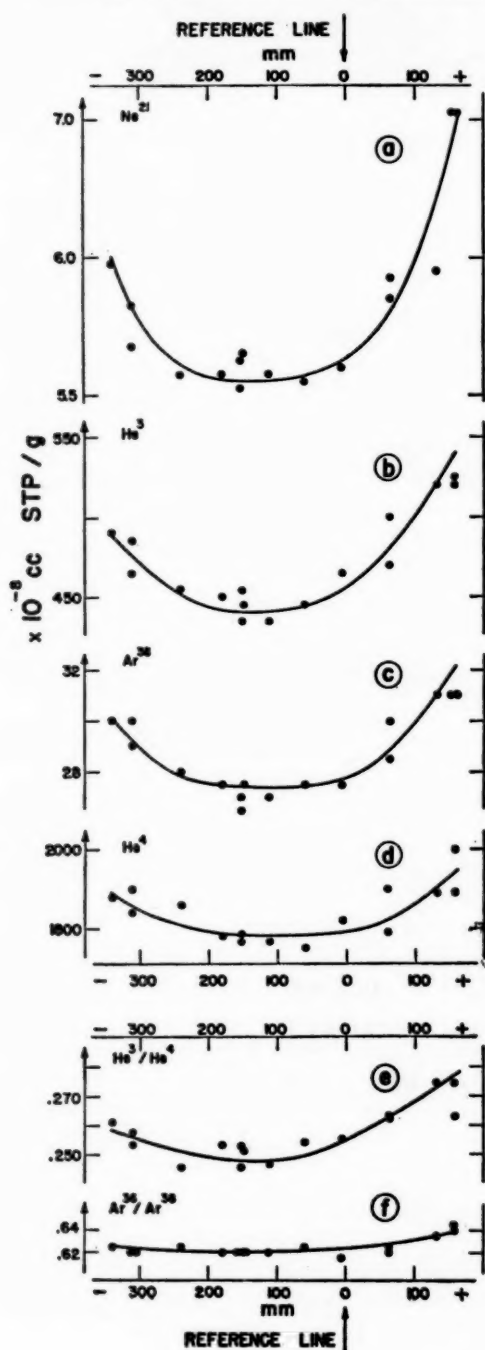


FIG. 3. Variation with position along bar *F* of Grant of Ne²¹, He³, Ar³⁸, He³/He⁴, Ar³⁶/Ar³⁸ (lower curves). See Figure 4 for locations (24).

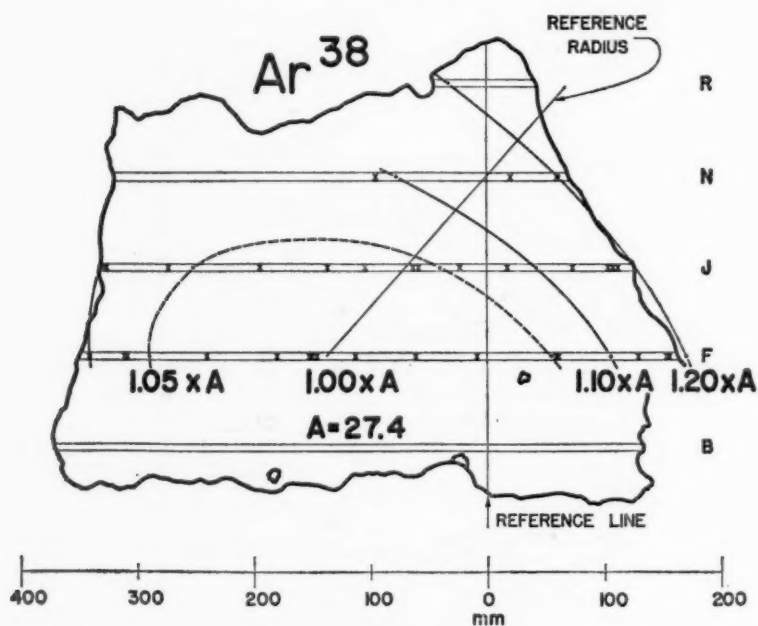
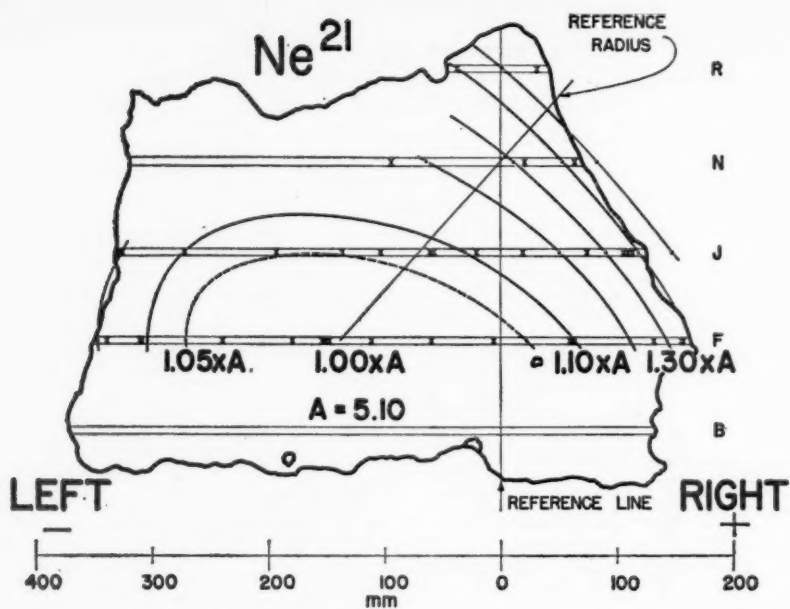


FIG. 4. Contours of equal concentration for Ne²¹ and Ar³⁸. Bar designations at right. Crosses indicate location of measured samples (24).

TABLE I(A)
LONG-LIVED ACTIVITIES IN SOME SMALL IRONS
[Data of Honda, Shedlovsky & Arnold (34, 39)]

	Be ¹⁰	Al ²⁶	Cl ³⁶	Mn ⁵³
Aroos	4.1 dpm/kg	3.6 dpm/kg	14, 16.5 dpm/kg	515 dpm/kg
Grant	4.0	4.3	12.4 ^a	380
Williamstown	3.5	3.4	3.5 ^b	360

^a Reference (56).

^b This low value is ascribed to a great terrestrial age (see text).

TABLE I(B)
ARGON 39 IN SOME CHONDRITES
[Data of Stoenner, Schaeffer & Davis (67)]

	Ar ³⁹ (at time of fall)	Per cent Fe	Per cent Ca
Benton	9.0 ± 0.3	20.2	
Forest City	11.9 ± 0.5	29.9	1.41
Richardton	7.1 ± 0.6		
Murray	9.4 ± 0.5	21.5	1.37
Hamlet	7.8 ± 0.2	19.5	

A still more rapid increase with size and depth should occur in the case of (n, γ) products such as nickel 59 and cobalt 60. The average production increases several times in going from 10 to 20 cm radius, while the concentration gradient in the outer 8 cm is very steep (68). This variation is convenient for ablation studies. It is interesting that the production of chlorine 36 by Cl³⁵(n, γ)Cl³⁶ in iron meteorites, first suggested by Geiss, has not been observed. Capture of neutrons appears to take place at energies far above thermal levels.

In a large meteorite the depth gradient will appear much steeper after the outer 10 to 20 cm have been passed. Below this depth the production rate for any species will decrease exponentially about as $e^{-x/150}$ (where x is in g/cm²), as it does in the earth's atmosphere. This has been observed in the large iron Sikhote-Alin (69, 70).

SPACE VARIATION IN COSMIC RAY INTENSITY

We come finally to the question of the constancy of the cosmic ray intensity in space and time. The space variation will be dealt with first.

The commonly held idea that meteorite orbits extend to the asteroid belt is supported by the one well-established orbit, that of the chondrite Luhy or Pribram (71). The period of this orbit is 3.8 years; the time average distance from the sun is 3.1 astronomical units. Let us assume that these values are typical. Then nuclides of half life long compared to 3.8 years have accumulated over many periods. The bombardment which produced them occurred mainly beyond the orbit of Mars. Nuclides of half life less than a few months have been produced in the same way, but only those atoms which were made in the portion of the orbit near the earth survive to reach us. If we measure the activities of suitable pairs and compare them with those expected from laboratory experiment or theory, the results give a measure of the space variation. Appropriate pairs should be as similar as possible except for half life; best of all would be isobars. Possible choices are $\text{Ar}^{37}\text{--Ar}^{39}$, $\text{Be}^7\text{--Be}^{10}$, $\text{P}^{32}\text{--Si}^{32}$, $\text{Ar}^{37}\text{--Cl}^{36}$, $\text{Ti}^{44}\text{--Sc}^{44}$, and $\text{Mn}^{52}\text{--Mn}^{54}$. Only the first of these has been used. The chondrite Hamlet (67, 72) and the iron Aroos (72) have been studied.

The conclusions of the two studies differ considerably. Stoenner, Schaeffer & Davis (67) find an experimental ratio $\text{Ar}^{37}:\text{Ar}^{39}$ of 2.0 ± 0.3 . By bombarding a piece of the same meteorite and a number of the major constituent elements at Brookhaven, under conditions somewhat similar to the natural ones, they derived an expected value of 1.5 ± 0.2 . Fireman & de Felice (72) report the experimental ratio as 2.3 ± 0.2 , and an expected value (based on another bombardment) of 1.2 ± 0.3 . In Aroos the latter authors find the activity ratio to be 1.4 ± 0.3 , while the expected value is 0.8 ± 0.1 . The error in the expected value is less for an iron meteorite. Thus one group finds little or no space variation in cosmic ray intensity, while the other concludes that the cosmic ray flux near the earth is of the order of twice that in the asteroid belt. It is worth noting that the data of Honda & Arnold (34) on many species of short and long life in Aroos show no trend with half life.

The accuracy of present data on this subject is adversely affected by the interval of months between meteorite fall and counting measurements. Much better measurements could be made with samples obtained more quickly. In any case direct measurements of cosmic ray intensity in the region of Mars and beyond will probably be made in a few years.

TIME VARIATION

In studies of the time variation of cosmic ray intensity, one tests the assumption that the intensity has been constant since the start of the bombardment. On this assumption each radioactive nuclide whose half life is a small fraction of the duration of bombardment is in secular equilibrium. The decay rate A equals the rate of formation R . The cosmic ray age is the true duration of the bombardment; the same age must result whatever pair of species is used. If the half life of a nuclide is comparable to the bombardment

age, the decay rate is given by $\Lambda = R(1 - e^{-\lambda t})$. The only present example of a partially saturated species is potassium 40.

Comparisons of the rate of formation and decay are most easily carried out for isobaric or neighboring pairs. Here experimental or calculated values of production cross sections at a typical energy may be used to fix the production ratio, since the ratio of cross sections is nearly independent of energy. Thick-target bombardments which simulate natural conditions are also more likely to give correct results for such pairs. A comparison was carried out by Honda & Arnold (34) for the pairs Mn^{54} — Mn^{53} , Ti^{44} — Sc^{46} — Ca^{45} , and Al^{28} — Na^{23} in the iron meteorite Aroos. They concluded that the observed ratios of activities were in agreement within a factor of two or three with expected re-

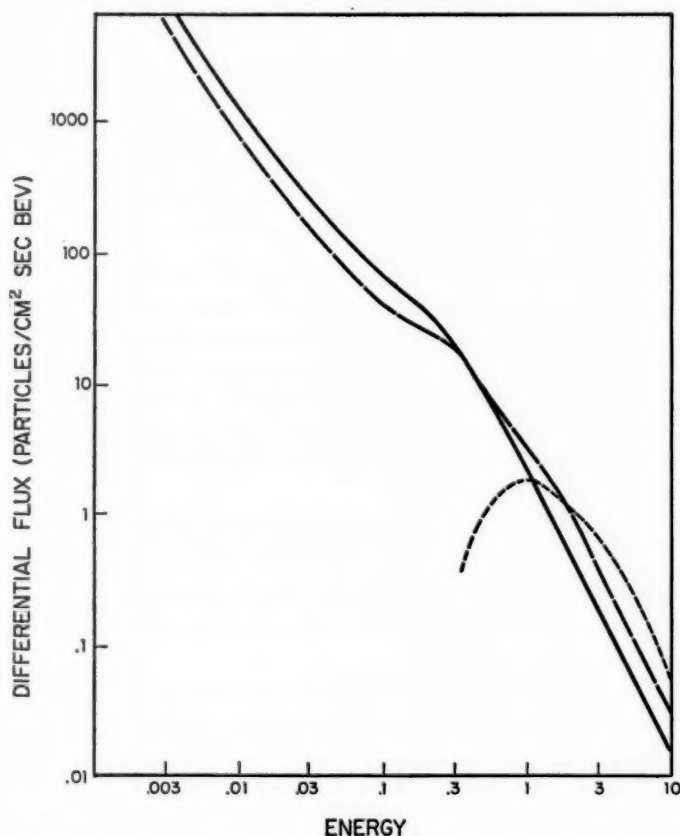


FIG. 5. Calculated energy distribution of the effective flux of nuclear particles in a "small" iron meteorite. — at a depth of 100 g/cm², - - - at a depth of 10 g/cm² (58). The primary spectrum - · - · - (80) is given for comparison. Energy in BeV.

sults for secular equilibrium. Thus the variations in intensity, averaged over the half lives of each species, have not been great.

The most thorough study yet carried out on this question is that of Arnold, Honda & Lal (58). They derived a spectrum of effective particles at a depth of 100 g/cm² in a typical "small" iron meteorite. The spectrum is shown in Figure 5 along with that derived for a depth of 10 g/cm², and the primary spectrum of McDonald & Webber (80). The integral over energy of the product of the spectrum and the excitation function for each species gives its production rate. It was shown that the absolute production rate of chlorine 36 was well reproduced when the present-day flux was used (23 dpm/kg calculated versus 14-18 dpm/kg experimental). All other species for which good data exist were compared with chlorine 36. An abbreviated and modified version of their Table V is shown in Table II. The experimental data for vanadium 50 (31) and calcium isotopes (73) have been added since the original publication. Stable species are compared to argon 36, taken as 1.2. The calculations agree well with the results, including the new ones. The scatter is of the order of 40 per cent, and no trend is apparent with charge or mass of the product nuclide. This gives ground for confidence that, within the accuracy of data and calculations, the cosmic ray intensity, averaged over the half life of each species, has been constant. The longest half life represented is that of manganese 53.

For the region of 10⁹ years, potassium 40 is the only useful nuclide. The short bombardment age of most irons, 5×10⁸ years, permits only a small amount of decay to occur—13 per cent on the assumption of steady state. At present, from the work of Voshage & Hintenberger (74) and Honda *et al.* (31, 75), it can only be concluded that the flux over the time of bombardment has been similar to the present one within a large error, perhaps a factor of two or three. Studies of meteorites of longer bombardment age are in progress.

The use of meteorites of finite, known terrestrial age would allow a more detailed study of cosmic ray time variations, a comparison being made of the saturation activities of a given species in bombardments ending at different times. Studies of argon 39 in old "falls," for instance, might shed light on the observed small variation with time in carbon-14 activity (corrected for decay) of terrestrial plants (76, 77).

Short-term variations in the intensity of high-energy particles must also be considered. The 11-year solar cycle should have only a small effect on production rates, except in very small meteorites. Bursts of particles associated with solar flares are sometimes intense enough to be capable of causing increases in the activities of short-lived radioactive species.

The conclusion that the cosmic ray intensity has been much the same for millions, and perhaps hundreds of millions, of years has not been greeted with astonishment. While theories of the origin of cosmic rays are still numerous and controversial, they tend more and more to give the phenome-

TABLE II
PRODUCTION RATES OF RADIOACTIVE AND STABLE NUCLIDES
IN THE IRON METEORITE AROOS
($\text{Cl}^{36} = 1$, $\text{Ar}^{36} = 1.2$)

Nuclide	Half life	Exptl. ^a	Calc. ^f
H ³	12 yr		12
He ³	stable	34	27
He ⁴	stable	128	135
Be ¹⁰	2.5×10^6 yr	0.29	0.31
ΣNe	stable	1.2	0.73
Na ²²	2.6 yr	0.15	0.11
Al ²⁶	7.4×10^5 yr	0.26 ^b	0.10
Si ³²	~ 700 yr	0.06	0.05
Cl ³⁶	3.1×10^5 yr	(1)	(1)
Ar ³⁶	stable	(1.2)	(1.2)
Ar ³⁷	35 days	1.3 ^c	0.65
Ar ³⁸	stable	1.9	1.6
Ar ³⁹	325 yr	0.9–1.0 ^c	0.90
Ca ⁴²	stable	3.5 ^d	3.1
Ca ⁴³	stable	4.2 ^d	3.6
Ca ⁴⁵	164 days	0.3	0.28
Ca ⁴⁶	stable	0.10 ^d	0.05
Sc ⁴⁵	stable	6.2 ^e	5.0
Sc ⁴⁶	84 days	2.1	1.5
Ti ⁴⁴	~ 200 yr	0.31	0.38
V ⁴⁸	16 days	6	7.3
V ⁴⁹	330 days	12	9.6
V ⁵⁰	stable	9.5 ^d	5.2
Cr ⁵¹	28 days	20	19
Mn ⁵³	$\geq 2 \times 10^6$ yr	38	33
Mn ⁵⁴	308 days	34	38
Fe ⁵⁵	2.6 yr	120	220
Co ⁵⁶	77 days	(4.4)	4.5
Co ⁵⁷	270 days	6.4	5.5
Co ⁵⁸	71 days	(4.4)	17

^a All data on radioactive species are from (34), unless otherwise noted. Stable rare gas data are from P. Signer (unpublished).

^b Production from P and S is estimated to account for half of this quantity.

^c Fireman & de Felice (72), H. Wänke (unpublished), D. Heymann & O. A. Schaeffer (unpublished).

^d Data of M. Honda and H. Stauffer.

^e Calculated from data of H. Wänke on similar meteorites.

^f Calculated using spectrum S(100), appropriate to a depth of 100 g/cm².

non a general galactic character. The production rate in the galaxy of supernovae (78), and still more of contact binary stars (79) and other common types (84), should not have varied much over these periods. If, on the other hand, as Shklovsky (81) suggested, the solar system may have passed through the remnants of supernova clouds in which an extremely high cosmic ray flux must persist, a different result might have been expected. Even passage near the region of an old supernova might have produced a measurable change (82).

LITERATURE CITED

1. Libby, W. F., *Radiocarbon Dating*, 2nd ed. (Univ. of Chicago Press, Chicago, Ill., 1955)
2. Lal, D., and Peters, B., *Progr. in Elementary Particle Phys. and Cosmic Ray*, 6 (In press)
3. Geiss, J., *Chimia (Switz.)*, 11, 349 (1957)
4. Eberhardt, P., and Geiss, J., Lecture (Varenna Summer School, Varenna, Italy, September 1960)
5. Krinov, E. L., *Principles of Meteoritics* (Vidizivnas, I., and Brown, H., Transl., Pergamon Press, London, Engl., 1960)
6. Urey, H. C., and Craig, H., *Geochim. et Cosmochim. Acta*, 4, 36 (1953)
7. Prior, G. T., and Hey, M. H., *Catalogue of Meteorites*, 2nd ed. (British Museum, London, Engl., 1953)
8. Peters, B., in *Handbook of Physics*, Chap. 12 (Condon and Odishaw, Eds., McGraw-Hill, New York, N. Y., 1958)
9. Rossi, B., *High Energy Particles* (Prentice-Hall, New York, N. Y., 1952)
10. Waddington, G. J., in *Progr. in Elementary Particle and Cosmic Ray Phys.*, 6 (In press)
11. Paneth, F. A., Gehlen, H., and Guenther, P. L., *Z. Elektrochem.*, 34, 465 (1928)
12. Arrol, W. F., Jacobi, R. B., and Paneth, F. A., *Nature*, 149, 235 (1942)
13. Bauer, C. A., *Phys. Rev.*, 72, 354 (1947)
14. Bauer, C. A., *Phys. Rev.*, 74, 225 (1948); also *Phys. Rev.*, 74, 501 (1948)
15. Burbidge, E. M., Burbidge, G. R., Fowler, W. A., and Hoyle, F., *Revs. Mod. Phys.*, 29, 547 (1957)
16. Huntley, H. E., *Nature*, 161, 356 (1948)
17. Paneth, F. A., Reasbeck, P., and Mayne, K. I., *Geochim. et Cosmochim. Acta*, 2, 300 (1952)
18. Singer, S. F., *Nature*, 170, 728 (1952)
19. Martin, G. R., *Geochim. et Cosmochim. Acta*, 3, 288 (1953)
20. Reasbeck, P., and Mayne, K. I., *Nature*, 176, 733 (1955)
21. Gentner, W., and Zähringer, J., *Z. Naturforsch.*, 10a, 498 (1955)
22. Fireman, E. L., and Schwarzer, D., *Geochim. et Cosmochim. Acta*, 11, 252 (1957)
23. Begemann, F., Geiss, J., and Hess, D. C., *Phys. Rev.*, 107, 540 (1957)
24. Signer, P., and Nier, A. O., *J. Geophys. Research*, 65, 2947 (1960)
25. Hoffman, J. H., and Nier, A. O., *Phys. Rev.*, 112, 2112 (1958)
26. Schaeffer, O. A., and Zähringer, J., *Geochim. et Cosmochim. Acta*, 19, 94 (1960)
27. Eberhardt, P., and Eberhardt, A., *Helv. Phys. Acta*, 33, 593 (1960)
28. Stauffer, H., *Geochim. et Cosmochim. Acta* and *J. Geophys. Research* (In press, 1961)
29. Fireman, E. L., *Nature*, 181, 1725 (1958)
30. Wänke, H., *Z. Naturforsch.*, 13a, 645 (1958)
31. Stauffer, H., and Honda, M., *J. Geophys. Research* (In press)
32. Anders, E., *Geochim. et Cosmochim. Acta*, 19, 53 (1959)
33. Van Dilla, M. A., Arnold, J. R., and Anderson, E. C., *Geochim. et Cosmochim. Acta*, 20, 115 (1960)
34. Honda, M., and Arnold, J. R., *Geochim. et Cosmochim. Acta*, 23, 219 (1961)
35. Gfeller, C., Herr, W., Houtermans, F. G., and Oeschger, H., *Helv. Phys. Acta*, 32, 277 (1959)
36. Lal, D., and Schink, D. R., *Rev. Sci. Instr.*, 31, 395 (1960)
37. Sugihara, T. T., Wolfgang, R. L., and Libby, W. F., *Rev. Sci. Instr.*, 24, 511 (1953)
38. Fireman, E. L., and de Felice, J., *Geochim. et Cosmochim. Acta*, 18, 183 (1960)
39. Honda, M., Shedlovsky, J. P., and Arnold, J. R., *Geochim. et Cosmochim. Acta*, 22, 133 (1961)
40. Turkevich, A. (Unpublished)
41. Sunderman, D. N., Ackermann, I. B., and Meinke, W. W., *Anal. Chem.*, 31, 40 (1959)
42. De Voe, J. R., and Meinke, W. W., *Anal. Chem.*, 31, 1426 (1959)
43. Fireman, E. L., *Nature*, 181, 1613 (1958)
44. Geiss, J., Hirt, B., and Oeschger, H., *Helv. Phys. Acta*, 33, 590 (1960)
45. Schaeffer, O. A., and Zähringer, J., *Phys. Rev.*, 113, 674 (1959)
46. Eberhardt, P., and Hess, D. C., *Astrophys. J.*, 131, 38 (1960)
47. Öpik, E. J., *Proc. Roy. Irish Acad.*, 54, 165 (1951)
48. Charters, A. C., *Sci. Am.*, 128 (October 1960)
49. Wänke, H. (Private communication)
50. Murayama, S., *Meteoritics*, 1, 99 (1953)
51. Geiss, J., Oeschger, H., and Signer, P., *Z. Naturforsch.*, 15a, 1016 (1960)
52. Whipple, F. L., and Fireman, E. L., *Nature*, 183, 1315 (1959)
53. Urey, H. C., *J. Geophys. Research*, 64, 1721 (1959)

54. Honda, M., and Arnold, J. R. (Unpublished)
55. Sprenkel, E. L., Davis, R., Jr., and Wiig, E. O., *Bull. Am. Phys. Soc. [II]*, **4**, 223 (1959)
56. Heymann, D., and Schaeffer, O. A., *Abstr. Am. Geophys. Union* (Washington, D. C., April 1961)
57. Davis, R., Jr. (Unpublished)
58. Arnold, J. R., Honda, M., and Lal, D., *J. Geophys. Research* (In press)
59. Miller, J. M., and Hudis, J., *Ann. Rev. Nuclear Sci.*, **9**, 159 (1959)
60. Rudstam, G., *Spallation of Medium Weight Elements* (Doctoral thesis, Univ. of Uppsala, Uppsala, Sweden, 1956)
61. Honda, M., and Lal, D., *Phys. Rev.*, **118**, 1618 (1960)
62. Baker, E., Friedlander, G., and Hudis, J., *Phys. Rev.*, **112**, 1319 (1958)
63. Fireman, E. L., *Planetary and Space Sci.*, **1**, 66 (1959)
64. Hoffman, J. H., and Nier, A. O., *Geochim. et Cosmochim. Acta*, **17**, 32 (1959)
65. Maringer, R. E., and Manning, G. K., *Geochim. et Cosmochim. Acta*, **18**, 157 (1960)
66. Ebert, H. H., and Wänke, H., *Z. Naturforsch.*, **12a**, 766 (1957)
67. Stoenner, R. W., Schaeffer, O. A., and Davis, R., Jr., *J. Geophys. Research*, **65**, 3025 (1960)
68. Lingenfelter, R. (Private communication)
69. Gerling, E. K., and Levskii, L. K., *Doklady Akad. Nauk USSR*, **123**, 420 (1958)
70. Vinogradov, A. P., Zadoeshnye, I. K., and Florenskii, K. P., *Geokhimiya*, **6**, 443 (1957)
71. Cepiecha, Z., *Bull. Astron. Inst. Czechoslovakia*, **12**, 21 (1961)
72. Fireman, E. L., and de Felice, J., *J. Geophys. Research*, **65**, 3035 (1960)
73. Stauffer, H., and Honda, M. (Unpublished)
74. Voshage, H., and Hintenberger, H., *Z. Naturforsch.*, **14a**, 194 (1959)
75. Honda, M., *Geochim. et Cosmochim. Acta*, **17**, 148 (1959)
76. Broecker, W. S., Olson, E. A., and Bird, J., *Nature*, **183**, 1582 (1959)
77. Suess, H. E., in *Natl. Acad. Sci.—Natl. Research Council, Publ. No. 845* (1960)
78. Ginzburg, V. I., *Progr. Elementary Particle and Cosmic Ray Phys.*, **4**, Chap. V (1958)
79. Hayakawa, S., and Koshiba, M., *Progr. Theoret. Phys. (Kyoto)*, **21**, 473 (1959)
80. McDonald, F. B., and Webber, W. R., *Phys. Rev.*, **115**, 194 (1959)
81. Shklovsky, I. S., *Cosmic Radio Waves* (Harvard Univ. Press, Cambridge, Mass., 1960)
82. Oda, M. (Private communication)
83. Vilček, E., and Wänke, H., *Z. Naturforsch.*, **16a**, 379 (1961)
84. Tandon, J. N., *Nature*, **190**, 246 (1961)

DETECTION OF NUCLEAR EXPLOSIONS^{1,2}

BY R. LATTER

The RAND Corporation, Santa Monica, California,

AND

R. F. HERBST AND K. M. WATSON

*The Lawrence Radiation Laboratory, University of California
Berkeley and Livermore, California*

INTRODUCTION

The Geneva negotiations on the discontinuance of nuclear weapon tests have focused considerable scientific attention on the problem of detecting nuclear explosions. The present paper reviews the detection problem broadly and describes in detail some of the more important aspects of the problem. There has been no attempt at completeness, and no attempt at evaluating the specific detection capabilities of the international detection system which were discussed at the Geneva political negotiations.

Detection will be discussed separately for each environment in which explosions could be undertaken—in the atmosphere, underwater, underground, and in space. The underground and space environments will be treated in greater detail than the atmosphere and underwater environments, since the more difficult problems for detection arise in the case of underground and space nuclear explosions.

ATMOSPHERIC NUCLEAR EXPLOSIONS

Detection of atmospheric nuclear explosions (1) depends primarily upon observing acoustic signals generated by the explosions and upon collecting radioactive debris. Radio signals are also generated by nuclear explosions, but are less useful for detection because of the intense background of similar signals from natural lightning which may be confused with explosion signals.

DETECTION OF ACOUSTIC SIGNALS

In the period immediately following detonation, the energy generated by a nuclear explosion appears primarily in the form of thermal radiation. This radiation diffuses out from the exploding device and into the surrounding air, heating up the air and forming an "isothermal sphere." As the sphere expands, it engulfs more air; it cools, and its rate of expansion decreases. When the sphere cools to a temperature of about 30 ev, the speed of expansion becomes subsonic with respect to the heated air in the sphere, and a shock wave develops at the surface of the sphere. For a one-kiloton

¹ The survey of literature pertaining to this review was concluded in June 1961.

² This work was supported in part by the United States Atomic Energy Commission and, in the case of Dr. Watson, the Institute of Defense Analysis.

explosion,³ the shock wave forms when the sphere has a radius of about 10 m, which occurs at a time of about 0.2 msec after the explosion. Shortly after this time, hydrodynamic effects dominate and the shock wave propagation becomes independent of the source mechanism. The propagation is found to be the same as it would have been if the isothermal sphere had had zero radius. For a zero-radius isothermal sphere it can be shown from the equations of hydrodynamics that the shock pressure is a function only of its radius R divided by the explosion yield Y to the one-third power.

As the shock wave moves outward, its strength and speed decrease. Eventually the shock wave degenerates into an acoustic wave, whose overpressure follows the law

$$p_m = CY^{1/3}/R \quad 1.$$

in a homogeneous atmosphere, where C is a constant independent of Y .

In the real atmosphere, inhomogeneities strongly affect the propagation of the acoustic signal and, thus, the dependence of p_m on R . The most important inhomogeneity is the variation of the sound speed with altitude. The temperature of the atmosphere decreases from sea level to about 10 km altitude, remains constant between 10 and 30 km, and then increases. Since the speed of sound is proportional to the square root of the temperature of the atmosphere, the region between 10 and 30 km forms a low-velocity wave guide for sonic propagation. The acoustic signals from explosions propagate to great distances principally in this wave guide. At great distances the combined effects of cylindrical divergence and waveguide dispersion lead approximately to the same dependence of overpressure p_m on distance R from the explosion as that given by Equation 1. The principal periods in the acoustic signal are from about one half second to several minutes.

The wind speeds at altitudes between 10 and 30 km strongly affect the acoustic-signal overpressure. Since wind speeds vary randomly with time, the coefficient in Equation 1 also varies randomly with time. If p_m is measured in dynes/sq cm, Y in kilotons, and R in thousands of kilometers, then the average value of C is about seven, and C is less than two about 10 per cent of the time. In winter and summer, when the winds are predominantly in one direction, the average downwind signal overpressure is about twice the upwind overpressure.

Since background acoustic noise is rarely greater than 5 dynes/sq cm, a one-kiloton explosion can with high probability be detected up to distances of about 1400 km.⁴ To locate an acoustic source, at least three signals at widely separated points must be detected. Source location is possible only to within a radius of about 100 km from the source.

Since chemical explosions and some natural events generate distant sig-

³ One kiloton (KT) equals 4.18×10^{10} ergs.

⁴ The detection capability of a network of acoustic detectors can be determined by the method described in the section on underground detection.

nals similar to nuclear explosions, identification of a nuclear explosion is not possible by acoustic signals alone. Natural volcanic and meteoritic explosions similar to nuclear events occur about 100 times each year.

DETECTION OF ELECTROMAGNETIC SIGNALS

A nuclear explosion in air generates a strong electromagnetic signal. Several processes contribute to the generation of this signal. Probably the most important processes result from Compton-recoil electrons which have been scattered by explosion γ rays [Christy & Gell-Mann (2), Kompagnets (3)].

The Compton-electron current at a distance R from an explosion is

$$J \sim -\frac{eL\mu}{\tau} N \frac{e^{-\mu R}}{4\pi R^2} e_r, \quad \text{for } \frac{R}{c} \lesssim t \lesssim \frac{R}{c} + \tau, \quad 2.$$

$$\sim 0, \quad \text{otherwise,}$$

where N is the total number of γ rays from the nuclear explosion, τ is the duration of the γ -ray pulse, μ is the air absorption coefficient for γ rays, and L is the range of the Compton electrons. Each Compton electron ionizes the air, producing a large number of ion pairs ($p \sim 3 \times 10^4$ for γ -ray energies of about 2 Mev). The electrons from these pairs attach to O_2 to form O_2^- at a rate α , where α is about $10^8/\text{sec}$. In equilibrium the density of free electrons is

$$n = \frac{p\mu}{\alpha\tau} N \frac{e^{-\mu R}}{4\pi R^2} \quad 3.$$

The electronic conductivity σ of the ionized air is

$$\sigma = te(ne^2/2m) \quad 4.$$

where t_e , the time between collisions, is about 3×10^{-12} sec.

The electric field produced by the Compton current and the back current of ionization electrons is determined by

$$-(\partial E/\partial t) = 4\pi\sigma E + 4\pi J \quad 5.$$

neglecting magnetic effects. When $\tau \gg 1/4\pi\sigma$,

$$E \sim -\frac{J}{\sigma} = \frac{2m\alpha L}{e\mu t_e} \sim 3 \text{ v/cm} \quad 6.$$

This voltage is generated over the entire region around the explosion for which $\tau \gg 1/4\pi\sigma$. For a one-kiloton explosion this region extends out to a radius of about 600 m. Within this region it is found that $\sigma E + J \sim 0$ and the net radiating current is zero. Outside, $\sigma E \ll J$ and the net radiating current is approximately J .

The electric field radiated to large distances is determined from J by

$$E = -\frac{1}{c^2 R} \frac{\partial}{\partial t} \int dr J\left(r, t - \frac{R}{c}\right) \quad 7.$$

If J is spherically symmetric, there is no radiated field. In general, asymmetries are present—the γ -ray emission from the nuclear device, the varia-

tion of atmospheric density, and the density discontinuity at the air-ground interface being the principal asymmetries. In the case of a surface explosion for which the γ rays are emitted uniformly into one hemisphere, approximate evaluation of Equation 7 gives for the maximum field strength at R km from the explosion

$$E = Ee_s \sim 10^4/R \text{ v/m} \quad 8.$$

In this estimate of E the radiation resulting from the disappearance of the dipole moment formed by the negative oxygen ions and the positive ions created by the γ rays has been omitted. The intensity of this radiation is comparable to the direct Compton-recoil radiation but is of lower frequency, being determined by ionic mobility.

Because of the presence of the earth's ionosphere, the electromagnetic field propagates to great distances dispersively with cylindrical divergence. Empirically, it is found that as a result of propagation effects, the maximum electric field at distances greater than about 1000 km from kiloton explosions is approximately

$$E \sim 10^3/R \text{ v/m} \quad 9.$$

in the frequency range 10 to 100 kc/sec.

In the case of an explosion at altitudes above about one kilometer, the asymmetry in J produced by the ground is no longer present. The remaining asymmetries are less than the ground asymmetry and, consequently, the radiated signal is expected to have a reduced amplitude. Above a few kilometers the asymmetry caused by the variation in atmospheric density is expected to become increasingly important and the signal magnitude is expected to increase. This variation of signal strength with altitude has been observed experimentally.

The radius of the region over which the net radiating current $\sigma E + J$ is approximately zero depends very insensitively on the explosion yield in view of the exponential absorption of the γ rays by the air. Outside this region the current itself also depends only slightly on yield. The net result is that the distant radiated signal is expected to vary slowly with yield. Careful analysis suggests that the distant signal varies as the logarithm of the yield. Experimental observations are consistent with this conclusion.

The electromagnetic signal can under ordinary circumstances be detected at distances of many thousands of kilometers. However, there are two important limitations of this method of detection. First, there is an intense background of electromagnetic signals from natural lightning (about 2000/sec throughout the world). Explosion signals detected near the source can be distinguished from lightning signals by their wave forms, but for detection distances greater than about 1000 km from the source the wave form becomes more a function of the propagation path and less a property of the source. Thus identification becomes unfeasible. Second, it is possible to suppress the electromagnetic signal by surrounding the device with material to absorb the explosion γ rays and neutrons. Experimentally, it has

been observed that several hundred grams per sq cm of absorbing material around the device can reduce the electromagnetic signal by about an order of magnitude. Also, it has been observed that the electromagnetic signal from an explosion carried out at about 20 m below the ground surface was not detectable even at very close distances.

DETECTION OF RADIOACTIVE DEBRIS

While acoustic and radio signals provide a sensitive means of detecting nuclear explosions, similar signals are generated by natural events. Only the collection of radioactive debris constitutes positive identification of nuclear explosions.

A kiloton fission explosion produces about 1.5×10^{23} fissions. Radiochemical techniques can identify the radioactive fission fragments from fewer than 10^8 fissions. If a sample of radioactive fragments from 10^{10} fissions is examined radiochemically, the age of the sample can be determined.

The amount of radioactive debris produced by an explosion which can travel great distances in the atmosphere depends upon the height of the burst point. A low-yield explosion which takes place near the bottom of the troposphere, but whose fire ball does not touch the ground, will leave most of its fission products as very small particles suspended in the troposphere. If the explosion is carried out on the ground, about 20 per cent or so of the fission products are in the form of particles which are too small to settle out onto the ground in less than a day.

Shortly after the explosion, the fission products which remain in the troposphere are confined to a relatively small volume of air. With time, the volume of air containing the fission products increases because of tropospheric winds; and, depending upon the wind patterns, it moves to great distances. In some wind fields it is possible for the volume of air containing the radioactive fission products to increase from its initial small volume to a volume as large as 10^6 cu km by the time the debris has moved a few hundred kilometers. If initially there were, for example, about 10^{22} fission fragments left suspended in the troposphere, then a volume of 10^6 cu km would contain a density of about 10^7 fission fragments/cu m. Nominally, the concentration of fission fragments at ground level is at least 1 per cent of the average concentration. Since it takes a day or so for such a large volume of air to cross any particular point on the ground, a filter which could filter up to 10^8 cu m/hr of air would be able to collect sufficient fission fragments for identification. It is possible that the volume of air containing the fission fragments remains sufficiently small to miss all ground filter stations in one hemisphere even with station separations of as little as 1000 km. To avoid this possibility, aircraft carrying suitable filters can be used to sample the air which might contain fission activity missed by ground filters.

For low-yield explosions in the upper troposphere, the fission fragments may rise into the stratosphere. For these explosions, and for explosions in the stratosphere, insufficient debris may reach the ground to permit identi-

cation. Aircraft carrying filters can then be used to collect debris. The aircraft may either fly regular search paths or be dispatched upon the detection of unidentified acoustic or radio signals. In many cases the trajectory of the air carrying the radioactivity can be backtracked. In such cases if the radioactive debris can also be dated, the approximate location of the explosion can be determined.

DETECTION OF UNDERWATER EXPLOSIONS

An underwater explosion generates a strong hydroacoustic signal. The signal consists of a series of pressure spikes which become progressively smaller and closer together with time. Willis (4) has shown that these spikes are generated by radial pulsations of the gas bubble formed by the explosion. The combustion products in the case of a chemical explosion and the vaporized water in the case of a nuclear explosion expand, converting their internal energy into kinetic energy of the water. Because of the inertia of the water, the expansion does not stop at that volume for which the pressure in the bubble equals the hydrostatic pressure, but rather overshoots its equilibrium position. The hydrostatic pressure decelerates the bubble and recompresses it, again overshooting. This process continues until the explosion energy is lost by radiation or dissipation.

The hydroacoustic signals so generated are transmitted to great distances in the SOFAR channel [Ewing & Worzel (5)], a low-velocity wave guide in the deep ocean. Detection of these signals appears possible at great distances. However, no precise estimate of sensitivity is available. The hydroacoustic wave can itself generate a seismic signal at the water-earth interface. This seismic signal is larger than the signal from an underground explosion of the same yield. Seismic detection methods thus apply to underwater as well as underground explosions. For explosions in inland bodies of water, only the seismic methods are useful for detection at great distances.

UNDERGROUND NUCLEAR EXPLOSIONS

The only signals known to propagate to great distances from underground nuclear explosions are seismic signals. Ideally, detection and identification of underground nuclear explosions would be based entirely on these signals. Unfortunately, seismic signals from underground nuclear explosions are similar to those from some earthquakes, and therefore explosions cannot be distinguished from earthquakes by seismic signals alone. For this reason seismic signals can only serve to identify some earthquakes as earthquakes without, it is hoped, misidentifying explosions as earthquakes. For unidentified events, inspection at the site is required to determine cause.

The problem of detection is further complicated because deliberate modification of the explosion environment can reduce the strength of the seismic signal by a large factor or alter the explosion signal so that it will be misidentified as an earthquake signal. Consequently, underground detection is forced to a limited scope: to detect and identify earthquakes and to detect

explosions carried out under special conditions. Evaluating underground detection even within this limited scope is difficult and uncertain because data are incomplete on many aspects of the problem.

GENERATION OF SEISMIC SIGNALS

The sudden release of energy from an underground nuclear explosion creates in microsecond times a small spherical "cavity" (a few meters in radius for kiloton explosions) containing vaporized materials from the ambient medium and from the nuclear device itself. The temperature and pressure of this vapor as well as its subsequent history depend upon the amount of energy released and the equation of state of the vapor. The creation of a high pressure in the neighborhood of the explosion sends a shock into the surrounding medium. As the shock propagates outward, the central cavity grows in volume and the vaporized materials expand adiabatically and lower in temperature, and the cavity pressure decreases.

As the pressure decreases, the cavity growth is inhibited by the tectonic stresses in the medium. The nature of these stresses depends upon the geological history of the medium and therefore varies from one region to another. In many regions the stresses result simply from the weight of the material above the explosion cavity (the overburden) and, for these regions, the pressure resisting the cavity growth increases linearly with the depth of the explosion.

When ambient stresses balance the pressure in the cavity, the cavity growth stops. Actually the cavity may overshoot its equilibrium position slightly because of residual kinetic energy in the surrounding medium which must radiate away or dissipate before static equilibrium is reached. In media for which tectonic stresses result only from the overburden, the final cavity pressure is expected to exceed the overburden pressure by an amount which depends upon the equation of state of the vapor and the physical properties of the medium. In a liquid, for example, the final cavity pressure is equal to the overburden pressure, and therefore the cavity size is determined entirely by the equation of state of the vapor. For an ideal elastic medium the cavity pressure can be arbitrarily large, and the cavity size is determined both by the elastic constants of the medium and the equation of state of the vapor. In the case of the Rainier explosion [Johnson, Higgins & Violet (6)] which took place in a tuff⁵ medium, there is evidence that the final pressure was approximately equal to the overburden, suggesting that the tuff medium behaved somewhat like a liquid in the immediate neighborhood of the explosion.

In view of the dependence of the final cavity size on the equation of state of the vaporized materials, it is clear that nuclear explosions will behave differently from chemical explosions. Moreover, the dependence of cavity size on medium and tectonic stress indicates that these factors also affect the

⁵ Tuff is a silicon dioxide rock formed from volcanic ash. The Rainier tuff was saturated with water.

generation of seismic waves from explosions. Experiments are required to determine the quantitative dependence.

Within the cavity the pressure is initially considerably greater than the elastic limit of the medium. As the shock wave propagates outward, the pressure is at first so great that the medium behaves hydrodynamically. After a while, the shock strength decays and the medium begins to behave plastically. Finally, when the shock pressure falls below the elastic limit of the medium, the shock wave becomes a simple elastic wave. The quantitative treatment of the nonelastic phases of the motion involves complicated and incompletely understood behavior of the medium. As a result it has not been possible to make reliable theoretical predictions of the signals generated. It has, however, been possible, without detailed knowledge of the non-elastic motion of the medium, to determine the dependence of the amplitude of the elastic wave (and hence the seismic signal) on the energy released by the explosion [Latter, Martinelli & Teller (7)].

To determine this relationship, it may be assumed for simplicity that the explosion occurs in an infinite homogeneous medium. The effect of inhomogeneities can be shown to be small. Let r_0 be the radius at which the shock wave becomes elastic and $p(t, r_0)$ the pressure history at r_0 . A straightforward solution of the elasticity equations [Jeffreys (8), Blake (8a)] gives for the displacement $z(t, r)$ of the medium at $r > r_0$

$$z(t, r) = \frac{1}{2\pi} \int_{-\infty}^{\infty} d\omega e^{i\omega t} \hat{z}(\omega, r) \quad 10.$$

where

$$\hat{z}(\omega, r) = \hat{p}(\omega, r_0) \frac{r_0^3}{4\mu} \left(\frac{i\omega}{rc} + \frac{1}{r^2} \right) \frac{e^{-i(\omega/c)(r-r_0)}}{1 + i \frac{\omega}{\omega_0} - \frac{\lambda + 2\mu}{4\mu} \left(\frac{\omega}{\omega_0} \right)^2} \quad 11.$$

and $\hat{p}(\omega, r_0)$ is the Fourier transform of $p(t, r_0)$. The symbols λ and μ are the Lamé constants, and $\omega_0 = c/r_0$ is the natural elastic frequency of the region $r < r_0$.

It is known that high-frequency waves are rapidly attenuated in the earth and cannot propagate to great distances. In those cases for which the unattenuated frequencies ω are much smaller than ω_0 , Equation 11 gives for the wave zone

$$\hat{z}(\omega, r) \sim \hat{p}(\omega, r_0) r_0^3 \frac{i\omega}{rc} \quad 12.$$

From observation on the Rainier explosion it appears that so far as the low frequencies are concerned [Perret (9)], $p(t, r_0)$ is essentially a step-function,⁶ so that

$$\hat{p}(\omega, r_0) = p_0/i\omega \quad 13.$$

⁶ The essential part of this argument is the assumption of a step function pressure. There are no data on nuclear explosions in media other than tuff to confirm the general validity of this assumption.

where p_0 is the shock pressure below which the medium behaves elastically and therefore a property only of the medium, independent of the energy release of the explosion. From Equations 12 and 13 it follows that

$$\hat{z}(\omega, r) \sim r_0^3 \quad 14.$$

where only quantities dependent on the energy have been retained. Note that \hat{z} is independent of frequency for low frequencies.

It is plausible to assume that the equations of motion for the region around the explosion are based on some combination of hydrodynamics, elasticity, and plasticity. In this case the equations for a point-source explosion do not involve a fundamental length or time; and therefore, as is well known, all lengths scale like the cube root of the energy. With this scaling law it follows from Equation 14 that the amplitude of the elastic wave scales linearly with the energy of the explosion.

This result depends upon the requirement that only frequencies small compared to ω_0 are unabsorbed during propagation. For low-yield explosions, ω_0 is large and the result valid. For high-yield explosions, however, frequencies of the order of ω_0 and greater do propagate to great distances. In this case the scaling law is changed. When only frequencies $\omega \gg \omega_0$ are absorbed, the amplitude of the elastic wave is given directly by substituting Equations 11 and 13 into Equation 10. A straightforward evaluation gives

$$z(t, r) \sim r_0^2 \quad 15.$$

and the amplitude scales as the two-thirds power of the energy release.⁷ Figure 1 shows the comparison of the theoretical and experimental results for the Nevada underground nuclear explosions.

A further consequence of the assumed similarity of the motion in the region $r < r_0$ is that the cavity volume produced by the explosion scales linearly with the energy release. This result combined with the scaling law for the amplitude of the elastic wave implies that, for a given explosion environment, the seismic signal from a low-yield explosion is directly proportional to the cavity volume and for a high-yield, proportional to the two-thirds power of the volume.

So far as the generation of seismic signals from natural earthquakes is concerned, neither the mechanism for triggering an earthquake nor the detailed mechanism by which energy is released is adequately understood. Qualitatively, however, earthquakes are generated by a spontaneous release of stored tectonic energy. The release usually takes the form of a rapid displacement of the region on one side of a plane—the so-called fault plane—relative to the region on the other side. This type of motion is equivalent in

⁷ For some components of the distant seismic signal, the amplitude of the signal is not simply proportional to the amplitude of the ground displacement in the neighborhood of the source. For example, the headwave which propagates along the Mohorovicic discontinuity is proportional to the integral of the displacement. In this case, obvious changes in the scaling laws are required.

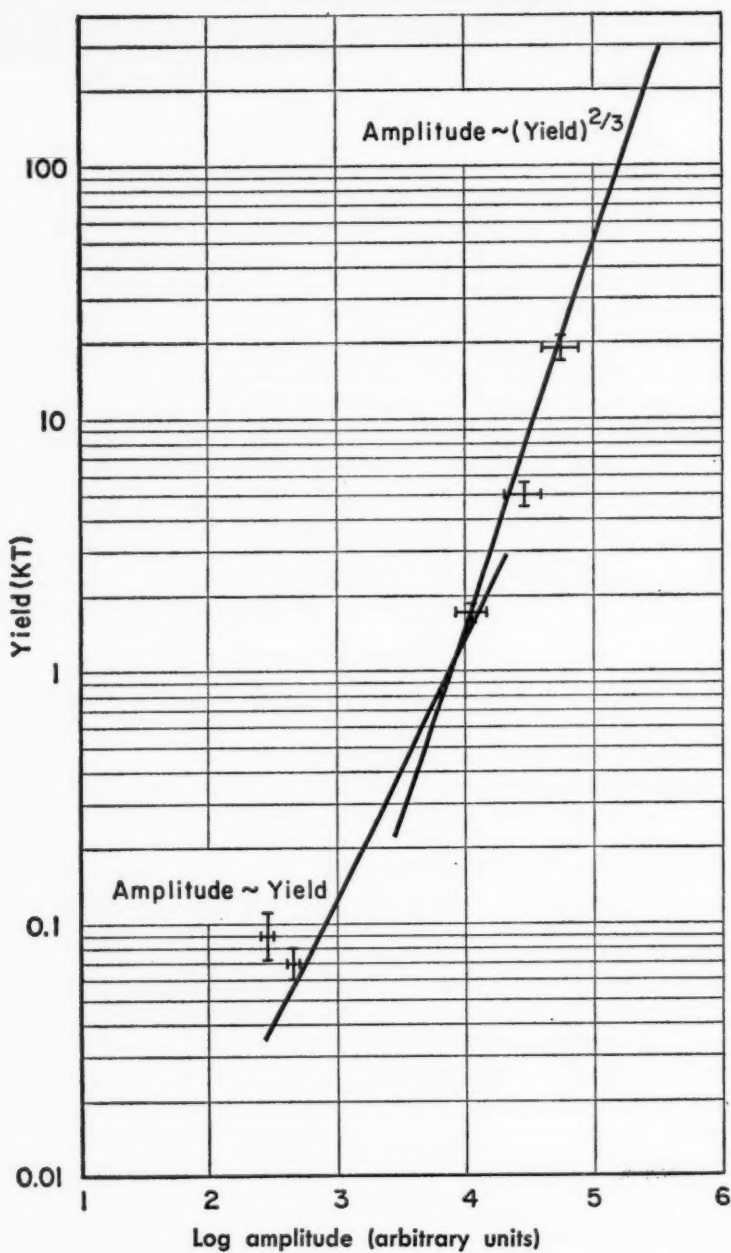


FIG. 1. Yield-amplitude relation from Rainier-Hardtack data.

the case of an ideal elastic medium to a quadrupole source—as contrasted to the monopole behavior of an explosion.

Analyses of the faulting motions of earthquakes have shown that in restricted geographical regions the direction of the earth motion generating earthquakes is approximately constant and is correlated with tectonics. The dip (angle with the horizontal) of the earthquake fault plane is, however, essentially random. From region to region the direction of earth motion varies as the local tectonics change, so that over sufficiently large regions the direction of earth motion is essentially random. In large seismic regions there is a tendency for earthquakes to be predominantly either strike-slip (vertical or oblique fault plane and horizontal displacement) or dip-slip (oblique fault plane and displacement perpendicular to a horizontal line). For almost all important seismic regions of the world, strike-slip faulting predominates. About 75 per cent of the world's shallow earthquakes are strike-slip [Scheidegger (10)].

Earthquakes may also be generated by nonfaulting earth motions. A volcanic eruption produces an earthquake similar to an explosion. An upward or downward thrust of a large tectonic block will produce an earthquake whose seismic signal is cylindrically symmetric. Such earthquakes are observed, but are relatively rare.

PROPAGATION OF SEISMIC SIGNALS

In an infinite homogeneous medium, the seismic wave generated by an explosion is a pure compressional wave (P wave) radiating outwardly [(11), Richter (12)]. In a finite homogeneous earth, the presence of a free surface leads to partial conversion of the P wave into a shear wave polarized perpendicular to the surface (SV wave) and to a surface shear wave (Rayleigh wave) vibrating in a plane perpendicular to the surface. An earthquake in a finite homogeneous earth produces not only P , SV , and Rayleigh waves but also horizontally polarized shear waves (SH waves) and horizontally polarized surface shear waves (Love waves).

If the earth were homogeneous, it would accordingly be possible to discriminate an explosion from a natural earthquake by the absence of SH waves and Love waves. However, the real earth is heterogeneous, and some types of heterogeneities can lead to mode conversion of P and SV waves into SH and Love waves. For example, a velocity discontinuity at an oblique angle to the radial direction from the explosion and to the earth's surface will partially convert SV or P waves into SH waves which by reflection at the surface can generate Love waves. The occurrence of SH waves and Love waves from nuclear explosions has been verified experimentally (11).

There is, however, a question of the relative efficiency with which earthquakes and explosions generate SH waves and Love waves. The only data bearing on this question suggest that Love and SH waves may be generated more efficiently by some earthquakes. Considerably more experimental data are needed to substantiate this preliminary result.

At large distances from the source, seismic signals consist of three distinct waves arriving at different times. The first arrival is the *P* wave, which has the greatest velocity, followed by the *S* wave and finally by the surface waves. While the surface waves radiate from the source and propagate on the surface, diverging essentially cylindrically, the *P* and *S* waves follow complicated paths determined by the variation of elastic velocity in the earth's interior. Very crudely, the *P* and *S* waves follow paths which, for shallow sources and great distances, pass steeply through the earth's crust, are refracted at the Mohorovicic discontinuity (about 30 to 60 km depth), follow the discontinuity (head wave) or refract slowly in the earth's mantle, and finally return again to the earth's surface steeply through the crust. If the earth were homogeneous, the successive *P*-, *S*-, and surface-wave trains would be short, corresponding to the short signal generation time (modified, of course, by absorption of high frequencies). Actually the earth's crust is extensively layered with regions of varying elastic velocities. A seismic signal is reflected and refracted many times by these layers; and the resultant distant signal, having a total duration up to minutes, is a superposition of many waves. In view of this complicated propagation, the properties of the distant seismic signals tend to be determined more by the nature of the earth than by the characteristics of the source.

The only property of the source which is known to propagate to great distances is the direction of the initial source motion. For explosions, the initial earth motion is expected to be outward from the source (compressive) in all directions. Earthquakes produced by faulting motion, however, are expected to exhibit compressive motions in some directions and rarefactive (inward) motions in others. The distribution of compressive and rarefactive initial motions depends upon the orientation of the earthquake fault plane and the direction of earth displacement.

Those relatively rare earthquakes which are generated by block motions can produce outward or inward motions in all directions. The occurrence of rarefactive initial motions can therefore serve to distinguish some earthquakes from explosions. But the existence of "explosive" type earthquakes makes positive identification of explosions impossible.

The initial earth motion radiates from the source in the *P*-wave portion of the seismic wave. Although inhomogeneities and absorption along the propagation path tend to distort the initial *P*-wave motion, in general the first-arrival *P* wave can be shown to correspond to the initial source motion. It is possible to construct inhomogeneities which can invert the initial direction of the *P* wave, but the existence of such inhomogeneities is a matter of conjecture. For strike-slip faulting, rarefactions and compressions of the *P*-wave first motion occur over equal areas of the earth's surface. For dip-slip faulting with dip angles near 45° it is possible for all *P*-wave signals beyond about 2000 km to show the same first motion (all compressions for "thrust" faulting, all rarefactions for "normal" faulting). *P*-wave signals within about

1000 km from dip-slip faults will more nearly conform to equal areas for compressions and rarefactions characteristic of strike-slip faulting.

The initial source motion is also contained in the surface-wave portion of the seismic signal. Mode conversion of the *P* wave at the surface directly above the source generates a Rayleigh wave whose initial motion is determined by the initial motion of the *P* wave. Propagation of the surface waves, however, is highly dispersive and, consequently, the direction of initial motion is obscured at great distances. In principle, if the transfer function of the propagation path is known, the source motion can be deduced by applying the inverse of the transfer function to the distant signal. This procedure, known as phase equilization, has proved practical and has had some success recently, but results are still preliminary [Aki (13)].

MICROSEISMIC NOISE

In the previous section it was pointed out that the most reliable method for identifying earthquakes is based on the sign of the first *P*-wave motion. The sign of this motion must be observed in the presence of background noise at detection stations. Noise may be characterized by a probability that the peak amplitude of the noise over a specified interval of time is less than a given amplitude. The nature and probability distribution of microseismic noise vary from region to region and with the time of year. The variations can be as much as ten or more. As an illustrative example, Figure 2 shows a typical noise distribution for a rather quiet site.

EXPERIMENTAL DATA ON EXPLOSION AND EARTHQUAKE SIGNALS

The amplitude of first motion from explosions appears in general smaller than the peak *P*-wave amplitude, and therefore some signals which are clearly detected by the signal peak will have their first motions submerged in the noise. To avoid misidentifying as first motion the first portion of the signal which happens to exceed the noise, a criterion for recognizing genuine first motion must be made in terms of the ratio of the peak amplitude of the *P*-wave signal to that of the noise. The stipulated ratio must be large enough to guarantee that the actual first motion is readable above the noise.

The principal data for exploring the *P*-wave signal from explosions are the seismic measurements obtained from the Rainier shot and the HARD-TACK II series. Actually, only the data from the Blanca (19 kilotons) and Logan (5 kilotons) explosions are sufficiently complete for analysis, and these explosions have several possibly vital limitations. They were both conducted in the same environment, at the same depth below the surface, and under the same geological conditions. It is not known whether these explosions are characteristic of unconcealed underground explosions or whether they generate an atypical signal which will be different for explosions under other conditions. Nonetheless, they provide the only available

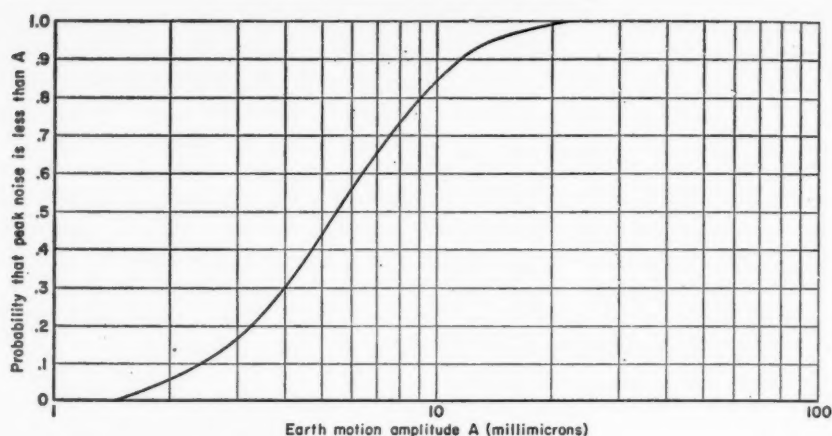


FIG. 2. Noise distribution.

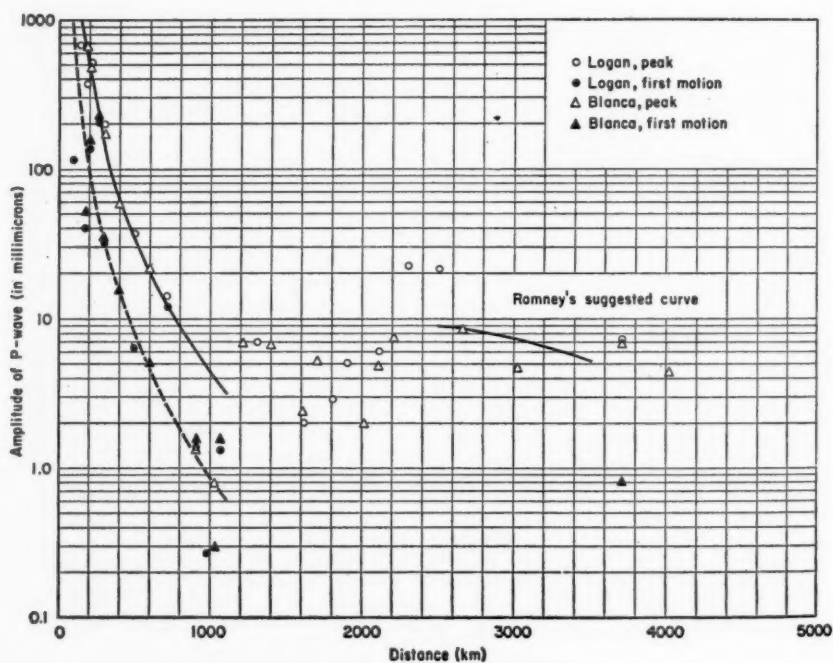


FIG. 3. Peak and first-motion amplitudes versus distance for one kiloton explosion. Solid curve refers to peak amplitude. Dashed curve refers to first-motion amplitude. Amplitude data from Blanca and Logan were divided by their yields to the two-thirds power in order to scale to one kiloton. The first-motion amplitude for Blanca at 3717 km is uncertain due to low signal-to-noise ratio.

extensive data on which to base detection capability. Quantitative data reported by Romney on the first motion and peak amplitude of the *P*-wave signal from these nuclear explosions are summarized in Figure 3 [Romney (14)].

For analyzing these data it has been convenient to define distance zones as follows: the near zone, 0 to 1100 km from the epicenter; the shadow zone, 1100 to 2500 km; and the far zone, 2500 to 3500 km. The basis for this definition is the conjecture that in the near and far zones, seismic signals are characterized by having a clear onset time, while in the shadow zone the signals grow only slowly out of the noise. It is not possible on the basis of the Blanca and Logan data to verify this conjecture, but there is some indication that the seismic signals from these shots do have this general behavior in the near and shadow zones. Moreover, there is some evidence that the predominant periods of the shadow-zone signals from Blanca and Logan are longer than those in the near and far zones.

While the Blanca and Logan data define rather accurately the variation of the peak *P*-wave amplitude as a function of distance in the near zone, there are only three readable records in the far zone. These records are insufficient to determine the far-zone amplitude-distance curve for the peak *P*-wave motion. Romney has suggested the far-zone amplitude-distance relation which is shown in Figure 3.

First motion for the Logan and Blanca explosions was clearly recorded only in the near zone. In the shadow zone, because of the somewhat indefinite onset of the signal, first motion was indefinite. Beyond 2500 km the signal-to-noise ratio for the experimental measurements was so small that first motion was unreadable except for a station at 3717 km where a compressive first motion may have been observed. Some question arises, therefore, as to the possibility of far-zone detection of first motion.

In trying to distinguish between earthquakes and nuclear explosions, it is necessary also to know the properties of earthquake signals. Good data on peak- and first-motion amplitudes of earthquake signals as a function of distance are at present not available. Richter has made a statistical study of earthquake peak amplitudes as a function of distance, shown in Figure 4 [Richter (12)]. However, in the near zone his analysis treated the peak amplitude of the earthquake signal in the entire wave train rather than just in the *P* wave as was done for explosions; moreover, the peak amplitude was measured on the standard Wood-Anderson torsion seismograph⁸ rather than on the Benioff seismograph used for recording the explosion signals. While the variation of peak amplitude with epicentral distance which he deduces is in reasonable agreement with that obtained from *P*-wave analysis on the nuclear explosions, it is not known whether this agreement is more than ac-

⁸ The Wood-Anderson seismograph has a broad-band frequency response, while the Benioff has a narrow response, peaked in the neighborhood of two cycles per second.

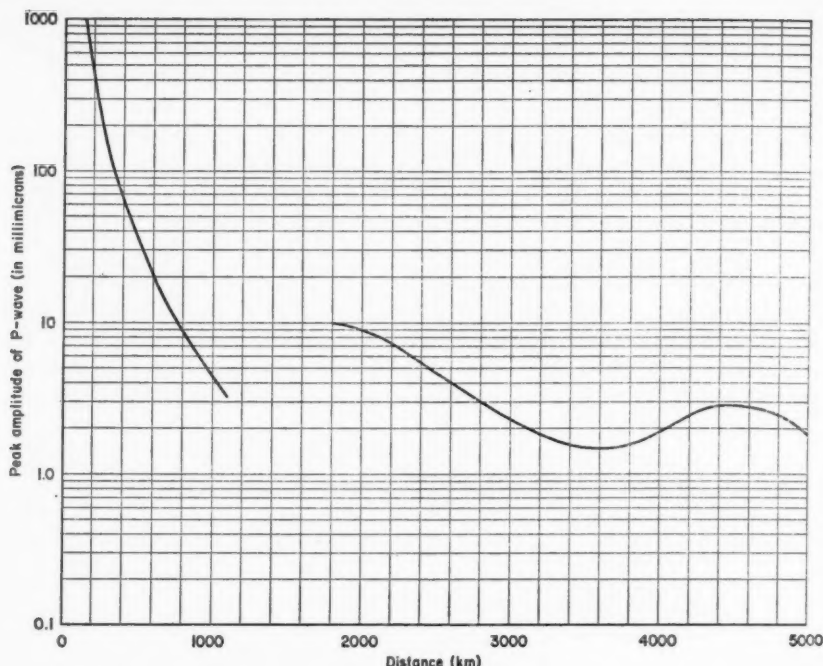


FIG. 4. Peak amplitude (scaled to 1 KT) versus distance based on Gutenberg and Richter earthquake data.

cidental in view of the differences in the measurement technique. In the far zone an analysis by Gutenberg applies to large earthquakes, of magnitude greater than 6, as shown in Figure 4 [Richter (12)]. At present there are no experimental data on which to base an extrapolation of Gutenberg's far-zone amplitude-distance relationship to low magnitudes. However, in estimating detection capability it is necessary to assume a peak amplitude-distance relationship for earthquakes. Quite arbitrarily this has been taken in the past to be the same as for explosions. This is consistent within a factor of two or three with an extrapolation of Gutenberg's *P*-wave amplitude-distance curve for large magnitude earthquakes down to low magnitudes. It should be pointed out that Romney's limits of 2500 to 3500 km for the far zone were dictated primarily by the requirements of first-motion observation; it is probable that the Gutenberg limits, about 1800 to 5000 km, are more reasonable for the detection problem which is primarily concerned with the peak signal. The data are not sufficient at the present time to decide between the Romney and Gutenberg amplitude-distance curves though it is clear that all detected signals, not just those in the near and far zones, are useful for detection and epicentral location.

So far as the first motion from earthquakes is concerned, the only anal-

ysis to date consists of studies on the use of the sign of the first motion to determine the nature of the faulting sources. The ratio of *P*-wave amplitude to the first-motion amplitude has not been studied. In the past, it has been arbitrarily assumed that the ratio of earthquake first motion to peak *P*-wave motion is no smaller than for explosions.

A METHOD FOR ESTIMATING DETECTION AND IDENTIFICATION CAPABILITY

A simplified but quite accurate method for estimating the capability for detection and identification of a network of seismic stations was developed at the 1958 Geneva Conference of Experts [Latter (15)]. This method is essentially statistical and depends on considering the recording of seismic events by a large number of stations as independent and random events. If out of a large number *N* of stations in a network, a number *n* of them records signals, then the number of recorded signals is

$$n = \sum_{i=1}^N x_i \quad 16.$$

where the sum extends over all the stations and x_i assumes the value 1 if the *i*th station records and 0 if it does not. In the present context, "signal" refers either to first motion or to peak amplitude depending upon whether identification or detection is being considered.

If x_i has the value 1 with a probability q_i and has the value 0 with a probability $1 - q_i$ and if the x_i 's are independent and random, then, by the central limit theorem, the probability $p(n)$ that *n* stations record signals is given by

$$p(n) = \frac{1}{\sqrt{2\pi\sigma^2}} \exp [-(n-\bar{n})^2/(2\sigma^2)] \quad 17.$$

where

$$\bar{n} = \sum_i q_i \quad 18.$$

and

$$\sigma^2 = \sum_i \sigma_i^2 = \sum_i q_i(1 - q_i) \quad 19.$$

Here \bar{n} is the expected number of stations which record signals and σ is the standard deviation of \bar{n} .

The expected number \bar{n} of stations recording signals may be estimated by approximating the sum of the q_i 's over the discrete set of stations by an integral,

$$\bar{n} = \sum_i q_i \approx 2\pi \int \rho(R)q(R)RdR \quad 20.$$

where $\rho(R)$ is the density of stations in the net at the distance *R* from an epicenter, and $q(R)$ is the probability that at *R* the signal-to-noise ratio meets the criterion for recording a signal. This clearly depends upon the

amplitude-distance relation and upon the assumed noise distribution at the station. In a similar fashion, the variance is approximated by

$$\sigma^2 \approx 2\pi \int \rho(R)q(R)[1 - q(R)]RdR \quad 21.$$

Since the likelihood that an explosion can produce a false rarefactive first motion is unknown, earthquake identification is based on the probability of finding a specified minimum number of rarefactive first motions among those recorded. An approximate expression for the probability of finding at least r rarefactive first motions out of a total of n recorded first motions may be derived by assuming the a priori probability that a station is in a rarefactive region is one-half. (This assumption leads to negligible error.) The expression is

$$\begin{aligned} \hat{p}_r(n) &= 1 - \frac{1}{2^n} \sum_{s=0}^{r-1} \frac{n!}{(n-s)!s!}, & n \geq r, \\ &= 0, & n < r \end{aligned} \quad 22.$$

The average earthquake identification probability P_r may be determined by summing the above expression weighted by $p(n)$, the probability that n stations record first motion. That is,

$$P_r = \sum_{n=r}^N p(n)\hat{p}_r(n) \quad 23.$$

The sum may be evaluated approximately by assuming σ small compared to n . Since the important contribution to the sum comes from values of n near n , the average earthquake identification probability P_r is approximately given by

$$P_r \approx \hat{p}_r(n) = 1 - \frac{1}{2^n} \sum_{s=0}^{r-1} \frac{n!}{(n-s)!s!} \quad 24.$$

In the special case that only near-zone recording of first motion is assumed, the above analysis can be carried out simply and explicitly. Letting R_1 ($= 1100$ km) denote the limiting radius of the near-zone contribution, the expression for n is

$$n = 2\pi\rho \int_0^{R_1} q(R)RdR \quad 25.$$

where the density of stations, ρ , is assumed constant. Since the amplitude of the P -wave signal in the near zone varies approximately as $1/R^3$, n may be written

$$n = \pi R_1^3 \rho H(A) \quad 26.$$

where $\pi R_1^3 \rho$ is the total number of stations in the near zone and

$$H(A) = \frac{2}{3} A^{2/3} \int_A^\infty q(x) \frac{dx}{x^{5/3}} \quad 27.$$

The amplitude of the signal at R_1 , A , is given by

$$A = \frac{4.2 \times 10^9 FGY^{2/3}}{R_1^3}, \quad Y > 1KT, \quad 28.$$

$$A = \frac{4.2 \times 10^9 FGY}{R_1^3}, \quad Y < 1KT \quad 29.$$

where the seismic amplitude has been assumed to scale linearly with equivalent explosion yield⁹ below 1 KT and as the two-thirds power, above (see Fig. 1). The inverse of F is the required peak signal-to-noise ratio for recording a signal; and G is the noise reduction factor achievable, for example, by an array of seismographs. Figure 5 shows $H(A)$, evaluated using the noise distribution of Figure 2.

In a similar fashion, the standard deviation σ of the expected number n may be written

$$\sigma = (\pi R_1^2 \rho)^{1/2} S(A) \quad 30.$$

where

$$S(A) = \left\{ \frac{2}{3} A^{2/3} \int_A^\infty q(x) [1 - q(x)] \frac{dx}{x^{5/3}} \right\} \quad 31.$$

with the previous definition of A . Figure 6 shows $S(A)$, also evaluated using the noise distribution of Figure 2.

The density of stations depends on the geometry of the net. In particular, for a triangular grid of spacing s , the density of stations is given by

$$\rho = (2\sqrt{3})/(3s^2) \quad 32.$$

With this expression for the density, n and σ are given by

$$n = 3.6H(A)(R_1^2/s^2) \quad 33.$$

and

$$\sigma = 1.9S(A)(R_1/s) \quad 34.$$

Detection and location capability may be evaluated by examining n as a function of yield. For location, P -wave recording at four stations is necessary, so that $n \geq 4$.¹⁰

Based on these results, near-zone detection and identification capability are shown in Figures 7 to 11 where the criterion on peak signal-to-noise ratio was taken as three to one for detection and as ten to one for identification; and for identification two rarefactions were required.

⁹ The "equivalent explosion yield" of an earthquake is defined as that yield nuclear explosion carried out under Rainier conditions which produces a signal of the same magnitude as the earthquake.

¹⁰ Three recordings are adequate provided the two antipodal epicentral locations determined by only three recordings can be distinguished, for example, by recording two components of the signal with different velocities simultaneously at one or more stations.

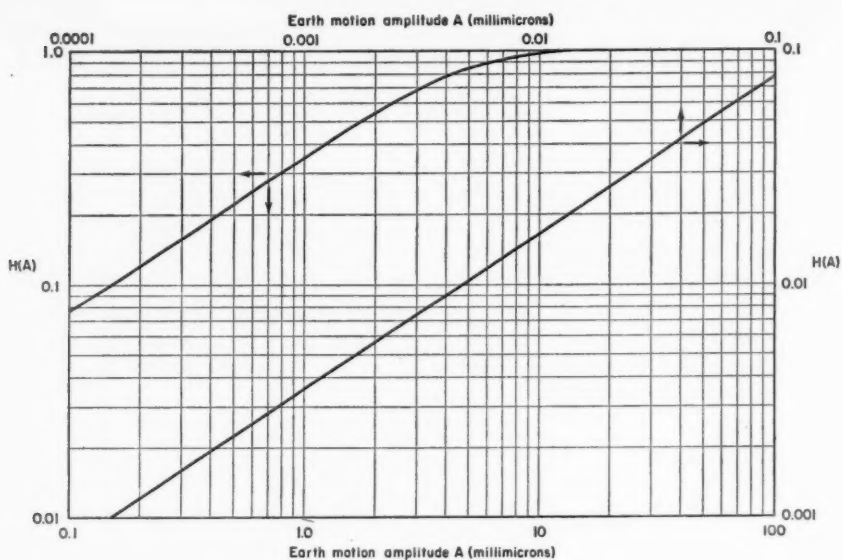


FIG. 5. $H(A)$ versus A for noise distribution of Fig. 2.

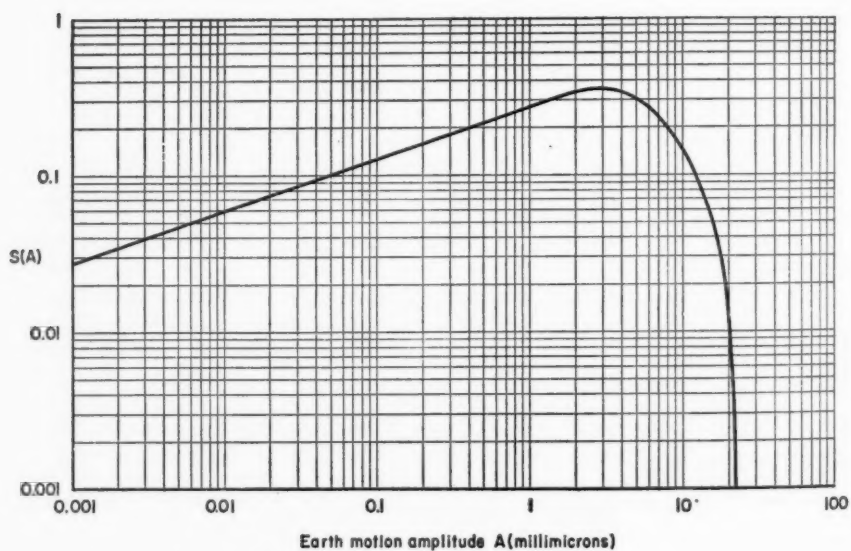


FIG. 6. $S(A)$ versus A for noise distribution of Fig. 2.

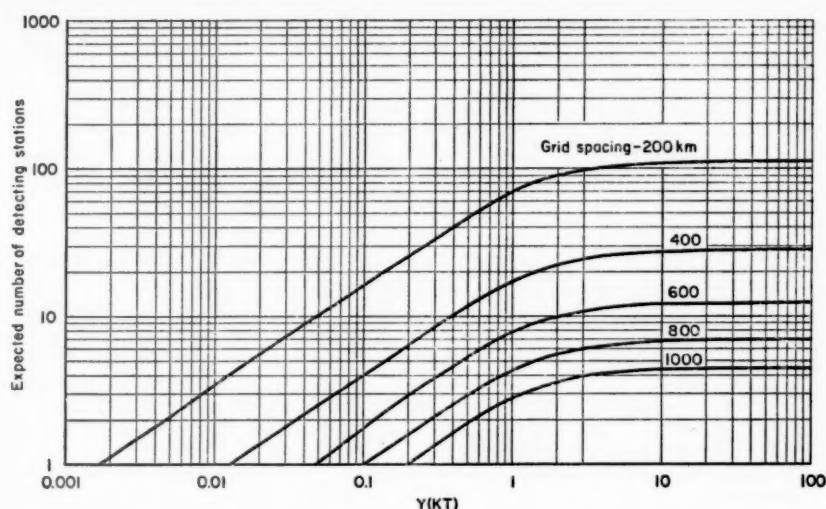


FIG. 7. Expected number of stations detecting P -wave motion as a function of equivalent explosion yield for triangular grids of indicated grid spacing. Noise distribution of Fig. 2. $F=0.33$, $G=2.5$.

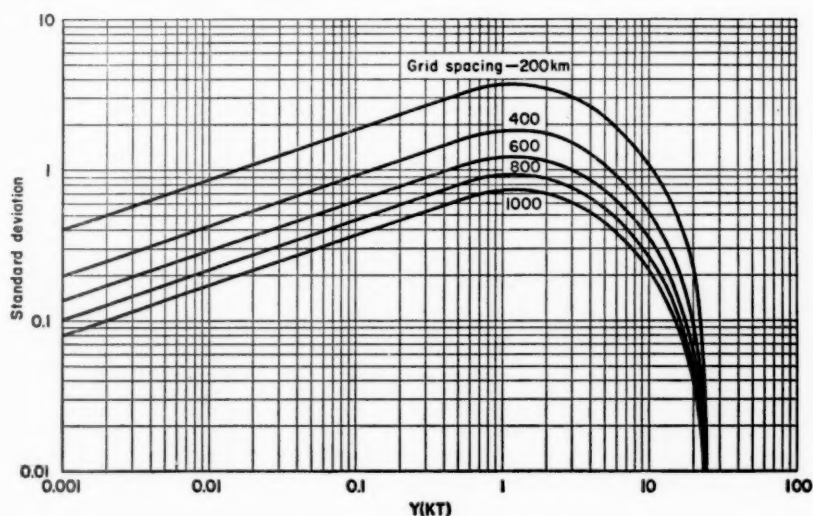


FIG. 8. Standard deviation of expected number of stations detecting P -wave motion as a function of equivalent explosion yield for triangular grids of indicated grid spacing. Noise distribution of Fig. 2. $F=0.33$, $G=2.5$.

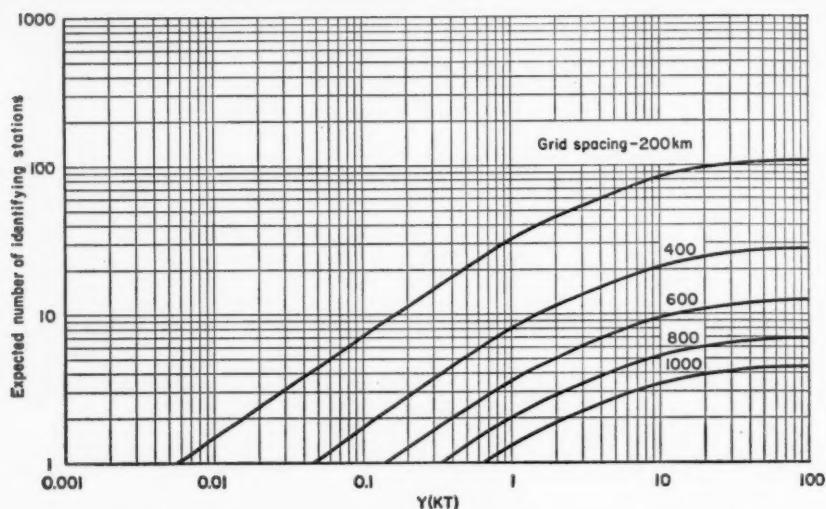


FIG. 9. Expected number of stations identifying first motion as a function of equivalent explosion yield for triangular grids of indicated grid spacing. Noise distribution of Fig. 2. $F=0.1$, $G=2.5$.

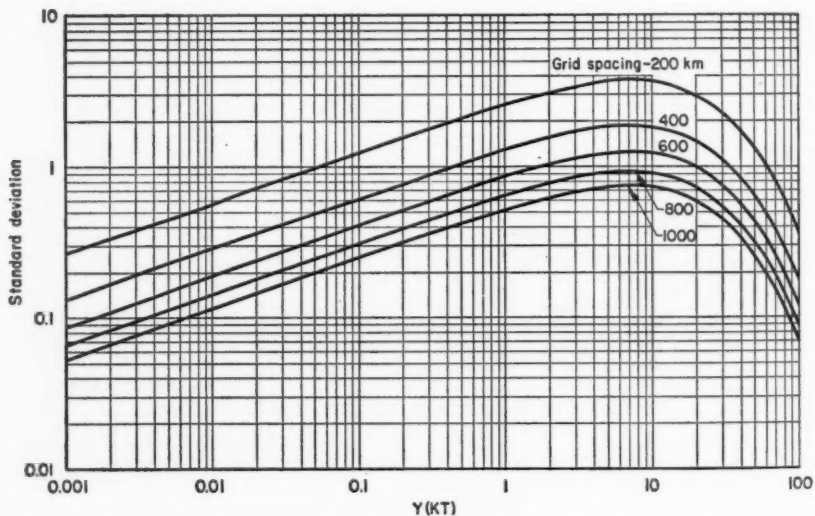


FIG. 10. Standard deviation of expected number of stations identifying first motion as a function of equivalent explosion yield for triangular grids of indicated grid spacing. Noise distribution of Fig. 2. $F=0.1$, $G=2.5$.

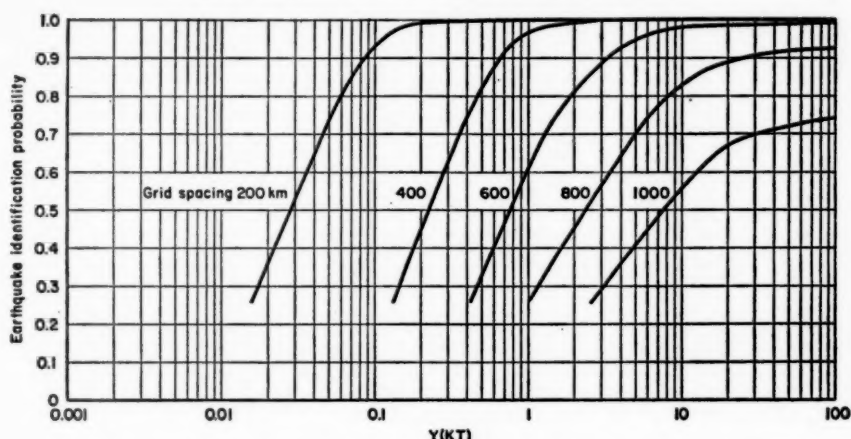


FIG. 11. Earthquake identification probability as a function of equivalent explosion yield for triangular grids of indicated grid spacing. Noise distribution of Fig. 2. $F=0.1$, $G=2.5$. Two rarefactions.

FREQUENCY AND DISTRIBUTION OF EARTHQUAKES

In order to relate the capability of a system to the number of earthquakes which can be identified, it is necessary to determine the seismicity distribution throughout the world. Only shallow continental earthquakes need be considered. Shallow continental earthquakes have been defined as those occurring on or near land (that is, on continents or on islands, but not in inland seas) and having hypocentral depth less than about 60 km. Deeper earthquakes can be identified by their seismic signals.

Seismicity estimates are based on information from Gutenberg & Richter (16). These authors provide an extensive tabulation of large earthquakes (magnitude $M > 6$) from which it is possible to infer the frequency and geographic distribution of these earthquakes throughout the world. Some data on the frequency of both small and large magnitude earthquakes occurring in limited geographical regions are also reported in this reference. These latter data apply to the annual number of earthquakes in Southern California and in New Zealand, and are plotted in Figure 12.

Such limited data are clearly inadequate in themselves to determine the seismicity of all regions of the world. However, an important empirical observation provides the basis for extrapolating the known data to any region. It is observed from Figure 12 that both for Southern California and for New Zealand, the variation of earthquake frequency as a function of magnitude is the same—namely, the number of earthquakes per year above a given magnitude increases by a factor of eight for each unit decrease in magnitude. It is assumed that this relationship between earthquake frequency

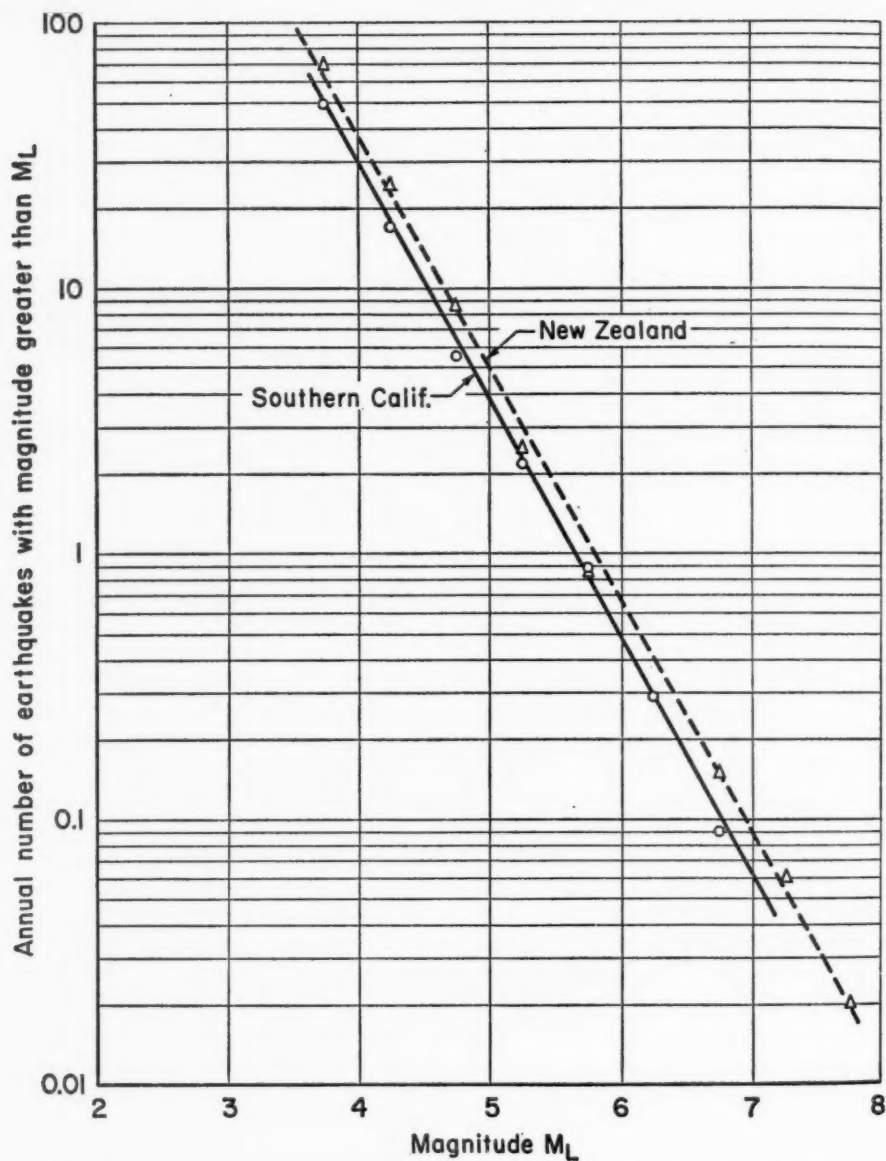


FIG. 12. Seismicity data for small magnitude earthquakes based on local studies.

and magnitude holds for all areas of the world. Consequently, using the data from Gutenberg & Richter on the world-wide distribution of large-magnitude earthquakes, and applying the assumed relationship, the frequency distribution of earthquakes of lower magnitude for all regions may be deduced.

There is, however, a difficulty in employing this procedure. Gutenberg & Richter give earthquake magnitudes in terms of the magnitude scale M , which is based on observations of teleseismic surface waves [Richter (12)]. Studies of local geographic regions generally determine earthquake magnitudes in terms of the local magnitude M_L [Richter (12)], based on the maximum amplitude in the entire seismic wave train as observed on a Wood-Anderson seismograph. It is therefore necessary to relate M and M_L . This can be done by expressing all magnitudes in terms of a third scale, the m scale which is based on P -wave observations [Richter (12)]. This is convenient also because explosion magnitudes have been determined experimentally on this m scale; namely, $m \sim 3.9 + \frac{2}{3} \log_{10} Y$ (kilotons) for $Y \gtrsim 1$ kiloton, $m \sim 3.9 + \log_{10} Y$ (kiloton), $Y \lesssim 1$ kiloton [Geneva (17)]. The basis for relating M to m is an empirical rule, $m = 2.5 + 0.63 M$, determined for the large-magnitude earthquakes, $M > 6$. The basis for relating M_L to m is first that M_L has been observed to be approximately equal to m for earthquakes of magnitude between 5 and 6 and second that measurements of the magnitude of Blanca and Logan indicate that this equality is true also for magnitudes 4.4 to 4.8. It is assumed, therefore, that $m = M_L$ for the entire range of magnitudes below 6. Thus the Southern California-New Zealand data can be used directly to extrapolate from data on larger earthquakes.

Seismicity estimates for any particular region are made by extrapolating, with the aid of the Southern California-New Zealand data, the data from Gutenberg & Richter for the annual number of shallow continental earthquakes with magnitudes $m > 6.3$. The geographic distribution of earthquakes in a given region is determined from the large earthquake data of these authors, if it is assumed that the same geographic distribution holds for smaller earthquakes. As an example, Figure 13 shows the annual number of earthquakes occurring throughout the world. The earthquake magnitudes are expressed in terms of the equivalent explosion yield derived from the relation between m and Y .

It should be noted that there are no systematic earthquake data for magnitudes below about four, and thus any estimates for the frequency of very small earthquakes are purely extrapolations.

ON-SITE INSPECTION

A seismic event which cannot be identified by its seismic signals requires inspection at the site of the event to determine whether a nuclear explosion has occurred. To identify a nuclear explosion, a sample of radioactive debris must be obtained. In the event that radioactivity is not located, the question remains whether the activity was overlooked or the event was natural. In this

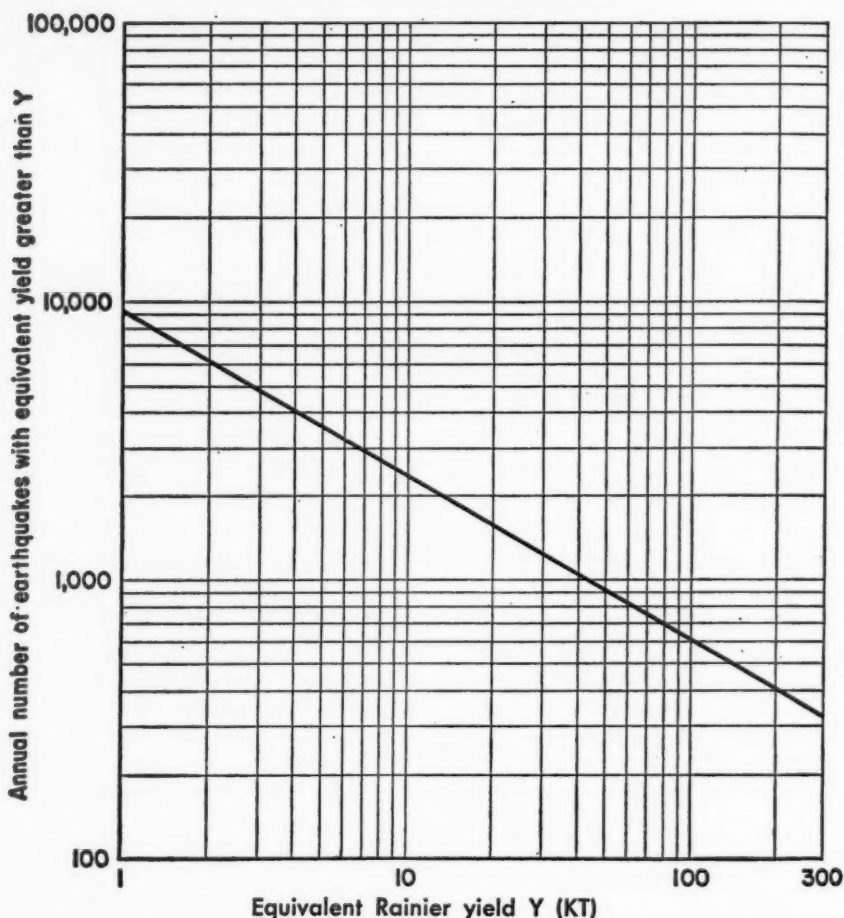


FIG. 13. Seismicity estimates. Annual number of shallow continental earthquakes with equivalent yield greater than Y occurring throughout the world.

situation indications that the event was of natural origin are required. There are, however, no known unique indications of a natural event.

To undertake an on-site inspection requires locating the source of the seismic event. The accuracy of location by distant seismic signals has only been partially evaluated. On the basis of existing travel-time data for seismic waves, a seismic event probably cannot be located more accurately than within a few hundred square kilometers. This inaccuracy is almost independent of distance since the main error in time results from the uncertainties in the propagation of the P wave through the crust, which propagation path is known to be essentially independent of distance. Existing techniques do

not permit determining source depth to better than a few tens of kilometers from the earth's surface. Since the radioactive debris from a nuclear explosion is contained within a few tens of meters of the explosion point, the problem of inspection is evidently quite difficult [Johnson, Higgins & Violet (6)].

The techniques of inspection are all rather primitive. They consist of a search for unusual human activity which might be associated with a nuclear explosion, observation of surface disturbances which might be produced by shallow explosions, and various geophysical prospecting techniques as well as detection of aftershocks for locating underground cavities.

CONCEALMENT

Perhaps the most difficult problem for detection was discovered early in 1959 when it was concluded theoretically and on the basis of the Rainier explosion that the seismic signal from an explosion in a large underground hole is several hundred times less than that from a tamped explosion—the so-called decoupling effect [Latter *et al.* (18)]. The basis for that conclusion will be described here.

For a nuclear explosion in a large spherical hole of radius a , the energy released is converted rapidly into internal energy of the gas in the hole, and a uniform pressure quickly results. The magnitude of the pressure is related to the energy release Y , the radius of the hole a , and the γ constant of the gas by

$$p = (\gamma - 1) [Y / (4/3\pi a^3)] \quad 35.$$

The medium surrounding the hole is required to remain elastic under the pressure p . Then, from Equation 11, the Fourier transform of the displacement at large distances from the hole is

$$\hat{z}_h(\omega, r) = \frac{pa^3}{4\mu_h c_h r} \frac{e^{-i(\omega/c_h)(r-a)}}{1 + i \frac{\omega}{\omega_{oh}} - \frac{\lambda_h + 2\mu_h}{4\mu_h} \left(\frac{\omega}{\omega_{oh}}\right)^2} \quad 36.$$

where the subscript h refers to the medium surrounding the hole. At the low frequencies which propagate to large distances,

$$\hat{z}_h(\omega, r) = \frac{pa^3}{4\mu_h c_h r} = \frac{3(\gamma - 1)Y}{16\pi\mu_h c_h r} \quad 37.$$

For a tamped explosion, it is possible to relate the displacement at large distances to the displacement near the explosion in the induction zone of the elastic wave—namely, from Equation 11,

$$\hat{z}_t(\omega, r) = i\omega \frac{r_0^2}{rc_t} \hat{z}_t(\omega, r_0) \quad 38.$$

where $r \gg c_t/\omega \gg r_0$ and the subscript t refers to the medium in which the tamped explosion is carried out. In the Rainier explosion the ground displacement was measured [Perret (9)] at distances of 371 ft and 451 ft from the explosion. These distances are in the elastic region of the explosion which

is estimated to extend beyond about 300 ft from the explosion point. The displacements at 371 ft and 451 ft were essentially step functions for low frequencies, so that

$$\hat{z}_i(\omega, r_0) = d_0/i\omega \quad 39.$$

Thus

$$\hat{z}_i(\omega, r) = r_0^2 d_0 / r c_t \quad 40.$$

Comparing with $\hat{z}_h(\omega, r)$,

$$\frac{\hat{z}_i(\omega, r)}{\hat{z}_h(\omega, r)} = \frac{16\pi}{3(\gamma - 1)} \frac{c_h}{c_t} \frac{\mu_h r_0^2 d_0}{Y} \quad 41.$$

From Rainier $r_0^2 d_0 \sim (2 \text{ to } 2.4) \times 10^9 \text{ cu cm}$; $Y = 7 \times 10^{10} \text{ ergs}$; $\gamma \sim 1.2$ for air. Thus

$$\frac{\hat{z}_i(\omega, r)}{\hat{z}_h(\omega, r)} = 2.4 \frac{c_h}{c_t} \mu_h \quad 42.$$

where μ_h is in kilobars. If the hole is in the same tuff medium as Rainier, $c_h = c_t$ and $\mu_h \sim 20$ kilobars; and the seismic signal from the hole is about 50 times less than from the tamped explosion. If the hole is in salt, $c_h \sim 2.5 c_t$ and $\mu_h \sim 100$ kilobars. In this case the hole signal is 600 times less. Other effects not included in the above derivation, such as the influence of local geology, may affect the magnitude of the signal reduction. How large these other effects may be is not known precisely, but they have been estimated to be less than a factor of two.

From Equation 37 it is seen that the seismic amplitude from a hole explosion is independent of hole size provided that the medium surrounding the hole remains elastic. If p_m is the maximum pressure at which the hole remains elastic, then the minimum volume of the hole is

$$V = 10^4 (Y/p_m) \text{ cu m} \quad 43.$$

where Y is in kilotons and p_m in kilobars. Roughly, p_m must be set equal to the overburden pressure on the hole in order to keep the medium from going into tension. Rock cannot sustain tension without fracturing.

The preceding theoretical considerations were verified experimentally in late 1959 by a series of chemical explosions in a salt medium—Project Cowboy [Herbst, Werth & Springer (19)]. An important result of these experiments was that even if the pressure in the hole exceeded the elastic limit of the surrounding medium there was still a reduction of the seismic signal. The magnitude of the reduction, however, decreased with increasing hole pressure. Simple models of the nonelastic region—based on plasticity, cracking, etc.—give a reasonably good account of the observations.

Additional techniques for concealment of underground nuclear explosions have been suggested [Latter *et al.* (18)]. One of these is to introduce some heat-absorbing material, such as carbon-black, into the decoupling hole. Such a heat absorber has the effect of decreasing the “ γ ” of the gas in the

hole which from Equation 41 is seen to lead to an increase in decoupling. Another concealment technique is to use an array of explosions to produce apparent rarefactive first motions. This can be achieved by suitable choice of relative magnitude, location, and timing of the explosions. And, finally, the triggering of a nuclear explosion by a larger earthquake could mask the explosion signal, leaving only the earthquake signal distinguishable.

RECENT RESEARCH

Because of the primitive state of the science of detecting underground nuclear explosions, the United States in 1959 initiated a program of research, known as Project VELA-Uniform, for the purpose of improving knowledge on all aspects of the underground detection problem. The program is still in its early stages, and only a few preliminary results have been obtained.

Instrument development for noise reduction has shown some fruitful results. Deep-well seismographs have been operated at great depths below the earth's surface where microseismic noise is less. Improved seismic instrumentation for stations throughout the world will soon be installed. These instruments will enable observation of earthquakes on a world-wide basis with common instruments. More quantitative studies of seismicity and earthquake characteristics will be possible. Some hopeful suggestions for improving accuracy of epicentral location are being explored. A great deal of study is being devoted to methods for determining source depth more accurately.

Finally, nonseismic methods of detecting underground explosions are being studied. The most interesting of these methods is the detection of the electromagnetic signal radiated by the explosion as the expanding diamagnetic plasma produced by the vaporized materials in the central explosion cavity pushes aside the earth's magnetic field. This signal, however, can be suppressed by surrounding the explosion with a simple Helmholtz coil to neutralize the earth's magnetic field.

SPACE NUCLEAR EXPLOSIONS¹¹

The energy released by a nuclear explosion in space is radiated to great distances in the form of γ rays and neutrons from nuclear reactions, X rays and visible light from the high-temperature material of the nuclear device, high-frequency radio signals from Compton-recoil electrons produced by γ -ray scattering in the device, and kinetic energy of the exploding materials [Geneva (21)]. These direct signals may produce other radiations by interaction with interplanetary matter, with the earth's atmosphere, or with the earth's magnetic field. X rays accelerate interplanetary electrons which radiate low-frequency radio waves. X rays also photo-eject electrons from

¹¹ The feasibility of carrying out nuclear explosions in space has been demonstrated by the five high-altitude explosions conducted by the United States in 1958 (20).

air atoms and these electrons excite nitrogen molecules producing visible fluorescent light. X rays and γ rays ionize the atmosphere at high altitudes and the resultant ionization is observable by effects on radio-wave propagation. Explosions occurring in the earth's magnetic field produce low-frequency magnetic disturbances by distorting the magnetic field. Debris from the device is at least partially contained by the magnetic field, and some of the β -decay electrons from fission products are trapped by the field. β -decay electrons which are not trapped spiral into the atmosphere along the earth's magnetic field producing limited regions of intense ionization at magnetic conjugate points in the upper atmosphere. Beta-decay electrons from neutrons similarly ionize the upper atmosphere, but with low intensity. Explosions in the ionosphere produce hydrodynamic disturbances by X-ray heating and kinetic energy of the exploding device, which interfere with radio-wave propagation or reflect radar waves.

All of the above signals are known to be generated by nuclear explosions in space. However, not all these signals are useful for detection. Natural background noise is the primary factor limiting the detectability of explosion signals. For some types of explosion signals the background noise is so intense that the explosion signals are completely obscured. A second factor limiting the usefulness of certain explosion signals is the lack of sufficient theoretical and experimental information to allow prediction of the form and intensity of the explosion signals. This limitation can probably be removed by continued research.

These limitations, however, presently restrict useful signals to direct X rays, γ rays, neutrons and visible light, and indirect air fluorescence, radio-wave absorption by X-ray and γ -ray ionization of the upper atmosphere, and magnetic trapping of β -decay electrons from fission products. Ionospheric disturbances detectable by radar appear to be more useful as confirmatory signals than as primary detection signals.

Direct visible light, X-ray induced fluorescence, ionization of the atmosphere, and ionospheric disturbances are detectable by ground-based instrumentation. X rays, γ rays, and neutrons are absorbed by the atmosphere and consequently require satellite-based instruments for detection. Detection instruments must be designed to minimize false signals arising from natural noise backgrounds. Complete elimination of false signals is not possible since fluctuations in noise backgrounds will always have some probability of producing false signals. In order to decrease this possibility, stronger explosion signals are required and detection ranges are reduced.

Since false alarms cannot be completely eliminated, positive identification of signals from explosions in space is not possible. By reducing sufficiently the probability of false signals, say, to one per hundred years or so, detection of a signal can raise a strong presumption that a nuclear explosion has occurred. If, however, natural events also produce signals similar to space explosions, like earthquakes in the underground case, identification of a space nuclear explosion will be entirely unfeasible.

A further difficulty with detecting nuclear explosions in space is the possibility of suppressing explosion signals. Signals from explosions behind the moon are completely shielded from earth-based instrumentation. Solar satellites are required for detection. Explosions in the direction of the sun are detected with reduced capability because of intense solar backgrounds. By inserting a thin metallic sheet between the explosion and detectors, the X rays, which are believed to have the greatest detectable range, can be suppressed. A shield, weighing 100 kg or so, can reduce the X-ray intensity in a prescribed direction from megaton explosions by a factor of 100 or more and reduce the temperature of the X rays to less than 100 ev. If solar satellites are used, shields must be heavier and more complicated.

SATELLITE-BASED DETECTION TECHNIQUES

Since most of the energy of a nuclear explosion is radiated in the form of X rays, detection of X rays appears to be the most promising method for detecting nuclear explosions at very great distances. Consequently, in the following sections the X-ray method will be described in the greatest detail, while other methods of detecting space explosions will be treated only briefly.

Detection of X rays.—At a distance R km from a nuclear explosion, the X-ray energy flux is

$$F = Y_x[(3 \times 10^9)/R^2] \text{ ergs/sq cm} \quad 44.$$

where Y_x is the total X-ray yield (kilotons) of an explosion of total yield Y . The X-ray yield Y_x , the time interval over which the X rays are emitted, and the energy spectrum of the X rays all depend sensitively upon the design of the nuclear device. Nominally, $Y_x \sim \frac{1}{2} Y$ for $Y > 10$ KT, the emission time is less than one microsecond; and X-ray energies are distributed as a Planck distribution corresponding to the temperature of the heated materials of the device which, for unshielded explosions,¹² are in the range from one to a few kev. X rays from shielded explosions may have energies in the range from 10 to 100 ev¹¹.

X rays may be detected by scintillation counters or by photomultipliers. Thin foils covering the detectors may be used to screen out background noise, but this results in some loss of detection sensitivity. Some of the charged-particle backgrounds may be screened out by electric grids placed around the detectors. The effectiveness of this method of screening backgrounds depends sensitively on the energy spectrum of background charged particles, which at present is quite uncertain.

To estimate X-ray detectability, backgrounds which might be confused with explosion signals must be determined. The most troublesome known backgrounds are: cosmic ray showers induced in the satellite carrying the detectors by primary cosmic rays; solar radiation such as the visible light, the high-temperature coronal radiation, solar flares, and the solar wind;

¹² See the discussion of concealment of space nuclear explosions.

auroral radiations; solar and stellar radiation scattered by interplanetary atoms; and micrometeorites.

The omnidirectional flux of primary cosmic rays is about 1 proton/sq cm sec above 1 Bev (with a relatively smaller flux of heavier primaries). The flux of primary cosmic ray protons having an energy greater than E (measured in Bev) is

$$F(E) \sim 1/E^{1.8} \text{ protons/sq cm sec, for } E > 1 \quad 45.$$

For a satellite of 1 sq m area, about 10^4 primary protons (with $E > 1$) per second are incident on it and can cause nuclear interactions in the materials of the satellite. At proton energies of 25 Bev, about 6π mesons are produced per nuclear interaction¹³ while, at much higher energies, 10 mesons are typically produced [Edwards *et al.* (22)]. On the average, one-third of these mesons are π^0 mesons, each of which decays into two energetic γ rays, which in turn generate cascade showers in the satellite.

Within a few radiation lengths, the energy from a shower-producing γ ray is shared by a relatively large number of electrons, positrons, and γ rays, each having an energy in the neighborhood of the critical energy of the shower. Since the satellite thickness is likely to be about two radiation lengths and since a significant fraction of showers is well developed within about two radiation lengths, a significant fraction of the 10^4 showers per sec that are produced in a satellite may contain hundreds to thousands of electrons, positrons, and γ rays of energies ranging from a few Mev to a few tens of Mev.

Except for very near explosions, the energy in a single shower will greatly exceed the energy in the explosion signal. Cosmic ray showers can, therefore, cause serious difficulty for the detection of nuclear explosions. This difficulty can possibly be overcome by employing detectors in multiple coincidence and anticoincidence within each satellite and between satellites.

The exact rate at which cosmic ray showers produce false signals similar to nuclear explosions depends sensitively on the distribution of matter and of detectors in the satellite. Approximately, however, with n detectors in coincidence, the shower counting rate is

$$r = Ip^n \quad 46.$$

where I is the rate of shower production and p is the probability that a single counter will register a count. As an example, in a satellite containing n counters of area $\sigma = 100$ sq cm separated by a distance d and in which 10^3 showers with $N_p = 10^3$ isotropic secondaries¹⁴ are produced each second, the coincidence counting rate is about

$$r \sim 10^2 \left(\frac{N_p \sigma \epsilon}{4\pi d^2} \right)^n \sim 10^2 \left(\frac{10^4 \epsilon}{d^2} \right)^n \text{ per sec} \quad 47.$$

¹³ We are indebted to Professor V. Fitch for this comment.

¹⁴ The assumption of isotropy may be too extreme. On the other hand, large showers may have 10^4 to 10^6 secondaries of which those at the critical energy tend to be isotropic.

where it is assumed that a single particle is counted with an efficiency ϵ and one particle can trigger a counter. It is clear that if r is to be kept less than, say, one count per hundred years, the separation d should be of the order of meters and n should be in the range of 10 to 20. If more than one particle per counter is required for a count, the separation distance and the number of counters can be decreased. However, this leads to a decrease in detection distance, since higher incidence fluxes are required to provide a coincidence. Alternatively, additional counters in anticoincidence may assist in suppressing the cosmic ray counting rate. Anticoincidence has the difficulty that close explosions could be discriminated against.

An important consequence of Equation 47 is that the counting rate is proportional to the rate at which showers form, times the number of particles per shower to the n th power. This means that the rare showers with very large numbers of particles determine the counting rate; thus reliable quantitative analysis of the shower problem is difficult. Despite this difficulty, it may reasonably be concluded that cosmic ray showers do not make X-ray detection impossible. However, elimination of this background will probably lead to a complicated detector system and consequently to a decreased detection range and system reliability.

Radiation from the sun provides an extremely intense background which must be suppressed if X-ray detection of nuclear explosions is to be possible at great distances. The total solar flux at the earth's orbit is 1.3×10^6 ergs/sq cm sec, and the portion in the high-energy range above a few tens of electron volts is $1.5 \times 10^9 d\epsilon/\epsilon$ photons/sq cm sec, where ϵ is the photon energy [Friedman, Chubb & Kreplin (23)]. During solar flares, the flux of solar X rays in the energy range from 100 ev to kv may be of the order of 1 erg/sq cm sec [Chubb, Friedman & Kreplin (24)]. For these intense backgrounds, the counting rate is

$$r = nIP_p^{n-1}p_{p-1} \quad 48.$$

where $p_{p-1} = e^{-q}q^{p-1}/(p-1)!$ is the probability that in the resolving time τ of the coincidence a single counter will register $p-1$ counts; I is the rate at which a single counter registers a count; and

$$P_p = \sum_{l=p}^{\infty} e^{-q}q^l/l!$$

is the probability that a single counter registers p counts or greater in the time τ . Approximately

$$r \sim nI \frac{e^{-(p-q)/2q}}{\sqrt{2\pi q}} \left(\frac{q}{p-q} \frac{e^{-(p-q)/2q}}{\sqrt{2\pi q}} \right)^{n-1} \quad 49.$$

If the false alarm rate from the total solar flux is not to exceed one per hundred years, then evaluation of Equation 49 for a coincidence-resolving time of one microsecond and a counter area of 10^2 sq cm leads to the requirement that the explosion signal must exceed about 10^{-6} ergs/sq cm, which corresponds to a maximum detection range of about $10^7 \sqrt{Y_s}$ km.

There are two possible methods for suppressing the solar radiation. Thin

foils can be placed over the counters, or a screen oriented toward the sun can shade the detectors. This screen has the difficulty that complicated equipment is required for orienting, and explosions in the direction of the sun cannot be seen. Covering the counters with foils has the disadvantage that shielding of explosions becomes simpler and more effective since only high-energy X rays can penetrate the foils.

Moreover, if thin foils are placed over the counters to suppress solar radiation, they may be punctured by micrometeorites. The flux of micrometeorites of mass greater than m (grams) has been estimated to be [Lapaz & Whipple (25)]

$$F_{>m} = 10^{-12}/m \text{ particles/sq m sec} \quad 50.$$

This flux is determined for large particles by visual and radar observations. It is presumably cut off for $m < 10^{-9}$ g because of the effect of solar radiation on the orbits of very light particles.

The average velocity of micrometeorites is 30 to 40 km/sec. On striking a solid surface, such a fast particle produces a crater. A rough estimate [Whipple (25)] of the crater size is obtained by equating the kinetic energy W of the micrometeorite to the mass of material vaporized from the crater times the heat of vaporization L per unit mass. Assuming a 60° angle for the crater, the crater depth D is approximately

$$D = W^{1/3}(9/\pi\rho L)^{1/3} \quad 51.$$

where ρ is the density of the material which is struck by the micrometeorite.¹⁵ If D is greater than the thickness of the surface which is hit, penetration will occur. For the flux given in Equation 50, foils sufficiently thick to stop photons with energies of a few tens of electron volts would last on the order of a month. Thicker foils, however, seriously degrade detection efficiency for shielded explosions.

Auroral streams have been observed to contain large fluxes of high-energy particles. The flux of electrons with energies greater than 50 kev in auroral streams is approximately [Brown (26)]

$$F_{\text{electron}} \sim 10^6 - 10^8 \text{ electrons/sq cm sec} \quad 52.$$

The flux of protons with energies greater than 30 Mev has been observed to be of the order of

$$F_{\text{proton}} \sim 10^3 \text{ protons/sq cm sec} \quad 53.$$

It seems likely that the performance of X-ray detectors will be seriously degraded while in an auroral stream. However, it is not yet known to what extent auroral particles are accelerated at the sun, in the space between the sun and earth, or in the geomagnetic field. If auroral streams are confined to the space near the earth, it would appear desirable to place detection satellites in orbits above the auroral particles. If auroral streams originate at the sun or in space, however, it is not possible to do this. In fact, it is not even

¹⁵ More accurate calculations of D indicate that Equation 51 is a significant underestimate of the penetration depth.

possible to shade the satellite from auroral particles by a sun screen since the solar magnetic field will presumably cause their orbits to be unpredictable.

The solar wind may also adversely affect detection. Although the magnitude (and even the existence) of the solar wind is uncertain, the solar wind [Bierman (27)] is believed to consist of a steady stream of protons and electrons emitted by the sun. The proton flux is estimated to be

$$F_{\text{solar wind}} \sim 10^8 - 10^9 \text{ protons/sq cm sec} \quad 54.$$

where the protons have energies from 1 to 10 kev. Comparable fluxes of electrons having energies below 100 ev are expected. These solar-wind particles may easily be stopped by thin foils placed over counters. For open counters it may be possible that electric or magnetic fields may be used to screen out the solar wind particles.

The greatest ranges for detection are obtained by assuming that the X-ray detectors are not covered, but are protected from solar radiation by a sun screen and from the solar wind by electromagnetic means. In this case when the detectors are not in an auroral stream, the principal source of background is probably starlight and sunlight scattered by free atoms in interplanetary space. The omnidirectional flux from starlight corresponds to a few times 10^8 photons/sq cm sec in the visible range. The solar Lyman-radiation scattered by interplanetary hydrogen produces an omnidirectional flux of about 2×10^9 photons/sq cm sec [Friedman, Chubb & Kreplin (23)]. The 40-ev radiation scattered by helium has a comparable flux [Van Allen & Frank (28)]. The total flux of photons on a counter with area $\sigma = 100$ sq cm is then expected to be of the order of

$$f \sim 10^{12} \text{ photons/sec} \quad 55.$$

If the resolving time of the counters is $\tau = 1 \mu\text{sec}$ (equal to the duration of the explosion signal), the mean counting rate of background is

$$q \equiv f\tau \sim 10^6 \quad 56.$$

This should be compared with the corresponding X-ray signal from a nuclear explosion. According to Equation 44, for a yield of Y_x kilotons of 1 kev X rays,

$$\sigma F \sim 2 \times Y_x (10^{10}/R^2) \text{ photons} \quad 57.$$

If the average flux, Equation 56, can be biased out, and if the bias is set at about four standard deviations, the minimum detectable signal is

$$F\sigma \sim 4\sqrt{q} = 4 \times 10^3 = 2 \times Y_x (10^{10}/R^2) \quad 58.$$

and the maximum detection range for an unshielded explosion is

$$R \sim 10^3 \sqrt{Y_x} \text{ km} \quad 59.$$

In this case the rate of false signals is about one per hundred years.

In summary, the maximum X-ray detection range is determined by ran-

dom fluctuations in the continuous background of scattered sunlight and starlight. To achieve this maximum range, elaborate engineering is required to suppress the background arising from cosmic ray showers, auroral particles, and solar radiations. Further complications may of course develop if new sources of background (or of fluctuations) are found.

Since X rays from an explosion can reach the top of the atmosphere only if the explosion takes place above altitudes of 80 to 100 km, X-ray detectors cannot detect explosions taking place below this altitude.

Detection of prompt γ rays.—Prompt γ rays are produced in times of about 10^{-7} sec by fission reactions and by inelastic scattering of neutrons within the device. The yield and spectrum of the γ rays depend upon device design. Nominally, the total γ -ray energy is about 3×10^{-4} of the total explosion energy, and the mean energy of a single γ ray is about 1 Mev. At a distance of R km from an explosion, the total γ -ray flux is

$$F = Y_F(10^{10}/R^2) \gamma \text{ rays/sq cm} \quad 60.$$

where Y_F is the fission yield of the explosion in kilotons.

Because γ rays from a nuclear explosion are quite penetrating, γ -ray detectors (possibly scintillation counters) may be covered with thick foils to stop soft radiation. The principal source of background then is cosmic ray showers generated within the satellite. To suppress this background it is again necessary to use multiple-coincidence counting and to separate the counters. The precise number of counters in coincidence and their separation distance cannot be determined without specification of the detailed distribution of matter in the satellite. Under similar assumptions to those made in the discussion of X-ray detection, it appears likely that five to ten counters in coincidence separated a few meters (having a resolving time of a few times 10^{-8} sec) will reduce the false signals from showers to about one per hundred years.

The probability P of detecting a pulse of γ rays is

$$P = (1 - e^{-m\epsilon})^n \quad 61.$$

where n is the number of counters in coincidence, ϵ the counting efficiency of a counter, and m the mean number of incident γ rays per counter. For $P \sim 0.9$, $\epsilon \sim \frac{1}{3}$, and $n \sim 5$ to 10, it is found that $m \sim 10$ to 15. A reasonable counter area for a satellite is about 10^2 sq cm. In this case the detection range is

$$R \sim 3 \times 10^5 \sqrt{Y_F} \text{ km} \quad 62.$$

Detection of delayed γ rays.—Delayed γ rays are produced by the radioactive decay of fission products. According to the well-known fission-decay law, the γ -ray intensity is approximately constant for the first second after the explosion and then decreases as $t^{-1.2}$. Only the first second is therefore important, and during this time the total flux of delayed γ rays from an explosion is about 100 times as great as that of prompt γ rays. However, the rate of emission of delayed γ rays is less by a factor of 10^5 than that of prompt γ rays. This small rate makes background effects more serious for delayed γ rays.

The principal known backgrounds which interfere with detection of delayed γ rays arise from the cosmic ray shower albedo from the earth's atmosphere and from showers in the satellite itself. Since the shower background is intense, being perhaps 10^4 to 10^5 per sec in the satellite, it is doubtful that this method has a great detection range. In fact, if all these showers were counted by the delayed γ -ray detector, the range of detection would be less than about $10^5 \sqrt{Y_F}$ km for a counter of 10^2 to 10^3 sq cm, even if only the fluctuations in the background rate were detected.

Detection of neutrons.—Neutrons are produced both by fission and by thermonuclear reactions. Nominally, of the order of one neutron per fission escapes the device. The neutron flux at a distance of R km from an explosion of Y kilotons is then

$$F \sim Y(10^{12}/R^2) \text{ neutrons/sq cm} \quad 63.$$

Because of the wide spectrum of neutron velocities emitted by the device, the neutrons arrive at distant counters over a time interval of the order of seconds to minutes.

Neutrons are detected by uranium 235 or boron trifluoride counters placed within a moderating medium. Sources of background are cosmic ray showers and the cosmic ray albedo from the earth's atmosphere. For the same reasons discussed in the case of delayed γ -ray detection, the intense shower background produced within the satellite itself makes it unlikely that neutrons can be detected beyond $10^5 \sqrt{Y}$ km and more likely that neutron detection is possible only at considerably smaller ranges.

General remarks.—Since the necessary experimental observations are lacking, little reliance can be placed on detection of neutrons or delayed γ rays. The estimates of detectability of X rays and prompt γ rays are probably reasonably reliable, but require detailed experimental and engineering study to determine feasibility.

It is desirable that the satellites for detecting X rays, γ rays, and neutrons not be placed in the Van Allen radiation belts where radiation is trapped by the geomagnetic field. To avoid false signals from the intense radiation in these belts, stronger explosion signals would be required, and detection ranges would consequently be reduced.

In the inner belt the electron flux is of the order of 10^9 electrons/sq cm sec with energy greater than 20 kev and 10^7 electrons/sq cm sec with energy greater than 600 kev [Van Allen & Frank (28)]. The proton flux in the inner belt, corresponding to an energy greater than 40 Mev, is 2×10^4 protons/sq cm sec [Van Allen & Frank (28), Freden & White (29)]. The energy spectrum of these protons is

$$F(e) \sim (1.55 \times 10^2)/E^{0.72} \text{ protons/Mev sq cm sec} \quad 64.$$

where E is the proton energy measured in Mev. The outer radiation belt consists of soft electrons and is subject to wide temporal variations. The particle flux in this belt falls to that of the cosmic ray background at altitudes above about 60,000 km and is small in the auroral zones (corresponding to latitudes greater than 60° north or south). The inner belt extends from about 700 km

to about 6000 km above the surface of the earth and is confined to a region above the equator extending to $\pm 30^\circ$ to 40° latitude.

If satellites are placed at an altitude of 700 km, from 50 to 70 satellites are required for complete earth surveillance. (If, for example, 10 satellites were used, the system could survey reliably only the volume of space above 2000 km altitude.) At altitudes above 50,000 km, only 5 or 6 satellites are required. However, the cost of putting satellites into such distant orbits is greater.

A suitably instrumented satellite placed in the radiation belt can detect the fission-decay electrons from the explosion which are trapped by the earth's magnetic field. This satellite will not be able to detect explosions occurring in the auroral zone since electron trapping does not occur in this region.

GROUND-BASED DETECTION TECHNIQUES

There are several possible ground-based techniques for detecting space explosions. Although the maximum range for ground-based detection is less than that for satellite-based detection, the lower cost and greater reliability in operation of ground-based detectors make them quite important.

Detection of visible light.—The details of the visible light emission from space nuclear explosions are not completely known [Latter (30)]. They depend upon device design, upon interactions with the atmosphere and with the ambient magnetic fields, and upon poorly understood physical processes and physical properties of materials. Consideration will be given only to that portion of the visible light emitted by the explosion debris during the first 10 or 20 μ sec after the explosion—before the debris can interact appreciably with the atmosphere or with ambient magnetic fields. During these times the principal emission mechanisms are reasonably understood. With this limitation to the early explosion phase, it is simple to estimate the fraction of the total explosion yield emitted as visible light and the effective time for this emission; these are the only parameters that enter into the detectability.

The detection of the visible light from the nuclear explosion must be made in the presence of natural sources of light. The largest of these backgrounds are:

Sun:	2×10^{10} ergs/sq cm sec ster.
Moon:	2×10^4 ergs/sq cm sec ster.
Skylight (day):	10^4 ergs/sq cm sec ster.
Stars:	Total starlight is equivalent to about 1100 magnitude —one ¹⁶ stars. The brightest stars are magnitude —2 to —4.

¹⁶ Stellar magnitude is related to the intensity I (ergs/sq cm sec) of visible light from a star by

$$\text{Magnitude} = -2.5 \log_{10}[I/(3 \times 10^{-6})].$$

The capability for detection against the noise backgrounds depends upon the specific design of the detection instrumentation. To specify this instrumentation, it should be noted that the signal from the explosion is essentially a point source, while the largest backgrounds (except for starlight) are extended sources. By well-known principles it is possible by means of a lens system to increase the amount of light gathered from a point source without increasing the brightness of the extended source backgrounds. This effect implies that the amount of light received from the explosion and focused on a given area can be increased arbitrarily while the amount of light on this same area received from the background is maintained constant. The only limitations on the increase in strength of the point source image are the size of the lens system and its inherent optical aberrations. The simplest system for achieving this effect is a single lens with a detector at its focus.

To permit observation of a large portion of the sky from a single ground station with a minimum number of lens systems, each lens system should have as large a field of view as possible. However, a large field of view requires a large detector area. This leads to a greater amount of background light being detected without increasing the light gathered from the point source. This disadvantage can be circumvented by dividing the detector into a number of cells each of which acts as an independent detector of reduced field of view while the total ensemble has the desired field of view. To work effectively, such a scheme must minimize spaces between the individual detectors to avoid dead spots. One possibility is to replace the simple detector array by a diverging lens backed up at a distance by an array of square focusing lenses which focus the light on the detector array. Another is to use a separate lens for each individual detector. In these ways, the detectors may have dead spaces between them without degrading the signal.

The individual detectors require special design. These will be assumed to be photocells or photomultipliers which have a conversion efficiency ϵ for converting photons to photoelectrons. The associated counting circuits will be assumed to have a memory time τ . To insure no loss of signal strength while minimizing the noise background, τ should be adjusted to equal the maximum explosion emission times which are expected.

The parameters which specify the detector system are the area σ and radius $a = \sqrt{\sigma/\pi}$ of the focusing lens, the focal length l of the lens, and the area σ_d and radius $a_d = \sqrt{\sigma_d/\pi}$ of the detector ensemble, the number N of individual detectors, and the conversion efficiency ϵ and memory time τ of the detectors.

The number of photoelectrons generated in the detector system by an explosion of yield Y kilotons at a distance R km is

$$F = 6.6 \times 10^{19} \epsilon \sigma (fY/R^2) \quad 65.$$

where f is the fraction of the yield radiated as visible light. The mean energy of the visible light from the explosion is taken to be 3 ev. This average results from noting that only photons of energy less than 4 ev penetrate the

atmosphere and that the visible light emitted by the explosion is in the "tail" of the Planck spectrum.

The number of photoelectrons generated by extended-source backgrounds in one resolving time τ of the detector is

$$B = 3 \times 10^{11} \tau F_b \frac{\sigma_d}{N} \left(\frac{a}{l} \right)^2 \epsilon \quad 66.$$

where the mean energy of background photons is 2 ev and F_b is the background intensity in ergs per sq cm sec ster. In the case of starlight,

$$B = 3 \times 10^{11} \tau F_b \epsilon \sigma \quad 67.$$

where F_b is the intensity in ergs per sq cm sec reaching the detector. The probability that the background generates before a time t a level of n_0 photoelectrons during one memory time τ of the detectors is

$$P(t) = 1 - e^{-qt} \quad 68.$$

where

$$q \sim \frac{B}{\tau} \frac{1}{\sqrt{2\pi B}} e^{-(n_0 - B)^2/2B} \quad 69.$$

If it is required that

$$P(3 \times 10^9 \text{ sec}) = 1 - (1/e) \quad 70.$$

then

$$n_0 \lesssim B + 10\sqrt{B} \quad 71.$$

With this condition the detection distance is given by

$$F = 10\sqrt{B} \quad 72.$$

or

$$R = 2.51 \times 10^6 (\epsilon \sigma f Y / \sqrt{B})^{1/2} \text{ km} \quad 73.$$

To estimate the detection distance quantitatively the parameters of the detection system must be specified. A set of reasonable values which leads to interesting detection ranges is: $\sigma = 10^4$ sq cm, $\sigma_d = 1.5 \times 10^4$ sq cm, $l = 120$ cm, $\epsilon = 0.1$, and $N = 100$. These values correspond to a field of view of 30° . This field avoids the problems of atmospheric attenuation when the lenses are pointed vertically.

Values of f and τ have been estimated to be $fY \sim 10^{-6} - 10^{-5}$ kilotons for unshielded low-yield explosions, $fY \sim 10^{-5} - 10^{-4}$ kilotons for unshielded high-yield explosions, and $\tau \lesssim 2 \times 10^{-5}$ sec.

Using $fY = 10^{-6}$ kilotons and $\tau = 2 \times 10^{-5}$, one finds that for low-yield explosions the detection range exceeds 10^5 km during the day or night. Against the direct solar background the detection range is less than 10^4 km. For high-yield explosions, these ranges may be as much as a factor of 10 greater.

Each lens system observes about $4\pi/15$ steradians. To observe the entire sky within the detection range and beyond 50 km requires approximately 250,000 lens systems—such a number is completely unfeasible. However, using 60 such lens systems, all points of the sky beyond about 6400 km will be seen.

Several points should be considered. First, it is desirable to be able to locate the source of the signals. This requires two or more widely spaced detectors with high optical resolving power or three or more with high temporal resolutions observing the same point in the sky. The previously described detectors have insufficient optical resolving power to locate a signal within 10^6 km. To obtain adequate optical resolving power while maintaining the same value of σ_d , it would be necessary to increase N to about 10^4 . To achieve threefold observation of the sky requires an excessive number of stations. Secondly, increasing N with the same σ_d does not increase the detection ranges significantly. For example, increasing N by a factor of 16 increases ranges by a factor of only 2. Clearly, this leads to considerable complication and increased cost of the system. Another point—in order to extend the coverage of the system below 6400 km, the number of lens systems needed increases rapidly. Specifically, complete coverage above altitude h km requires $15[(6400+h)/h]^2$ uniformly spaced lens systems.

The short range in those detector cells observing the sunlight can be improved somewhat by using supplementary moving lens systems which observe continuously only in the direction of the sun. By excluding the sun from the central region of the remaining systems and by suitable placement of the lenses, it will be possible to avoid "looking" at the sun and thereby reducing the detection range. Finally, it should be recognized that this means of detection is not useful at all in the presence of cloud cover. On the other hand, shielding of the visible light appears difficult.

Detection of air fluorescence.—The X rays from a space nuclear explosion are stopped in the earth's atmosphere above altitudes of about 70 km. Photoelectrons ejected by the X rays produce molecular excitations of nitrogen. The excitation decays by emission of visible radiation and provides a possible means for detecting explosions [(1), Westervelt (31)].

The X-ray photoelectrons produce a particularly strong excitation in the P branch of the (0, 0) band in the N_2^+ (1N) system which emits a line of wavelength 3914 Å. Approximately 5×10^{-3} of the X-ray energy deposited in the atmosphere is reradiated in this particular line over a time interval of about one microsecond, corresponding to the slowing-down time of the photoelectrons. Thus the fluorescent flux at a distance R km from an explosion radiating Y_x kilotons of X-ray energy is

$$F \sim 10^6(Y_x/R^2) \text{ ergs/sq cm} \quad 74.$$

This radiation may be detected by photomultipliers mounted behind a well-collimated optical system. The range of detection depends upon the specific design of the detection instrumentation and the magnitude of the back-

ground noise. The background noise in the neighborhood of the 3914-A line is about 0.25 to 0.5 μ watts/A sq cm ster. Assuming a reasonably feasible detector system and assuming that the explosion signals must be at least 10 times the statistical fluctuations in the average background, the detection range is approximately $10^5 \sqrt{Y_z}$ km for an unshielded explosion.

Atmospheric ionization.—Atmospheric ionization by nuclear explosions results from deposition of X-ray and γ -ray energy [Latter & LeVier (32); (1)]. The energy is deposited by X-ray photoejection of electrons from air atoms and by Compton scattering of electrons by γ rays. The secondary electrons transfer energy to air atoms by slowing down, thereby inducing ionization. One ion pair is produced for each 33 ev of energy transferred to the air.

In the case of X rays and prompt γ rays, the energy is essentially deposited instantaneously. The slowing-down time of the secondary electrons is about one microsecond and therefore ionization is produced essentially instantaneously. The rate of disappearance of the ionization depends sensitively upon its altitude and the chemistry of the air. X rays in the kilovolt-energy range deposit energy at altitudes above about 70 or 80 km where ionization persists for seconds to minutes. Gamma rays in the Mev range deposit energy at altitudes of 20 to 30 km or so and their ionization vanishes in the order of milliseconds. Delayed γ rays deposit energy slowly with time at the same altitudes as prompt γ rays. The intensity and duration of the delayed γ -ray ionization are therefore determined by competition between the mechanisms of production and of decay. The intensity is comparable to that produced by prompt γ rays but persists for about one to a few seconds.

Since X rays constitute over half the energy of nuclear explosions, X-ray induced ionization is more intense and more persistent than that arising from γ rays and is, therefore, the important ionization for detection.

To determine quantitatively the intensity of X-ray ionization, some simplifying but accurate assumptions can be made. The air density will be assumed to vary with altitude exponentially,

$$\rho(z) = \rho_0 e^{-z/H} \quad 75.$$

where H is the scale height of the atmosphere over the region of induced ionization. Multiple scattering of the X rays will be neglected. The X rays will be assumed to be emitted as a Planck distribution with temperature T corresponding to the average temperature of the exploding device. Under these assumptions, the X-ray-induced ionization at altitude z from a nuclear explosion of X-ray yield Y_z kilotons at distance R km from the deposition point is

$$n(z) = 6.7 \times 10^{18} \frac{Y_z}{R^2} \frac{15}{\pi^4} \rho_0 e^{-z/H} \int_0^\infty \frac{du u^3 K(u)}{e^u - 1} \exp \left[-\frac{\rho_0 K(u) H e^{-z/H}}{\Psi(\theta) u^3} \right] \quad 76.$$

The expression $K(u)$ denotes the mass absorption coefficient for air and is approximately

$$\begin{aligned}
 K(u) &= \frac{1.8 \times 10^3}{T^3} \frac{1}{u^3} \text{ sq cm/g}, & u < \frac{0.4}{T}, \\
 &= \frac{3.4 \times 10^3}{T^3} \frac{1}{u^3} \text{ sq cm/g}, & u > \frac{0.4}{T}
 \end{aligned} \quad 77.$$

where $u = h\nu/kT$ and T is in kilovolts. The quantity $\Psi(\theta)$ is a geometrical factor given by

$$\Psi(\theta) = \cos \theta \left[\frac{2H \tan^2 \theta}{\pi(R_E + z)} \right]^{1/2} e^{-(R_E + z)/(2H \tan \theta)} \left\{ \frac{2}{\sqrt{\pi}} \int_{\sqrt{(R_E + z)/(2H \tan \theta)}}^{\infty} e^{-t^2} dt \right\}^{-1} \quad 78.$$

where θ is the angle between the radius vector from the earth's center to the deposition point and the vector from the deposition point to the explosion point, and R_E is the radius of the earth. For $\theta = 90^\circ$,

$$\Psi(90^\circ) = \sqrt{\frac{2H}{\pi(R_E + z)}} \quad 79.$$

For temperatures greater than about 0.5 kev, saddle-point evaluation of Equation 76 gives

$$\begin{aligned}
 n(z) &= 6.7 \times 10^{18} \frac{Y_x}{R^2} \frac{15}{\pi^4} \sqrt{\frac{\pi}{2}} \frac{\Psi(\theta)}{3H} \left(\frac{3K_0 \rho_0 H}{\Psi(\theta)} e^{-z/H} \right)^{9/8} \\
 &\cdot \exp \left[-\frac{4}{3} \left(\frac{3K_0 \rho_0 H}{\Psi(\theta)} e^{-z/H} \right)^{1/4} \right]
 \end{aligned} \quad 80.$$

where $K_0 = u^3 K(u)$ for $u > 0.4/T$.

Ionization is most simply detected by effects on the propagation of radio-frequency electromagnetic waves. A particularly simple method of detecting one such effect is by observing the amplitude of radiofrequency noise from galactic sources. Any sudden depression of the noise amplitude can be interpreted as absorption by atmospheric ionization. The magnitude of this absorption for a wave propagating vertically through the atmosphere is

$$A = 0.46 \int \frac{\nu(z)n(z)}{\omega^2 + \nu^2(z)} dz \text{ decibels} \quad 81.$$

where $\nu(z)$ is the collision frequency of electrons with air atoms and ω is the angular frequency of the observed radio signals.

Substituting $n(z)$ from Equation 76 into Equation 81 and noting that for frequencies above about 10 Mc/sec which penetrate the ionosphere $\nu(z) \ll \omega$, the absorption produced by X rays of temperature greater than about 0.5 kev is found to be

$$A \sim 2.1 \times 10^{25} \frac{\Psi^2(\theta) T^3}{\omega^2} \frac{Y_x}{R^2} \text{ decibels} \quad 82.$$

where the electron collision frequency is taken equal to $1.5 \times 10^{11} \text{ sec}^{-1}$ at sea level.

For a frequency of about 30 Mc/sec, a one-decibel absorption of galactic noise appears easily detectable. At this absorption level the ionization from an explosion radiating one kiloton of X-ray energy in the temperature range from 0.5 to 2 kev at distances of 10^4 to 10^5 km is detectable by a ground-based vertically directed receiver. Since the magnitude of the absorption varies inversely as the square of the explosion distance, an absorption sensitivity of 0.01 decibels at 30 Mc/sec would be required to increase the detection range by a factor of 10. Such an improved sensitivity appears difficult to achieve.

For explosions at altitudes below a few hundred kilometers, X rays are absorbed by the atmosphere before they can propagate to regions of the atmosphere far from the point directly below the explosion. Consequently, the area of the atmosphere over which ionization occurs decreases and the number of detection stations required to observe the ionization increases.

Intense ionization of the atmosphere is known to occur from natural sources. Occurrence of ionization therefore does not prove that a nuclear explosion has taken place. There is, however, a possible distinction between explosion-induced ionization and natural ionization, namely, the onset time of the ionization. For explosions the onset time is less than about one microsecond. Observations just recently begun suggest that the onset time of natural ionization is very much greater than one microsecond, but these results are still preliminary.

Ionospheric disturbances.—Backscatter radars have detected nuclear explosions above a few tens of kilometers to a few hundred kilometers. The specific explosion effects detectable by this technique are uncertain. However, there is little doubt that explosions near the ionosphere produce, by hydrodynamic processes, by interaction with the earth's magnetic field, and by ionizing radiations, major disturbances in the neighborhood of the explosion and in the ionosphere. These disturbances produce strong variations in dielectric constant of the atmosphere, and such variations are known to be detectable by backscatter radar.

The backscatter radar technique is probably limited to detecting only those explosions carried out below a few hundred to perhaps a few thousand kilometers. It has the advantage that this entire region of space can be observed with only a few radars. The principal disadvantage of this technique is its sensitivity to the background of natural events, particularly in the auroral regions.

CONCEALMENT OF SPACE EXPLOSIONS

The most obvious method for concealing space nuclear explosions from earth-based detectors (earth satellites or ground-based systems) is to carry them out behind the moon. The moon shields all prompt radiations from the detectors, and only delayed γ rays which are emitted from the fission debris after the debris moves out from behind the moon are detectable. However, material can be distributed around the device in such a way as to

direct the fission debris toward the moon's surface allowing only the inactive materials to move out from behind the moon. Explosions behind the sun are completely undetectable by earth-based detectors. Detectors in solar satellites would be required.

It is possible to construct artificial shielding against detection of prompt γ rays and X rays. It does not appear possible, however, to shield against delayed γ rays and visible light.

X-ray shields.—The simplest X-ray shield consists of a thin sheet of lead or lead-loaded plastic (a lead balloon) placed a few meters from the explosion and between the explosion and the X-ray detectors. The shield must be large enough to screen the expanding explosion debris until the temperature of the debris has fallen below the X-ray detection level.

Such an X-ray shield operates as follows. The X rays emitted by the explosion are deposited in a very shallow layer on the surface of the shield facing the explosion. This thin layer becomes hot and begins to reradiate the energy which it absorbed back toward the explosion and away from the X-ray detectors. At the same time deeper layers of the shield will be heated by radiation diffusing into the shield. If the shield is thick enough, the radiation will not diffuse all of the way through. In this case the detector side of the shield will be heated to less than 10 ev by a hydrodynamic shock generated by the initial X-ray deposition.

However, the shield is further heated when the explosion debris collides with it. Most of the kinetic energy of the debris intercepted by the shield will be converted into internal energy and will radiate in the form of low-energy X rays. For a shield placed several meters from the explosion, only a small fraction of the total kinetic energy of the debris will be intercepted by the shield. Moreover, since the kinetic energy of the debris is only a fraction of the total explosion yield, the total energy of the explosion which can radiate in the direction of the X-ray detectors can be reduced by a factor of at least 100 and perhaps 1000 or more.

During the time that the explosion emits its X rays, the shield will be heated on the side toward the explosion and will reradiate most of the incident energy. The surface temperature T_0 on that side of the shield can be calculated approximately by equating the incident flux to the reradiated flux,

$$\sigma T_0^4 = Y_x / 4\pi R^2 \tau \quad 83.$$

where τ is the time of emission of the X rays; R , the distance from the explosion to the shield; and σ , the Stefan-Boltzmann constant. The amount of mass penetrated by radiation in the time τ for a driving temperature T_0 is

$$\Delta m \approx \left[\frac{c}{3} \frac{1}{\kappa} \frac{a T_0^4}{b T_0} \tau \right]^{1/2} \quad 84.$$

where κ is the opacity of the shield; b , its specific heat; and $a T_0^4$ the energy density of the radiation. If, for example, $Y_x = 80$ kilotons for an explosion of

100 kilotons total yield, $\tau = 10^{-7}$ sec and $R = 10$ m, then $T_0 \sim 230$ ev. For reasonable choices of κ and b , $\Delta m \sim 0.05$ g. After the time τ , the shield will cool by radiating back through the hot, expanded explosion debris. If the thickness of the shield is about 0.1 or 0.2 g, then the detector side of the shield will not become hot because of the direct X-ray heating.

The average rate per unit area at which kinetic energy from the explosion debris is delivered to the shield is

$$F = \frac{1}{2} [Mv^2 / (4\pi R^2 t_c)] \quad 85.$$

where M is the mass of the bomb, v the root mean square velocity of the debris, and t_c the time of the collision of the debris with the shield. This energy does not radiate away faster than it is delivered so that

$$\sigma T_1^4 + \sigma T_2^4 \lesssim F \quad 86.$$

where T_1 is the temperature on detector side of the shield and T_2 the temperature on the explosion side.

As an example, if the exploding device has a mass of about 200 kg, the debris will be less than 0.02 g/sq cm thick when it collides with the shield. Since the shield is much thicker than the debris, the energy radiates back through the debris more easily than through the shield. Thus $T_2 > T_1$ and $\sigma T_1^4 < \frac{1}{2} F$. For this type of explosion v is about 10^8 cm/sec and t_c , about 4×10^{-6} sec. Thus $T_1 < 60$ ev. At this temperature, X rays are strongly attenuated by covered X-ray detectors.

If detection satellites were restricted to orbits around the earth, the above shield which need only weigh about 100 lb would reduce detection distances by about two or three orders of magnitude. If solar satellites were used for detection, the shield would have to be heavier in order to shield X rays in all directions from the explosion in which satellites might be located. Such heavy shields and shields which reduce the radiating temperature to even less than ~ 60 ev have also been designed. The design of such shields is quite dependent upon the design of the nuclear device, and complicated calculations are required to determine their effectiveness [Herbst & Wainwright (33)].

Gamma-ray and neutron shields.—A few inches of lead can reduce the γ -ray flux from an explosion by a factor of 100 or more. However, neutrons from the explosion can produce γ rays in the lead by inelastic scattering. If the shield need be effective only over a limited solid angle, it can be separated from the explosion, thereby reducing the neutron flux on the shield sufficiently to allow only a negligible number of γ rays to be produced by inelastic scattering.

If a shield is required to reduce both the neutron and γ -ray fluxes or to be effective over a large solid angle, it would have to be a mixture of a moderating material such as hydrogen and absorbing materials such as boron and lead. Such a shield would be extremely heavy if high attenuations of the neutrons and γ rays are required.

RECENT RESEARCH

In addition to Project VELA-Uniform for underground explosions, the United States in 1959 initiated Projects VELA-Sierra and -Hotel for research on the detection of space explosions. VELA-Sierra deals with ground-based detection techniques and VELA-Hotel, with satellite-based techniques. The primary emphasis of this research program is on the nature and intensity of natural background noise affecting detection, on design feasibility of detection instruments, and on exploring new detection techniques and evaluating old ones more carefully.

Measurement of natural background noise by ground-based instrumentation is currently under way. Measurement of space backgrounds requires satellite-based instrumentation. Some limited measurements have been completed, but the required extensive measurements await the design of suitable instruments and the availability of rockets.

Instruments to detect optical fluorescence and galactic noise absorption have been built and are currently being tested by measuring natural backgrounds. Backscatter radars for measuring ionospheric disturbances are a standard geophysical tool, and have been in operation for some time. Design of instruments for detecting the direct visible light is currently being studied. Instrumentation for measuring X rays, γ rays, and neutrons in space has been designed and, as a preliminary test, will be mounted on balloons to measure backgrounds at high altitudes. The principal problem involved in this instrumentation is the discrimination of cosmic ray showers. The balloon tests, combined with laboratory tests using high-energy accelerators, are expected to contribute vital data on this difficult problem. The electromagnetic signal from Compton-recoil electrons produced by γ -ray scattering in the device or in X-ray shields has recently been estimated to be less than about 10^6 km, independent of the explosion yield [Karzas & Latter (34)].

Only a few new detection techniques have been suggested. Observation of changes in phase of a low-frequency radio wave appears to be a sensitive measure of changes in ionospheric ionization—how sensitive remains to be determined. Balloon- or aircraft-borne instrumentation appears to be a possible method for detecting γ rays. The sensitivity of this approach is less than for satellites, because of atmospheric absorption of γ rays. Moreover, the feasibility of maintaining sufficient balloons or aircraft at high altitudes to permit continuous observation of space is somewhat questionable. A particularly interesting suggestion is to observe resonance scattering of sunlight from the debris of the exploding device. Preliminary estimates suggest that this approach has no better detection capability than other techniques, but considerably more research is necessary.

ACKNOWLEDGMENTS

The authors wish to thank Drs. R. E. LeLevier and W. J. Karzas for many helpful discussions on underground detection.

LITERATURE CITED

1. *Verbatim Records and Report of the Geneva Conference of Experts* (1958)
2. Christy, R. F., and Gell-Mann, M. (Unpublished, 1958)
3. Kompaneets, A. S., *Soviet Phys. JETP*, **38**, 1076 (1959)
4. Willis, H. F., *Underwater Explosion Research*, **II**, 761 (Office of Naval Research, 1950)
5. Ewing, M., and Worzel, S. I., "Long-range Sound Transmission," *Geol. Soc. Am.*, Memoir 27 (1948)
6. Johnson, G. W., Higgins, G. H., and Violet, C. E., *J. Geophys. Research*, **64**, 1457 (1959)
7. Latter, A. L., Martinelli, E. A., and Teller, E., *Phys. Fluids*, **2**, 280 (1959)
8. Jeffreys, H., "On the cause of oscillatory movement in seismograms," *Monthly Notices Roy. Astron. Soc., Geophys. Suppl.* **2**, 407 (1931)
- 8a. Blake, F. R., Jr., *J. Acoust. Soc. Am.*, **24**, 211 (1952)
9. Perret, W. R., "Subsurface motion from a confined underground detonation," Part I, *Sandia Corp. Rept. ITR-1529* (October 1957)
10. Scheidegger, A. E., *Bull. Seismol. Soc. Am.*, **49**, 337 (1959)
11. *Report of the Panel on Seismic Improvement*, "The Need for Fundamental Research in Seismology" (Department of State, 1959)
12. Richter, C. F., *Elementary Seismology*, (W. H. Freeman and Co., San Francisco, Calif., 1958)
13. Aki, K., *J. Geophys. Research*, **65**, 729 (1960); **65**, 2405 (1960)
14. Romney, C., *J. Geophys. Research*, **64**, 1489 (1959); (Private communication)
15. Latter, R. (Unpublished, 1958)
16. Gutenberg, B., and Richter, C. F., *Seismicity of the Earth* (Princeton University Press, Princeton, N. J., 1954)
17. *Verbatim Records of the Technical Working Group 2 of the Geneva Conf. on Discontinuance of Nuclear Weapons Tests* (1959)
18. Latter, A. L., LeLevier, R. E., Martinelli, E. A., and McMillan, W. G., *J. Geophys. Research*, **66**, 943 (1961)
19. Herbst, R. F., Werth, G. C., and Springer, D. L., *J. Geophys. Research*, **66**, 959 (1961)
20. *Hearings Joint Comm. on Atomic Energy of the US Congr.*, "Technical Aspects of Detection and Inspection Controls of a Nuclear Weapons Test Ban," April 19-22, 1960 (US Govt. Printing Office, Washington, D.C., 1960)
21. *Verbatim Records of the Technical Working Group 1 of the Geneva Conf. on Discontinuance of Nuclear Weapons Tests* (1959)
22. Edwards, B., Losty, J., Perkins, D. H., Pinkau, K., and Reynolds, J., *Phil. Mag.*, **3**, 237 (1958)
23. Friedman, H., Chubb, T., and Kreplin, R., *Sky and Telescope* (Sky Publishing Co., July 1958)
24. Chubb, T. A., Friedman, H., and Kreplin, R. W., *J. Geophys. Research*, **65**, 1831 (1960)
25. Lapaz, L., and Whipple, F., *Physics and Medicine of the Upper Atmosphere* (Univ. of New Mexico Press, Albuquerque, N. M., 1952)
26. Brown, R. R., *J. Geophys. Research*, **66**, 1379 (1961), has reported a flux of 5×10^9 electrons/sq cm sec.
27. Bierman, L., *Mém. soc. roy. sci. Liège*, **13**, 29 (1953)
28. Van Allen, J. A., and Frank, L. A., *Nature*, **183**, 430 (1959); **184**, 219 (1959)
29. Freden, S. C., and White, R. S., *Phys. Rev. Letters*, **3**, 9 (1959)
30. Latter, R. (Unpublished RAND Report, 1959)
31. Westervelt, D. R., *Los Alamos Rept. J-10-351* (1959)
32. Latter, R., and LeLevier, R. (Unpublished, 1958)
33. Herbst, R., and Wainwright, T. (Unpublished, 1959)
34. Karzas, W. J., and Latter, R. (To be published)

HEAVY-ION ACCELERATORS¹

BY EDWARD L. HUBBARD

Lawrence Radiation Laboratory, University of California, Berkeley, California

INTRODUCTION

Since the pioneering work around 1930 that led to the disintegration of atomic nuclei by accelerated ions, much effort has been expended on the development of particle accelerators. The primary objective of this development has always been the acceleration of electrons, protons, deuterons, and α particles to higher and higher energies. Recent progress in the acceleration of these particles to high energies has been reviewed by Judd (1).

Until recently relatively little work was done on the acceleration of ions heavier than helium. In 1940 Alvarez reported the acceleration of six-times-ionized carbon ions to an energy of 50 Mev in the 37-inch cyclotron at Berkeley (2). Further work with the 60-inch cyclotron at Berkeley led, in 1950, to the detection of nuclear reactions produced with carbon ions by Miller and co-workers (3). Soon afterwards, the usefulness of accelerated carbon ions for the production of transuranic elements was demonstrated by Ghiorso *et al.* (4), and a paper pointing out the possibilities of nuclear research with accelerated heavy ions was published by Breit, Hull & Gluckstern (5). The interest in research with heavy ions created by this work led to the acceleration of heavy ions with other cyclotrons designed for deuterons, and the construction of machines designed specifically for the acceleration of heavy ions. Carbon ions with an energy as high as 1.1 Bev have been produced in the FM cyclotron at Chicago (6). However, the emphasis has been on the production of ions with energies of 10 Mev/*A* or less for use in low-energy nuclear physics experiments.²

Review articles describing recent nuclear research with accelerated heavy ions have been published by Breit (7), Flerov (8), Fremlin (9), and Zucker (10). A detailed discussion of much of the recent work was presented at the

¹ The survey of literature pertaining to this review was concluded in January 1961.

² The term "heavy ion" as used here refers to any ion heavier than helium, and by most standards the particles now being accelerated in heavy-ion accelerators would be considered light ions. The ions produced by a linear accelerator or a cyclotron with a fixed $H\rho$ all have the same velocity. Therefore the energy of the ions depends on their mass, but the energy per unit mass is the same for all ions. For this reason, the energy per nucleon in the nucleus of the ion (Mev/*A*) is a unit often used in heavy-ion work, rather than the total energy of the ions. When a beam current of multiply charged heavy ions is measured with a Faraday cup, the current reading must be divided by the charge on the ions to obtain a current representing the same number of particles per second as the same current of protons. However, experimenters in this field customarily do not divide by the charge, and the term "meter μa " is sometimes used to indicate this.

Second Conference on Reactions Between Complex Nuclei (11). In addition to their use in nuclear research, accelerated heavy ions are being used in biological studies (12).

The accelerator required for heavy ions is quite large if singly ionized ions are used. For example, a cyclotron that accelerates singly charged neon ions to 10 Mev/ A would have at least 360-in.-diameter poles. A large reduction in the size of the accelerators results from the use of multiply charged ions. However, the higher the state of ionization of the ions, the more difficult it is to get a large beam from an ion source. Therefore, in some machines the ions are accelerated to a moderate energy in a low charge state and then stripped to a higher charge state by being passed through a thin layer of matter. The ion sources used for multiply charged ions and the techniques of electron stripping are discussed in the next sections before the various types of heavy-ion accelerators are described.

ION SOURCES

Arc discharge sources.—During the early experiments on the acceleration of heavy ions at Berkeley, spark-type ion sources similar to those used in spectroscopy were tried (13), and a source of this type has been used on the heavy-ion linac at Kharkov (14). However, for ions of elements available in gaseous form, larger beams are produced by arc-type sources, and this type is used in most heavy-ion accelerators.

To produce ions in a given charge state, the electrons in the arc discharge must have an energy greater than the ionization potential of the electrons to be removed from the ion. The cross section for ionization reaches a maximum when the energy of the electrons in the discharge is three to five times the ionization potential. The ionization potentials of the ions commonly used in heavy-ion accelerators are listed in Table I. It is seen, for example, that the ionization potential for Ne^{+6} is about 10 times that for hydrogen, while for Ne^{+10} the ratio is 100. The commonly used proton sources operate with rather low arc voltages and are not suitable for the production of multiply charged ions; therefore, special arcs that operate with high arc voltages have been developed for this purpose.

The most successful sources of multiply charged ions use a dc discharge that is collimated by a magnetic field. The ionizing electrons make multiple traversals through the discharge as in a Penning or Phillips ionization gage (PIG). Figure 1 is a sketch of the source developed for the cyclotron at Moscow by Morozov, Makov & Ioffe (15). One of the cathodes is heated by electron bombardment and emits thermionic electrons. With an arc voltage of 750 to 800 v and arc currents of 4 to 5 amp, beams of 0.1 ma of N^{+5} and 2 ma of N^{+4} are produced. A similar source was built recently by Papineau, Benezech & Maillard (15a).

Sources of this type that depend on secondary emission of electrons from cold cathodes to sustain the discharge were developed for the Oak Ridge 63-inch cyclotron by Jones & Zucker (16) and for the heavy-ion linear accel-

TABLE I
IONIZATION POTENTIALS (VOLTS)

Charge	H	He	B	C	N	O	F	Ne	Si	S	A
1	13.5	24.5	8.3	11.3	14.5	13.6	17.4	21.6	8.1	10.4	15.8
2		54.1	25.0	24.4	29.6	35.1	35.0	41.1	16.3	23.4	27.6
3			37.8	47.9	47.4	54.9	62.6	63.4	33.5	34.7	40.9
4			258.1	64.5	77.4	77.4	87.2	97.2	45.1	47.3	59.8
5			338.5	392.0	97.9	113.9	114.2	126.4	166.7	72.5	75.0
6				498.8	551.9	138.1	157.1	157.9	205.1	88.0	91.4
7					666.8	739.1	185.1	207.3	246.4	281.0	124.2
8						871.1	935.6	239.0	303.7	328.8	143.5
9							1196	351.0	379.0	422.6	
10								1360	401.3	448.6	480.0
11									476.0	506.4	539.5
12									523.2	564.6	621.1
13									2436	651.7	688.5
14									2666	706.4	755.5
15										3220	854.4

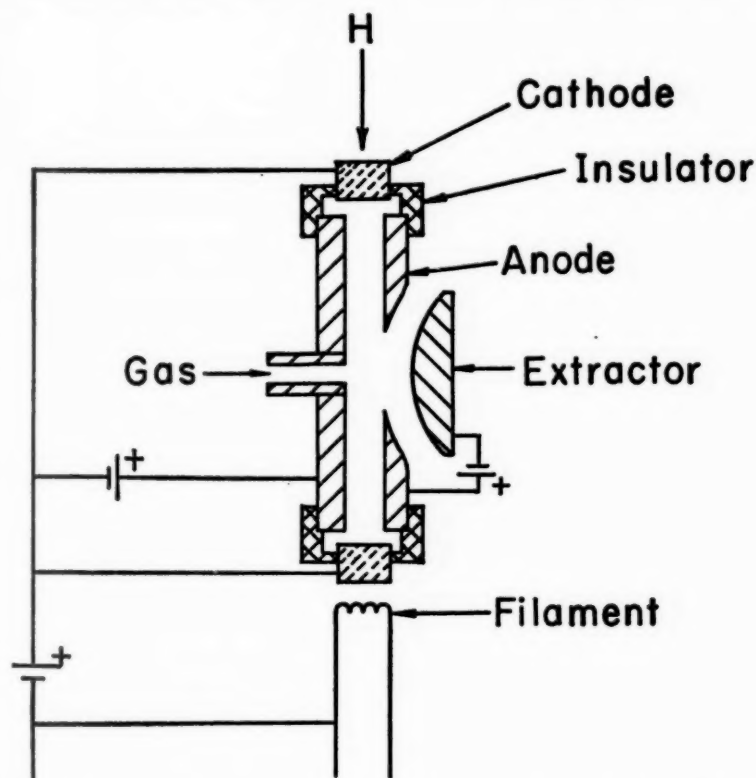


FIG. 1. Schematic drawing of the Penning ionization gauge (PIG)-type ion source used in the 150-cm cyclotron at Moscow (15).

erators at Berkeley and Yale by Anderson & Ehlers (17). The Oak Ridge source produces several ma of N^{+3} with an arc voltage of 600 v and 3 to 5 amp of arc current. The Berkeley-Yale source operates with 1 kv arc drop and 1.5 amp arc current and produces ma beams of many ions in the He-Ne mass region with $e/m \geq 0.15$.³

Jones & Zucker also developed a source using a hot filament (16, 18). In this source the lower cathode in Figure 1 is omitted, and the electrons emitted by the filament are used to sustain the discharge. The upper cathode is allowed to float instead of being held at a fixed negative potential. With 250 v of arc voltage and 3.5 amp of arc current this source produces a few ma of N^{+3} ions.

Figure 2 shows how the number of argon ions produced in various charge states by the Berkeley source depends on the arc current. Similar curves were obtained for nitrogen ions by Morozov, Makov & Ioffe (15). The rapid increase in the yield of ions in higher charge states with higher arc current suggests that several ionizing collisions are involved in the formation of multiply charged ions and that single collisions in which several electrons are removed are relatively unimportant.

The fraction of the ions in higher charge states is also increased by lowering the pressure in the discharge. Curves showing this effect have been published by Morozov, Makov & Ioffe (15). The processes responsible for this effect seem to be the capture of electrons in collisions with neutral gas atoms in the discharge chamber and the change in mean free path (and therefore the energy) of the ionizing electrons. It is difficult to determine the gas pressure in the discharge chamber, but estimates indicate that it is of the order of 1μ with the gas consumption in the operating region of about 1 cc/min (at atmospheric pressure). The high gas flow used by these sources and the low pressure needed in the region outside the source to prevent capture of electrons by the multiply charged ions mean that high-speed vacuum pumping is required.

The ions are extracted radially through a slit in the side of the anode. Ions from the slit are accelerated by the extractor electrode. In cyclotrons, the extractor is mounted on the dee and the radiofrequency (rf) voltage on the dee is used for extraction of ions from the source. In the linear accelerators at Berkeley and Yale, a dc voltage of about 15 kv is applied to the extractor electrode.

PIG discharges have also been used as proton sources for linear accelerators (19). In these sources, the protons are extracted in the axial direction through a hole in a cathode. In preliminary experiments this type of extraction of heavy ions at Berkeley and Manchester did not yield as favorable a ratio of multiply charged ions to singly charged ions as did the sources using radial extraction. Radial extraction also has the advantage that the magnet

³ In this article the charge-to-mass ratio e/m of the ions is expressed in units of the charge-to-mass ratio of the proton.

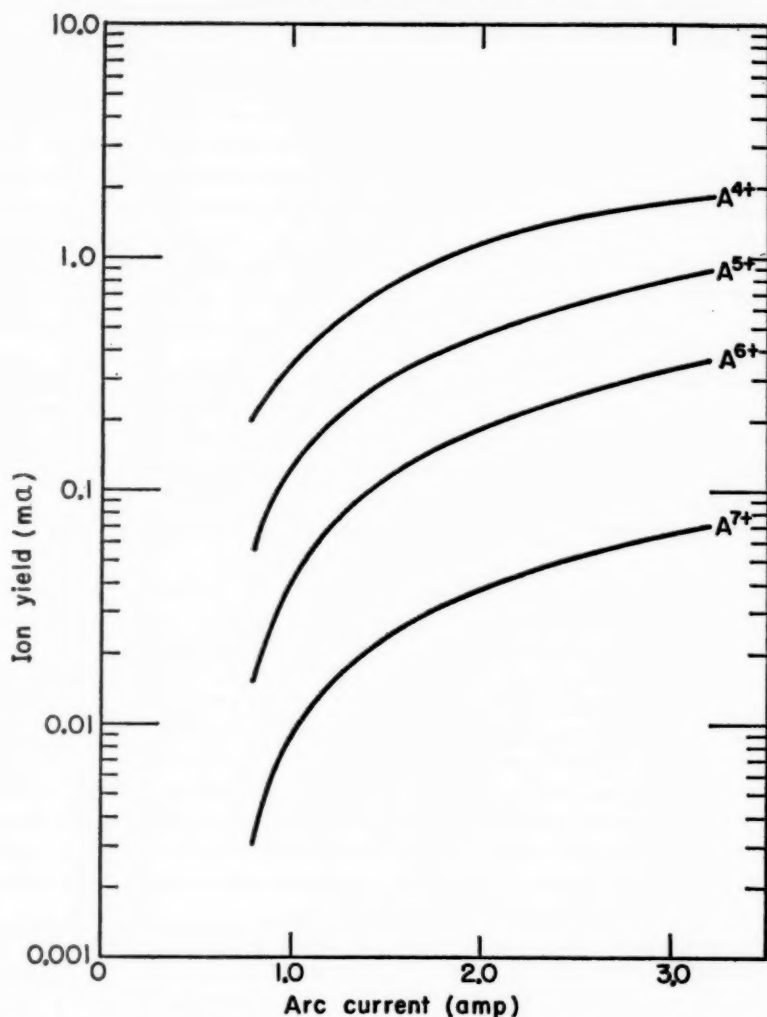


FIG. 2. Yield of multiply charged argon ions as a function of the arc current. The data were obtained by Gavin, using a constant arc drop of 1000 v in the Berkeley source. (B. F. Gavin, private communication.)

used to collimate the PIG discharge separates the ions to be accelerated from the ions in other charge states. Elimination of ions with the wrong charge reduces the space-charge defocusing in the accelerating column of the dc injector accelerator. However, radial extraction has the disadvantage that the beam is astigmatic.

As in all types of ion sources, good performance depends on a number of

details, many of which are not clearly understood. For instance, Anderson & Ehlers tried many different cathode materials and chose tantalum and titanium as the best. Jones & Zucker also used tantalum, but Morozov *et al.* used tungsten in the heated cathode and molybdenum in the cold one. For elements available in the gaseous state only in compounds, different compounds give different performances. Compounds that work well for some commonly used ions are BF_3 for boron and fluorine ions, CO_2 for carbon ions, and H_2S for sulfur ions.

In linear accelerators where the rf accelerating fields are pulsed with a duty factor of about 3 per cent, the life of the source is increased by pulsing the arc discharge. The problems encountered in pulsed operation and their solutions are described by Anderson & Ehlers (17).

A different type of arc discharge, similar to the duoplasmatrons that are coming into wide use as proton sources, has been used by von Ardenne to produce multiply charged ions (20). In operation with an arc drop of 750 v, 0.95 ma of N^{+3} and 0.06 ma of N^{+4} ions were obtained during a 10- μsec pulse. These yields are not quite as large as those obtained from the PIG sources, and the use of this type of source in a heavy-ion accelerator has not been reported.

Sources for ions of solid materials.—In the PIG discharge sources of the type shown in Figure 1, bombardment of the cathodes by ions in the discharge causes the cathode material to be sputtered away. Ions of the sputtered cathode material are observed in the beam extracted from the source. For most materials the beam currents obtained are too small to be useful. However, Anderson has used this method to obtain 1-ma beams of singly charged ^6Li and 0.1 ma of doubly charged ^6Li from the ion source at Yale (21). The lithium was loaded into a pocket in the lower titanium cathode, and the source was operated in the usual way, using nitrogen to sustain the discharge. Boron nitride insulators were used in the source since they are not damaged by lithium vapor. The $^6\text{Li}^{+1}$ ions have a high enough charge-to-mass ratio to be accepted by the Yale linear accelerator.

A 0.5- μa beam of singly charged lithium ions has been obtained from a standard rf ion source by Cornides, Roósz & Siegler (22). The rf discharge was produced in hydrogen, and then lithium was introduced from a heated tube on the side of the discharge chamber.

When certain lithium compounds are heated to temperatures over 1000°C, singly charged lithium ions are emitted. This phenomenon has been used for many years to make lithium ion sources. Recently, using a source of this type, Norbeck obtained 5 to 10 μa of lithium ions from an electrostatic accelerator (23). A powder of the mineral β -eucryptite, a lithium-aluminum silicate eutectic mixture, was suspended in amyl acetate and painted onto a filament.

The methods used to produce lithium ions can also be used for heavier alkali metals, but the charge on the ions is too small for them to be used in resonance accelerators.

ELECTRON STRIPPING

Equilibrium charge distribution.—When fast ions pass through matter, they lose and capture electrons in collisions with atoms of the material they are going through. The way in which a beam of 8.7-Mev O^{+8} ions changes charge while passing through argon is illustrated in Figure 3. The distribution of the ions among the various charge states changes until equilibrium is established between capture and loss of electrons. After the ions have gone through enough stripping material to establish equilibrium, no further change in the charge-state distributions occurs as they pass through more material. Equilibrium is reached before any significant degradation of the energy or multiple scattering of the ions takes place.

The ratio of the capture to the loss cross section for a given electron depends on the orbital velocity of the electron within the ion and the velocity of the ion. The electron-loss cross sections are greater than the capture cross sections if the ion velocity is larger than the orbital electron velocity, and vice versa. If the ion velocity equals the orbital velocity of a given electron, the capture and loss cross sections are nearly equal, and at equilibrium some of the ions will carry this electron and some will not. Using an approximate form of the Fermi-Thomas distribution of orbital electron velocities, Bohr obtained the formula $\bar{e}/Z = v/(v_0 Z^{2/3})$ for the average charge \bar{e} carried by a beam of ions at equilibrium (25). In this equation, v is the ion velocity, v_0 is the velocity of the electron in the ground state of hydrogen, and Z is the atomic number of the ion.

For ions in the mass region carbon to neon, Bohr's formula gives values

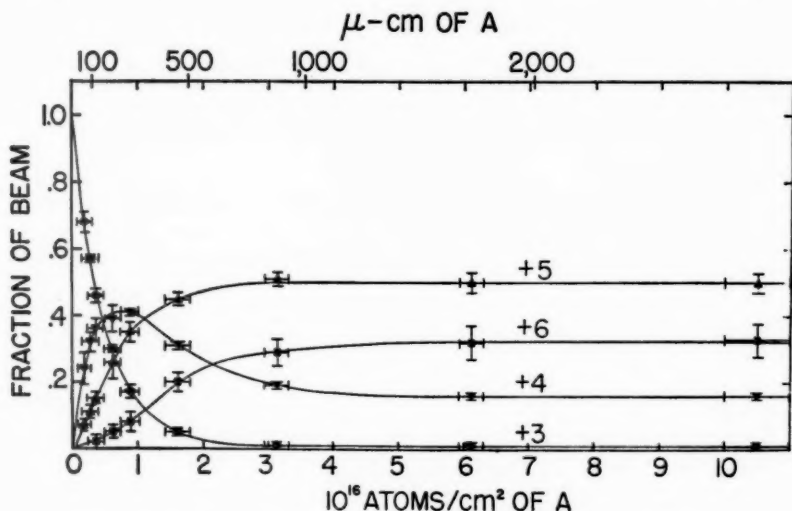


FIG. 3. Stripping of a beam of 8.7-Mev O^{+8} ions in argon (24).
The thickness of argon is given in micron (Hg)-cm.

of \bar{e} that are too high, especially for highly ionized ions. Brunings, Knipp & Teller (26) have used two methods for determining the appropriate orbital electron velocities and obtained more complicated relations between \bar{e}/Z and $v/Z^{2/3}$. An empirical-empirical relation between \bar{e}/Z and $v/Z^{2/3}$ was obtained from experimental equilibrium charge distributions by Papineau (27). Papineau's curve, extended to higher energies with the data of Heckman *et al.* (28), is plotted in Figure 4, with the energy per nucleon in the abscissa.

For many light ions, the ratio e/m which determines the parameters of the accelerator is equal to half the ratio e/Z . For these ions, the energy per nucleon required for stripping to a given e/m increases as $Z^{4/3}$. For heavier ions, in which e/m becomes less than half e/Z , the stripping energy increases as a slightly higher power of Z . At a given velocity, \bar{e}/m decreases with the mass of the ion. Therefore, the choice of the velocity at which stripping is done in an accelerator can be optimum for only one ion. For lighter ions, the accelerator is larger than is necessary and for heavier ions a large fraction of the beam is not stripped to a high enough e/m and is lost.

As shown in Figure 3, most of the stripped beam is distributed over three charge states. As a result, some loss of beam occurs unless the section of the accelerator that follows the stripper accepts the beam in more than one charge state and unless the lowest charge accepted is one charge lower than the average charge.

There is some evidence that the average equilibrium charge \bar{e} is slightly

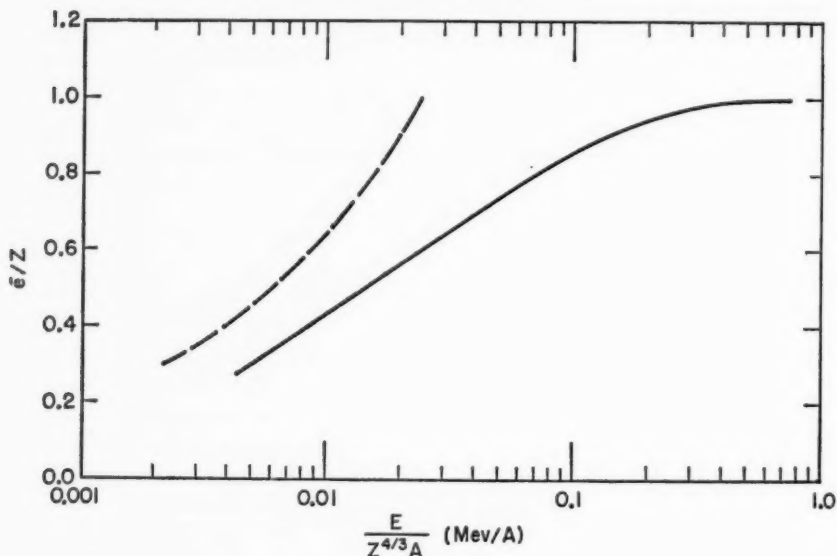


FIG. 4. Dependence of the average equilibrium charge \bar{e} on the energy per nucleon, E/A , of ions of atomic number Z . For comparison, the values given by Bohr's formula (25) are indicated by the dashed curve. See text for details.

higher for solid stripper materials than for gaseous ones (29, 30). According to Bohr & Lindhard (31), stripping should be more probable in solid materials because many of the electrons of the ion are in excited states, whereas in gases there is sufficient time between collisions for the ions to return to the ground state. There are also some indications of a slight dependence of \bar{e} on the atomic number of the stripper material. However, the dependence of \bar{e} on the stripper material is not large enough to be important in the choice of a material to be used in a stripper for an accelerator.

The experimental equilibrium charge distributions determine only the ratios of the capture to the loss cross sections. To determine the thickness of stripper material required, it is necessary to know the absolute values of the cross sections. The absolute cross sections can be determined from measurements of the charge distributions under nonequilibrium conditions. However, only a few experiments of this type have been performed (24, 32, 33).

Cross sections for capture and loss of electrons by oxygen, neon, phosphorus, and argon ions passing through argon have been calculated by Gluckstern in the energy range from 0.2 to 1.2 Mev/A (34). The calculated loss cross sections are in good agreement with experiment, but the capture cross sections are too high. The theory does not consider collisions in which more than one electron is exchanged, although Gluckstern suggests that these may be significant. To determine the thickness of stripper material needed, one can use the velocity dependence of the cross sections obtained by Gluckstern together with the experimental measurements available and get a fair estimate. For ions in the nitrogen-to-neon region with 1 Mev/A, about $10 \mu\text{g}/\text{cm}^2$ of stripper material is sufficient.

Foil strippers.—A stripper $10 \mu\text{g}/\text{cm}^2$ thick introduces an energy spread of the order of 10^{-5} Mev/A, and the root mean square multiple scattering angle is of the order of 0.1 degree. These values are considerably smaller than the acceptance limits of an accelerator following the stripper. However, if the stripper is more than $100 \mu\text{g}/\text{cm}^2$ thick, the multiple scattering angle begins to be an appreciable fraction of the angular acceptance.

Although in principle a foil is the simplest kind of stripper one can use, some difficulty is involved in making foils less than $100 \mu\text{g}/\text{cm}^2$ thick that will stand up in an intense beam of ions. However, several laboratories have succeeded in producing suitable foils and are using them for strippers in accelerators.

Nickel foils $45 \mu\text{g}/\text{cm}^2$ (500 A) thick are available commercially from the Chromium Corporation of America (35). The nickel is electrodeposited on a 0.1-mil copper backing which can be removed with activated chromic acid. Nickel foils of this type were used at first on the Yale heavy-ion accelerator, but they were later abandoned in favor of aluminum oxide foils.

Aluminum oxide foils are prepared by anodizing a thin sheet of aluminum (36). The oxide coating is removed from one side of the anodized sheet with NaOH, and then the excess aluminum is removed with HCl. Foils with thickness from 25 to $250 \mu\text{g}/\text{cm}^2$ (700 to 7000 A) can be prepared this way. The

thickness of the oxide layer is determined by the anodization voltage and is independent of the electrolytic concentration. Aluminum oxide foils $40 \mu\text{g}/\text{cm}^2$ thick stand up for weeks in the Yale accelerator.

Carbon foils from $4 \mu\text{g}/\text{cm}^2$ to $1 \text{ mg}/\text{cm}^2$ (200 \AA to 5μ) thick can be prepared by evaporating carbon from a carbon arc. The carbon is evaporated onto a glass plate and then the film is floated off on water. Carbon foils $5 \mu\text{g}/\text{cm}^2$ thick used for stripping in the Harwell tandem electrostatic accelerator stand up in the beam almost indefinitely (37).

Gas strippers.—A gas-filled chamber with an opening in each end and a differential pumping system has been used in many studies of the capture and loss of electrons. A gas-filled tube was used by Bittner to strip a beam of 400-keV He^{+1} ions inside the high-voltage terminal of a Van de Graaff generator (38), and a system of this type is used for stripping in the tandem Van de Graaff accelerators at Chalk River and Aldermaston.

To reach equilibrium in a gas-filled tube 20 inches long, a pressure of about 50μ is required at the center of the tube. In a system where axial length is not limited or where a small-diameter tube can be used, a differential pumping system is feasible. However, in a linac, where the axial length available is limited by phase debunching of the beam and the diameter of the beam tube is about half an inch, the differential pumping problem is severe, and systems of this type have not been used.

Jet strippers.—Stripping can also be done with a supersonic jet of gas directed transversely to the beam direction. If a jet of a condensable vapor is used, the problem of pumping out the gas introduced can be eliminated by collecting it on a cold trap. A jet of carbon dioxide was used to strip a beam of He^{+1} ions from a Van de Graaff accelerator by Geller & Prevot (39). The carbon dioxide was solidified in the cold trap.

The heavy-ion linac (Hilac) at Berkeley uses a jet of mercury similar to the one developed by Beringer & Rall (40). The mercury vapor is supplied to the jet nozzle from a boiler and then condensed to a liquid and returned to the boiler. For surface densities in the jet of $10 \mu\text{g}/\text{cm}^2$ the boiler pressure is about 50 mm Hg, while the vacuum chamber surrounding the jet is at 10^{-5} mm Hg. With a pressure drop this large, the jet is underexpanded for any practical nozzle design, and the jet expands into the low-pressure region. Therefore, it is necessary to put cold traps around the beam tube near the jet to prevent mercury from streaming into the linac cavities. Diffusion pump oil could be used in this type of jet; however, in linacs any oil that gets onto the drift tube surfaces increases the tendency to spark.

DIRECT-CURRENT HIGH-VOLTAGE ACCELERATORS

Conventional dc accelerators.—The standard dc high-voltage accelerators that have been in use for many years accelerate any ion in any charge state. At Chicago, Minnesota, and Saclay, Li^{+1} ions accelerated in machines of this type are being used to study nuclear reactions with very light targets. The only unusual feature of these accelerators is the ion source discussed above.

For ions heavier than lithium, the energy is too low for the study of nuclear reactions unless multiply charged ions are used. In principle, it would be possible to use one of the special sources for multiply charged ions. In a 6-Mv Van de Graaff generator, ions with charge $+5$ would be accelerated to 30 Mev. However, the sources for multiply charged ions require more power and more space than is customarily available in such a machine. Moreover, these sources need frequent maintenance, which would be inconvenient for a source located in a pressure vessel. For these reasons, the use of the standard dc machines for ions heavier than lithium has been very limited.

Tandem Van de Graaff accelerators.—When a very-low-energy beam of atomic ions passes through matter, many of the ions capture electrons. Most of the ions in the equilibrium charge distribution are neutral, but a few of them carry a negative charge. Also, when a beam of molecular ions is dissociated by being passed through matter, some of the atomic ions formed are negative. Negative ions formed in either of these processes can be accelerated from ground to the positive high-voltage terminal of a dc accelerator. In the high-voltage terminal, electrons can be stripped off and the resultant positive ions accelerated from the terminal back to ground. This type of accelerator was first suggested by Bennett in 1937 (41), but little interest in the idea developed until the possibilities were pointed out again by Alvarez in 1951 (42). The first Van de Graaff accelerator using this principle was built by the High Voltage Engineering Corporation for the laboratory at Chalk River (43). Recently, other machines of this design were put into operation at Florida State University and the University of Wisconsin. Similar accelerators built by Metropolitan-Vickers are in use at Aldermaston and at Harwell (44). Several more machines of this type, now known as "tandem" Van de Graaff accelerators, are under construction.

One of the advantages of the tandem Van de Graaff over the conventional one is that the ion source and its associated equipment are at ground potential where there is no limitation on the space or power available. An ion source that produces $25\text{ }\mu\text{a}$ of negative ions was developed by Weinman & Cameron (45). Positive ions are produced in a PIG discharge using a hot filament and axial extraction. The extractor electrode is a tube with hydrogen introduced into the center of it. About 2 per cent of the positive ions extracted at 10 kev are converted to negative ions. The yield of negative ions from dissociation of molecular ions turned out to be larger than the yield from capture by atomic ions. Fogel, Koval & Timofeev used a similar ion source with a mercury jet and obtained $40\text{ }\mu\text{a}$ of O^{-1} ions (46). The British machines use a rf source developed by Collins & Riviere (47). The negative ions are produced by introducing gas into the exit canal. The Chalk River machine also uses a rf source.

The negative ions are magnetically separated from other components of the ion source beam and accelerated to an energy of from 40 to 120 kev before entering the accelerating column of the Van de Graaff. In the machines that use gas strippers in the high-voltage terminal, the gas is pumped down

the high-energy accelerating column to avoid stripping the negative ions in the low-energy column.

To date, oxygen ions have been used for most of the heavy-ion work with tandem accelerators. However, carbon ions have also been accelerated at Chalk River, and it is expected that a large variety of ions will eventually become available.⁴ In a 6-Mv tandem Van de Graaff accelerator, a large fraction of the negative oxygen ions is stripped to the +5 charge state in the high-voltage terminal, and the final energy is 36 Mev. For energies below 36 Mev, the tandem Van de Graaff accelerators have the advantages over resonance accelerators of continuously variable energy and precision energy control. Beam currents of a few tenths of a μ a are available with a $\frac{1}{8}$ -in diameter.

A further extension of the tandem scheme that uses two high-voltage generators, one positive and one negative, is now under development. The negative ion source is mounted in the negative high-voltage terminal. The negative ions are accelerated to ground, then to the positive high-voltage terminal, where they are stripped, and then to ground again. With 6 Mv on each terminal, the ions would have 12 Mev at the stripper, and a good yield of O^{+6} ions should be obtained. The final energy of the oxygen ions would be 48 Mev, or 3 Mev/A.

CYCLOTRONS

Cyclotrons using stripping.—The radiofrequency for many fixed-frequency cyclotrons is chosen for the acceleration of deuterons and α particles which have an e/m of $\frac{1}{2}$. Completely stripped ions of ^{12}C , ^{14}N , ^{16}O , and ^{20}Ne also have an e/m of $\frac{1}{2}$ and can be accelerated in these machines. Completely stripped ions of ^{12}C were used in the early cyclotron experiments of Alvarez (2), Tobias (48, 49), and Condit (50, 51). The ion sources in use at that time operated with an arc voltage of 200 volts. As seen in Table I, the electrons in the arc were well below the ionization potential for the sixth electron in carbon. Tobias suggested that the completely stripped ions were produced by high-energy electrons that oscillate between the dees.

When further ion source development (13) still did not yield enough external carbon beam to permit detection of nuclear reactions, bombardments using the internal circulating beam were tried. Not only were nuclear transmutations detected, but also the yield indicated that the circulating beam of carbon ions was 10^3 to 10^4 times greater than the external beam (52). The ratio of circulating beam to external beam for light ions such as deuterons was about 10 to 1 at that time. The reason for the low efficiency of the deflector for C^{+6} ions turned out to be a large spread in the energy at the deflector radius. The intensity of the C^{+6} beam increased rapidly for lower energies, and only the high-energy tail of the energy distribution received the right amount of deflection in order to go through the external beam channel.

The early experiments of Condit (50, 51) had established the existence of

⁴ The recent use of He^{-1} ions in a tandem accelerator indicates that small beams of ions of even the noble gases are possible (66).

a C^{+2} beam accelerated with the third harmonic of the orbital frequency of the ions equal to the cyclotron radiofrequency. Further experiments led to the conclusion that the C^{+6} ions were formed from C^{+2} ions that were pre-accelerated by harmonic acceleration and stripped in collisions with residual gas atoms in the cyclotron tank (52). After an electron has been lost, the center of curvature of the ion's orbit would not be at the center of the cyclotron, and the orbital motion would not be synchronized with the dee voltage. As the ions crossed the dee gaps they would sometimes be accelerated and sometimes decelerated. Some of the ions would undergo further collisions while their energy was high enough to produce C^{+6} ions. Some of the C^{+6} ions formed in this way would be accelerated to full radius, but ions formed at different points in the cyclotron would have orbits with different centers of curvature and reach a given radius with different energies. Subsequent experiments with the acceleration of heavy ions in the 60-inch cyclotron at Birmingham by Walker and associates (53, 54) support this explanation of the production of high-energy C^{+6} ions. It is possible, however, that the high-energy electrons between the dees are significant in the stripping process.

This method of accelerating heavy ions in cyclotrons designed for deuterons has also been used at Stockholm (55) and Saclay (56). Further work at Berkeley resulted in internal beams of $0.2 \mu a$ of carbon ions with energy greater than 100 Mev, and an external beam of $0.001 \mu a$ of 120-Mev carbon ions (57). By increasing the magnetic field of these cyclotrons above the design values, smaller beams of high-energy N^{+6} , O^{+6} , and Ne^{+6} ions have been obtained.

At full radius, the intensity of the 1-Mev/ A beam of doubly charged ions is about 500 times the intensity of the high-energy $+6$ beam, and the heating of internal targets by it is a serious problem. The large energy spread in the internal beam makes it impossible to do precise experiments, and the external beams are too small for most experiments. For these reasons, this method of accelerating heavy ions has largely been abandoned since the advent of accelerators designed specifically for heavy ions.

Cyclotrons without stripping.—Since no method for stripping in a controlled manner in a cyclotron has yet been developed, several laboratories have built cyclotrons that accelerate multiply charged ions obtained directly from the ion source. After leaving the source, the ions are accelerated in the conventional manner.

The 120-cm cyclotron at the Physical-Technical Institute in Leningrad (58) and the 63-in. cyclotron at Oak Ridge (59) have accelerated triply charged nitrogen ions for some time. At Leningrad $0.5 \mu a$ of 16-Mev N^{+3} ions is obtained on a 3-mm-diameter external target. At Oak Ridge the energy of the external beam is 28 Mev and the current is $2 \mu a$. Recently, quadruply charged ions of carbon, nitrogen, oxygen, and neon have been accelerated in the Leningrad cyclotron (60). Energies up to 40 Mev are obtained, and the external beam current varies from 10^{-9} to 3×10^{-7} amp. These machines have

proved very useful for the study of Coulomb and nuclear interactions with light elements.

At the Atomic Energy Institute in Moscow, the ion source developed by Morozov, Makov & Ioffe (15) has been used with a 150-cm cyclotron to accelerate N^{+5} ions to 110 Mev or 7.8 Mev/A (8). A circulating beam of 1 μ a is obtained, but an external beam has not been reported. C^{+4} and O^{+6} have also been accelerated to 8 Mev/A. This machine has been used for many studies of nuclear reactions with heavy targets, but the necessity of using the internal beam has limited the complexity of the experiments. The Moscow group has recently moved to Dubna, where it is building an immense cyclotron designed to produce large currents of carbon, nitrogen, and oxygen ions with energies of 12 Mev/A.

Advances in cyclotron technology made in the last few years have led to the initiation of several projects to build cyclotrons that can be used to accelerate heavy ions to energies up to 10 Mev/A. The development of cyclotron rf systems whose frequency can be varied over a wide range, and of magnets whose field can be varied between wide limits, allows the acceleration of ions with a wide variety of e/m values. Also, the energy of the ions at the entrance to the deflector channel can be varied to obtain a variable-energy external beam. The use of azimuthally varying magnetic fields allows these machines to be used also for the acceleration of light ions to relativistic energies without frequency modulation and the resultant loss in beam intensity. Very versatile cyclotrons of this type with pole diameters of 76 inches and 88 inches are nearing completion at Oak Ridge and Berkeley, respectively. A detailed account of these and many other new cyclotrons is given in the proceedings of the Conference on Sector-Focused Cyclotrons (61).

LINEAR ACCELERATORS

Introduction.—Standing-wave linear accelerators of the type Alvarez developed for protons (62) have several advantages over cyclotrons for the acceleration of heavy ions. The size and complexity of the ion source are not as restricted. Stripping can be used without the large loss in intensity and the large energy spread that occur with stripping in a cyclotron. It is easier to obtain a well-focused mono-energetic external beam. Ions with different e/m can be accelerated by changing only the rf voltage, whereas in a cyclotron a variable-frequency rf system or a magnet that retains the proper field shape at different field strengths is required to accomplish this.

Very similar linear accelerators that produce beams of heavy ions with 10 Mev/A are in operation at Berkeley and at Yale University (63), and a somewhat different machine is operating at the Physical-Technical Institute in Kharkov (14). The injection system for a fourth heavy-ion linac is operating at Manchester, and the main part of the linac is under construction.

Radiofrequency cavities.—The main part of these linear accelerators consists of a long cylindrical cavity resonator. Ions are injected into the main cavity with an e/m of about 0.3 and energy of about 1 Mev/A. The length

of the cavity required for energies of 10 Mev/A depends on the accelerating electric field that can be achieved without sparking, as well as the e/m of the ions. The sparking limit depends somewhat on the frequency of the rf fields. In the 70-Mc machines at Berkeley, Yale, and Manchester, the design value of the average electric field over the length of the cavity is 0.5 Mv/ft, resulting in a cavity length of 90 ft. The Kharkov machine operates at 140 Mc with a higher average cavity field and uses a cavity 60 ft long.

In the Kharkov machine, focusing is done with grids as in the early proton linacs. However, since this accelerator has 101 drift tubes, the beam loss from interception by the grids is considerable. Because of the lower frequency, only 67 drift tubes are used in the main cavity of the Berkeley, Yale, and Manchester linacs. In these machines, interception of the beam by focusing grids is eliminated by the use of alternating-gradient focusing. The focusing fields are provided by quadrupole magnets placed inside the drift tubes. With this focusing system nearly all the beam injected is transmitted.

To achieve the correct value of the accelerating fields at all points in long cavities such as these, it is necessary to control the dimensions to very close tolerances or to use a number of tuners. This problem is eased considerably in the Manchester design by dividing the main cavity into two sections each 45 ft long. Dividing the cavity into sections also has the advantage that a half-energy beam can be obtained merely by turning off the rf field in the second cavity and allowing the beam to drift through it; the quadrupole magnets in the drift tubes of the second cavity can then be used to focus the beam drifting through it, and very little beam is lost in this process.

The main cavity requires 2.5 Mw of rf power to excite it. The machines are pulsed to reduce the average rf power consumption. The length of the pulses is 400 μ sec at Kharkov and 2 msec at Berkeley and Yale. The pulse rate is 10 to 15 pulses per second. At Berkeley and Yale the rf power is supplied by four large shielded-grid triodes, while at Kharkov it is supplied by a larger number of smaller tubes.

Injection.—Beam is injected into the linac at Kharkov with a 2.5-Mv Van de Graaff accelerator. The multiply charged ions are formed directly in the ion source. The charge states required are +4 for carbon and nitrogen and +5 for oxygen. These ions are injected into the linac with an energy of 0.7 Mev/A.

In the Berkeley-Yale and the Manchester designs, the ions are accelerated to the injection energy in a lower charge state and then stripped to an e/m of 0.3 or more before being injected into the main cavity of the linac. The large range of allowable synchronous phases resulting from the use of quadrupole focusing magnets in the main cavities permits the simultaneous acceleration of ions in several charge states to the same energy.

At Berkeley and Yale the e/m of the ions before stripping must be at least 0.15. Therefore the ion source is required only to produce doubly charged ions for carbon and lighter ions, and triply charged ions in the nitrogen-to-neon region. In the Manchester machine the minimum e/m of the

ions from the source is $\frac{1}{2}$, and doubly charged ions can be used for ions as heavy as oxygen.

The intense arcs used as sources of multiply charged ions require frequent maintenance work. The use of these sources in a pressure-insulated electrostatic accelerator means that considerable time and effort is required each time access to the source is necessary. For this reason the Berkeley, Yale, and Manchester machines use Cockcroft-Walton accelerators, insulated with air at atmospheric pressure, for the first stage of acceleration. The ions are then accelerated with a short section of rf linac to the energy of 1 Mev/A required for stripping and injection into the main linac. This short linac is often referred to as the prestripper linac and the main linac cavity, as the poststripper linac.

At Berkeley and Yale the maximum voltage of the Cockcroft-Walton accelerator is 470 kv and the energy of the ions injected into the prestripper linac is 70 kev/A. At this low input velocity the drift tubes become very short for the rf frequency of 200 Mc usually employed in proton linacs. The rf fields penetrate into the bore of the drift tubes, and the tubes lose their effectiveness for shielding the ions from the fields during the reverse part of the cycle. In addition, the space inside the drift tubes is too small for quadrupole focusing magnets, and the magnetic fields required are very high.

At the frequency of 70 Mc used at Berkeley and Yale, the length of the first drift tube in the prestripper is 1.7 in. With the $\frac{3}{4}$ -in. bore used, this length is sufficient to shield the ions from the rf field adequately, and it would be possible to fit a quadrupole magnet inside. However, when these accelerators were designed there was little experience with alternating-gradient linacs. It was felt that if quadrupole magnets were used for focusing, a larger bore should be used and the radial motion should remain stable for all allowable phases of the ions. Magnetic fields higher than those attainable were required under these conditions. Therefore, focusing grids are used in the prestripper sections of these linacs.

The diameter of the 70-Mc cavities used in the Berkeley and Yale linacs is 10 ft, and construction of cavities of the Alvarez type for lower frequencies is unattractive because of the large diameter of the cavities. Considerable work was done on the problem of injection into linacs at 70 kev/A during the development of the high-current linear accelerator at the Lawrence Radiation Laboratory in Livermore (64).

One solution was the use of an Alvarez-type cavity with extra-long drift tubes, so that the ions cross an accelerating gap only once in every two cycles of the rf frequency. In this scheme, plenty of room for the focusing magnets is provided inside the drift tubes, but the loss of accelerating efficiency caused by penetration of the rf fields into the bore region is not improved.

Another solution is to use a lower frequency and to keep the size down by using another type of cavity. In the first section of the high-current linac, the first two drift tubes were mounted on 24-Mc quarter-wave stubs. In Manchester, the prestripper linac is a 25-Mc Sloane-Lawrence accelerator.

These types of accelerators are not suitable for acceleration of ions to high energy because they require more rf power than the Alvarez type. However, the phase bunching is good enough for them to be used as injectors into a linac of the Alvarez type operating at a frequency that is a multiple of the frequency of the low-energy linac. In the high-current linac the main accelerator cavity operated at twice the frequency of the quarter-wave input section. At Manchester the frequency of the poststripper linac will be three times the frequency of the Sloane-Lawrence prestripper linac. The high voltage of the Cockcroft-Walton injector for this machine is only 200 kv, and the energy of the ions at injection into the prestripper cavity is 25 kev/nucleon.

Performance.—The total peak-beam currents during the pulse from the Berkeley and Yale linacs is in the neighborhood of 50 meter μ a for ions² in the boron-to-neon region. For a pulse rate of 15 pulses per second the total-time average beam is 1.7 meter μ a. About half of the total beam can be focused onto a $\frac{1}{8}$ -in.-diameter spot. Because the multiply charged ions must be formed in the ion source rather than in a stripper, and because of the interception of beam by the large number of focusing grids, the beam current from the machine in Kharkov is somewhat smaller. Work on the installation of a stripper and alternating-gradient focusing on this machine is under way.

Although ions as heavy as argon can be accelerated in the Berkeley and Yale machines, the beam current is lower by a factor of 50 than it is for ions in the boron-to-neon region. The reasons are that the yield of the A^{+6} ions required from the ion source is smaller than the yield of the doubly and triply charged lighter ions and that the velocity at the stripper is too low to strip a large fraction of the argon ions to the +12 charge state required for acceleration in the poststripper linac. Stripping at a higher velocity in these machines would increase the beam interception on the focusing grids in the prestripper linac and result in smaller beams of the lighter ions.

FUTURE POSSIBILITIES

Variable energy.—The tandem Van de Graaff accelerators already offer variable-energy beams in the lower energy region. Cyclotrons that produce variable-energy external beams of light ions have been in operation for several years and the application of the same principles to heavy-ion cyclotrons seems straightforward. It is possible to vary the energy of a linac in discrete steps by dividing it into several separate cavities and turning off the rf power in one or more of the cavities at the output end. In the last cavity of the linac at Manchester, it is planned to install a movable diaphragm that will cut off the rf field in the output end of the cavity. This system will allow variation of the energy in steps equal to the energy gain in one accelerating gap or about 200 kev/A. A similar proposal is being studied at Berkeley.

Higher currents.—External beam currents of 2 μ a of 28-Mev N^{+3} ions have been obtained from the 63-inch cyclotron at Oak Ridge. Similar currents at higher energies should be obtained from the larger cyclotrons that

are being built. Larger currents could be obtained from a cyclotron by accelerating ions with a lower charge, but for high energies the size of the magnet required makes this approach unattractive.

The Livermore high-current linac was not pulsed, and produced time-average beam currents of 200 ma of 0.5-Mev protons (67).⁵ Although beam currents of heavy ions as large as this do not appear practical with the present technology, the average beam currents from the Berkeley and Yale machines could be increased by a factor of 30 by supplying enough rf power to operate them constant-wave. Experience with alternating-gradient linacs obtained during the last few years indicates that it would be possible to put quadrupole magnets in the prestripper cavities of these machines. Elimination of beam loss on the grids should increase the beam transmitted by a factor of about six. Use of higher-voltage dc injectors for linacs, and further exploitation of the techniques of low-velocity rf acceleration used in the high-current linac, would lower the e/m required of the ions from the source and give increased beam currents, especially of ions heavier than neon. These techniques could also be used to accelerate ions that are heavier than argon.

Higher energies.—Acceleration of heavy ions to energies higher than 10 Mev/A in a cyclotron involves the use of a very large and expensive magnet. The extension of linear accelerators to energies of 20 to 30 Mev/A appears straightforward. Above these energies, the linacs become too long and the rf power consumption too high to be very attractive, although use of linac cavities of the Alvarez design appears possible for energies up to a few hundred Mev/A.

The use of a linac to inject fully stripped heavy ions into a cyclotron or synchrotron has been suggested by Tobias (65). The feasibility of building a synchrotron to accelerate heavy ions to energies in the region of 125 Mev/A for use in biophysical research is being studied at Berkeley.

⁵ When protons were accelerated to the full energy of 3.7 Mev, it was necessary to limit the beam current to 30 ma to avoid exceeding the maximum power dissipation on the target of 30 kw/in.² (68).

LITERATURE CITED

1. Judd, D. L., *Ann. Rev. Nuclear Sci.*, **8**, 181 (1958)
2. Alvarez, L. W., *Phys. Rev.*, **58**, 192 (1940)
3. Miller, J. F., Hamilton, J. G., Putnam, T. M., Haymond, H. R., and Rossi, G. B., *Phys. Rev.*, **80**, 486 (1950)
4. Ghiorso, A. Thompson, S. G., Street, K., Jr., and Seaborg, G. T., *Phys. Rev.*, **81**, 154 (1951)
5. Breit, G., Hull, M. H., Jr., and Gluckstern, R. L., *Phys. Rev.*, **87**, 74 (1952)
6. Chou, C. N., Fry, W. F., and Lord, J. J., *Phys. Rev.*, **87**, 671 (1952)
7. Breit, G., *Encyclopedia of Physics*, **XLI/I**, 367-406 (Springer-Verlag, Berlin, Germany, 1959)
8. Flerov, G. N., *Proc. Intern. Conf. Peaceful Uses Atomic Energy*, 2nd, *Geneva*, **14**, 151 (1958)
9. Fremlin, J. H., in Endt, P. M., and Demur, M., Eds., *Nuclear Reactions*, **I**, Chap. III (North Holland Publishing Co., Amsterdam, Netherlands, 502 pp., 1959)
10. Zucker, A., *Ann. Rev. Nuclear Sci.*, **10**, 27 (1960)
11. Zucker, A., Howard, F. T., and Halbert, E., Eds., *Reactions Between Complex Nuclei* (Wiley, New York, N.Y., 319 pp., 1960)
12. Tobias, C. A., and Brustad, T., in Benson, O. O., and Strughold, H., Eds., *Physics and Medicine of the Atmosphere and Space*, 193-207 (Wiley, New York, N. Y., 1960)
13. York, H., Hildebrand, R., Putnam, T., and Hamilton, J. G., *Phys. Rev.*, **70**, 446 (1946)
14. Bolotin, L. I., Revutskij, E. I., Chernyak, L. L., Bomko, V. A., Kulygin, Y. F., Ovsyannikov, V. M., and Suprunenko, V. A., *Proc. Intern. Conf. High-Energy Accelerators and Instrumentation*, 643, 644 (CERN, Geneva, 1959)
15. Morozov, P. M., Makov, B. N., and Ioffe, M. S., *Soviet J. Atomic Energy*, **2**, 327 (1957) (Transl., Consultants Bureau Inc., New York, N.Y.)
- 15a. Papineau, A., Benezech, P., and Mailard, R., *J. phys., radium*, **21**, 410 (1960)
16. Jones, R. J., and Zucker, A., *Rev. Sci. Instr.*, **25**, 562 (1954)
17. Anderson, C. E., and Ehlers, K. W., *Rev. Sci. Instr.*, **27**, 809 (1956)
18. Reynolds, H. L., and Zucker, A., *Rev. Sci. Instr.*, **26**, 894 (1955)
19. Gow, J. D., and Foster, J. S., Jr., *Rev. Sci. Instr.*, **24**, 606 (1953)
20. von Ardenne, M., *Atomkernenergie*, **4**, 121 (1956)
21. Anderson, C. E., in Zucker, A., Howard, F. T., and Halbert, E., Eds., *Reactions Between Complex Nuclei*, 67-76 (Wiley, New York, N. Y., 315 pp., 1960)
22. Cornides, I., Roósz, J., and Siegler, A., *Nuclear Instr.*, **1**, 94 (1957)
23. Norbeck, E., Jr., *Phys. Rev.*, **105**, 204 (1957)
24. Hubbard, E. L., and Lauer, E. J., *Phys. Rev.*, **98**, 1814 (1955)
25. Bohr, N., *Kgl. Danske Videnskab. Selskab, Mat.-fys. Medd.*, **18**, No. 8 (1948)
26. Brunings, J. H., Knipp, J., and Teller, E., *Phys. Rev.*, **60**, 657 (1941)
27. Papineau, A., *Compt. rend.*, **242**, 2933 (1956)
28. Heckman, H. H., Hubbard, E. L., Perkins, B. L., and Simon, W. G., *Bull. Am. Phys. Soc. [II]*, **4**, 367 (1959)
29. Nikolaev, V. S., Dmitriev, I. S., Fateeva, L. N., and Teplova, Ia. A., *Soviet Phys. JETP*, **6** (33), 1019 (1958)
30. Lassen, N. O., *Kgl. Danske Videnskab. Selskab, Mat.-fys. Medd.*, **26**, No. 12 (1951)
31. Bohr, N., and Lindhard, J., *Kgl. Danske Videnskab. Selskab, Mat.-fys. Medd.*, **28**, No. 7 (1954)
32. Reynolds, H. L., Wyly, L. D., and Zucker, A., *Phys. Rev.*, **98**, 1825 (1955)
33. Nikolaev, V. S., Fateeva, L. N., Dmitriev, I. S., and Teplova, Ia. A., *Soviet Phys. JETP*, **6** (33), 239 (1958)
34. Gluckstern, R. L., *Phys. Rev.*, **98**, 1817 (1955)
35. Bashkin, S., and Goldhaber, G., *Rev. Sci. Instr.*, **22**, 112 (1951)
36. Hauser, U., and Kerler, W., *Rev. Sci. Instr.*, **29**, 380 (1958)
37. Dearnaley, G., *Rev. Sci. Instr.*, **31**, 197 (1960)
38. Bittner, J. W., *Rev. Sci. Instr.*, **25**, 1058 (1954)
39. Geller, R., and Prevot, F., *Compt. rend.*, **238**, 1578 (1954)
40. Beringer, R., and Rall, W., *Rev. Sci. Instr.*, **28**, 77 (1957)

41. Bennett, W. H., *Rev. Sci. Instr.*, **24**, 915 (1953)
42. Alvarez, L. W., *Rev. Sci. Instr.*, **22**, 705 (1951)
43. Danforth, J. L., *Can. Electron. Engr.*, **2**, 18 (1958)
44. Allen, K. W., Jilian, F. A., Allen, D. W., Pyrah, A. E., and Blears, J., *Nature*, **184**, 303 (1959)
45. Weinman, J. A., and Cameron, J. R., *Rev. Sci. Instr.*, **27**, 288 (1956)
46. Fogel, Ia. M., Koval, A. G., and Timofeev, A. D., *Soviet J. Atomic Energy*, **5**, 1518 (1958) (Transl., Consultants Bureau, Inc., New York, N. Y.)
47. Collins, L. E., and Riviere, A. C., *Nuclear Instr.*, **4**, 121 (1959)
48. Tobias, C. A., *High Energy Carbon Particles* (Ph.D. thesis, Univ. Calif., Berkeley, 1940)
49. Tobias, C. A., and Segrè, E., *Phys. Rev.*, **70**, 89 (1946)
50. Condit, R., *Phys. Rev.*, **62**, 301 (1942)
51. Condit, R. I., *A Cloud Chamber Study of Heavy Particles Accelerated in the Cyclotron* (Ph.D. thesis, Univ. Calif., Berkeley, 1942)
52. Miller, J. F., *Reactions of Fast Carbon Nuclei in Photographic Emulsions* (Univ. Calif. Rad. Lab., Berkeley, Calif., Rept. UCRL-1902, 258 pp., 1952)
53. Walker, D., and Fremlin, J. H., *Nature*, **171**, 189 (1953)
54. Walker, D., Fremlin, J. H., Link, W. T., and Stephens, K. G., *Brit. J. Appl. Phys.*, **5**, 157 (1954)
55. Atterling, H., *Arkiv Fysik*, **7**, 503 (1954)
56. Debraine, P., *L'Onde Électrique*, **35**, 1048 (1955)
57. Rossi, G. B., Jones, W. B., Hollander, J. M., and Hamilton, J. G., *Phys. Rev.*, **93**, 256 (1954)
58. Alkhazov, D. G., Andreyev, D. S., Greenberg, A. P., and Lemberg, I. Kh., *Nuclear Phys.*, **2**, 65 (1956)
59. Livingston, R. S., *Nature*, **173**, 54 (1954)
60. Lemberg, I. Kh., in Zucker, A., Howard, F. T., and Halbert, E., Eds., *Reactions Between Complex Nuclei*, 112-26 (Wiley, New York, N. Y., 315 pp., 1960)
61. Howard, F. T., Ed., *Sector-Focused Cyclotrons* (Publ. 656, Natl. Acad. Sci.—Natl. Research Council, Washington, D. C., 310 pp., 1959)
62. Alvarez, L. W., Bradner, H., Franck, J. V., Gordon, H. S., Gow, J. D., Marshall, L. C., Oppenheimer, F., Panofsky, W. K. H., Richman, C., and Woodyard, J. R., *Rev. Sci. Instr.*, **26**, 111 (1955)
63. Hubbard, E. L., Baker, W. R., Ehlers, K. W., Gordon, H. S., Main, R. M., Norris, N. J., Peters, R., Smith, L., Van Atta, C. M., Voelker, F., Anderson, C. E., Beringer, R., Gluckstern, R. L., Knox, W. J., Malkin, M. S., Quinnton, A. R., Schwarcz, L., and Wheeler, G. W., *Rev. Sci. Instr.* (To be published)
64. Lawrence, E. O., *Science*, **122**, 1127 (1955)
65. Tobias, C. A., *Phys. Rev.*, **85**, 764 (1952)
66. Carter, E. B., and Davis, R. H., *Bull. Am. Phys. Soc.* [II], **6**, 253 (1961)
67. Clark, A. F., Jopson, R. C., Lamb, W. A. S., Smith, L., and Van Atta, C. M., *High Current Linear Accelerators* (Lawrence Rad. Lab., Livermore, Calif., Rept. UCRL-3057, 5 pp., 1955)
68. Chupp, E. L., Clark, A. F., DuMond, J. W. M., Gordon, F. J., and Mark, H., *Phys. Rev.*, **107**, 745 (1957)

ISOTOPE EFFECTS IN CHEMICAL REACTIONS¹

BY RALPH E. WESTON, JR.²

*Chemistry Department, Brookhaven National Laboratory,
Upton, Long Island, New York*

The isotope effects to be discussed in this article are those which result from differences in atomic masses, with a subsequent alteration of molecular partition functions. For a chemical system at equilibrium, the framework for the theory of such effects is provided by statistical thermodynamics. This is the procedure by which microscopic properties of individual molecules (vibrational force constants, molecular configurations, and atomic masses) can be converted to macroscopic properties of the system (free energy, entropy, etc.). The feasibility of making such a computation depends on the availability and accuracy of molecular data; the shortcomings of the latter make the experimental study of isotopic systems at equilibrium a subject of continuing interest. In particular, the statistical thermodynamics of systems with strong intermolecular interactions, i.e., condensed phases, is in a far from satisfactory state. It is in this region that one may expect to see the most active interest in equilibrium isotope effects.

The extension of statistical mechanical methods to chemically reacting systems has been made through the transition state method, which is a quasi-equilibrium approach to the problem. The principles are the same as those of the equilibrium case; the application of these is more difficult since it requires a knowledge of "molecular" properties of that elusive beast, the activated complex. Influenced by this fundamental difficulty, as well as by differences in scientific taste, work on kinetic isotope effects lies somewhere between two extremes. At one end of the spectrum is the work in which such effects are used in a qualitative way to aid in the elucidation of a reaction mechanism; at the other end is the type of study in which a detailed knowledge of a transition state is sought.

The most recent review article with this same title to appear in the *Annual Review of Nuclear Science* was published in 1953, and the last general review included in the *Annual Review of Physical Chemistry* appeared in 1956. Obviously the above title is more all-inclusive than it deserves to be, and I have had to restrict the scope of the review to some particular aspects. Fortunately, some recent reviews have appeared which help to fill the remaining gap. Numerous examples of isotope effect studies continue to appear in the *Annual Review of Physical Chemistry*, particularly in chapters on reaction kinetics. An excellent compilation of deuterium isotope effects appeared

¹ Literature through December 1960 was surveyed for this review.

² The preparation of this review was carried out in part under the auspices of the United States Atomic Energy Commission, and in part while the author was a visiting scientist at the Service des Isotopes Stables, Centre d'Études Nucléaires de Saclay, Gif-sur-Yvette (Seine-et-Oise), France.

in 1955 [Wiberg (1)], and I have tried to avoid duplicating this. A critical appraisal of both theoretical and experimental aspects of kinetic effects has appeared fairly recently [Bigeleisen & Wolfsberg (2)]. These authors stress particularly the relation between kinetic isotope effects and the transition state theory, and the accurate prediction of rate constants. A complementary approach is taken by Melander in his recent book (3), since he is more interested in the application of such effects to the study of reaction mechanisms. This has the distinction of being the first book on the subject of kinetic isotope effects; in addition, it presents the theoretical background in an admirably clear and comprehensible style.

Finally, a word of apology to both the neglected authors and readers for the large range of interesting topics which has not been included—isotope exchange systems (both kinetic and equilibrium measurements), many examples of primary isotope effects, isotope separation methods, isotopic geochemistry—any one of which demands a review article of its own.

SECONDARY ISOTOPE EFFECTS

An increase in the utilization of an experimental method invariably stimulates interest in the more subtle aspects of the technique. Thus, in the field of isotope chemistry, secondary effects of isotopic substitution have attracted increasing attention during the past few years. In a primary effect, a bond involving the isotopic substituent is broken during the reaction; in a secondary effect, this bond remains intact. Secondary effects are generally smaller than primary ones, but in principle they should be calculable on the basis of the theory developed by Bigeleisen, which permits the a priori calculation of an equilibrium or kinetic isotope effect provided all the necessary vibrational frequencies are known [cf., for example, Bigeleisen & Wolfsberg (2)]. This ideal situation is seldom attained, and one resorts to approximations in the nature of educated guesses. This becomes particularly difficult when small effects are concerned; in particular, anharmonicity corrections may make significant contributions when hydrogen isotopes are involved.

Wolfsberg (4) has made some interesting calculations for model systems in order to estimate a lower limit for secondary deuterium isotope effects. He has calculated partition function ratios for ethylene, ethylene- d_4 , and the corresponding hypothetical transition states with the force constant for the carbon-carbon stretching vibration set equal to zero. The force constants involving hydrogen motion were the same for the original molecule and the transition state. He finds a rate constant ratio k_H/k_D of 1.11 to 1.12 at 300°K, corresponding to $\Delta\Delta F^\ddagger$ of 16 cal/mole.³ From a similar calculation for ethane and ethane- d_6 , $\Delta\Delta F^\ddagger$ is 15 cal/mole. This gives some idea of the magnitude of

³ The quantity $\Delta\Delta F^\ddagger$ is defined as $(RT/n)\ln(k_H/k_D)$, where n is the number of deuterium atoms per molecule. This function facilitates the comparison of experimental data obtained at different temperatures and for differing extents of isotopic substitution. At 300° K, with $n=1$, a value of 10 cal/mole for $\Delta\Delta F^\ddagger$ corresponds to k_H/k_D of 1.017. The corresponding function for an equilibrium is $\Delta\Delta F$.

the effect to be expected, if there is no change in the bonding of the hydrogen atoms in going from the ground state to the transition state.

A different point of view has been suggested by Halevi (5), who has proposed that secondary effects result from a difference in the electron-donating capacities of hydrogen and deuterium atoms. Thus, for example, there is a measurable difference between the dipole moments of HCl and DCl (0.003-.007 Debye) or of NH_3 and ND_3 (0.012-.015 Debye). Halevi has shown that this polarity difference can be accounted for by consideration of the change in dipole moment with internuclear distance (6). Because of the anharmonicity of molecular vibrations, isotopic substitution produces small changes in average internuclear distances. A small dipole moment ($<10^{-3}$ Debye) has also been estimated for the HD molecule by Blinder (7).

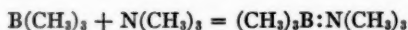
A similar sort of phenomenon has been found in nuclear magnetic resonance spectroscopy, where deuterium substitution produces a small effect on observed chemical shifts [Tiers (8, 9), Kusumoto *et al.* (10)]. This has been explained by Gutowsky (11), again on the basis of a difference in mean internuclear distances resulting from isotopic substitution.

Halevi and co-workers (12, 13), using molecular-orbital wave functions obtained by the method of linear combinations of atomic orbitals, have attempted to calculate the effect of isotopic substitution on ground-state electronic energies for toluene and toluene- α - d_3 , as well as for the ethylcarbonium ion and its methyl-deuterated analogue. They find that the effects of changes in the overlap integrals, and of nonbonding interactions are in opposing directions, so that it is difficult to estimate even the sign of the over-all effect.

If Halevi's approach implies a difference in electronic partition functions, this difference should be extremely small, according to the Born-Oppenheimer approximation [Weston (14)]. More recently, Halevi has suggested a general relation between his inductive-effect model and the more conventional one (15).

Still another point of view has been adopted by Bartell (16), who has suggested that secondary effects are caused by repulsions between nonbonded atoms. These repulsions will change with isotopic substitution and its resulting influence on mean internuclear distances. This is already taken into account as an effect on vibrational frequencies, provided that they are known with sufficient accuracy. It has been proposed that differences in molar volume produced by isotopic substitution can be calculated from amplitudes of vibration; these volume differences will produce a pressure dependence of equilibrium constants for isotope exchange [Joy & Libby (17)].

Secondary isotope effects on equilibrium constants.—The equilibrium constants for the reaction



and the analogous reaction with $\text{B}(\text{CD}_3)_3$ have been determined in the gas phase [Love *et al.* (18)]. The value of $\Delta\Delta F = -17$ cal/mole is explicable if

the vibrational frequencies of the methyl groups on boron are raised in the complex; this is reasonable in view of the change from a trigonal configuration to a more crowded tetrahedral one.

Several dissociation constants of deuterated acids have been compared with those of the normal compounds. For formic acid and formic-*d* acid, two values have been found: $\Delta\Delta F$ is 30 cal/mole [Ropp (19)] or 68 cal/mole [Bell & Jensen (20)]. Halevi & Nussim (21) have found $\Delta\Delta F$ is 31 cal/mole for $C_6H_5CH_2COOH$ compared with $C_6H_5CD_2COOH$; similar values are reported for acetic-*d*₃ acid and the benzyl-*d*₂-ammonium ion [Halevi (15)].

The ionization constants for ion-pair formation from mono-*p*-methyl triphenyl methyl chloride and the corresponding methyl-*d*₃ compound in liquid sulfur dioxide have been determined [Lichtin *et al.* (22)] and are essentially the same. A similar comparison of ionization constants for $(C_6D_5)_3CCl$ and $(C_6H_5)_3CCl$ leads to a value of -7 cal/mole for $\Delta\Delta F$ [Kresge *et al.* (23)]. The direction of this effect is in agreement with observed frequency shifts (particularly in the out-of-plane C—H vibrations).

The formation of carbonium ions in sulfuric acid from diphenylcarbinol, di-*p*-methoxyphenylcarbinol, *p*-chlorobenzaldehyde, and the analogous compounds deuterated in the α position has been studied [Stewart *et al.* (24)]. From the equilibrium constants, values of $\Delta\Delta F$ of 166 cal/mole, 99 cal/mole, and -55 ± 40 cal/mole are obtained. The explanation for this type of effect was first suggested by Streitwieser and co-workers (25) in connection with kinetic experiments. When the bonds around a carbon atom change from a tetrahedral (sp^3) to a trigonal (sp^2) configuration, the major change in the C—H vibrational frequencies is in one of the bending modes. In the trigonal configuration, this is an out-of-plane mode which is lower by about 500 cm^{-1} than the corresponding motion in the tetrahedral configuration. This would lead to an isotope effect with $\Delta\Delta F$ equal to 180 cal/mole. The values cited above for the first two compounds are within this range; for the aldehyde, little change in the bonding is expected upon formation of the carbonium ion.

Halevi & Nussim (26) have found an effect corresponding to a $\Delta\Delta F$ of 14 cal/mole in the formation of complexes between chloranil and toluene- α -*d*₃ or *m*-xylene-*d*₃. A partial comparison of vibrational frequencies leads to a prediction in the opposite direction.

The dissociation constants of the methanol hemiketal of acetone-*d*₆ in dioxane and of the methanol hemiketal of cyclopentanone-2,2,5,5-*d*₄ in methanol have been measured [Jones & Bender (27)]. The effects correspond to $\Delta\Delta F$ of 25 cal/mole for acetone and 61 cal/mole for cyclopentanone. The authors relate them to an increase in hyperconjugation in going from the hemiketal to the ketone; this is in accord with substituent effects previously found for the stability of ketones relative to their cyanohydrin addition complexes.

Effect of isotopic substitution in the α position on rate constants.—Data from the large number of papers dealing with these effects in S_N1 solvolytic

reactions (in which the rate-determining step is the formation of a carbo-nium ion) are summarized in Table I. This type of effect has been exploited considerably in the two years since it was found by Streitwieser and co-workers (25). The explanation has been discussed in the previous section, and it will be noted that the values of $\Delta\Delta F^\ddagger$ in Table I are largely in the

TABLE I
EFFECT OF α -DEUTERIUM SUBSTITUTION IN S_N1 SOLVOLYSES

Substrate	Solvent	$\Delta\Delta F^\ddagger$, cal/mole	Ref
Cyclopentyl- <i>d</i> <i>p</i> -toluenesulfonate	Acetic acid	90	(25)
Cyclopentyl- <i>d</i> <i>p</i> -toluenesulfonate	Acetic acid	103	(28)
Cyclohexyl- <i>d</i> <i>p</i> -toluenesulfonate	Acetic acid	117	(28)
Cyclodecyl- <i>d</i> <i>p</i> -toluenesulfonate	Acetic acid	90	(28)
Cyclopropylmethyl- <i>d</i> ₂ benzenesulfonate	Ethanol	102	(29)
Cyclopropylmethyl- <i>d</i> ₂ benzenesulfonate	Acetic acid	86	(29)
(CH ₃) ₂ CD <i>p</i> -bromobenzenesulfonate	Acetic acid	76	(28)
C ₇ H ₁₅ CDCl(CH ₃)	Methanol	60	(30)
C ₆ H ₅ CH ₂ CD ₂ <i>p</i> -toluenesulfonate	Formic acid	59	(31)
C ₆ H ₅ CH ₂ CD ₂ <i>p</i> -toluenesulfonate	Acetic acid	12	(31)
C ₆ H ₅ CH ₂ CD ₂ <i>p</i> -toluenesulfonate	Acetic acid	55	(28)
C ₆ H ₅ CHD <i>p</i> -toluenesulfonate	Acetic acid	72	(28)
C ₆ H ₅ CD ₂ <i>p</i> -toluenesulfonate	Acetic acid	71	(28)
(C ₆ H ₅) ₂ CHCD ₂ <i>p</i> -toluenesulfonate	Acetic and formic acids	66	(32)
<i>p</i> -MeOC ₆ H ₄ CH ₂ CD ₂ <i>p</i> -toluenesulfonate	Acetic and formic acids	58	(32)
<i>p</i> -MeC ₆ H ₄ CDCl(CH ₃)	Aq. acetone	69	(33)

range of 55 to 80 cal/mole. This relative constancy is to be expected if the proposed explanation is correct and if the substituent groups have little effect on the C—H bending frequencies. The effects are consistently larger for the reactions involving cycloalkyl groups, but there is no obvious reason for this.

In the case of S_N2 solvolyses, where both the incoming nucleophilic agent and the leaving group are included in the transition state, the effects are relatively small and often inverse ($k_H < k_D$). Johnson & Lewis (30) have suggested that the decrease in $\Delta\Delta F^\ddagger$ with increasing S_N2 character results from a steric effect of entering and leaving groups, which raises C—H bending frequencies in the transition state.

For series of methyl-*d*₃ compounds hydrolyzing in water, values of -6 to -32 cal/mole were found for $\Delta\Delta F^\ddagger$ [Llewellyn, Robertson & Scott (34)]. Robertson and co-workers (35) have also measured α effects for ethyl-*d*₂ (-12 to 12 cal/mole), isopropyl-*d* (32 – 75 cal/mole), and *n*-propyl-*d*₂ (-6 to 12 cal/mole) compounds undergoing hydrolysis. Steric effects arising

from nonbonded interactions appear to be the best explanation for these observations.

Other related reactions include the reaction of methoxide ion with methyl- d_3 *p*-bromobenzenesulfonate, with an effect of -8 cal/mole (30), and the reaction of ethoxide ion with isopropyl- d bromide with no measurable effect [Shiner (36)].

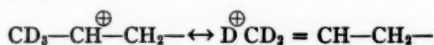
Since a normal ($k_H > k_D$) α -deuterium effect is found when there is a change from sp^3 to sp^2 in the carbon bond hybridization, an inverse effect should be found when the hybridization change is in the opposite direction. This has been confirmed by Seltzer (37), who found a $\Delta\Delta F^\ddagger$ of -43 cal/mole in the isomerization of maleic- d_2 acid catalyzed by thiocyanate ion. The transition state presumably involves bond formation to the ion with simultaneous reduction in the bond order of the carbon-carbon bond. Similar effects ($\Delta\Delta F^\ddagger$ ranging from -14 to -53 cal/mole) were found in several additions to the double bond in $C_6H_5CD:CD_2C_6H_5$ [Denney & Tunkel (38)]. Conversely, in the bromination of biphenyl-4,4'- d_2 , a normal effect of 41 cal/mole has been found [Berliner & Schueller (39)]; in the bromination of benzene- d_6 , no effect at all is found [De la Mare *et al.* (40)]. These last two reactions are examples of electrophilic substitution, in which the rate-determining step is the formation of an intermediate. The resultant change in hybridization from sp^2 to sp^3 for one of the ring carbon atoms should favor an inverse effect.

The rates of reaction of aniline-N,N- d_2 , aniline-2,4,6- d_3 , and aniline-2,4,6-N,N- d_8 with benzoyl chloride have been measured [Elliott & Mason (41)]. The effects of -45 , -15 , and -25 cal/mole were explained by an increase in both N—H and C—H frequencies upon quaternization of aniline. The quaternization of pyridine with methyl- t iodide is a similar example; in this case, k_H/k_T is 0.96 [Simon & Palm (42)]. The same authors report a value of k_H/k_T of 1.12 for the esterification of CH_2TOH with *p*-nitrobenzoyl-chloride, and k_{12}/k_{14} is 1.00 for the same reaction involving $^{14}CH_3OH$. While the mass of the methyl group is the same in both cases, there is no reason to expect the isotope effects to be equal. The formation of phenylhydrazones between β -naphthaldehyde- t and phenylhydrazine or *p*-nitrophenylhydrazine gave relative rates (k_H/k_T) of 0.77 and 0.78; in the corresponding reaction between 3-phenylpropionaldehyde-1- t and *p*-nitrophenylhydrazine, a normal isotope effect ($k_H/k_T = 1.12$) was found [Simon & Palm (43)]. There is no evident explanation for the difference in sign in these two cases.

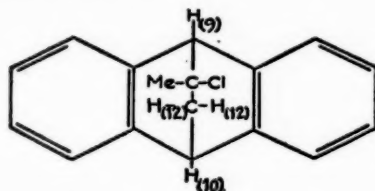
In the hydration of acetaldehyde- d , Pocker (44) has found that $\Delta\Delta F^\ddagger$ is -11 cal/mole. The direction is reasonable, since the slow step is believed to involve a change in the carbon bond configuration from trigonal to tetrahedral.

Secondary effects from isotopic substitution farther from the reaction center.—The secondary deuterium effects which first attracted attention were found in S_N1 solvolyses of compounds substituted in the β position [Shiner (45), Lewis & Boozer (46)]. The generally accepted interpretation invokes

the effect of hyperconjugation in stabilizing the transition state, which resembles a carbonium ion; e.g.,



It is assumed that the no-bond resonance contributions will lead to a decrease in C—H force constants, so that a normal isotope effect is to be expected. The evidence for this interpretation has been summarized by Lewis (47) and by Shiner (48). Thus, substituent effects that parallel the expected contributions from hyperconjugation are found, isotope effects are transmitted across aromatic systems from the para position, and steric effects are important. A striking example of the latter is given by the substituted 9,10-dihydro-9,10-ethanoanthracene:



When both H_{12} 's are substituted by deuterium, a normal effect of 46 cal/mole is observed in the solvolysis, but no effect is found when H_9 and H_{10} are substituted [Shiner (49)]. In the latter case, hyperconjugation involving the bridgehead carbon is essentially ruled out by steric considerations. The data in Table II also show that there are solvent influences, which tend to obscure the comparison of isotope effects in different systems.

Further evidence for the hyperconjugation argument concerns the decomposition of *p*-toluene- α,α,α - d_3 -diazonium fluoborate [Lewis *et al.* (55)]. The observed effect is very small (−2.5 cal/mole), but in the expected direction, since the ground state can be stabilized by hyperconjugation, while symmetry considerations prohibit this in the carbonium ion produced in the slow step.

In the base-catalyzed hydrolysis of ethyl acetate- d_3 an inverse effect of −22 cal/mole has been found [Bender & Feng (56)]. This is understandable in view of other evidence that hyperconjugation is less important for tetrahedrally-bonded than for trigonally-bonded carbon, together with the formation of a tetrahedral intermediate in the rate-determining step of the hydrolysis. Similar arguments apply to the hydration of acetaldehyde-2,2,2- d_3 , with $\Delta\Delta F^\ddagger$ of −12 cal/mole [Pocker (44)]. The inverse of this situation is exemplified by the decomposition of diacetone alcohol to acetone; here the effect is 10 cal/mole [Pocker (57)]. However, for the basic hydrolysis of methyl *p*-methyl-*t*-benzoate, an effect in the normal direction was observed, with k_H/k_T equal to 1.05 [Hodnett *et al.* (58)]. No effect was found for the acid hydrolysis of the same compound, which proceeds through a quite different intermediate.

TABLE II
EFFECT OF β - AND γ -DEUTERIUM SUBSTITUTION IN S_N1 SOLVOLYSES

Substrate	Solvent	$\Delta\Delta F^\ddagger$, cal/mole	Ref
$\text{CH}_3\text{CD}_2\text{CCl}(\text{CH}_3)_2$	Aq. ethanol	110	(45)
$\text{CH}_3\text{CH}_2\text{CCl}(\text{CD}_3)_2$	Aq. ethanol	58	(45)
$\text{CH}_3\text{CD}_2\text{CCl}(\text{CD}_3)_2$	Aq. ethanol	64	(45)
$\text{CH}_3\text{CH}_2\text{CD}_2\text{CHBrCD}_3$	Formic acid	56	(50)
$\text{CH}_3\text{CH}_2\text{CD}_2\text{CH}(\text{p-toluenesulfonate})\text{CD}_3$	Aq. ethanol	51	(50)
$\text{CH}_3\text{CH}_2\text{CD}_2\text{CH}(\text{p-toluenesulfonate})\text{CD}_3$	Formic, acetic acids	75	(50)
$(\text{CH}_3)_2\text{CDCCl}(\text{CH}_3)_2$	Aq. ethanol	146	(51)
$\text{CH}_3\text{CH}_2\text{CD}_2\text{CCl}(\text{CH}_3)_2$	Aq. ethanol	93	(48)
$(\text{CH}_3)_2\text{CHCD}_2\text{CCl}(\text{CH}_3)_2$	Aq. ethanol	108	(48)
$(\text{CH}_3)_2\text{CHCH}_2\text{CCl}(\text{CH}_3)\text{CD}_3$	Aq. ethanol	58	(48)
$(\text{CH}_3)_2\text{CCH}_2\text{CCl}(\text{CH}_3)\text{CD}_3$	Aq. ethanol	66	(52)
$(\text{CH}_3)_2\text{CCD}_2\text{CCl}(\text{CH}_3)_2$	Aq. ethanol	23	(52)
$\text{CD}_3\text{C}(\text{OC}_2\text{H}_5)_2\text{CD}_3$	Aq. dioxane	13	(53)
$\text{CD}_3\text{C}(\text{OC}_2\text{H}_5)_2\text{CD}_2\text{CH}_3$	Aq. dioxane	20	(53)
$\text{CD}_3\text{C}(\text{OC}_2\text{H}_5)_2\text{CD}(\text{CH}_3)_2$	Aq. dioxane	23	(53)
$\text{CD}_3\text{C}(\text{OC}_2\text{H}_5)_2\text{CD}_2\text{COC}_6\text{H}_5$	Aq. dioxane	31	(53)
<i>trans</i> -Cyclopentyl-2- <i>d</i> <i>p</i> -toluenesulfonate	Acetic acid	95	(25)
<i>cis</i> -Cyclopentyl-2- <i>d</i> <i>p</i> -toluenesulfonate	Acetic acid	127	(25)
Cyclopentyl-2,2,5,5- <i>d</i> <i>p</i> -toluenesulfonate	Acetic acid	114	(25)
$\text{C}_6\text{H}_5\text{CD}_2\text{CH}_2$ <i>p</i> -toluenesulfonate	Formic acid	0	(31)
$\text{C}_6\text{H}_5\text{CD}_2\text{CH}_2$ <i>p</i> -toluenesulfonate	Acetic acid	18	(31)
<i>p</i> - $\text{CH}_3\text{OC}_6\text{H}_4\text{CD}_2\text{CH}_2$ <i>p</i> -toluenesulfonate	Formic acid	-11	(32)
<i>p</i> - $\text{CH}_3\text{OC}_6\text{H}_4\text{CD}_2\text{CH}_2$ <i>p</i> -toluenesulfonate	Acetic acid	0	(32)
$(\text{C}_6\text{H}_5)_2\text{CDCH}_2$ <i>p</i> -toluenesulfonate	Formic acid	7	(32)
$(\text{C}_6\text{H}_5)_2\text{CDCH}_2$ <i>p</i> -toluenesulfonate	Acetic acid	14	(32)
<i>p</i> - $\text{CH}_3\text{C}_6\text{H}_4\text{CHClCD}_3$	Acetic acid	50	(33)
<i>p</i> - $\text{CH}_3\text{C}_6\text{H}_4\text{CHClCD}_3$	Aq. acetone	35	(33)
<i>p</i> -($\text{CH}_3)_2\text{CDC}_6\text{H}_4\text{CHCl}(\text{C}_6\text{H}_5)$	Aq. acetone*	4	(54)
<i>p</i> - $\text{CD}_3\text{C}_6\text{H}_4\text{CHCl}(\text{C}_6\text{H}_5)$	Aq. acetone*	12	(54)
<i>p</i> - $\text{CH}_3\text{CD}_2\text{C}_6\text{H}_4\text{CHCl}(\text{C}_6\text{H}_5)$	Aq. acetone*	7	(54)
<i>p</i> -($\text{CH}_3)_2\text{CHCD}_2\text{C}_6\text{H}_4\text{CHCl}(\text{C}_6\text{H}_5)$	Aq. acetone*	6	(54)
<i>p</i> - $\text{CD}_3\text{C}_6\text{H}_4\text{CHClCH}_3$	Aq. acetone*	2	(33)
<i>m</i> - $\text{CD}_3\text{C}_6\text{H}_4\text{CHClCH}_3$	Aq. acetone*	-3	(33)
<i>p</i> - $\text{CHD}_2\text{C}_6\text{H}_4\text{CHClCH}_3$	Acetic acid	27	(33)

* For other solvents, see original paper.

A small but experimentally significant secondary effect caused by ^{14}C substitution has been found in the reaction of phenylmethyl- ^{14}C ketone with 2,4-dinitrophenylhydrazine [Raaen *et al.* (59)]. The rate ratio k^{14}/k^{12} is $1.0085 \pm .0004$ and can be explained if hyperconjugation is important in the transition state relative to the ground state. The hyperconjugative resonance forms which lead to a weakening of a C—H bond also lead to a strengthening of a C—C bond. It would be worth investigating other reactions to see if there is an inverse correlation between hydrogen and carbon isotope effects.

Boozer and co-workers (60) have used secondary isotope effects in a study of the air oxidation of deuterated cumene to see if the mechanism involves a radical intermediate stabilized by hyperconjugation. The isotope effect on the chain termination step was separated out by the addition of inhibitors, and in this way values of 13–74 cal/mole were found for $\Delta\Delta F^\ddagger$. Hyperconjugation has also been cited as responsible for an effect observed in the acid hydrolysis of $\text{Co}(\text{ND}_3)_6\text{Cl}^+$ and $\text{Co}(\text{NH}_3)_6\text{Cl}^+$; $\Delta\Delta F^\ddagger$ is 9 cal/mole [Pearson *et al.* (61)].

The rates of the acid- and base-catalyzed enolizations of cyclopentyl-2,2,5,5- d_4 phenyl ketone and the acid-catalyzed reaction of cyclohexyl-2,2,6,6- d_4 phenyl ketone have been determined [Emmons & Hawthorne (62)]. The results are: 42 cal/mole for base catalysis of the cyclopentyl ketone, 35 cal/mole for acid catalysis with the same compound, and 62 cal/mole for acid catalysis of the cyclohexyl compound. These effects were explained on the basis of a concerted acid-base attack on the ketone, with a transition state resembling the enol. The results obtained in the base-catalyzed reaction cannot be explained (if hyperconjugation is the cause) if an enolate ion mechanism is followed.

The reader should not be left with the impression that there is no evidence against the importance of hyperconjugation in determining secondary isotope effects. One contrary piece of evidence is the lack of an isotope effect in the ionization of mono-*p*-methyl triphenyl methyl chloride previously mentioned (22); in other work, the substituent effects in such ionizations have been found to parallel those in solvolysis reactions. There is also the case of electrophilic aromatic substitution, in which the carbonium ion intermediate would be expected to be stabilized by hyperconjugative resonance contributions. Nevertheless, no effect was found in the acid-catalyzed tritium exchange between 10 *M* H_2SO_4 and toluene- α,α,α - d_3 [Kresge & Satchell (63)]. On the other hand, a small effect of 12 cal/mole was found for the aromatic hydrogen exchange between the same substrate and trifluoroacetic acid in heavy water [Lauer & Koons (64)]. No effects were found in the nitration or mercuration of the same compound, or in the nitration of toluene- α - t . The bromination of the same compounds gave a $\Delta\Delta F^\ddagger$ value of 15 cal per mole and a $k_{\text{H}}/k_{\text{T}}$ value of 1.05 [Swain *et al.* (65)].

The present status of the importance of hyperconjugation in organic reaction mechanisms is far from clear [cf. *Tetrahedron*, **5**, 105–274 (1959)]. However, a large body of pertinent evidence has been accumulated in the

study of secondary isotope effects, and whatever the fate of hyperconjugation theory may be, it will have to accommodate these facts.

A large number of S_N2 hydrolysis reactions of β - and γ -deuterated compounds have been measured by Leffek, Llewellyn & Robertson (66, 67), with the following results for $\Delta\Delta F^\ddagger$ (in cal/mole):

	Tosylate	Methane-sulfonate	Bromide	Iodide
Ethyl- β - d_3	4	6	8	9
<i>i</i> -Propyl- β - d_3	44	44	32	30
<i>n</i> -Propyl- β - d_3	26	26	20	24
<i>n</i> -Propyl- γ - d_3	-11	-13	-19	-18

These effects parallel to some extent the effects found by these authors for the same compounds substituted in the α position (35). Hyperconjugation apparently still has an important influence, since the effects increase with increasing carbonium ion stability and S_N1 character of the solvolysis. Steric influences are also involved, and the inverse effects for the γ -substituted compounds were explained on that basis.

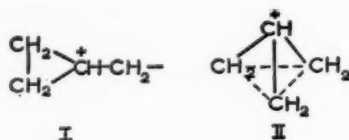
In the reaction of ethoxide ion with isopropyl- d_3 or isopropyl- d_3 bromide, an effect of -12 cal/mole was found [Shiner (36)]. The solvolysis of ethyl- β - d_3 *p*-bromobenzenesulfonate in acetic acid leads to a small effect of 6 cal per mole [Lewis (47)].

Winstein & Takahasi (68) have studied the solvolysis of $(CH_3)_2CDCH(p\text{-toluenesulfonate})CH_3$, which involves a competition between an S_N2 mechanism and an S_N1 mechanism proceeding through a cyclic carbonium ion. The effect for the latter reaction is about twice that for the former.

Very small β effects have been observed for the acetolysis and formolysis of arylethyl tosylates [Saunders *et al.* (31, 32)]. By comparison with the larger α effects, a symmetrical transition state of the type



can be ruled out. A similar comparison between α (Table I) and γ effects (negligible) in the ethanolysis and acetolysis of cyclopropyl- d_4 -methyl benzenesulfonate and cyclopropylmethyl- d_2 benzenesulfonate has given evidence that the intermediate is a carbonium ion of the form (I) rather than (II) [Borčič *et al.* (29)].



An effect of 19 cal/mole was found in the S_N1 hydrolysis of the sulfonium salt $\text{CH}_3\text{CD}_2\text{C}(\text{CD}_3)_2\text{S}(\text{CH}_3)_2\text{I}$, which is considerably smaller than the result obtained with analogous reactions when carbon is at the reaction center [Ašperger & Ilakovac (69)].

A large inverse effect of -53 cal/mole was found in the aqueous hydrolysis of sodium borohydride [Davis *et al.* (70)]. The proposed mechanism involves a transition state similar to BH_3 , with a resultant increase in B—H stretching frequencies (such as that found in B_2H_6 by comparison with BH_4^-).

Lewis (47) reports a value of 0.93 for k_H/k_D (temperature not stated) in the reaction of $\text{Et}_3\text{NCD}_2\text{CH}_3$ with methyl *p*-bromobenzenesulfonate; this effect appears to be related to that found in the reaction of aniline and benzoyl chloride (41).

A very small effect (9 cal/mole) was found in the deoxymercuration of $\text{CH}_3\text{OCD}_2\text{CD}_2\text{HgI}$ ([Kreevoy & Ditsch (71)]; on this basis, a transition state with appreciable resemblance to a carbonium ion is unlikely.

In the gas-phase pyrolysis of ethyl- d_4 and ethyl- d_6 acetates, a very large effect is observed [Blades & Gilderson (72)]; there is probably some contribution from a primary effect. Ethyl acetate- d_3 pyrolyzed at the same rate as the normal compound.

ISOTOPE EFFECTS PRODUCED BY THE USE OF HEAVY WATER AS A SOLVENT

Within the ten-year period following the discovery of deuterium in 1932, a large amount of research was devoted to investigating the solvent properties of heavy water in equilibria and in kinetic systems, in spite of the relative scarcity of heavy water at that time, which made it necessary to carry out many of the experiments on a semi-micro scale. This activity was diverted to more immediate objectives during World War II. Now that heavy water is available in large quantities at a price not much higher than that of some organic solvents, there has been a considerable revival of activity in fundamental studies of solvent properties of heavy water. As such studies are important to an understanding of the solvent properties of water itself, it is surprising to note the large gaps in the data for heavy water. For example, the only accurate measurement of the activity coefficient of an alkali halide in D_2O seems to be that of La Mer & Noonan, made in 1939 (73).

Present theories of the structure of water suffer from the usual difficulties of liquid-state problems, which are increased because of the unusually strong intermolecular forces in this case. These forces produce a quasicrystalline structure with a degree of order between that of ice and that of a more conventional liquid. Properties which reflect the extent of this "structure" indicate a higher degree of order in heavy water than in light water at the same temperature; this can be related to differences in vibrational energies. The interaction of solutes with water can be considered as an effect on its structural properties: nonelectrolytes tend to increase the degree of order, while electrolytes generally have the opposite effect. These effects will be different in magnitude for light and heavy water, so that solubilities, heats of solution,

etc., differ in the two solvents. Since there is less than 1 per cent difference between dielectric constants of H_2O and D_2O , a continuum model is not likely to explain the observed differences.

These ideas have been formulated more explicitly by Swain & Bader (74), who have calculated differences between several thermodynamic functions of H_2O and D_2O . Using essentially an Einstein model for the liquid, they obtained the ratio of partition functions at 25°C ., and the value thus calculated is in excellent agreement with the experimental one. In my opinion, this agreement is partly fortuitous: there is some question about their choice of frequencies for intramolecular and intermolecular vibrations (75, 76). More serious is the neglect of anharmonicity corrections, which are not known for the liquid, but which contribute 35 per cent to the partition function ratio in the gas phase.

Swain & Bader have extended their calculations to a model for ionic solutions, in which an ion is supposed to perturb the librational frequencies of four adjacent water molecules. They correlate observed librational frequencies and differences in heats of solution calculated with this model with experimental differences in heats of solution. The agreement is good, but the infrared bands are extremely broad and weak. At present, there are not sufficient data in the literature to provide an adequate quantitative verification of Swain & Bader's model.

Spectra in light and heavy water.—The electronic absorption spectra of several complexes of transition metal ions have been measured in H_2O and D_2O [Halpern & Harkness (77)]. For ions such as $\text{Cr}(\text{H}_2\text{O})_6^{+++}$, which contain water molecules in the inner coordination sphere, absorption maxima are 30 to 70 cm^{-1} higher in D_2O than in H_2O ; such an effect is not found in ions like $\text{Cr}(\text{C}_2\text{O}_4)_3^{---}$. The authors relate this effect to differences in ligand field splittings caused by the different dipole moments of H_2O and D_2O . An alternate explanation based on a coupling of electronic levels with intermolecular vibrational levels of water molecules has been proposed [Bigeleisen (78)]. A similar shift in electronic absorption bands has been found for $(\text{NH}_3)_5\text{CoOH}_2^{+++}$ (in H_2O) compared with $(\text{ND}_3)_5\text{CoOD}_2^{+++}$ (in D_2O) and for $(\text{NH}_3)_5\text{CoCl}^{++}$ compared with $(\text{ND}_3)_5\text{CoCl}^{++}$ [Taube (79)].

Ultraviolet spectra of H_2O , HDO , and D_2O have been compared [Barrett *et al.* (80), Price *et al.* (81)]. Isotopic varieties of water have been particularly useful for the assignment of vibrational frequencies in both the liquid and solid states [Ceccaldi *et al.* (75), Giguère & Harvey (76), Haas & Hornig (82), Hornig *et al.* (83), Ockman (84)].

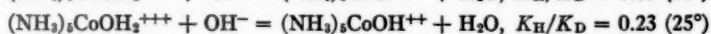
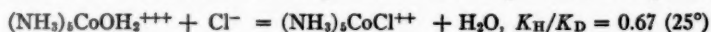
Ionic systems in heavy water.—The effect of dissolved electrolytes on the vapor pressure ratio $P(\text{H}_2\text{O})/P(\text{HDO})$ was investigated by Googin & Smith (85). In all cases, the ratio was lower than it was for water itself.

A number of complex ion systems have been studied in heavy water. Hudis & Dodson (86) measured the rate of the electron transfer reaction between $\text{Fe}(\text{II})$ and $\text{Fe}(\text{III})$, and found the rate lower by a factor of 2 in

heavy water at 7°C while the equilibrium constant for the reaction



is the same in H_2O and D_2O at 21°C. These results were considered to be evidence for the importance of hydrogen atom or ion transfer during the exchange reaction. In the reaction of Cr^{++} with $(\text{NH}_3)_5\text{CrCl}^{++}$, $k_{\text{H}}/k_{\text{D}}$ is 1.37 at 26°C [Ogard & Taube (87)]. Since there is almost certainly no hydrogen transfer in this reaction, the argument of Hudis & Dodson is weakened. An even larger effect is found in the reaction of Cr^{++} with the corresponding aquo complex $(\text{NH}_3)_5\text{CrOH}_2^{+++}$ [Zwickel & Taube (88)]. Taube (79) has also determined the solvent effect on equilibria involving similar complexes:



The difference in the two ratios emphasizes the importance of the internal structure of OH^- in producing the larger effect. Equilibria of this type have also been discussed by Bigeleisen (78).

Rates of hydrolysis of $(\text{NH}_3)_5\text{CoCl}^{++}$ and $(\text{ND}_3)_5\text{CoCl}^{++}$ have been measured in light and heavy water [Pearson *et al.* (61)]. The hydrolysis of the trans- $\text{Co}(\beta\text{-picoline})_4\text{Cl}_2^+$ complex was also studied. Relative rates $k_{\text{H}}/k_{\text{D}}$ of about 1.3–1.4 (49°C) were found for the aquation reaction. This can be explained by effects of the ion on the solvating properties of surrounding molecules, and it does not appear necessary to invoke a mechanism involving differences in hydrogen bonding, which was originally suggested [Adamson & Basolo (89)]. In the case of hydrolysis catalyzed by hydroxyl ion, the rate constant ratio is 1.7 (2.5–18°C). An isotope effect of similar magnitude is reported for the aquation of $(\text{NH}_3)_2\text{Cr}(\text{NCS})_4^-$; $k_{\text{H}}/k_{\text{D}}$ is 1.9 at 60°C [Adamson (90)].

Krishnamurthy & Harris (91) have studied the kinetics of the aquation of trisoxalatochromium (III); the reaction is subject to specific hydrogen-ion catalysis. The rate constant ratio is 0.38 at 50°C, and the applicability of the Gross-Butler expression in H_2O – D_2O mixtures provides further evidence for the mechanism (cf. following section).

The heavy-water solvent effect in the oxidation of Pu (III) by oxygen in aqueous sulfate solutions has been determined [Baker & Newton (92)]. The reaction is 17 to 30 per cent more rapid in H_2O at 23°C; this relatively small effect is evidence that a hydrogen-atom transfer is not involved in the oxidation. In the oxidation of Np (IV) to Np (VI) in sulfate and perchlorate solutions, the rate is higher in light water by a factor of about 5 at 25°C [Hindman *et al.* (93)]. The same authors found a rate ratio of 0.4 for the disproportionation of Np (V) to Np (IV) and Np (VI).

Turning to organic systems, one finds a large body of data concerning $\text{S}_{\text{N}}2$ solvolyses of organic halides, nitrates, sulfonates, etc., obtained by Robertson & Laughton (94, 95, 96). They have varied the organic groups over a wide structural range and have used quite different anionoid groups.

However, in all cases the isotope effect is rather small, with the rate constant in light water about 20 per cent higher than that in heavy water. This effect may be linked to structural changes in the solvating molecules: stronger solvation around the reactant molecule will give a larger zero-point energy difference between H_2O and D_2O than the weakened solvation expected for the transition state, which has more ionic character.

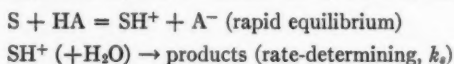
Dissociation of acids and bases in heavy water.—The use of the glass electrode to measure the hydrogen-ion activity in heavy water has been discussed by two groups [Glasoe & Long (97), Mikkelsen & Nielson (98)]. Both groups found that the " pD " in D_2O is given by the value measured with a conventional glass electrode, if a constant factor of 0.40 to 0.44 pH units is added.

Dissociation constant ratios in light and heavy water have been determined for a number of acids: maleic acid, fumaric acid, bimalate ion, bifumarate ion, ethyl hydrogen maleate, and ethyl hydrogen fumarate [Dahlgren & Long (99)]; trifluoroethanol and chloroethanol [Ballinger & Long (100, 101)]; glycine, alanine, phenylalanine, threonine, and glutamic acid [Hyman *et al.* (102)]; the hexaminoplatinum (IV) complex [Pearson *et al.* (61)]; acetaldehyde hydrate, glucose, and tetramethylglucose [Pocker (44, 103)]. The pK_A values for these acids range from 2 to 13, while the ratio of dissociation constants varies from 2 to 5.

Högfelt & Bigeleisen (104) have investigated the behavior of a series of Hammett indicators in solutions of DCl from 10^{-4} to 1 M , and in D_2SO_4 solutions from 10^{-4} to 12 M . The Hammett acidity function in the deuterium systems is the same as that in the corresponding protium systems, except in sulfuric acid of 10^{-3} to 10^{-1} M , a region in which the dissociation of HSO_4^- becomes important. The dissociation constants of the indicators in D_2O , with pK_A values ranging from -5.5 to 3.3 , were determined and compared with those in H_2O : a range of 2 to 4 was found for K_H/K_D . The authors re-examined the frequently used empirical rule relating $pK_A(\text{D}_2\text{O}) - pK_A(\text{H}_2\text{O})$ and $pK_A(\text{H}_2\text{O})$. They find neither theoretical nor experimental justification for this assumption, although there is a small dependence of ΔpK_A on pK_A within a family of similar acids.

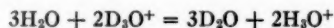
Acid-base catalysis in heavy water.—Because of the influence of heavy water on ionization equilibria, one expects to find kinetic differences in reactions proceeding by acid or base catalysis mechanisms. Long & Bigeleisen (105) have surveyed this situation and have shown that some general predictions can be made on the basis of reasonable assumptions about relative rate and equilibrium constants. In the following discussion, their generalizations will be compared with available data.

For the case of specific hydronium-ion catalysis, the reaction scheme is



The rate constant ratio is $k_H/k_D = (k_{sH}/k_{sD})(K_{SD^+}/K_{SH^+})$ and has values of about 0.3 to 0.4; it differs from unity largely because of the ionization constant ratio.

A frequently used test of specific hydronium-ion catalysis is the effect of solvent deuterium concentration on the rate constant. Because the equilibrium constant L for the reaction



is not unity, the mole fraction of deuterium in the hydronium-ion species will differ from that in the water species. This in turn affects the concentration of protonated substrate in such a way that the rate constant k_N is not a linear function of deuterium concentration N in the solvent. The theory of this effect was derived by Gross and by Butler some 25 years ago and has recently been re-examined by Purlee (106). From electrochemical data, and independently from rate constants and dissociation constants in $\text{H}_2\text{O}-\text{D}_2\text{O}$ mixtures, he finds a value of 11.0 for L , which gives better agreement between experimental data and calculated values of k_N/k_H than did the former value of 15.3. This theory has also been discussed by Swain and co-workers (74, 107) who obtained a value of 8.2 for L from observed vibrational frequencies of water and the hydronium ion. The frequency assignment for the latter is not known with great certainty.

Finally, Purlee's re-examination of the Gross-Butler theory has been re-examined by Gold (108). He finds that values of k_N/k_H are not very sensitive to the choice of L , but depend strongly on the formulation of the solvated proton as H_3O^+ . Also, he finds that k_N/k_H in a reaction with slow proton transfer from a hydronium ion will be similar to that in a reaction with a rapid pre-equilibrium proton transfer. This is a point to be kept in mind when the rest of this section is read.

We now turn to some experimental examples of reactions following specific hydronium ion catalysis mechanisms. In the hydration of 2-methyl-2-butene and of 1-methyl-cyclopentene, the rate ratios are 0.82 (30°C) and 1.08 (35°C) [Purlee & Taft (109)]; both of these are significantly higher than the predicted values. Perhaps this is caused by a primary isotope effect produced when the π -bonded proton forms a normal covalent C—H bond. Both of these reactions were studied in mixed solvents, and the Gross-Butler equation was followed; however, the rate ratio is so nearly unity that the deviation from linearity is scarcely outside experimental error.

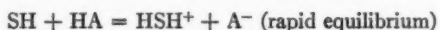
In an extension of studies on aromatic hydrogen exchange reactions, the loss of tritium from *p*-cresol-*o*-*t* to aqueous HCl at 25°C has been measured in light and heavy water [Gold *et al.* (110)]. The rate ratio is 0.62, slightly higher than that predicted for a mechanism involving specific hydronium-ion catalysis. In mixed solvents, the Gross-Butler equation was found applicable. These facts are consistent with a mechanism previously proposed by Gold & Satchell in which an unsymmetrical intermediate is formed in a rapid equilibrium, followed by a slow rearrangement and rapid proton loss to the solvent. On the other hand, the possibility of a slow proton transfer to give a symmetrical intermediate is not ruled out.

Pritchard & Long (111, 112) have studied the hydronium-ion-catalyzed hydrolysis of ethylene oxide, trimethylene oxide, epichlorohydrin, and β -

methylglycidol in H_2O and D_2O . For all of these, the observed rate ratio is near 0.5 at $25^\circ C$, in agreement with the predicted value. Rate measurements in mixed solvents are also in accord with the proposed mechanism. The neutral hydrolyses of propylene oxide and isobutylene oxide were studied by the same authors, and a mechanism involving rapid proton transfer was ruled out by the small isotope effect (k_H/k_D is 1.1–1.2 at $50^\circ C$) and the behavior in mixed solvents.

Kreevoy and co-workers have used heavy water as a tool for investigating deoxymercuration reactions, which are subject to specific hydronium-ion catalysis. For both α - and β -2-methoxycyclohexylmercuric iodide the rate ratio is 0.3 (113). Essentially the same effect was found for 2-methoxy-1-iodomercuriethane at $25^\circ C$, and in addition, the Gross-Butler equation was obeyed (114). For 1-iodomercuri-2-propanol and its methyl ether, rate ratios of 0.45 and 0.35 at $25^\circ C$ were determined (115). In the latter case the agreement with the Gross-Butler curve is somewhat poorer.

A second type of reaction is one involving general acid catalysis, with the mechanism



In this case,

$$k_H/k_D = (k_{sH}/k_{sD})(K_{DSH^+}/K_{HSH^+})(K_{HA}/K_{DA}) \simeq 1.0 \text{ to } 1.5$$

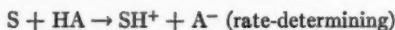
or, if the catalyzing acid is H_3O^+ ,

$$k_H/k_D = (k_{sH}/k_{sD})(K_{DSH^+}/K_{HSH^+}) \simeq 0.3 \text{ to } 0.4$$

(105). Thus the rate ratio is expected to be larger by a factor of ~ 2 to 4 for catalysis by a weak acid compared with catalysis by the hydronium ion. In this type of reaction there may be a hydrogen exchange in the equilibrium, which will lead to a sizable primary isotope effect in the slow proton transfer, and to larger values of the rate constant ratio. This primary effect is probably responsible for the results found for the mutarotation of glucose and tetramethylglucose [Challis *et al.* (116)]. In the case of glucose, rate ratios at $25^\circ C$ for various catalysts are: 1.37 (H_3O^+), 2.6 (CH_3COOH), and 3.2 to 3.8 (H_2O). For tetramethylglucose, values of 1.3 (H_3O^+) and 3.2 (H_2O) were found. [See, however, the discussion of this reaction by Purlee (106).]

Pocker (44) has studied the general acid-catalyzed dehydration of acetaldehyde hydrate, a reaction with a mechanism analogous to that for glucose mutarotation. Rate ratios at $0^\circ C$ for various catalysts are: 1.4 (H_3O^+), 2.8 (CH_3COOH), and 3.9 (H_2O), which are very close to those for the glucose reaction.

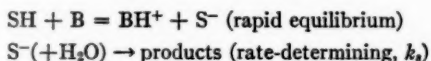
The reverse reaction, the hydration of acetaldehyde, has also been studied by Pocker (44). In this case, the mechanism is a general acid-catalyzed slow proton transfer:



The rate constant ratio will be sensitive to the differences in bonding of hydrogen in the acid HA and in the transition state $S \cdots H \cdots A$, and is difficult to predict. However, Long & Bigeleisen point out that the difference in rate ratios produced by changing HA from a strong to a weak acid will be similar to that found in the rapid pre-equilibrium mechanism. This is confirmed by Pocker's data for k_H/k_D at 0°C: 1.3 (H_3O^+), 2.5 (CH_3COOH), and 3.6 (H_2O).

Another example of general acid catalysis without a pre-equilibrium is found in the hydrolysis of *p*-methoxybenzeneboronic acid to phenylmethyl ether and boric acid [Kuivila & Nahabedian (117)]. The rate constant ratio for catalysis by H_3O^+ is rather large (3.7 at 25°C) and, furthermore, a linear relation between rate and deuterium concentration is observed, contrary to the predictions of Gold. This appears to be the single published case of such a reaction which has been studied in light and heavy water mixtures.

Turning now to base-catalyzed systems, one finds a situation quite analogous to that for acid catalysis. If the mechanism is



the reaction is subject to specific hydroxyl-ion catalysis, and the rate constant ratio is (105)

$$k_H/k_D = (k_{sH}/k_{sD})(K_{SH}/K_{SD})(K_{D_2O}/K_{H_2O}) \simeq 0.5 \text{ to } 0.7$$

Two groups have studied the hydroxyl-ion catalysis of the formation of ethylene oxide from ethylene chlorohydrin [Ballinger & Long (101), Swain *et al.* (118)]. Their results are in excellent agreement, with a k_H/k_D ratio of 0.65 at 25°C; this value is within the predicted range. For propylene chlorohydrin, Ballinger & Long find a rate ratio of 0.63, almost identical. From the measured ratio of acid ionization constants of ethylene chlorohydrin in H_2O and D_2O , the latter authors found that k_{sH}/k_{sD} is 0.87. This small inverse ratio is attributed to a general solvent effect. The rate constant in mixed solvents is not a linear function of the deuterium concentration.

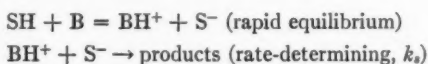
Pocker (57) has used the solvent isotope effect to show that the decomposition of diacetone alcohol to acetone proceeds through a mechanism of the above type, and not through a mechanism involving the slow formation of a carbanion. The rate constant ratio is 0.67 at 25°C, and the Gross-Butler equation is applicable.

The benzylic acid rearrangement in a dioxane-water (H_2O or D_2O) mixture has been investigated by Hine & Haworth, who found a rate constant ratio of 0.54 at 50°C for hydroxyl-ion catalysis (119). This is evidence against a rate-determining step involving the simultaneous shift of a phenyl group and a hydrogen atom, since this step should have a large primary isotope effect.

A different type of mechanism was proposed by Pritchard & Long (112) for the hydroxyl-ion catalysis of the hydrolysis of epoxides. For ethylene

oxide, propylene oxide, and isobutylene oxide, k_H/k_D is in the range 0.88 to 0.96 at 25°C, and the rate is linearly dependent on deuterium concentration. The reaction must involve the slow addition of a hydroxyl ion to the substrate, with a subsequent rapid proton transfer to the resulting anion. The small effect is probably a pure solvent effect.

We consider now the case of general base catalysis involving a rapid equilibrium step, i.e.:



Here the predictions are parallel to those for the analogous case of acid catalysis, with

$$k_H/k_D = (k_{sH}/k_{sD})(K_{HS}/K_{DS})(K_{BD^+}/K_{BH^+})$$

The partial compensation of equilibrium constant ratios will diminish the effect, but there will generally be a normal primary isotope effect in the second step. If the catalyzing base is the hydroxyl ion, the ratio will be

$$k_H/k_D = (k_{sH}/k_{sD})(K_{HS}/K_{DS})(K_{D_2O}/K_HO)$$

so it will be slightly smaller than for a weak base.

In the special case where water is the base,

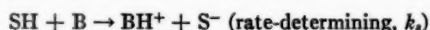
$$k_H/k_D = (k_{sH}/k_{sD})(K_{HS}/K_{DS})$$

so that a large ratio (3 to 5) is predicted. This is confirmed by the analysis Pocker has made of the neutral mutarotation of glucose and tetramethylglucose (103). For the former compound k_H/k_D is 3.8 and for the latter it is 3.2. Pocker has now measured the acid dissociation constants for each compound at 25°C. These can be combined with the observed rates to obtain k_{sH}/k_{sD} , which is 0.85 for glucose and 0.78 for tetramethylglucose.

The base-catalyzed dehydration of acetaldehyde, mechanistically similar to the foregoing reaction, has a rate constant ratio of 2.5 at 0°C for catalysis by acetate ion (44), a large fraction of which is probably due to the primary effect in the slow proton transfer. The neutral reaction has a ratio of 3.9, but it is not possible to separate the acid- and base-catalyzed reaction paths.

There is some disagreement about the interpretation of solvent effects found in the neutral hydrolysis of several acid anhydrides and acyl chlorides, although the experimental agreement is good [Butler & Gold (120, 121), Bunton *et al.* (122)]. The observed effects range from 1.5 to 3.5 for k_H/k_D . Butler & Gold propose a mechanism with two molecules of water and a substrate molecule involved in a rapid equilibrium, followed by a slow proton transfer. The observed rate ratios are thus somewhat below the predicted one, but not unreasonably so. Catalysis by acetate gives a smaller effect, as predicted. The observed effects certainly appear too large to be explained as pure solvent influences, as Bunton and co-workers have done.

The final category of reactions to be considered is the rather large class which involve a slow proton transfer from the substrate to a basic catalyst:



As in the corresponding acid-catalyzed reaction, the rate ratio is sensitive to differences in the bonding of hydrogen in the substrate and in the transition state, and no general prediction is possible.

Returning again to the water-acetaldehyde system (which is unique in exhibiting several mechanisms), one finds that Pocker has determined the rate ratio for acetate-ion catalysis of the hydration; the value is 2.3 at 0°C (44).

In the case of the enolization of acetone (as determined by the rate of bromination), the slow step is the removal of a proton from a methyl group. This is shown by the large isotope effect for acetone- d_6 [Pocker (123)]. For normal acetone, the rate constant ratio is 0.67 at 25°C for hydroxyl-ion catalysis, i.e., OD^- is more effective in removing a proton than is OH^- . The reverse step, transfer of a proton from water to the enolate ion, is about five times faster in H_2O than in D_2O . This latter effect is about the same as the one for relative rates of proton transfer from H_2O and D_2O to the $^-\text{CH}_2\text{CHO}$ carbanion involved in the aldol condensation [Pocker (124)].

For the hydrogen isotope exchange and the racemization of the mandelate ion, a mechanism exactly analogous to that of the enolization of acetone has been found [Pocker (125)]. The solvent effect gives $k_{\text{H}}/k_{\text{D}}$ equal to 0.72 at 100°C, which is close to that for the acetone reaction.

Long & Watson (126) have made a careful study of the enolization of 3-methylpentane-2:4-dione and its 3-deutero analogue in light and heavy water, again by measuring the bromination rate. They did not study the catalysis by hydroxyl ion, but the rate constant ratios (at 25°C) are 1.25 with acetate catalysis, and 1.37 for catalysis by water. They explain this as a solvent influence, but since such an effect would also be present in the corresponding hydroxyl-ion catalysis of acetone enolization, there must be other factors involved.

Finally, it is in order to mention the renaissance now taking place in the study of biological systems in heavy water (and vice versa) with a wide spectrum of research ranging from physical biochemistry to effects on the reproductive capacity of mice. An introduction to this rapidly growing field may be obtained from "Deuterium Isotope Effects in Chemistry and Biology," *Annals of the New York Academy of Sciences*, **84**, 573-781 (1960), edited by Kritchevsky.

LITERATURE CITED

1. Wiberg, K. B., *Chem. Revs.*, **55**, 713 (1955)
2. Bigeleisen, J., and Wolfsberg, M., *Advances in Chemical Physics*, **1**, 15 (Prigogine, I., Ed., Interscience Publishers, Inc., New York, N. Y., 426 pp., 1958)
3. Melander, L., *Isotope Effects in Reaction Rates* (Ronald Press Co., New York, N. Y., 181 pp., 1960)
4. Wolfsberg, M., *J. Chem. Phys.*, **33**, 2 (1960)
5. Halevi, E. A., *Tetrahedron*, **1**, 174 (1957)
6. Halevi, E. A., *Trans. Faraday Soc.*, **54**, 1441 (1958)
7. Blinder, S. M., *J. Chem. Phys.*, **32**, 105 (1960)
8. Tiers, G. V. D., *J. Phys. Chem.*, **64**, 373 (1960)
9. Tiers, G. V. D., *J. Chem. Phys.*, **29**, 963 (1958)
10. Kusumoto, H., Itoh, J., and Hiruta, K., *J. Phys. Soc. Japan*, **15**, 728 (1960)
11. Gutowsky, H. S., *J. Chem. Phys.*, **31**, 1683 (1959)
12. Halevi, E. A., and Pauncz, R., *J. Chem. Soc.*, 1974 (1959)
13. Ron, A., Halevi, E. A., and Pauncz, R., *J. Chem. Soc.*, 630 (1960)
14. Weston, R. E., Jr., *Tetrahedron*, **6**, 31 (1959)
15. Halevi, E. A., *Intern. J. Appl. Radiation and Isotopes*, **7**, 192 (1960)
16. Bartell, L. S., *Tetrahedron Letters*, No. 6, 13 (1960)
17. Joy, H. W., and Libby, W. F., *J. Chem. Phys.*, **33**, 1276 (1960)
18. Love, P., Taft, R. W., Jr., and Wartik, T., *Tetrahedron*, **5**, 116 (1959)
19. Ropp, G. A., *J. Am. Chem. Soc.*, **82**, 4252 (1960)
20. Bell, R. P., and Jensen, M. B., *Proc. Chem. Soc.*, 307 (1960)
21. Halevi, E. A., and Nussim, M., *Bull. Research Council Israel*, **5A**, 263 (1956)
22. Lichtin, N. N., Lewis, E. S., Price, E., and Johnson, R. R., *J. Am. Chem. Soc.*, **81**, 4520 (1959)
23. Kresge, A. J., Rao, K. N., and Lichtin, N. N., *Chem. & Ind. (London)*, 53 (1961)
24. Stewart, R., Gatzke, A. L., Mocek, M., and Yates, K., *Chem. & Ind.*, 331 (1959)
25. Streitwieser, A., Jr., Jagow, R. H., Fahey, R. C., and Suzuki, S., *J. Am. Chem. Soc.*, **80**, 2326 (1958)
26. Halevi, E. A., and Nussim, M., *Tetrahedron*, **5**, 352 (1959)
27. Jones, J. M., and Bender, M. L., *J. Am. Chem. Soc.*, **82**, 6322 (1960)
28. Mislow, K., Borčić, S., and Prelog, V., *Helv. Chim. Acta*, **40**, 2477 (1957)
29. Borčić, S., Nikoletić, M., and Sunko, D. E., *Chem. & Ind. (London)*, 527 (1960)
30. Johnson, R. R., and Lewis, E. S., *Proc. Chem. Soc.*, 52 (1958)
31. Saunders, W. H., Jr., Ašperger, S., and Edison, D. H., *J. Am. Chem. Soc.*, **80**, 2421 (1958)
32. Saunders, W. H., Jr., and Glazer, R., *J. Am. Chem. Soc.*, **82**, 3586 (1960)
33. Lewis, E. S., Johnson, R. R., and Copinger, G. M., *J. Am. Chem. Soc.*, **81**, 3140 (1959)
34. Llewellyn, J. A., Robertson, R. E., and Scott, J. M. W., *Can. J. Chem.*, **38**, 222 (1960)
35. Lefk, K. T., Llewellyn, J. A., and Robertson, R. E., *Can. J. Chem.*, **38**, 1505 (1960)
36. Shiner, V. J., Jr., *J. Am. Chem. Soc.*, **74**, 5285 (1952)
37. Seltzer, S., *Chem. & Ind. (London)*, 1313 (1959)
38. Denney, D. B., and Tunkel, N., *Chem. & Ind.*, 1383 (1959)
39. Berliner, E., and Shueller, K. E., *Chem. & Ind.*, 1444 (1960)
40. De La Mare, P. B., Dunn, T. M., and Harvey, J. T., *J. Chem. Soc.*, 923 (1957)
41. Elliot, J. J., and Mason, S. F., *Chem. & Ind.*, 488 (1959)
42. Simon, H., and Palm, D., *Chem. Ber.*, **92**, 2701 (1959)
43. Simon, H., and Palm, D., *Chem. Ber.*, **93**, 1289 (1960)
44. Pocker, Y., *Proc. Chem. Soc.*, 17 (1960)
45. Shiner, V. J., Jr., *J. Am. Chem. Soc.*, **75**, 2925 (1953)
46. Lewis, E. S., and Boozer, C. E., *J. Am. Chem. Soc.*, **74**, 6306 (1952)
47. Lewis, E. S., *Tetrahedron*, **5**, 143 (1959)
48. Shiner, V. J., Jr., *Tetrahedron*, **5**, 243 (1959)
49. Shiner, V. J., Jr., *J. Am. Chem. Soc.*, **82**, 2655 (1960)
50. Lewis, E. S., and Boozer, C. E., *J. Am. Chem. Soc.*, **76**, 791 (1954)
51. Shiner, V. J., Jr., *J. Am. Chem. Soc.*, **76**, 1603 (1954)
52. Shiner, V. J., Jr., *J. Am. Chem. Soc.*, **78**, 2653 (1956)
53. Shiner, V. J., Jr., and Cross, S., *J. Am. Chem. Soc.*, **79**, 3599 (1957)

54. Shiner, V. J., Jr., and Verbanic, C. J., *J. Am. Chem. Soc.*, **79**, 373 (1957)
55. Lewis, E. S., Kinsey, J. L., and Johnson, R. R., *J. Am. Chem. Soc.*, **78**, 4294 (1956)
56. Bender, M. L., and Feng, M. S., *J. Am. Chem. Soc.*, **82**, 6318 (1960)
57. Pocker, Y., *Chem. & Ind. (London)*, 89 (1959)
58. Hodnett, E. M., Taylor, R. D., Tormo, J. V., and Lewis, R. E., *J. Am. Chem. Soc.*, **81**, 4528 (1959)
59. Raaen, V. F., Tsiomis, A. K., and Collins, C. J., *J. Am. Chem. Soc.*, **82**, 5502 (1960)
60. Boozer, C. E., Ponder, B. W., Trisler, J. C., and Wightman, C. E., III, *J. Am. Chem. Soc.*, **78**, 1506 (1956)
61. Pearson, R. G., Stellwagen, N. C., and Basolo, F., *J. Am. Chem. Soc.*, **82**, 1077 (1960)
62. Emmons, W. D., and Hawthorne, M. F., *J. Am. Chem. Soc.*, **78**, 5593 (1956)
63. Kresge, A. J., and Satchell, D. P. N., *Tetrahedron Letters*, No. 13, 20 (1959)
64. Lauer, W. M., and Koons, C. B., *J. Org. Chem.*, **24**, 1169 (1959)
65. Swain, C. G., Knee, T. E. C., and Kresge, A. J., *J. Am. Chem. Soc.*, **79**, 505 (1957)
66. Leffek, K. T., Llewellyn, J. A., and Robertson, R. E., *Can. J. Chem.*, **38**, 2171 (1960)
67. Leffek, K. T., Llewellyn, J. A., and Robertson, R. E., *J. Am. Chem. Soc.*, **82**, 6315 (1960)
68. Winstein, S., and Takahasi, J., *Tetrahedron*, **2**, 316 (1956)
69. Ašperger, S., and Ilakovac, N., *Chem. & Ind. (London)*, 1191 (1960)
70. Davis, R. E., Kibby, C. L., and Swain, C. G., *J. Am. Chem. Soc.*, **82**, 5950 (1960)
71. Kreevoy, M. M., and Ditsch, L. T., *J. Am. Chem. Soc.*, **82**, 6127 (1960)
72. Blades, A. T., and Gilderson, P. W., *Can. J. Chem.*, **38**, 1407 (1960)
73. La Mer, V. K., and Noonan, E., *J. Am. Chem. Soc.*, **61**, 1487 (1939)
74. Swain, C. G., and Bader, R. F. W., *Tetrahedron*, **10**, 182 (1960)
75. Ceccaldi, M., Goldman, M., and Roth, E., *Colloq. Spectrosc. Intern. VI (Amsterdam, 1956)*, 623 (Pergamon Press, Ltd., London)
76. Giguère, P. A., and Harvey, K. B., *Can. J. Chem.*, **34**, 798 (1956)
77. Halpern, J., and Harkness, A. C., *J. Chem. Phys.*, **31**, 1147 (1959)
78. Bigeleisen, J., *J. Chem. Phys.*, **32**, 1583 (1960)
79. Taube, H., *J. Am. Chem. Soc.*, **82**, 524 (1960)
80. Barrett, J., Mansell, A. L., and Goldring, R. M., *Nature*, **187**, 138 (1960)
81. Price, W. C., Harris, P. V., Beaven, G. H., and Johnson, E. A., *Nature*, **188**, 45 (1960)
82. Haas, C., and Hornig, D. F., *J. Chem. Phys.*, **32**, 1763 (1960)
83. Hornig, D. F., White, H. F., and Reding, F. P., *Spectrochim. Acta*, **12**, 338 (1958)
84. Ockman, N., *Advances in Phys.*, **7**, 199 (1958)
85. Googin, J. M., and Smith, H. A., *J. Phys. Chem.*, **61**, 345 (1957)
86. Hudis, J., and Dodson, R. W., *J. Am. Chem. Soc.*, **78**, 911 (1956)
87. Ogard, A. E., and Taube, H., *J. Am. Chem. Soc.*, **80**, 1084 (1958)
88. Zwickel, A., and Taube, H., *J. Am. Chem. Soc.*, **81**, 1288 (1959)
89. Adamson, A. W., and Basolo, F., *Acta Chem. Scand.*, **9**, 1261 (1955)
90. Adamson, A. W., *J. Am. Chem. Soc.*, **80**, 3183 (1958)
91. Krishnamurty, K. V., and Harris, G. M., *J. Phys. Chem.*, **64**, 346 (1960)
92. Baker, F. B., and Newton, T. W., *J. Phys. Chem.*, **61**, 381 (1957)
93. Hindman, J. C., Sullivan, J. C., and Cohen, D., *J. Am. Chem. Soc.*, **81**, 2316 (1959)
94. Laughton, P. M., and Robertson, R. E., *Can. J. Chem.*, **34**, 1714 (1956)
95. Robertson, R. E., and Laughton, P. M., *Can. J. Chem.*, **35**, 1319 (1957)
96. Laughton, P. M., and Robertson, R. E., *Can. J. Chem.*, **37**, 1491 (1959)
97. Glasoe, P. K., and Long, F. A., *J. Phys. Chem.*, **64**, 188 (1960)
98. Mikkelsen, K., and Nielsen, S. O., *J. Phys. Chem.*, **64**, 632 (1960)
99. Dahlgren, G., and Long, F. A., *J. Am. Chem. Soc.*, **82**, 1303 (1960)
100. Ballinger, P., and Long, F. A., *J. Am. Chem. Soc.*, **81**, 1050 (1959)
101. Ballinger, P., and Long, F. A., *J. Am. Chem. Soc.*, **81**, 2347 (1959)
102. Hyman, H. H., Kaganove, A., and Katz, J. J., *J. Phys. Chem.*, **64**, 1653 (1960)
103. Pocker, Y., *Chem. & Ind. (London)*, 968 (1960)
104. Högfeldt, E., and Bigeleisen, J., *J. Am. Chem. Soc.*, **82**, 15 (1960)

105. Long, F. A., and Bigeleisen, J., *Trans. Faraday Soc.*, **55**, 2077 (1959)
106. Purlee, E. L., *J. Am. Chem. Soc.*, **81**, 263 (1959)
107. Swain, C. G., Bader, R. F. W., and Thornton, E. R., *Tetrahedron*, **10**, 200 (1960)
108. Gold, V., *Trans. Faraday Soc.*, **56**, 255 (1960)
109. Purlee, E. L., and Taft, R. W., Jr., *J. Am. Chem. Soc.*, **78**, 5807 (1956)
110. Gold, V., Lambert, R. W., and Satchell, D. P. N., *J. Chem. Soc.*, 2461 (1960)
111. Pritchard, J. G., and Long, F. A., *J. Am. Chem. Soc.*, **80**, 4162 (1958)
112. Pritchard, J. G., and Long, F. A., *J. Am. Chem. Soc.*, **78**, 6008 (1956)
113. Kreevoy, M. M., and Kowitt, F. R., *J. Am. Chem. Soc.*, **82**, 739 (1960)
114. Kreevoy, M. M., and Ditsch, L. T., *J. Org. Chem.*, **25**, 134 (1960)
115. Kreevoy, M. M., *J. Am. Chem. Soc.*, **81**, 1099 (1959)
116. Challis, B. C., Long, F. A., and Pocker, Y., *J. Chem. Soc.*, 4679 (1957)
117. Kuivila, H. G., and Nahabedian, K. V., *Chem. & Ind.*, 1120 (1959)
118. Swain, C. G., Ketley, A. D., and Bader, R. F. W., *J. Am. Chem. Soc.*, **81**, 2353 (1959)
119. Hine, J., and Haworth, H. W., *J. Am. Chem. Soc.*, **80**, 2274 (1958)
120. Butler, A. R., and Gold, V., *Proc. Chem. Soc.*, 15 (1960)
121. Butler, A. R., and Gold, V., *Chem. & Ind. (London)*, 1218 (1960)
122. Bunton, C. A., Fuller, N., Perry, S. G., and Shiner, V. J., Jr., *Chem. & Ind.*, 1130 (1960)
123. Pocker, Y., *Chem. & Ind.*, 1383 (1959)
124. Pocker, Y., *Chem. & Ind.*, 599 (1959)
125. Pocker, Y., *Chem. & Ind.*, 1117 (1958)
126. Long, F. A., and Watson, D., *J. Chem. Soc.*, 2019 (1958)

INDUSTRIAL USES OF ISOTOPES¹

By W. F. LIBBY

Department of Chemistry, University of California, Los Angeles, California

USES AS ISOTOPES

By isotopes is meant the radioactive and stable nuclides that are of the same element and are distinguishable one from another either by their radioactive radiations or by their mass as measured in the mass spectrometer. In this first section the uses in industry which exist because the isotopes are chemically identical, or nearly identical, with the ordinary nuclides constituting the main part of the element will be discussed.

Nutrition of farm animals.—By the use of radioisotopes, the metabolism of many elements in farm animals can be followed conveniently from their uptake in food in the form of elements and compounds, through their incorporation into various regions of the body, and finally to their degradation and excretion. Tracer techniques are of extreme value in such nutritional studies. For example, an element which occurs in amounts of only a few parts per 100,000,000 parts of feed can be traced from the feed, through the digestive tract, and finally to its location in the tissues of a 1000-pound animal. All this can be done without interference with the normal physiology of the animal.

Many elements are required in small amounts by farm animals. For example, a lack of cobalt in the diet decreases the formation of vitamin B₁₂. Tracer techniques also showed that high levels of molybdenum in cattle feed inhibit synthesis of vitamin B₁₂. Vitamin B₁₂ labeled with cobalt 60 has been used for many types of investigation with farm animals. For example, it is transferred from the body of the cow to its milk during lactation, and the vitamin B₁₂ content of milk may be used as an indication of the status of the cobalt nutrition. Vitamin B₁₂ also is transferred from the hen to the egg; the amount deposited in the egg actually is the principal source for the chick up to several weeks after hatching. Even 12 weeks after hatching, the original vitamin in the egg represents an appreciable part of the total vitamin in the bird.

Sulfur is rapidly metabolized by animals. For example, the milk proteins of goats contained radioactivity within three hours after the goats were fed sodium sulfate labeled with radioactive sulfur 35. Until recently it was thought that chickens could not use sulfur in the form of inorganic sulfate for synthesizing sulfur-containing organic compounds such as the amino acid cystine. Again, with the use of radioactive sulfur, it has been possible to show

¹ The survey of literature pertaining to this review was concluded September 30, 1960.

that both hens and growing chicks can utilize inorganic sulfur. In fact, under certain conditions, the addition of sulfate to certain poultry feed increases the rate of chicken growth. The growth of cattle and sheep on a low-protein diet can be increased by feeding them inorganic sulfur.

Isotope techniques have permitted important practical studies on the absorption and utilization of calcium from feed by farm animals. These studies are complicated by the loss of endogenous calcium from the blood through the intestinal wall into the feces. The availability of radioactive calcium 45 has made such studies much simpler. It has been shown, for example, that the level of endogenous calcium in feces changes appreciably with age, becoming progressively greater in older animals, and that both calves and adult cattle can obtain large amounts of calcium from powdered limestone in the feed. It was found further that calves could absorb and retain significantly more calcium from milk than from hay or grain. Other tracer studies permit livestock feeders to get more efficiency from feed by more careful control of the calcium-phosphorus ratio of the diet and by eliminating high concentrations of materials which adversely affect absorption of these elements.

As indicated in the selected examples, radioactive tracer techniques have been of great importance in studying the mineral nutrition of farm animals. Tracer methods have been perhaps even more important in studying the uptake and metabolism of organic foodstuffs. In the past, most detailed nutritional studies on animals were carried out with small laboratory mammals; large farm animals have not been widely used because of the expense of purified diets. The use of tracer techniques, however, has permitted nutritional studies in livestock as well as in the smaller animals. Studies with tagged compounds have been carried out with vitamin A, the lack of which sometimes produces impaired vision in cattle. Other tracer studies have led to techniques for correcting deficiencies in the amino acid methionine in dry plant livestock feeds by the addition of compounds such as choline and betaine.

Milk production.—A study of the biochemical functions of microorganisms that inhabit the stomachs of grazing animals may result in methods of controlling the chemical composition of milk. Grazing animals that chew their own cud (ruminants) depend for their existence on billions of bacteria and other microbes contained in the rumen (first compartment of the ruminant stomach). These microbes produce materials necessary to the life of ruminant animals. In this way, the tiny organisms are in effect a "fluid tissue" and are just as vital to the animal as the tissues of solid organs, i.e., the heart, liver, and kidneys.

The ruminant is dependent upon a supply of fatty acids for its existence; these acids are the fermentation end-products of carbohydrates taken into the animal system in feed such as hay. Some complex carbohydrates are manufactured and stored by the microbes in the rumen. The complex carbohydrates made by rumen microbes are called polysaccharides and constitute

a reserve source of energy for the microbes. This storage polysaccharide is chemically identical regardless of which species of microbes is involved in its production; and the same end-products, fatty acids, are formed from the storage polysaccharide and from rapidly used external energy materials. This means the ruminant is assured of a continuous supply of the fatty acids upon which it depends.

Once the role of this "fluid tissue" in manufacture of milk components is understood, as well as what the animal system does with products formed by the rumen bacteria, controlling the type of milk produced by the ruminant may be possible. For example, milk low in fat might be obtainable directly from the cow, making unnecessary the mechanical processing to reduce fat content.

Control of end-products formed by the rumen microflora also may result in regulation of the chemical composition of milk. Scientists must first understand what substances go into manufacture of the milk component they want to control, and they must know what substances are produced from the materials that the animal is fed. Then the principle of physiological control might be extended to include regulation of other animal products, such as proteins.

Cattle breeds of temperate areas (such as the Shorthorn) do very poorly in tropical areas. As environmental temperatures approach 80°F, food consumption, milk production, and growth rate begin to fall off, and at 100°F these processes drop to perhaps one-quarter the ordinary values. The thyroid secretory activity of cattle, as studied with radioactive iodine, showed a temperature dependence that paralleled the processes listed above. On the other hand, the thyroid activity of Zebu cattle (a tropical breed) remained the same over a very wide environmental temperature range; also the food consumption and growth of these cattle are essentially independent of temperature. Basic studies of this type may some day permit the raising of high-productivity temperate zone cattle in tropical regions, perhaps as the result of appropriate hormone treatments (1).

Detergent residues on food products.—Detergents are frequently difficult to remove completely, and it is important that the degree of removal be measurable because of possible deleterious effects upon foodstuffs. Alkylbenzene sulfonate labeled with sulfur 35 is used in a typical case. In general, over 98 per cent of the total detergent can be followed in the washing process by using the radioactive sulfur radiation as detected by a Geiger counter, whereas ordinary methods keep track of only 85 per cent, some 15 per cent being lost. All relevant experiences today demonstrate the superiority of the radioisotope tracer method in sensitivity and reliability.

Use of potassium-40 gammas to estimate lean meat content.—A rapid, objective, and nondestructive method using natural potassium-40 radiation for determining the amount of lean meat present in live animals, carcasses, and cuts of meat is of considerable value in improving the pricing efficiency in-

volved in the marketing of livestock and meat. Objective evaluation of the amount of lean meat present makes it possible to set a price that better reflects the desirability of the product (2, 3).

Potassium 40 occurs naturally, so it may be thought to be different from those isotopes which are synthetic and short lived. Potassium 40, with its half life of 1.3 billion years, is left over from the original genesis of the elements. It is naturally present in ordinary potassium at .0119 per cent. Table I, taken from (3), shows the results for various kinds of meat and fat. This application seems to be particularly promising.

TABLE I
K⁴⁰ MEASUREMENTS OF LEAN AND FAT HAM

Sample	Weight (lb.)	K ⁴⁰ (cpm/lb) counting rate	Chemical analysis		
			Water (%)*	Fat (%)*	Lean (%)*,†
100% lean	59.50	44.1 ± 0.6	73.3	5.9	91.8
55% lean	51.00	24.2 ± 0.7	43.5	45.6	52.3
50% lean	58.13	22.5 ± 0.5	39.7	49.5	50.0
45% lean	61.13	21.1 ± 0.5	36.8	53.8	46.9
100% fat	57.56	0.4 ± 0.5	6.1	92.3	7.3
Fat jacket‡	47.31	22.7 ± 0.6	41.3	47.7	53.7
Fat and lean§	58.81	22.5 ± 0.5	42.0	47.1	52.2

* These percentages are by weight. Fat and lean should add up to 100%. They fail to do so only because of experimental error.

† Estimate from nitrogen measurement.

‡ Roll of lean surrounded by roll of fat.

§ Roll of lean end-on to roll of fat.

Isotope dilution.—Isotope dilution can be used with either stable or radioactive isotopes. The procedure involves introduction of a known weight of material with a known amount of radioactivity into a sample of a compound to be assayed. By thorough mixing, the known concentration that was added is diluted by an amount proportional to the unknown amount of material present in the original sample. A small amount of the pure compound is separated and its final concentration of radioactivity determined. It then is possible to calculate the amount of material present in the original sample that produced the change in the specific activity, the concentration of the radioactivity, in the sample.

This method is used quite extensively in a wide variety of problems, for example, in chemical research to determine the amount of six different sulfur-containing compounds in the same mixture. The same technique can be used to determine the volume of liquid in a complex industrial system (4).

Particularly important in the isotope dilution method are the compounds

of radioactive carbon (carbon 14) and tritium (radioactive hydrogen), for from them can be made the radioactive molecules for application of the isotope dilution technique in organic analyses. The synthetic problems may be of considerable difficulty. They have been attacked by the classical method of synthetic organic chemistry, supported by two new techniques—the Wilzbach method of synthesis of tritium compounds by direct exposure to tritium gas (5)—and biosynthesis, the growing of the compounds in radioactive environment. The largest single biosynthesis installation is that at the Argonne National Laboratory (6). The combination of the three techniques mentioned makes it possible to synthesize most organic compounds, at least in a randomly labeled way.

Of course, after biosynthesis, or with any of the three methods, it is necessary to purify and separate out the particular compounds desired. This is usually done by chromatographic methods, either paper or gaseous. These techniques are particularly valuable, since counters can be used to detect the radiation, either on the paper or in the gas stream itself.

Water movement.—The ideal tracer for water is tritium (radioactive hydrogen). It occurs in nature and can be used to detect rain water, since rain water has a tritium concentration derived from the cosmic ray bombardment of the atmosphere and from nuclear weapons tests. After the rain water has stood for twelve years, it loses half its tritium content because of radioactive decay. It thus is possible to tell the age of water in the sense of the time lapse since it fell as rain. In this way the age of underground waters can be measured and their origin and flow patterns studied. The technique will be particularly valuable when it is supplemented with the injection of known amounts of tritium in known localities. This has not been done to any great extent. However, there is considerable information about cosmic ray and bomb tritium in ground, river, and ocean waters (7 to 24), so these can be used for tracer purposes.

USES AS RADIOACTIVE NONISOTOPIC TRACERS

There are many uses of radioactive isotopes that do not take advantage of the fact that the isotopes have the same chemical characteristics as the nonradioactive partner nuclides in the element, but merely use them as radiation sources in tracer applications.

Many applications have been made of isotopes carried in foreign bodies as radiation sources into slurries so that the mechanics of slurry mixing processes can be studied. In particular, this technique has proven useful in controlling and monitoring the operation of catalytic cracking units in oil refineries; radioactive pellets are introduced into the catalyst powder in order to trace its movement (25). The volume of liquid in a closed system may be measured with a radioactive tracer by the dilution method: a known volume of radioactive solution is introduced and allowed to mix (either by circulation or by internal stirring); the tracer concentration is measured after mixing in comparison with the initial concentration of the tracer; the

dilution ratio multiplied by the original volume gives the desired unknown volume (26). Another application of the technique is the Hull total-count method (26), which is based on the principle that the total number of gamma rays registered by a Geiger counter strapped to a pipe through which fluid containing a fixed amount of radioactive isotope is flowing varies inversely with the velocity of the flow. At the same time, the integrated count is independent of the way in which the radioactive intensity varies along the stream as long as it passes at constant speed. This principle, which can be demonstrated mathematically, is valuable in actual practice.

There are many applications of radioactive isotopes as nonisotopic tracers in attrition studies. One of the most celebrated is the use of radioactive engine parts to study wear as first proposed by Ferris (27) in 1943. In 1948, Hull and co-workers (28) showed the way to inexpensive and practical radioactive engine tests by neutron activation of standard piston rings inside a nuclear reactor. This technique has been used to study the influence of fuels, lubricants, and operating variables on engine wear rates. It has also been applied to field tests and ordinary passenger car service using a radioactive ring in the top front cylinder in each car; these tests demonstrate the efficacy of a high detergent-type oil for reducing ring wear in cars. The radioactive ring technique is about fifty times as fast as the weight loss method used before, and the reproducibility of wear rates obtained is much better.

A similar technique has been used in measuring gear wear, using neutron-irradiated gears. Other examples of engine parts that have been irradiated for wear lubricant testing are combustion cylinder liners, ball bearings, and piston-ring rest pins for Diesel locomotives.

The diversion of any fluid stream from one channel to another can be readily detected with radioactive tracers. Sometimes the extent of such a leak can be measured quantitatively. This technique of leak detection has wide applicability.

A significant application of the isotopic tracer technique is to the measurement of the movement of oil in pipelines. When two different stocks are adjacent in a pipeline, the introduction of a gamma-emitting tracer in one of these or at the interface between them allows the position of the interface to be fixed by means of its radioactivity. It is thus possible to distinguish between the two stocks, or rather to locate the interface, and Geiger counters attached to the pipeline can tell when the interface passes. Antimony 124 in the form of triphenylstibine is most widely used for this purpose, but cobalt-60 naphthenate is also used. A millicurie of a radioisotope provides a satisfactory signal in most cases.

Other examples are the determination of the uniformity of mixing of cement, the following of littoral drift using radioactive glass sand, and the full-scale measurements of siltation in estuaries. In the manufacture of paper pulp, wood chips are treated with cooking liquor for a suitable period in digesters, with a forced liquor circulation to ensure uniform treatment. The circulation carries the process heat, and the circulation characteristics thus

are important for the quality of the pulp produced. One tracer used is sodium 24; about 5 mc have been found by experience to be suitable. It is injected into the system as an aqueous solution by means of a simple apparatus, and the activity of the circulating liquor after the injection is recorded continuously at a point in the external part of the circulation system. A series of evenly spaced activity maxima corresponding to each cycle of circulation is found. These peaks broaden increasingly for each cycle, and finally successive peaks start to overlap as the process continues.

Material flow in sponge iron furnaces.—Sponge iron is produced in a continuous process, involving reduction of sintered iron ore concentrate with gas. Because of its high reactivity the sponge iron must be cooled before meeting the open air, and it is therefore collected in closed containers, which are kept closed for several days before opening. The sponge pellets can only be inspected through a small window as they leave the furnace; it is thus difficult to study the transport of single pellets through the furnace and to find the transport rate by, for instance, the addition of colored pellets at different points in the furnace and visual determination of the time of their appearance at the outlet. Radioactive tracer methods have, however, been used successfully for this purpose. Chamotte balls were made of the same size as the iron ore pellets, and small pieces of irradiated platinum-iridium wire were enclosed in the balls. These were added to the charge at different points in the furnace, and the time when they left the furnace was determined with a scintillation detector connected to a recorder. The furnace outlet was connected to the container by a tube. The detector was mounted outside this tube. Experiments had shown that an activity of 100 μc of Ir^{192} gave significant signals to the recorder if the labeled ball was dropped in front of the detector. The pellets were supposed to pass the detector at a constant distance as the tube was not vertical. These balls labeled with different amounts of active material should give different signals. Three balls labelled with 50, 150, and 500 μc Ir^{192} were placed at three different points at one level in the furnace. One ball was placed in the center, one close to the wall, and the third at a point between these two. The balls are unambiguously identified by the different heights of the peaks in the diagram. A certain difference in transport time was found, as expected from the construction of the furnace. The results from several series of investigations indicated, however, that the operation of the furnace showed excellent stability as far as the flow rate of the pellets was concerned and that the rates along different verticals were quite uniform.

Among these various applications, perhaps one of the most underdeveloped at this time is the total-count method for measuring flow. It depends on the principle, as stated above, that a finite amount of radioactivity introduced into a flowing stream and passing a counter gives a number of counts inversely proportional to its flow rate. After measurement of the geometrical factors involved, it is possible to make an absolute measurement of the flow rate (29).

USES AS RADIATION SOURCES FOR GAUGING

Some of the more important uses of isotopes in industry apply the penetrating power and absorbability of the isotopic radiations to measurements of thickness and locations in manufacturing processes. Of all these, probably the most important is the beta thickness gauge.

Beta-particle transmission gauges are used routinely for measurements from 1 to 1200 mg/cm². Several different sources are needed to cover this range adequately. For measuring a particular thickness of material with the best possible accuracy, it is desirable to choose a source of beta particles such that they are at least 50 per cent absorbed in the thickness to be measured. When this is done, since the emergent radiation falls off nearly exponentially with thickness, relatively small changes in thickness result in easily measurable changes in the number of emergent beta particles. The apparent advantages in sensitivity of using beta particles that are heavily absorbed are offset by statistical fluctuations when only a few particles emerge to the detector. Generally, beta particles from a given source can be used successfully for measurements from 0.2 to 4 times the "half thickness" for absorption of the particles, and best results (thickness to about 1%) are obtained at the equivalent of 0.5 to 2 half thicknesses. For low-energy beta particles, the range is further limited by absorption in air between the source and detector, and in the detector window.

Pure beta emitters are preferred as sources, especially for the smaller thicknesses, since the more penetrating gamma rays are only slightly absorbed and reduce the sensitivity of the system to changes in thickness. Long half life is desirable to avoid the need for frequent recalibration. High specific activity is required, especially when the beta-particle energy is low; otherwise self-absorption limits the effective strength of the source. For example, early attempts to employ Ca⁴⁵ (maximum beta-particle energy 0.25 Mev) have been superseded by the use of Pm¹⁴⁷, which is more easily produced in high specific activity (as a fission product) and has a longer half life. Table II shows a series of beta emitters in popular use for thickness gauges.

Most of these sources are now available as foils containing the radioactive material sealed between thin sheets of silver. Thallium 204 is supplied as an electroplated deposit, covered with a thin protective plating of cadmium. Activities from 5 to 20 mc are commonly used in conjunction with ionization chambers as detectors.

Much greater thicknesses up to several inches of steel can be measured by use of gamma-ray sources. A typical application is to the gauging of hot-rolled metal strips. A useful series of gamma emitters is given in Table III (30).

One of the important applications of isotopes in industry is radiography. The isotopes most commonly used for radiographic testing of such products as castings and welds are cobalt 60, cesium 137, and iridium 192.

The level gauge is similar in operation to thickness and density gauges in that it measures changes in radiation intensity produced by an intervening

TABLE II
SOURCES OF BETA PARTICLES USED IN THICKNESS GAUGES

Isotope	Half life	Maximum energy (Mev)	Approximate half thick- ness mg/cm ² (Al)	Approximate useful range of operation mg/cm ²
S ³⁵	87 days	0.167	2.0	0.5-5
Pm ¹⁴⁷	2.6 yr	0.23	4.5	1-12
Tl ²⁰⁴	4 yr	0.77	35	10-150
Sr ⁹⁰	20 yr	0.53	17	
+Y ⁹⁰	(in equilibrium)	2.2	160	50-650
Ce ¹⁴⁴	280 days	0.30	7.5	
+Pr ¹⁴⁴	(in equilibrium)	3.0 (+ γ rays)	220	100-1000
Ru ¹⁰⁶	1.0 yr	0.03		
+Rh ¹⁰⁶	(in equilibrium)	3.5 (+ γ rays)	270	130-1200

material. Commonly, the radioisotope source is attached to one side of a tank or vessel, and the detecting instrument is attached to the other side. When the content rises, it cuts off or reduces the beam of radiation to the radiation-measuring instrument. When it is desirable to read variations in level from a gauge, the source and detection instruments are placed so that the beam passes directly or diagonally from top to bottom of the vessel. Changes in level can then be read from a calibrated instrument activated by variations in beam intensity reaching the detector.

Level gauges are most useful where heat, pressure, corrosive substances, or the difficulties of maintenance make it impossible or undesirable to use level measuring devices of the contact type. Liquid-level gauges are widely used in the petroleum industry to measure the level of hydrocarbons in cracking units and tank farms, and in the chemical industry for determining the height of various materials in closed vessels or reactors. The levels of molten glass, molten metals, and paper pulp slurries in closed vessels are also

TABLE III
GAMMA EMITTERS USED IN THICKNESS GAUGES

Isotope	Half life	Gamma-ray energy (Mev)
Tm ¹⁷⁰	127 days	0.085
Se ⁷⁶	127 days	0.40-0.067 many γ rays
Ir ¹⁹²	74 days	0.61-0.14 many γ rays (mean about 0.5 Mev)
Cs ¹³⁷ + Ba ^{137m}	33 yr	0.66
Co ⁶⁰	5.23 yr	1.33, 1.17

being measured in this manner. In addition, the heights of solids, such as catalysts in hoppers or scrap metal in cupolas, are being controlled with radioisotope-level gauges (31).

INDUSTRIAL USES OF RADIATION

The industrial uses of radiation from radioactive isotopes are important and promise to become more important as the present uses are further applied and new uses developed. The radiation from isotopes falls into two general classes: the soft and readily absorbed beta radiation and the hard and more penetrating gamma radiation. The isotopes differ in the particular proportions of beta and gamma radiation, and each must be considered for its own properties, but it is generally true that convenient and inexpensive sources of both kinds of radiation are supplied from the atomic energy plants either as waste products—that is, fission products—or as a result of neutron irradiation in reactors, such as cobalt 60. A third source of radiation, of course, is the reactor itself. And in some of the future uses of radiation it is to be expected that reactors will be the source, for they are the cheapest source per unit of radiation delivered. One can envisage the possible utilization of a reactor for four products—power, heat, isotopes, and reactor radiation; i.e., reactors might be constructed in the future to deliver these four products and furnish these four kinds of income.

The principal present industrial uses of isotopic radiation are plant mutations for production of superior crop plants, pest control, and power sources.

PLANT MUTATIONS FOR PRODUCTION OF SUPERIOR CROP PLANTS

The production of improved agricultural and ornamental plant varieties requires many years of deliberate breeding and selection to obtain desired characteristics. The breeder needs a large pool of genetically variable source material for selective combination into a new variety. Ionizing radiation helps to provide this pool, since it produces rapidly a great variety of genetic changes in plant stocks.

With the use of radiation-altered stocks, abrupt improvements in resistance to disease have been produced. Small improvements in yield or in maturation time of crops have been achieved. The synthesis of small, independent, but scattered changes into one new variety can give surprisingly good results. Favorable genetic changes make up, of course, only a tiny fraction of all the changes produced by radiation, and the plant breeder still must eliminate and select with patience and care.

Irradiation of seeds used extensively in the United States has produced a number of promising mutations. Two new plant varieties obtained in this way have been formally released to plant breeders for practical agricultural use. One, the "Sanilac" bush navy bean, in several years of testing, out-produced the parent variety by approximately 30 per cent per acre and required fewer days from planting to harvesting. The other is an improved

variety of peanut released to commercial sources two years ago; this peanut has higher yield and greater disease resistance.

Ionizing radiation also is used to produce somatic mutations in plants, such as fruit trees, that can be propagated with cuttings or grafts. Another technique involves using radiation to fragment chromosomes—genetic materials in reproductive cells—to permit recombining genes or sections of chromosomes in desired crosses. This technique has been successfully used in introducing genes for leaf rust resistance into wheat.

Disease-resistant strains have been reported in experiments with wheat, oats, and flax. High-yield dwarf forms of cereal grasses have been observed which suffer less wind damage than do customary strains. Encouraging results are reported from attempts to use mutation to eliminate a factor toxic to livestock from certain otherwise useful forage plants. Fruit trees grown in low levels of gamma radiation for several years and permitted to return to normal growth are being analyzed for possible useful mutations.

Two beneficial mutations have been reported in such experiments on peach trees: one branch on a Fairhaven peach tree bears fruit which ripens approximately ten days earlier than normal; a branch on a different tree ripens its fruit some three weeks later than normal. These two radiation-induced mutations may lead to increasing by more than a month the season over which the fresh fruit can be available (32).

Some of the useful and potentially useful plant mutations induced by irradiation are summarized in Table IV.

PEST CONTROL

A fundamentally new method for controlling animal populations—one that enlists the reproductive process of the species in its own extinction—has entirely eradicated a major agricultural insect pest throughout a large continental region. The pest is the screw-worm fly which infests livestock; not a single screw-worm fly has been seen in the southeastern United States for almost two years. This unprecedented achievement was effected within a few months, the first time the self-eradication method was tried on such a large scale, and suggests that this method may be applied with the same results to other insect species and to rodents and other pests.

Entomologists and veterinarians of the Agricultural Research Service of the U. S. Department of Agriculture and the Florida Livestock Board reared millions of screw-worm flies in what was literally a screw-worm factory. The insects were made sexually sterile by exposure to high-energy radiation. They were then released in the infested area. The sterile males, mating with the females in the natural population, nullified their reproductive capacity. The result was the complete elimination of the natural population.

The new method offers obvious advantages over conventional techniques directed at killing the living generations of the pest. In the first place, it is highly selective, involving only the single target species and leaving the rest of the ecological system completely undisturbed. Secondly, no species can

TABLE IV

MUTATIONS INDUCED (33)

(Some Examples of Useful or Potentially Useful Mutations or Sports Obtained in Plants by Irradiation*)

Character improved or modified	Character or direction of change	Plant
IN CROP PLANTS		
Disease resistance	To stem rust	Barley, oats, wheat
	To stripe rust	Wheat
	To Victoria blight	Oats
	Leafspot	Peanut
Insect resistance	To gall fly	Sesame
Growth habit	Shorter	Barley, flax, oats, rice, wheat
	Taller	Flax, jute
	Dwarf	Sorghum, bean
	Giant	Pea, peanut, red clover
Maturity	Earliness	Barley, oats, soybean
	Lateness	Barley, oats, wheat
Self-incompatibility	To self-fertility	Red and white clovers
Quality	Improved	Tobacco, wheat
Yield	Increased	Oil mustard, peanut, peas, sesame, barley, oats, wheat
Hardiness	Increased	Oats, wheat
IN HORTICULTURAL PLANTS		
Disease resistance	To rust	Black currant
Flower color, shape, size	Various	African violet, carnation, cyclamen, petunia, phlox, snapdragon, tulip
Self-incompatibility	Self-fertility	Sweet cherry
Growth habit	Varied	Black currant
Leaf shape and color	Various	African violet, apple, phlox
Quality	Varied improvement	Black currant
Fruit size	Increased	Black currant
Fruit color	Improved	Apple, pear
Time of ripening	Earlier and later	Peach

* Some of these mutants have been induced at Brookhaven, but the majority are summarized from published articles. Space does not allow references to the original literature citations, but most of these may be found in articles (34 to 37).

Source: Sparrow, A. H., and Konzak, C. F. (1958) (38).

acquire immunity to sterile matings as it can to the insecticides used in the past. There is a third and not so apparent advantage. Killing agents tend to become progressively less efficient as the pest population declines, and so leave a few survivors to begin the cycle of geometric population increase all over again. The sterile-male method has the theoretical and, as shown with the screw-worm fly, practical capability of becoming increasingly efficient as the pest population reaches the vanishing point.

There are nonetheless disadvantages inherent in the method when it comes to planning campaigns against certain species and throughout large geographic regions. But eradication of the screw-worm fly surely urges the search for similar uses. The screw-worm fly itself remains a major objective. It continues to infest the livestock of the Southwest, where losses are estimated at \$25 million each year (39).

The adult screw-worm fly lays a compact mass of two to three hundred eggs in the wounds of warm-blooded animals. The insect is especially damaging to newborn animals, infesting their navels; in fact, in areas heavily populated with screw-worm flies, few newborn calves, lambs, kids, pigs, or other young escape attack. Tiny maggots hatch from the eggs in 12 to 24 hr, becoming full-grown in about five days and reaching a length of about $\frac{3}{4}$ in. Then they drop out of the wound, burrow into the ground, and change to the pupal or resting stage in about one day. The adults emerge from the pupal case after about eight days during the summer months, live for two or three weeks, and range for many miles. They mate on about the third day after emergence, and the females are ready to lay eggs four days later. The generation period may thus be as short as three weeks; and in areas where the insect survives the year round, there may be ten to twelve generations during each year. The principle by which this eradication of the screw-worm fly is conducted is that sterile male flies made sterile by cobalt-60 irradiation are released in sufficient numbers to exceed the natural population. For example, even under conditions that are favorable to a fivefold increase in insect population per generation, it seems that the release of sterile male flies in an initial 9 to 1 ratio to the natural population could eliminate the fly in five generations. It was found that with this initial ratio, the eggs from the mated females were 83 per cent sterile; this was sufficiently close to the 90 per cent expected for the case of nondiscrimination between irradiated and nonirradiated males to justify the hope that the method would work. The first tests were conducted on Sanibel Island off the west coast of Florida, which has an area of 15 square miles and has a natural population of screw-worm flies. Irradiated sexually sterile screw-worm males were released at the rate of 100 per square mile per week for a period of three months. Within two months, 80 per cent of the screw-worm fly egg masses were sterile, and by the third month the natural population had virtually vanished.

The screw-worm fly precedent inspires people to think about application of the technique to other areas and to other varieties of pests, such as the oriental melon, Mediterranean and Mexican fruit flies, the pink bollworm,

the boll weevil, the sugar cane borer, European corn borer, the gypsy moth, and the codling moth. Basic information and experience are still inadequate to determine just how far the technique can be applied and further developed. It does seem clear, however, that such dramatic success as that experienced in the southeastern United States with the screw-worm fly strongly indicates many other equally successful applications to be made in the future.

ISOTOPIC POWER SOURCES ✓

While there are several methods known for producing electricity from radioactive atoms, the most promising technique is based on the thermopile principle, which was investigated years ago as a means of converting ordinary heat into electricity but was abandoned as uneconomical. With the advent of new semiconductor materials and the availability of large quantities of radioisotopes, a new type of battery has become practical, and means to extend its usefulness are being investigated. Conversion of the by-product material, strontium 90, into a safe and useful isotopic power source will provide a unique source of electrical energy.

During the past year it has been proved practical to use large quantities of strontium 90 in this way to produce electricity. The first requirement was to find a compound of strontium with proper thermal conductivity, strontium density, compressibility, and solubility characteristics. Strontium titanate meets the requirements. Strontium titanate melts at 3038°F and is soluble in sea water at 60°C to only 10 parts per billion. The solubility in fresh wash is not detectable by tracer techniques. As additional protection against environmental contamination, the material is triply encapsulated in 0.75 in. of Hastaloy C, which has a salt-water corrosion rate of 0.0001 in. per year. In addition 1.25 in. of tungsten surround the encapsulated strontium.

A 5-watt generator has been designed and is under construction to power an automatic data telemetering station. The construction of the battery is simple: strontium titanate ceramic pellets (containing about 20,000 curies of Sr^{90}) are encapsulated and sealed in a tungsten heat sink; 72 pairs of lead telluride thermocouples are placed around the heat sink and connected electrically.

The generator is capable of continuously delivering 5 watts at 4.0 volts dc for two years unattended. Even then its limit is the electronic equipment rather than the isotopic generator. The equipment will be capable of telemetering data at programmed times or on call from remote regions and will collect information such as meteorological observations from previously inaccessible regions (40).

The ultimate capability for producing power by isotope radiation is small. Since only a minute fraction of the total fission energy resides in the decay energy of the long-lived fission products and since production of radioactive isotopes, such as cobalt 60, by neutron irradiation is a highly inefficient process, large amounts of power can probably never be made from isotope radiation sources. There are, however, many instances in which the

light weight and small need for maintenance are commanding features. An example is distant weather stations where the isotope power source will serve to charge batteries which, on occasion, send back weather information to the home station. The isotope power source is unique. Of course, the most important application and the most obvious one is to space-exploration problems requiring light-weight power sources capable of delivering up to several hundred watts of electric power. Above this power level, it is necessary to use nuclear reactors. Early in the program, it was recognized that the development of the radioisotope power source for space uses would take a relatively short time, and in January 1959 the first success was reported with a $4\frac{3}{4}$ -in. diameter, 5-lb device generating 5 watts of electricity, fueled in this instance, however, with the natural isotope polonium 210. This device was a "proof of principle" effort. The next stage is, of course, to use fission products, such as strontium 90, and there seems to be no doubt that these sources will be completely successful in those applications where the small amounts of power they can deliver will suffice.

POTENTIAL NEW USES

FOOD PRESERVATION BY IRRADIATION

Research on the radiation processing of foods commenced over ten years ago. Within the past six years a full-scale development program has been concentrated in the United States on this new concept in food technology. Work on radiation-processed foods in other countries has also been initiated and is being pursued actively. Major effort in the United States has been supported by the government, primarily the Department of Defense, through contractual research projects at universities, research institutes, and private companies. Current selected information on radiation-processed foods technology can be found in the report on the Massachusetts Institute of Technology International Conference on the Preservation of Foods by Ionizing Radiation. A comprehensive survey of the field through 1957 is contained in the U. S. Army Quartermaster Corps publication entitled *Radiation Preservation of Food* (41). However, the rate of accumulation of information in this subject area has increased sharply since the latter book was published. A good general reference is the material contained in the *Hearings on the National Food Irradiation Research Program—Jan. 14 and 15, 1960—held before the Joint Committee on Atomic Energy of the Congress, Parts I and II* (42).

The comprehensive research and development program on radiation processing of food has revealed some products having a potential for commercialization. However, the radiation sterilization of some meats, such as beef, still poses major problems. Other items, such as chicken, fish, and pork products, show promise as completely sterile products. Generally, however, substerilization offers more immediate promise since effects on quality (flavor, texture, and color) are minimized and the processing costs more

nearly approach those of conventional processing methods. The sub-sterilization of marine products, chicken, and some selected fruit products, such as strawberries, to extend shelf-life appears promising (42).

In the development of radiation as a general processing agent, we are concerned with putting to work the millions of curies of fission products and other sources of radiation energy being produced in our atomic energy program. Already radiation energy is being used to yield several products of im-

TABLE V
ESTIMATED COSTS OF PROCESSING WITH RADIATION SOURCES

	Exposure	
	2.5×10 ⁶ rep	10 ⁶ rep
Spent fuel elements	2.050¢/lb	0.0820¢/lb
Gaseous fission products	0.360¢/lb	0.0144¢/lb
Separated cesium 137*	0.379¢/lb	0.0152¢/lb
Sodium 24	0.648¢/lb	0.0260¢/lb
Reactor-activated indium	1.402¢/lb	0.0560¢/lb
Electron accelerator (7.5-kw)	0.548¢/lb	0.0722¢/lb
Electron accelerator (50-kw)	0.235¢/lb	0.0854¢/lb

* Does not include the cost of the cesium source.

portance in our space and missile program. These specific advances were developed by private industry but are based largely upon technology which emerged in government programs in the early '50's. A concerted effort is being made to broaden the scientific base of this technology so that additional promising applications of radiation energy can be achieved.

The costs are potentially quite low. A reasonable set of estimates is given in Table V (43).

As the atomic power reactors become more common and the handling of reactor radiation and fission products is better understood, the cost will fall even further; e.g., in the sodium graphite reactor being built at Hallam, Nebraska, it was hoped at one time to incorporate a loop which took the radioactive sodium out of the reactor proper and passed it into an adjacent room, where the gamma radiation from the 15-hr half-life radioactivity could be used to sterilize food.

The question of the wholesomeness of irradiated food is a serious one, but, in general, the indications are favorable. However, the taste of various foods is altered somewhat, and it now seems likely that the program using less intense radiations than those required for complete sterilization will be followed, particularly with certain kinds of fish, as a beginning attack on the whole problem of getting the atom to work on the problem of food preservation.

ORGANIC CHEMICALS

Radiation can be used to cause chemical reactions which, in the case of certain organic chemicals, are unique. The hardening of polyethylene plastic by irradiation is a case in point. Cross-links are induced that cause a structure to become rigid and glassy, so the plastic can be heated to higher temperatures before it softens. Similarly, rubber can be vulcanized with irradiation in a way that produces a superior product. None of these processes as yet is commercially economic or practical, but the whole idea of using radiation as a chemical reagent is catching on to a considerable degree. One of the barriers to the development of a radiation chemical industry is the lack of understanding of radiation effects on matter. This understanding is coming slowly; but as it does come, it seems likely that it will be possible to develop important chemical uses for radiation. The subject is still in the research and development stage, and it appears it will be some years before a fully practical process emerges. The properties of radiation which cause chemical reaction are fairly well understood, but the nature of the chemical entities that react is not clear. It is quite certain in many instances that the free radicals produced are responsible; but in other instances the ions produced seem to be responsible, at least in part, and it is probable that both are involved to a certain degree in almost every case. Radiation is cheap enough in the internal parts of an atomic reactor to indicate that if we had any process which appeared to be reasonably efficient, the chemical use of radiation might be important; in other words, a reactor might operate both as a chemical factory and as a power source.

LIMITATIONS (HEALTH AND REGULATORY)

Isotopic tracer uses are based on the fact that matter otherwise indistinguishable can be distinguished by virtue of the radioactivity contained in the isotopes, or by virtue of the difference in mass, as in the case of deuterium tracing or in a few instances by other characteristics of the atomic nuclei, such as fissionability; in most industrial applications of isotopes, the radiations of radioactive isotopes are used. There are two general subclasses of the uses—those in which the tracing is the main thing and those in which the radiation itself is the main thing, either for purposes of gauging or for purposes of radiation treatment or radiation chemical uses. The principles of isotopes, of course, contain the seeds for the limitations of the method, and these are simple. The radiations can be dangerous. So, in this section, the matter of the limitations on isotope uses which the public health demands will be discussed.

The safe handling and use of isotopes has been given a great deal of attention by the federal government, particularly the Atomic Energy Commission, which dealt wisely with the problem by using education as well as regulatory techniques. The law vests the Atomic Energy Commission with the power to control the products of the atomic fission reaction and those

isotopes which can be made by neutron irradiation, but it does not give it the power to regulate the use of X rays or natural isotopes, such as radium. This characteristic of the law has made the work of the Commission somewhat more specialized than it otherwise would have been, but the broad sweep of its responsibility, nevertheless, has meant that the Atomic Energy Commission has had to deal with the matter of the public health in connection with radioactive isotopes since its very inception. Recently, the Public Health Service and the Department of Health, Education, and Welfare have also had to pay increasing attention to this potential hazard.

The great benefits from isotopes are such that we will want to tolerate as general a use of isotopes as is reasonable and safe. So we must become educated about them and understand the hazards of radiation, in order to judge just how far it is possible to go in living with radiation and isotopes. There are various aspects of the problem; the most immediate one is the use of isotopes and the hazard that they constitute. Of course, there is a broad, general, and underlying hazard of radioactive fallout in time of war, but we are not dealing with it here. The question is: "Can you safely use isotopes for a particular application?" And this question is immediate and definite and important, and there must be an answer for it. Otherwise, progress in the direction of isotope use will stop.

The basic threat that radiation constitutes is that it does change tissue. It will cause somatic effects, i.e., damage to the health, and it will also cause genetic effects, i.e., changes in the characteristics inherited in the children and grandchildren and subsequent generations. Now, as stated, these facts have their beneficial aspects; e.g., in the treatment of cancer, the excision of tissue by irradiation is a standard and useful technique, and in the development of new kinds of plants, the horticulturist finds it useful to irradiate to get improved types. The hazard also lies in the same facts, and it must be dealt with against the background of the usefulness. A useful guide in this connection is the amount of radiation which is normally received from uranium, thorium, and potassium naturally present in the ground, and from the cosmic rays. The regulations have been set on the basis of the general feeling that the tolerable steady dose should not exceed a few times the natural dose rate and that even this should be restricted to a relatively small fraction of the total population, so that the genetic effects will be minimal. (It is a point in principle, of course, in genetics that the genetic effects require that large numbers of individuals be exposed in order that they may be manifested; i.e., the exposure of a few individuals will not cause widespread genetic effects.) On the matter of health, however, it is a matter of the individual. In general, effects on health are very hard to observe for radiation exposures below several roentgens in amount, whereas the natural dose rate is about .1 to .2 r per year. So one sees that at levels of radiation which are a few times the natural dose rate, the "permissible" dose can cause no immediately observable effects on health. However, there is a widespread feeling among certain life scientists who have studied the problem

that some possibility exists that in a large number of individuals exposed to a very small dose, there is a certain probability of the development of serious maladies such as cancer. It has not been demonstrated that this is so, nor has it been demonstrated that it is not so; the known fact that cancer and other maladies can be caused by higher doses leads one to assume for reasons of safety that the effects are linear at low dose rates. So most of the regulations are set up on the linear basis. It is better to play safe in this way than to take an unwarranted chance. Further information and further research in this area are most important. Of course, we pay a price in having to live with regulations which are unnecessarily restrictive in the use of such valuable and generally applicable tools as radioactive isotopes; but until we know about the nature of the somatic and genetic effects of low dose rates it is difficult to do anything other than to take the linear assumption. On the linear assumption, the rules are made so that the tolerances are essentially of the order of the natural dose effects. And it can be said with certainty that, living with these regulations, the effects of radiation will certainly be minimal. It is, however, possible that the regulations are unnecessarily restrictive and that as we learn more about the nature of the effects of radiation on matter, particularly human tissue and the human genes, we will be able to relax somewhat. Conceivably, of course, the trend would go the other way, but the general consensus of opinion is that levels of exposure that are considered tolerable at present are really safe.

Practical problems, such as the granting of permission for a proposed use of radioactive isotopes or the disposal of radioactive waste, involve the people in the community and require the informing of public health officials about the effects of radiation on matter, especially on human tissue. And this general information is not as widely known as it should be, and so for some considerable time there will be a shortage of trained public officials. This need is recognized widely, and as the States get into the business of helping the Atomic Energy Commission and the Department of Health, Education, and Welfare police the atomic energy industry, we will require more and more trained people. So there is an educational program now under way to train public health officials for the type of inspection and regulatory activities required. The general literature on the subject of radiation hazard is voluminous. A few items, however, might be cited. They are:

Living with Radiation, Vol. I and II, and *General Handbook for Radiation Monitoring* (US Atomic Energy Commission); *Disposal of Radioactive Waste*, Vol. I and II; *Proceedings of International Atomic Energy Agency* (Vienna, 1960); *Selected Materials on Radiation Protection Criteria and Standards: Their Basis and Use* (Joint Committee on Atomic Energy Congress of the US, Govt. Printing Office Document 54561); and *Hearings before the Joint Committee on Atomic Energy—Jan. 28, 29, and 30; Feb. 2 and 3, 1959—on the Industrial Radioactive Waste Disposal (1959)*, 1 and 2 (Govt. Printing Office—No 0-37457).

One problem of the atomic age is that radioactive material becomes widely disseminated in very small amounts, and though it constitutes essentially no health hazard, it may become a problem technically. Apparatus for the sensitive measurements of small amounts of radioactivity requires clean materials of construction, and it is necessary now in writing specifications for equipment of this sort to specify clean materials, materials free of radioactivity to specified levels. The problem is not yet serious, but could become so. For example, lead is normally radioactive because of the natural radioisotope, Radium D, but old lead which has lost its RaD (half life 19.4 years) by decay is not appreciably radioactive and can be used for the construction of low-level counting equipment whereas young lead cannot. The problem of assuring radioactive cleanliness in materials used in photography is another example.

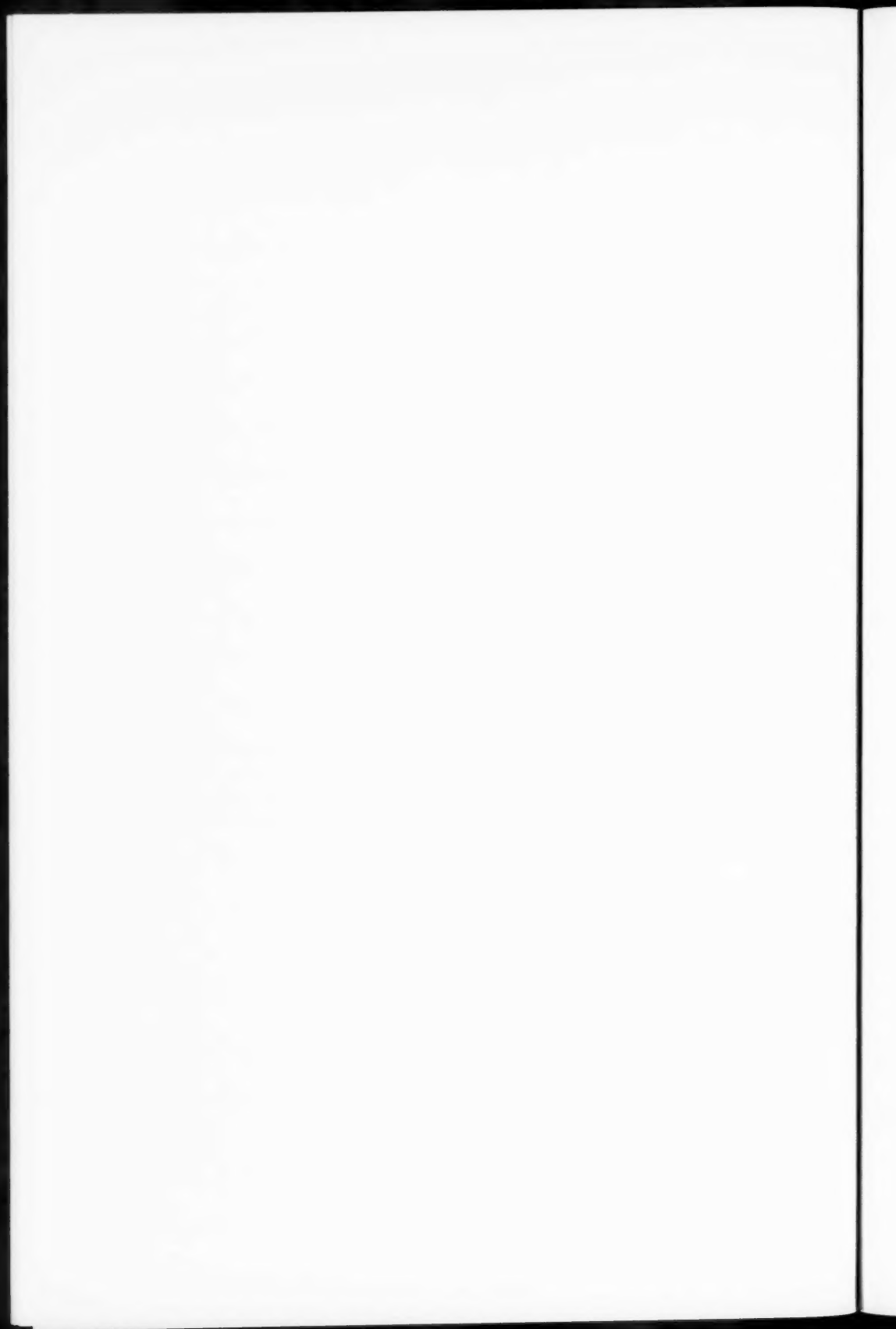
LITERATURE CITED

1. "Radioisotopes in Science and Industry," *US Atomic Energy Commission Document, 0-512688*, 14-16 (January 1960)
2. Kulwich, R., Feinstein, L., and Anderson, E. C., *Science*, **127**, 338 (1958)
3. Pringle, D. H., and Kulwich, R., *Nucleonics*, **19** (No. 2), 74 (1961)
4. "Physical and Chemical Research Utilizing Radioisotopes," *US Atomic Energy Commission Document, 0-512688*, 32-33 (January 1960)
5. Wilzbach, K. E., *J. Am. Chem. Soc.*, **79**, 1013 (1957)
6. Scully, N. J., Stavely, H. E., Skok, J., Stanley, A. R., Dale, J. K., Craig, J. T., Hodge, E. B., Chorney, W., Watanabe, R., and Baldwin, R., *Science*, **116**, 87-89 (1952)
7. Grosse, A. V., Johnston, W. H., Wolfgang, R. L., and Libby, W. F., *Science*, **113**, 1 (1951)
8. Kaufmann, S., and Libby, W. F., *Phys. Rev.*, **93**, 1337 (1954)
9. Von Buttlar, H., and Libby, W. F., *J. Inorg. & Nuclear Chem.*, **1**, 75 (1955)
10. Brown, R. M., and Grummitt, W. E., *Can. J. Chem.*, **34**, 220 (1956)
11. Gilletti, B. J., and Kulp, J. L., *Trans. Am. Geophys. Union*, **37**, 345 (1956)
12. Kaufman, W. J., and Orlob, G. T., *J. Am. Waterworks Assoc.*, **48**, 559 (1956)
13. Findel'shtein, Y. B., Filonov, U. A., Soifer, U. N., and Obukhova, M. P., *Doklady Akad. Nauk SSSR*, **116**, 671 (1957)
14. Alekseev, F. A., Soifer, U. N., Filonov, U. A., and Findel'shtein, Y. B., *Soviet J. Atomic Energy (USSR)*, **4**, 396 (1958)
15. Begemann, F., *Intern. Conf. on Peaceful Uses of Atomic Energy*, 15/P/1963 (1958)
16. Bolin, B., *Intern. Conf. on Peaceful Uses of Atomic Energy*, 15/P/176 (1958)
17. Gilletti, B. J., Bazan, F., and Kulp, J. L., *Trans. Am. Geophys. Union*, **39**, 807 (1958)
18. Suess, H. E., *Ann. Rev. Nuclear Sci.*, **8**, 243 (1958)
19. Von Buttlar, H., *Erdöl und Kohle*, **11**, 376 (1958)
20. Von Buttlar, H., and Wendt, I., *Trans. Am. Geophys. Union*, **39**, 660 (1958)
21. Begemann, F., *Z. Naturforsch.*, **14a**, 334-42 (1959)
22. Gilletti, B. J., and Kulp, J. L., *Science*, **129**, 901 (1959)
23. Brown, R. M., *Geochim. et Cosmochim. Acta* (To be published)
24. Wilson, A. T., and Fergusson, G. J., *Geochim. et Cosmochim. Acta*, **18**, 273 (1960)
25. Hull, D. E., and Bowles, R. R., *Oil and Gas J.*, **51**, 295 (1953)
26. Hull, D. E., *Nucleonics*, **13**, 18 (1955)
27. Ferris, S. W., *US Patent 2,315,845* (1943)
28. Pinotti, P. L., Hull, D. E., and McLaughlin, E. J., *SAE Journal*, **57**, 52 (1959)
29. Borsoff, V. N., Cook, D. L., and Otvos, J. W., *Nucleonics*, **10**, 67 (1952)
30. Putman, J. L., *Proc. Intern. Conf. Peaceful Uses Atomic Energy, Geneva, 1955*, **15**, Paper P/463, 119-20 (1955)
31. Hull, D. E., and Macomba, M., *Proc. Intern. Conf. Peaceful Uses Atomic Energy, 2nd, Geneva, 19*, Paper P/817 (1958)
32. "Use of Radioisotopes and Radiation in Agricultural and Plant Studies," *US Atomic Energy Commission Document, 0-512688*, 7-8 (January 1960)
33. Stanford Research Institute, "A Technical Report on Isotopes in Agriculture—Genetics," *Radioisotopes at Work for Agriculture*, 117 (October 1959)
34. MacKey, J., *Brookhaven Symposia in Biol.*, 141-56 (1956)
35. Smith, H. H., *Botan. Rev.*, **24** (No. 1), 1-23 (1958)
36. Konzak, C. F., *Quart. Rev. Biol.*, **32**, 27-45 (1957)
37. Sparrow, A. H., Binnington, J. P., and Pond, V., *US Atomic Energy Commission Document, BNL 504(L-103)* (1958)
38. Sparrow, A. H., and Konzak, C. F., *Camellia Culture* (Torje, E. C., Ed., Southern Calif. Camellia Soc., by MacMillan Co., N. Y., 1958)
39. Knipling, E. F., *Sci. Am.*, **203**, 54 (1960)
40. Aebersold, P. C., *The AEC Program for Radioisotopes Technology Development*, 10-11 (Presented at 1960 Nuclear Congr., New York, N. Y., April 4-7, 1960)
41. Available as *Rept. No. PB 151493*

- (Office of Tech. Services, US Dept. Commerce, Washington, D. C., price \$5)
42. *Hearing before Joint Committee on Atomic Energy Congr. of the US, 86th, 2nd Session, on Natl. Food Irradiation Research Program—Jan. 14 and 15, 1960, Part I, p. 137*
- (Washington, D. C., 1960)
43. Beeley, R. J., *Logistic and Economic Feasibility Study on Radiation Sterilization of Foods, PB 121961, p. 2* (Period: 28 June 1955–28 August 1956) (Chicago: US Dept. Commerce, Office of Tech. Services)

RELATED ARTICLES APPEARING IN OTHER ANNUAL REVIEWS

1. Gerstner, H. B., "Reaction to Short-Term Radiation in Man," *Ann. Rev. Med.*, **11**, 289-302 (1960)
2. Kligerman, M. M., "High Voltage Radiation Therapy," *Ann. Rev. Med.*, **11**, 303-14 (1960)
3. Hempelmann, L. H., "Evaluation of Hazards of Radiation Exposure in Medical Practice," *Ann. Rev. Med.*, **12**, 151-64 (1961)
4. Schwichtenberg, A. H., "Medical Aspects of Space Flight," *Ann. Rev. Med.*, **12**, 299-322 (1961)
5. Taylor, J. H., "Physiology of Mitosis and Meiosis," *Ann. Rev. Plant Physiol.*, **12**, 327-44 (1961)
6. Levinthal, C., and Davison, P. F., "Biochemistry of Genetic Factors," *Ann. Rev. Biochem.*, **30**, 641-68 (1961)
7. Mazia, D., "Biochemistry of the Dividing Cell," *Ann. Rev. Biochem.*, **30**, 669-88 (1961)
8. Hine, J., "Physical Organic Chemistry," *Ann. Rev. Phys. Chem.*, **11**, 65-86 (1960)
9. Bersohn, R., "Nuclear and Electron Resonance," *Ann. Rev. Phys. Chem.*, **11**, 369-90 (1960)
10. Goldberg, E. D., "Marine Geochemistry," *Ann. Rev. Phys. Chem.*, **12**, 29-48 (1961)
11. Weissman, S. I., "Nuclear Electron Spin Resonance," *Ann. Rev. Phys. Chem.*, **12**, 151-70 (1961)
12. Zwolinski, B. J., and Danti, A., "Thermochemistry and Thermodynamic Properties of Substances," *Ann. Rev. Phys. Chem.*, **12**, 325-54 (1961)
13. Kunin, R., "Ion Exchange," *Ann. Rev. Phys. Chem.*, **12**, 381-88 (1961)
14. Magee, J. L., "Radiation Chemistry," *Ann. Rev. Phys. Chem.*, **12**, 389-410 (1961)



AUTHOR INDEX

A

Aamodt, R. L., 104
 Abashian, A., 165
 Abragam, A., 180, 183, 186, 187
 Abraham, M., 182, 183
 Ackermann, I. B., 353
 Adair, R. K., 270
 Adamson, A. W., 451
 Adelson, E., 338
 Adyasevich, B. P., 261, 278
 Aebersold, P. C., 474
 Ageev, N. V., 335
 Agnew, L. E., Jr., 22, 23, 29, 33
 Aki, K., 383
 Akimov, Yu. K., 44
 Akimova, M. K., 282, 283
 Alaga, G., 283
 Alder, K., 283
 Alekseev, A. I., 128
 Alekseev, F. A., 465
 Alexeff, I., 158
 Alikhanian, A. I., 44
 Alkhazov, D. G., 431
 Allcock, G. R., 128
 Allen, D. W., 429
 Allen, K. W., 429
 Alles, W., 71, 76, 158
 Allison, S. K., 312
 Alston, M., 80, 81, 82
 Alvarez, L. W., 42, 48, 61, 68, 69, 70, 71, 72, 75, 76, 79, 80, 81, 82, 419, 429, 430, 432
 Amal, S., 20, 29
 Amaldi, E., 14, 17, 22, 23, 42
 Amati, D., 22, 29, 41, 46, 49, 58, 59, 60, 82, 83, 163
 Ambler, E., 176, 179, 182, 183, 186, 195, 196, 197
 Ammar, R. G., 59
 Anders, E., 353
 Anderson, A. C., 189
 Anderson, C. E., 422, 424, 432
 Anderson, E. C., 353, 464
 Anderson, F., 48, 49
 Anderson, J. A., 156
 Anderson, P. W., 333
 Andresen, A., 340, 341
 Andresen, A. F., 321
 Andreyev, D. S., 431
 Araki, G., 134, 135
 Arfken, G. B., 266
 Arnold, J. R., 349-70; 353, 356, 357, 358, 360, 363, 364, 365, 366, 367

Arnous, E., 131
 Arnowitt, R., 113, 127, 129
 Arrol, W. F., 350
 Ashkin, J., 42
 Asperger, S., 443, 446, 448, 449
 Atterling, H., 431
 Auluck, F. C., 5
 Austin, A. E., 338
 Ayer, F., 27
 Azuma, S., 137

B

Bäckström, G., 260
 Bacon, G. E., 304, 312, 320, 321, 323, 326, 335
 Bader, R. F. W., 450, 453, 454
 Baender, R. G., 49, 68, 84
 Bagguley, D. M. S., 176, 194, 195
 Baker, E., 359
 Baker, F. B., 451
 Baker, W. R., 432
 Balazs, L., 102
 Baldin, A. M., 44
 Baldo-Ceolin, M., 42
 Baldock, D., 192
 Baldwin, R., 465
 Ball, J., 156, 165
 Ball, W. P., 221, 222, 223
 Ballinger, P., 452, 455
 Balzer, R., 261
 Bang, V. X., 156
 Barashenkov, V. S., 6, 7, 14, 17, 21, 28, 29, 30, 31, 32, 33
 Barbaro-Galtieri, A., 42
 Barbashov, B. M., 6, 7, 21, 32, 33
 Barkas, W. H., 14, 17, 22, 23, 42, 46
 Barnes, S. W., 242
 Baroncini, D., 121
 Baroni, G., 14, 17, 22, 23, 42
 Barrett, J., 450
 Barshay, S., 69
 Bartell, L. S., 441
 Bartholomew, G. A., 259-302; 260, 261, 264, 265, 271, 272, 273, 274, 276, 277, 278, 279, 283, 284, 290, 291, 294, 295, 296
 Bashkin, S., 427
 Basolo, F., 447, 451, 452
 Bastien, P., 80
 Bauer, C. A., 350
 Bauer, R. W., 201
 Baz, A., 51, 52
 Bazan, F., 465
 Beaven, G. H., 450
 Beebe, L., 226, 227, 228, 243
 Beeley, R. J., 476
 Begemann, F., 350, 356, 465
 Belenkii, S. Z., 6, 11, 12, 14, 16, 17, 18, 20, 21, 22, 23, 24, 27, 29, 33
 Belinfante, F. J., 11, 29
 Bell, R. E., 263, 265, 272
 Bell, R. P., 442
 Belyakov, V. A., 32
 Bender, M. L., 442, 445
 Benzezech, P., 420
 Bengston, J., 103, 139
 Bennett, R. G., 287, 292
 Bennett, W. H., 429
 Berge, J. P., 80
 Bergia, S., 27
 Bergqvist, I., 287, 297
 Bergsma, J., 321
 Beringer, R., 428, 432
 Berliner, E., 444
 Bernardini, C., 44
 Bernardini, G., 217, 232
 Berners, E. D., 141
 Bernstein, S., 190, 196
 Besson, C., 29
 Bethe, H. A., 97, 111, 126, 131, 278
 Bhatia, A. B., 102
 Biedenharn, L. C., 100, 266
 Bierman, L., 405
 Bigeleisen, J., 440, 450, 451, 452, 454, 455
 Bilenky, S. M., 47
 Binnington, J. P., 472
 Bird, J., 366
 Bird, J. R., 100, 287, 288, 289, 291, 292
 Birge, R. W., 14, 17, 22, 23, 46
 Biswas, N. N., 71, 76
 Biswas, S. N., 116, 128
 Bittner, J. W., 428
 Bivins, R., 217, 230, 232
 Blades, A. T., 449
 Blake, F. R., Jr., 378
 Blank, V. Z., 157
 Blankenbecler, R., 98, 159
 Blanpied, W. A., 158
 Blatt, J. M., 100, 139, 141, 163, 273, 274, 275, 281, 285, 304
 Bleaney, B., 176, 177, 178, 194, 195, 202, 203, 207

- Blears, J., 429
 Blinder, S. M., 441
 Blinowski, K., 344
 Blin-Stoyle, R. J., 64, 175, 178
 Blizzard, E. P., 225
 Bloch, C., 268
 Bloch, F., 305
 Block, M. M., 12, 16, 29, 48, 49, 66
 Block, R. C., 286
 Bloembergen, N., 184
 Bockelman, C. K., 287, 288, 292, 295
 Bogachev, N. P., 13, 31
 Bogolubov, N. N., 145
 Bohr, A., 47, 201, 208, 282, 283
 Bohr, N., 425, 426, 427
 Bokelman, C. K., 295
 Boldt, E., 45
 Bolin, B., 465
 Bollinger, L. M., 265, 286, 287, 288, 289, 290, 291, 292, 293
 Bolotin, H. H., 287, 289, 290, 291, 292
 Bolotin, L. I., 420, 432
 Bomko, V. A., 420, 432
 Bonnevey, G., 137
 Bonsignori, F., 27
 Boos, E. G., 20, 33
 Booth, E. T., 217, 232
 Booth, N. E., 165
 Booth, R., 221, 223
 Boozer, C. E., 444, 446, 447
 Borčić, S., 443, 448
 Borgardt, A. A., 132
 Borghini, M., 180, 183, 186
 Borsoff, V. N., 467
 Bosco, B., 82, 83
 Bostrom, C. O., 261, 289, 291
 Bouricius, W., 102
 Bowcock, J., 156, 164
 Bowen, T., 67
 Bowers, K. D., 176, 177, 194, 195, 202, 203
 Bowles, R. R., 465
 Boyle, A. J. F., 192
 Bradner, H., 432
 Braid, T. H., 261
 Bransden, B., 45
 Brautti, G., 49
 Breit, G., 51, 96, 100, 101, 102, 103, 130, 131, 139, 140, 141, 142, 163, 165, 294, 419
 Brickwedde, F. G., 318
 Brink, D. M., 285, 292, 293
 Brockhouse, B. N., 337, 344
 Brockman, F. G., 337
 Broecker, W. S., 366
 Brovetto, P., 33, 181
 Brown, N., 326
 Brown, R. R., 404, 465
 Brucker, E. B., 48, 49, 54, 66, 67
 Brueckner, K. A., 13, 101, 112, 117, 122, 123, 136, 137, 139, 141
 Brunings, J. H., 426
 Brussel, M. K., 287, 291
 Brustad, T., 420
 Bryan, R. A., 98, 143
 Bubelev, E. G., 6, 7, 32, 33
 Buechner, W. W., 276, 279, 295
 Buehler, E., 191
 Bugg, W. M., 13
 Bunbury, D. St. P., 192
 Bunton, C. A., 456
 Bunyatov, S. A., 13, 31
 Burbidge, E. M., 350
 Burbidge, G. R., 350
 Burgov, N. A., 261
 Burgy, M. T., 318, 339, 340
 Burke, P. G., 156
 Burkhardt, H., 44
 Burmeister, J., 35
 Burmistrov, V. R., 265, 279
 Busing, W. R., 313, 321
 Butler, A. R., 456
 Button, J., 42
 Byers, N., 50
 Bykov, V. N., 335
- C
- Cable, J. W., 329, 333, 335, 336, 338, 339, 341
 Caglioti, G., 310
 Caldwell, D. O., 45
 Call, R. L., 44
 Cameron, A. G. W., 274, 275, 276, 283, 284, 285, 296
 Cameron, J. R., 429
 Camnitz, H. G., 101
 Campion, P. J., 261, 264, 272, 273, 274, 277, 279, 283, 284, 290
 Campos, F. P., 311
 Cap, F., 131, 132
 Capps, R. H., 47, 60, 82, 84
 Carmony, D. D., 156
 Carpenter, R. T., 265, 287, 288, 289, 290, 291, 292, 293
 Carter, E. B., 430
 Carter, R. E., 262, 264, 272, 294
 Cartwright, W. F., 101
 Carver, T. R., 181
 Case, K. M., 101, 237, 238
 Cassels, J. M., 344
 Castagnoli, C., 14, 17, 22, 23, 42
 Ceccaldi, M., 450
 Ceccarelli, M., 71, 76
 Ceolin, C., 69
 Ceolin, M., 42
 Cepuleha, Z., 364
 Cerulus, F., 12, 13, 15, 17, 18, 21, 22, 23, 29, 30, 31
 Cester, R., 29
 Chadwick, G. B., 12, 30, 265
 Chagnon, P. R., 261
 Challis, B. C., 454
 Chamberlain, O., 101, 327
 Chang, C., 48, 49, 54, 67
 Chapman, C. J. S., 199
 Charap, J. M., 98, 106, 107, 135, 158, 159, 160
 Charon, J., 138
 Charters, A. C., 355
 Chasan, B. M., 28
 Chen, F. F., 221, 222
 Chernavskii, D. S., 2
 Chernyak, L. L., 420, 432
 Chew, G. F., 1, 23, 49, 50, 155, 156, 161, 162
 Child, H. R., 329, 333, 341
 Chinowsky, W., 68, 69
 Chorney, W., 465
 Chou, C. N., 419
 Chou, Kuang-Chao, 45
 Chraplyvy, Z. V., 127
 Chrien, R. E., 287, 289, 290, 291, 292
 Christian, R. S., 96, 101, 102
 Christy, R. F., 62, 373
 Chubb, T. A., 403
 Chupp, E. L., 262, 436
 Chupp, W. W., 14, 17, 22, 23
 Church, E. L., 263
 Chuvilo, I. V., 67
 Cini, M., 121, 146, 153, 154, 155, 158, 162, 163
 Ciok, P., 33, 34
 Citron, A., 248, 249
 Claesson, A., 129
 Clark, A. F., 436
 Clayton, G. T., 327
 Clementel, E., 102
 Cloud, W. H., 338
 Cocconi, G., 13, 28, 32, 33, 34
 Cocconi, V. T., 12, 13, 18, 29
 Coghen, T., 33, 34
 Cohen, D., 451
 Cohn, H. O., 48, 49, 54, 66, 67
 Collins, C. J., 447
 Collins, E. R., 286, 292
 Collins, G. B., 12, 30
 Collins, L. E., 429
 Combe, J. C., 32
 Compton, A. H., 312
 Condit, R., 430
 Condit, R. I., 430
 Condon, E. U., 100, 163
 Conversi, M., 44
 Cook, D. L., 467
 Cook, R. F., 10, 11, 24

Cooke, A. H., 195
 Cooper, L. N., 113
 Coor, T., 101, 221, 222
 Coppinger, G. M., 443, 446
 Corge, C., 287, 290, 291
 Cork, B., 101
 Corliss, L. M., 310, 326,
 332, 333, 335, 337, 338, 341
 Cornides, I., 424
 Cortellessa, G., 84
 Côté, R. E., 286, 287, 289,
 290, 291
 Cottingham, W. N., 156, 164
 Craig, H., 349
 Craig, J. T., 465
 Crawford, F. S., Jr., 54, 66, 84
 Crayton, N., 59
 Cresti, M., 59, 66, 84
 Cristu, M., 261
 Crosbie, E., 246
 Cross, S., 446
 Crowe, K. M., 165
 Crussard, J., 29, 71, 76
 Cumming, J., 226, 227, 228,
 243
 Curry, N. A., 321, 323, 325
 Curtis, R. B., 230, 231,
 233, 234
 Cuzcosky, R. E., 128, 139,
 151, 158
 Cvijanovich, G., 32
 Cziffra, P., 139, 140, 164
 Czyż, W., 2

D

Dabbs, J. W. T., 175-212;
 188, 190, 196, 202, 203,
 204, 207, 208, 210
 Dachs, H., 325
 Dadaian, A. T., 44
 Dagley, P., 195, 201
 Dahl, O., 54, 59, 69
 Dahlberg, D. A., 286
 Dahlgren, G., 452
 Dale, J. K., 465
 Dalitz, R. H., 41, 48, 49,
 59, 60, 68, 69, 70, 73, 74,
 75, 76, 77, 78, 79
 Dallaporta, N., 53, 56, 59, 68, 69
 Dancoff, S. M., 120, 260
 Danforth, J. L., 429
 D'Angelo, N., 266
 Daniel, R. R., 13, 15, 30
 Daniels, J. M., 194
 Danilian, G. V., 261
 Danner, H. R., 325
 Dascola, G., 59, 71, 76
 Da-tsao Hi-in Kim, 42
 Davidson, W. L., 318, 321
 Davis, D. H., 71, 76
 Davis, H. S., 253
 Davis, R., Jr., 356, 360,
 363, 364
 Davis, R. E., 449
 Davis, R. H., 430
 Day, T. B., 46, 48, 53, 75, 79

Daybell, M., 44
 Dayton, B., 32
 Dearnaley, G., 428
 De Benedetti, S., 12, 30
 Debraine, P., 431
 Debye, P., 326
 de Felice, J., 353, 357, 364,
 367
 De Hoffman, F., 97, 131,
 237, 238
 De La Mare, P. B., 444
 Demidov, A. M., 260, 261,
 262, 263, 274, 278, 279,
 280, 281, 282, 285, 294,
 295
 Denney, D. B., 444
 Derado, I., 12
 Deriagin, B. N., 44
 Desai, B. R., 24
 DeSantis, V., 69
 Deser, S., 113, 129
 De-Shalit, A., 21
 Desjardins, J. S., 286, 292
 d'Espagnat, B., 54, 59, 60
 de Swart, J. J., 139
 De Voe, J. R., 353
 Devons, S., 270
 Deutsch, M., 201
 Diamant, A. Ya., 287, 291
 Ditsch, L. T., 449, 454
 Diven, B. C., 286
 Dmitriev, I. S., 427
 Dobrotin, N. A., 34, 230
 Dodson, R. W., 450
 Domanic, F., 292
 Domokos, G., 20
 Donahue, D. J., 286
 Douglass, R. L., 54
 Downs, B., 48, 49
 Dragomirescu, D., 261
 Draper, J. E., 260, 261,
 265, 279, 285, 288, 289,
 292
 Dresner, L., 134
 Duke, P. J., 12, 30
 DuMond, J. W. M., 262, 436
 Dunmur, I. W., 335
 Dunn, T. M., 444
 Dunning, J. R., 318
 Durand, H., 188, 195
 Durand, L. III, 102, 141
 Dwight, K., 337
 Dyson, F. J., 121

E

Eberhard, P., 42, 46, 80,
 81, 82
 Eberhardt, A., 351
 Eberhardt, P., 349, 351,
 355, 356
 Eberle, E., 24
 Ebert, H. H., 360
 Eden, R. J., 98, 149
 Eder, G., 135
 Edison, D. H., 443, 446,
 448

Edwards, B., 402
 Edwards, C., 192
 Edwards, S. F., 128
 Egli, P., 32
 Ehlers, K. W., 422, 424,
 432
 Eisberg, R. M., 27
 Eisenbud, L., 99
 Eisenstein, J. C., 207, 210
 Ekspong, A. G., 14, 17, 22,
 23, 25
 Elloff, T., 22, 23, 29, 33
 Elliot, J. J., 444, 449
 Elliott, L. G., 263, 272
 Elliott, N., 332, 333, 335,
 341
 Elliott, R. J., 344
 Ely, R., 45, 46
 Ely, R. R., 44
 Emelyanov, A. A., 34, 35
 Emmons, W. D., 447
 Endt, P. M., 276, 279, 295
 Enge, H. A., 295
 Erb, E., 183
 Erickson, R. A., 314, 329,
 336, 338
 Ericson, T., 2, 283
 Espe, L., 100
 Esterman, I., 318
 Estle, T. L., 177, 188
 Estulin, I. V., 261, 265
 Evans, D., 44
 Everling, F., 271, 272
 Eversdijk Smulders, M. C.,
 198
 Ewing, M., 376

F

Fahey, R. C., 442, 443, 446
 Falk, C. E., 101
 Fano, U., 178
 Farley, F. J. M., 34
 Fateeva, L. N., 427
 Fazzini, T., 13
 Fedorov, V. N., 44
 Feinberg, E. L., 20, 34
 Feinberg, G., 50, 65, 67
 Feinstein, L., 464
 Feldman, D., 99, 102, 120,
 121, 128, 134
 Feldman, G., 50
 Feng, M. S., 445
 Fenstermacher, C. A., 287,
 288, 292
 Fergusson, G. J., 465
 Fermi, E., 4, 5, 7, 10, 14,
 19, 20, 21, 27, 29, 33, 62,
 305, 311
 Ferrari, F., 59, 70, 137
 Ferreira, E. M., 69
 Ferretti, B., 63
 Ferris, S. W., 466
 Ferro-Luzzi, M., 42, 80
 Ferroni, S., 33, 181
 Feshbach, H., 97, 102
 Fettweis, P., 265

Feynman, R. P., 138, 139
 Fialho, G. E. A., 17, 19
 Fidecaro, G., 13
 Fillmore, F. L., 101
 Filonov, U. A., 465
 Findel'shtein, Y. B., 465
 Finkelstein, R. J., 344
 Finn, C. B. P., 177
 Fiorini, E., 44
 Fireman, E. L., 350, 351,
 353, 354, 356, 357, 360,
 364, 367
 Firik, F. W. K., 287, 289,
 291, 292, 313
 Fischer, C. R., 142
 Fisher, P. C., 272
 Fleischer, A. A., 265, 279
 Flerov, G. N., 419, 432
 Florenskii, K. P., 363
 Fogel, Ia. M., 429
 Fogel, K. G., 100
 Foley, H. M., 102
 Fonda, L., 51, 137
 Foster, J. S., Jr., 422
 Fouché, V., 29
 Fowler, E. C., 29
 Fowler, P. H., 33
 Fowler, W. A., 350
 Fowler, W. B., 11, 12,
 14, 22, 23, 24, 27, 29, 33,
 46
 Fox, J. D., 287, 291
 Frahn, W. E., 129
 Franck, J. V., 432
 Frank, L. A., 405, 407
 Franzinetti, C., 14, 17, 22,
 23, 41, 44, 49, 54
 Frautschi, S. C., 23, 26,
 156
 Frazer, B. C., 323, 325
 Frazer, W. R., 156
 Freden, S. C., 407
 Fremlin, J. H., 419, 431
 Friedländer, E. M., 35
 Friedlander, G., 217, 230,
 232, 359
 Friedman, H., 403
 Frisch, D. M., 44
 Frisk, A., 22, 25
 Froman, P. O., 344
 Fry, W. F., 419
 Frye, G., 70
 Fubini, S., 64, 82, 83, 121,
 146, 153, 154, 155, 158
 162, 163
 Fubini, S. P., 98, 106, 107,
 135, 158, 159, 160
 Fujii, A., 84
 Fujii, S., 141
 Fujii, T., 12
 Fujii, Y., 68
 Fukuda, H., 20, 29
 Fukuda, N., 117, 121
 Fulco, J. R., 156
 Fuller, N., 456
 Fulton, T., 50, 103
 Furuichi, S., 161

G

Galinina, N. D., 287, 291
 Gammel, J. L., 96, 102,
 104, 141, 142
 Gardner, W. E., 321
 Garrett, B. S., 323
 Garrett, C. G. B., 189,
 194
 Garrison, J. D., 29
 Gartenhaus, S., 117, 123,
 139
 Gasiorowicz, S., 45, 127,
 129
 Gatto, R., 22
 Gatzke, A. L., 442
 Gavrilov, B. I., 261
 Geffen, D. A., 128
 Gehlen, H., 350
 Geilikman, B. T., 131
 Geiss, J., 349, 350, 354,
 356
 Gelernter, H., 141
 Geller, R., 428
 Geller, S., 338
 Gell-Mann, M., 41, 49, 58,
 82, 112, 143, 373
 Gentner, W., 248, 249, 350
 Gerling, E. K., 363
 Gessaroli, R., 48, 49, 54,
 66, 67, 71, 76
 Gettner, M., 44
 Gfeller, C., 353
 Ghiorso, A., 419
 Gibbons, J. H., 286
 Gibson, W. M., 32
 Gierula, J., 33, 34, 35
 Giguère, P. A., 450
 Gilderson, P. W., 449
 Giles, J. C., 194
 Gilletti, B. J., 465
 Gingrich, N. S., 326, 338
 Ginther, R. J., 313
 Ginzburg, V. I., 368
 Glaser, V., 129
 Glashow, S. L., 2
 Glasoe, P. K., 452
 Glauber, R. J., 344
 Glazer, R., 443, 446, 448
 Gluckstern, R. L., 96, 101,
 419, 427, 432
 Goebel, C., 22
 Goedkoop, J. A., 321
 Göing, M., 71, 76
 Gold, V., 453, 456
 Goldberger, M. L., 95, 98,
 112, 145, 157, 159, 160,
 164, 217, 232
 Goldfarb, L. J. B., 102
 Goldhaber, G., 11, 14, 17,
 22, 23, 24, 26, 68, 69,
 427
 Goldhaber, M., 62, 68, 263
 Goldhaber, S., 11, 14, 17,
 22, 23, 24, 26, 68, 69
 Goldman, J. E., 338
 Goldman, M., 450

Goldring, R. M., 450
 Goldstein, J. S., 100, 128
 Golovkina, V. S., 335
 Gomez, R., 44
 Good, M. L., 42, 46, 54,
 59, 66, 80, 81, 82, 84
 Good, R. H., 46
 Goodell, W. F., Jr., 242
 Goodenough, J. B., 333, 335
 Goodings, D. A., 192
 Googin, J. M., 450
 Gordon, F. J., 436
 Gordon, H., 432
 Gorter, C. J., 175, 177,
 187, 195, 201
 Goto, J., 105
 Goto, T., 23
 Gottstein, K., 71, 76, 84
 Gourdin, M., 69, 103, 116,
 128, 156
 Gove, N. B., 271
 Gow, J. D., 422, 432
 Grace, M. A., 175, 178,
 188, 192, 195, 199, 201
 Grashin, A. F., 164
 Graziano, W., 42, 80, 81,
 82
 Grechukhin, D. P., 268
 Green, G. K., 246, 248
 Green, H. S., 113, 116, 128
 Greenberg, A. P., 431
 Gregory, J. M., 199, 201
 Griffiths, G. M., 294
 Grisar, M. T., 157, 164
 Grobner, W., 132
 Groshev, L. V., 260, 261,
 262, 263, 264, 274, 278,
 279, 280, 281, 282, 283,
 285, 294, 295
 Grosse, A. V., 465
 Grummitt, W. E., 465
 Guenther, P. L., 350
 Guillaud, C., 336
 Gupta, M. L., 60
 Gupta, S. N., 65, 106, 117,
 135, 160
 Gürsey, F., 67
 Gustavi, S. G. M., 100
 Gutenberg, B., 393
 Gutowsky, H. S., 441

H

Haas, C., 450
 Haas, R., 270
 Haber-Schaim, U., 6, 33
 Hadjionnou, F. T., 139
 Hadley, J., 101, 104
 Haeblerl, W., 158
 Hafner, E. M., 101
 Hagedorn, R., 6, 7, 8, 9,
 12, 13, 14, 17, 18, 29, 30,
 32, 33
 Halban, H., 188, 195
 Halevi, E. A., 441, 442
 Hall, D., 164
 Hall, G. R., 202, 203, 207

- Hall, H. H., 100
 Halpern, I., 210
 Halpern, J., 318, 450
 Halpern, O., 266, 305, 311, 329
 Hamada, T., 98, 100, 112, 126, 137, 142, 143
 Hamermesh, B., 260, 261, 262, 279
 Hamilton, J., 157
 Hamilton, J. G., 419, 420, 430, 431
 Hamilton, W. C., 312, 325
 Hammermesh, M., 311
 Hanauer, S. H., 202, 203, 204
 Hanna, S. S., 192
 Hardy, J., Jr., 67
 Harkness, A. C., 450
 Harris, G. G., 44
 Harris, G. M., 451
 Harris, P. V., 450
 Harrison, B. K., 230, 231, 233, 234
 Hart, E., 12, 29
 Hart, E. W., 101
 Hart, H. E., 139
 Hart, H. R., Jr., 177, 188
 Hartsough, W., 101
 Harth, E. M., 12, 29, 48, 49, 54, 66
 Harvey, J. A., 272, 273, 276, 285, 288, 289, 291
 Harvey, J. T., 444
 Harvey, K. B., 450
 Hasegawa, H., 130
 Hasegawa, K., 137
 Hastings, J. M., 310, 326, 332, 333, 335, 337, 338, 341
 Hatcher, R. D., 139
 Hauser, U., 427
 Havens, W. W., 286, 292, 311
 Haworth, H. W., 454
 Haworth, L. J., 256
 Hawthorne, M. F., 447
 Hayakawa, S., 368
 Haymond, H. R., 419
 Hayward, E., 101
 Hayward, R. W., 196
 Heaton, L., 311, 321, 326, 327
 Heberle, J., 192
 Heckman, H. H., 14, 17, 22, 23, 426
 Heine, V., 192
 Heisenberg, W., 131
 Heller, L., 100
 Heller, R. B., 339
 Hemmendinger, A., 286
 Henley, E. M., 125, 136
 Hennessy, J., 29, 71, 76
 Henshaw, D. G., 327
 Herbst, R. F., 371-418; 398, 416
 Herman, R., 156
 Herpin, A., 336, 338
 Herr, W., 353
 Herschman, A., 139
 Hess, D. C., 350, 355, 356
 Hey, M. H., 349
 Heymann, D., 356, 363
 Hibdon, C. T., 263
 Hickok, R. L., 288
 Hiida, K., 136
 Hien, N. C., 12, 30
 Higgins, G. H., 377, 397
 Higgs, L. A., 260, 261, 274
 Hiida, K., 45
 Hildebrand, R., 226, 227, 229, 241, 420, 430
 Hill, D. A., 221, 222
 Hill, D. L., 201, 202, 207, 208
 Hill, J. S., 195, 201
 Hill, R. D., 71, 76
 Hindman, J. C., 451
 Hine, J., 454
 Hinman, C. W., 242
 Hintenberger, H., 351, 366
 Hirsch, W., 46
 Hirt, B., 354
 Hiruta, K., 441
 Hoang, T. F., 9, 11, 19, 22, 24, 26, 29
 Hobden, M. V., 188, 189, 190
 Hodge, E. B., 465
 Hodnett, E. M., 445
 Hoffman, J. H., 351, 360
 Hofstadter, R., 101, 156
 Hoge, H. J., 318
 Högfeldt, E., 452
 Holladay, W., 46
 Hollander, J. M., 431
 Holloway, L., 44
 Holyhski, R., 33, 34
 Honda, M., 351, 353, 356, 357, 358, 360, 363, 366
 Hoogenboom, A. M., 265
 Hoppes, D. D., 196
 Hornig, D. F., 450
 Hornyak, W. F., 101, 221, 222
 Horwitz, N., 22, 54, 59, 69
 Hoshizaki, N., 105
 Houtermans, F. G., 353
 Hoyle, F., 350
 Hsu, F. S. L., 191
 Hubbard, E. L., 419-38; 425, 426, 427, 432
 Hudis, J., 217, 218, 354, 357, 359, 450
 Hughes, D. J., 272, 273, 274, 276, 285, 287, 289, 318, 339, 340, 344
 Hughes, I. S., 48
 Huiskamp, W. J., 176, 198, 201
 Hulzenga, J. R., 282, 285
 Hull, D. E., 465, 466, 470
 Hull, M. H., Jr., 103, 139, 140, 141, 142, 158, 419
 Hultbén, L., 97, 100
 Hummel, V., 261
 Huntley, H. E., 350
 Hurst, D. G., 327
 Hurwitz, H., 278
 Huynh, V. D., 287, 290, 291
 Hwang, C., 186
 Hyman, H. H., 452
- I
- Ida, M., 128
 Igo, G., 292
 Ikeda, M., 62
 Ilakovac, N., 449
 Imamura, T., 159
 Inoue, K., 117, 122
 Ioffe, M. S., 420, 421, 422, 432
 Isaev, P. S., 157
 Ishida, S., 13
 Iso, C., 20, 29
 Rabashi, K., 121, 134
 Ito, D., 35
 Itoh, J., 441
 Ivanovskaya, I. A., 67
 Iwadare, J., 33, 103, 119, 135, 136, 138, 139, 141, 142
- J
- Jackson, J. D., 69, 70, 71, 73, 76, 139, 163, 278
 Jacob, M., 164
 Jacobi, R. B., 350
 Jacobs, I. S., 337
 Jagow, R. H., 442, 443, 446
 Jain, A. P., 292
 Jain, K. P., 59
 James, R. W., 317
 Janik, J., 344
 Jarrett, H. S., 338
 Jastrow, R., 97, 101, 141
 Jauch, J. M., 3, 42
 Jean, M., 130
 Jeffreys, H., 378
 Jeffries, C. D., 179, 181, 182, 183, 184, 185, 186
 Jensen, M. B., 442
 Jewell, R. W., 272
 Jilian, F. A., 429
 John, W., 272
 Johnson, C. E., 188, 192, 195, 201
 Johnson, E. A., 450
 Johnson, G. W., 377, 397
 Johnson, L., 101
 Johnson, M. H., 305, 311, 329
 Johnson, R. R., 442, 443, 445, 446, 447
 Johnston, W. H., 465
 Jones, B. D., 71, 76
 Jones, J. M., 442
 Jones, R. J., 420, 422
 Jones, W. B., 431

Jopson, R. C., 436
 Jordan, J. L., 129
 Jost, R., 103, 152
 Joy, H. W., 441
 Judd, D. L., 419
 Julien, J., 287, 290, 291
 Jurak, A., 33, 34
 Jurney, E. T., 272, 294

K

Kaganove, A., 452
 Kajfosz, J., 261
 Kalbach, R. M., 13, 15, 30
 Kalbfleisch, G. R., 42, 54, 67
 Kalinkin, L. F., 261, 265
 Kalogeropoulos, Th. E., 11, 24
 Kalos, M. H., 100, 141
 Kameswara Rao, N., 13, 15, 30
 Kane, W. R., 265
 Kaplan, T. A., 336
 Kapon, M., 41, 68, 69, 76
 Kardon, B., 261, 265, 277
 Karelitz, M., 244
 Karplus, R., 59, 145
 Karzas, W. J., 417
 Kasper, J. S., 335, 337
 Katsumori, H., 45, 46
 Katz, J. J., 452
 Kaufman, W. J., 465
 Kaufmann, S., 465
 Kawaguchi, M., 84
 Kawarabayashi, K., 60
 Kayas, G., 29
 Kazi, A. H., 262
 Kedzie, R. W., 182
 Keller, A., 100
 Kelly, E., 101
 Kemmer, N., 128
 Kennett, T. J., 287, 290
 Kerler, W., 427
 Kernan, A., 29
 Kerth, L. T., 49, 68, 84
 Ketley, A. D., 454
 Keuffel, J. W., 44
 Khuri, N. M., 98, 157, 159
 Khutsishvili, G. R., 183
 Kibby, C. L., 449
 Kikuchi, T., 49, 66
 Kikuta, T., 103
 King, D. T., 13
 Kinsey, B. B., 260, 261, 271, 272, 273, 276, 278, 286, 292, 294, 295
 Kinsey, J. L., 445
 Kirz, J., 80
 Kiss, D., 261, 265, 277
 Kittel, C., 337
 Kituchi, T., 48, 49, 54, 67
 Kladnitskaya, E., 42
 Klaiber, B., 13, 15, 30, 32
 Klein, A., 107, 117, 120, 121, 122, 125, 126, 127, 128, 129, 135, 136, 143, 165
 Kleiner, W. H., 305
 Knecht, D. J., 141
 Knee, T. E. C., 447
 Knipling, E. F., 473
 Knipp, J., 426
 Knoepfel, H., 261, 274
 Knowles, J. W., 261, 262, 263, 264, 272, 273, 274, 277, 279, 283, 284, 290
 Knox, W. J., 432
 Koba, Z., 2, 5, 10, 11, 20, 26, 34
 Kobayakawa, K., 14, 20, 23, 35
 Kobsarev, I. Yu., 164
 Koch, W., 13, 15, 30, 32
 Koehler, W. C., 303-48;
 312, 314, 319, 326, 329, 330, 333, 335, 336, 337, 338, 339, 340, 342
 Kohn, W., 103, 152
 Koide, S., 138
 Komoda, T., 139
 Kompaneets, A. S., 373
 König, L. A., 271, 272
 Konuma, M., 117, 125, 136
 Konzak, C. F., 472
 Koons, C. B., 447
 Kopecky, J., 261
 Kopylov, G. I., 19
 Koshiba, M., 368
 Kotani, T., 59, 196
 Kothari, D. S., 5
 Kothari, L. S., 33
 Kouvel, J. S., 335
 Kovacs, A., 48, 49, 54, 67
 Kovacs, J. S., 11, 13
 Koval, A. G., 429
 Kowitt, F. R., 454
 Kramers, H. A., 145, 333
 Kraus, D., 44
 Kraushaar, W. L., 34
 Kreevoy, M. M., 449, 454
 Kreplin, R. W., 403
 Kresge, A. J., 442, 447
 Kretzschmar, M., 1-40; 20, 21, 23, 33
 Krinov, E. L., 349
 Krishnamurty, K. V., 451
 Krone, R. W., 260, 261
 Kronig, R., 145
 Krueger, T. K., 286
 Kubitschek, H. E., 260
 Kudinov, B. S., 265
 Kuivila, H. G., 454
 Kulp, J. L., 465
 Kulwich, R., 464
 Kulygin, Y. F., 420, 432
 Kuni, F. M., 124, 157
 Kunzler, J. E., 191
 Kurnetsov, E. V., 67
 Kursunoglu, B., 121, 127
 Kurti, N., 175, 187, 188, 189, 190, 192, 195, 201
 Kusumoto, H., 441
 Kutznetov, A., 42
 Kycia, T. F., 49, 68, 84

L

Lagnaux, G. P., 71, 76
 Lal, D., 349, 353, 357, 358, 360, 366
 Lamb, W. A. S., 436
 Lambert, R. W., 453
 LaMer, V. K., 449
 Lancaster, T. H., 255
 Landau, L. D., 6, 20, 23, 33, 151
 Lande, K., 44
 Lander, R. L., 22, 23, 29, 33
 Landon, H. H., 287, 290, 291, 292
 Landshoff, P. V., 98
 Lane, A. M., 288, 294, 295
 Lane, J. A., 255
 Lanius, K., 35
 Lannutti, J., 42
 Lapaz, L., 404
 Larsen, R. R., 140
 Larson, M. O., 44
 Laserew, B., 189
 Lassen, N. O., 427
 Lassila, K., 103, 140
 Latter, A. L., 378, 397, 398
 Latter, R., 371-418; 387, 408, 412, 417
 Lattes, C. M. G., 104
 Laubenstein, R. A., 272
 Lauer, E. J., 425, 427
 Lauer, W. M., 447
 Loughton, P. M., 451
 Laurikainen, K. V., 100, 102
 Lawrence, E. O., 434
 Lea, R. M., 27
 Leader, E., 163
 Leavitt, C. P., 221, 222
 Lebedev, A. E., 12
 LeBlanc, M. A. R., 194
 Leboy, E., 44
 Lederman, L., 42
 Lee, B. W., 70
 Lee, J., 44
 Lee, T. D., 44
 Lee, W., 11, 24, 26, 68, 69
 Lee Whiting, G. E., 261
 Leffek, K. T., 443, 448
 Legros, M., 13
 Lehmann, H., 121
 Leifson, O. S., 183, 184, 185, 186
 Leipuner, L. B., 270
 Leiss, J. E., 253
 Leitner, J., 48, 49, 54, 66, 67
 Leitner, P. N., Jr., 66
 LeLevier, R. E., 397, 398
 Lemberg, I. Kh., 431
 Lemmer, H. R., 188, 195, 201
 Lendinara, L., 48, 49, 54, 67
 Lepore, J. V., 4, 9, 10, 11, 16, 19, 24, 119, 124, 136

- Levdik, V. A., 335
 Levin, J. S., 272, 273, 276, 285
 Levi-Setti, R., 59
 Levskii, L. K., 363
 Levy, H. A., 313, 320, 321, 323
 Levy, M. M., 108, 116, 117, 120, 126, 128, 138
 Lewis, E. S., 442, 443, 444, 445, 446, 447, 448, 449
 Lewis, H. W., 5, 11
 Lewis, R. E., 445
 Libby, W. F., 461-82; 349, 353, 441, 465
 Lichtenberg, D., 59
 Lichtin, N. N., 442, 447
 Liedtke, R. A., 260
 Lindenbaum, S. J., 213-58; 12, 27, 29, 30, 217, 218, 226, 227, 228, 232, 236, 237, 242, 243, 244, 245
 Lindhard, J., 427
 Lingelfelter, R., 363
 Link, W. T., 431
 Lipman, N. H., 13
 Litchtenberg, B., 59
 Littauer, R., 253
 Liu, L., 49
 Livingston, M. S., 250, 251, 253
 Livingston, R. S., 431
 Llewellyn, J. A., 443, 448
 Llewellyn, P. M., 202, 203, 207
 Lock, W. O., 32
 Loeb, A. L., 333
 Lomon, E. L., 98, 143
 Lomsadze, I. M., 131
 Long, F. A., 452, 453, 454, 455, 457
 Loopstra, L. H., 321
 Lopes, J. L., 138, 139
 Lord, J. J., 13, 15, 30, 419
 Losty, J., 402
 Louttit, R. I., 33
 Lovas, I., 261, 265, 277
 Love, P., 441
 Lowde, R. D., 310, 312, 344
 Lurie, D., 156, 164
 Lutsenko, V. N., 260, 262, 274, 278, 279, 281, 285, 294, 295
 Lyman, E., 84
 Lynch, G. R., 22, 24, 42
 Lynn, J. E., 294, 295
 Lynn Stevenson, M., 42
 Lyytikäinen, S., 100
- M
- McCausland, M. A. H., 183
 McCormick, B. H., 117, 125, 129, 135
 McDaniel, B. D., 84, 261
 McDonald, F. B., 366
 MacDowell, S. W., 154
 MacGregor, M. H., 97, 139, 140, 141, 143, 158, 221, 223
 McHargue, C. J., 329
 Machida, S., 104, 105, 107, 117, 118, 119, 122, 136, 137, 139, 161
 Macke, W., 126, 127, 128
 MacKey, J., 472
 Macklin, R. L., 286
 McLaughlin, E. J., 466
 McMillan, W. G., 397, 398
 Macomba, M., 470
 McReynolds, A. W., 340
 Maenchen, G., 27
 Magalinskii, V. B., 7, 17, 19, 20
 Maglit, B., 42
 Maier-Leibnitz, H., 263
 Maillard, R., 420
 Main, R. M., 432
 Makov, B. N., 420, 421, 422, 432
 Maksimenko, V. M., 6, 7, 14, 16, 17, 18, 21, 22, 24, 27, 28, 29, 30, 33
 Maleev, C. V., 344
 Malhotra, P. K., 13, 15, 30
 Malkin, M. S., 432
 Malov, A. F., 262
 Maltsev, V. M., 7, 14, 17, 29, 31, 32, 33
 Mandelstam, S., 98, 128, 144, 145, 150, 155, 156, 161
 Manfredini, A., 14, 17, 22, 23, 42
 Manley, J. H., 318
 Mann, A. K., 270, 274, 275
 Manning, G., 264, 265, 273, 274, 277, 279, 283, 284, 290
 Manning, G. K., 360
 Mansell, A. L., 450
 Marcinkowski, M. J., 326
 Maringer, R. E., 360
 Mark, H., 262, 436
 Markov, M. A., 41
 Marks, L. J., 34
 Marney, M. C., 313
 Marshak, R. E., 46, 84, 98, 99, 134, 135, 139, 142, 143
 Marshak, H., 193, 261
 Marshall, J., 242
 Marshall, L., 305, 311
 Marshall, L. C., 432
 Marshall, W., 344
 Martin, A., 59, 103, 141, 156, 162
 Martin, E. M., 69
 Martin, G. R., 350, 360
 Martinelli, E. A., 397, 398
 Mason, S. F., 444, 449
 Mateciuc, V., 261
- Matsen, R., 46
 Matsumoto, M., 102, 141
 Matsumoto, T., 137
 Matsuyama, S., 157
 Mattauch, J. H. E., 271, 272
 Matthews, P. T., 42, 45, 49, 69, 70, 130
 Mayne, K. I., 350, 359
 Meecham, W. C., 121
 Meinke, W. W., 353
 Melander, L., 440
 Melloranskii, A. S., 261, 265
 Melkanoff, M. A., 68, 69
 Melkonian, E., 318
 Meltzer, C. M., 48, 49, 54, 66, 67
 Meneghetti, D., 335
 Menke, H., 326
 Menon, M. G., 44
 Menyuk, N., 337
 Merekov, Yu. P., 13, 31
 Mèriel, P., 336, 338
 Mermoud, R. M., 32, 33
 Morrison, A. W., 13
 Messel, S., 141
 Metropolis, N., 102, 164, 217, 230, 232
 Meyer, H. W., 35
 Meyer, P., 51
 Michul, A., 42
 Miedema, A. R., 189, 198, 201
 Mięsowicz, M., 33, 34, 35
 Mikhul, E. K., 7, 14, 29, 31, 32
 Mikkelsen, K., 452
 Milburn, R. H., 4, 14, 16, 27, 28
 Milekhin, G. A., 20, 33
 Miller, D., 22, 42, 59, 69
 Miller, D. M., 54
 Miller, J. F., 419, 430, 431
 Miller, J. M., 217, 218, 230, 232, 354, 357
 Miller, P. D., 286
 Minguzzi-Ranzi, A., 66
 Mirza, S., 287, 290, 291
 Mislow, K., 443
 Mittelman, P. S., 260
 Miyazawa, H., 117, 125, 136, 157
 Mobley, R. C., 272
 Mocek, M., 442
 Moffat, J. W., 156
 Monahan, J., 261
 Monara, V., 54
 Monari, L., 48, 49, 54, 66, 67
 Moore, W., 226, 227, 228, 243
 Moore, W. M., 67
 Moorhouse, R. G., 45, 344
 Mora, S., 59, 71, 76
 Moravcsik, M. J., 95-174; 50, 84, 97, 103, 139, 140
 Morita, M., 196

- Morita, R. S., 196
 Morozov, P. M., 420, 421, 422, 432
 Morpurgo, G., 41-94; 41, 44, 54, 58, 65, 82, 121
 Morris, T. W., 29, 33
 Morrison, G. C., 217, 221, 232
 Morton, G. A., 318
 Moshinsky, M., 103
 Moszkowski, S. A., 103, 143
 Motchane, J. L., 183
 Moyer, B. J., 213, 215, 226, 227, 229, 230, 240, 242, 245
 Mueller, M. H., 321
 Muirhead, H., 217, 221, 232
 Murray, J., 22, 80
 Mott, J. E., 59
 Mottelson, B. R., 282, 283
 Motz, H. T., 261, 262, 263, 264, 272, 294
 Moxon, M. C., 287, 289, 291, 292
 Muchnik, M., 42
 Muehlhauser, C. O., 263, 285
 Muller, F., 46
 Munakata, Y., 127
 Murayama, S., 355
 Murray, J. J., 54, 59, 69
 Mutchler, G. S., 201
- N
- Nagai, H., 35
 Nahabedian, K. V., 454
 Naidenov, V. A., 263
 Nakabayashi, K., 124, 134
 Nakamura, S., 97, 107, 138
 Nambu, Y., 42, 44, 98, 124, 157
 Nanda, V. S., 5
 Nathans, R., 337, 340, 341
 Natsuyama, S., 157
 Nauenberg, M., 46, 82
 Néel, L., 332, 337
 Neiler, J. H., 286, 310
 Neilsen, G. C., 265
 Nesbitt, R. K., 333
 Netter, F., 287, 290, 291
 Neuman, M., 4, 6, 11, 19, 129
 Newton, R. G., 102, 103
 Newton, T. D., 282, 283, 284, 285
 Newton, T. W., 451
 Nielsen, S. O., 452
 Nier, A. O., 351, 360
 Nigam, B. P., 142
 Nikishov, A. I., 11, 14, 16, 17, 18, 21, 22, 23, 24, 27, 28, 29
 Nikitin, A., 42
 Nikolaev, V. S., 427
 Nikolett, M., 443, 448
 Nikolić, M., 13, 15, 30, 32
 Nilsson, S., 22, 25
- Nishijima, K., 106, 107, 119, 128, 134
 Niu, K., 34
 Nogami, Y., 82, 130
 Noonan, E., 449
 Norbeck, E., Jr., 424
 Norris, N. J., 432
 Northcliffe, L. C., 141
 Novozhilov, I. V., 125, 135
 Noyes, H. P., 95-174; 100, 101, 102, 103, 155, 161, 162, 163
 Nussim, M., 442
- O
- Obinakov, B. A., 261
 Obukhova, M. P., 465
 Occhialini, G. P. S., 104
 Ockman, N., 450
 Oda, M., 368
 Odier, S., 305, 342
 Oehme, R., 98, 157, 160
 Oeschger, H., 353, 354, 356
 Ogard, A. E., 451
 Ogawa, S., 62
 Ogievetskij, V. I., 45
 Ogimoto, T., 88
 Ohnuki, Y., 62
 Ohnuma, S., 138
 Okabayashi, T., 121
 Okubo, S., 46, 99, 117, 121, 122, 128, 134
 Okun, L., 48, 51, 52
 Olson, E. A., 366
 O'Malloran, T., 68, 69
 O'Neill, G. K., 230, 231, 233, 234
 Ono, K., 6
 Onuma, S., 117, 118, 119, 139
 Öpik, E. J., 355
 Oppenheimer, F., 432
 Oppenheimer, J. R., 11
 Orbach, R., 177
 Orear, J., 44
 Orlob, G. T., 465
 Ostrander, H., 262
 Oswald, L., 46
 Otsuki, S., 117, 125, 136, 138, 139, 141, 142
 Otvos, J. W., 467
 Overhauser, A. W., 180
 Ovsyannikov, V. M., 420, 432
 Owen, J., 176, 177, 194, 195, 202, 203
 Oxley, C. L., 101
- P
- Pais, A., 11, 22, 24, 26, 50, 55, 57, 58, 59, 60, 61, 67, 71, 88, 101
 Pal, Y., 45
 Palevsky, H., 287, 289, 290, 291, 344
 Palfrey, T. R., Jr., 253
 Palm, D., 444
 Pandya, S. P., 102
 Paneth, F. A., 350, 359
 Panofsky, W. K. H., 101, 104, 251, 252, 253, 432
 Paoletti, A., 310, 341
 Papineau, A., 420, 426
 Parikh, V. R., 29
 Paris, C. H., 276, 279
 Parker, G. W., 202, 203, 204, 208
 Parmley, T. J., 226, 227, 229, 241
 Patronis, E. T., 261
 Patterson, H. W., 226, 227, 241, 242, 254
 Pauli, W., 131, 134, 137
 Pauncz, R., 441
 Pauthenet, R., 338
 Pearlstein, L. D., 129
 Pearson, R. G., 447, 451, 452
 Pease, R. S., 323
 Peaslee, D. C., 11, 29
 Pekar, S. I., 137
 Peker, L. K., 295
 Pelekhov, V. I., 260, 274, 278, 280, 281, 282, 285, 294, 295
 Pepinsky, R., 323, 325
 Perkins, B. L., 426
 Perkins, D. H., 14, 17, 22, 23, 33, 402
 Perlow, G. J., 192
 Perneg, J., 34
 Perret, W. R., 378, 397
 Perring, J., 162
 Perring, J. K., 103
 Perry, S. G., 456
 Peterman, A., 45
 Peters, B., 349
 Peters, R., 432
 Peterson, S. W., 313, 316, 320, 321, 323
 Petrunkin, V. A., 12
 Petrziška, V., 28, 30
 Pevsner, A., 48, 49, 54, 66, 67
 Peyrou, C., 42
 Phillips, P., 162
 Phillips, R. J. N., 97, 103
 Piccioni, O., 46
 Pickart, S. J., 337
 Pickup, E., 27
 Pigott, M. T., 341
 Pilkuhn, H., 22
 Pines, D., 282
 Pinkau, K., 402
 Pinotti, P. L., 466
 Pinaki, G., 24
 Placzek, G., 237, 238, 344
 Pocker, Y., 444, 445, 452, 454, 455, 456, 457
 Polkinghorne, J. C., 98
 Pomeranchuk, I. Ya., 6, 23, 48, 137

Pond, V., 472
 Ponder, B. W., 447
 Pontecorvo, B., 44, 45
 Poole, M. J., 286
 Pope, N. K., 327
 Porter, C. E., 289, 290
 Postma, H., 193, 198
 Poulis, N. J., 177
 Pound, R. V., 195, 197
 Powell, C. F., 33, 104
 Powell, J. L., 100
 Powell, W. M., 11, 22, 23, 24, 26, 27, 29, 33, 46, 101
 Power, E. A., 135
 Prasad, N. O., 44
 Pratt, G. W., Jr., 333
 Prelog, V., 443
 Prentki, J., 51, 54, 59, 60
 Present, R. D., 100, 163
 Preston, M. A., 100, 101, 141
 Preston, R. L., 100
 Preston, R. S., 192
 Preston, W. M., 242
 Prevot, F., 428
 Price, E., 442, 447
 Price, W. C., 450
 Prince, E., 337
 Pringle, D. H., 464
 Pringle, R. W., 260, 261
 Prins, J. A., 326
 Prior, G. T., 349
 Pritchard, J. G., 453, 455
 Proctor, W. G., 183
 Prokesh, A., 67
 Prowse, D. J., 42, 44, 68, 69
 Pryce, M. H. L., 202, 203, 207, 210
 Puppi, G., 48, 49, 54, 66, 67
 Purlee, E. L., 453
 Püschel, W., 71, 76
 Pusterla, M., 70
 Putman, J. L., 468
 Putnam, T., 420, 430
 Putnam, T. M., 419
 Puzikov, L. D., 99
 Pyatt, K. D., Jr., 103, 140, 142
 Pyrah, A. E., 429

Q

Quarenì, G., 59, 71, 76
 Quarenì Vignudelli, A., 59
 Querzoli, R., 44
 Quinton, A. R., 432

R

Raas, V. F., 447
 Raboy, S., 261, 272
 Racah, G., 178
 Rae, E. R., 286, 287, 290, 291, 292
 Rahm, D. C., 33

Rainwater, L. J., 286, 311
 Rajopadhye, V. Y., 30
 Rall, W., 428
 Rao, K. N., 442
 Raphael, R., 135, 143, 165
 Raphael, R. B., 102, 103
 Rasmussen, J. O., 198, 199
 Rasmussen, N. C., 262
 Ratti, S., 44
 Rau, R. R., 33
 Ravenhall, D. G., 69, 70, 73
 Reardon, W. A., 260, 261
 Reasbeck, P., 350, 359
 Recksiedler, A. L., 279
 Redding, F. P., 450
 Reibel, K., 270, 274, 275
 Reier, M., 261
 Revutskij, E. I., 420, 432
 Reynolds, C. A., 193
 Reynolds, G. T., 67
 Reynolds, H. L., 422, 427
 Reynolds, J., 402
 Riazuddin, 101, 141, 157
 Ricci, F. P., 310
 Richman, C., 101, 432
 Richter, C. F., 381, 385, 386, 393, 395
 Riddell, R. J., Jr., 9, 16, 19
 Ringo, G. R., 261, 304, 318
 Riste, T., 344
 Riviere, A. C., 429
 Roberts, A., 12, 30
 Roberts, B. W., 335
 Roberts, F. F., 326
 Roberts, L. D., 175-212; 188, 190, 192, 196, 202, 203, 204, 207, 208, 210, 270
 Robertson, R. E., 443, 448, 451
 Robinson, F. N. H., 183, 186, 188, 189, 190, 201
 Robinson, K., 261
 Rodberg, L. S., 59, 68
 Rohrlisch, F., 3
 Romney, C., 385
 Ron, A., 441
 Ronne, B. E., 22, 25
 Roósz, J., 424
 Ropp, G. A., 442
 Rose, B., 186, 187
 Rose, D., 262
 Rose, M. E., 175, 178, 189, 195, 203, 266
 Rosen, J. L., 286, 292
 Rosenfeld, A. H., 41, 42, 46, 66, 70, 80
 Ross, M., 59, 60, 69
 Ross, M. H., 59
 Rosser, W. G. V., 217, 221, 232
 Rossi, B., 349
 Rossi, G. B., 419, 431
 Rossi, H. H., 213, 214, 216
 Rossi, V., 42
 Roth, B., 100

Roth, E., 450
 Roth, W. L., 326, 332
 Roulston, K. I., 260, 261
 Rouvina, J., 101
 Rozental, I. L., 2, 16, 17, 22, 33, 34, 35
 Rubbia, C., 44
 Ruderman, H., 44
 Ruderman, M. A., 125, 136, 145
 Rudstam, G., 357, 358
 Rukhadze, A. A., 121
 Runciman, W. A., 325
 Ruppel, H. M., 140
 Ruskin, V. I., 23, 27, 29
 Russel Stannard, F., 59
 Ryndin, R. M., 47, 99

S

Sachs, R. G., 311
 Sailor, V. L., 190, 193, 292
 Saint-James, D., 305, 342
 Sakata, S., 62
 Sakurai, J. J., 49, 58, 62, 63, 64, 165
 Salam, A., 42, 60, 69, 70, 126, 130
 Salant, E. O., 27
 Salinger, G. L., 189
 Salmeron, R., 66
 Salpeter, E. E., 100, 101, 126, 317
 Salvini, G., 44
 Salzman, F., 14
 Salzman, G., 14
 Samoilov, B. N., 193
 Sample, J. T., 265
 Sanders, T. M., 186
 Sandmann, W. H., 44
 Sands, M., 44
 Sandweiss, J., 14, 17, 22, 23
 Saniewska, T., 33, 34
 Sanjeevalah, B., 71, 76
 Saperstein, A. M., 102, 141
 Saplakoglu, A., 286
 Sasaki, M., 97, 107, 138, 139
 Satchell, D. P. N., 447, 453
 Sato, I., 124, 134
 Sato, M., 20, 29
 Sato, S., 134
 Saunders, W. H., Jr., 443, 446, 448
 Savchenko, O. V., 44
 Sawada, K., 117, 121
 Saylor, D. P., 143
 Scarf, F. L., 128
 Scatturin, V., 333
 Schaeffer, O. A., 351, 354, 356, 360, 363, 364
 Schectman, R. M., 28
 Scheidegger, A. E., 381
 Schenck, J., 310
 Scherrer, P., 261, 274
 Schiff, L. I., 13, 132

- Schink, D. R., 353
 Schleip, P. E., 48, 49, 54, 59, 66, 67
 Schooley, J. F., 198, 199
 Schmitz, N., 12, 156
 Schneeberger, M., 13, 15, 30, 32
 Schneeberger, R., 32
 Schofield, J. H., 102
 Schubnikow, L., 189
 Schultz, H. L., 287, 288, 292
 Schumacher, C. R., 116
 Schwäger, J. E., 265, 271
 Schwarcz, L., 432
 Schwartz, M., 42, 51, 53, 54, 88
 Schwartz, R. B., 273, 274
 Schwarzer, D., 350, 354
 Schweber, S. S., 121
 Schwinger, J., 101, 305, 317
 Scott, B. L., 103, 143
 Scott, J. M. W., 443
 Scully, N. J., 465
 Scurlock, R. G., 192
 Seaborg, G. T., 419
 Segel, R. E., 261, 265, 279
 Segre, E., 14, 17, 22, 23, 29, 33, 101, 430
 Selleri, F., 49
 Selove, W., 12, 44
 Seltzer, S., 444
 Senba, K., 137
 Sessler, A. M., 102
 Seth, K., 286
 Severi, M., 42
 Shah, S. M., 102
 Shamos, M. H., 261
 Shapiro, A., 221, 222
 Shapiro, J., 101, 141, 158
 Share, S., 165
 Sharma, O., 44
 Sharp, R. T., 125
 Sharrah, P. C., 327
 Shaw, G., 69
 Shaw, J. L., 60
 Shedlovsky, J. P., 353, 356, 360, 363
 Shephard, W. D., 27
 Shimizu, T., 88
 Shimoura, K., 45
 Shindo, M., 134
 Shiner, V. J., Jr., 444, 445, 446, 448, 456
 Shirane, G., 325, 340, 341
 Shirley, D. A., 198, 199
 Shklovsky, I. S., 368
 Shono, Y., 112
 Shore, F. J., 193
 Shostakovich, N. V., 44
 Shrivastava, P., 59
 Sneller, K. E., 444
 Shull, C. G., 304, 311, 312, 313, 314, 315, 318, 319, 320, 321, 326, 329, 330, 331, 332, 335, 337, 338, 340, 341
 Shut'ko, A. V., 295
 Shutt, R. P., 11, 12, 14, 27, 29
 Shvartsman, B. F., 287, 291
 Sidhu, S. S., 311, 321, 335
 Sidorov, V. M., 13, 31
 Siegel, R. T., 44
 Siegel, S., 326
 Siegler, A., 424
 Signell, P., 118, 140, 162
 Signell, P. S., 98, 135, 142
 Signer, P., 351, 356, 360
 Silberberg, R., 22, 26
 Silverman, A., 44, 84
 Simic, J., 287, 290, 291
 Simon, F., 175, 187, 188, 189, 190
 Simon, H., 444
 Simon, W. G., 426
 Simons, D. G., 201
 Simonsen, S. H., 323
 Simpson, O. C., 318
 Singer, S. F., 350
 Sirlin, A., 47
 Sittkus, A., 248, 249
 Skavlem, S., 100
 Skieggstad, O., 59
 Sklyarevskii, V. V., 193, 261
 Skok, J., 465
 Slater, W. E., 68, 69
 Slaughter, G. G., 313
 Slavatsky, S. A., 34
 Slichter, C. P., 181
 Slotnick, M., 329
 Slovatsky, S. A., 230
 Smith, D. P., 321
 Smith, F. M., 14, 17, 22, 23
 Smith, G. P., 327
 Smith, H. A., 450
 Smith, H. G., 316
 Smith, H. H., 472
 Smith, J. H., 335
 Smith, L., 221, 222, 432, 436
 Smith, R. L., Jr., 139
 Smorodinskii, Ya. A., 99
 Snow, G., 79, 101
 Snow, G. A., 46, 48, 50, 53, 75, 221, 222
 Soifer, U. N., 465
 Solnitz, F. T., 24, 59, 66, 84, 103
 Soloviev, M., 42
 Soloviev, M. I., 29, 45, 46, 82
 Soloviev, V. G., 65
 Soroko, L. M., 44
 Sowter, C. V., 195, 199
 Sparrow, A. H., 472
 Sperduto, A., 295
 Spitzer, R., 47
 Spohr, D. A., 188, 189, 190
 Sprengel, E. L., 356
 Springer, D. L., 398
 Springer, T. E., 285, 289, 292
 Squires, G. L., 318, 344
 Srivastava, P. P., 4, 19
 Stanford, C. P., 196
 Stanghellini, A., 27, 82, 83, 158, 162
 Stanisiz, O., 34
 Stanley, A. R., 465
 Stapp, H. P., 97, 102, 103, 139, 140, 164
 Starfeldt, N., 287, 297
 Stauffer, H., 351, 366
 Staveland, H. E., 465
 Steenland, M. J., 175, 178, 199, 201
 Stehn, J. R., 165
 Steinberger, J., 44, 84, 87
 Steiner, H. M., 22, 23, 29, 33
 Stellwagen, N. C., 447, 451, 452
 Stepanov, E. P., 193, 261
 Stephens, K. G., 431
 Stern, O., 318
 Sternheimer, R. M., 12, 27, 29, 30
 Stevens, K. W. H., 176, 177, 178, 194, 195
 Stevenson, M. L., 54, 59, 66, 84
 Stewart, A. T., 318, 344
 Stewart, R., 442
 Steyert, W. A., 189
 Stoenner, R. W., 360, 363, 364
 Stoll, H., 261
 Stoll, P., 261, 274
 Stolovy, A., 190, 194, 272, 273, 276, 285, 288, 292
 Stoppini, G., 44
 Stork, D. H., 14, 17, 22, 23, 68, 69
 Storm, M., 217, 230, 232
 Strand, R., 48, 49, 54, 66, 67
 Strauser, W. A., 329, 332, 338
 Street, K., Jr., 419
 Street, R., 335
 Streitwieser, A., Jr., 442, 443, 446
 Strutinski, V. M., 210, 282, 283
 Stuart, R. N., 4
 Stubbs, T., 68, 69
 Stückelberg, E. C. G., 63
 Stump, R., 260, 261
 Sturm, W. J., 311
 Succ, C., 44
 Sucher, J., 46, 48, 50, 53, 75, 79
 Sudarshan, E. C. G., 4, 19, 22, 46
 Suess, H. E., 366, 465
 Sugano, R., 127
 Sugawara, M., 97, 117, 122, 126, 134, 137, 139
 Sugie, A., 101

Sugihara, T. T., 353
 Sullivan, J. C., 451
 Sun, G. R., 67
 Sun, K. H., 313
 Sunderman, D. N., 353
 Sunko, D. E., 443, 448
 Suprunenko, V. A., 420, 432
 Suzuki, S., 442, 443, 446
 Swain, C. G., 447, 449, 450, 453, 454
 Swanson, D., 102
 Swartz, C. E., 12, 30, 226, 227, 228, 243
 Symanzik, K., 128, 145

T

Taffara, L., 69
 Taft, M., 54
 Taft, R. W., Jr., 441, 453
 Tagliaferri, G., 67
 Takagi, S., 2, 5, 11, 14, 34, 35
 Takahasi, J., 448
 Takeda, G., 26
 Taketani, M., 97, 104, 107, 117, 118, 119, 121, 122, 138, 139, 141
 Takibaev, Zh. S., 20, 33, 35
 Talman, R., 44
 Tamagaki, R., 138, 139, 141, 142
 Tamm, I., 120
 Tanaka, H., 45
 Tandon, J. N., 368
 Tani, S., 123, 141
 Taube, H., 450, 451
 Tausner, M. J., 158, 160
 Taylor, H. W., 260, 261
 Taylor, J. C., 98, 121
 Taylor, J. G., 49, 50
 Taylor, R. D., 445
 Taylor, R. T., 192
 Taylor, S., 44
 Teller, E., 317, 378, 426
 Ten-Gyn, 32
 Teplov, I. B., 279
 Teplova, Ia. A., 427
 Terent'ev, I. A., 125, 135
 Terletskii, Ya. P., 7, 17, 19, 20
 Terrell, J., 286
 Thaler, R. M., 68, 96, 102, 103, 104, 141, 142
 Thomas, G. E., 286
 Thomas, R. G., 289, 290, 294, 295
 Thompson, S. G., 419
 Thomson, J. O., 192
 Thorndike, A. M., 11, 12, 14, 27, 29, 33
 Thornton, E. R., 453
 Ticho, H. K., 42, 46, 54, 59, 68, 69, 80, 81, 82, 84
 Tiegte, J., 59, 71, 76
 Tiers, G. V. D., 441
 Timofeev, A. D., 429

Tiomno, J., 56, 88
 Tobias, C. A., 420, 430, 432, 436
 Tolhoek, H. A., 175, 176, 178, 199, 201
 Tolstov, K. D., 32
 Tomasini, A., 158
 Tomonaga, S., 129, 131
 Torelli, G., 44
 Tormo, J. V., 445
 Tosi, R., 49
 Touschek, B. F., 65, 121
 Toyota, T., 117, 122
 Trail, C. C., 261, 272
 Trammell, G. T., 305, 309, 342
 Treado, P. A., 261
 Treiman, S. B., 47, 50, 59, 61, 98, 159
 Trilling, G., 29
 Tripp, R. D., 22, 66
 Trisler, J. C., 447
 Trumpy, G., 265, 266, 277, 279
 Ts'ao, C. H., 13, 15, 30
 Tsao, C. J., 230, 231, 233, 234
 Tsiomis, A. K., 447
 Tsuzuki, Y., 13, 15, 30
 T-ty Nguen, 42
 Tuan, S., 69, 70, 73, 74, 75, 76, 77, 78, 79
 Tunkel, N., 444
 Turkevich, A., 217, 230, 232, 353
 Turkot, F., 84, 85, 87
 Turner, J. S., 100
 Tzoar, N., 135, 143, 165

U

Überall, H., 100
 Übersfeld, J., 183
 Umezawa, H., 128
 Urbanec, J., 261
 Uretsky, J., 45
 Urey, H. C., 349, 356
 Usik, P. A., 23, 29

V

Van Allen, J. A., 405, 407
 Van Atta, C. M., 432, 436
 Vandenbosch, R., 282, 285
 Vanderhaeghe, G., 32
 Van Dilla, M. A., 353
 Van Hove, L., 344
 Van Patter, D. M., 271, 295
 van Rossum, L., 14, 17, 22, 23
 Varho, O., 102
 Varshalovich, D. A., 277
 Veksler, V. I., 42
 Verbanic, C. J., 446
 Verlet, L., 141
 Vervier, J. F., 265, 267, 268, 269, 277, 279, 291

Videira, A., 88
 Vilcsek, E., 355
 Villain, J., 336
 Villi, C., 102
 Vincent, D. H., 192
 Vineyard, G. H., 327
 Vinogradov, A. P., 363
 Vinogradov, S. I., 335
 Violet, C. E., 377, 397
 Virgasov, N., 42
 Vishki, T., 31
 Vitale, B., 22, 29, 41, 46, 49, 58, 59, 60, 82, 83, 163
 Voelker, F., 432
 Vogt, E., 293
 Vogt, R. H., 292
 von Ardenne, M., 424
 von Behr, J., 13, 15, 31, 32
 Von Buttlar, H., 465
 von Dardel, G., 32, 33
 Voshage, H., 351, 366
 Vosko, S. H., 128
 Voss, R. G. P., 221, 222
 Vrana, I., 42

W

Waddington, G. J., 349
 Wainwright, T., 416
 Walecka, J. D., 64, 156
 Walker, D., 431
 Walker, R. L., 253, 261
 Walker, W. D., 27
 Walker, W. H., 295
 Wall, N. S., 279
 Wallace, J. W., 339
 Wallenmeyer, W. A., 29
 Waller, I., 344
 Walter, F. J., 202, 204
 Walters, A. E., 287, 292
 Waters, J. R., 287, 288, 289, 291
 Wanders, G., 127
 Wang, S. F., 32
 Wang Kan-chang, 42
 Wang Pei, 17, 31
 Wang Tau-tsen, 42
 Wänke, H., 351, 355, 356, 357, 360
 Wapstra, A. H., 271, 272
 Warner, C. III, 88
 Warren, J. B., 265
 Wartik, T., 441
 Watanabe, R., 465
 Watari, W., 102, 138, 139, 141, 142
 Waterstrat, R. M., 335
 Watson, D., 457
 Watson, K. M., 371-418; 117, 122, 123, 124, 136, 137, 139
 Watson, M., 59, 69
 Webber, W. R., 366
 Weber, G., 32, 33
 Weinman, J. A., 429
 Weinstock, R., 344
 Weiss, R. J., 310, 335

- Weisskopf, V. F., 125, 273,
 274, 275, 281, 285, 304
 Welsh, R. E., 286
 Wendt, I., 465
 Wentzel, G., 131
 Werbrouck, A. E., 67
 Werle, J., 116, 136
 Wernick, J. H., 191
 Werth, G. C., 398
 Wertheim, M. S., 141
 Westervelt, D. R., 411
 Weston, R. E., Jr., 439-60;
 441
 Whaling, W., 271
 Wheatley, J. C., 177, 188,
 189
 Wheeler, G. W., 432
 Wheeler, J. A., 201, 208
 Whipple, F., 404
 Whipple, F. L., 356
 White, D. H., 28
 White, H. F., 450
 White, H. S., 22, 23, 29,
 33, 46
 White, M. G., 246
 White, P., 54
 White, R. S., 407
 Whittemore, W. L., 11, 12,
 14, 27, 29
 Wiberg, K. B., 440
 Wiblin, E. R., 286, 292
 Wick, G. C., 127, 128,
 164, 344
 Wiegand, C., 22, 23, 29,
 33, 101
 Wightman, A. S., 164
 Wightman, C. E. III, 447
 Wigner, E. P., 51, 63, 99
 Wiig, E. O., 356
 Wilkinson, D. H., 295
 Wilkinson, M. K., 303-48;
 314, 320, 326, 329, 331,
 333, 335, 336, 338, 339,
 341
 Williams, R. W., 250, 251
 Willis, H. F., 376
 Willis, W. J., 33
 Wilson, A. T., 465
 Wilson, R., 84, 221, 222,
 260
 Wilzbach, K. E., 465
 Winstein, S., 448
 Winter, K., 32, 33
 Winzeler, H., 13, 15, 30,
 32
 Wojcicki, S., 42, 80, 81,
 82
 Wolf, W. P., 177
 Wolfenstein, L., 102
 Wolfgang, R. L., 353, 465
 Wölfl, W., 261
 Wolfsberg, M., 440
 Wollan, E. O., 303-48;
 304, 311, 312, 313, 314,
 315, 318, 319, 321, 326,
 329, 330, 332, 333, 335,
 336, 337, 338, 339, 340,
 341, 342
 Wong, D. Y., 100, 101,
 156, 162, 163, 164, 165
 Wong, H. S., 156
 Wood, R. E., 292
 Woodyard, J. R., 432
 Worsham, J. E., 320
 Worzel, S. I., 376
 Wouthuyzen, S. A., 11
 Wright, R. W., 27
 Wu, C. S., 311
 Wyld, H. W., Jr., 69, 70,
 71, 73, 76
 Wyly, L. D., 427
- Y
- Yafet, Y., 337
 Yajima, N., 14, 20, 23,
 35
 Yakovlev, L. G., 19
 Yamaguchi, Y., 42, 44, 51,
 62, 103
 Yamamoto, H., 128
 Yamamoto, Y., 12
 Yamanouchi, T., 44, 45
 Yang, C. N., 44, 62
 Yarb, V. A., 13, 31
 Yates, K., 442
 Yeivin, Y., 21, 33
 Yekutieli, G., 2, 6, 33
 Yoder, R., 162
 Yokoi, K., 6
 York, H., 101, 226, 227,
 229, 241, 420, 430
 Yoshimori, A., 336
 Yost, F. L., 294
 Young, H. D., 139, 158
 Young, J., 9, 19
 Yovits, M. C., 139
 Ypsilantis, T., 22, 23, 29,
 33, 102, 164
 Yuan, L. C. L., 29
 Yukawa, H., 104
- Z
- Zachariasen, W. H., 334
 Zadoeshnye, I. K., 363
 Zagury, L., 88
 Zähringer, J., 350, 351,
 354
 Zakrzewsky, J., 71, 76
 Zamori, Z., 261, 265, 277
 Zaretskii, D. F., 294, 295
 Zastavenko, L. G., 17
 Zaubers, D. D., 311, 321
 Zemach, A., 128
 Zernike, F., 326
 Zharkov, G. F., 103, 136
 Zichichi, A., 66
 Zielinski, P., 35
 Zimmerman, A. H., 45
 Zimmerman, R. L., 287,
 291
 Zimmerman, W., 127
 Zinn, R., 98, 135, 142
 Zorn, G. T., 71, 76
 Zucker, A., 419, 420, 422,
 427
 Zwickel, A., 451

SUBJECT INDEX

A

- Accelerators
 - for heavy ions, 419-38
 - see also Heavy-ion accelerators
- shielding
 - for high-energy machines, 213-58
 - see also Shielding
- Alpha-particle angular distribution
 - from oriented nuclei, 201-7, 210
 - see also Nuclear orientation
- Analyticity and unitarity
 - applied to nucleon-nucleon scattering, 143-66
 - see also Nucleon-nucleon scattering
- Angular correlation measurements
 - on neutron capture gamma-ray cascades, 265, 266, 276-78
 - see also Neutron capture gamma rays
 - in high-energy statistical methods, 11
 - see also Statistical methods
- Angular distribution
 - of alpha particles, 201-7, 210
 - of gamma rays, 175, 176, 179, 182, 193, 194, 198-201
 - of nuclear radiations, 175, 176
 - see also Nuclear orientation
- Antiferromagnetic materials
 - in nuclear orientation, 177
 - see also Nuclear orientation
- Antiferromagnetism studies
 - by neutron diffraction techniques, 332-36
 - see also Neutron diffraction
- Antihyperons
 - observation of, 42
 - see also Strange particles
- Atmospheric nuclear explosions
 - detection of, 371-76
 - see also Nuclear explosions

B

- Baryons
 - lack of evidence for new hyperons, 45
 - see also Strange particles
- Beam removal half-value thickness
 - of various shielding materials, 218, 221-29, 233, 235, 236
 - see also Shielding
- Bent-crystal spectrometer, 262, 263
- Beta-particle transmission gauges, 468, 469
 - see also Isotopes, industrial uses
- Beta-ray anisotropy
 - from aligned nuclei, 196-99
 - see also Nuclear orientation
- Biologic exposure to radiation, 213-17
- Bosons
 - heavy charged, 44, 45
 - neutral
 - hypercharge of, 42, 44
 - 62-64
 - pseudoscalar meson, 42, 44
 - vector ρ_0 meson, 44
- Bound nuclear levels
 - properties determined, 276-78
 - see also Neutron capture gamma rays
- Brookhaven AGS (alternating gradient synchrotron)
 - shielding layout, 247
 - see also Shielding
- collision, 230-31
 - see also Shielding
- Charged particles
 - search for mass 555 m_e mesons, 44
- Chemical reactions
 - isotope effects, 439-60
 - see also Isotope effects
- Circular polarization measurements
 - on gamma rays
 - in neutron capture cascades, 266-70, 276-78
 - see also Neutron capture gamma rays
- Clipper targets
 - in high-energy accelerators
 - use in controlling radiation distribution in, 247, 248
 - see also Shielding
- Coincidence measurements
 - on gamma rays, 265, 266
 - see also Neutron capture gamma rays
- Compound models
 - of strongly interacting particles, 62-64
 - see also Strange particles
- Compton spectrometer, 261, 262
- Cosmic-ray--induced nuclear effects
 - in meteorites, 349-70
 - activation analysis, 351
 - cosmic ray ages, 349, 350, 354-56
 - cosmogenic nuclide concentration in, 351-54
 - depth effects in cosmic ray bombardment, 350, 359-63
 - excitation functions for nuclide production, 358, 359
 - experimental methods, 351-54
 - long-lived activities in some irons, 363
 - low-energy nuclear reactions, 359
 - low-level counting techniques, 351, 353, 354
 - mass spectrometric methods, 351, 352
 - meteorite ablation, 349, 360, 363
 - meteorite collisions in

C

- Capture mechanisms
 - for neutrons, 293-97
 - see also Neutron capture gamma rays
- Cascade hyperon parity of, see Strange particles
- Cascades, 284, 285, 293
- Charged bosons
 - search for heavy mesons, 44, 45
- Charged particle multiplicity
 - per high-energy nucleon

- space, 355, 356
 meteorite erosion in space, 356
 neutron capture reactions, 359
 nuclear reactions in meteorites, 357-59
 space variation of cosmic ray intensity, 363, 364
 spallation reactions, 357-59
 tabulated production rates of nuclides, 367
 terrestrial ages of meteorites, 356, 357
 time variation of cosmic ray intensity, 364-68
 variation with depth and size, 350, 359-63
 space variation, 363, 364
 time variation, 364-68
 Crystal diffraction spectrometers, 261-63
 Crystalline electric field effects
 on electron spin, 176-78
 see also Nuclear orientation
 Crystallography and chemical binding studies
 by neutron diffraction, 319-27
 see also Neutron diffraction
 Cyclotrons
 for heavy-ion acceleration, 430-32, 435, 436
 see also Heavy-ion accelerators
- D**
- Delayed coincidence techniques, 266
 Deuteron binding energy, 100, 271, 272
 determinations, 271, 272
 and low-energy nucleon-nucleon interaction parameters, 100
 Deuteron polarization
 by nuclear resonance techniques, 187
 see also Nuclear orientation
 Deuteron stripping gamma-ray production
 compared to neutron capture gamma-ray production, 295
 Diffraction of neutrons, 303-48
 see also Neutron diffraction
 Direct current high-voltage accelerator, 428-30, 435
- see also Heavy-ion accelerators
 Dispersion relations
 applied to nucleon-nucleon scattering problem, 143-66
 see also Nucleon-nucleon scattering
- E**
- Earthquakes
 frequency and distribution of, 393-95
 see also Nuclear explosions
 "Effective" spin Hamiltonian for nuclear orientation, 176-79
 see also Nuclear orientation
 Electric quadrupole coupling, 195, 197, 198, 200, 203-7, 209, 210
 in alignment of iodine 131, 197, 198
 in alignment of promethium, 200
 see also Nuclear orientation
 Electromagnetic signals
 from atmospheric nuclear explosions, 373-75
 see also Nuclear explosions
 Electron accelerator
 shielding, 250-53
 see also Shielding
 Electron stripping
 for multiply charged ion production, 425-28
 see also Heavy-ion accelerators
 Elementary particles
 magnetic moments of, 43, 46
 masses of, 43, 45, 46
 properties of, 42-46
 spins of, 43, 46
 tabulated properties of, 42-46
 see also Strange particles
 Epithermal neutron capture, 286-93
 see also Neutron capture gamma rays
- F**
- Ferroelectric compounds
 neutron diffraction studies of, 323-25
 see also Neutron diffraction
 Ferromagnetism
 nuclear orientation studies, 177-78
 see also Nuclear Orientation
- Ferrimagnetism studies
 by neutron diffraction techniques, 330, 332, 336-38
 see also Neutron diffraction
 Field theory
 aspects of meson-nucleon problem, 108-13
 see also Nucleon-nucleon scattering
 Fission angular distributions
 from oriented nuclei, 201, 202, 207-10
 see also Nuclear orientation
 Flux density
 of penetrating particles through shielding walls, 227-28
 see also Shielding
 FM cyclotron shielding, 241-42
 see also Shielding
 Food preservation
 by irradiation, 475, 476
 see also Isotopes, industrial uses
 Form-factors, 305-6, 341-43
- G**
- Gamma-ray angular distribution
 in nuclear orientation studies, 175, 176, 179, 182, 193, 194, 198-201
 Gamma rays
 from neutron capture, 259-302
 resonance absorption of, 270, 274
 see also Neutron capture gamma rays
 Gauging
 by use of radioisotopes, 468-70
 see also Isotopes, industrial uses
 Genetic effects
 of radioisotopes
 in man, 478, 479
 see also Isotopes, industrial uses
 Global symmetry
 of strong interactions, see Strange particles
 and the Y resonance, 82, 83
- H**
- Half-value thicknesses
 for beam attenuation
 of shielding materials, 218, 221-29, 233, 235, 236

see also Shielding
 Hard core interaction
 in nucleon-nucleon scattering, 97, 116
 see also Nucleon-nucleon scattering
 Health problems
 concerned with radioisotopes, 477-79
 see also Isotopes, industrial uses
 Heavy-ion accelerators, 419-38
 aluminum oxide stripping foils, 427, 428
 arc discharge ion source, 420-24, 429, 430
 beam injection, 433-35
 carbon stripping foils, 428
 cathode materials
 for ion sources, 424
 charge distribution for O^{+3} ions in argon
 as a function of stripper thickness, 425
 Cockcroft-Walton accelerator
 for injection into linear accelerators, 434, 435
 conventional dc accelerators, 428, 429
 cyclotrons
 for heavy-ion work, 430-32, 435, 436
 using stripping, 430, 431
 without stripping, 431, 432
 direct current high-voltage accelerator, 428-30, 435
 duoplasmatron ion sources
 for multiply charged ions, 424
 equilibrium charge distribution
 of ions passing through matter, 425-27
 foil stripper, 427, 428
 future possibilities
 higher currents, 435, 436
 higher energies, 436
 variable energy, 435
 gas stripping methods, 428
 ionization potentials of ions
 commonly used, 420, 421
 jet stripping method, 428
 linear acceleration
 of different charge states, 433
 linear accelerator
 advantages of, 432
 performance, 435
 lithium arc discharge ion source, 424
 lithium ion production
 from rf ion source, 424
 multiply charged ion pro-

duction, 420-24
 by electron stripping, 425-28
 negative ion production
 for tandem Van de Graaff acceleration, 429, 430
 nickel stripping foils, 427
 Phillips ionization gauge-type ion source, 420-24
 PIG discharges
 as proton sources for linear accelerators, 422, 423
 poststripper linac, 432-35
 prestripper linac injection, 434, 435
 production of multiply charged ions
 for cyclotron acceleration, 420-24, 431, 432
 radial extraction
 from an ion source, 422, 423
 radiofrequency cavities
 for the heavy-ion linear accelerator, 432, 433
 secondary emission cold cathode-type ion sources, 420, 422
 sector-focused cyclotron
 for heavy-ion work, 432
 shielding, 213-55
 see also Shielding
 sources for ions of solid materials, 424
 stripper material
 dependence of average ion charge upon, 426-27
 stripping of ions
 for injection into linear accelerators, 433-35
 tandem Van de Graaff accelerators, 429, 430, 435
 Van de Graaff accelerator
 for injection into linear accelerators, 433
 variable energy cyclotron, 432
 Von Ardenne ion source
 for multiply charged ions, 424
 yield of higher charge
 states in arc discharge ion source
 as a function of current, 422, 423
 Heavy-ion linacs, 432-36
 see also Heavy-ion accelerators
 Heavy mesons
 strong interactions and reactions of, 41-94
 see also Strange particles
 High-energy physics
 statistical methods, 1-40
 see also Statistical methods

Hypercharge
 of neutral bosons, 42, 44
 see also Strange particles
 Hyperfine structure coupling
 in dilute paramagnetic salts, 194-210
 see also Nuclear orientation
 Hyperfine structure interaction, 177-79, 182, 195, 197, 198, 200, 202-7, 209, 210
 see also Nuclear orientation
 Hyperon nucleon scattering, 59, 60
 see also Strange particles
 Hyperons
 strong interactions and reactions of, 41-94
 see also Strange particles

I

Intermediate coupling
 in meson theories, 129-30
 see also Nucleon-nucleon scattering
 Internal conversion measurements, 263, 265
 see also Neutron capture gamma rays
 Ionization buildup factor
 for high-energy particle beams, 219-21
 Ionization density
 for various beam shielding thicknesses, 227-28
 see also Shielding
 Ion sources
 for heavy-ion accelerators, 420-24, 429, 430
 see also Heavy-ion accelerators
 Isobaric states
 of the nucleon
 in high-energy physics, 11-12, 27, 30-32
 see also Statistical methods
 Isomeric state yields
 in neutron capture, 284, 285
 see also Neutron capture gamma rays
 Isotope dilution techniques, 464, 465
 see also Isotopes, industrial uses
 Isotope effects in chemical reactions, 439-60
 absorption spectra
 of complexes of transition metal ions, 450
 acetolysis and formolysis
 of arylethyl tosylates, 448
 acid-base catalysis
 in heavy water, 453-57
 acid-catalyzed reaction

- of cyclohexyl 2, 2, 6, 6- d_4 phenyl ketone, 447
- aldol condensation, 457
- α - and β -2-methoxycyclohexyl mercuric iodide, 454
- aquation of trioxalatochromium (III), 451
- basic hydrolysis
 - of methyl p-methyl-t-benzoate, 445
- benzilic acid rearrangement, 455
- biological systems
 - in heavy water, 457
- bromination
 - of benzene- d_6 , 444
 - of biphenyl-4, 4'- d_2 , 444
- carbonium ion formations compared to analogous compounds deuterated in the α position, 442
- decomposition
 - of diacetone alcohol, 445, 455
 - of p-toluene- α , α , α - d_3 -diazonium fluoborate, 445
- dehydration
 - of acetaldehyde hydrate, 454, 456
- deoxymercuration reactions, 449, 454
- dipole moments
 - of HCl and DCl, 441
 - of NH_3 and ND_3 , 441
- disproportionation
 - of Np (V) to Np (IV) and Np (VI), 451
- dissociation constant ratios
 - in light and heavy water, 452
- dissociation constants
 - for formic acid and formic-d acid, 442
 - of Hammett indicators, 452
 - of methanol hemiketals, 442
- double bond
 - in $C_6H_5D:CDC_6H_5$, 444
- effect of α -deuterium substitution
 - in S_N1 solvolysis, 442-43
 - in S_N2 solvolysis, 443-44
- effects of β - and γ -deuterium substitution
 - in S_N1 solvolysis, 446
- electron transfer reaction
 - between Fe (II) and Fe (III), 450, 451
- electrophilic aromatic substitution, 447
- enolization, 447, 457
- equilibrium constants, 441
- esterification of CH_2TOH with p-nitrobenzoylchloride, 444
- ethanolysis and acetolysis, 448
- formation of ethylene oxide from ethylene chlorohydrin, 455
- formation of phenylhydrazones, 444
- ground state electronic energies
 - for the ethylcarbonium ion, 441
 - for toluene and toluene- α - d_3 , 441
- heavy water as a solvent, 449-50
- hydration, 445, 453
- hydrolysis, 445, 449, 451, 453-54, 455, 456
- hyperconjugation stabilization
 - of transition states, 444-45
- ionic systems
 - in heavy water, 450-52
- ionization constants, 442
- isomerization, 444
- isotopic substitution in the α position
 - effects on rate constants, 442-44
- mutarotation
 - of glucose and tetramethylglucose, 454, 456
- oxidation
 - of deuterated cumene, 447, 451
- partition function ratios
 - for ethane and ethane- d_6 , 440
- produced by heavy water as a solvent, 449-50
- pyrolysis
 - of ethyl- d_4 and ethyl- d_5 acetates, 449
- quarternization
 - of pyridine with methyl-t-iodide, 444
- racemization
 - of the mandelate ion, 457
- reaction rates, 444
- reactions
 - of Cr^{++} with $(NH_3)_5CrCl^{++}$, 444, 448, 451
- secondary isotope effects, 440-49
- S_N2 solvolysis, 448
 - of organic halides, nitrates, and sulfonates, 451-52
- spectra
 - in light and heavy water, 450
- substituted 9, 10-dihydro-9, 10-ethanoanthracene, 445
- tritium loss, 453
- ultraviolet spectra, 450
- vapor pressure ratio $P(H_2O)/P(HDO)$, 450
- vibrational frequencies
 - in liquid and solid water, 450
- Isotope identification
 - in neutron capture studies, 288
 - see also Neutron capture gamma rays
- Isotopes, industrial uses, 461-82
- beta-particle thickness gauges, 468, 469
- calcium utilization
 - in farm animal nutrition, 462
- carbon 14
 - in isotope dilution techniques, 464, 465
- as a chemical reagent, 477
- cobalt deficiency
 - in farm animal nutrition, 461
- dilution techniques
 - with isotopes, 464, 465-67
- eradication
 - of screw-worm fly, 471-73
- food preservation
 - by irradiation, 475, 476
 - possible cost, 476
- gamma-ray thickness gauging, 468, 469
- gauging, 468-70
- genetic effects in man, 478, 479
- isotopic power sources, 474-75
- lean meat assays
 - with potassium-40 gamma rays, 463-64
- level gauges, 468-70
- limitations, 477-80
- material flow in sponge iron furnaces
 - by tracer techniques, 467
- metabolism of sulfur
 - in farm animals, 461, 462
- molybdenum effect
 - on vitamin B₁₂ synthesis, 461
- pest control, 471-74
- plant mutations
 - for superior crops, 470-72
- radioactive nonisotopic tracer techniques, 465-67
- radioactivity contamination problem, 480
- radioisotope battery, 474, 475
- radioisotope studies

of farm animal nutrition,
461-63
radiography, 468
somatic effects
of radioisotopes in man,
477-79
strontium titanate
for radioisotope power
generators, 474, 475
substerilization
in food preservation by
irradiation, 475, 476
tracer techniques
applied to detergent resi-
dues on food, 463
and milk production, 462,
463
and oil flow in pipelines,
468
paper manufacture, 466,
467
and polysaccharide pro-
duction in cattle, 462,
463
and wear in machinery,
466
tritium
in isotope dilution tech-
niques, 464, 465
water-movement tracing,
465

K

K mesons
relative parity of K and \bar{K}
mesons, 88
see also Strange particles
K-meson charge exchange
cross sections, 70, 71,
73, 76
see also Strange particles
K⁻-meson reactions, 69-80
K-meson scattering
at low energy, 68, 69, 79
see also Strange particles

L

Lambda hyperon
parity of, see Strange
particles
Lambda-pion resonance,
79-83
see also Strange particles
Linear accelerators
for heavy-ion studies,
432-36
see also Heavy-ion accel-
erators
Linear energy transfer
dependence of RBE (rela-
tive biological effective-
ness), 214-15
see also Shielding
for high-energy accel-
erators

M

Magnetic form-factors
of atoms, 305-6, 341-43
see also Neutron diffrac-
tion
Magnetic investigations
by neutron diffraction
techniques, 327-44
see also Neutron diffrac-
tion
Magnetic moments
of elementary particles,
43, 46
see also Strange particles
Magnetic pair spectrometer,
261
Magnetic scattering
of neutrons, 305-6, 341-
43
see also Neutron diffrac-
tion
Mandelstam representation,
144-56
see also Nucleon-nucleon
scattering
Masses
of elementary particles,
43, 45, 46
see also Strange particles
Meson production
in nucleon-antinucleon
annihilation, 22-27
in nucleon-nucleon collis-
ions
at cosmic ray energies,
33-35
at energies below 30 Bev,
29-33
in pion-nucleon collisions,
27-30
see also Statistical methods
Meson-theoretic nucleon-
nucleon potentials,
104-43
Meson-theoretic potential
comparison with experiment,
138-43
see also Nucleon-nucleon
scattering
Meteorites
ablation, 349, 360, 363
achondrites, 350
chondrites, 350
depth effects
in cosmic ray bombard-
ment, 350, 359-63
"falls," 349
"finds," 349
"irons," 350
nuclear effects
of cosmic rays in, 349-70
see also Cosmic ray--
induced nuclear effects
nuclear reactions
induced by cosmic rays,
357-59

rare gases, 350
stone, 35
stony-iron, 350
see also Cosmic ray--
induced nuclear effects
Multiply charged ion pro-
duction
by electron stripping,
425-28
see also Heavy-ion accel-
erators
Muon shielding problems
for high-energy accel-
erators, 248-49
Mutations
produced in plants
by radioisotopes, 470-72
see also Isotopes, in-
dustrial uses

N

Neutral vector boson fields,
42, 44, 62-64
see also Strange particles
Neutron attenuation
in accelerator shielding,
218, 221-29, 233, 235,
236
see also Shielding
Neutron capture gamma rays,
259-302
absolute radiative neutron
capture cross sections,
271, 272
analysis
of capture gamma-ray
spectra, 282-84
angular correlation meas-
urements, 265, 266,
276-78
bent-crystal spectrometer,
262, 263
bound nuclear levels
properties of, 276-78
the capturing state
properties of, 271-76
cascades
multiplicity of, 284, 285,
293
circular polarization
of capture gamma rays,
266-70, 276-78
of gamma rays averaged
over cascade spectrum,
268
coincidence and angular
correlation meas-
urements, 265, 266, 276-78
Compton spectrometer,
261, 262
crystal diffraction spectrom-
eter, 261-63
(d,p) stripping reaction
comparison to neutron
capture gamma spectra,
295

- delayed coincidence techniques, 266
- deuteron binding energy determinations, 271, 272
- energy and intensity measurements, 260-63
- epithermal neutron capture, 286-93
- internal conversion measurements, 263, 265
- isotope identification, 288
- low-energy neutron capture theoretical description of, 294-97
- magnetic spectrometers, 261
- neutron capture mechanism, 293-97
- neutron separation energies, 271, 272
- Newton's level density formula, 283, 284
- 180° magnetic pair spectrometer, 261
- partial radiation widths of gammas from neutron capture, 272-76, 288-90, 297
- resonance absorption of gamma rays, 270, 274
- scintillation spectrometers, 260, 261, 289
- spectral distribution of gammas, 278-86
- spin assignments of epithermal neutron capture resonances, 290-93
- spin determinations from angular correlations and circular polarization measurements, 276-78
- sum coincidence method, 265, 266
- techniques in epithermal neutron capture studies, 287
- thermal neutron capture, 260-86
- thin-lens β spectrometer, 261
- total radiation widths, 285, 286, 292, 293-97
- yields of isomeric states in neutron capture, 284, 285
- Neutron capture mechanisms, 293-97
- Neutron diffraction, 303-48
 - antiferromagnetic crystals domain properties of, 338-39
 - auxiliary experimental equipment, 313-14
 - chemical binding effects upon neutron scattering, 306
 - coherent nuclear scattering amplitudes, 306, 307, 315-19
 - coherent scattering from a crystal, 307-8
 - composite crystals with heavy and light atoms, 319-23
 - compounds with special chemical or magnetic properties, 325-26
 - critical reflection from mirrors, 303, 305, 315
 - crystallography and chemical binding, 306, 319-27
 - equipment, 309-10
 - experimental procedures, 309-14
 - ferrimagnetism, 336-38
 - ferroelectric compounds, 323-25
 - ferromagnetic crystals domain properties of, 338, 339
 - ferromagnetism, 330-32
 - hydrogen-containing substances, 319-23
 - ice structure studies, 321, 323-24
 - incoherent scattering from a crystal, 308-9
 - indirect magnetic interaction, 332, 333
 - inelastic neutron scattering in solids, 242, 344
 - isotopic effects upon neutron scattering, 307
 - liquids and amorphous materials, 326-28
 - long-range modulation-type antiferromagnetic structures, 335-36
 - magnetic field effects, 338-39
 - magnetic form-factors of atoms, 305-6, 341-43
 - magnetic inelastic scattering, 344
 - magnetic investigations, 327-44
 - magnetic moments of atoms in magnetic alloys, 330-32
 - magnetic ordering studies, 338
 - magnetic scattering of neutrons by atoms, 305-6, 341-43
 - magnetic transitions, 338
 - "magnon" processes in magnetic structure, 344
 - "metamagnetics," 333-35, 339
 - monochromators, 310
 - neutron detection, 310, 313
 - neutron polarization, 340, 341
 - nuclear potential scattering, 304-5
 - neutron-proton interaction, 317-19
 - neutron scattering by an atom, 304-6
 - by atomic nuclei, 304-7, 315-19
 - neutron source, 309
 - nuclear scattering amplitudes, 306, 307, 315-19
 - nuclear scattering effects, 304-7, 315-19
 - nuclear spin dependence of neutron scattering, 306
 - nuclear studies, 306, 307, 314-19
 - order-disorder phenomena in alloy systems, 326
 - paramagnetism, 327-30
 - "phonon" processes in solids, 342, 344
 - photographic techniques, 313
 - powder method, 311-12
 - scattering of neutrons by crystals, 307-9
 - single-crystal method, 312, 313
 - super exchange in magnetic structures, 332-33
 - tabulated neutron scattering data for elements and isotopes, 316
 - techniques, 311-14
 - theoretical considerations, 304-9
- Neutron inelastic cross sections, 221-25
 - see also Shielding
- Neutron mean free path for removal in shielding materials, 218, 222-29, 233, 235, 236
- Neutron-nucleon cross sections relevant to shielding, 221-25
- Neutron polarization in neutron diffraction techniques, 340-41
 - see also Neutron diffraction
- Neutron-proton scattering amplitudes at thermal energies, 317-19

- Neutrons
 - RBE (relative biological effectiveness)
 - as a function of neutron energy, 215-17
- Nonlocal interactions
 - in nucleon-nucleon scattering, 97
 - see also Nucleon-nucleon scattering
- Nuclear demagnetization, see Nuclear orientation
- Nuclear explosions, detection of, 371-418
 - acoustic signals
 - detection of, 371-73
 - acoustic wave propagation in a real atmosphere, 372
 - age determination
 - of radioactive samples from nuclear explosions, 375-76
 - air fluorescence
 - produced by explosions in space, 411-12
 - amplitude of elastic waves
 - dependence on energy in underground explosion, 379-80
 - atmospheric disturbances
 - produced by explosions in space, 414
 - atmospheric ionization
 - produced by explosions in space, 412-14
 - atmospheric nuclear explosions, 371-76
 - background acoustic noise, 372-73
 - background electromagnetic signals, 374-75
 - Compton electron current
 - as source of electromagnetic signals, 373-74
 - detection techniques
 - recent research on, 399, 417
 - earthquakes
 - frequency and distribution of, 393-96
 - generation of seismic signals by, 379, 381-83
 - generation of signals by nonfaulting earth motion, 381, 382
 - electromagnetic signals
 - dependence on explosion asymmetry, 373-74
 - detection of, 373-75
 - estimation of detection and identification capability of seismic detection network, 387-93
 - experimental data
 - on explosion and earthquake signals, 383-87
 - explosions in space, 399-417
 - concealment of, 414-16
 - ground-based detection techniques for, 408-14
 - new detection techniques for, 417
 - shielding of delayed gamma rays and visible light from, 414-15
 - signals generated by, 398-401
 - visible light from, 408-11
 - X-ray shields for, 415-16
 - first P-wave motion, 382-87
 - generation of SH and Love waves by earthquakes and explosions
 - relative efficiency of, 381
 - initial source motion
 - propagation of, 382-87
 - microseismic noise, 383, 384
 - near-zone detection and identification capability, 391-93
 - network of seismic stations, 387-93
 - on-site inspection, 395-97
 - peak and first motion amplitudes
 - as a function of distance from the Blanca and Logan test explosions, 384-85
 - study of, from earthquakes, 385-87
 - peak P-wave amplitude of seismic signals, 383-87
 - Project VELA-Hotel, 417
 - Project VELA-Sierra, 417
 - Project VELA-Uniform, 399
 - radioactive debris
 - detection of, 375-76
 - satellite-based detection techniques, 401-8
 - seismicity
 - for a given geographical region, 395
 - seismic signals
 - generation of, 377-81
 - propagation of, 381-87
 - theoretical analysis, 387-93
 - shock wave propagation
 - in atmosphere, 371-72
 - sign of first P-wave motion, 382, 383, 386, 387
 - underground nuclear explosions, 376-99
 - cavity formation in, 377-78
 - concealment of, 397-99
 - decoupling method for, 397-99
 - shock waves from, 377-79
 - seismic methods for detecting, 376-99
 - seismic signals generated by, 377-81
 - underwater explosions
 - detection of, 376
 - generation of seismic signals by, 376
 - yield seismic signal amplitude relation
 - from Rainier-Hardtack data, 380
- Nuclear orientation, 175-212
 - angular distribution
 - of alpha particles, 201-7, 210
 - of beta particles, 196-99
 - of gamma rays, 175, 176, 179, 198-201
 - of nuclear radiations, 175, 176
 - antiferromagnetism, 177
 - "axial" alignment
 - of promethium isotopes, 199, 200
 - beta anisotropy
 - from aligned nuclei, 196-99
 - beta and gamma emission
 - from oriented holmium 166(m), 198, 199
 - "Bleaney" alignment, 195
 - "brute force" polarization method, 187-91
 - "crystal field" wave functions, 176, 177
 - crystalline electric field effects
 - on electron spin, 176-78
 - deuteron polarization
 - by nuclear resonance techniques, 187
 - of diamagnetic atoms
 - in ferromagnetic materials, 193
 - diffusion
 - of proton polarization, 185, 186
 - dipole-dipole coupling, 182, 183
 - dynamic method for producing, 179-87
 - dynamic polarization
 - of cobalt 60, 182
 - dynamic proton polarization
 - experiments, 180
 - effective spin Hamiltonian, 176-79
 - electric quadrupole coupling, 197, 198
 - electric quadrupole hyperfine structure, 195, 197, 198, 200, 203-7, 209, 210
 - fission angular distribution, 201, 202, 207-10
 - forbidden "R" and "S"

- transitions, 183, 184, 186, 187
- gamma-ray anisotropy, 175, 176, 179, 182, 193, 194, 198-201
- hydrocarbons
 - for proton polarization, 186, 187
- hyperfine structure coupling, 177-79, 182, 194-210
- interaction of polarized neutrons
 - with polarized holmium and gadolinium, 193, 194
- manganese isotopes, 200, 201
- methods for producing, 176-79
- nuclear alignment
 - of promethium isotopes, 199, 200
- nuclear demagnetization
 - use for obtaining extremely low temperatures, 189-91
- of nuclei
 - included in ferromagnetic or antiferromagnetic materials, 192-94
- Overhauser method for producing, 180, 181
- paramagnetic salts
 - use in production of, 194-210
- parity nonconservation
 - experiments, 196, 197
- partially forbidden transitions
 - saturation of, 181-83
- "planar" alignment
 - of promethium isotopes, 200
- polarization
 - of gamma rays, 198, 199, 201
 - of protons, 180, 183, 185-87, 188
- "Rose-Gorter" polarization, 195
- polarization
 - by saturating "forbidden" electron resonances, 182, 183, 184-87
- "Pound" alignment, 195
- scattering of polarized neutrons
 - from polarized target nuclei, 189, 190
- spin-Hamiltonian
 - for magnetically dilute materials, 176, 177
- static method for producing, 178, 179, 187-210
- thermal-neutron fission
 - of oriented uranium nuclei, 207-10
- uranium and neptunium isotope experiments, 201-10
 - using a relaxation process, 180, 181
- Nuclear scattering effects
 - in neutron diffraction studies, 304-7, 315-19
 - see also Neutron diffraction
- Nucleon-antinucleon annihilation
 - meson production, 22-27
 - see also Statistical methods
- Nucleon beams
 - mean free path
 - in shielding materials, 218, 221, 229, 233, 235, 236
- Nucleon-nucleon collisions
 - at cosmic ray energies
 - meson production, 33-35
 - at energies under 30 Bev
 - meson production, 29-33
 - see also Statistical methods
- Nucleon-nucleon scattering
 - "adiabatic potential," 107
 - analyticity and causality relationship between, 144-45
 - analyticity and unitarity, 143-66
 - "anomalous threshold," 150
 - Bethe-Salpeter equation, 126-29
 - boundary condition models, 102-3
 - Brueckner-Watson method
 - for constructing mean potentials, 122-24
 - Brueckner-Watson (BW) potential, 117, 123-24
 - canonical transformation method
 - for obtaining potentials, 118-19
 - Cap potential, 132-33
 - charge independence
 - in low-energy interactions, 100-1, 163
 - Chew cutoff theory, 125
 - "classical" meson field model, 130-31
 - Clementel-Villi ambiguity, 157-58
 - connection among nucleon-nucleon, nucleon-pion, and pion-pion scattering, 151-54
 - coupling
 - of pseudoscalar mesons to nucleons, 111-13
 - D-state percentage
 - in the deuteron, 100, 139
 - depolarization measure-
 - ments, 98
 - deuteron binding energy, 100
 - deuteron magnetic moment, 100
 - deuteron quadrupole moment, 100
 - dispersion relations applied to, 143-66
 - in energy, 157-58
 - double spectral representation, 144-56
 - early high-energy phenomenology, 101-2
 - effective-range treatment, 98
 - Feynman graphs
 - general substitution rule for, 147
 - location of singularities, 151
 - field theory, 108-13
 - Foldy-Wouthuysen transformation
 - applied to the Bethe-Salpeter equation, 127
 - Frazer-Fulco amplitude, 164
 - Fukuda-Sawada-Taketani (FST) potentials, 117, 122
 - Gammel-Thaler potential, 102
 - Gartenhaus potential, 117, 123-24
 - Hamada potential, 134, 142-43
 - "hard core" interaction, 97, 116
 - helicity amplitudes, 164
 - interaction between pseudoscalar mesons and nucleons, 111-13
 - intermediate boson
 - between nucleon and pion, 137-38
 - intermediate coupling theories, 129-30
 - isobar model effects upon, 102, 103, 137
 - Klein-McCormick (KMCC) potential, 117, 125, 129
 - Konuma-Miyazawa-Otsuki (KMO) potential, 117, 125
 - "ladder" approximation
 - to two-body equation, 126, 128
 - logarithmic derivative
 - in phenomenological models, 102-3
 - low-energy parameter, 100-1, 138-39
 - L. S potentials, 142-43, 165, 166
 - Mandelstam representation, 144-56
 - meson field theory, 108-13

- meson-potential calculations
at high energy, 140-42
meson-theoretic potentials,
104-43
calculation of corrections
to, 125, 133-38
comparison with experi-
ment, 138-43
general requirements for,
106
methods for constructing,
124-25, 126-29
modified phase-shift an-
alysis, 142-43
neutron-proton scattering,
101
"new Tamm-Dancoff"
schemes, 121
Nogami-Hasegawa poten-
tial, 130
nonlinear meson theories,
131-33
nonlocal interactions, 97
nonrelativistic limit of
scattering theory
in terms of potentials, 99
nonrenormalizability
of pseudovector coupling
meson theory, 113
"nonstatic" or recoil
corrections, 133-35
nonweak coupling theories,
129-33
one-dimensional dispersion
relations, 157-58
one-pion-exchange inter-
action
proof of validity, 138-40
 3P_0 and 3P phases
and the tensor force, 103,
104
pair processes
in weak coupling theories,
113-14
pair suppression
in meson theory, 112,
156
partial-wave dispersion
relations, 160-63
phase-shift analysis, 97,
103, 104, 140-43
phenomenological models,
99-104, 143
phenomenological poten-
tials, 103-4
photodisintegration
of the deuteron, 139
pion-nucleon coupling,
111-13
pion-nucleon coupling con-
stant, 152
pion-nucleon scattering
pole, 152
pion-pion interaction effects
on nucleon-nucleon poten-
tial, 137, 155, 156
pion-pion and pion-nucleon
scattering, 137, 154-56
pion-pion resonance, 155-
56
potentials
derived from weak cou-
pling meson theory, 114-
17
potentials from field-
theoretic amplitudes
construction of, 158-60
proton-proton scattering,
101
pseudoscalar and pseudo-
vector couplings, 111-
13
equivalence of, 111-13
P-wave phase shifts, 103,
104, 140-42
radiative corrections, 136
recoil corrections, 133-35
renormalization
of pseudoscalar coupling
meson theory, 113
of the Tamm-Dancoff
theory, 121-22
repulsive hard core
from meson theory, 116
scattering amplitudes
singularities in, 145-66
scattering description
in the nonrelativistic
limit, 99
Schrödinger equation
used to obtain potentials,
118-24
semiphenomenological
potential models, 143
separable potentials, 103
singlet effective range,
100-1, 139
singlet scattering lengths,
100-1, 139
 1S_0 n-p and p-p scattering
lengths, 103-4
static meson potentials
graphs contributing to,
114
static potential or μ/M
limit, 106-7
strong coupling theories,
130-31
Sugawara-Okubo (SO) po-
tential, 122-27
Taketani-Machida-Onuma
(TMO) potential, 117-
18, 124, 141
Tamm-Dancoff method,
119-22, 126-27
tensor force
between nucleons, 102
theories of, 95-174
triplet effective range, 100
triplet scattering length,
100
two-pion-exchange inter-
action, 163-65
unitarity and analyticity,
143-66
unphysical region, 152
vacuum polarization
in nonlinear theories, 131
vector mesons
in strong interactions,
165-66
velocity-dependent inter-
actions, 97, 102, 103,
106
weak coupling potentials,
114-17, 127-29
weak coupling theories,
113-29
Nucleonic cascades in
shielding materials
Monte Carlo calculation of,
232-35
see also Shielding
- O
- One-meson exchanges
in high-energy events, 13,
14
see also Statistical methods
Orientation
of nuclear spins, 175-212
of nuclei
in ferromagnetic or anti-
ferromagnetic materials,
192-94
using a relaxation process,
180, 181
see also Nuclear orientation
Overhauser method
for producing nuclear
orientation, 180, 181
see also Nuclear orientation
- P
- Paramagnetic impurity atoms
use for producing nuclear
orientation, 182-87
see also Nuclear orientation
Paramagnetic salts
use in production of nuclear
orientation, 194-210
see also Nuclear orientation
Paramagnetism studies
by neutron diffraction tech-
niques, 327-30
see also Neutron diffrac-
tion
Parities
of the strange particles,
46-53, 88
see also Strange particles
Parity conservation
in strong interactions,
64-68
see also Strange particles
Parity nonconservation
nuclear orientation experi-
ments, 196, 197
Partial radiative widths

- for gamma-ray emission
 - in neutron capture, 272-76, 288-90, 297
 - see also Neutron capture gamma rays
 - Particle buildup factor
 - for high-energy particle beams, 220-22, 229-35
 - see also Shielding
 - Particles
 - elementary
 - tabulated properties of, 42-46
 - see also Strange particles
 - Phase-shift analysis
 - for nucleon-nucleon scattering, 97
 - see also Nucleon-nucleon scattering
 - Phenomenological models
 - in nucleon-nucleon scattering, 99-104, 143
 - see also Nucleon-nucleon scattering
 - "Phonon" processes
 - in solids, 342, 34
 - Photodisintegration
 - of the deuteron, 139
 - Pion-hyperon scattering, 60-61, 77-83
 - Pion-nucleon coupling, 111-13
 - Pion-nucleon system
 - interaction Hamiltonian densities for, 111-13
 - see also Nucleon-nucleon scattering
 - Polarization
 - of deuterons
 - by nuclear resonance techniques, 187
 - of gamma rays
 - from oriented nuclei, 198, 199, 201
 - see also Nuclear orientation
 - of protons
 - by the "brute force" method, 188
 - by nuclear resonance techniques, 180, 183, 185-87
 - see also Nuclear orientation
 - Polarized beams
 - in neutron diffraction techniques, 340-41
 - see also Neutron diffraction
 - Power production
 - from radioisotopes, 474, 475
 - see also Isotopes, industrial uses
 - Proton-nucleon cross sections
 - relevant to shielding, 221-25
 - see also Strange particles
 - Proton polarization
 - diffusion of, 185, 186
 - by nuclear resonance techniques, 180, 183, 185-87
 - see also Nuclear orientation
 - Proton synchrotrons
 - shielding, 242-46
 - see also Shielding
 - Pseudoscalar boson with
 - T equal to zero, 42, 44
- R
- Radiation
 - as chemical reagent
 - in organic chemistry, 477
 - see also Isotopes, industrial uses
 - Radiation dosage
 - maximum permissible limits, 215-16
 - for nonoccupational exposures, 216
 - for occupational personnel, 216
 - nominal tolerance level, 216-17
 - in terms of particle fluxes, 216-17
 - see also Shielding
 - Radiation pest control methods, 471-74
 - see also Isotopes, industrial uses
 - Radiation from radioisotopes
 - industrial uses of, 470-77
 - see also Isotopes, industrial uses
 - Radiation widths
 - for gamma-ray emission
 - in neutron capture, 272-76, 285, 286, 288-90, 292, 293-97
 - see also Neutron capture gamma rays
 - Radioactive debris
 - from nuclear explosions
 - detection of, 375-76
 - see also Nuclear explosions
 - Radiographic uses of radioisotopes, 468
 - see also Isotopes, industrial uses
 - Radioisotopes
 - genetic effects
 - in man, 478, 479
 - health problems in use of, 477-79
 - regulations pertaining to use of, 477-79
 - see also Isotopes, industrial uses
 - Radioisotope tracer applications
 - in farm animal nutrition studies, 461-63
 - Radioisotopic level gauges, 468-70
 - see also Isotopes, industrial uses
 - Radioisotopic power sources, 474, 475
 - see also Isotopes, industrial uses
 - Radioisotopic thickness gauges, 468, 469
 - see also Isotopes, industrial uses
 - RBE (relative biological effectiveness)
 - dependence on linear energy transfer
 - of a radiation, 214-15
 - of minimum ionizing particles, 214-15
 - of neutrons
 - as a function of energy, 215
 - see also Shielding
 - of radiations
 - encountered at high-energy accelerators, 213-17
 - Relative parities
 - of the strange particles, 46-53, 88
 - see Strange particles
 - Resonance absorption
 - of gamma rays, 270, 274
 - Resonances
 - in strong interactions, 42, 50, 51, 79-83
 - see also Strange particles
- S
- Satellite-based detection techniques
 - for nuclear explosions in space, 401-8
 - see also Nuclear explosions
 - Scattering
 - of neutrons
 - by atoms, 304-6
 - see also Neutron diffraction
 - of neutrons
 - by crystals, 307-9
 - see also Neutron diffraction
 - of thermal neutrons
 - by nuclei, 304-7, 315-19
 - see also Neutron diffraction, Nuclear explosions, Nucleon-nucleon scattering, Strange particles
 - Schroedinger equation, 118-24
 - Scintillation spectrometers
 - for gamma-ray measure-

ments, 260, 261, 289
 Seismic signals
 generated by natural earthquakes, 379, 381-83
 generated by underground nuclear explosions, 377-81
 propagation of, 381-87
 first P-wave motion, 382-87
 peak P-wave amplitude, 383-87
 see also Nuclear explosions
 Shielding, for high-energy accelerators, 213-58
 attenuation lengths
 for electron-photon showers, 250
 for nucleon removal, 218, 221-29, 233, 235-36
 Berkeley shielding measurements, 226-27
 for the Bevatron, 245-46
 biologic exposure to radiation, 213-17
 biologic requirements, 213-17
 Brookhaven shielding measurements, 227-29
 buildup factors
 for various secondary beam components, 220, 221, 222, 229-35
 cascade neutron production in shielding, 230-32
 charged particle multiplicity
 per high-energy nucleon collision, 230-31
 clipper targets, 247-48
 concretes
 properties and cost of, 253-56
 cost versus density
 for high-density concrete shielding, 255
 cracks in, 256-57
 for a deuteron cyclotron (200-Mev), 241-42
 effective mean free path for particle removal, 218, 221-29, 233, 235, 236
 effective removal
 of the primary component, 219
 for electron accelerators, 250-53
 equilibrium buildup factor, 221-22
 evaporation neutron production in, 230-32
 external beam experiments at the Cosmotron, 244-45
 FM cyclotron, 241-42

ground leakage
 of radiation, 241
 half attenuation thickness of neutrons in heavy concrete, 233
 for high-intensity target areas
 at the Cosmotron, 244
 high-temperature damage effects
 in concrete, 255
 ionization attenuation problem
 with muons, 248-49
 ionization buildup factors, 219-21
 ionization density
 as a function of shielding thickness, 227-28
 ionization density dependence
 of RBE, 214-16
 layout for Brookhaven alternating gradient synchrotron, 247
 macroscopic inelastic cross sections
 for shielding materials, 253
 materials for shielding, 253-57
 maximum permissible radiation dose, 215-17
 mean free path for high-energy nucleon removal, 218, 221-29, 233, 235, 236
 muon shielding problem, 248-49
 neutron attenuation in, 218, 221-29, 233, 235, 236
 neutron flux for given dosage
 as a function of energy, 217
 neutron-nucleon cross section, 221-25
 neutron production
 from Stanford two-mile electron accelerator, 252
 nucleon cascades
 in heavy concrete, 233
 from high-energy electron and gamma radiation, 250-53
 Monte Carlo calculations of, 232-35
 in target and shielding materials, 217-19, 232, 235
 nucleon interactions
 with lithium hydride at 300 Bev, 230
 one-dimensional infinite slab problem, 218-25,

235, 236
 particle buildup factor, 220-21
 penetrating particle flux density
 as a function of shielding thickness, 227-28
 phenomenological shielding calculations, 235-36
 for proton accelerators
 in several hundred Mev to several Bev energy range, 217-49
 proton-nucleon cross section, 221-25
 radiation damage limit on lifetime of concrete, 255
 radiation dosage
 in terms of particle fluxes, 216-17
 radiation lengths
 in various materials, 253-54
 radiation source characteristics
 for the AGS machines, 247-48
 for weak-focusing proton synchrotrons, 242-44
 RBE dependence
 on the LET of a radiation, 214-15
 RBE of minimum ionizing particles, 214-15
 RBE of neutrons
 as a function of energy, 215
 RBE of various radiations, 213-17
 removal half-value thickness
 of shielding materials, 218, 221-29, 233
 roof shielding, 236-42, 244
 for FM cyclotron, 242
 shielding attenuations required, 218
 shielding block designs, 256-57
 "sky shine" and roof shielding, 236-42, 244
 Stanford two-mile linear electron accelerator, 251-53
 strong-focusing synchrotrons, 246-49
 tolerance level
 for radiation dosage, 216-17
 transition region
 for attenuation of high-energy nucleon beams, 222-23
 water content of concrete, 255

- for weak-focusing proton synchrotrons, 242-46
- Sigma hyperon
 - parity of, 50-53, 88
- "Sky shine," 236-42, 244
 - see also Shielding
- Somatic effects of radiation
 - from radioisotopes, 477-79
 - see also Isotopes, industrial uses
- Spectral distribution of gamma rays
 - in neutron capture, 278-86
 - see also Neutron capture gamma rays
- Spin assignments of epithermal neutron capture resonances, 290-93
- Spin-Hamiltonian for magnetically dilute materials, 176-77
 - see also Nuclear orientation
- Spin orientation of nuclei, 175-212
 - see also Nuclear orientation
- Spins of elementary particles, 43, 46
 - see also Strange particles
- Stanford two-mile electron accelerator
 - neutron production from, 252
- Static methods for producing nuclear orientation, 178, 179, 187-210
 - see also Nuclear orientation
- Statistical methods, in high-energy physics, 1-40
 - angular correlations, 11
 - angular momentum conservation, 3, 7, 9-11
 - applications to special processes, 22-35
 - calculational methods for phase-space integrals, 14-19
 - data
 - on nucleon-nucleon collisions at 6.2 Bev, 15
 - deuteron production at high energy, 32
 - Fermi model, 2-11
 - final state interactions, 11-13
 - formulation in terms of spherical waves, 10-11
 - inelasticity and peripheral collisions, 6, 13, 14, 28, 31-32, 34
 - interaction volume, 4-13
 - isobar formation, 11-12, 27, 30-32
 - isotopic spin conservation in statistical models, 20-22
 - limits
 - to validity of model, 6-7
 - meson production
 - in nucleon-antinucleon annihilation, 22-27
 - in nucleon-nucleon collisions at cosmic ray energies, 33-35
 - in nucleon-nucleon collision at energies below 30 Bev, 29-33
 - in pion-nucleon collisions, 27-30
 - Monte Carlo method for evaluating phase-space integrals, 17-19
 - peripheral collisions and inelasticity, 6, 13, 14, 28, 31, 32, 34
 - phase-space integrals, 4, 9, 14-19
 - physical picture corresponding to statistical model, 5-6
 - production volume, 4-13
 - prong distribution in pion-nucleon collisions, 28
 - recurrence relation for phase-space integrals, 19
 - scattering theory formulation of the problem, 2, 3
 - statistical hypothesis, 3-7
 - strange particles in, 6-8, 23-24, 26, 29, 33
 - theoretical formulation, 2-22
 - thermodynamic approximation for very high-energy events, 19-20
 - "two-center" model of nucleon-nucleon collisions, 34-35
- Strange particles
 - in high-energy statistical theory, 6-8, 23-24, 26, 29, 33
 - see also Statistical methods
 - magnetic moments of, 46
 - masses of, 43, 45, 46
 - new symmetries, 54-68
 - relative parities of, 46-53
- cascade hyperon, 47
- correlations of polarizations and momenta, 50
- "cusp" method, 51-53
- Dalitz's method, 48, 49
 - determination for Λ , N , K , 47-50
 - determination for Λ and Σ hyperons, 50-53, 88
- dispersion relations, 49
- extrapolation method, 49, 50
- of K and \bar{K} mesons, 88
- Okun and Pomeranchuk's method, 47, 48
- the Y - π resonance method, 50-51
- spins of, 43, 46
- strong interactions and reactions of, 41-94
 - angular distributions in associated production, 84-88
 - associated production by photons and pions, 85-89
 - baryonic charge, 63, 64
 - comparison of scattering length approximation to K - N interactions, 76-77
 - compound models, 62-64
 - Coulomb effects in K - p elastic scattering, 75, 76
 - Dalitz-Tuan K - N scattering amplitudes, 74
 - doublet symmetry, 55-62, 67
 - dynamic problems, 68-89
 - global symmetry and the Y^* resonance, 82, 83
 - heavy mesons, 41-94
 - hypercharge, 62-64
 - hyperon-nucleon scattering, 59, 60
 - hyperons, 41-94
 - isotopic spin assignments under doublet symmetry, 56-62
 - K -meson charge exchange cross section, 70, 71, 73, 76
 - K -meson reactions, 69-80
 - K - N interactions, 70-80
 - K - n scattering, 68, 69, 79
 - K - p absorptive processes, 79, 80
 - K -proton elastic scattering, 68-71, 73-80
 - neutral vector boson fields, 42, 44, 62-64
 - new symmetries, 54-68
 - parity conservation by,

54-68
 parity nonconservation in
 associated production,
 66, 67
 pion-hyperon scattering,
 60-61, 77-83
 reaction matrix treatment,
 77-80
 relative parity of the cas-
 cade particle and
 nucleon, 47
 relative parity of K and
 K mesons, 88
 relative parity of lambda
 and sigma hyperons,
 50-53, 88
 resonances, 42, 50, 51,
 79-83
 restricted and global
 symmetry, 58-61
 scattering length approxi-
 mation to K-N inter-
 actions, 73-77
 Σ and Σ^+ production
 cross sections, 69, 70,
 72, 73-80
 time reversal invariance,
 63-67
 vector bosons, 42, 44,
 62-64
 weak doublet symmetry,
 61, 62
 Y- π (and K- π) resonance,
 79, 80-83
 Strong coupling theories
 of nucleon-nucleon in-
 teraction, 130-31
 see also Nucleon-nucleon
 scattering
 Strong-focusing proton syn-
 chrotrons
 shielding, 246-49
 see also Shielding
 Strong interactions
 see Strange particles

Sum coincidence method,
 265, 266
 Symmetries
 in the strong interactions
 of the strange particles,
 54-68
 see also Strange particles

T

Tamm-Dancoff methods
 in meson theory, 119-22,
 126-27
 see also Nucleon-nucleon
 scattering
 Theories of nucleon-nucleon
 scattering, 95-174
 see also Nucleon-nucleon
 scattering
 Thermal neutron capture,
 260-86
 fission of oriented uranium,
 207-10
 Time reversal invariance
 of strong interactions, 65-67
 see also Strange particles
 Total radiative widths
 of neutron capturing states,
 285, 286, 292, 293-97
 see also Neutron capture
 gamma rays
 Tracer techniques
 with radioisotopes, 461-64
 see also Isotopes, in-
 dustrial uses
 Transition region
 for attenuation of high-
 energy nucleon beams,
 222-23
 see also Shielding
 Tritium
 as a tracer
 for water movement, 465
 see also Isotopes, in-
 dustrial uses

Two-body equation, 126-
 29

U

Underground nuclear ex-
 plosions
 detection of, 376-99
 see also Nuclear explos-
 ions
 Underwater nuclear explo-
 sions
 detection of, 376
 see also Nuclear explo-
 sions
 Unitarity and analyticity
 applied to nucleon-nucleon
 scattering, 143-66
 see also Nucleon-nucleon
 scattering

V

Vector bosons, 42, 44, 62-
 64
 see also Strange particles
 Velocity-dependent inter-
 actions
 in nucleon-nucleon scat-
 tering, 97, 102, 103,
 106
 see also Nucleon-nucleon
 scattering

W

Weak coupling theories
 of nucleon-nucleon inter-
 actions, 113-29
 see also Nucleon-nucleon
 scattering
 Weak-focusing proton syn-
 chrotrons
 shielding, 242-46
 see also Shielding

CUMULATIVE INDEX OF CONTRIBUTING AUTHORS

VOLUMES 7 TO 11

A	J	Powers, E. L., 7:63
Ajzenberg-Selove, F., 10:409	Judd, D. L., 8:181	Q
Aldrich, L. T., 8:257	K	Quastler, H., 8:387
Alper, T., 10:489	Kendall, H. W., 9:343	R
Anders, E., 9:203	Koch, L. J., 9:437	Rainwater, J., 7:1
Arnold, J. R., 11:349	Koehler, W. C., 11:303	Reines, F., 10:1
Atwood, K. C., 9:553	Konopinski, E. J., 9:99	Roberts, L. D., 11:175
B	Kraus, K. A., 7:31	Robertson, J. S., 7:135
Bartholomew, G. A., 11:259	Kretschmar, M., 11:1	Rosenfeld, A. H., 7:407
Beckerley, J. G., 10:425	L	Rugh, R., 9:493
Bond, V. P., 7:135	Lane, J. A., 9:473	S
Bradner, H., 10:109	Latter, R., 11:371	Segrè, E., 8:127
C	Lauritsen, T., 10:409	Stapp, H. P., 10:292
Cameron, A. G. W., 8:299	Libby, W. F., 11:461	Stocken, L. A., 9:523
Chamberlain, O., 10:161	Lindenbaum, S. J., 7:317; 11:213	Storer, J. B., 10:561
Chew, G. F., 9:29	Lushbaugh, C. C., 7:163	Suess, H. E., 8:243
Church, E. L., 10:193	M	T
D	MacGregor, M. H., 10:313	Talmi, I., 10:353
Dabbs, J. W. T., 11:175	Miller, J. M., 9:159	Thompson, R. C., 10:531
DuMond, J. W. M., 8:163	Moravcsik, M. J., 10:324; 11:95	U
F	Morpurgo, G., 11:41	Unna, I., 10:353
Feshbach, H., 8:49	Morrison, G. H., 9:221	V
Freiser, H., 9:221	Moyer, B. J., 8:327	Villars, F., 7:185
Fry, W. F., 8:105	N	W
G	Neher, H. V., 8:217	Watson, K. M., 11:371
Garden, N. B., 7:47	Nelson, F., 7:31	Weneser, J., 10:193
Gell-Mann, M., 7:407	Ney, E. P., 10:461	Weston, R. E., Jr., 11:439
Grahn, D., 10:561	Nielsen, E., 7:47	Wetherill, G. W., 8:257
Greisen, K., 10:63	Nierenberg, W. A., 7:349	Wick, G. C., 8:1
H	Noyes, H. P., 11:95	Wilkinson, D. H., 9:1
Halpern, I., 9:245	O	Wilkinson, M. K., 11:303
Harvey, B. G., 10:235	Okun', L., 9:61	Wolf, A. P., 10:259
Herbst, R. F., 11:371	Ord, M. G., 9:523	Wollan, E. O., 11:303
Hofstadter, R., 7:231	P	Wood, T. H., 8:343
Holmes, B. E., 7:89	Paxton, H. C., 9:437	Z
Hubbard, E. L., 11:419	Post, R. F., 9:367	Zucker, A., 10:27
Hudis, J., 9:159		

CUMULATIVE INDEX OF CHAPTER TITLES

VOLUMES 7 TO 11

ACCELERATORS		
Conceptual Advances in Accelerators	D. L. Judd	8:181-216
Optics of High-Energy Beams	O. Chamberlain	10:161-92
Heavy-Ion Accelerators	E. L. Hubbard	11:419-38
CHEMISTRY, NUCLEAR AND RADIO-		
Radiochemical Separations by Ion Exchange	K. A. Kraus, F. Nelson	7:31-46
Equipment for High Level Radiochemical Processes	N. B. Garden, E. Nielsen	7:47-62
Technetium and Astatine Chemistry	E. Anders	9:203-20
Solvent Extraction in Radiochemical Separations	H. Freiser, G. H. Morrison	9:221-44
Labeling of Organic Compounds by Recoil Methods	A. P. Wolf	10:259-90
Isotope Effects in Chemical Reactions	R. E. Weston, Jr.	11:439-60
COSMIC RAYS		
The Primary Cosmic Radiation	N. V. Neher	8:217-42
Cosmic Ray Showers	K. Greisen	10:63-108
Experiments on Cosmic Rays and Related Subjects during the International Geophysical Year	E. P. Ney	10:461-88
Nuclear Effects of Cosmic Rays in Meteorites	J. R. Arnold	11:349-70
DETECTORS		
Gamma-Ray Spectroscopy by Direct Crystal Diffraction	J. W. M. DuMond	8:163-80
Electronics Associated with Nuclear Research	H. W. Kendall	9:343-66
Bubble Chambers	H. Bradner	10:109-60
FISSION (REACTORS)		
Nuclear Fission	I. Halpern	9:245-342
High-Temperature Plasma Research and Controlled Fusion	R. F. Post	9:367-436
Fast Reactors	L. J. Koch, H. C. Paxton	9:437-72
Economics of Nuclear Power	J. A. Lane	9:473-92
INTERACTION OF NUCLEAR RADIATIONS AND MATTER		
Nuclear Methods for Subsurface Prospecting	J. G. Beckerley	10:425-60
Industrial Uses of Isotopes	W. F. Libby	11:461-82
LOW TEMPERATURES		
Nuclear Orientation	L. D. Roberts, J. W. T. Dabbs	11:175-212
MESONS AND ELEMENTARY PARTICLES		
Mu-Meson Physics	J. Rainwater	7:1-30
Hyperons and Heavy Mesons (Systematics and Decay)	M. Gell-Mann, A. H. Rosenfeld	7:407-78
Invariance Principles of Nuclear Physics	G. C. Wick	8:1-48
Hyperfragments	W. F. Fry	8:105-26
Antinucleons	E. Segrè	8:127-62
The Pion-Nucleon Interaction and Dispersion Relations	G. F. Chew	9:29-60
Strange Particles	L. Okun'	9:61-98
Neutrino Interactions	F. Reines	10:1-26
Statistical Methods in High-Energy Physics	M. Kretzschmar	11:1-40
Strong Interactions and Reactions of Hyperons and Heavy Mesons	G. Morpurgo	11:41-94

NEUTRONS [SEE ALSO FISSION (REACTORS)]		
Neutron Capture Gamma Rays	G. A. Bartholomew	11:259-302
Neutron Diffraction	M. K. Wilkinson, E. O. Wollan, W. C. Koehler	11:303-48
NUCLEAR GEOLOGY, COSMOLOGY		
Radioactivity of the Atmosphere and Hydrosphere	H. E. Suess	8:243-56
Geochronology by Radioactive Decay	L. T. Aldrich, G. W. Wetherill	8:257-98
Nuclear Astrophysics	A. G. W. Cameron	8:299-326
NUCLEAR MOMENTS, NUCLEAR MODELS AND STRUCTURE		
Collective Model of Nuclei	F. Villars	7:185-230
Measurement of the Nuclear Spins and Static Moments of Radioactive Isotopes	W. A. Nierenberg	7:349-406
Optical Model and Its Justification	H. Feshbach	8:49-104
Experimental Clarification of the Laws of β -Radioactivity	E. J. Konopinski	9:99-158
Theoretical Interpretation of Energy Levels of Light Nuclei	I. Talmi, I. Unna	10:353-408
Appendix: Energy Levels of Light Nuclei	F. Ajzenberg-Selove, T. Lauritsen	10:409-24
Nuclear Structure Effects in Internal Conversion	E. L. Church, J. Weneser	10:193-234
NUCLEAR REACTIONS		
Nuclear and Nucleon Scattering of High-Energy Electrons	R. Hofstadter	7:231-316
Collision of π Mesons with Nuclei (Excluding Electrons and Photons)	S. J. Lindenbaum	7:317-48
Nuclear Photodisintegration	D. H. Wilkinson	9:1-28
High-Energy Nuclear Reactions	J. M. Miller, J. Hudis	9:159-202
High-Temperature Plasma Research and Controlled Fusion	R. F. Post	9:367-436
Nuclear Interactions of Heavy Ions	A. Zucker	10:27-62
Recoil Techniques in Nuclear Re- action and Fission Studies	B. G. Harvey	10:235-58
Nucleon-Nucleon Scattering Experi- ments and Their Phenomenological Analysis	M. H. MacGregor M. J. Moravcsik H. P. Stapp	10:291-352
Statistical Methods in High- Energy Physics	M. Kretzschmar	11:1-40
Strong Interactions and Reactions of Hyperons and Heavy Mesons	G. Morpurgo	11:41-94
Theories of Nucleon-Nucleon Elastic Scattering	M. J. Moravcsik, H. P. Noyes	11:95-174
POSITRONIUM, ANTIPARTICLES		
Invariance Principles of Nuclear Physics	G. C. Wick	8:1-48
Antinucleons	E. Segrè	8:127-62
RADIATION EFFECTS AND HAZARDS		
Biochemical Effects of Ionizing Radiation	B. E. Holmes	7:89-134
Practical Control of Radiation Hazards in Physics Research	M. G. Ord, L. A. Stocken	9:523-52
Detection of Nuclear Explosions	B. J. Moyer R. Latter, R. F. Herbst, K. M. Watson	8:327-42 11:371-418
RADIOACTIVITY		
Neutrino Interactions	F. Reines	10:1-26
RADIOBIOLOGY		
Cellular Radiobiology	E. L. Powers T. H. Wood K. C. Atwood T. Alper H. Quastler	7:63-88 8:343-86 9:553-92 10:489-530 8:387-400
Information Theory in Radiobiology		

Vertebrate Radiobiology		
Embryology	R. Rugh	9:493-522
Lethal Actions and Associated Effects	V. P. Bond, J. S. Robertson	7:135-62
Pathology of Radiation Exposure	C. C. Lushbaugh	7:163-84
Metabolism of Internal Emitters	R. C. Thompson	10:531-60
Late Effects	J. B. Storer, D. Grahm	10:561-82
SHIELDING		
Shielding of High-Energy Accelerators	S. J. Lindenbaum	11:213-58
(See also RADIATION HAZARDS)		
SPECTROSCOPY		
Gamma-Ray Spectroscopy by		
Direct Crystal Diffraction	J. W. M. DuMond	8:163-80